AD NUMBER
ADC018374
CLASSIFICATION CHANGES
TO: **unclassified**
FROM: **secret**
LIMITATION CHANGES
TO: **Approved for public release, distribution unlimited**
FROM: **Controlling DoD Organization: U.S. Naval Electronic Systems Command, Washington, DC 20360.**
AUTHORITY
ONR ltr, 31 Jan 2006; ONR ltr, 31 Jan 2006

AD-C018374

~~4. TITLE (and Subtitle)~~

MOORED SURVEILLANCE SYSTEM FIELD VALIDATION TEST
SENSOR PERFORMANCE ANALYSIS, [redacted]
~~VOL. III~~, VERNIER RESOLUTION DATA PRODUCTS (U).
Volume III,

~~7. AUTHOR(s)~~

(9)

SECRET (This page is UNCLASSIFIED.)

SECURITY CLASSIFICATION OF THIS PAGE (When Data Entered)

REPORT DOCUMENTATION PAGE

READ INSTRUCTIONS BEFORE COMPLETING FORM

1. REPORT NUMBER

2. GOVT ACCESSION NO.

3. RECIPIENT'S CATALOG NUMBER

(9)

4. ~~TITLE (and Subtitle)~~

(6) MOORED SURVEILLANCE SYSTEM FIELD VALIDATION TEST SENSOR PERFORMANCE ANALYSIS, [redacted]

~~VOL. III~~, VERNIER RESOLUTION DATA PRODUCTS (U).

Volume III.

5. ~~TYPE OF REPORT & PERIOD COVERED~~

final rep[redacted]t,

10 JAN 77 - 31 MAR 78,

6. PERFORMING ORG. REPORT NUMBER

ARL-TR-78-3

7. ~~AUTHOR(s)~~

(10) Steven L./Watkins

Judith L./Winterkamp

(8)

8. ~~CONTRACT OR GRANT~~ NUMBER(s)

N00039-77-C-0003

(15)

9. PERFORMING ORGANIZATION NAME AND ADDRESS

Applied Research Laboratories

The University of Texas at Austin

Austin, Texas 78712

10. PROGRAM ELEMENT, PROJECT, TASK AREA & WORK UNIT NUMBERS

Items 0003 and 0004

11. CONTROLLING OFFICE NAME AND ADDRESS

Naval Electronic Systems Command

Department of the Navy

Washington, DC 20360

12. REPORT DATE

31 December 1978

13. NUMBER OF PAGES

403

14. MONITORING AGENCY NAME & ADDRESS(if different from Controlling Office)

(14) ARL-TR-78-3

15. SECURITY CLASS. (of this report)

SECRET

15a. DECLASSIFICATION/DOWNGRADING SCHEDULE

See reverse side.

16. DISTRIBUTION STATEMENT (of this Report)

None (12) 314 p.

17. DISTRIBUTION STATEMENT (of the abstract entered in Block 20, if different from Report)

18. SUPPLEMENTARY NOTES

19. KEY WORDS (Continue on reverse side if necessary and identify by block number)

rapidly deployable surveillance system

moored surveillance system

DIFAR

20. ABSTRACT (Continue on reverse side if necessary and identify by block number)

(U) Volume III of this report contains the detailed vernier frequency resolution data products used to analyze candidate sensor performance based on the Moored Surveillance System Field Validation Test. In addition, this volume contains a brief discussion of each type of display and the methods used to generate it.

DD FORM 1 JAN 73 1473 EDITION OF 1 NOV 65 IS OBSOLETE 404 434 **SECRET**

(This page is unclassified)

SECURITY CLASSIFICATION OF THIS PAGE (When Data Entered)

UNCLASSIFIED

SECURITY CLASSIFICATION OF THIS PAGE(When Data Entered)

15a.

DD 254, 12/10/76,
Cont. N00039-77-C-0003

CLASSIFIED BY OPNAVINST S5510.72C, 4 Sep 73
EXEMPT FROM GDS OF E.O. 11652
EXEMPTION CATEGORY 3
DECLASSIFIED ON 31 Dec 2007

"NATIONAL SECURITY INFORMATION"

"Unauthorized Disclosure Subject to Criminal Sanctions"

Accession For	
NTIS GRA&I	☐
DDC TAB	☒
Unannounced	☐
Justification	
By	
Distribution/	
Availability Codes	
Dist.	Avail and/or special
9	

UNCLASSIFIED

SECURITY CLASSIFICATION OF THIS PAGE(When Data Entered)

TABLE OF CONTENTS

	Page
LIST OF TABLES	v
LIST OF FIGURES	vii
I. INTRODUCTION	1
II. cw DATA PRODUCTS	3
III. AMBIENT SOUND FIELD DATA PRODUCTS	17
IV. DISCUSSION	21
REFERENCES	23
APPENDICES	25

(The reverse of this page is blank.)

LIST OF TABLES

Table	Title	Page
III-1	Vernier Resolution Data Base (U)	4
III-2	Vernier Resolution Processing Parameters (U)	5
III-3	cw Projector Characterisitics for Vernier Resolution Data Products	6
III-4	Vernier Resolution Line History Plots	8
III-5	Vernier Resolution Propagation Loss or Signal, Noise, and Array Gain versus Range Plots	10
III-6	Vernier Resolution Probability of Detection versus Range Plots	12
III-7	Vernier Resolution Bearing Error versus Signal-To-Noise: Ratio Plots	14
III-8	Vernier Resolution Signal-To-Noise Ratio versus Range Plots	15
III-9	Lines Deleted from Clutter Measurements (U)	19

LIST OF FIGURES

Figure No.	Title	Appendix
III-1 - III-23	Summary Detection Curves (U)	A
III-24 - III-163	Line History Curves (U)	B
III-164 - III-171	Propagation Loss versus Range Curves (U)	C
III-172 - III-199	Array Gain versus Range Curves (U)	D
III-200 - III-235	Percentage Detection versus Range Curves (U)	E
III-236 - III-257	Bearing Error versus Signal-to-Noise Ratio Curves (U)	F
III-258 - III-293	Signal-to-Noise Ratio versus Range Curves (U)	G
III-294 - III-301	Noise Gain Timeseries Curves (U)	H
III-302 - III-312	Clutter Timeseries Curves (U)	I
III-313 - III-354	Ambient Sound Field Level versus Frequency Curves (U)	J

(The reverse of this page is blank.)

I. INTRODUCTION

(C) During November 1975, the Moored Surveillance System (MSS) Field Validation Test (FVT) was conducted under the sponsorship of the MSS Project Office (PME 124-30) of Naval Electronic Systems Command. Applied Research Laboratories, The University of Texas at Austin (ARL:UT), participated in the processing and analysis of the acquired ACODAC data.

(C) The results of this work, performed under Contract N00039-77-C-0003, are contained in a four volume report describing the measurements and analyses of candidate sensor performance based on data from the MSS-FVT. Volume I describes the data collection system and the measurement system used to obtain the results. Volume II contains data products obtained with standard frequency resolution processing. This volume, Volume III, contains the data products obtained with vernier frequency resolution processing. Volume IV contains the background information, summary data products, and analysis.

(U) Since the MSS-FVT was completed, the name of the MSS program has been changed to Rapidly Deployable Surveillance System (RDSS). To avoid ambiguity, the term MSS will be used throughout this report. However, the issues addressed here are those specified by the MSS Project Office and are those issues that were of current interest to RDSS at the time that this report was written.

(U) This volume, III, which contains the detailed vernier frequency resolution data products, is partitioned into four sections. The first is this introduction. The second section describes the cw data products. The third section describes the ambient sound field (ASF) data products. The fourth and final section briefly discusses the utilization of these data products. Much of the text in this volume is similar to that found

(U) in Volumes I and II, but it is repeated here so that each volume can be used independently of the others.

II. cw DATA PRODUCTS

(U) The detailed vernier frequency resolution cw data products contained in this volume were extracted from the data intervals shown in Table III-1. A summary of the processing parameters is shown in Table III-2. The cw projector characteristics used in performing these measurements are summarized in Table III-3. The cw projector source levels for the CFAV KAPUSKACING are higher than those reported previously (Ref. 1). These revisions were made in order to reconcile the propagation loss curves from the CFAV KAPUSKACING with those from the other sources. A detailed description of the measurement system can be found in Volume I.

(C) Several different types of cw data products are contained herein. Each type is described briefly, and a table of the curves is given. The abbreviations used in these tables and the text are:

- QT CFAV QUEST
- KP CFAV KAPUSKACING
- CH R/V CHAIN
- O Omnidirectional Sensor
- SC Single Cardioids Sensor
- MGL Maximum Gain Limacons Sensor
- VD Vertical Dipole Sensor
- DC Differenced Cardioids Sensor

These curves were included in this report to substantiate the observations in Volume IV, and to furnish a data base for future issues not addressed by this report. For completeness, each curve containing any data was included, even though the small number of samples may minimize its statistical significance.

(C) TABLE III-1

VERNIER RESOLUTION DATA BASE (U)

Low Band (46 to 84 Hz) Single and Differenced Arrays

Site A1	1200Z	17 Nov[321]	- 0039Z	18 Nov[322]
Site A2	1200Z	17 Nov[321]	- 1859Z	17 Nov[321]
Site A3	1200Z	17 Nov[321]	- 2359Z	21 Nov[325]

Midband (145-183 Hz) Single and Differenced Arrays

Site A1	1200Z	17 Nov[321]	- 2359Z	17 Nov[321]
Site A2	1200Z	17 Nov[321]	- 1859Z	17 Nov[321]
Site A3	1200Z	17 Nov[321]	- 2359Z	17 Nov[321]
	1200Z	21 Nov[325]	- 2359Z	21 Nov[325]

High Band (300-338 Hz) Single Array

Site A1	1200Z	17 Nov[321]	- 0529Z	18 Nov[322]
Site A2	1200Z	17 Nov[321]	- 1859Z	17 Nov[321]
Site A3	1200Z	17 Nov[321]	- 2359Z	21 Nov[325]

[] Julian Day

Z Greenwich Mean Time

(S) TABLE III-2

VERNIER RESOLUTION PROCESSING PARAMETERS (U)

Parameter	Value
Sample Rate:	100 Hz (obtained from zero crossings of tape servo signal)
Frequency Range	46 to 84 Hz (low band) 145 to 183 Hz (midband) 300 to 338 Hz (high band)
FFT Length	81.92 sec (8192 samples)
Spectral Window	Hanning
Frequency Spacing	0.0122 Hz
3 dB Bandwidth	0.0176 Hz
Equivalent Noise Bandwidth	0.0183 Hz
FFT Overlap	50%
ALI Interval	5 min
ALI Type	Rectangular Integration
FFT/ALI	7
Time Bandwidth Product	5.76
Equivalent Degrees of Freedom	13.4
Probability of False Alarm	10^{-3}
Detection Threshold	-14.6 dB//Hz

TABLE III-3

cw PROJECTOR CHARACTERISTICS FOR VERNIER RESOLUTION DATA PRODUCTS

TOW PLATFORM	NOMINAL FREQUENCY (Hz)	NOMINAL LEVEL (dB//µPa)	17 NOV FIELD EVENT ON/OFF TIMES (Z)	17 NOV FIELD EVENT NOMINAL DEPTH (m)	19 NOV FIELD EVENT ON/OFF TIMES (Z)	19 NOV FIELD EVENT NOMINAL DEPTH (m)	21 NOV FIELD EVENT ON/OFF TIMES (Z)	21 NOV FIELD EVENT NOMINAL DEPTH (m)
CFAV	55	141	1230/2230	110	1224/2215	95	1217/2030	110
QUEST	155	134	1230/2230	110	---	---	1217/2030	110
	305	136	1230/2230	110	1224/2215	95	1217/2030	110
CFAV	64	162	1230/2318	110	1230/2230	115	1230/2030	120
KAPUSKACING	160	161	1230/2318*	110	---	---	1230/2030	120
R/V	70	166	1225/2200	100	1225/2200	95	1230/2030	85
CHAIN	170	156	1225/2200	100	---	---	1230/2030	85
	335	154	1645/2200	100	1225/2200	95	1230/2030	85

*FREQUENCY VARYING 1 CYCLE

(C) Data products of the first type are termed summary detection plots (Appendix A, Figs. III-1 - III-23). These are plots of each detected line within a frequency band as a function of time. The solid symbols indicate that the line was detected in multiple cells and/or on multiple beams of the sensor. The X symbols indicate that the line was only detected in a single cell on a single beam of the sensor. The solid line emanating from each symbol indicates the maximum signal-to-noise ratio (S/N) of any cell of the line. If the sensor provides bearing information, the solid line also indicates the estimated bearing, north being toward the top of the plot. The dashed lines indicate which of the detections were linked by the tracking algorithm. These displays are intended to provide qualitative information about the environment in which the processor must function in terms of line loading and relative clutter density between sensors and frequency regimes. More quantitative information will be found in section III of this volume.

(C) Data products of the next type (Appendix B, Figs. III-24 - III-163) are termed line history plots, and are cataloged in Table III-4. These are plots of the estimated cw signal parameter values as a function of time. The top portion of the plot contains a solid line indicating ground truth source-to-receiver range in nautical miles and X's indicating the number of equivalent degrees of freedom for each ALI. The second portion contains a solid line denoting ground truth receiver-to-source bearing, X's indicating the estimated signal bearing and □'s indicating the estimated noise bearing. Gaps in the solid ground truth lines indicate intervals of missing data, such as calibration signal intervals. The third portion contains the estimated ambient sound field (ASF) levels in dB//μPa/Hz$^{1/2}$. The omnidirectional (O) and vertical dipole (VD) sensor curves contain a single trace of connected X's. The single cardioids (SC), maximum gain limacons (MGL) and differenced cardioids (DC) curves contain a trace for each beam. Each beam is labeled by the first letter of its main axis bearing (north, east, south, and west). ASF level estimates were displayed only when the signal was detected. The fourth portion of the plot contains the estimated sound pressure level (SPL) in dB//μPa of the received signal. The O and VD sensor curves each contain

(U)

TABLE III-4

VERNIER RESOLUTION LINE HISTORY PLOTS

		17 NOV (321)															19 NOV (323)				21 NOV (325)			
		Site A1					Site A2					Site A3					Site A3				Site A3			
Source Platform	Source Frequency	0	SC	MGL	VD	DC	0	SC	MGL	VD	DC	0	SC	MGL	VD	DC	0	SC	VD	DC	0	SC	VD	DC
QT	55	24	25	26	27	28	60	61	62	ND	63	95	96	97	98	99	ND	ND	ND	ND	ND	141	ND	142
KP	64	37	38	39	40	41	72	73	74	75	76	108	109	110	111	112	131	132	133	134	146	147	148	149
CH	70	47	48	49	50	51	82	83	84	85	86	118	119	120	121	122	135	136	137	138	154	155	156	157
QT	155	29	30	31	32	33	64	65	66	67	68	100	101	102	103	104	---	---	---	---	ND	143	ND	ND
KP	160	42	43	44	45	46	77	78	79	80	81	113	114	115	116	117	---	---	---	---	150	151	152	153
CH	170	52	53	54	55	56	87	88	89	90	91	123	124	125	126	127	---	---	---	---	158	159	160	161
QT	305	34	35	36	--	--	69	70	71	--	--	105	106	107	---	---	ND	ND	---	---	144	145	---	---
CH	335	57	58	59	--	--	92	93	94	--	--	128	129	130	---	---	139	140	---	---	162	163	---	---

ND - Not Detected

(C) two traces: the X's denote the levels for the cell with the highest S/N (most detectable); the +'s denote the levels summed over all detected cells, as is normally done when computing propagation loss. The SC, MGL, and DC sensor curves each contain four traces, each giving the levels for the most detectable cell on a beam and annotated in the same manner as the ASF levels. The fifth portion of the plot contains the S/N in decibels relative to a 1 Hz noise band. The traces are defined in the same manner as the SPL curves. The dashed line denotes the detection threshold. The bottom portion of the plot contains two traces: the X's denote the estimated signal frequency, and the □'s denote the line's bandwidth. These displays contain all of the information known about the signal. All of the remaining cw data products are derived from these data.

(C) Data products of the next type (Appendix C, Figs. III-164 - III-171) are termed propagation loss plots, and are cataloged under the 0 sensor columns of Table III-5. These plots contain curves of the estimated cw propagation loss in decibels as a function of range in nautical miles. Below these are other traces denoting the associated signal excess, (S+N)/N, at each range bin in decibels relative to the noise level in the analysis bandwidth. These traces indicate the confidence associated with the measurements. The bottom traces denote the estimated background ASF levels associated with each range bin. These measurements were derived for a 1 nmi range bin, and smoothed with a 3-bin sliding average. The received signal power was estimated from that cell with the highest S/N of any detected cell on any beam. Since these are single cell measurements, they will show more loss than the total received SPL technique, such as was used in Ref. 2. This difference is discussed in Volume IV.

(C) Data products of the next type (Appendix D, Figs. III-172 - III-199) are termed signal, noise, and array gain plots, and are cataloged in Table III-5 under the sensors other than 0. These are plots of measured

(U)

TABLE III-5

VERNIER RESOLUTION PROPAGATION LOSS OR SIGNAL, NOISE, AND ARRAY GAIN VERSUS RANGE PLOTS

Source Platform	Source Frequency	17 NOV (321)															19 NOV (323)				21 NOV (325)			
		Site A1					Site A2					Site A3					Site A3				Site A3			
		O	SC	NGL	VD	DC	O	SC	NGL	VD	DC	O	SC	NGL	VD	DC	O	SC	VD	DC	O	SC	VD	DC
QT	55	164	172	173	174	175	164	172	173	ND	175	164	172	173	174	175	ND	ND	ND	ND	ND	172	ND	175
KP	64	165	176	177	178	179	165	176	177	178	179	165	176	177	178	179	165	176	178	179	165	176	178	179
CH	70	166	180	181	162	183	166	180	181	182	183	166	180	181	182	183	166	180	182	183	166	180	182	183
QT	155	167	184	185	186	187	167	184	185	186	187	167	184	185	186	187	---	---	---	---	ND	184	ND	ND
KP	160	168	188	189	190	191	168	188	189	190	191	168	188	189	190	191	---	---	---	---	168	188	190	191
CH	170	169	192	193	194	195	169	192	193	194	195	169	192	193	194	195	---	---	---	---	169	192	194	195
QT	305	170	196	197	---	---	170	196	197	---	---	170	196	197	---	---	ND	ND	---	---	170	196	---	---
CH	335	171	198	199	---	---	171	198	199	---	---	171	198	199	---	---	171	198	---	---	171	198	---	---

ND - Not Detected

(C) sensor signal, noise, and S/N levels relative to those of an omnidirectional sensor (0) as a function of range. The top portion of the plot indicates how many samples (0 sensor detections) occurred in each range bin. The next portion contains traces denoting the measured signal gain of the sensor, where signal gain is the ratio of the received SPL of this sensor over that of the 0 sensor. The next portion contains traces denoting the measured array gain of the sensor, where array gain is the ratio of the S/N of this sensor over that of the 0 sensor. The bottom portion contains traces denoting the measured noise gain of the sensor, where noise gain is the ratio of the ASF level of this sensor over that of the 0 sensor. Since signal gain is primarily a function of range, whereas noise gain is a function primarily of time, this display allows array gain to be interpreted in terms of both range and time. All of the traces were computed with 1 nmi range bins and smoothed with a 3 nmi sliding average.

(C) When computing average S/N as a function of range, if the signal is not detected during every ALI, the resultant average will be biased high. This bias occurs because only the highest S/N ratios are detected. In order to reduce this bias, the detection threshold (Table III-2) has been substituted for the missing S/N wherever the target was not detected. This debiasing technique was used both for computing array gain and for generating curves of S/N versus range.

(C) Data products of the next type (Appendix E, Figs. III-200 - III-235) are termed percentage detection plots, and are cataloged in Table III-6. These curves of single line detection percentages were calculated as the number of independent detection opportunities (ALI intervals) that the specified source was within a given integer 1 mile range interval and that resulted in detection, divided by the number of such opportunities. For multibeam sensors, detection on any beam was considered a detection for the sensor. If the number of equivalent degrees of freedom for an ALI was less than that specified in Table III-2 (some portion of the ALI interval was missing), and the signal was not detected,

(U)

TABLE III-6

VERNIER RESOLUTION PROBABILITY OF DETECTION VERSUS RANGE PLOTS

		17 NOV (321)															19 NOV (323)				21 NOV (325)			
		Site A1					Site A2					Site A3					Site A3				Site A3			
Source Platform	Source Frequency	0	SC	MGL	VD	DC	0	SC	MGL	VD	DC	0	SC	MGL	VD	DC	0	SC	VD	DC	0	SC	VD	DC
QT	55	200	201	202	203	204	200	201	202	ND	204	200	201	202	203	204	ND	ND	ND	ND	ND	201	ND	204
KP	64	213	214	215	216	217	213	214	215	216	217	213	214	215	216	217	213	214	216	217	213	214	216	217
CH	70	223	224	225	226	227	223	224	225	226	227	223	224	225	226	227	223	224	226	227	223	224	226	227
QT	155	205	206	20[illegible]	208	209	205	206	207	208	209	205	206	207	208	209	---	---	---	---	ND	206	ND	ND
KP	160	218	219	220	221	222	218	219	220	221	222	218	219	220	221	222	---	---	---	---	218	219	221	222
CH	170	228	229	230	231	232	228	229	230	231	232	228	229	230	231	232	---	---	---	---	228	229	231	232
QT	305	210	211	212	---	---	210	211	212	---	---	210	211	212	---	---	ND	ND	---	---	210	211	---	---
CH	335	233	234	235	---	---	233	234	235	---	---	233	234	235	---	---	233	234	---	---	233	234	---	---

ND - Not Detected

(C) then the ALI was not counted as a valid detection opportunity. These editing criteria were required because the detection threshold for each ALI was determined by its number of degrees of freedom. All of the traces were smoothed with a 3 nmi sliding average. If the sensor furnished a bearing estimate, its rms bearing error was also plotted as a function of range.

(C) Data products of the next type (Appendix F, Figs. III-236 - III-257) are termed bearing error plots, and are cataloged in Table III-7. These are curves of the number of bearing estimates (detections), the mean bearing error (estimated bearing *minus* ground truth bearing), the rms bearing error, and the bearing error standard deviation, all plotted as a function of S/N in dB//1 Hz noise band. The ground truth bearing was computed from the navigation reconstruction as the great circle receiver-to-source bearing at the receiver and at the beginning of the ALI. The estimated bearings were corrected for magnetic variation and acoustically debiased (see Volume I). Each trace was smoothed with a 3 dB sliding average.

(C) Data products of the last type (Appendix G, Figs. III-258 - III-293) are curves of S/N (dB//1 Hz noise band) versus range (nmi), and are cataloged in Table III-8. These measurements were obtained from the detected cell with the highest S/N on any beam. As described earlier, these results are partially debiased by substitutions of the detection threshold during ALI intervals without signal detections. The detection threshold is drawn on each plot. Each trace was smoothed with a 3 nmi sliding average.

(U)

TABLE III-7

VERNIER RESOLUTION BEARING ERROR
VERSUS SIGNAL-TO-NOISE RATIO PLOTS

		17 NOV (321)															19 NOV (323)				21 NOV (325)			
		Site A1					Site A2					Site A3					Site A3				Site A3			
Source Platform	Source Frequency	O	SC	MGL	VD	DC	O	SC	MGL	VD	DC	O	SC	MGL	VD	DC	O	SC	VD	DC	O	SC	VD	DC
QT	55	---	236	237	---	238	---	236	237	---	238	---	236	237	---	238	---	ND	---	ND	---	236	---	238
KP	64	---	244	245	---	246	---	244	245	---	246	---	244	245	---	246	---	244	---	246	---	244	--	246
CH	70	---	250	251	---	252	---	250	251	---	252	---	250	251	---	252	---	250	---	252	---	250	---	252
QT	155	---	239	240	---	241	---	239	240	---	241	---	239	240	---	241	---	---	---	---	---	239	---	ND
KP	160	---	247	248	---	249	---	247	248	---	249	---	247	248	---	249	---	---	---	---	---	247	---	249
CH	170	---	253	254	---	255	---	253	254	---	255	---	253	254	---	255	---	---	---	---	---	253	---	255
QT	305	---	242	243	---	---	---	242	243	---	---	---	242	243	---	---	---	ND	---	---	---	242	---	---
CH	335	---	256	257	---	---	---	256	257	---	---	---	256	257	---	---	---	256	---	---	---	256	---	---

ND - Not Detected

UNCLASSIFIED

(U)

TABLE III-8

VERNIER RESOLUTION SIGNAL-TO-NOISE RATIO VERSUS RANGE PLOTS

Source Platform	Source Frequency	17 NOV (321) Site A1					Site A2					Site A3					19 NOV (323) Site A3				21 NOV (325) Site A3			
		0	SC	MGL	VD	DC	0	SC	MGL	VD	DC	0	SC	MGL	VD	DC	0	SC	VD	DC	0	SC	VD	DC
QT	55	258	259	260	261	262	258	259	260	ND	262	258	259	260	261	262	ND	ND	ND	ND	ND	259	ND	262
KP	64	271	272	273	274	275	271	272	273	274	275	271	272	273	274	275	271	272	274	275	271	272	274	275
CH	79	281	282	283	284	285	281	282	283	284	285	281	282	283	284	285	281	282	284	285	281	282	284	285
QT	155	263	264	265	266	267	263	264	265	266	267	263	264	265	266	267	---	---	---	---	ND	264	ND	ND
KP	160	276	277	278	279	280	276	277	278	279	280	276	277	278	279	280	---	---	---	---	276	277	279	280
CH	170	286	287	288	289	290	286	287	288	289	290	286	287	288	289	290	---	---	---	---	286	287	289	290
QT	305	268	269	270	---	---	268	269	270	---	---	268	269	270	---	---	ND	ND	---	---	268	269	---	---
CH	335	291	292	293	---	---	291	292	293	---	---	291	292	293	---	---	291	292	---	---	291	292	---	---

ND - Not Detected

(The reverse of this page is blank.)

III. AMBIENT SOUND FIELD DATA PRODUCTS

(U) Three types of ambient sound field (ASF) measurements were performed: sound pressure levels at an omnidirectional sensor, noise gains of directional sensors, and clutter (processor loading) statistics of each sensor. The vernier frequency resolution ASF data products herein span an interval of 4 1/2 days, but have limited frequency coverage. The standard frequency resolution ASF data products in Volume II cover a wide frequency range (40 to 600 Hz), but are of only 12 hours duration. Each data product set can be used to extrapolate the other to different frequencies or times.

(U) Data products of the first type (Appendix H, Figs. III-294 - III-301), are termed timeseries plots, and reveal the time dependence of the ASF measured in selected 1 Hz bands. The first three figures contain the omnidirectional ASF levels ($dB//\mu Pa/Hz^{1/2}$) in each vernier band. The remaining figures contain the noise gains (dB) where noise gain is the ratio of the ASF level of this sensor over that of the omnidirectional sensor. These timeseries plots were derived from ASF meaurements summed over 1 Hz bands. The noise gains were derived for a 1 Hz band which was relatively free from contamination by tonals. The 1 Hz summation increased the number of equivalent degrees of freedom, and thus decreased the variance of the measurments.

(C) Data products of the second type (Appendix I, Figs. III-302 - III-312), are termed clutter timeseries plots. These are plots of the number of detected cells, the number of lines formed, and the number of lines linked, for each ALI interval as a function of time. These measurements were obtained during field events only, and a separate curve is provided for each such event. The measurements were performed for three contiguous 10 Hz bands of 819 cells each. The results for each band were similar and have been combined into a single 30 Hz band for these curves.

(C) The clutter timeseries plots are intended to portray the shore link and processor capacity required for operations in the absence of targets. In order to provide accurate clutter measurements, it is necessary to first eliminate the loading incurred due to the presence of the exercise vessels and projectors. Table III-9 lists those lines which have been deleted from the clutter measurements, along with their probable source.

(U) Data products of the last type (Appendix J, Figs. III-313 - III-354), are termed 3D plots. These are 3-dimensional representations of omni-directional ASF levels (dB//μPa/Hz$^{1/2}$) as a function of time and frequency. Each trace represents the average over a 10 min interval and has been smoothed so as to maintain a constant number of equivalent degrees of freedom. Plots of data from the vertical dipole sensor are also included. These displays serve as a roadmap of the data since they reveal signatures, tones, artifacts, and broadband trends.

(C) TABLE III-9

LINES DELETED FROM CLUTTER MEASUREMENTS (U)

LOW FREQUENCY VERNIER (50 to 80 Hz)

55 Hz	Scheduled QUEST Projector Line
64 Hz	Scheduled KAPUSKACING Projector Line
70 Hz	Scheduled CHAIN Projector Line
76 Hz	ARL:UT Translator Artifact
79 Hz	ARL:UT Translator Artifact

MIDFREQUENCY VERNIER (150 to 180 Hz)

155 Hz	Scheduled QUEST Projector Line
160 Hz	Scheduled KAPUSKACING Projector Line
170 Hz	Scheduled CHAIN Projector Line

HIGH FREQUENCY VERNIER (305 to 335 Hz)

305 Hz	Scheduled QUEST Projector Line
320 Hz	KAPUSKACING Projector Harmonic (5×64 or 2×160)
324 Hz	KAPUSKACING Projector Sum Frequency (64+260)
335 Hz	Scheduled CHAIN Projector Line

(The reverse of this page is blank.)

IV. DISCUSSION

(U) The analysis of these data is contained in Volume IV. However, a brief discussion of some of their limitations may prevent those readers not having access to Volume IV from drawing unwarranted conclusions.

(C) The curves in this volume denote the estimated averages of complex stochastic processes. The estimates are displayed as a function of a single variable, such as range, even though they may be highly dependent on another variable, such as the time dependence of S/N or array gain. The signal, noise, and array gain displays allow the time and range dependencies to be somewhat separated, whereas the percentage detection and S/N versus range displays do not. Even though the propagation loss and signal, noise, and array gain displays separate the time dependence of the ASF from the range dependence of the signal field, they do not isolate the time dependence of the signal field. However, since these curves are in good agreement for all three data intervals at Site A3, the day-to-day time dependence of the signal field, as observed with a 5 min ALI, is probably small.

(U) Since the curves are estimated averages of complex stochastic processes (assumed to be stationary in a wide sense), the variance of these estimates is highly dependent on the number of sample measurements. For most of the cw curves, and particularly for the lower level signals, the number of samples is small (<10). The variance of each curve has been decreased by a smoothing window which effectively tripled the number of samples in each bin, but also decreased the resolution of the curve. However, the statistical fluctuation of these estimates does not entirely account for the apparently anomalous results from the low level signals. As is discussed in Volume IV, these results are sometimes severely biased. This is because a fixed threshold detection process

(U) was used to extract signal measurements, and thus only that portion of the signal SPL distribution lying above the threshold was used to estimate its average. For the higher level sources, more of the SPL distribution was detected and used to estimate its average. As was discussed earlier, a simple technique was used to partially debias the S/N results.

(C) The results that appear most anomalous are those at 55 Hz, where the entire SPL distribution is undetectable. The 55 Hz detections occurred only when the ASF level in the signal cell exceeded the estimated ASF mean level sufficiently that it forced the signal-plus-noise level above the detection threshold. This results in erroneous cw measurements (Ref. 3). This phenomenon is discussed more fully in Volume IV. (pp. 62-65).

REFERENCES

1. Steven L. Watkins, "MSS/FVT cw Projector Reconstruction," Applied Research Laboratories Technical Report No. 76-16 (ARL-TR-76-16), Applied Research Laboratories, The University of Texas at Austin, October 1976. UNCLASSIFIED

2. Steven L. Watkins, "MSS/FVT Ambient Sound Field and cw Propagation Measurements for Near-Bottom Sensors at Site A3" (U), Applied Research Laboratories Technical Report No. 76-52 (ARL-TR-76-52), Applied Research Laboratories, The University of Texas at Austin, December 1976. CONFIDENTIAL

3. Jack A. Shooter and Steven L. Watkins, "Estimation of Background Ambient Noise Level from the Spectral Analysis of Time Series with Application to cw Propagation Loss Measurements," J. Acoust. Soc. Am. 62, 84-90 (1977). UNCLASSIFIED

APPENDIX A

SUMMARY DETECTION CURVES (U)

(FIGURES III-1 - III-23)

(The reverse of this page is blank.)

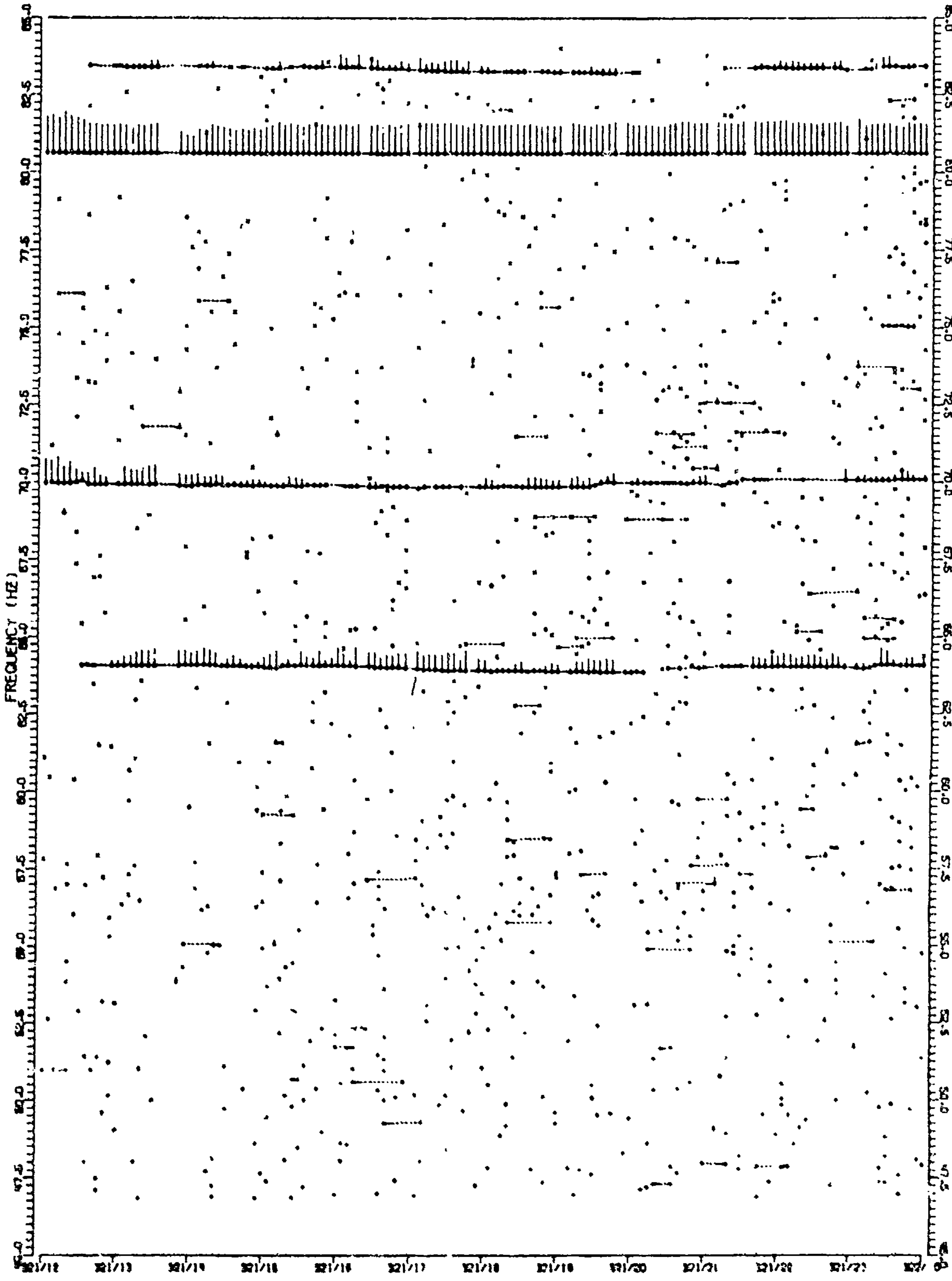

FIGURE III-1
BSS-FVT LOW-BAND DETECTION OVERVIEW DURING THE 17 NOV FIELD EVENT AT SITE A1 OBTAINED VIA THE OMNIDIRECTIONAL SENSOR WITH VERNIER RESOLUTION (U)

AS-77-2601

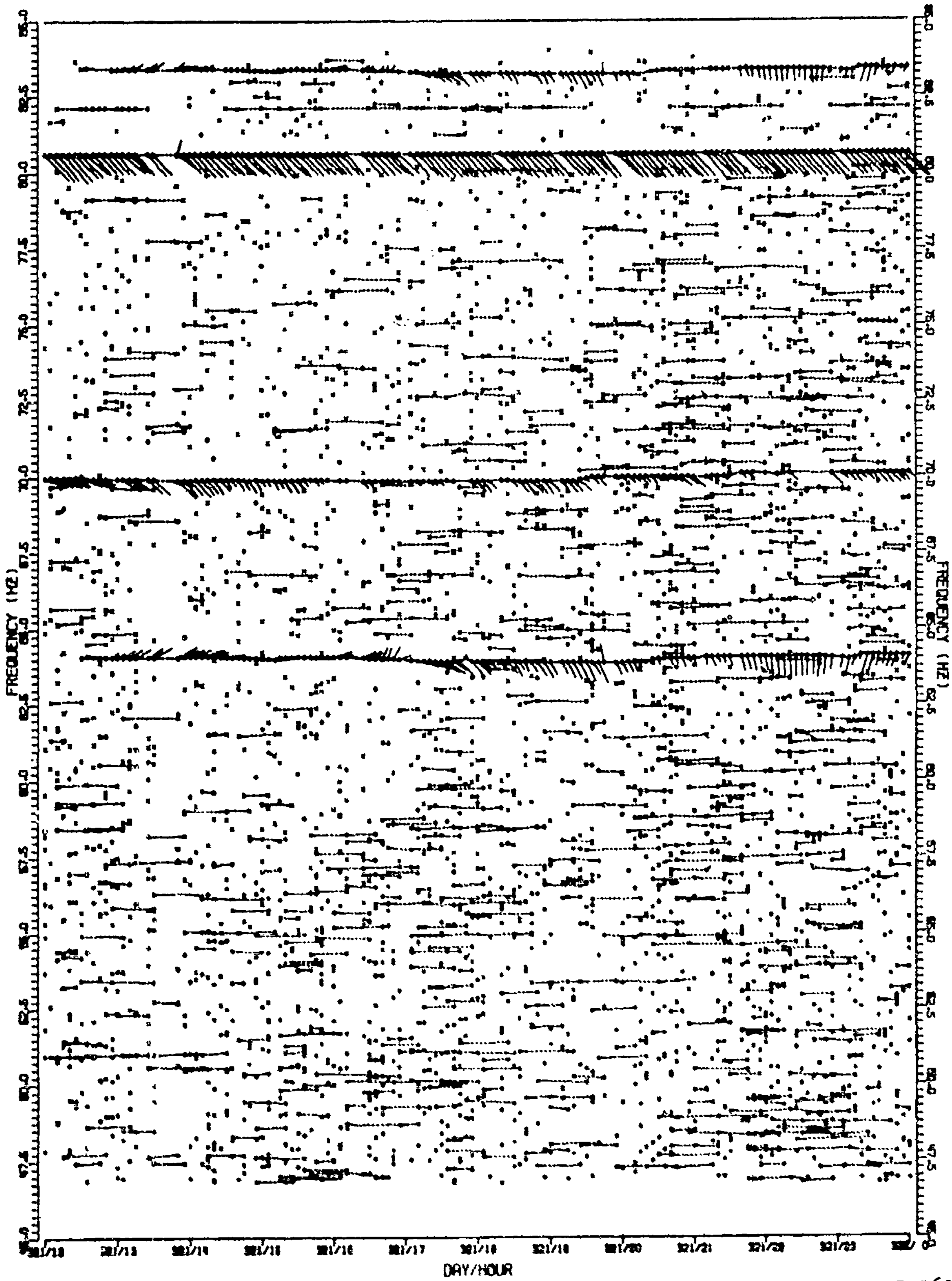

FIGURE III-2
MSS-FVT LOW-BAND DETECTION OVERVIEW DURING THE 17 NOV FIELD EVENT AT SITE A1
OBTAINED VIA THE SINGLE CARDIOIDS SENSOR WITH VERNIER RESOLUTION (U)

AS-77-2602

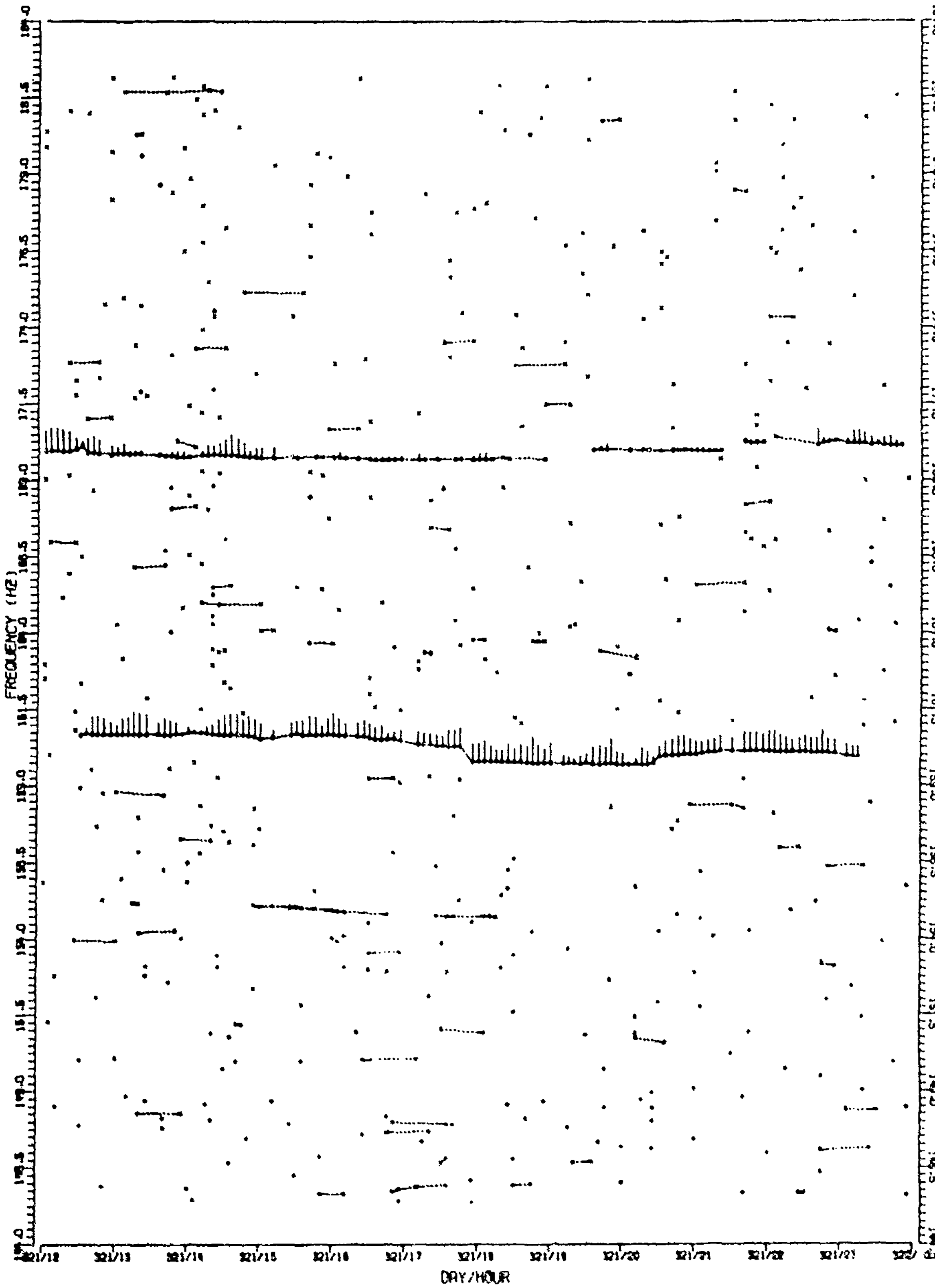

FIGURE III-3
MSS-FVT MID-BAND DETECTION OVERVIEW DURING THE 17 NOV FIELD EVENT AT SITE A1 OBTAINED VIA THE OMNIDIRECTIONAL SENSOR WITH VERNIER RESOLUTION (U)

AS-77-2603

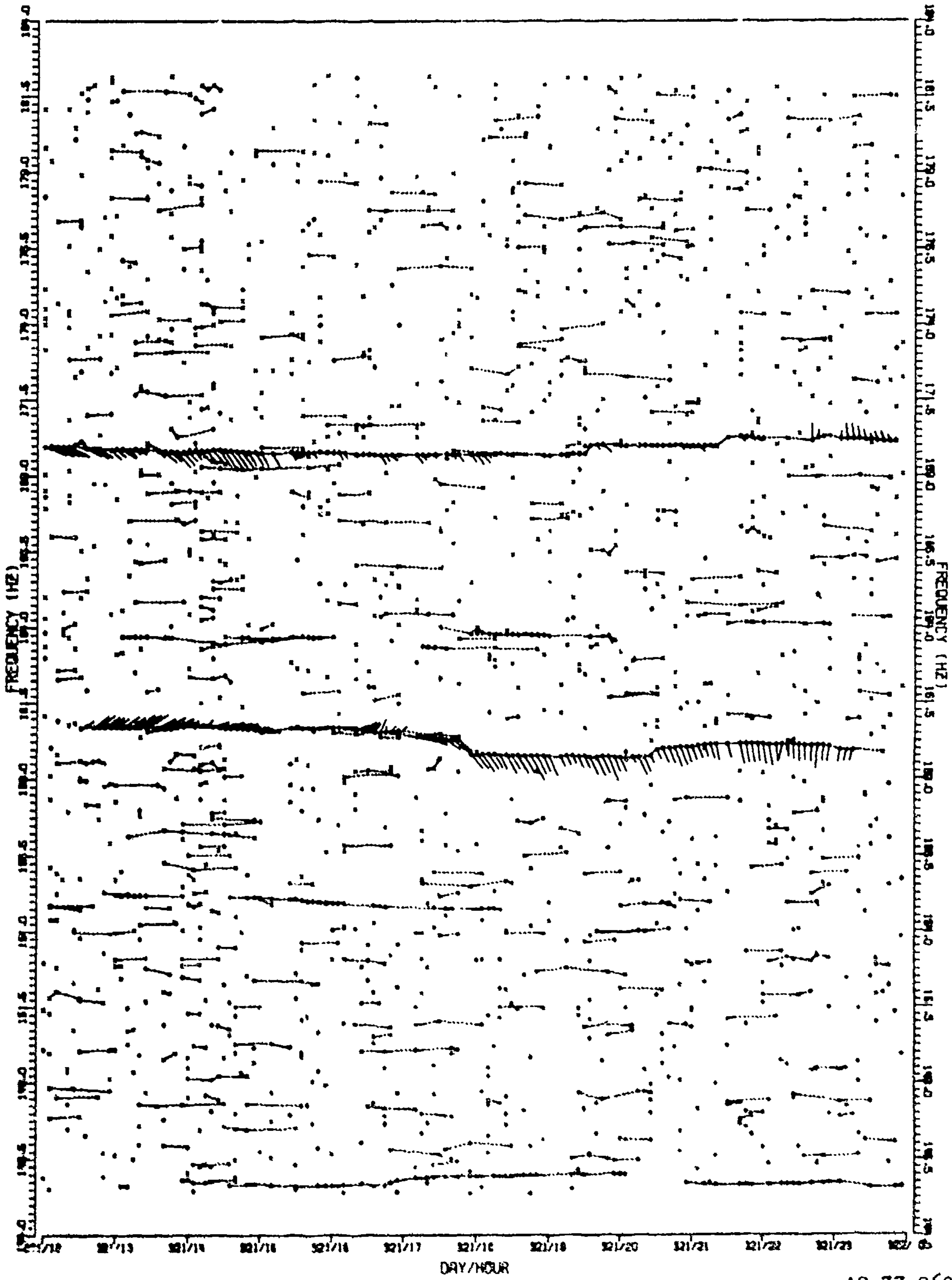

AS-77-2604

FIGURE III-4
NSS-FVT MID-BAND DETECTION OVERVIEW DURING THE 17 NOV FIELD EVENT AT SITE A1
OBTAINED VIA THE SINGLE CARDIOIDS SENSOR WITH VERNIER RESOLUTION (U)

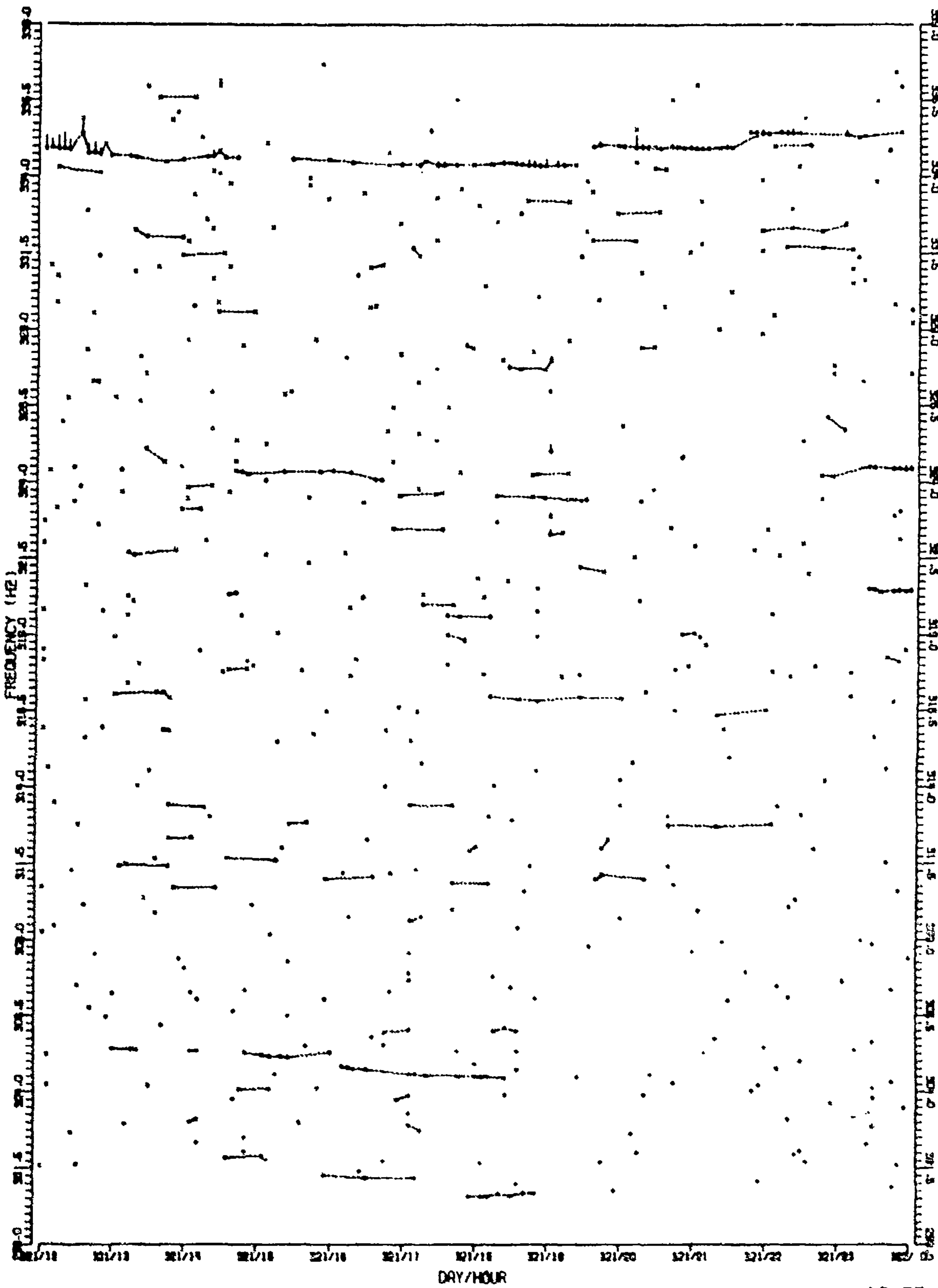

AS-77-2605

FIGURE III-5
MSS-FVT HIGH-BAND DETECTION OVERVIEW DURING THE 17 NOV FIELD EVENT AT SITE A1 OBTAINED VIA THE OMNIDIRECTIONAL SENSOR WITH VERNIER RESOLUTION (U)

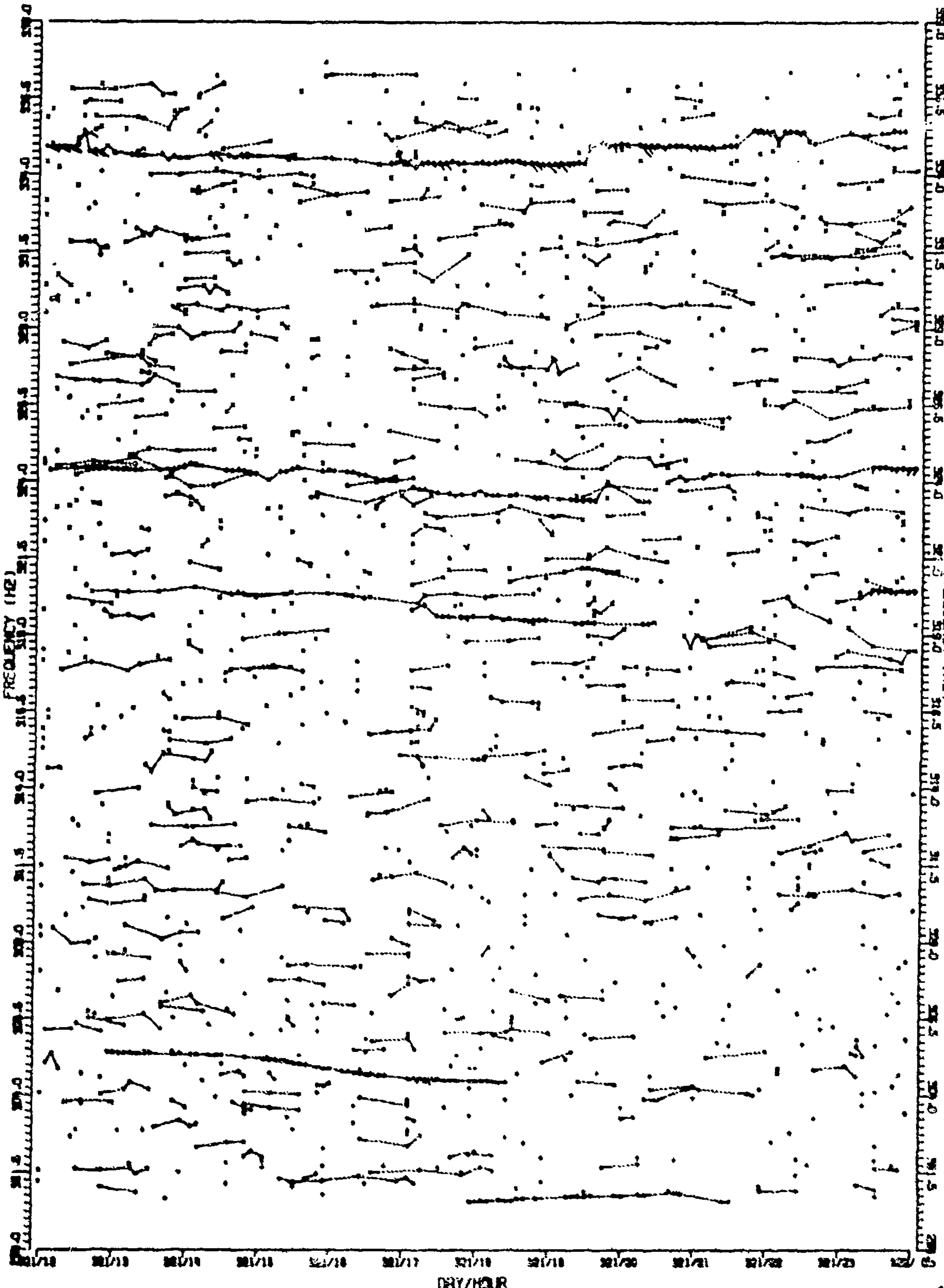

AS-77-2606

FIGURE III-6
MSS-FVT HIGH-BAND DETECTION OVERVIEW DURING THE 17 NOV FIELD EVENT AT SITE A1
OBTAINED VIA THE SINGLE CARDIOIDS SENSOR WITH VERNIER RESOLUTION (U)

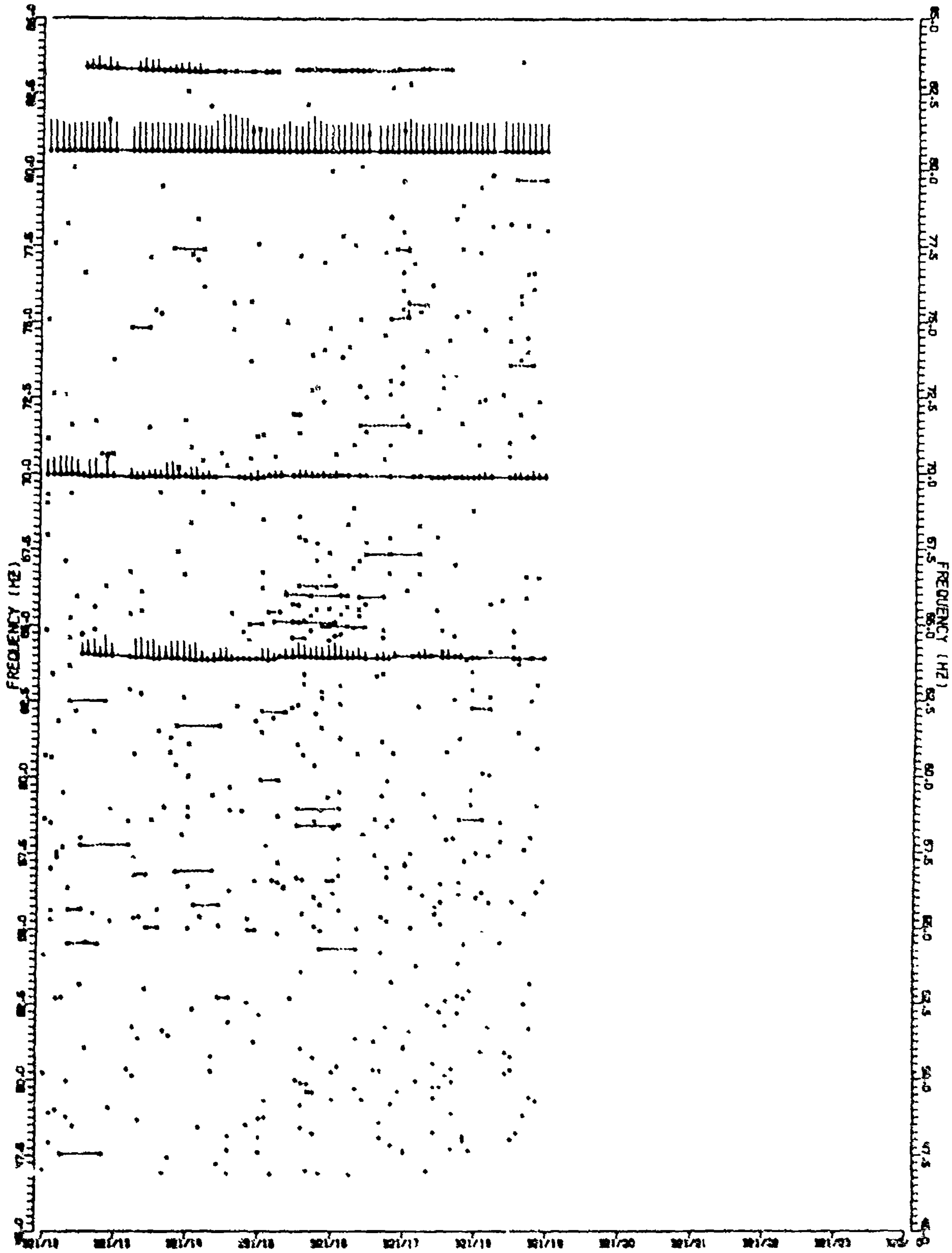

AS-77-2607

FIGURE III-7
MSS-FVT LOW-BAND DETECTION OVERVIEW DURING THE 17 NOV FIELD EVENT AT SITE R2 OBTAINED VIA THE OMNIDIRECTIONAL SENSOR WITH VERNIER RESOLUTION (U)

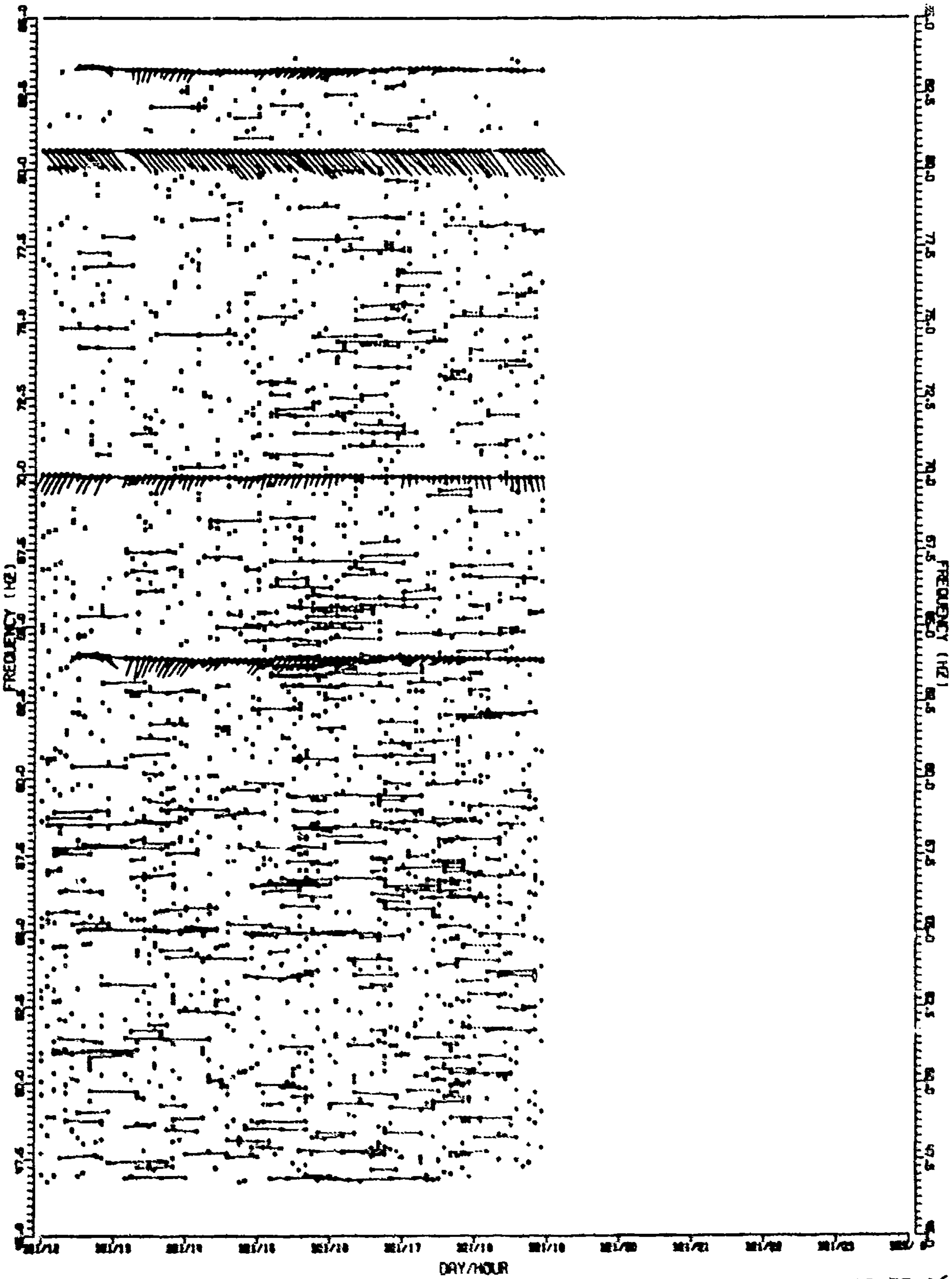

FIGURE III-8
NSS-FVT LOW-BAND DETECTION OVERVIEW DURING THE 17 NOV FIELD EVENT AT SITE A2
OBTAINED VIA THE SINGLE CARDIOIDS SENSOR WITH VERNIER RESOLUTION (U)

AS-77-2608

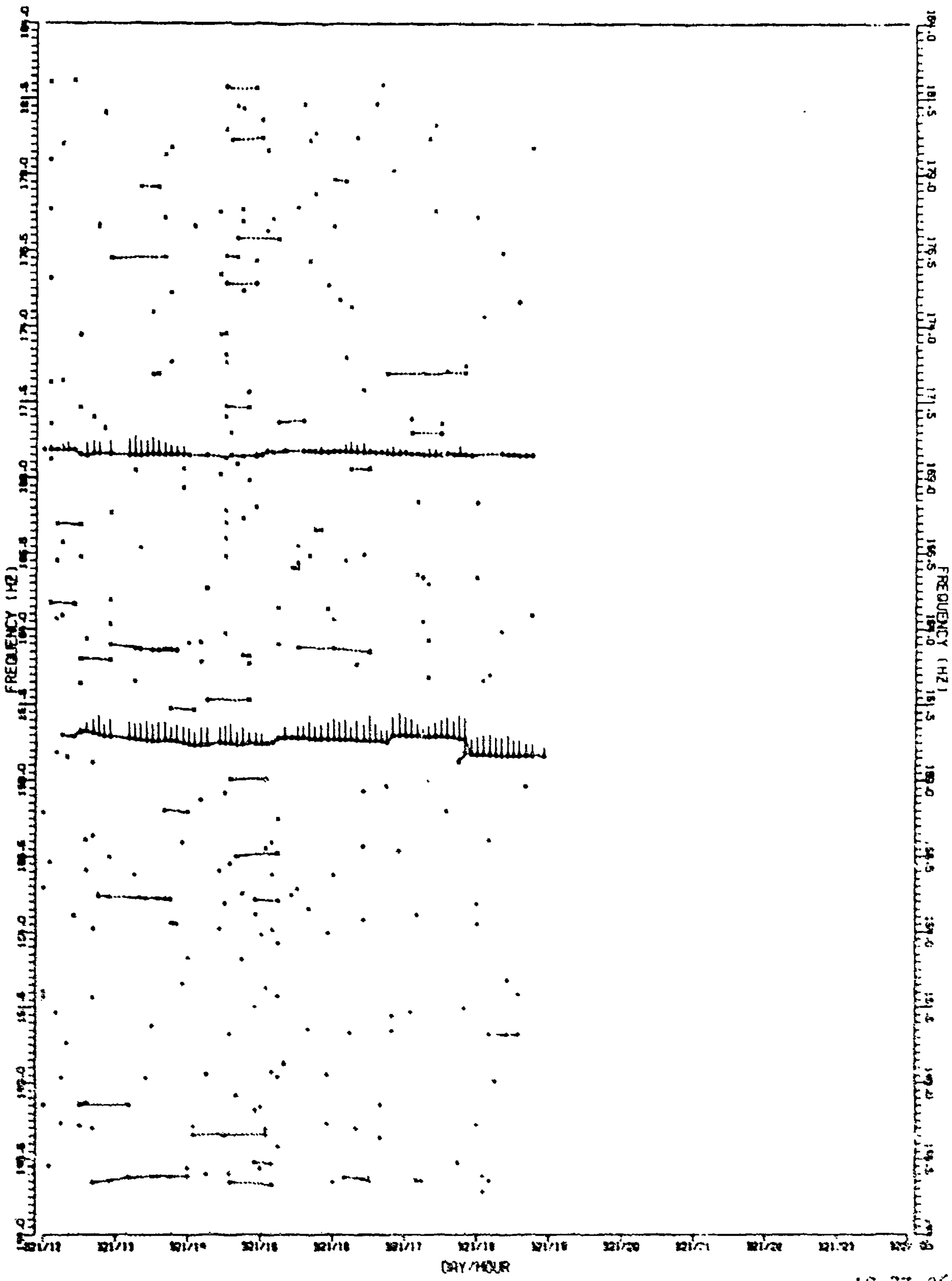

AS-77-2609

FIGURE III-9
HSS-FVT MID-BAND DETECTION OVERVIEW DURING THE 17 NOV FIELD EVENT AT SITE A2
OBTAINED VIA THE OMNIDIRECTIONAL SENSOR WITH VERNIER RESOLUTION (U)

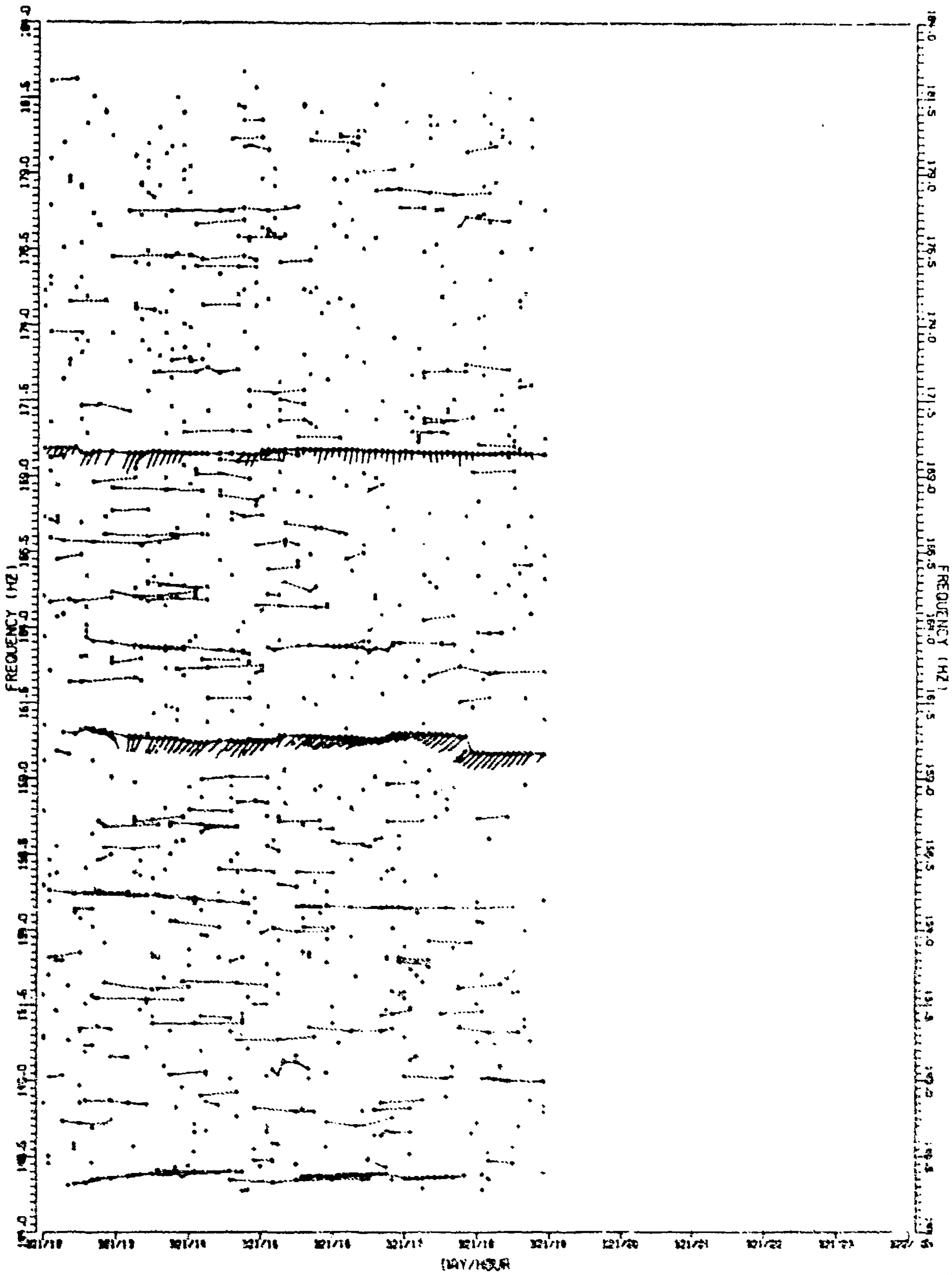

FIGURE III 10
MSS-FVT MID-BAND DETECTION OVERVIEW DURING THE 17 NOV FIELD EVENT AT SITE A2
OBTAINED VIA THE SINGLE CARDIOIDS SENSOR WITH VERNIER RESOLUTION (U)

AS-77-2610

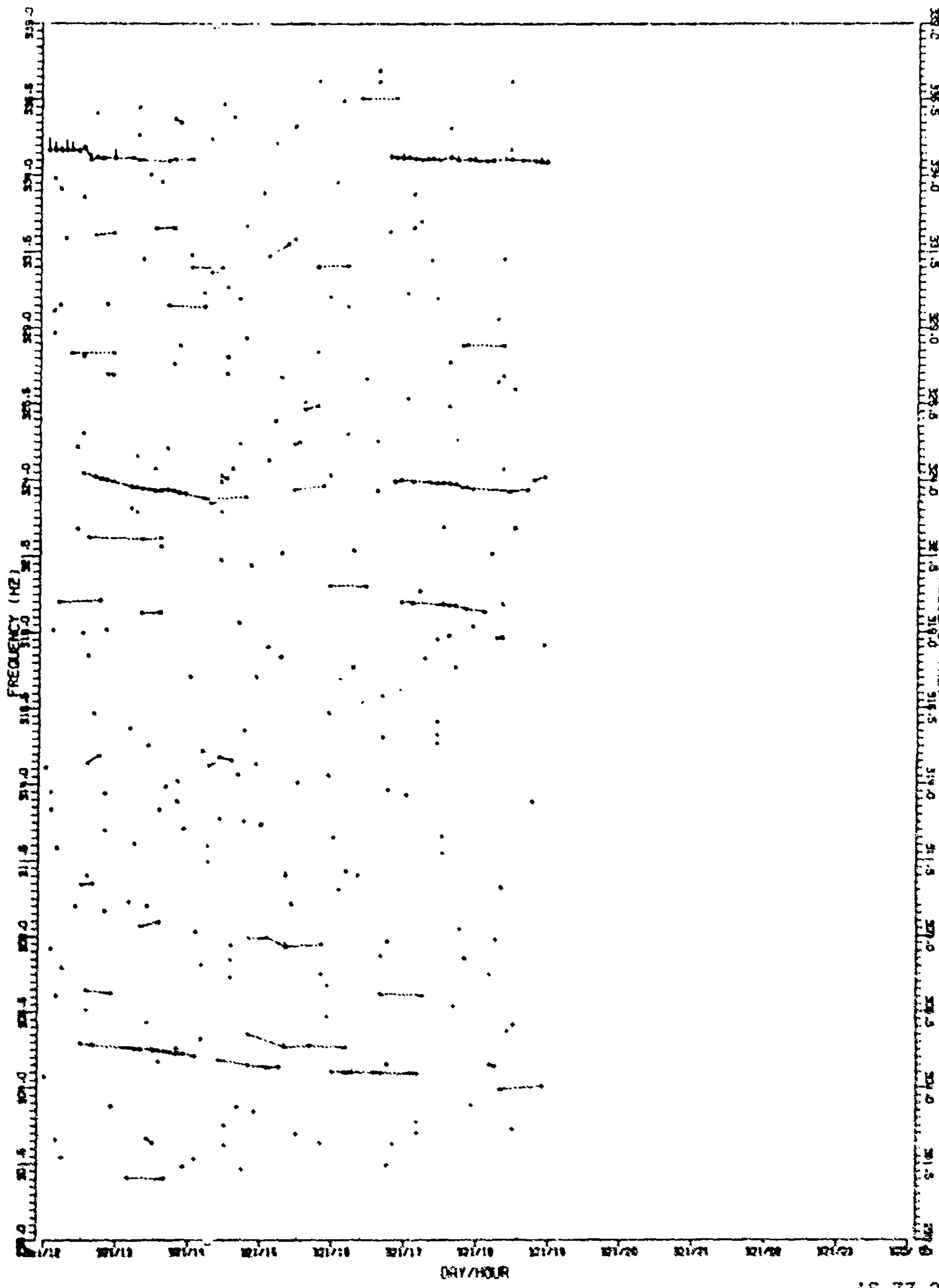

AS-77-2611

FIGURE III-11
NSS-FVT HIGH-BAND DETECTION OVERVIEW DURING THE 17 NOV FIELD EVENT AT SITE A2 OBTAINED VIA THE OMNIDIRECTIONAL SENSOR WITH VERNIER RESOLUTION (U)

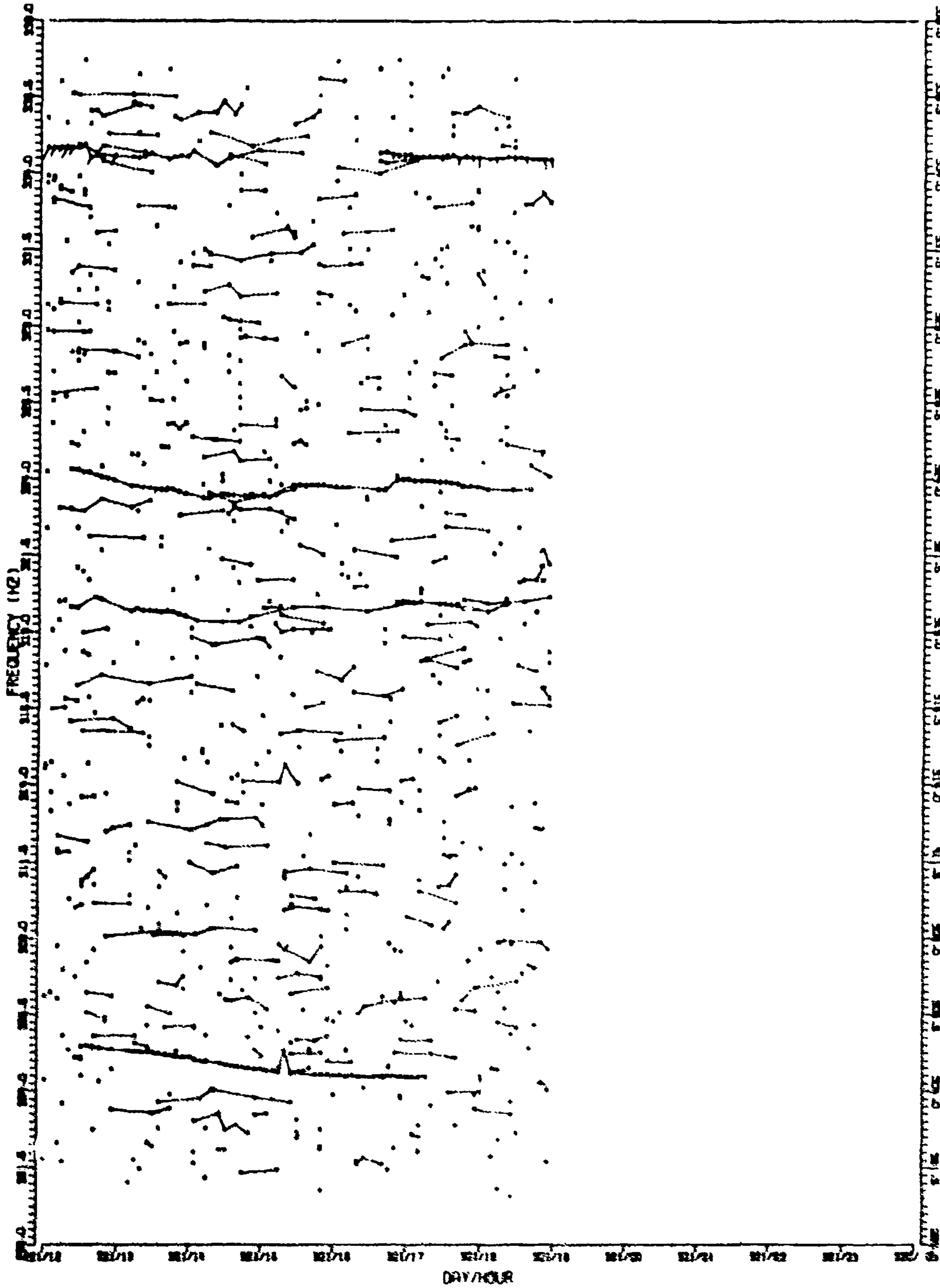

FIGURE III-12
MSS-FVT HIGH-BAND DETECTION OVERVIEW DURING THE 17 NOV FIELD EVENT AT SITE A2
OBTAINED VIA THE SINGLE CONTINUOUS SENSOR WITH VERNIER RESOLUTION (U)

AS-77-2612

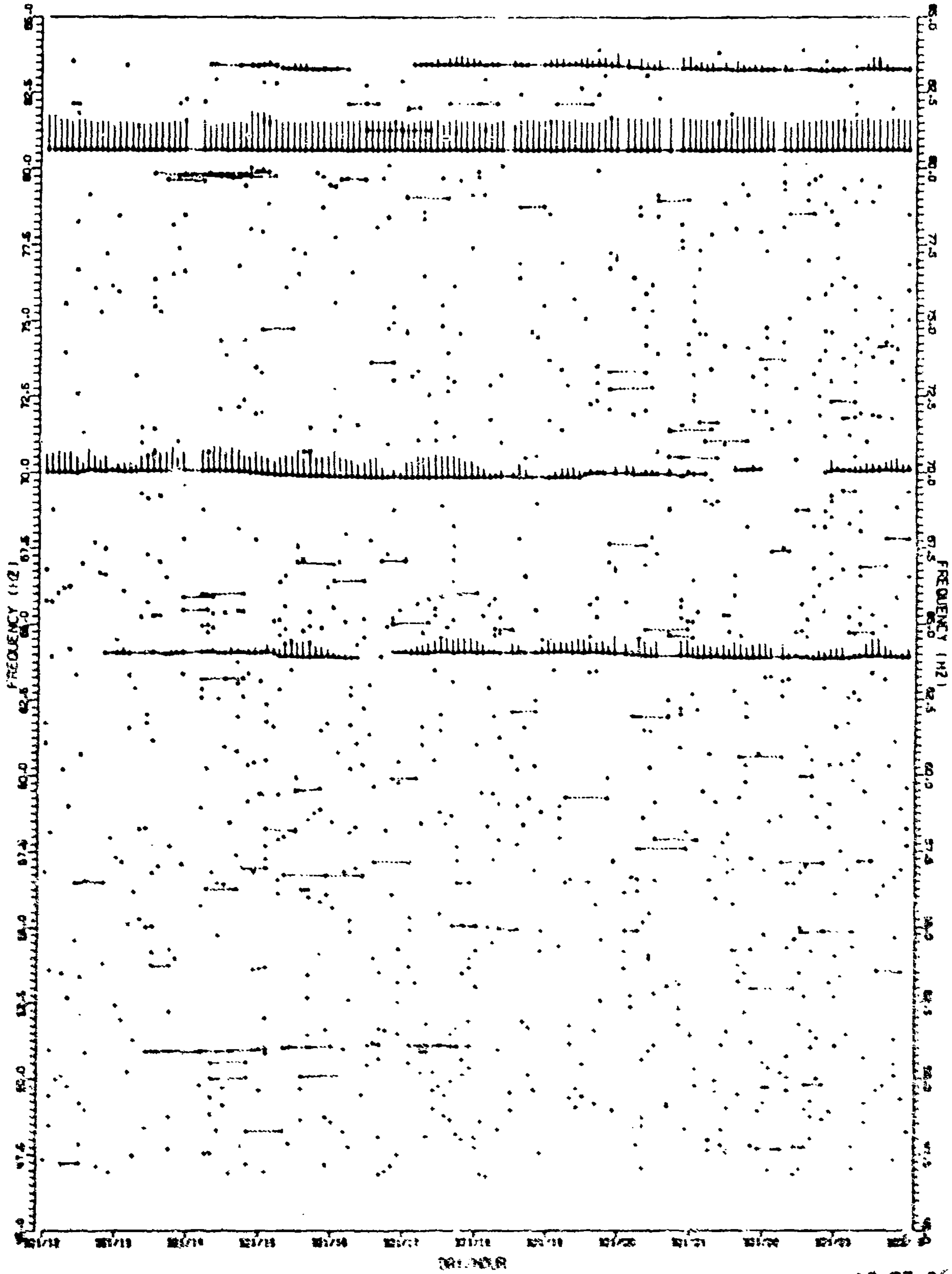

AS-77-2613

FIGURE III-13
NSS-FVT LOW-BAND DETECTION OVERVIEW DURING THE 17 NOV FIELD EVENT AT SITE AG
OBTAINED VIA THE OMNIDIRECTIONAL SENSOR WITH VERNIER RESOLUTION (U)

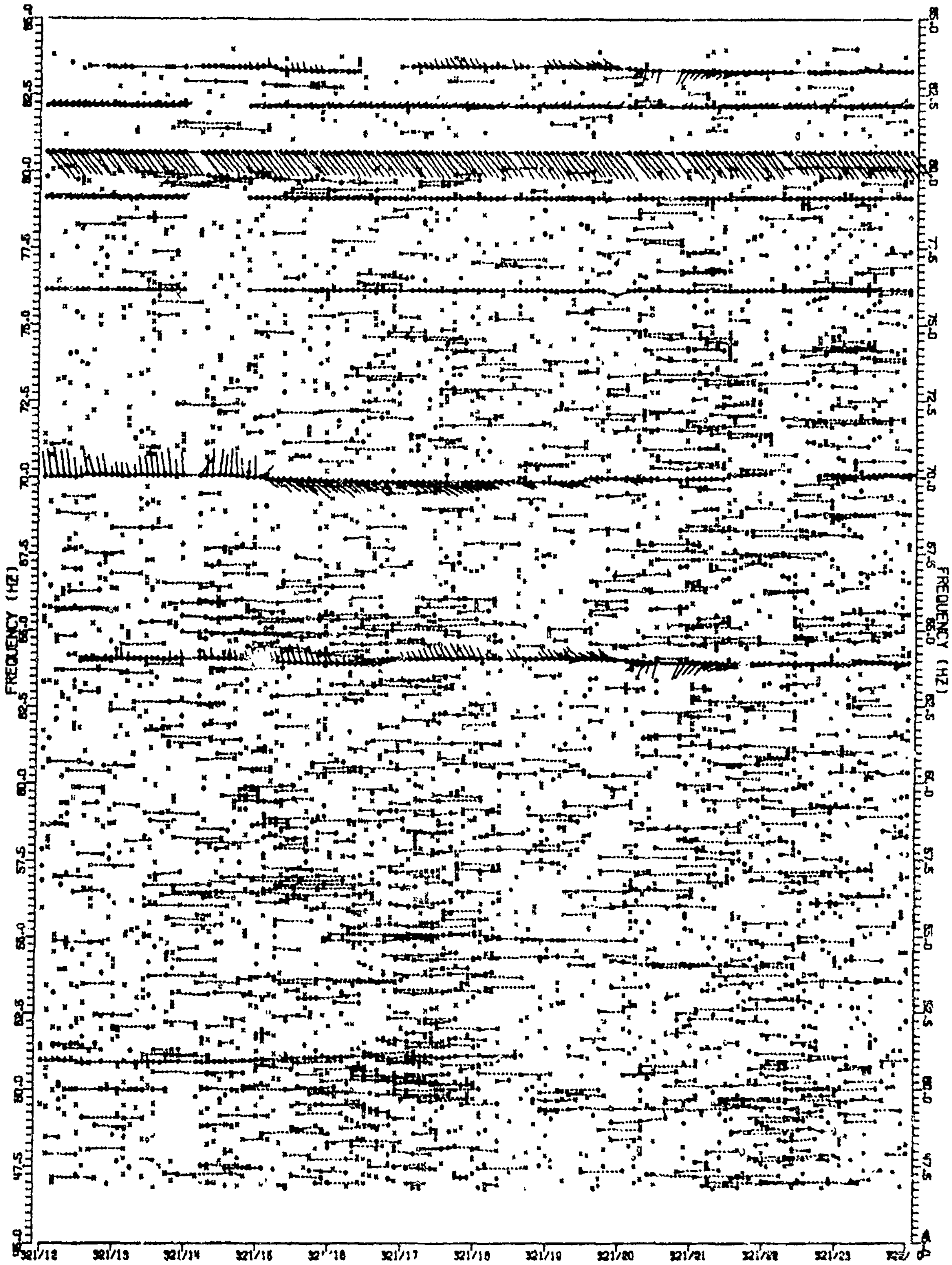

AS-77-2614

FIGURE III-14
MSS-FVT LOW-BAND DETECTION OVERVIEW DURING THE 17 NOV FIELD EVENT AT SITE A3
OBTAINED VIA THE SINGLE CARDIOIDS SENSOR WITH VERNIER RESOLUTION (U)

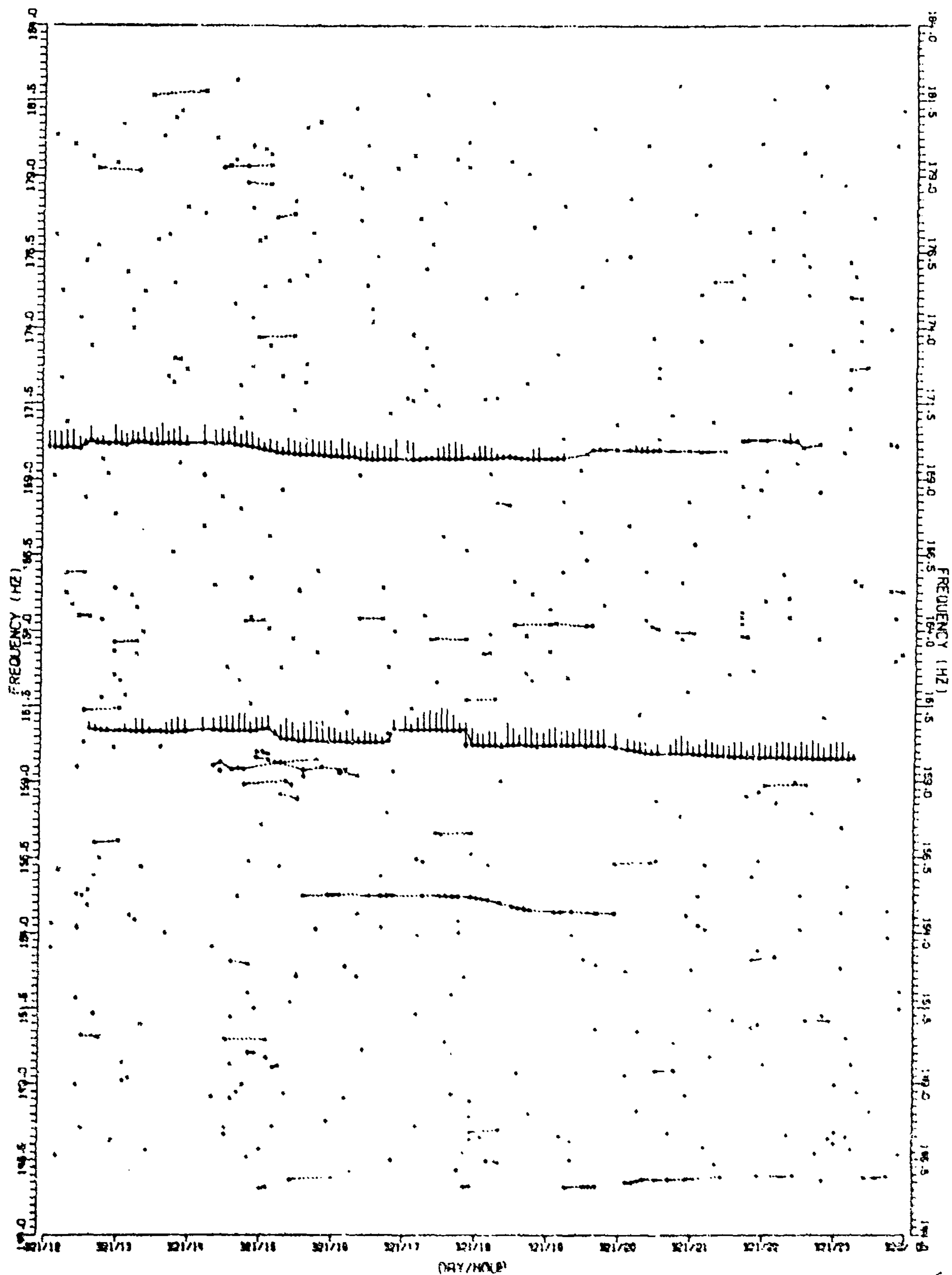

FIGURE III-15
NSS-FVT MID-BAND DETECTION OVERVIEW DURING THE 17 NOV FIELD EVENT AT SITE A3
OBTAINED VIA THE OMNIDIRECTIONAL SENSOR WITH VERNIER RESOLUTION (U)

AS-77-2615

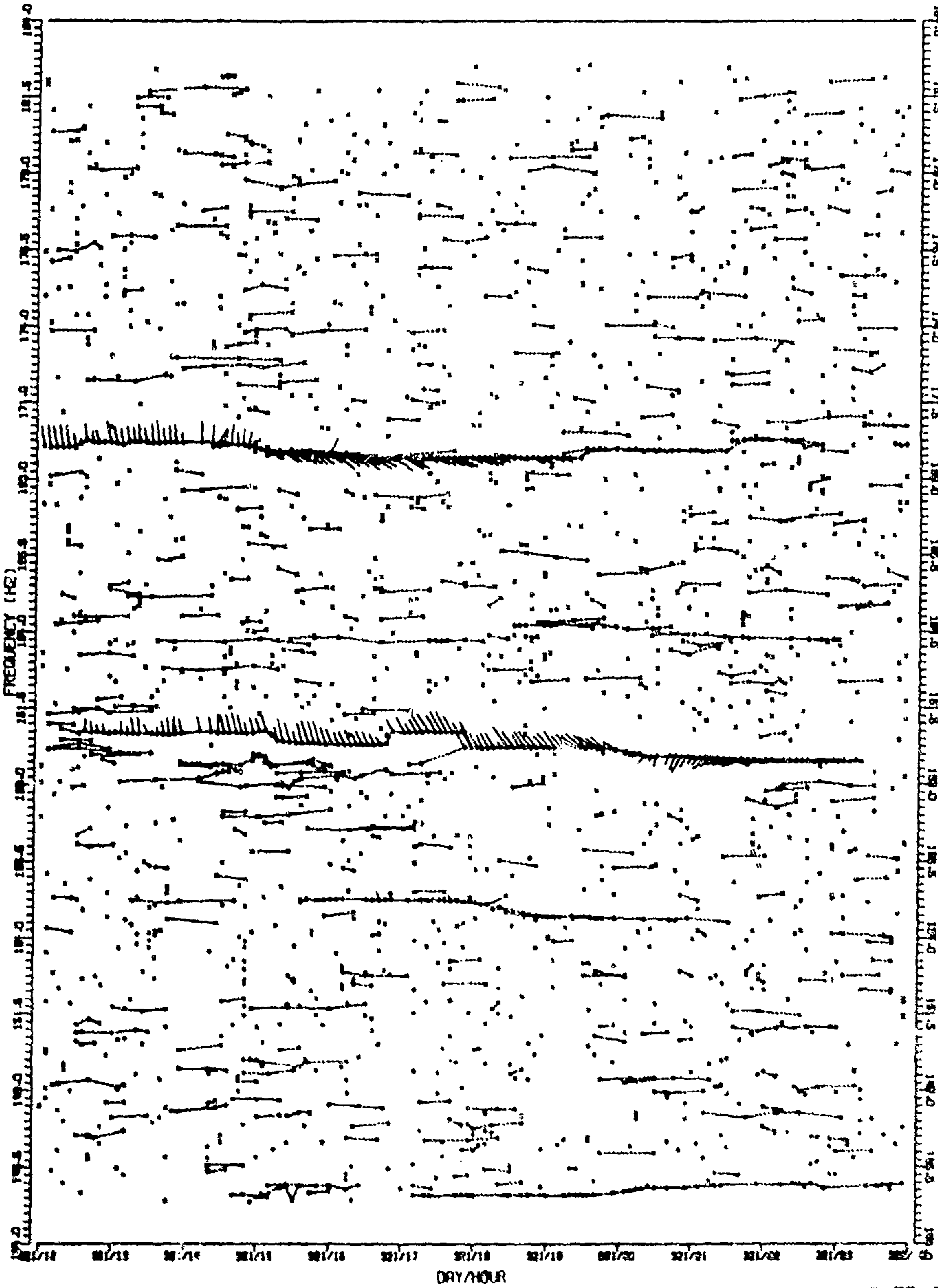

AS-77-2616

FIGURE III-16
MSS-FVT MID-BAND DETECTION OVERVIEW DURING THE 17 NOV FIELD EVENT AT SITE A3 OBTAINED VIA THE SINGLE CARDIOIDS SENSOR WITH VERNIER RESOLUTION (U)

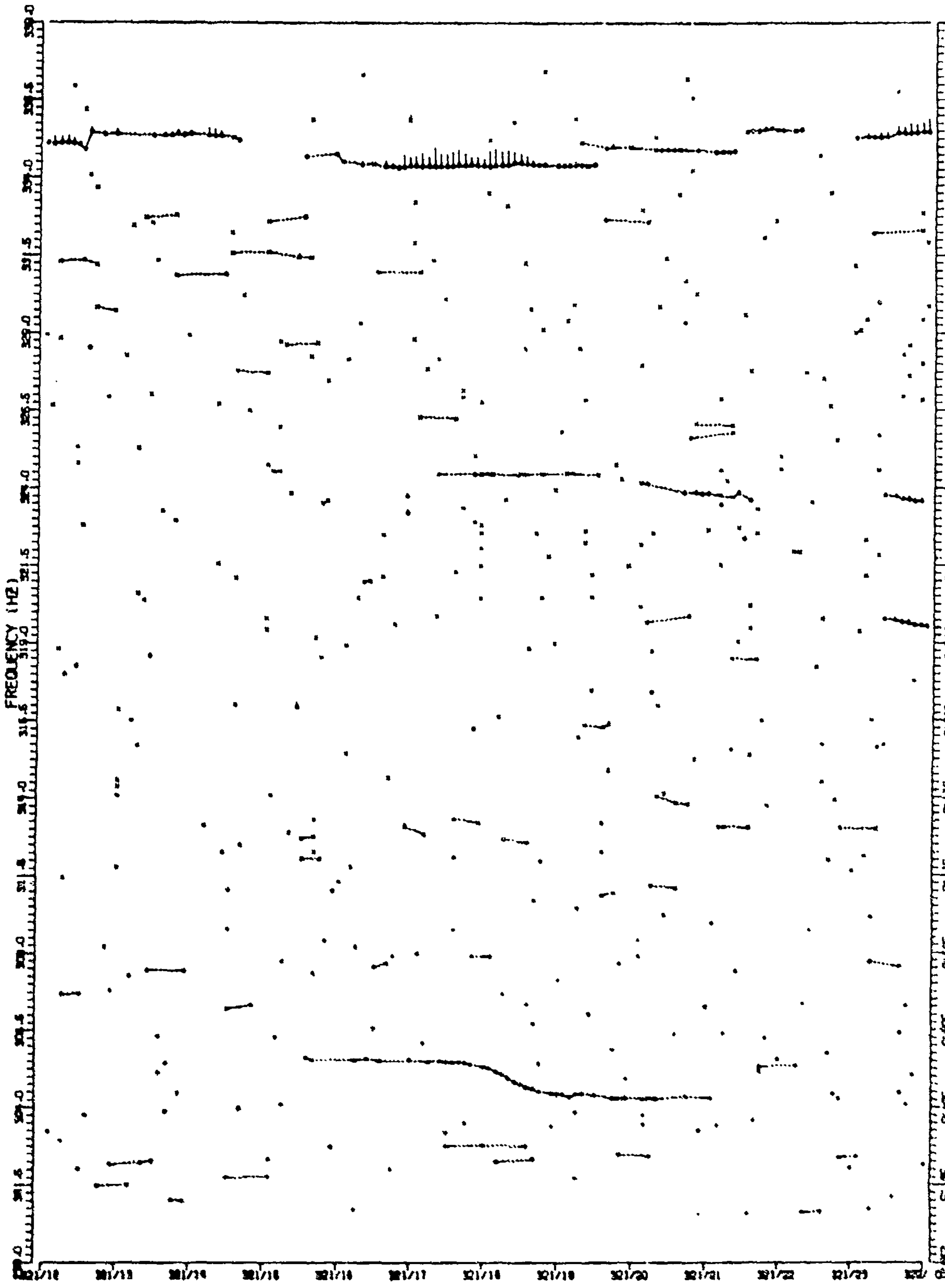

AS-77-2617

FIGURE III-17
NSS-FVT HIGH-BAND DETECTION OVERVIEW DURING THE 17 NOV FIELD EVENT AT SITE A3
OBTAINED VIA THE OMNIDIRECTIONAL SENSOR WITH VERNIER RESOLUTION (U)

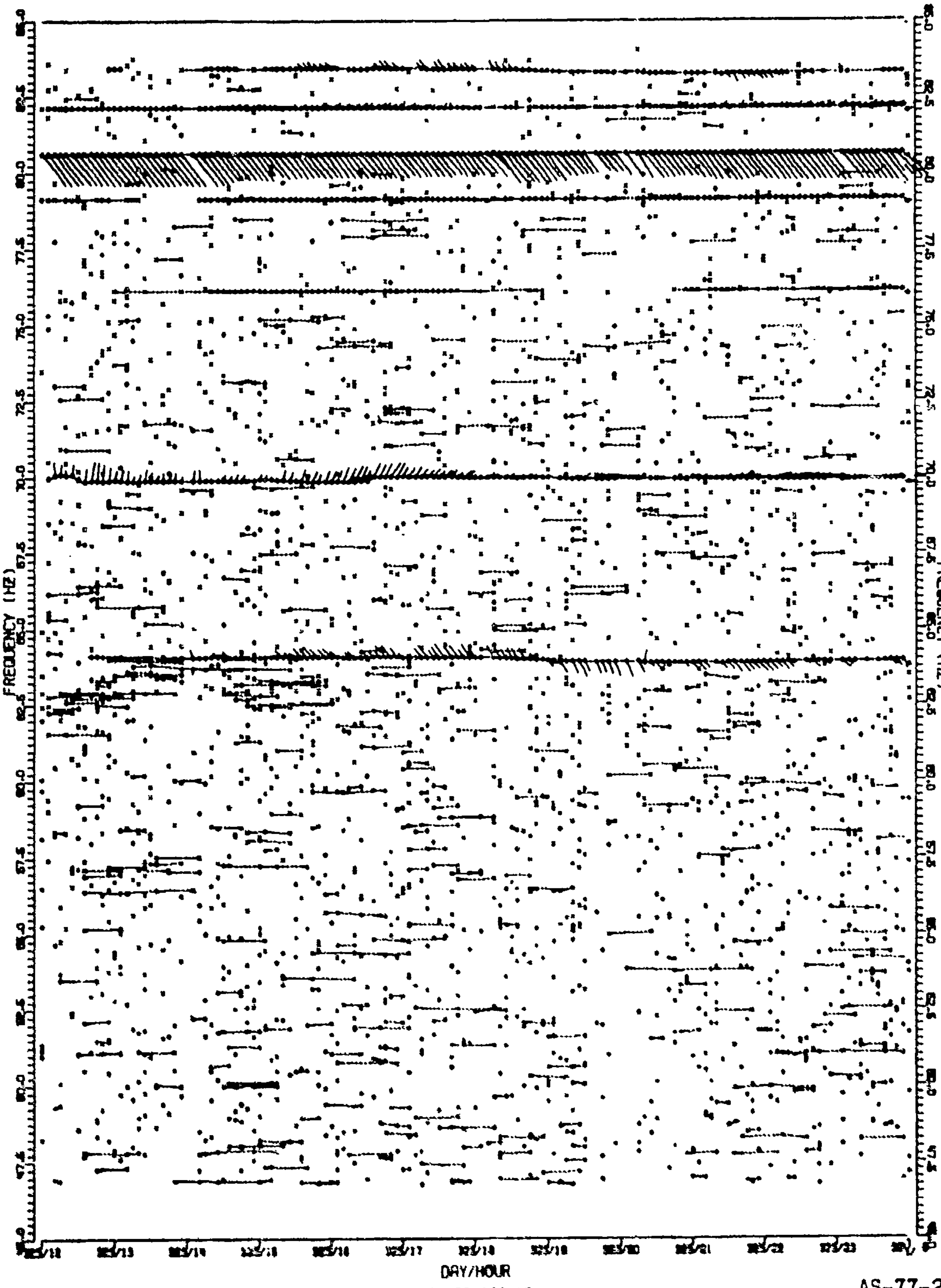

AS-77-2619

FIGURE III-19
NSS-FVT LOW-BAND DETECTION OVERVIEW DURING THE 19 NOV FIELD EVENT AT SITE A3
OBTAINED VIA THE SINGLE CARDIOIDS SENSOR WITH VERNIER RESOLUTION (U)

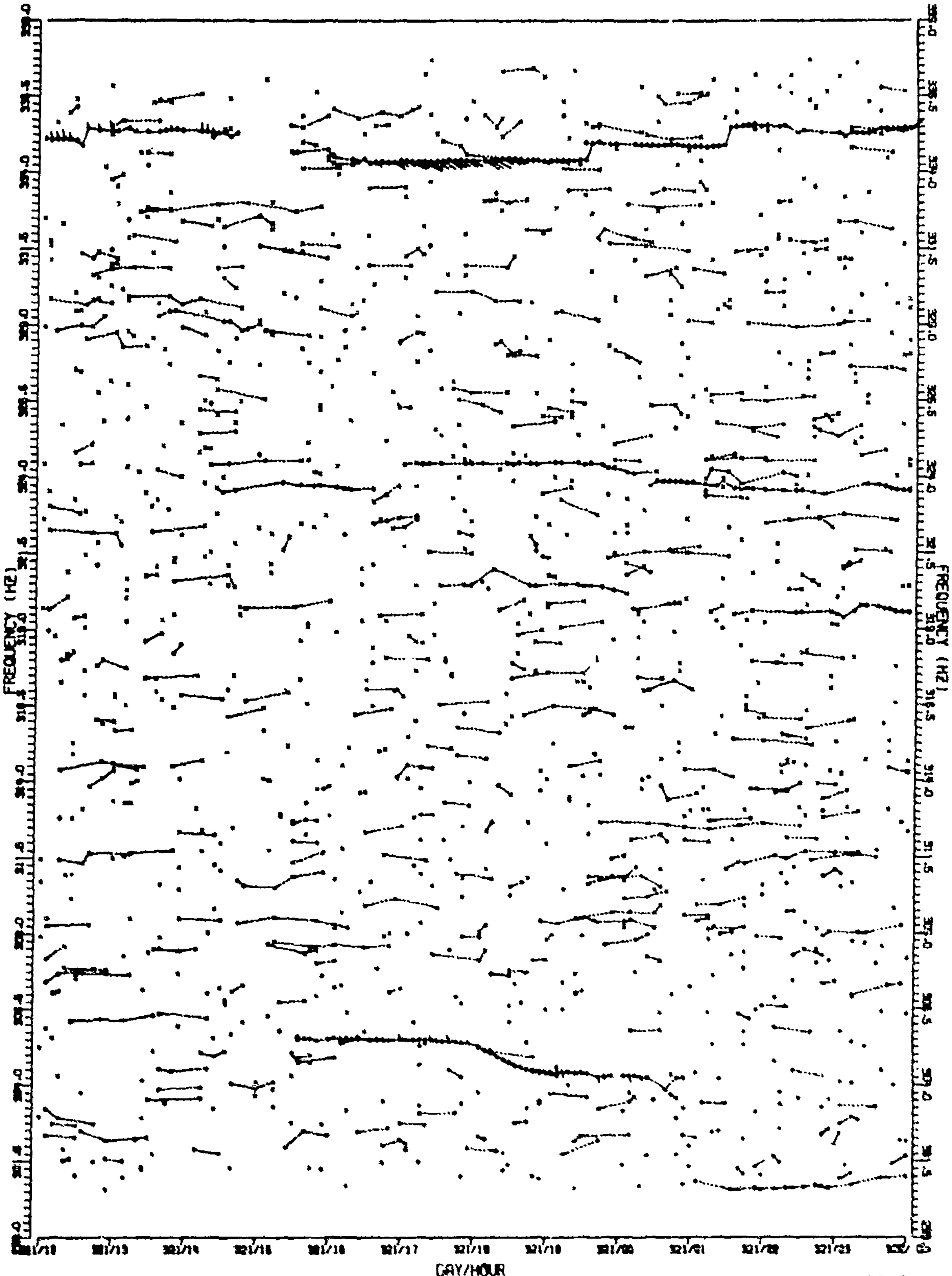

AS-77-2618

FIGURE III-18
NSS-FVT HIGH-BAND DETECTION OVERVIEW DURING THE 17 NOV FIELD EVENT AT SITE A3 OBTAINED VIA THE SINGLE CARDIOIDS SENSOR WITH VERNIER RESOLUTION (U)

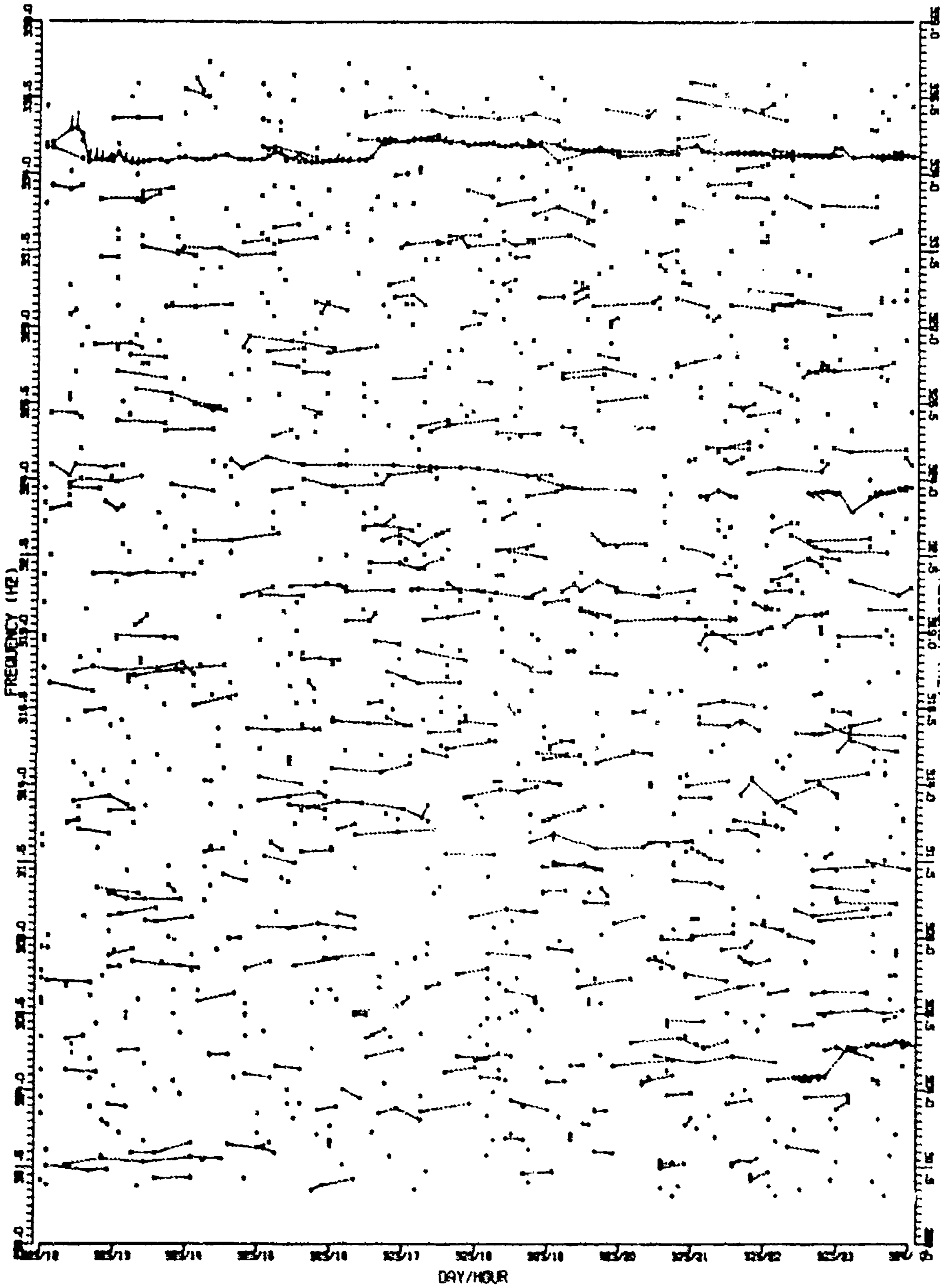

AS-77-2620

FIGURE III-20
NSS-FVT HIGH-BAND DETECTION OVERVIEW DURING THE 13 NOV FIELD EVENT AT SITE A3
OBTAINED VIA THE SINGLE CARDIOIDS SENSOR WITH VERNIER RESOLUTION (U)

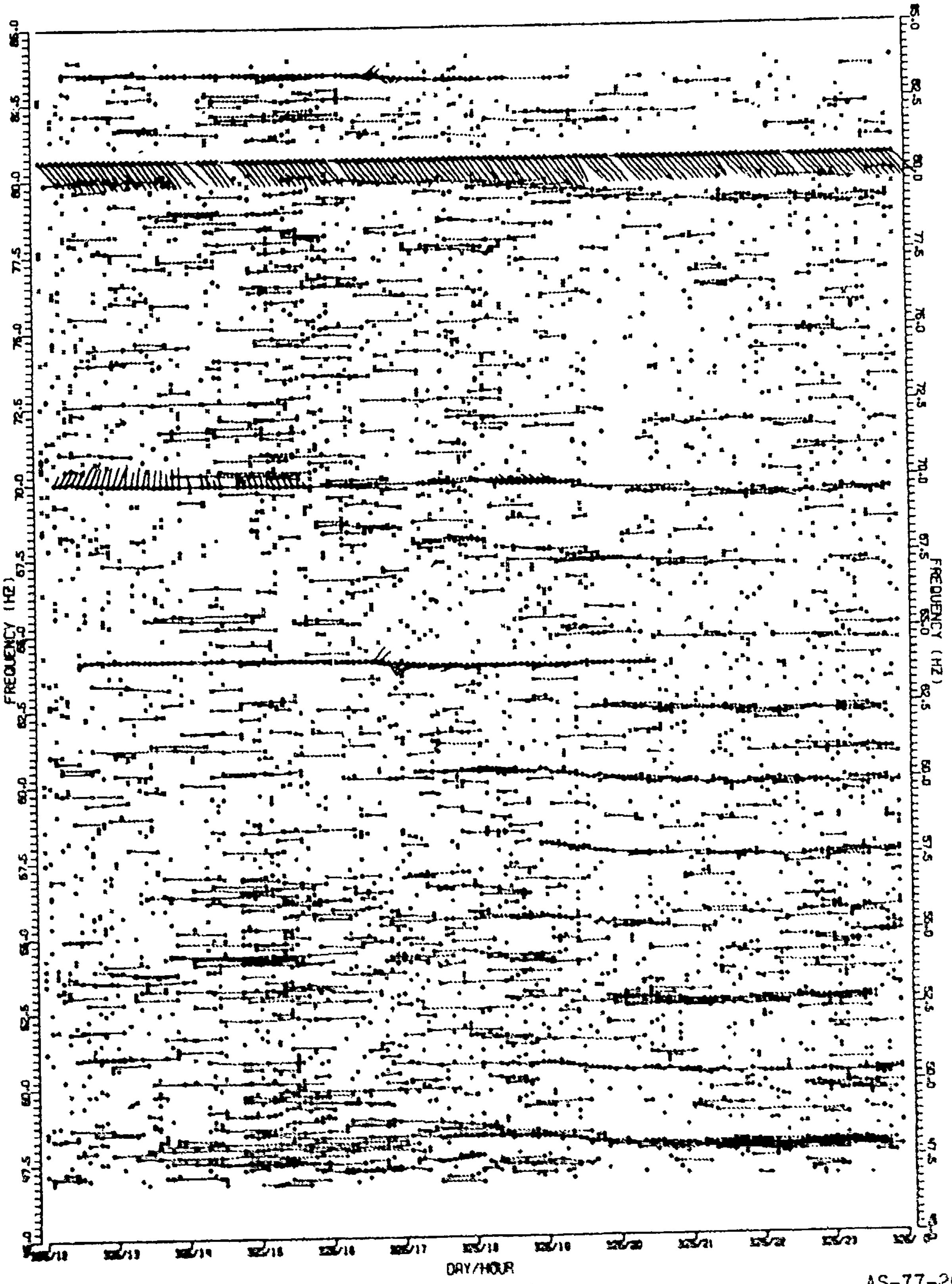

AS-77-2621

FIGURE III-21
MSS-FVT LOW-BAND DETECTION OVERVIEW DURING THE 21 NOV FIELD EVENT AT SITE A3 OBTAINED VIA THE SINGLE CARDIOIDS SENSOR WITH VERNIER RESOLUTION (U)

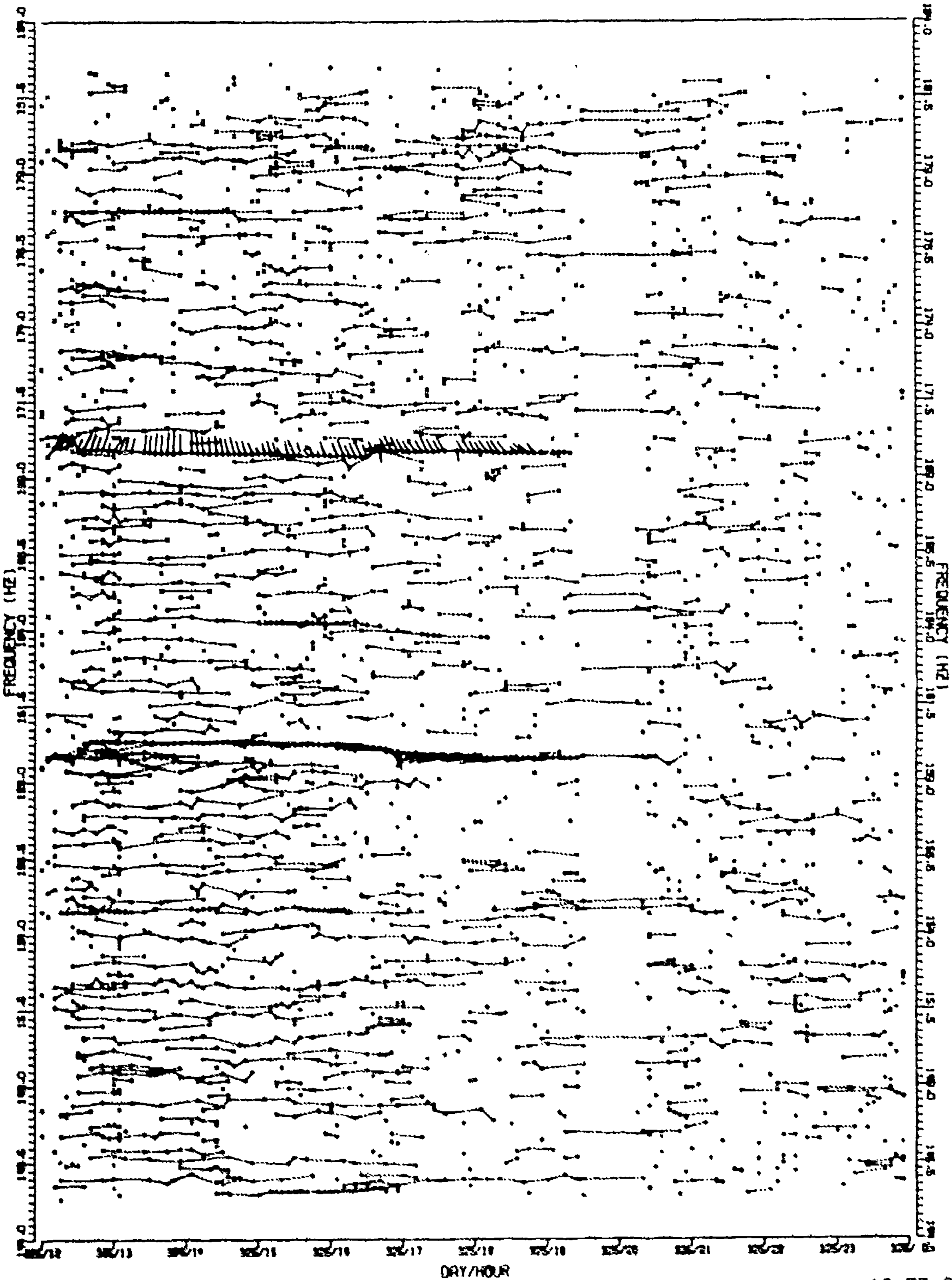

AS-77-2622

FIGURE III-22
MSS-FVT MID-BAND DETECTION OVERVIEW DURING THE 21 NOV FIELD EVENT AT SITE A3
OBTAINED VIA THE SINGLE CARDIOIDS SENSOR WITH VERNIER RESOLUTION (U)

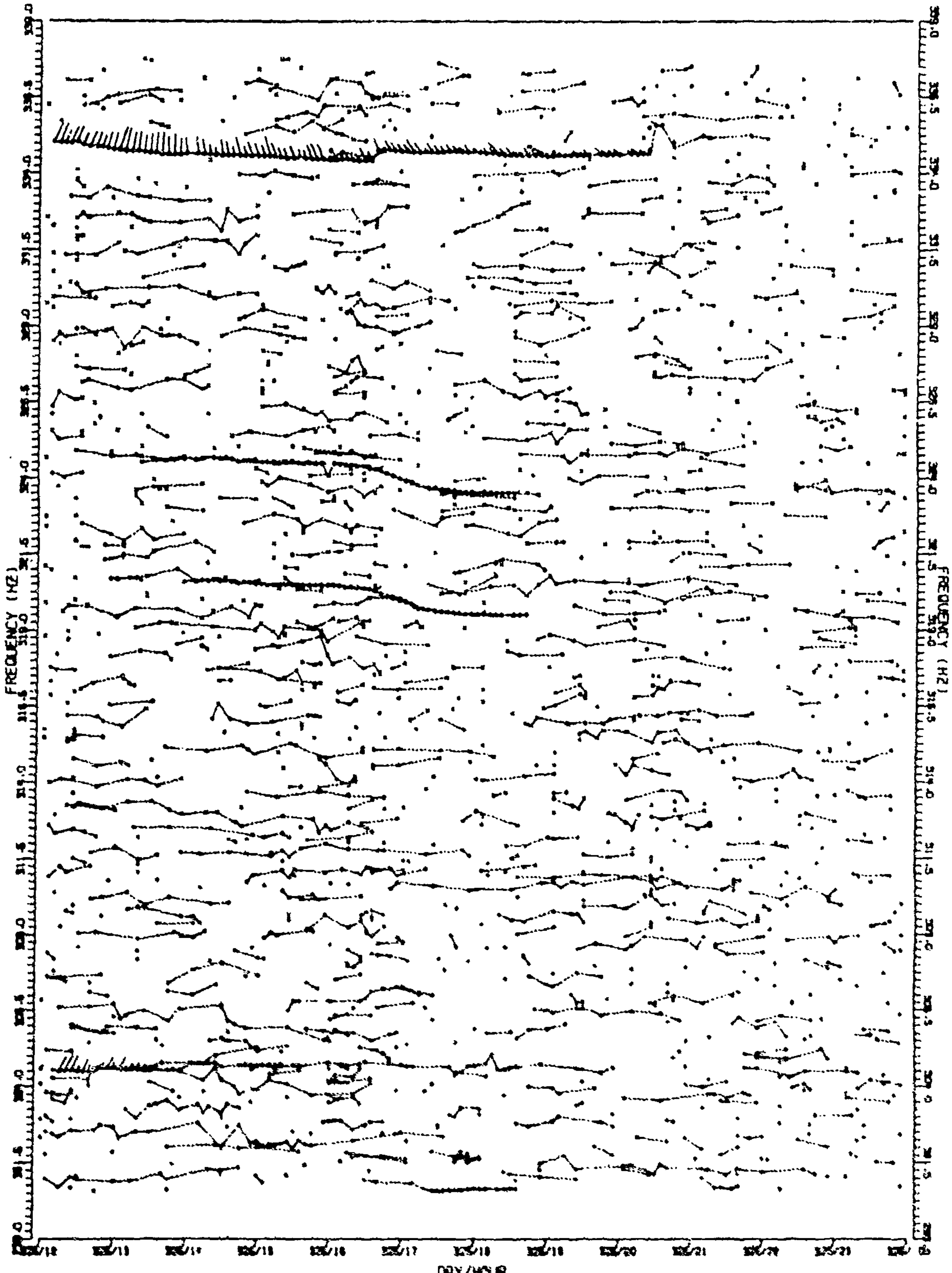

AS-77-2623

FIGURE III-23
MSS-FVT HIGH-BAND DETECTION OVERVIEW DURING THE 21 NOV FIELD EVENT AT SITE A3
OBTAINED VIA THE SINGLE CARDIOIDS SENSOR WITH VERNIER RESOLUTION (U)

(The reverse of this page is blank.)

APPENDIX B

LINE HISTORY CURVES (U)

(FIGURES III-24 - III-163)

(The reverse of this page is blank.)

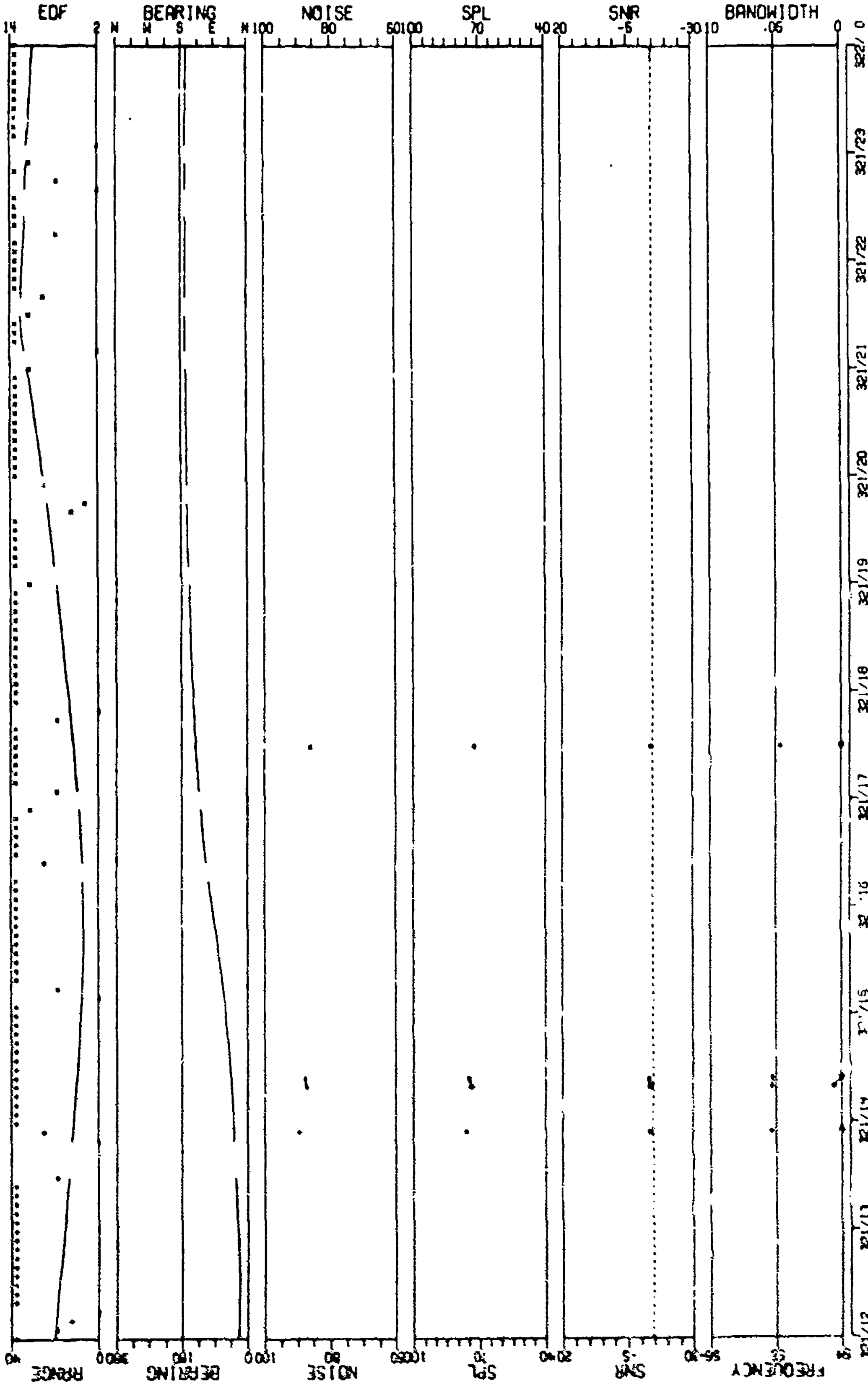

FIGURE III-24
MSS-FVI 55 HZ LINE HISTORY AS OBSERVED VIA THE OMNIDIRECTIONAL SENSOR AT SITE A1 DURING THE 17 NOV FIELD EVENT WITH VERNIER RESOLUTION (U)

AS-77-2624

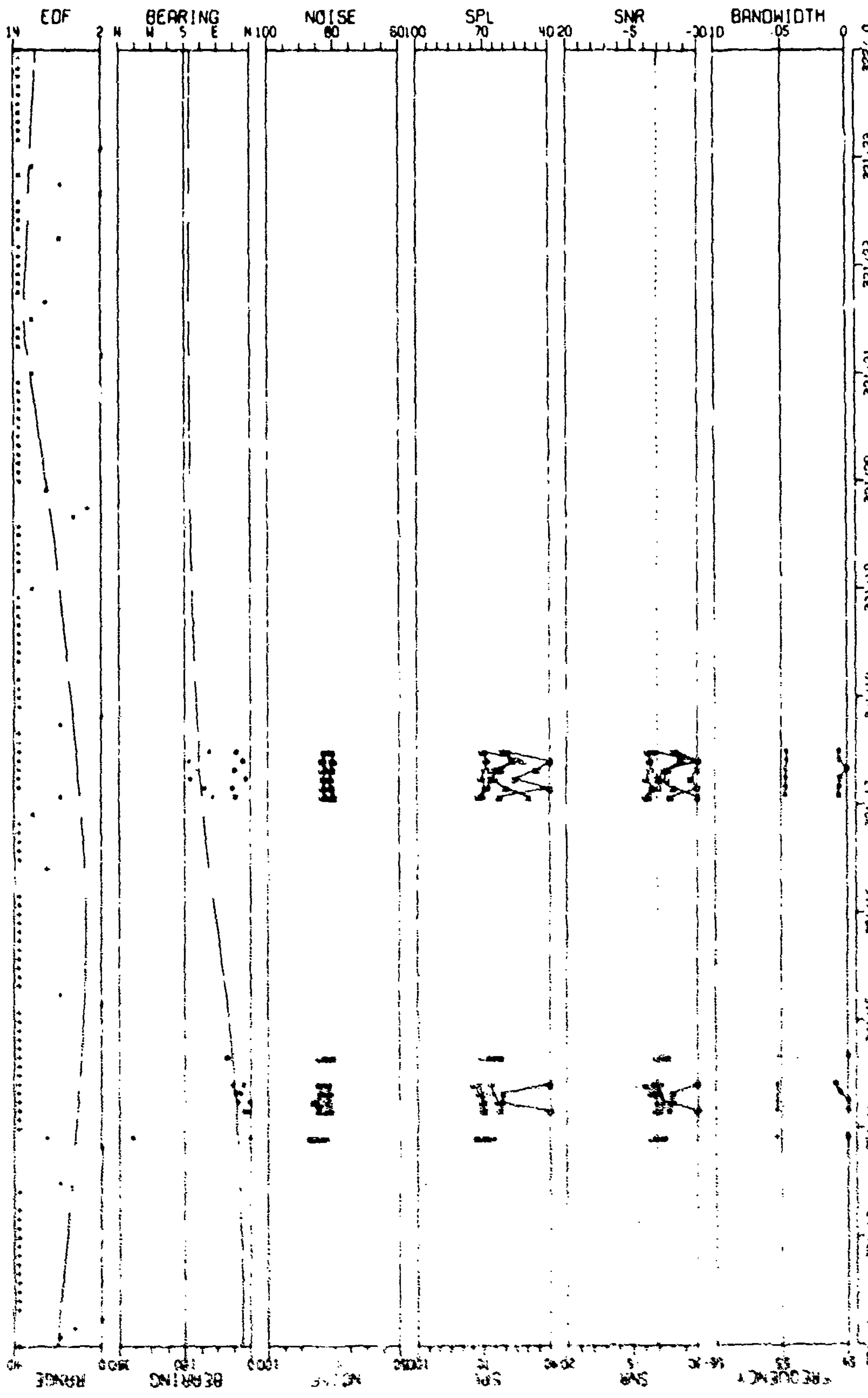

FIGURE III-25
MSS-FVT 55 HZ LINE HISTORY AS OBSERVED VIA THE SINGLE CARDIOIDS SENSOR AT SITE A1 DURING THE 17 NOV FIELD EVENT WITH VERNIER RESOLUTION (U)

AS-77-2625

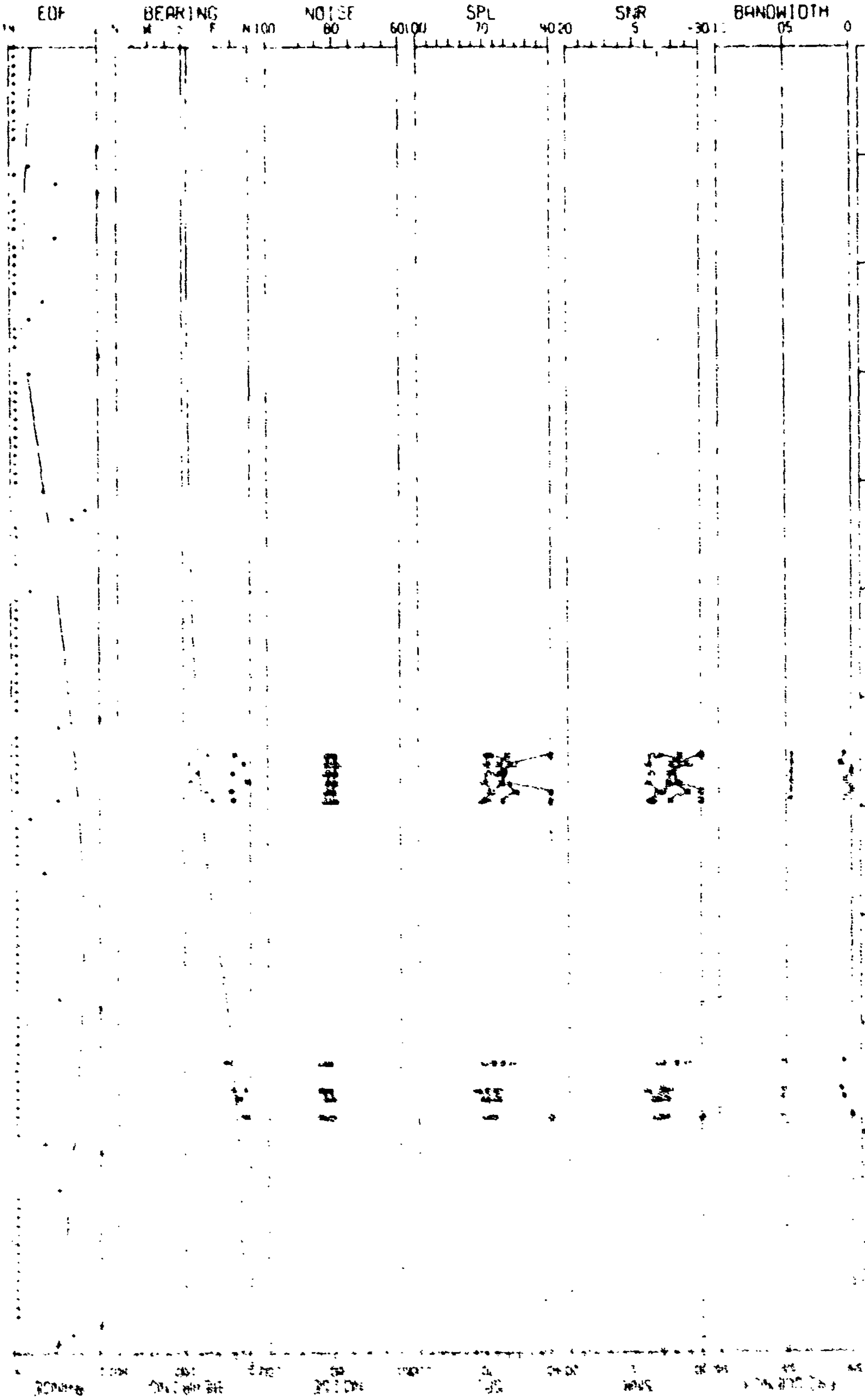

FIGURE III-26
[illegible] HZ LINE HISTORY [illegible] OBSERVED VIA THE MAX GAIN LIMACONS SENSOR
[illegible] DURING THE 17 NOV FIELD EVENT WITH VERNIER RESOLUTION (U)

AR-77-2626

CONFIDENTIAL

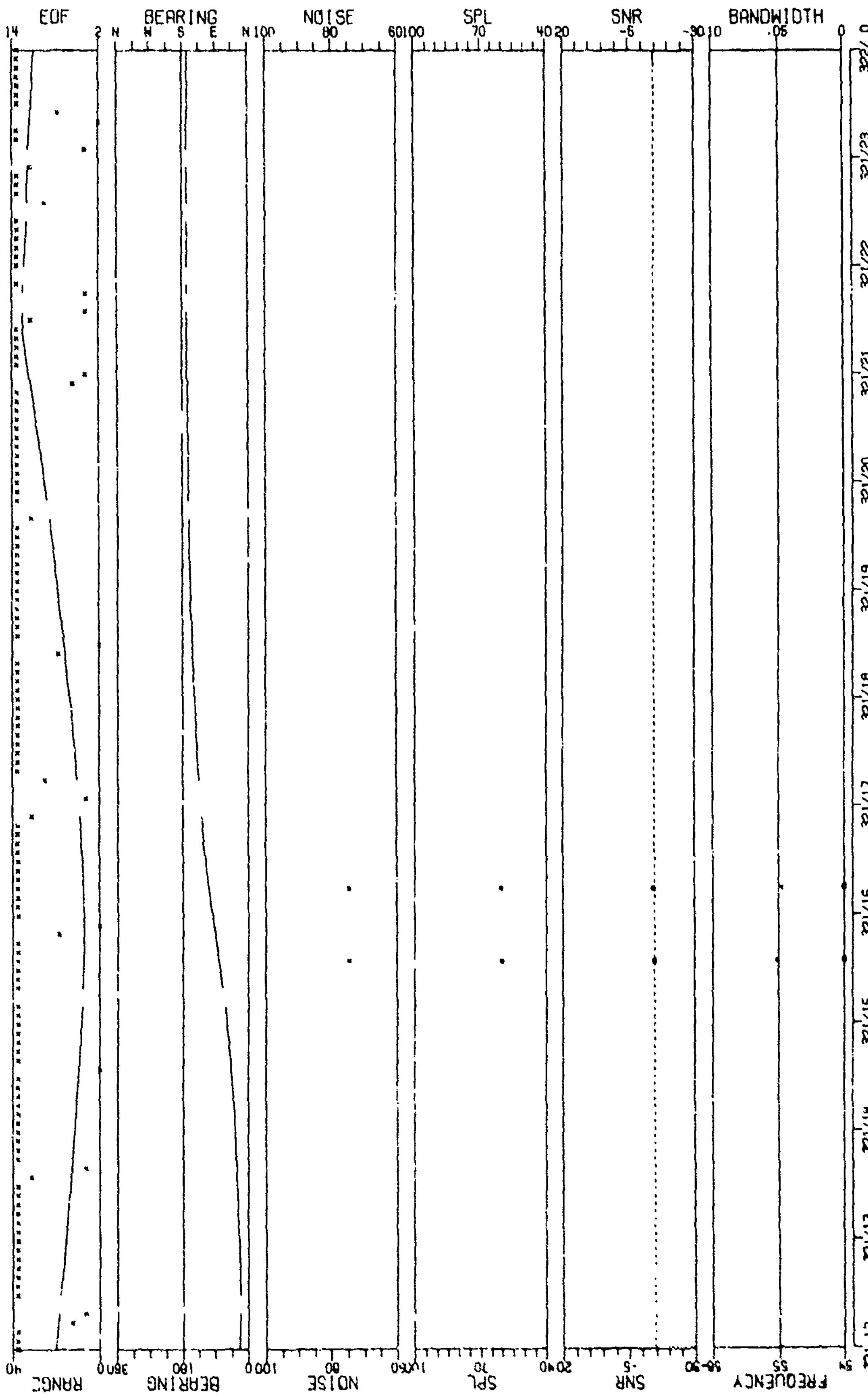

FIGURE III-27
MSS-FVT 55 HZ LINE HISTORY AS OBSERVED VIA THE VERTICAL DIPOLE SENSOR
AT SITE A1 DURING THE 17 NOV FIELD EVENT WITH VERNIER RESOLUTION (U)

AS-77-2627

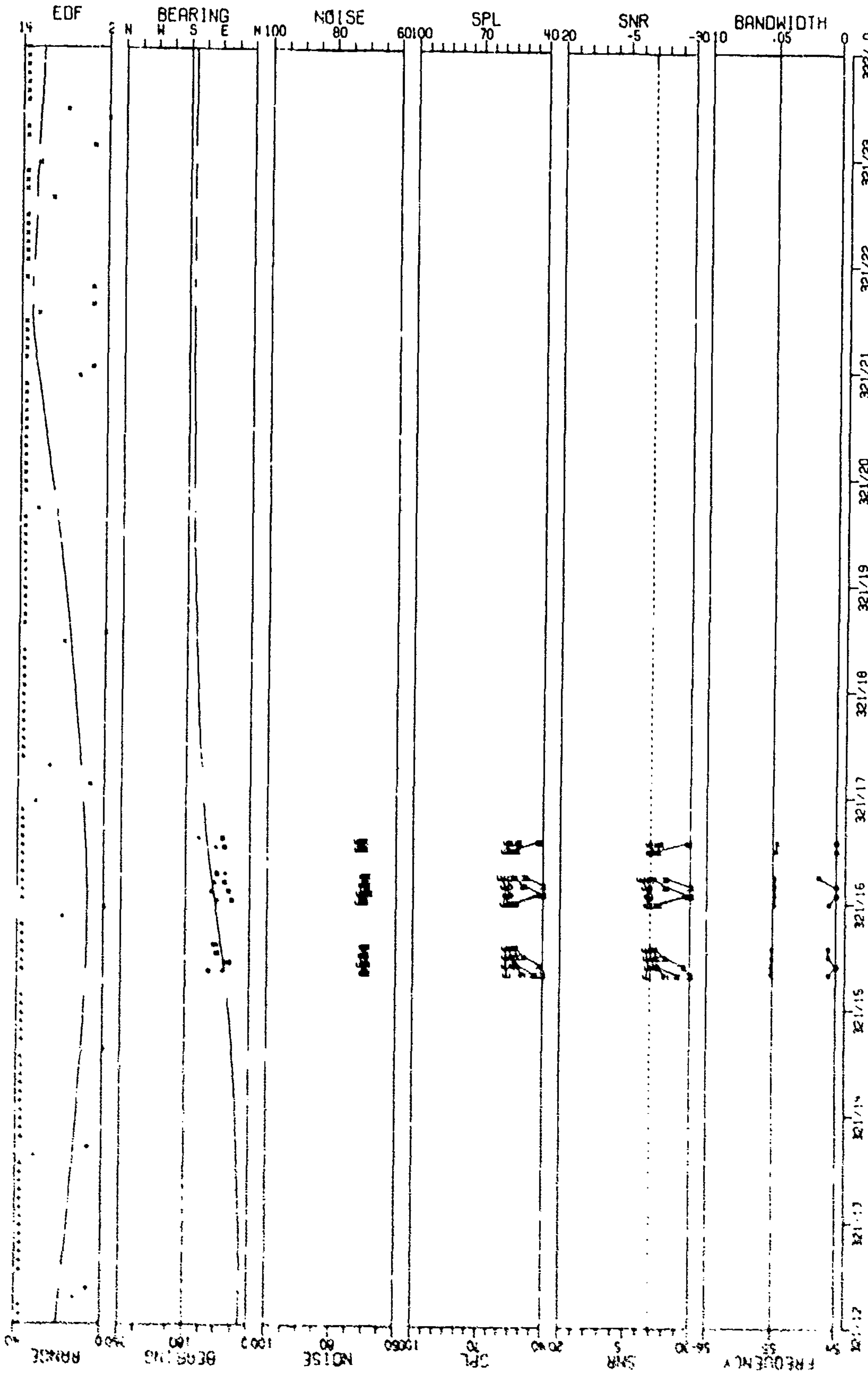

FIGURE III-28
MSS EVT 55 HZ LINE HISTORY AS OBSERVED VIA THE DIFFERENCED CARDIOIDS SENSOR AT SITE A1 DURING THE 17 NOV FIELD EVENT WITH VERNIER RESOLUTION (U)

AS-77-2628

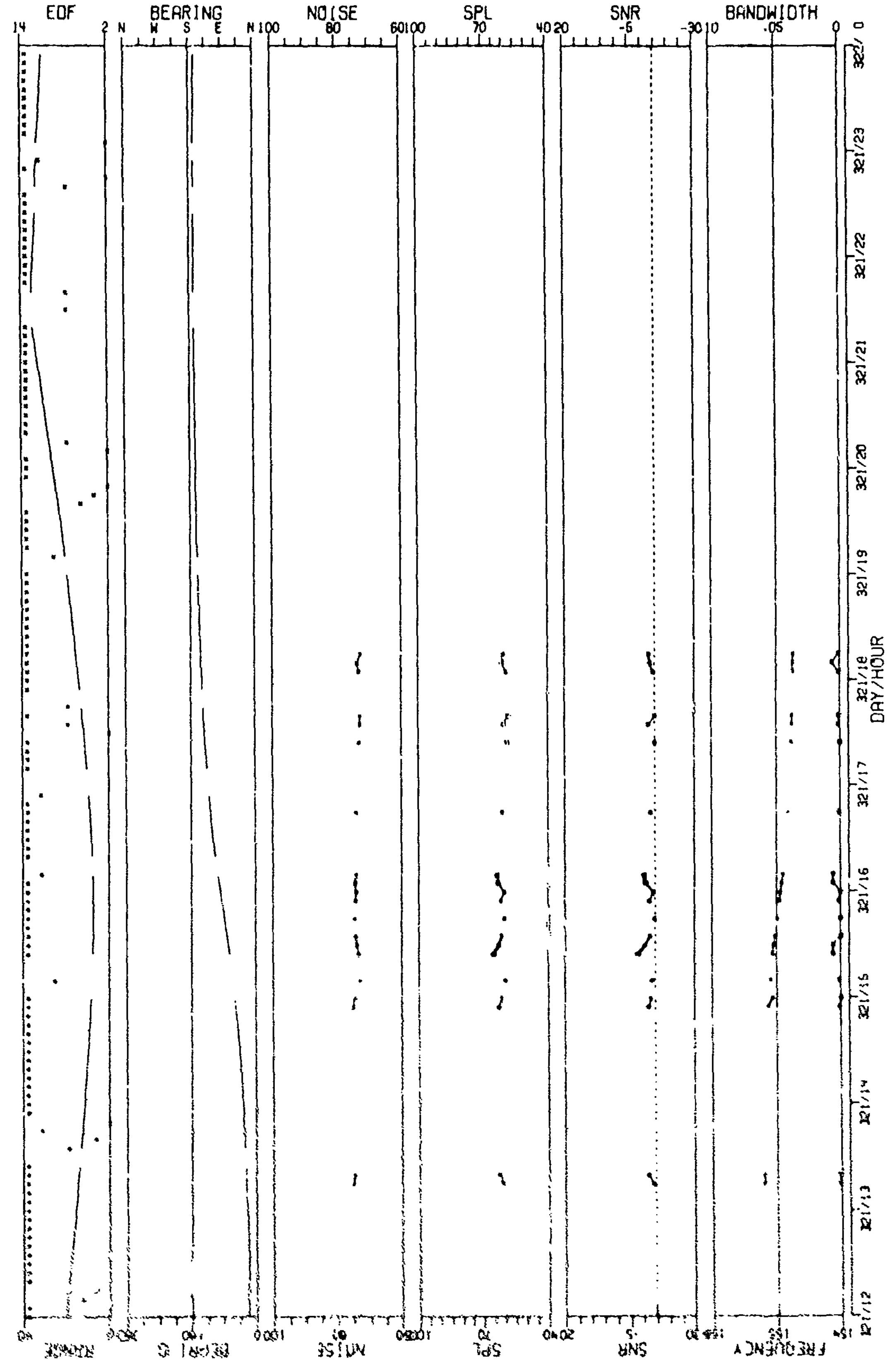

FIGURE III-29
MSS-FVT 155 Hz LINE HISTORY AS OBSERVED VIA THE OMNIDIRECTIONAL SENSOR AT SITE A1 DURING THE 17 NOV FIELD EVENT WITH VERNIER RESOLUTION (U)

AS-77-2629

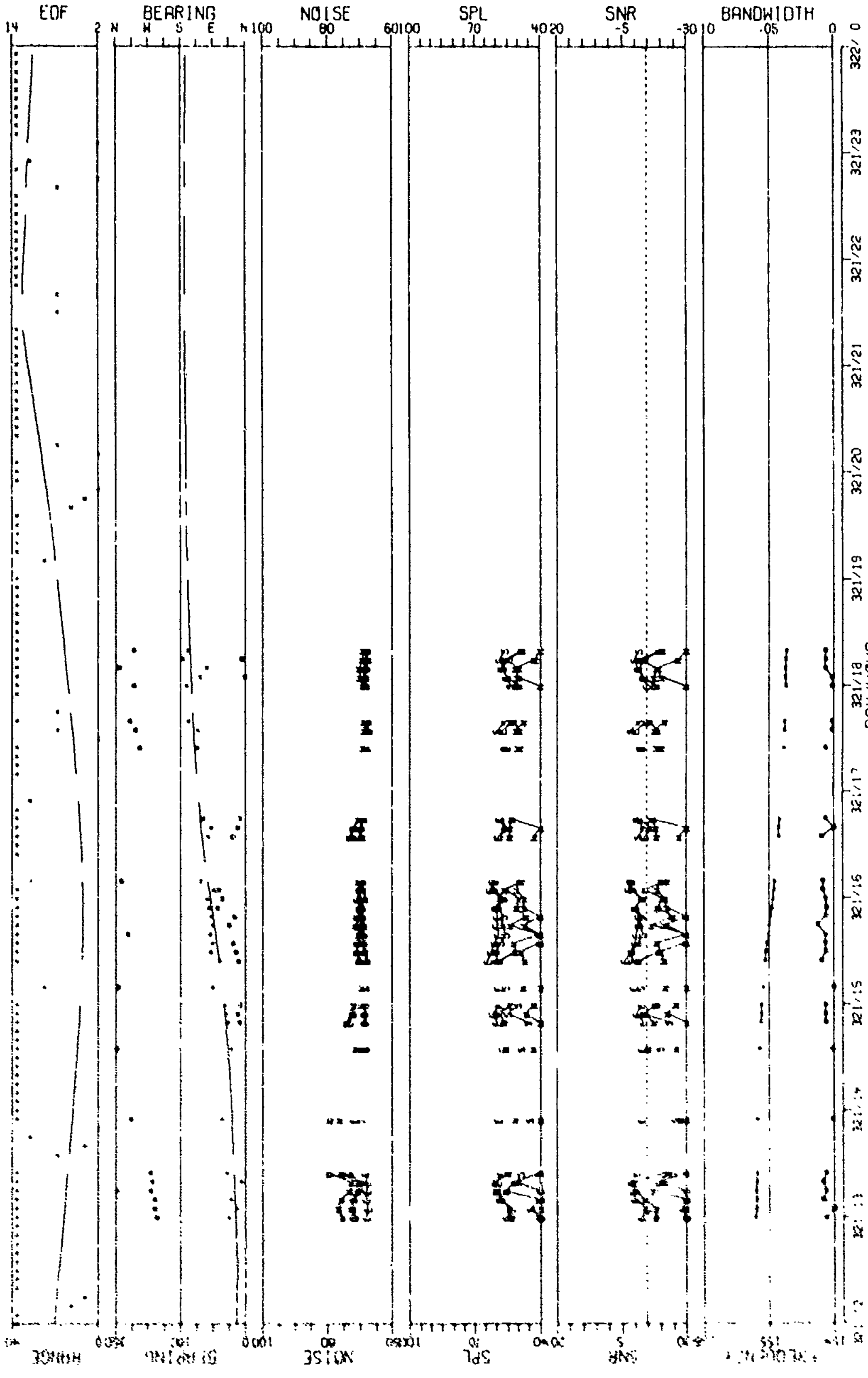

FIGURE III-30
MSS-FVT 155 HZ LINE HISTORY AS OBSERVED VIA THE SINGLE CARDIOIDS SENSOR AT SITE A1 DURING THE 17 NOV FIELD EVENT WITH VERNIER RESOLUTION (U)

AS-77-2630

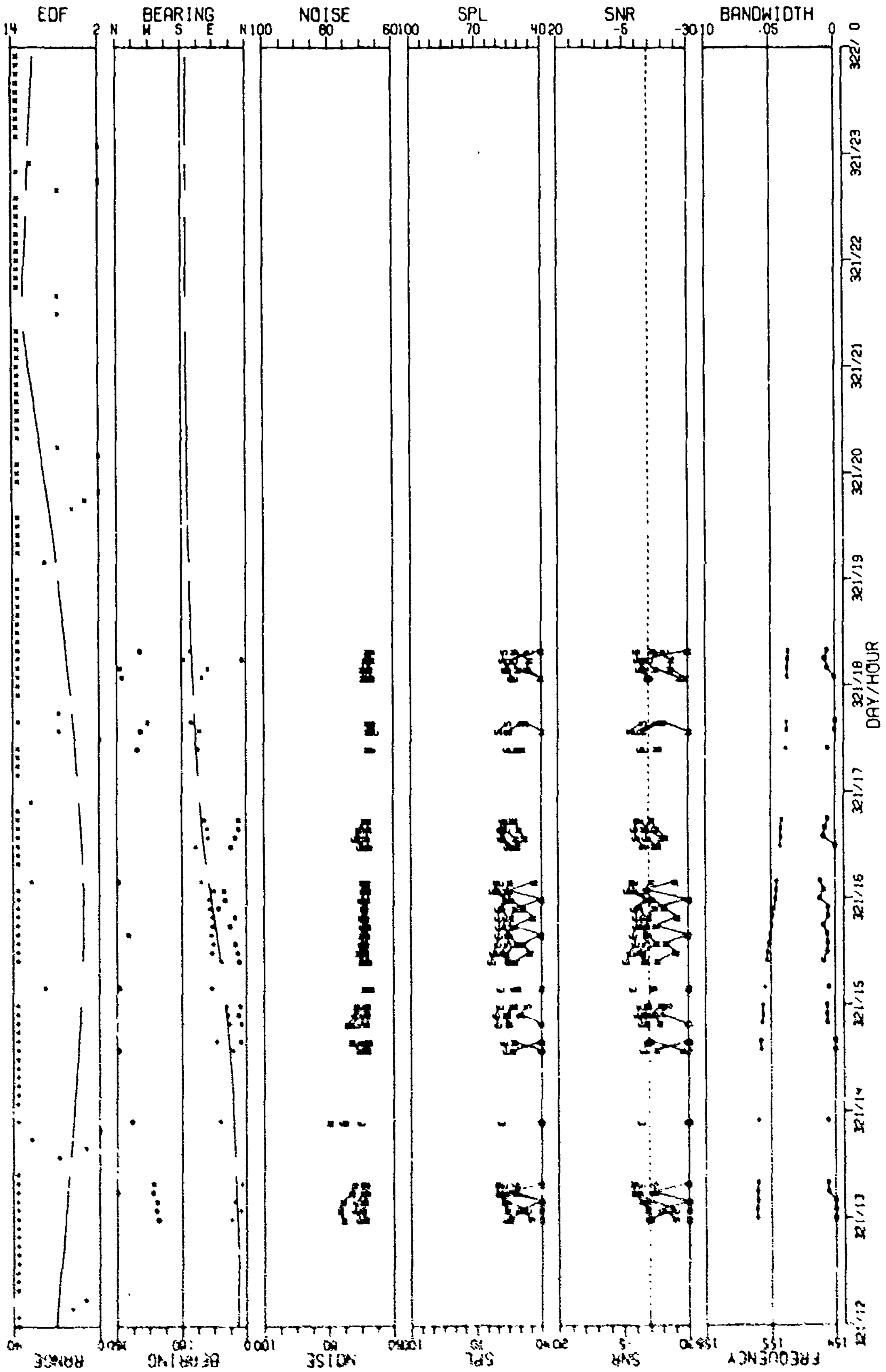

FIGURE III-31
MSS-FVT 155 HZ LINE HISTORY AS OBSERVED VIA THE MAX GAIN LIMACONS SENSOR AT SITE A1 DURING THE 17 NOV FIELD EVENT WITH VERNIER RESOLUTION (U)

AS-77-2631

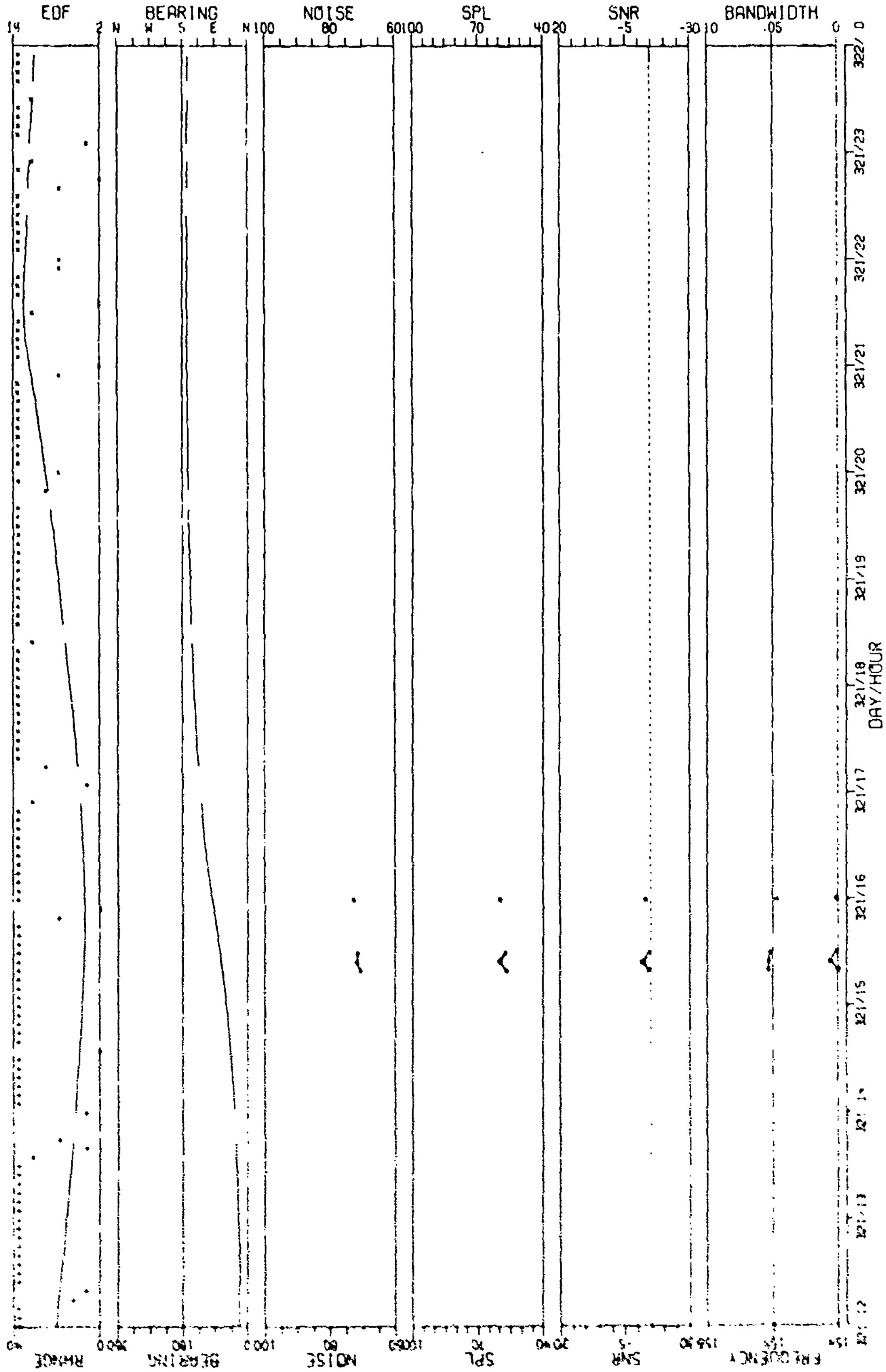

FIGURE III-32
MSS-EVT 155 HZ LINE HISTORY AS OBSERVED VIA THE VERTICAL DIPOLE SENSOR AT SITE A1 DURING THE 17 NOV FIELD EVENT WITH VERNIER RESOLUTION (U)

AS-77-2632

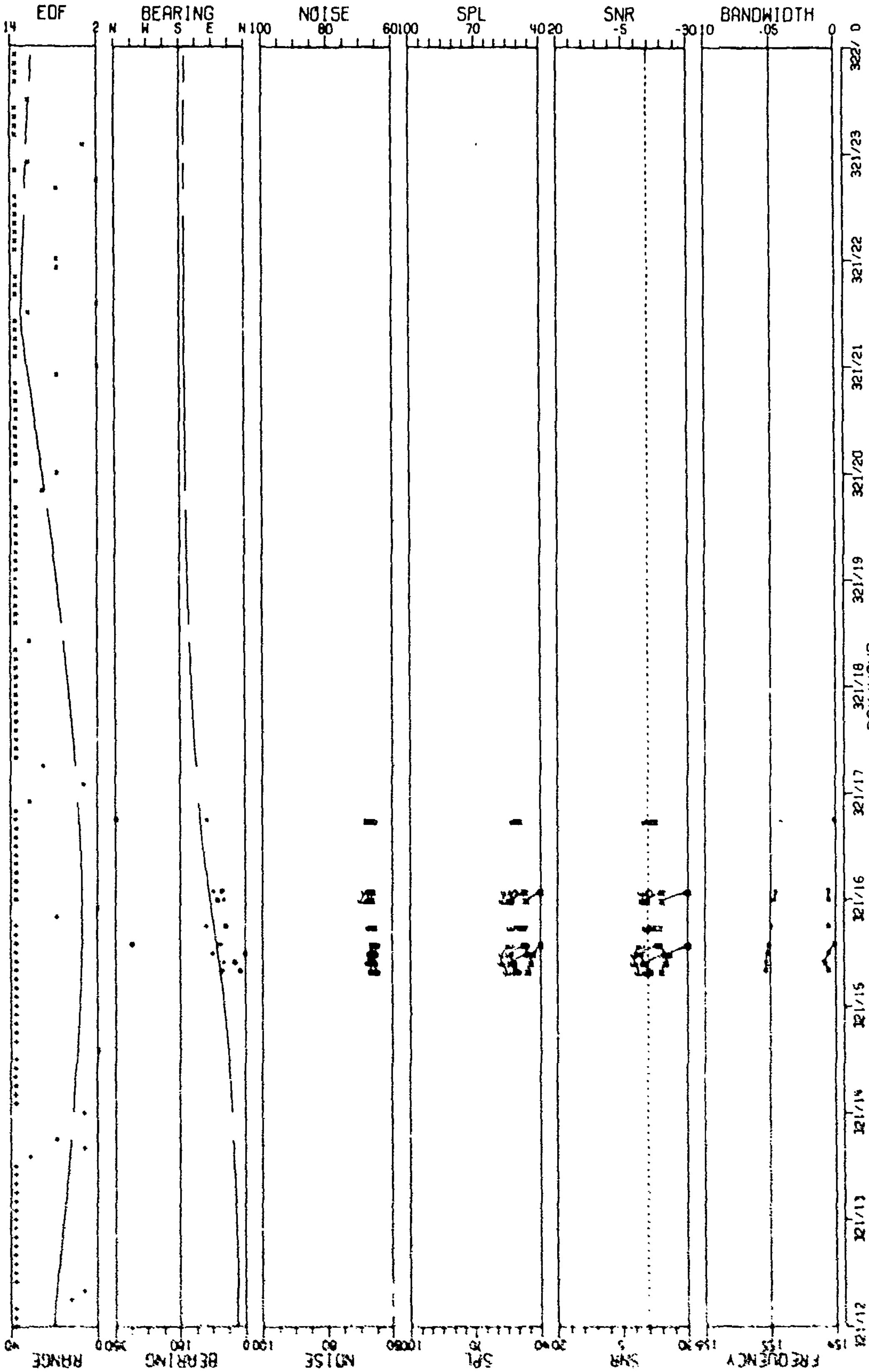

FIGURE III-33
WCS-FVT 155 HZ LINE HISTORY AS OBSERVED VIA THE DIFFERENCED CARDIOIDS SENSOR AT SITE A: DURING THE 17 NOV FIELD EVENT WITH VERNIER RESOLUTION (U)

AS-77-2633

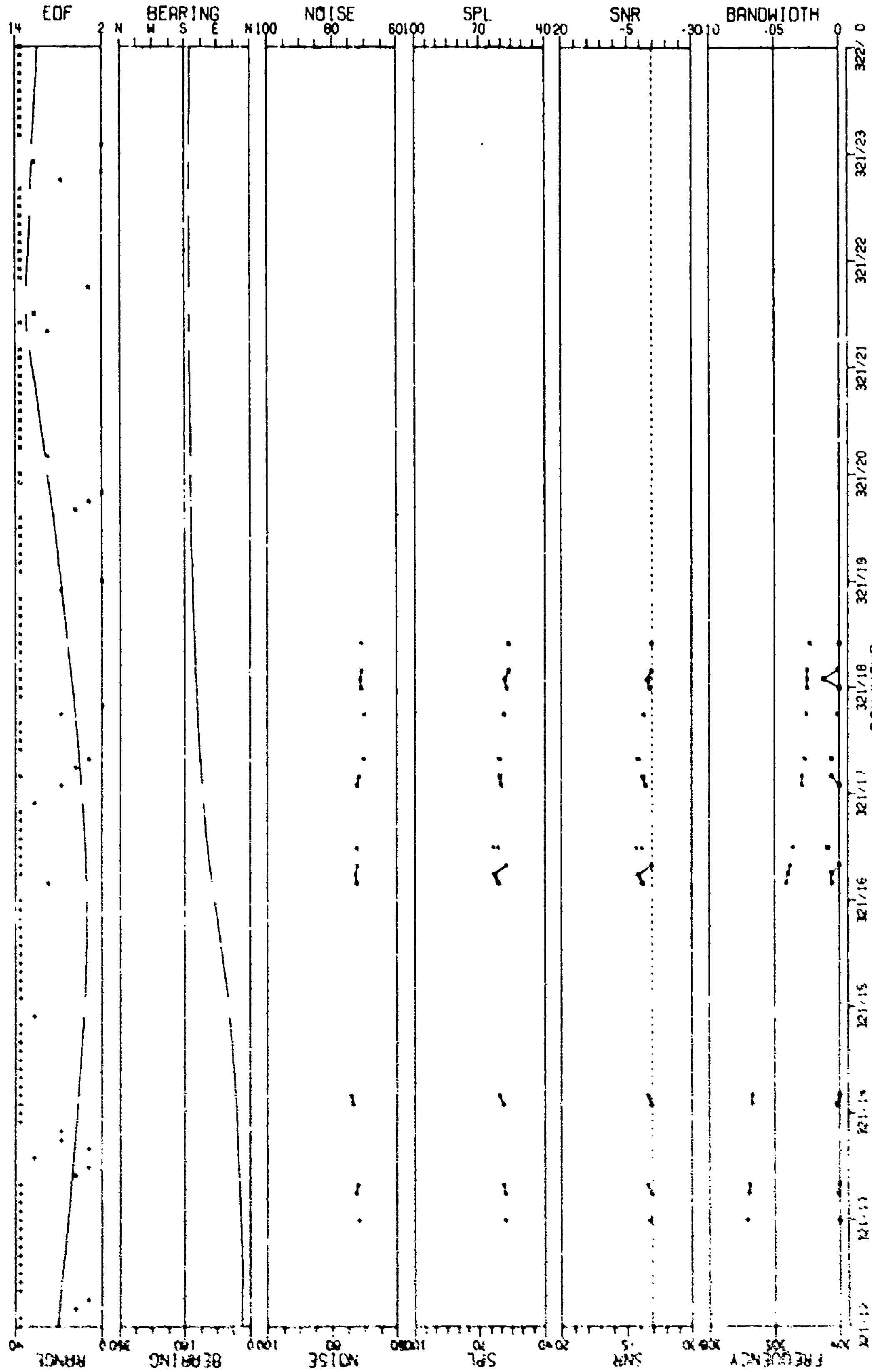

FIGURE III-34
WSS-FVT 305 HZ LINE HISTORY AS OBSERVED VIA THE OMNIDIRECTIONAL SENSOR AT SITE A1 DURING THE 17 NOV FIELD EVENT WITH VERNIER RESOLUTION (U)

AS-77-2634

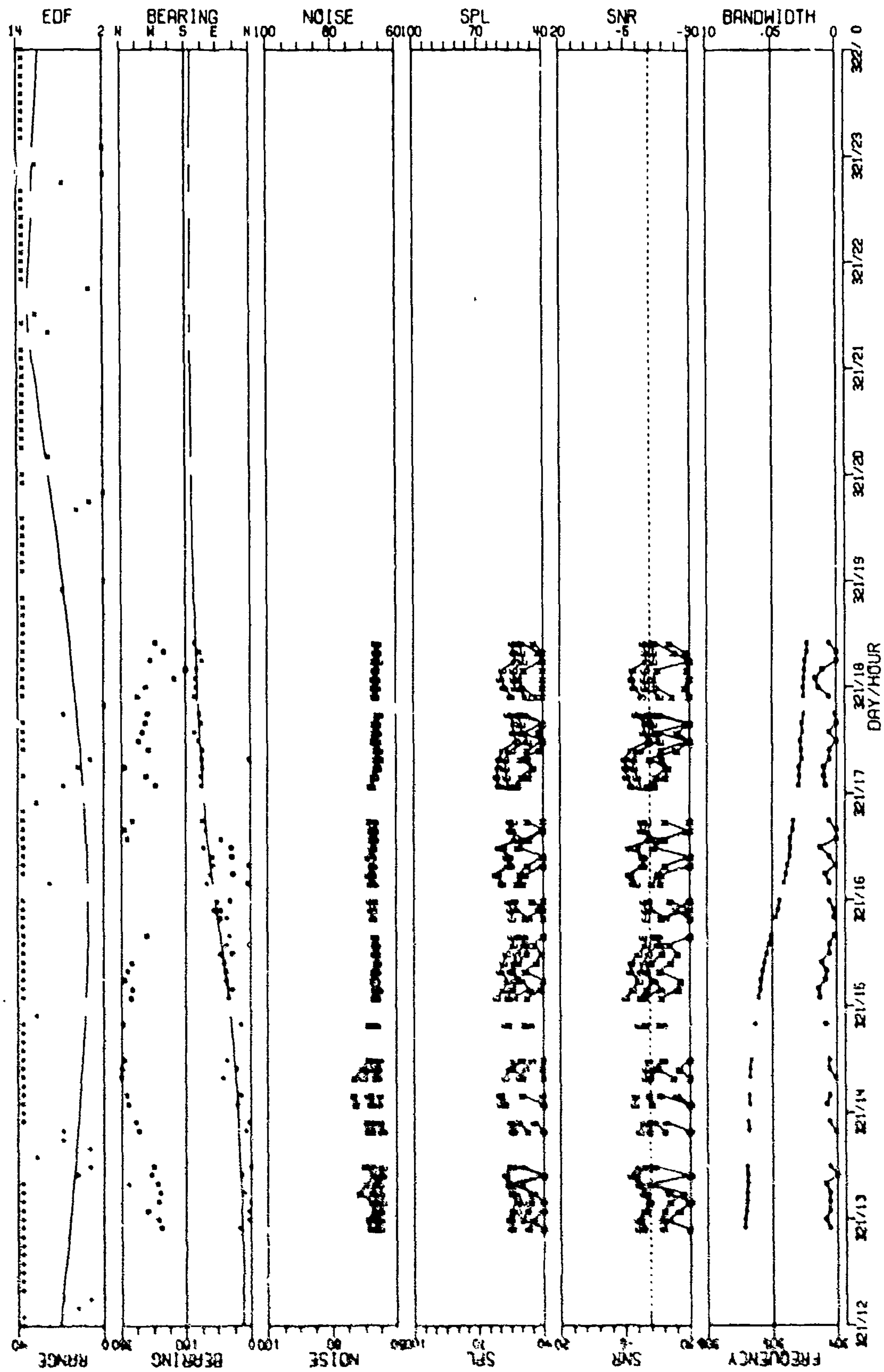

FIGURE III-35
MSS-FVT 305 HZ LINE HISTORY AS OBSERVED VIA THE SINGLE CARDIOIDS SENSOR
AT SITE A1 DURING THE 17 NOV FIELD EVENT WITH VERNIER RESOLUTION (U)

AS-77-2635

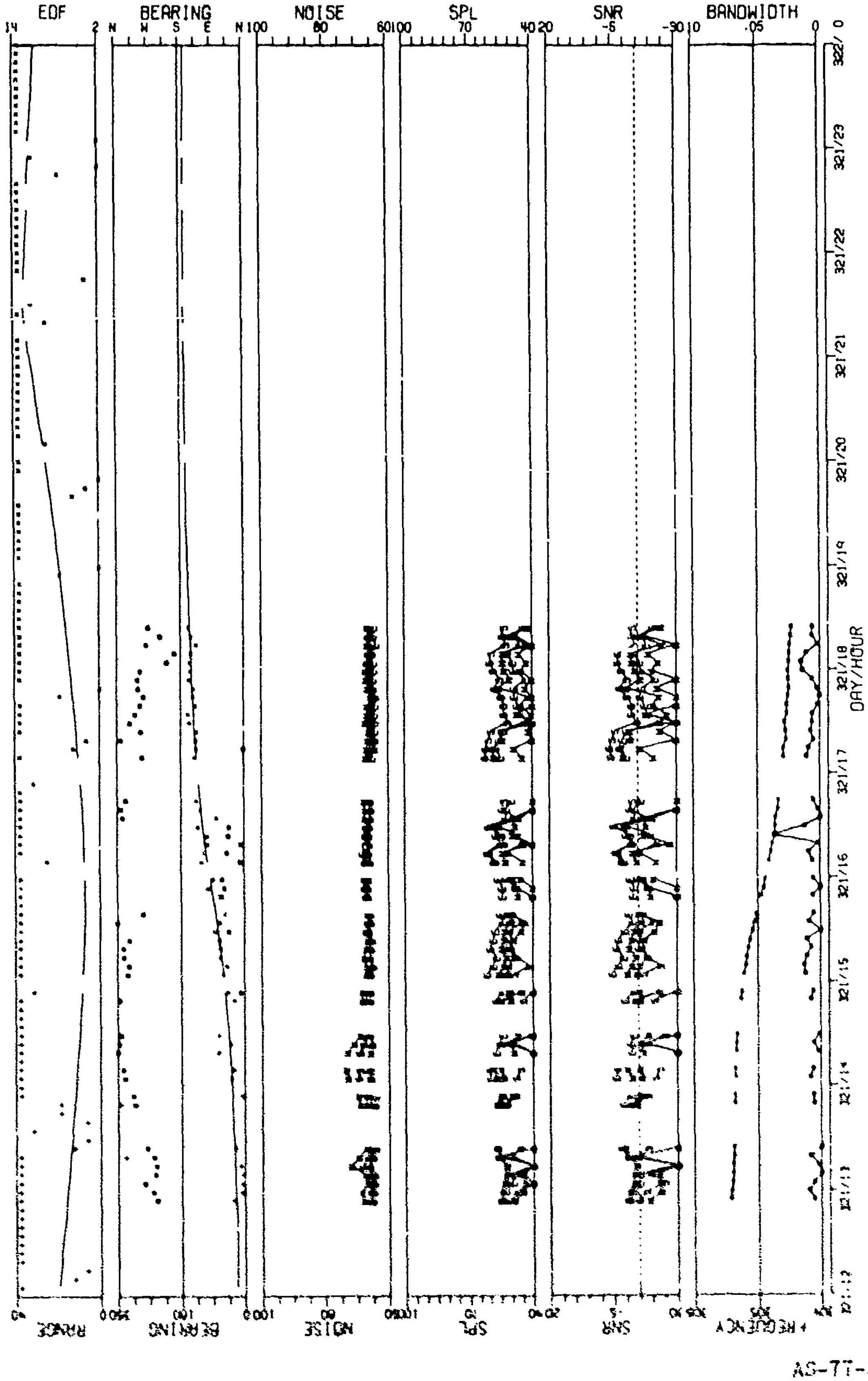

FIGURE III-36
MSS-FVT 305 HZ LINE HISTORY AS OBSERVED VIA THE MAX GAIN LIMACONS SENSOR AT SITE A1 DURING THE 17 NOV FIELD EVENT WITH VERNIER RESOLUTION (U)

AS-77-2636

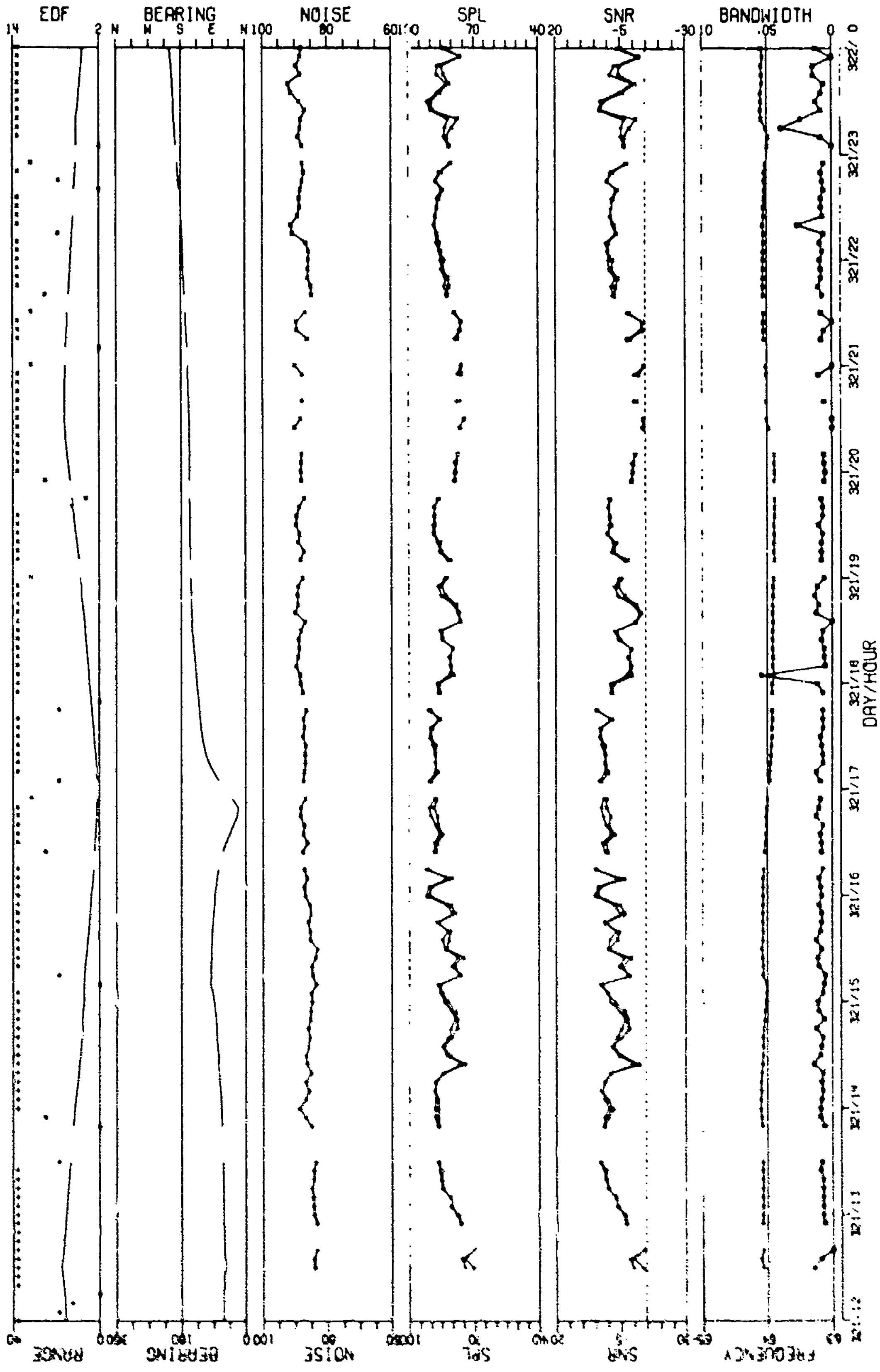

FIGURE III-37
MSS-FVT 64 HZ LINE HISTORY AS OBSERVED VIA THE OMNIDIRECTIONAL SENSOR AT SITE A1 DURING THE 17 NOV FIELD EVENT WITH VERNIER RESOLUTION (U)

AS-77-2637

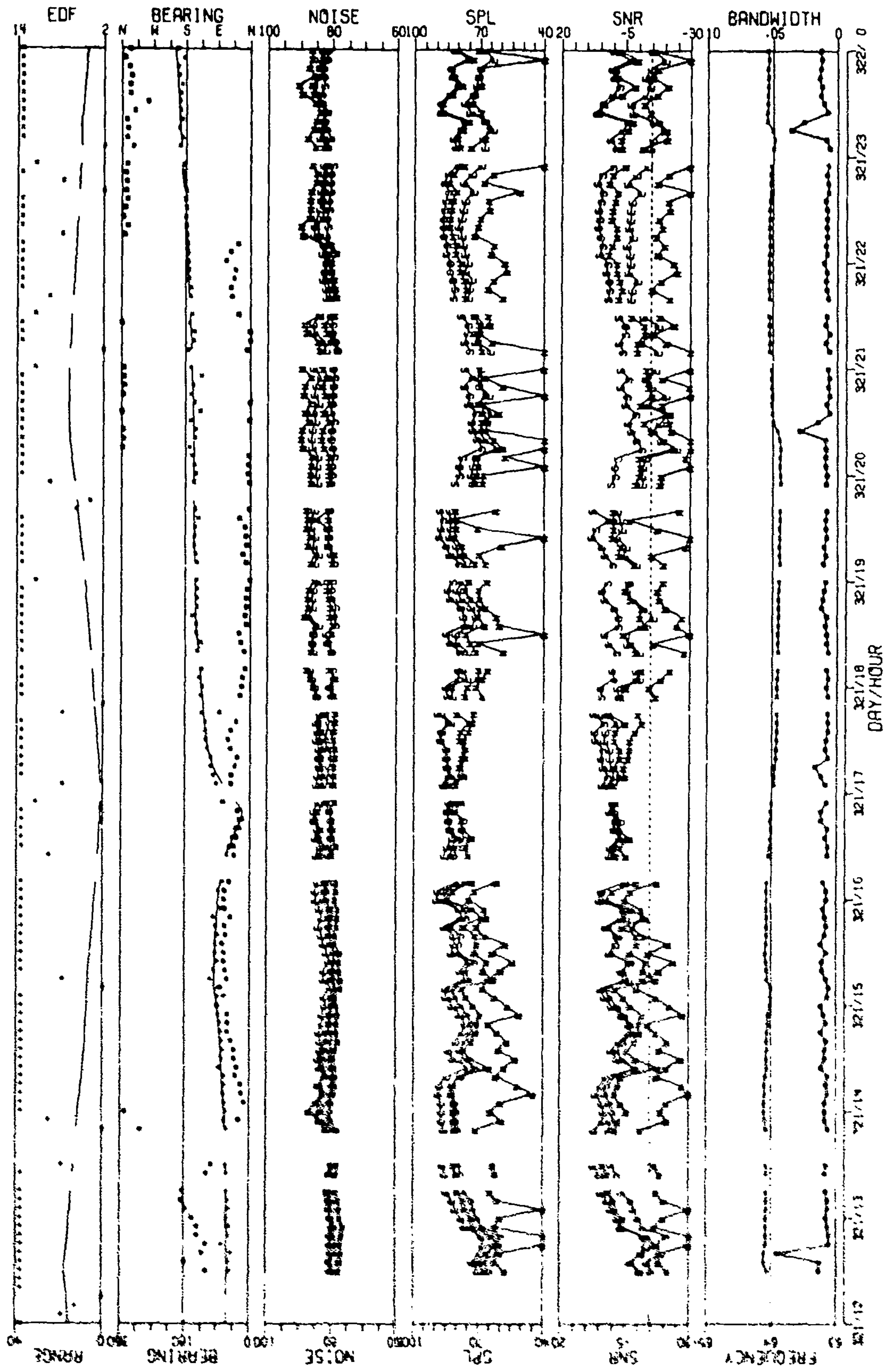

FIGURE III-38
MSS FVT 64 HZ LINE HISTORY AS OBSERVED VIA THE SINGLE CARDIOIDS SENSOR AT SITE A1 DURING THE 17 NOV FIELD EVENT WITH VERNIER RESOLUTION (U)

AS-77-2638

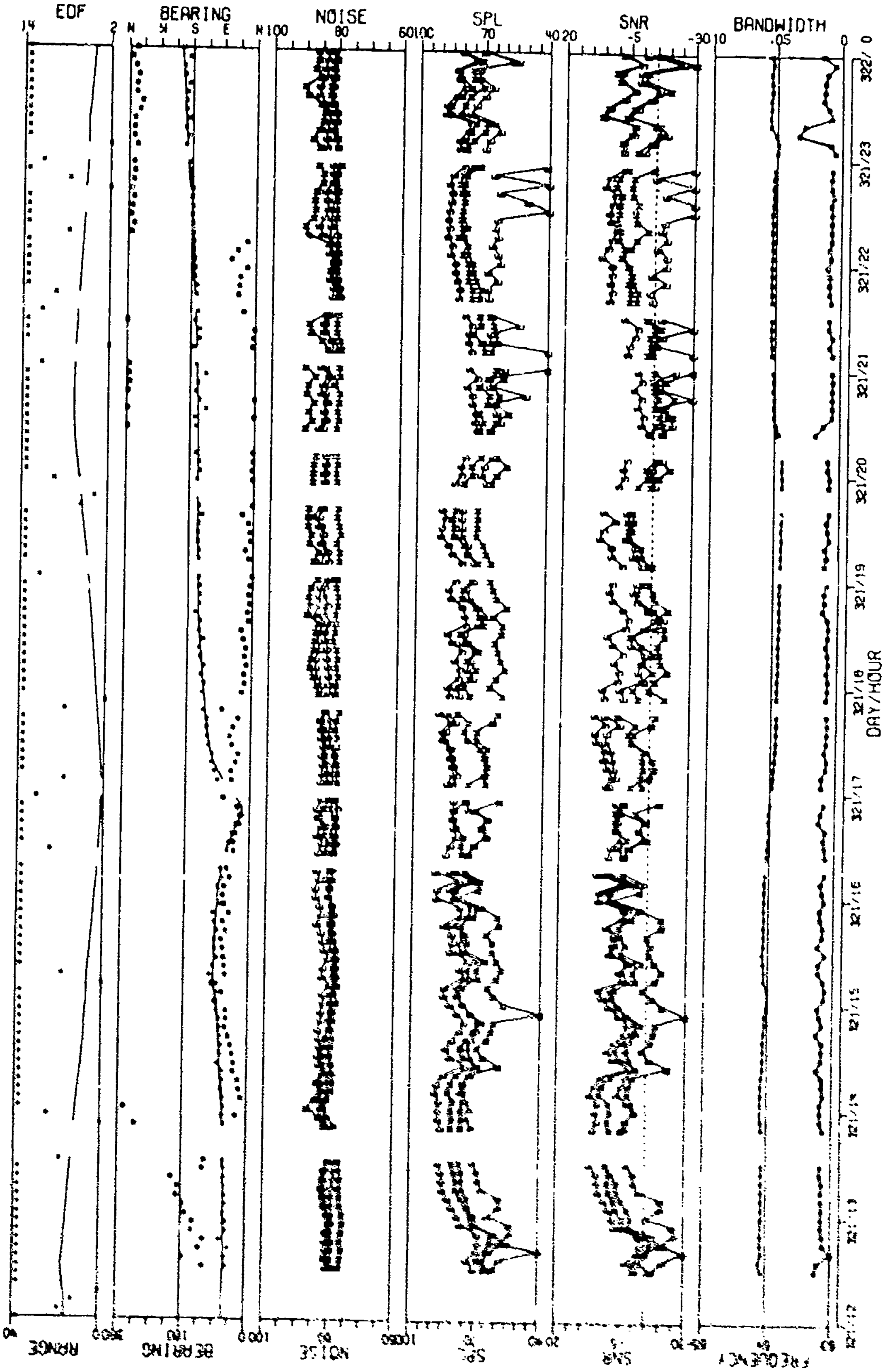

FIGURE III-39
MSS-EVT 64 HZ LINE HISTORY AS OBSERVED VIA THE MAX GAIN LIMACONS SENSOR AT SITE A1 DURING THE 17 NOV FIELD EVENT WITH VERNIER RESOLUTION (U)

AS-77-2639

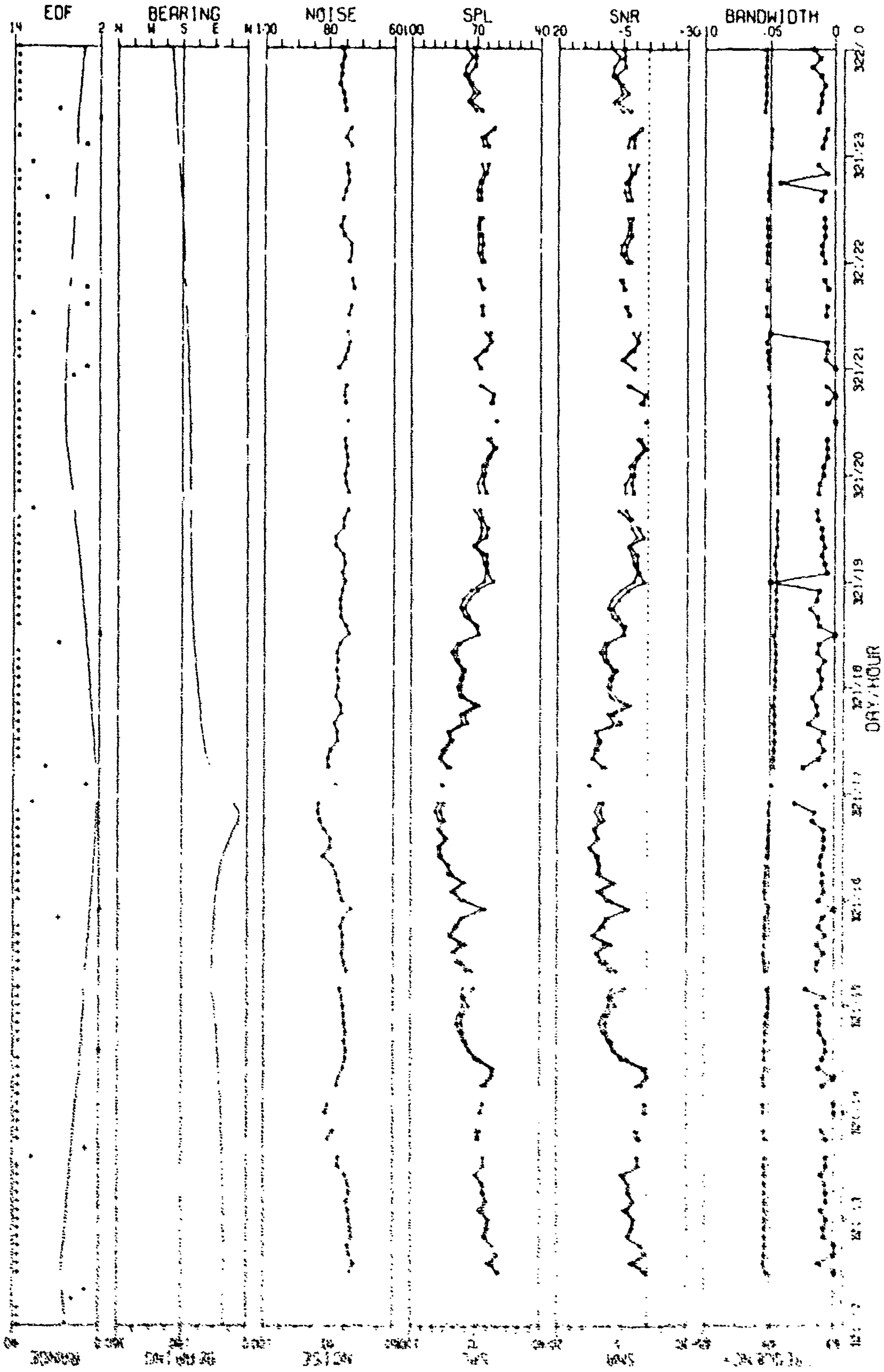

FIGURE III-40
[illegible] 50 HZ LINE HISTORY AS OBSERVED VIA THE VERTICAL DIPOLE SENSOR [illegible] DURING THE 17 NOV FIELD EVENT WITH VERNIER RESOLUTION (U)

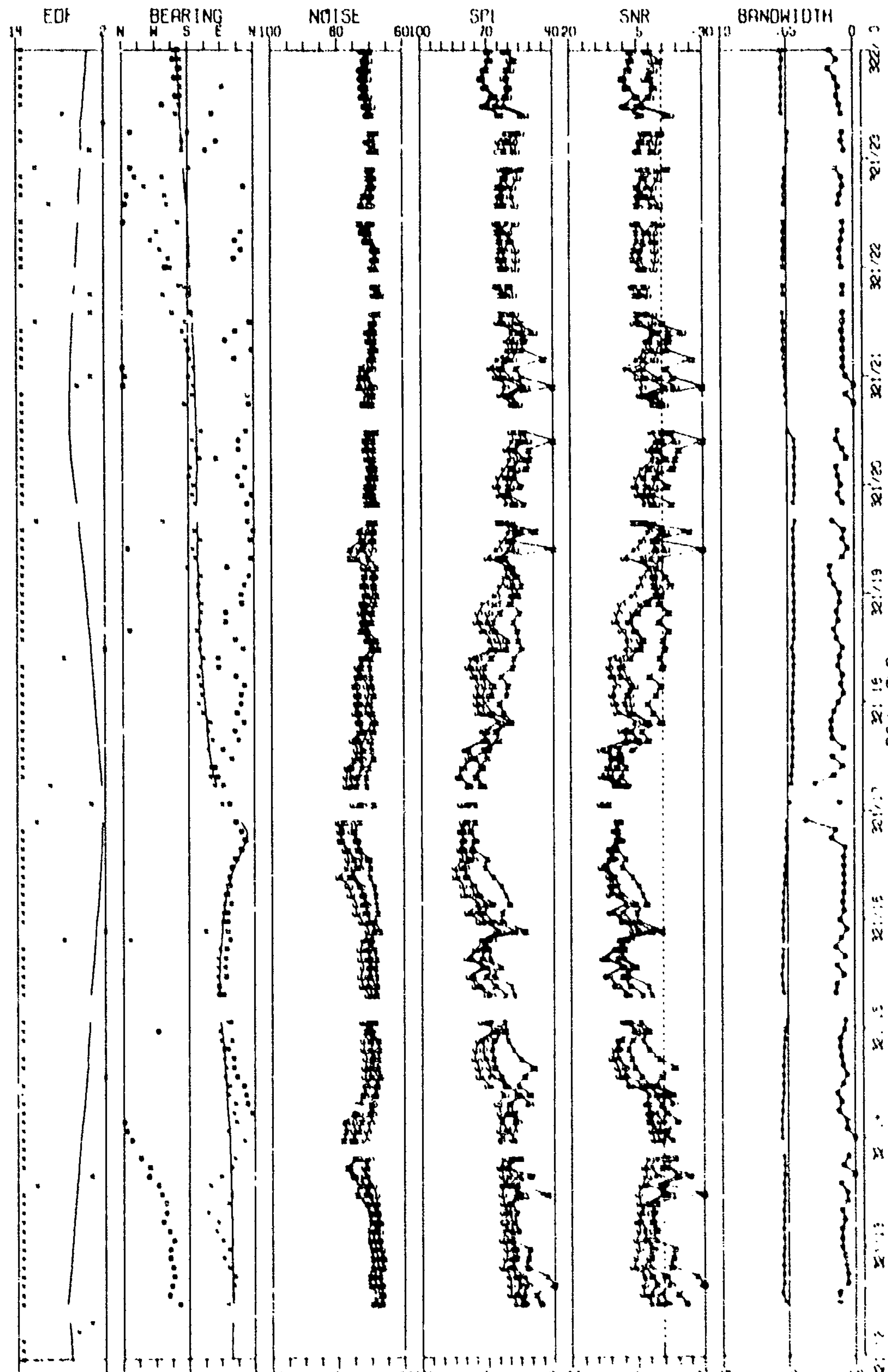

FIGURE III-41

AS-77-2641

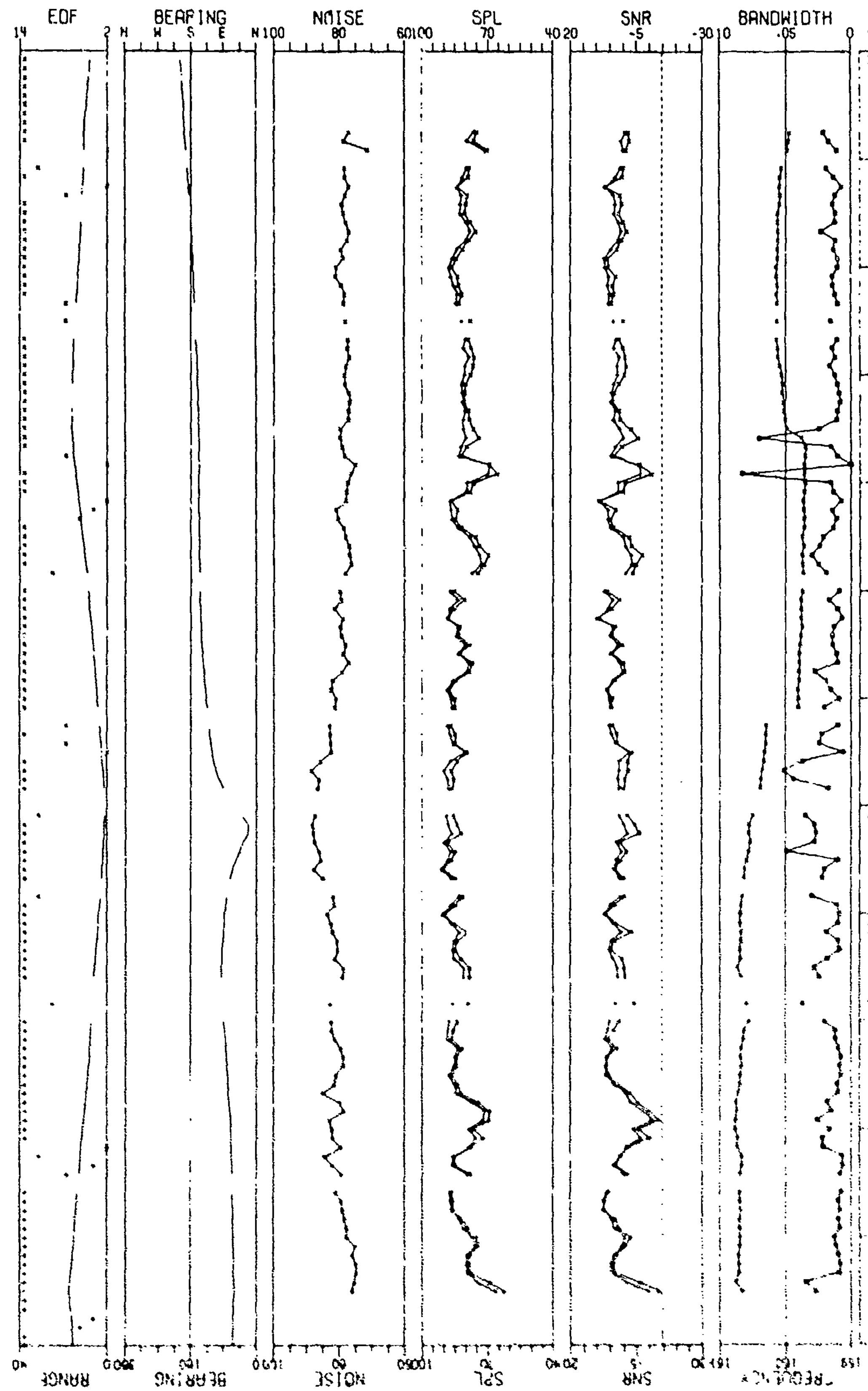

FIGURE III-42
160 HZ LINE HISTORY AS OBSERVED VIA THE OMNIDIRECTIONAL SENSOR DURING THE 17 NOV FIELD EVENT WITH VERNIER RESOLUTION (U)

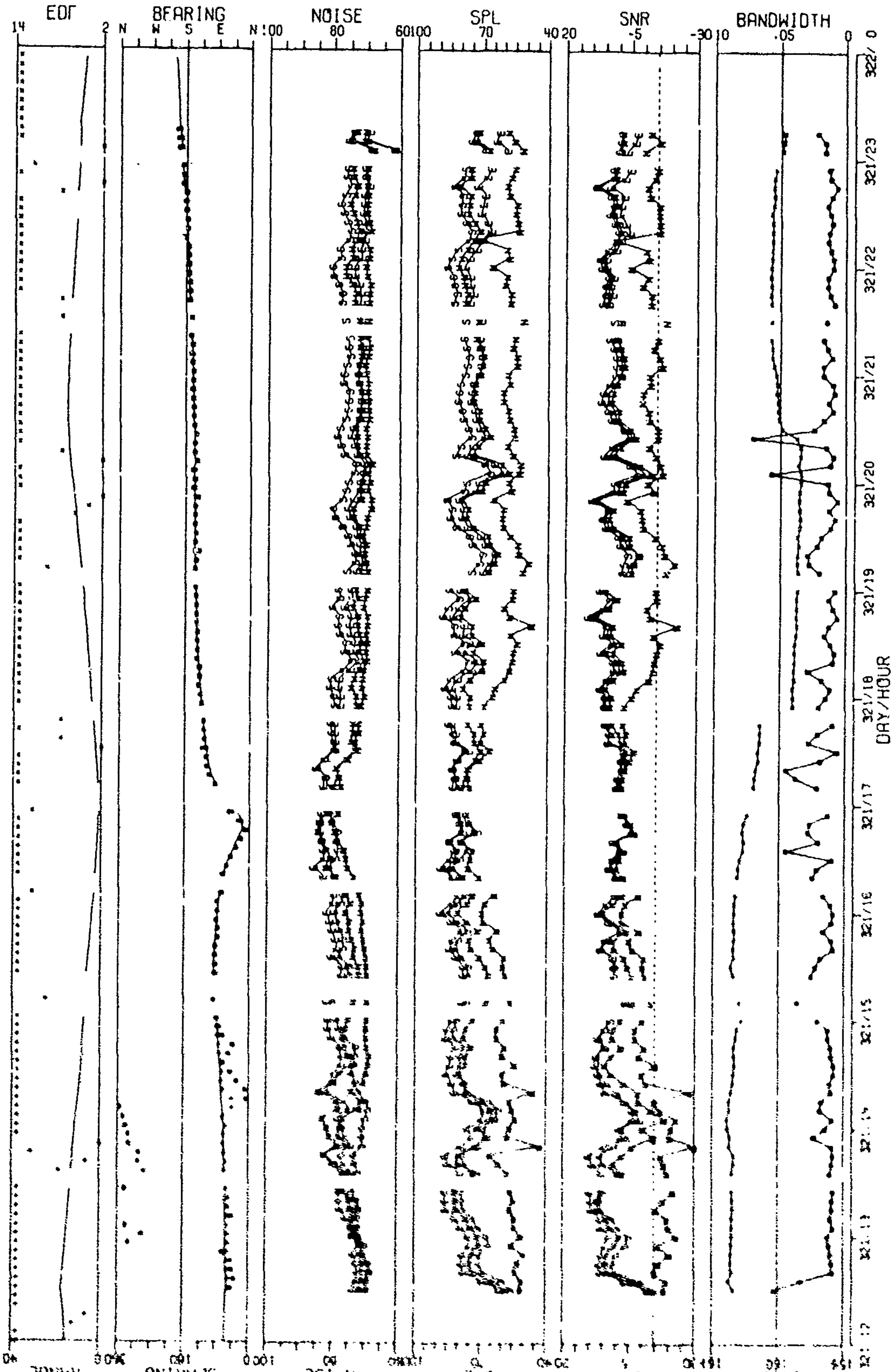

FIGURE III-43
MSS-FVT 160 HZ LINE HISTORY AS OBSERVED VIA THE SINGLE CARDIOIDS SENSOR AT SITE A1 DURING THE 17 NOV FIELD EVENT WITH VERNIER RESOLUTION (U)

AS-77-2643

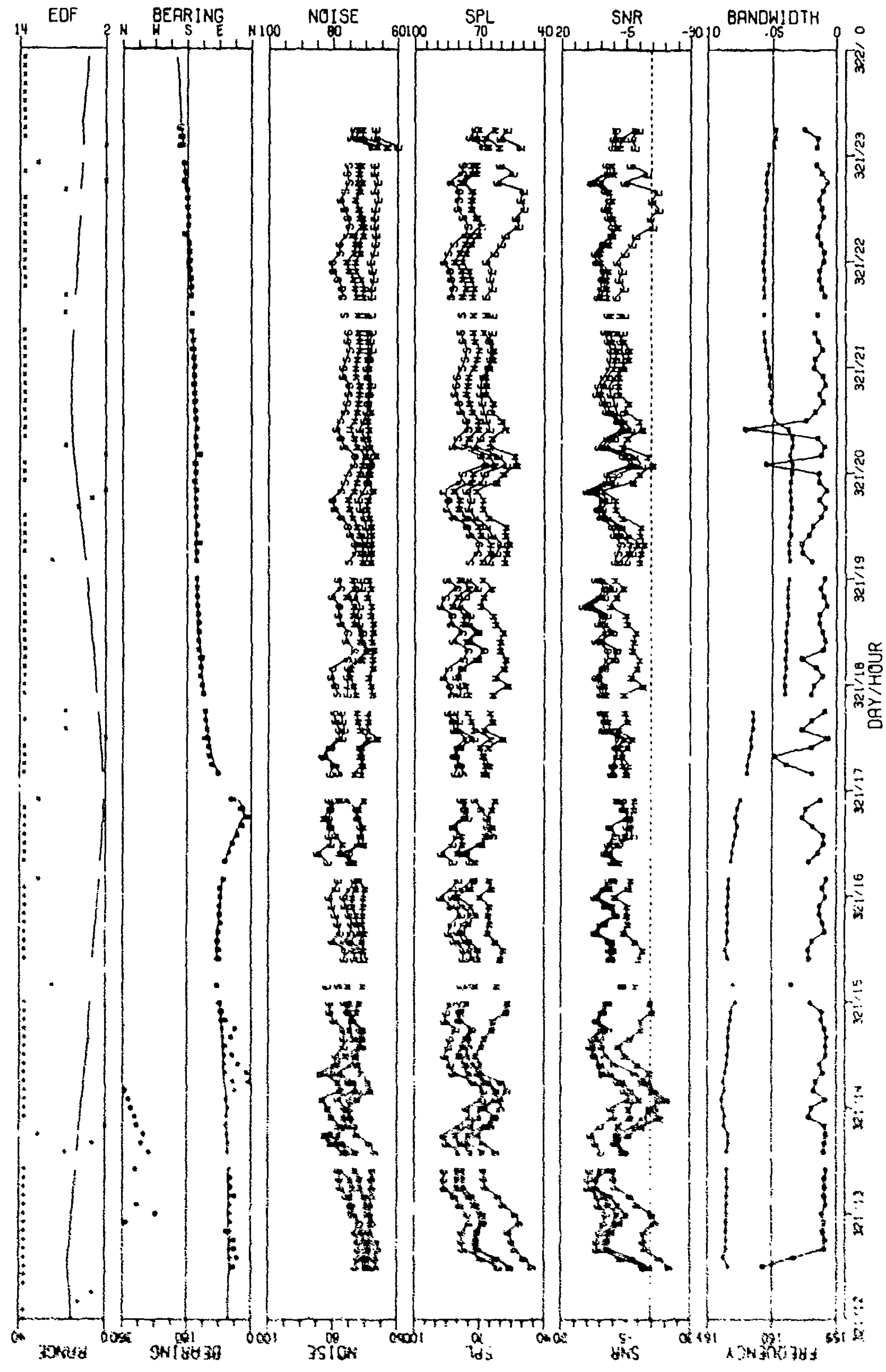

FIGURE III-44
MSS-FVT 160 HZ LINE HISTORY AS OBSERVED VIA THE MAX GAIN LIMACONS SENSOR AT SITE A1 DURING THE 17 NOV FIELD EVENT WITH VERNIER RESOLUTION (U)

AS-77-2644

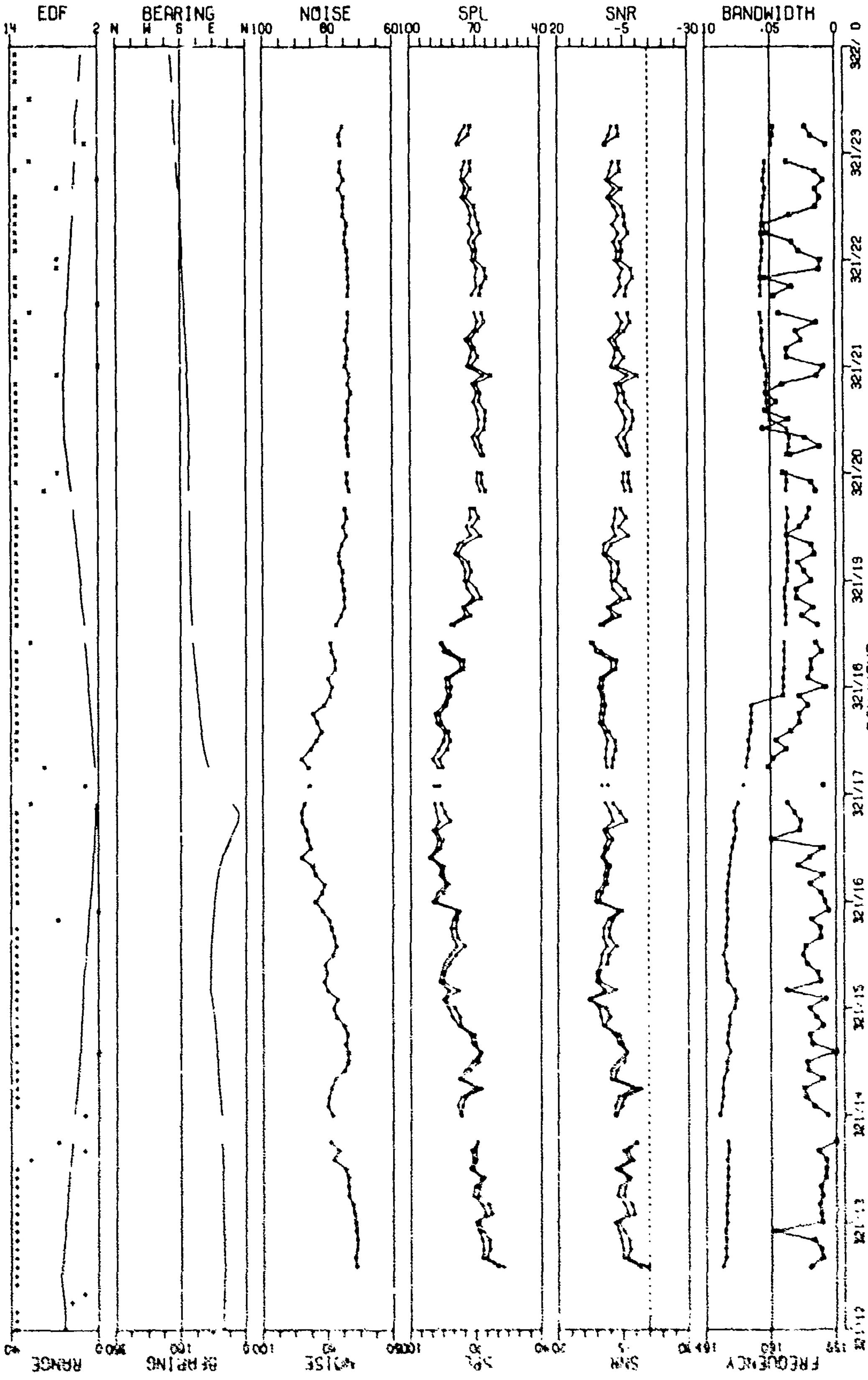

FIGURE III-45
MSS-FVT 160 HZ LINE HISTORY AS OBSERVED VIA THE VERTICAL DIPOLE SENSOR
AT SITE A1 DURING THE 17 NOV FIELD EVENT WITH VERNIER RESOLUTION (U)

AS-77-2645

FIGURE III-46
MSS EVT 150 HZ LINE HISTORY AS OBSERVED VIA THE DIFFERENCED CARDIOIDS SENSOR AT SITE A1 DURING THE 17 NOV FIELD EVENT WITH VERNIER RESOLUTION (U)

AG-77-2646

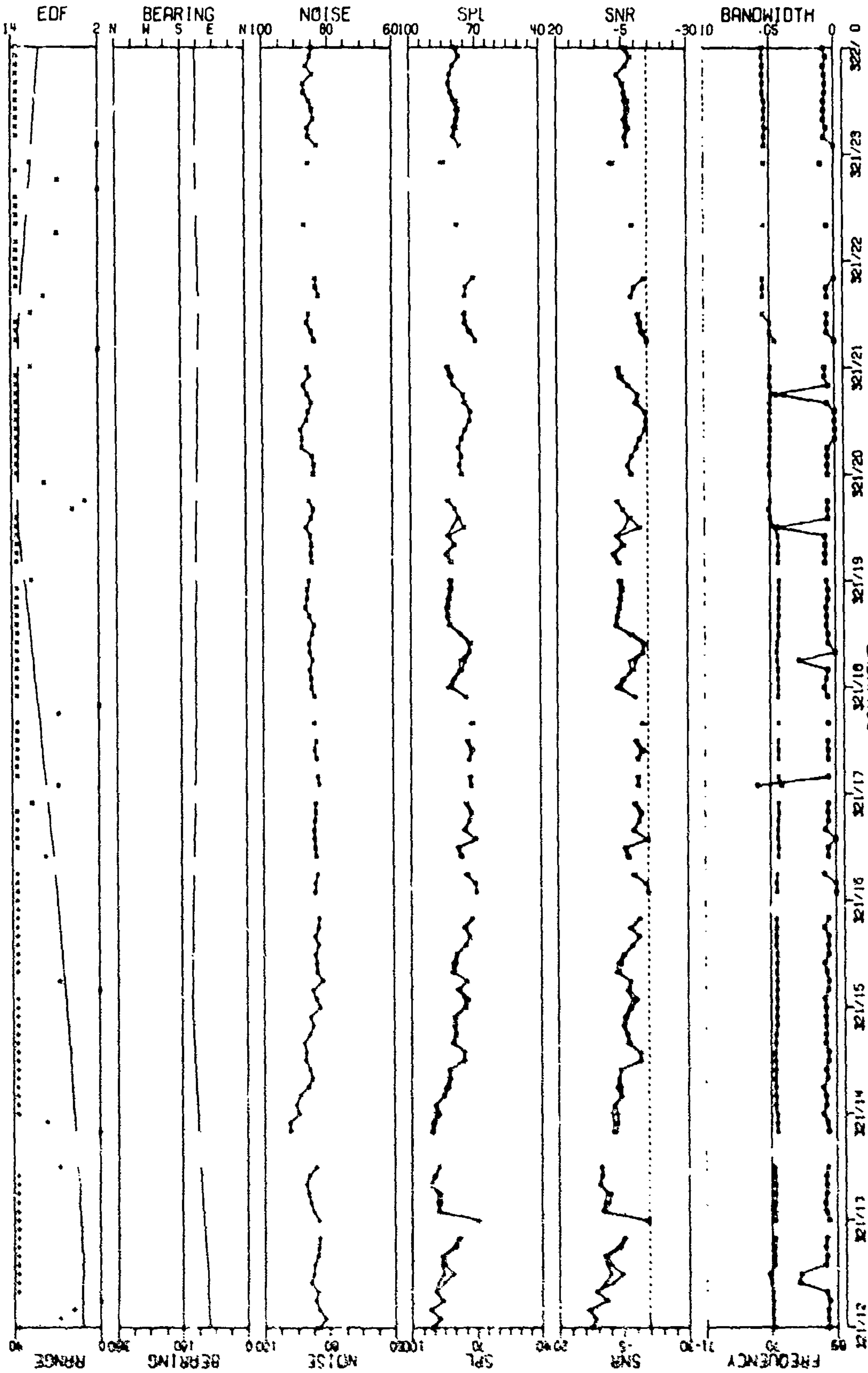

FIGURE III-47
MSS-FVT 70 HZ LINE HISTORY AS OBSERVED VIA THE OMNIDIRECTIONAL SENSOR AT SITE A1 DURING THE 17 NOV FIELD EVENT WITH VERNIER RESOLUTION (U)

AS-77-2647

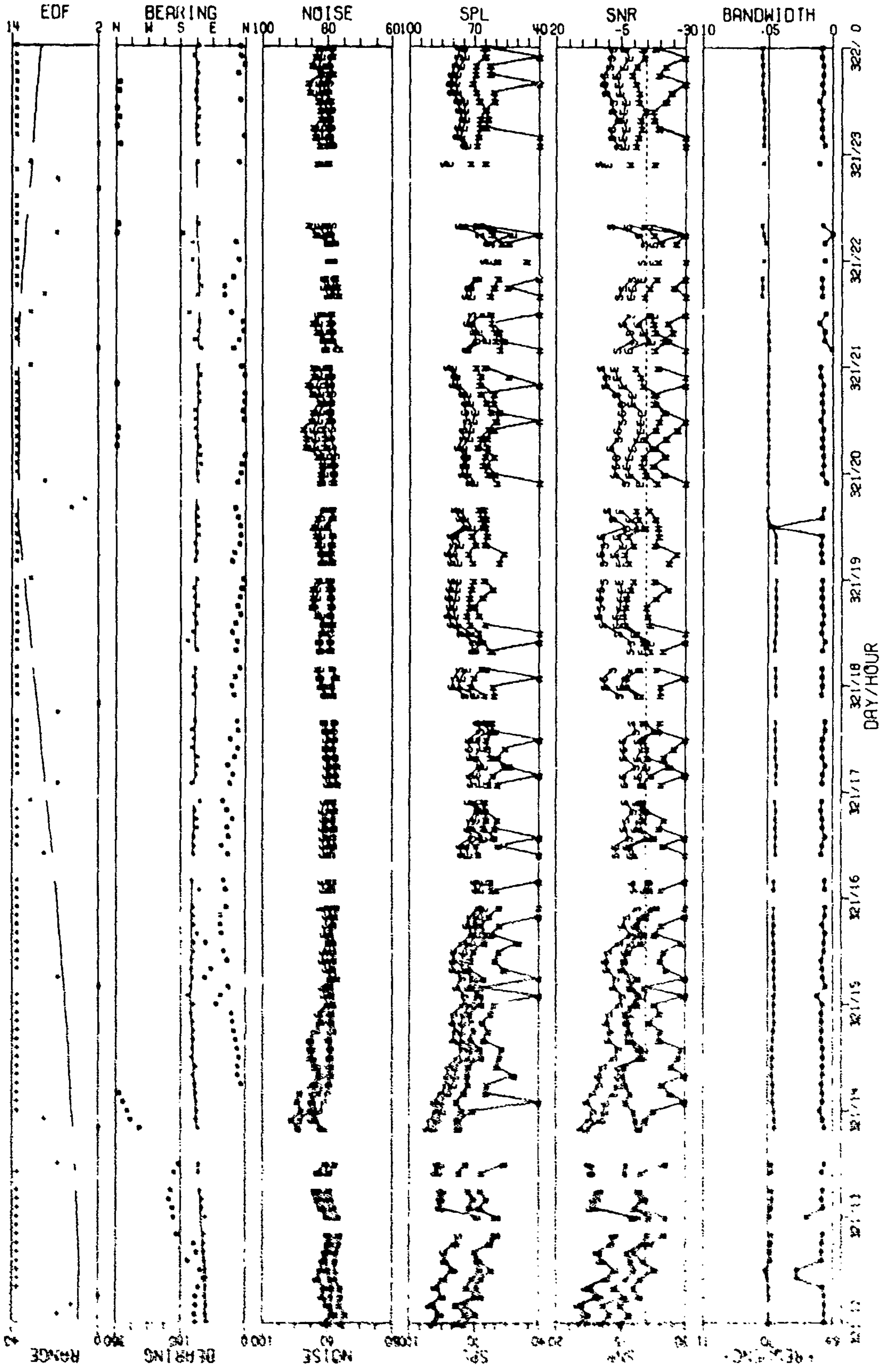

FIGURE III-48
MSS-FY? 70 HZ LINE HISTORY AS OBSERVED VIA THE SINGLE CARDIOIDS SENSOR AT SITE A, DURING THE 17 NOV FIELD EVENT WITH VERNIER RESOLUTION (U)

AS-77-2646

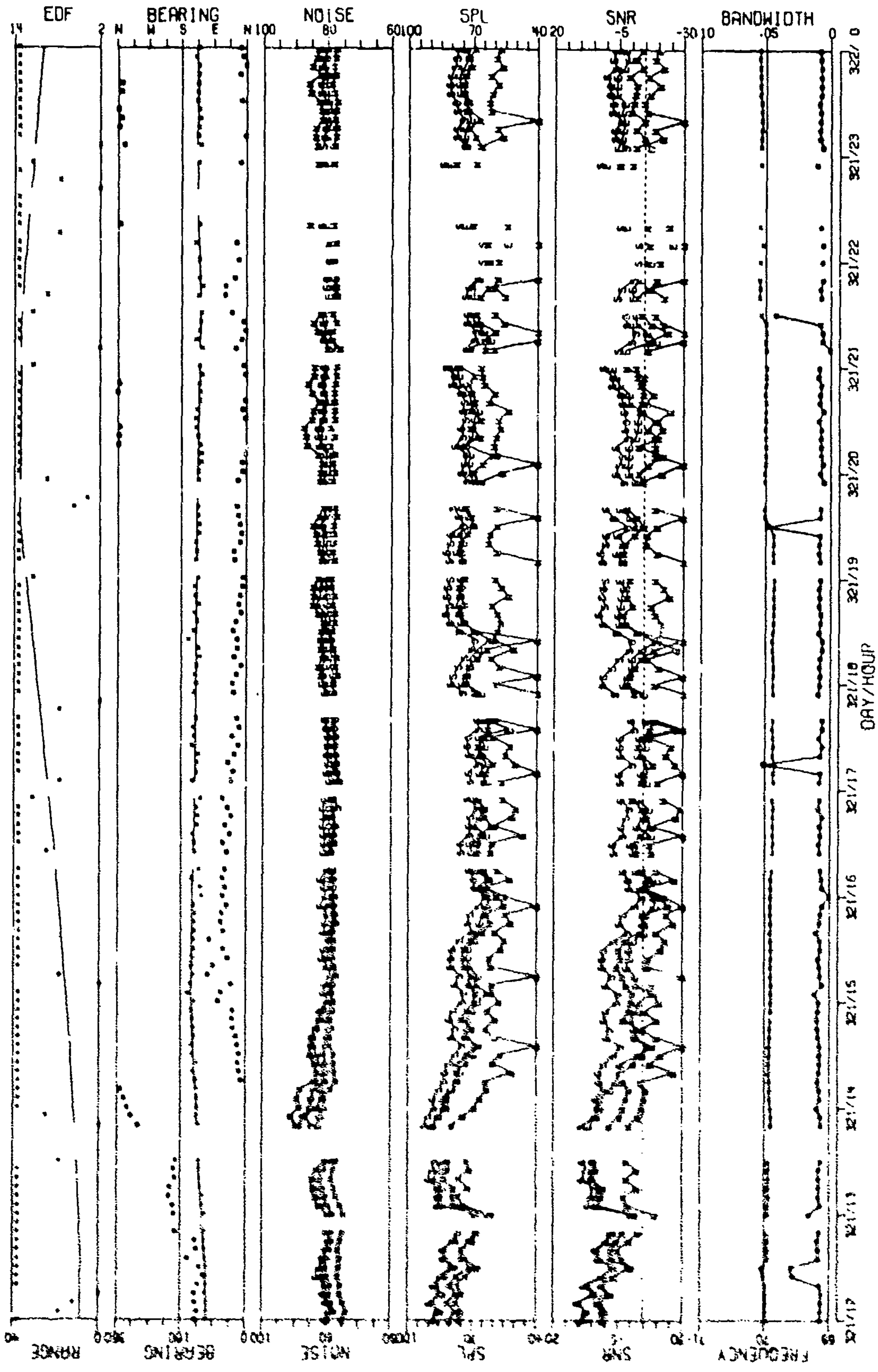

FIGURE III-49
MSS-FVI 70 HZ LINE HISTORY AS OBSERVED VIA THE MAX GAIN LIMACONS SENSOR
AT SITE A1 DURING THE 17 NOV FIELD EVENT WITH VERNIER RESOLUTION (U)

AS-77-2649

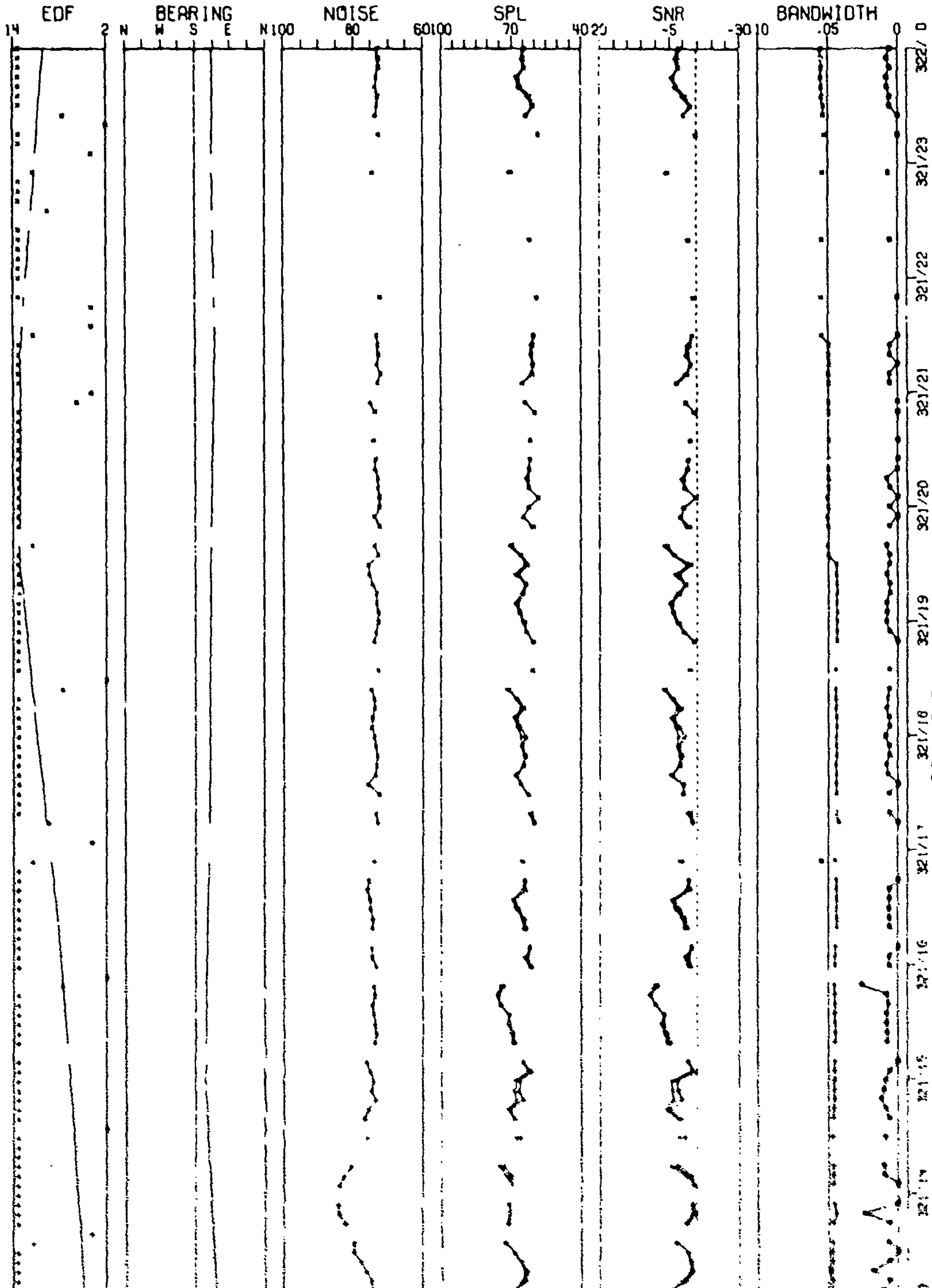

FIGURE III-50
MCS-FVI 70 HZ LINE HISTORY AS OBSERVED VIA THE VERTICAL DIPOLE SENSOR AT SITE A! DURING THE 17 NOV FIELD EVENT WITH VERNIER RESOLUTION (U)

AS-77-2650

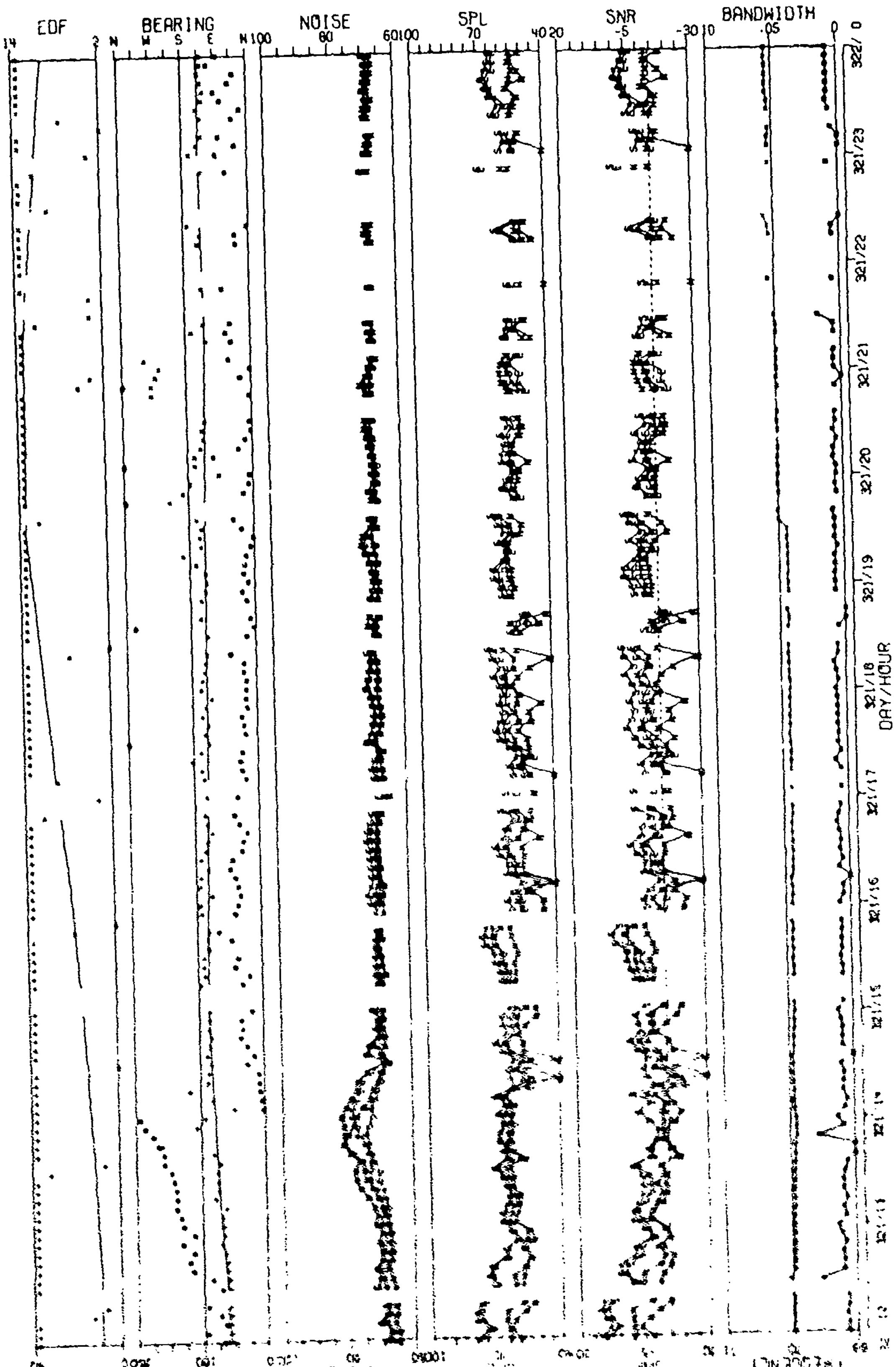

FIGURE III-51
MOB-EVT 70 HZ LINE HISTORY AS OBSERVED VIA THE DIFFERENCED CARDIOIDS SENSOR AT SITE A1 DURING THE 17 NOV FIELD EVENT WITH VERNIER RESOLUTION (U)

AS-77-2651

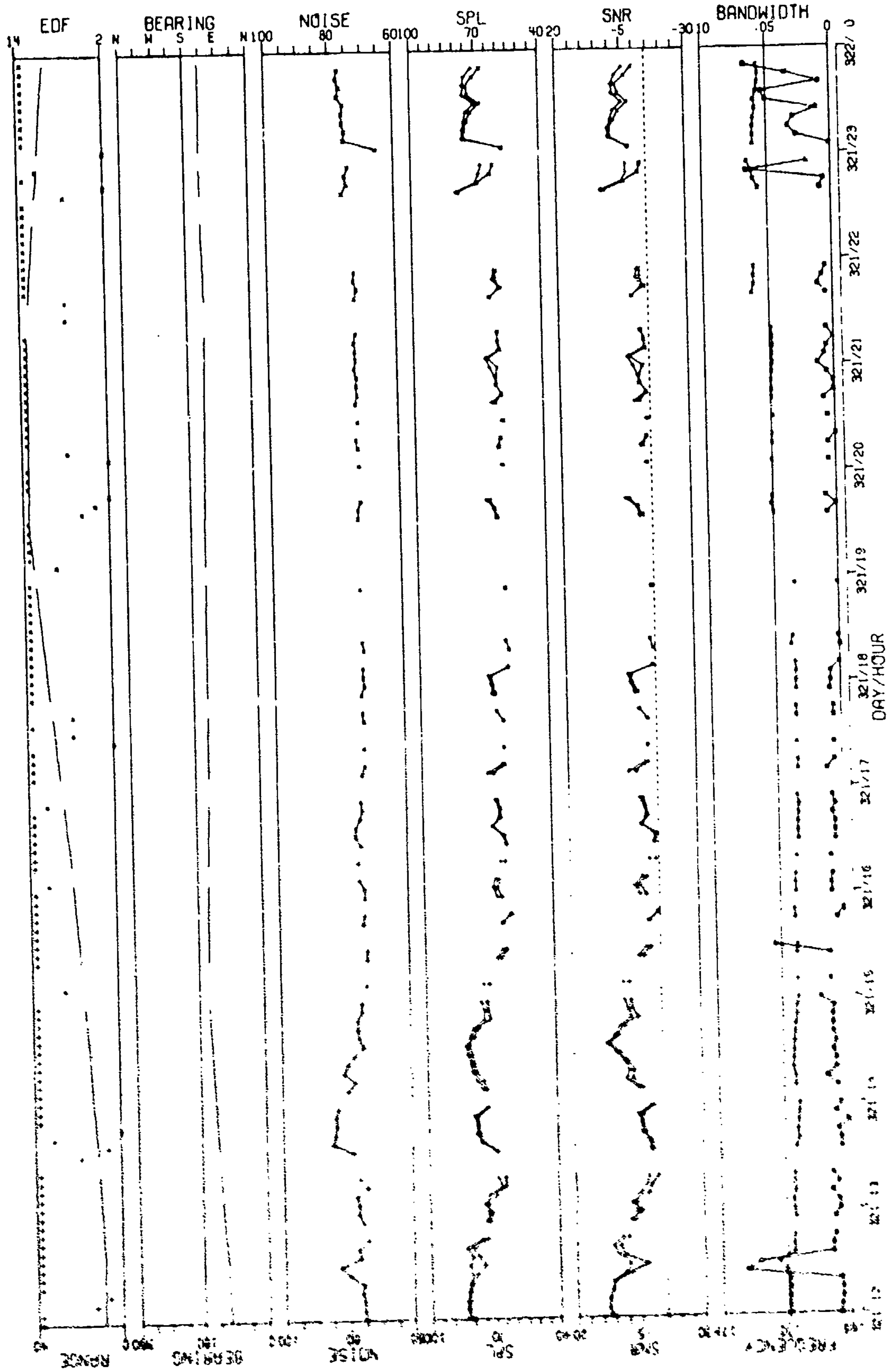

FIGURE III-52
MCS FVT 170 HZ LINE HISTORY AS OBSERVED VIA THE OMNIDIRECTIONAL SENSOR AT SITE A1 DURING THE 17 NOV FIELD EVENT WITH VERNIER RESOLUTION (U)

AG-77-2652

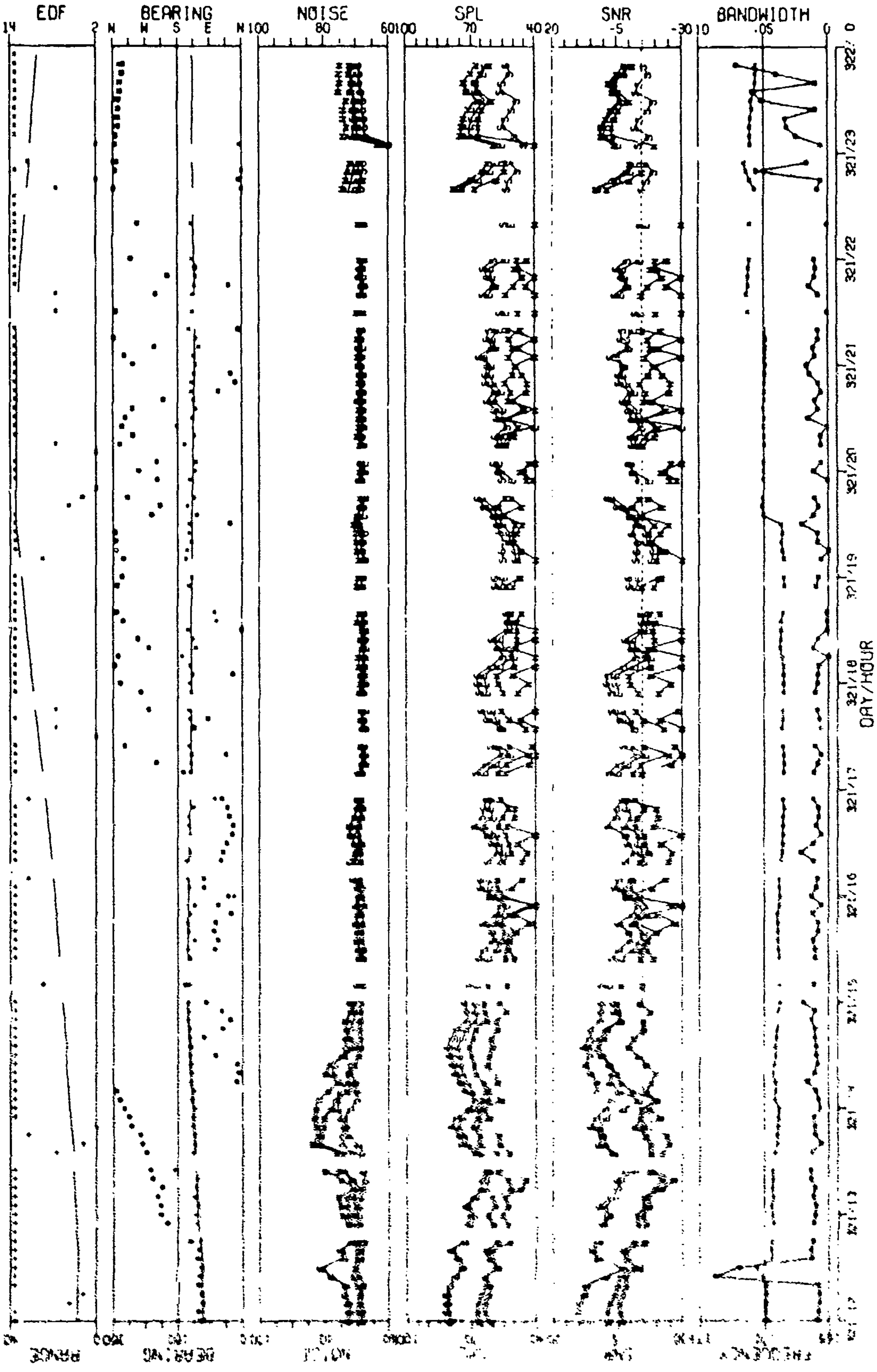

FIGURE III-53
MSS-FIX 170 HZ LINE HISTORY AS OBSERVED VIA THE SINGLE CARDIOIDS SENSOR
AT SITE R1 DURING THE 17 NOV FIELD EVENT WITH VERNIER RESOLUTION (U)

AG-77-2653

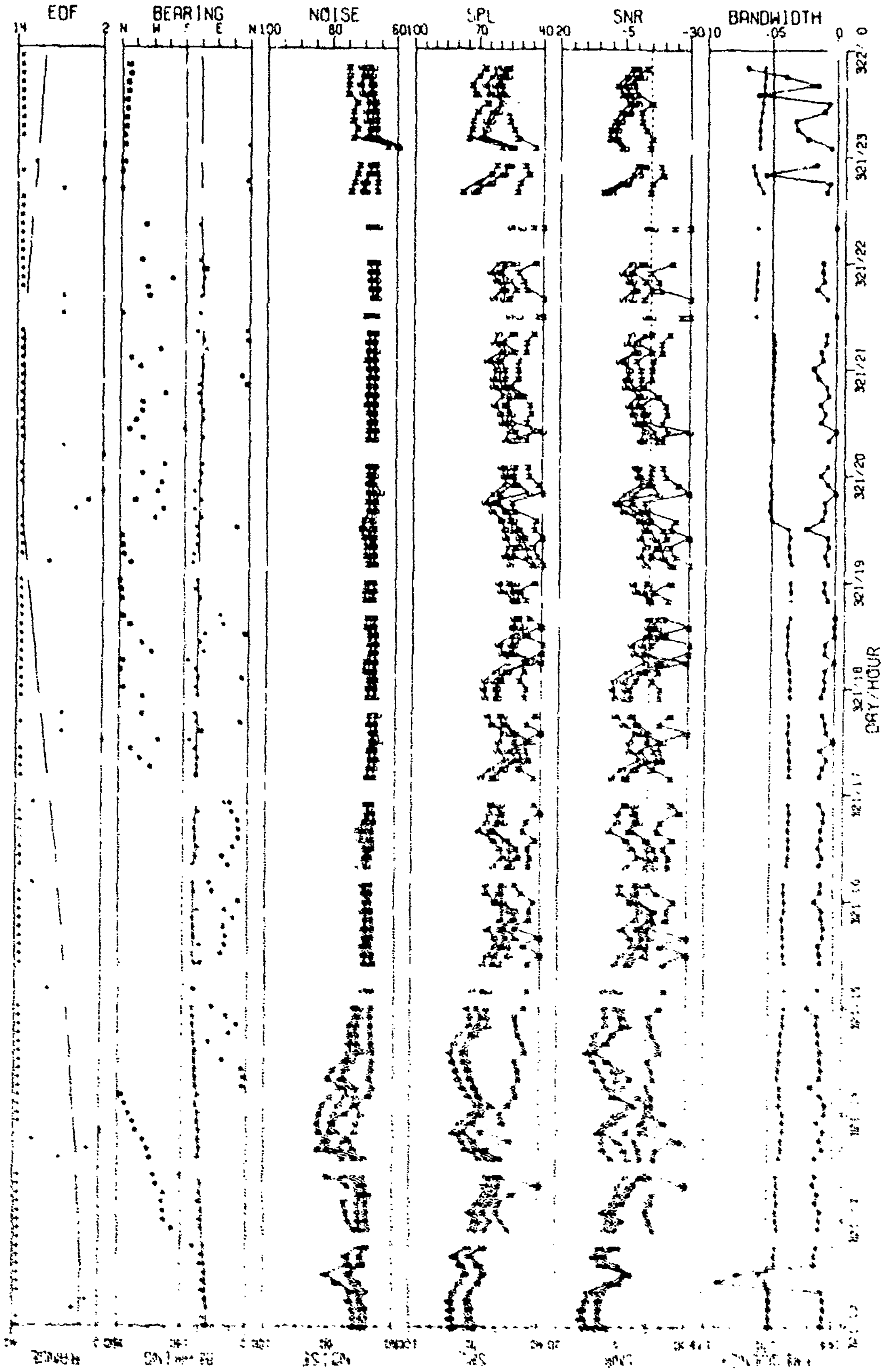

FIGURE III-54
[illegible] LINE HISTORY AS OBSERVED VIA THE MAX GAIN LIMACONS SENSOR
[illegible] DURING THE 17 NOV. FIELD EVENT WITH VERNIER RESOLUTION (U)

FIGURE III-55
MSS-F/T 170 HZ LINE HISTORY AS OBSERVED VIA THE VERTICAL DIPOLE SENSOR AT SITE A1 DURING THE 17 NOV FIELD EVENT WITH VERNIER RESOLUTION (U)

AS-77-2655

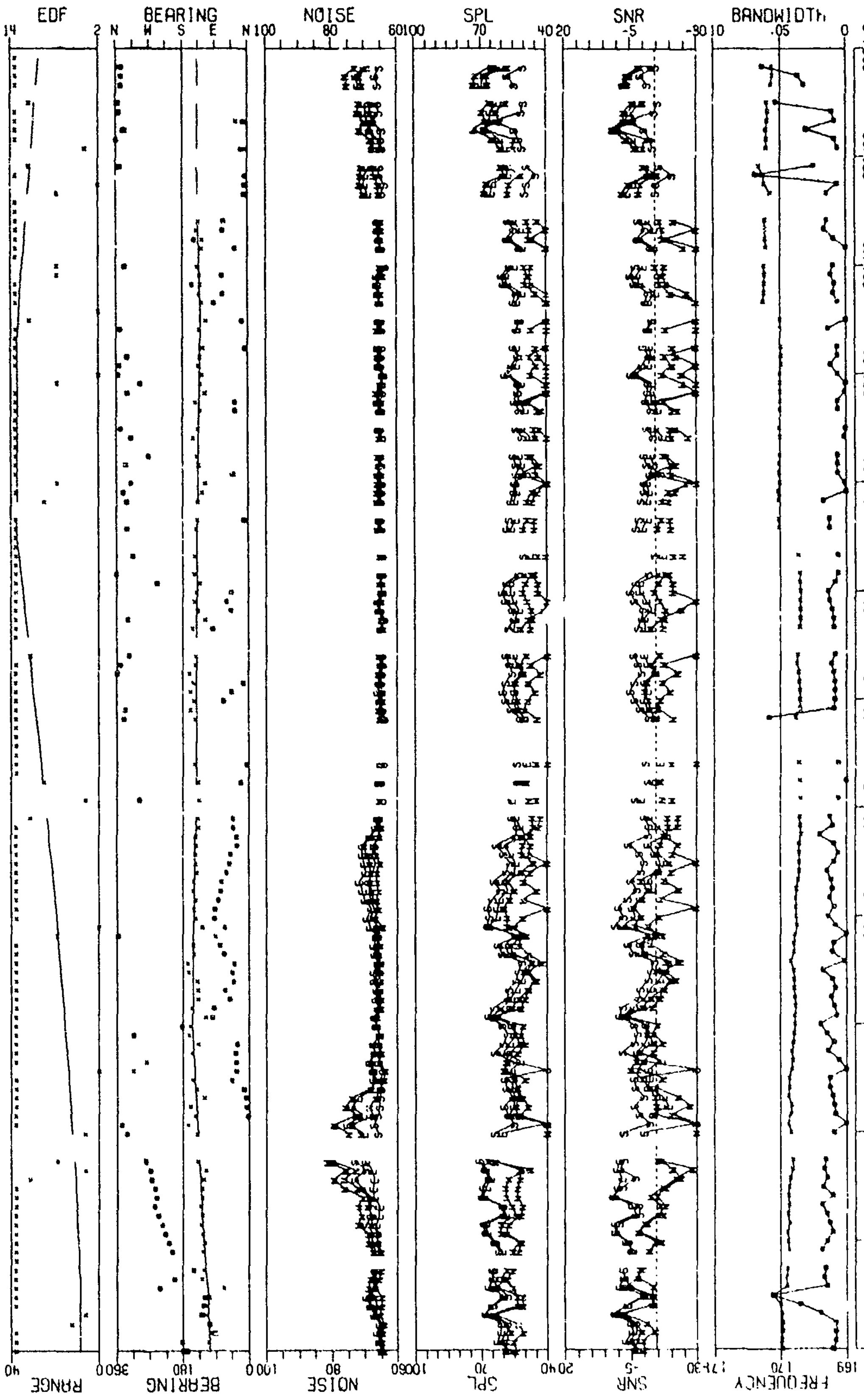

FIGURE III-56
MSS-FVT 170 HZ LINE HISTORY AS OBSERVED VIA THE DIFFERENCED CARDIOIDS SENSOR AT SITE A1 DURING THE 17 NOV FIELD EVENT WITH VERNIER RESOLUTION (U)

AS-77-2656

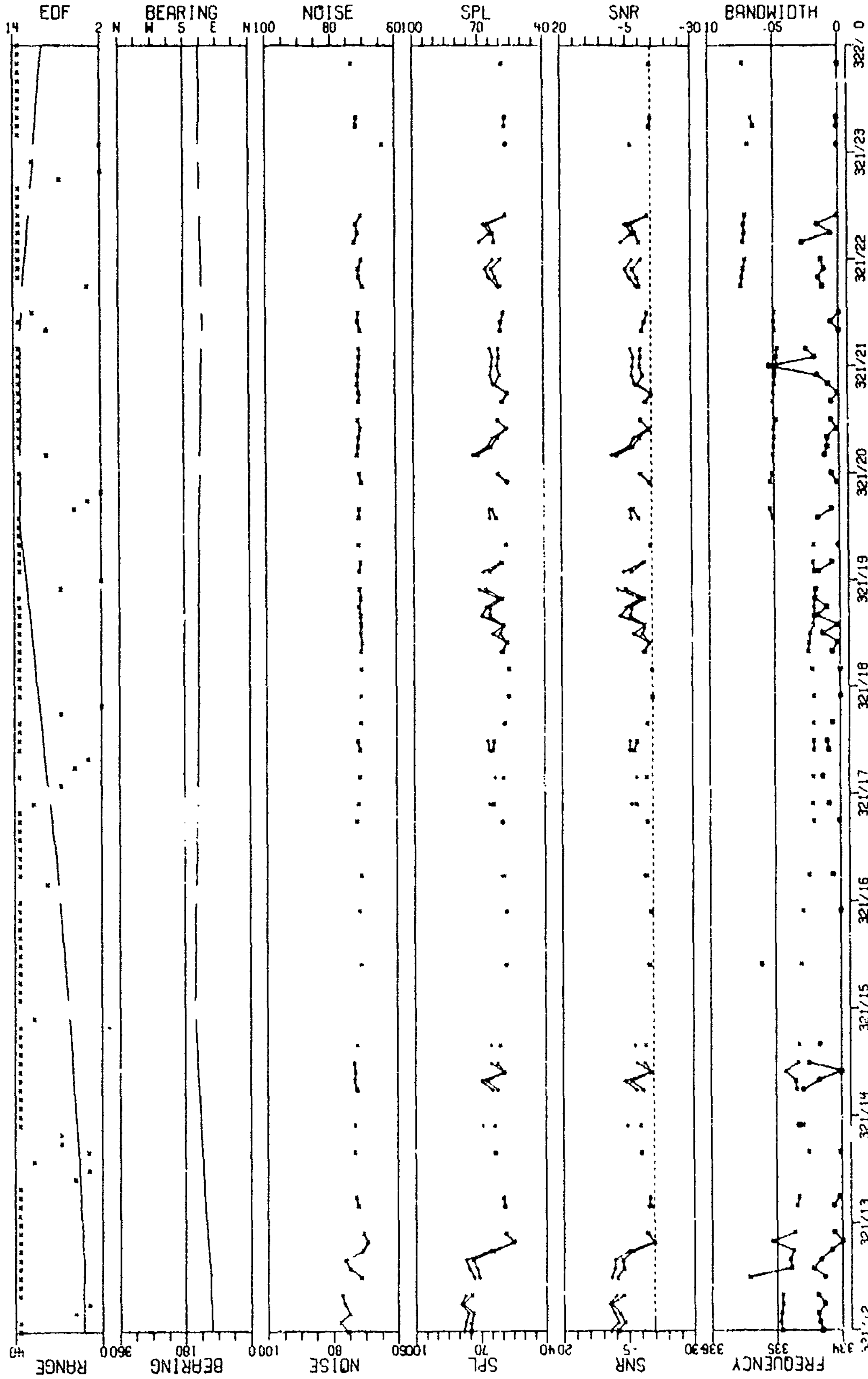

FIGURE III-57
MSS-FVT 335 HZ LINE HISTORY AS OBSERVED VIA THE OMNIDIRECTIONAL SENSOR
AT SITE A1 DURING THE 17 NOV FIELD EVENT WITH VERNIER RESOLUTION (U)

AS-77-2657

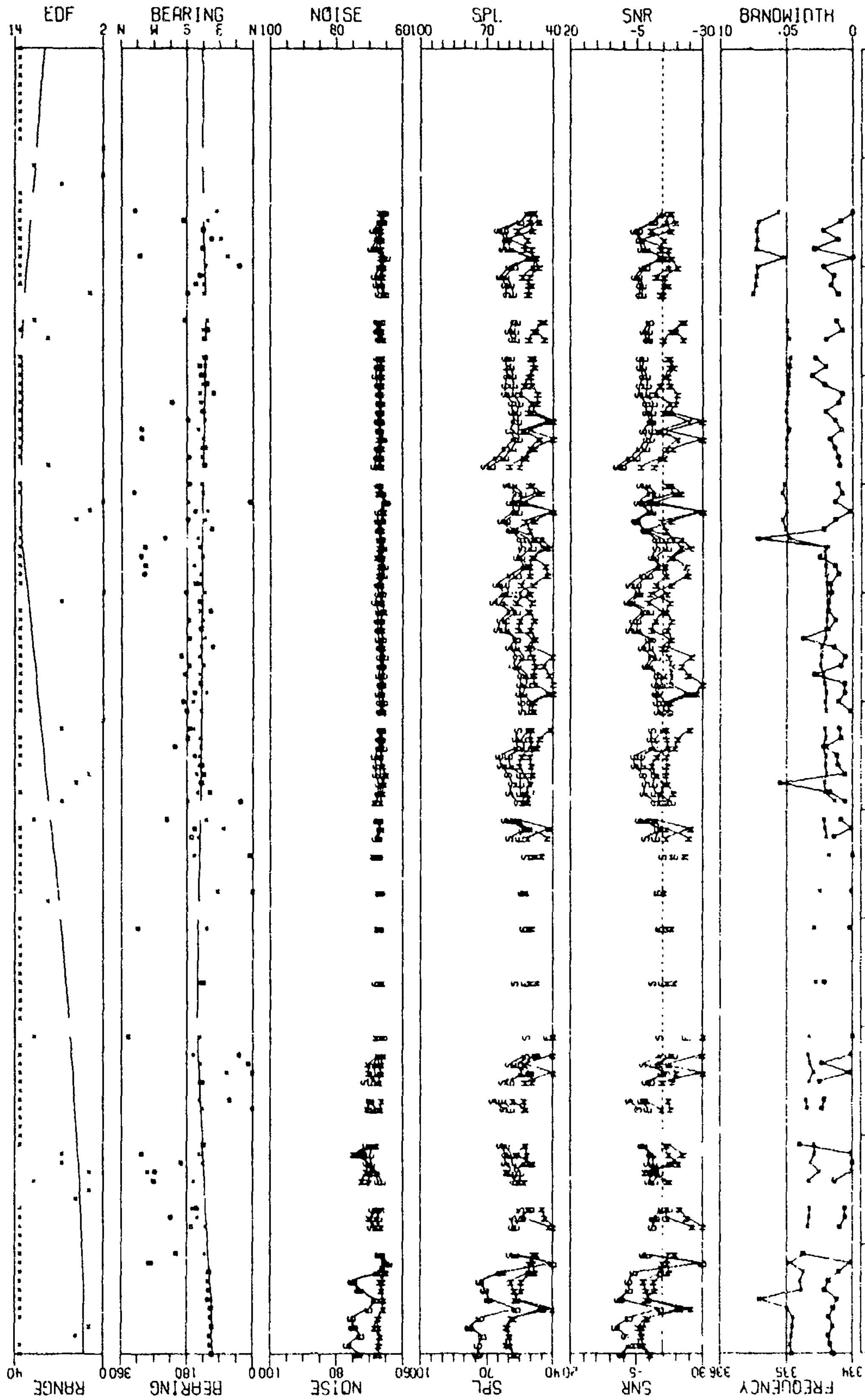

FIGURE III-58
MSS-FVT 335 HZ LINE HISTORY AS OBSERVED VIA THE SINGLE CARDIOIDS SENSOR AT SITE A: DURING THE 17 NOV FIELD EVENT WITH VERNIER RESOLUTION (U)

AS-77-2658

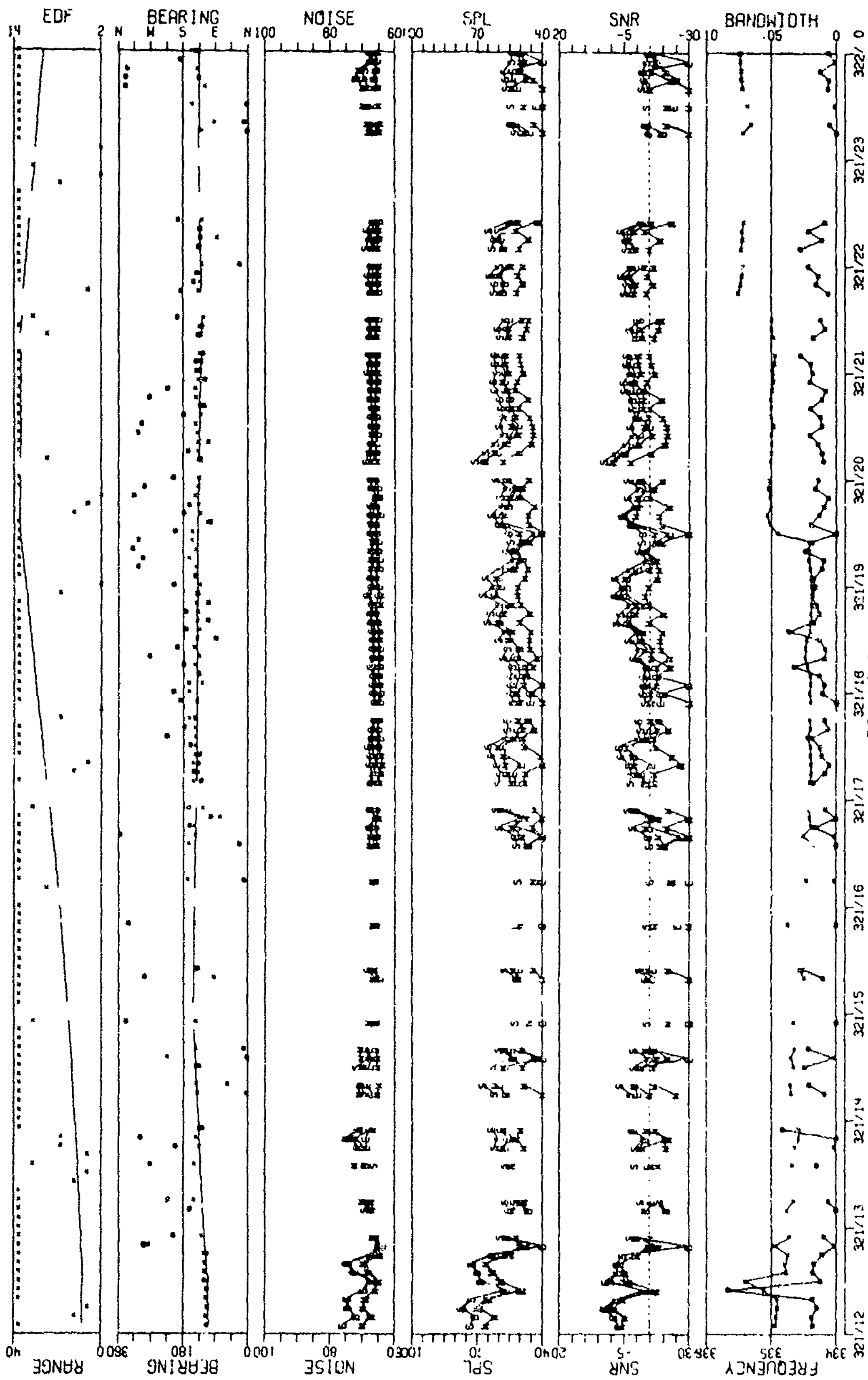

FIGURE III-59
MSS-FVT 335 HZ LINE HISTORY AS OBSERVED VIA THE MAX GAIN LIMACONS SENSOR
AT SITE A1 DURING THE 17 NOV FIELD EVENT WITH VERNIER RESOLUTION (U)

AS-77-2659

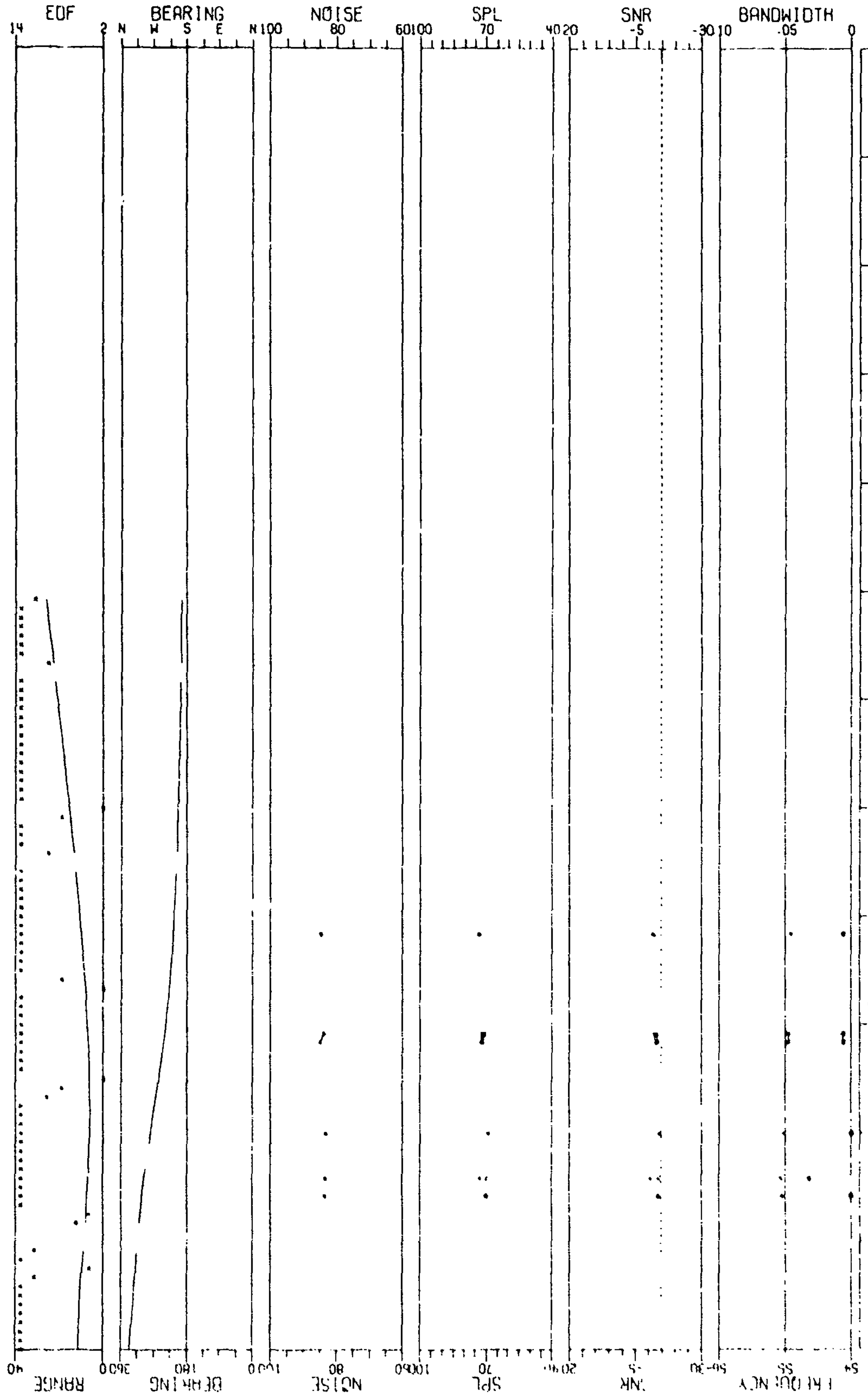

FIGURE III-60
MSS-EVT 55 HZ LINE HISTORY AS OBSERVED VIA THE OMNIDIRECTIONAL SENSOR AT SITE A2 DURING THE 17 NOV FIELD EVENT WITH VERNIER RESOLUTION (U)

AS-77-2660

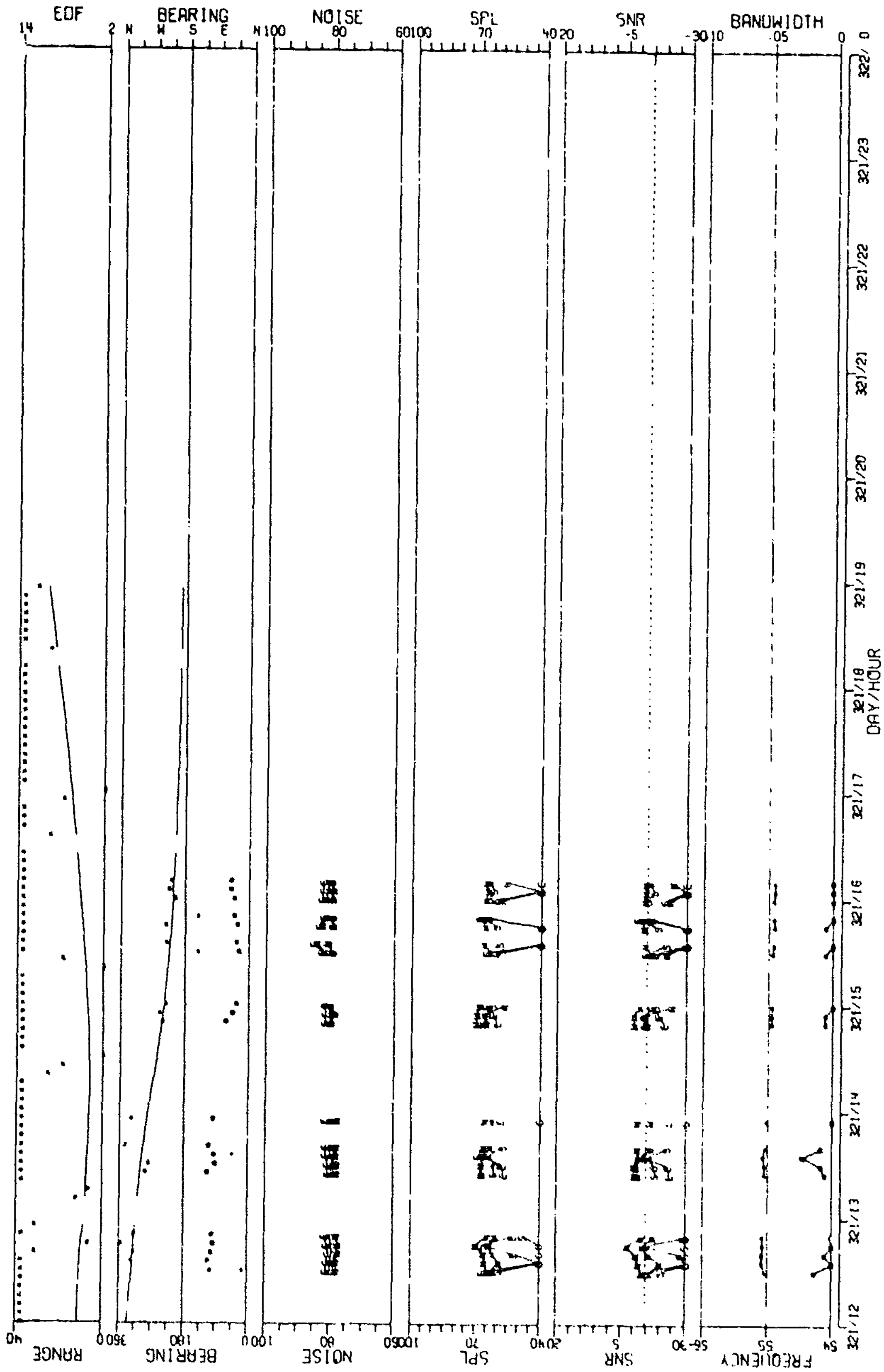

FIGURE III-61
MSS-FVT 55 HZ LINE HISTORY AS OBSERVED VIA THE SINGLE CARDIOIDS SENSOR
AT SITE A2 DURING THE 17 NOV FIELD EVENT WITH VERNIER RESOLUTION (U)

AS-77-2661

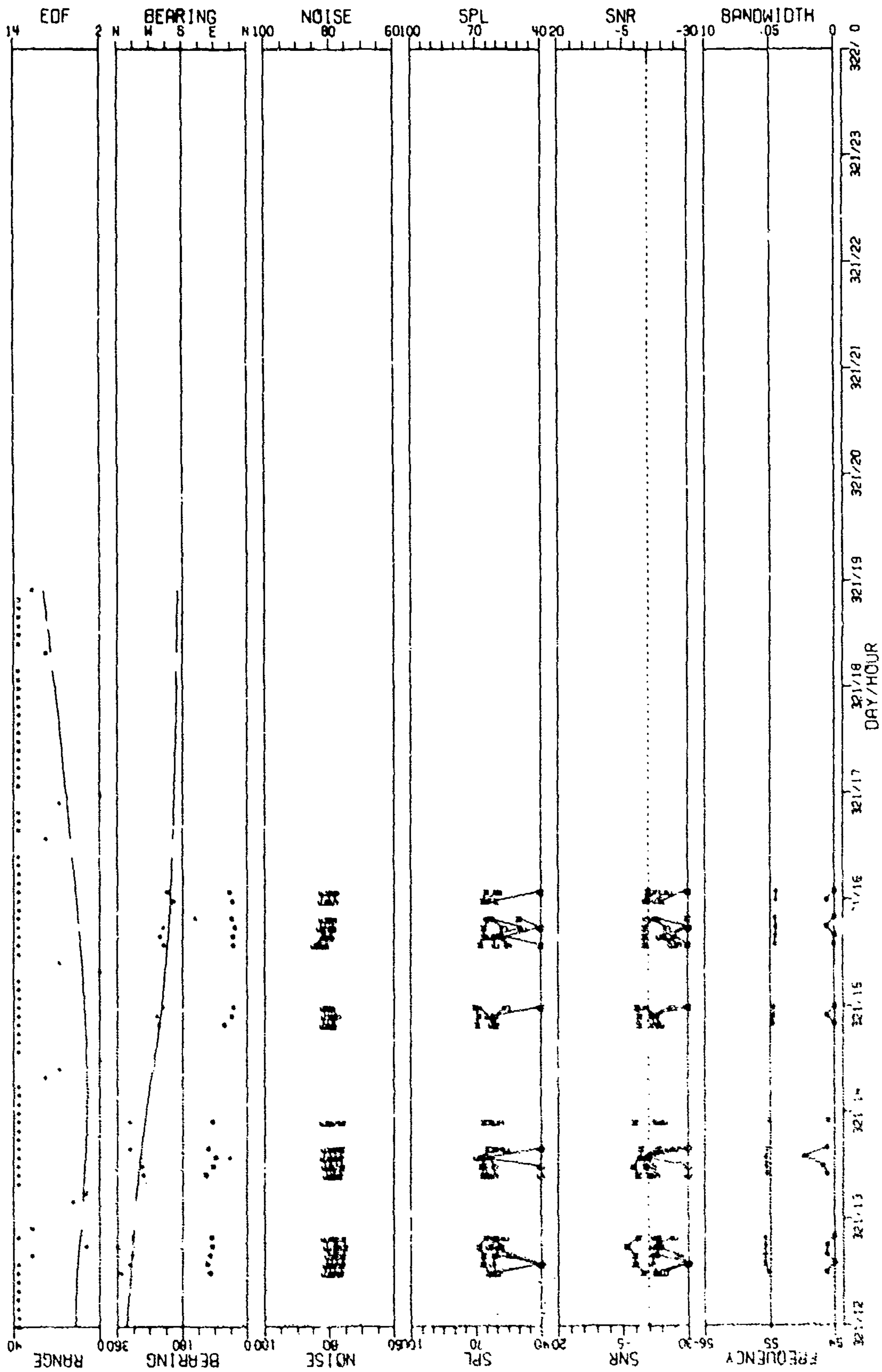

FIGURE III-62
[illegible] 55 HZ LINE HISTORY AS OBSERVED VIA THE MAX GAIN LIMACONS SENSOR AT SITE A2 DURING THE 17 NOV FIELD EVENT WITH VERNIER RESOLUTION (U)

AS-77-2662

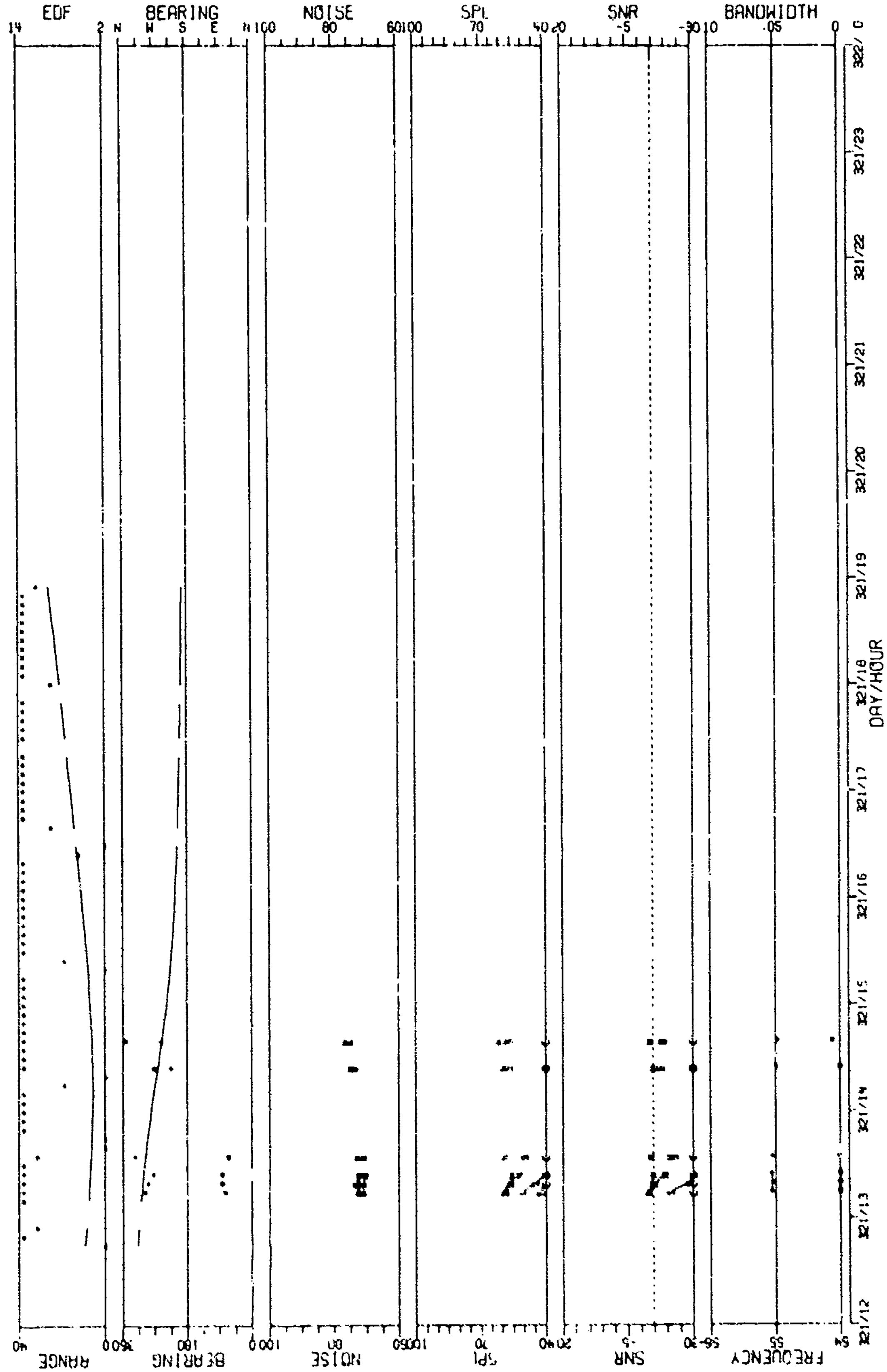

FIGURE III-63

MSS-FVT 55 HZ LINE HISTORY AS OBSERVED VIA THE DIFFERENCED CARDIOIDS SENSOR AT SITE A2 DURING THE 17 NOV FIELD EVENT WITH VERNIER RESOLUTION (U)

AS-77-2663

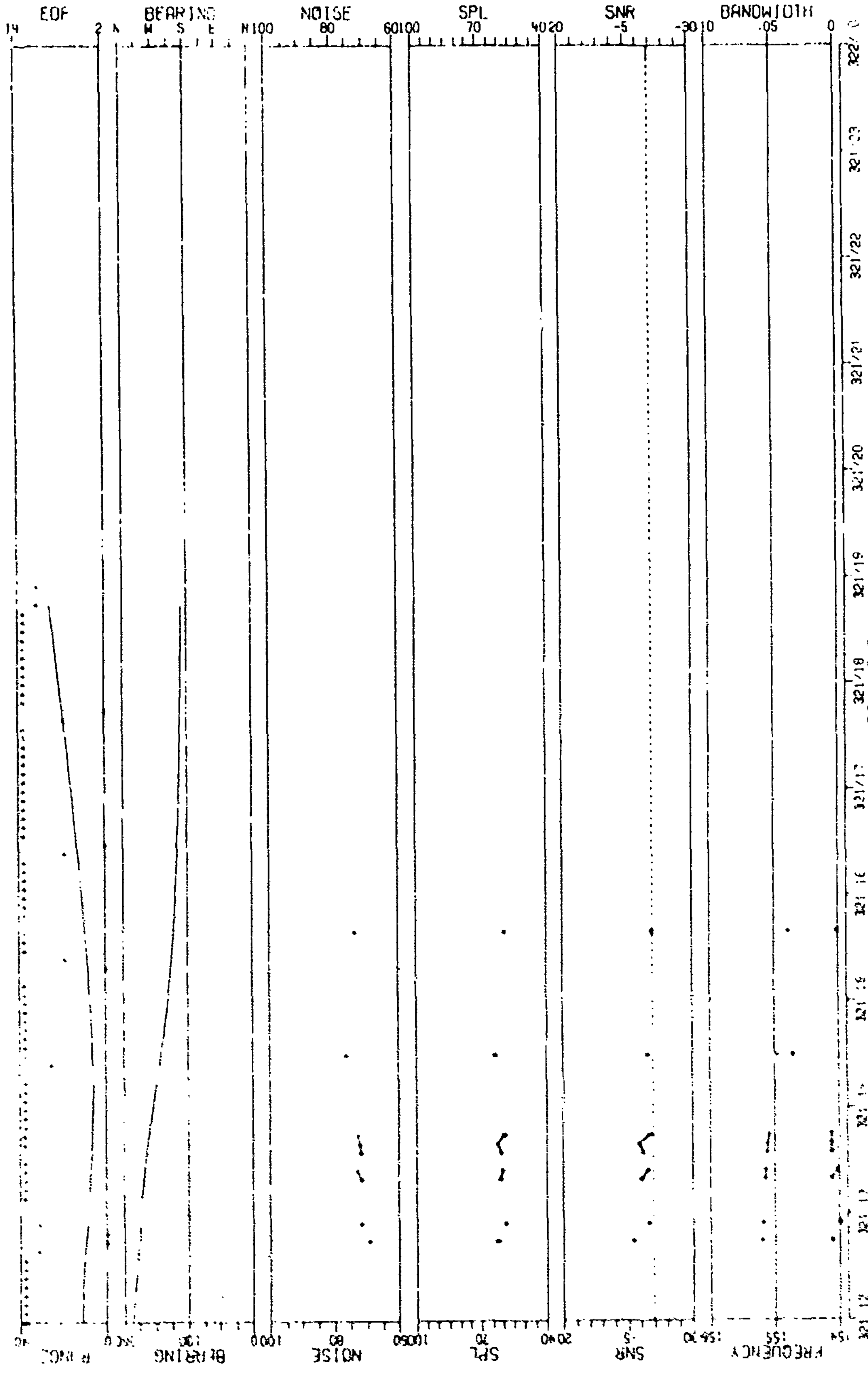

FIGURE III-64
MSS-FVT 155 HZ LINE HISTORY, AS OBSERVED VIA THE OMNIDIRECTIONAL SENSOR
AT SITE A2 DURING THE 17 NOV FIELD EVENT WITH VERNIER RESOLUTION (U)

AS-77-2664

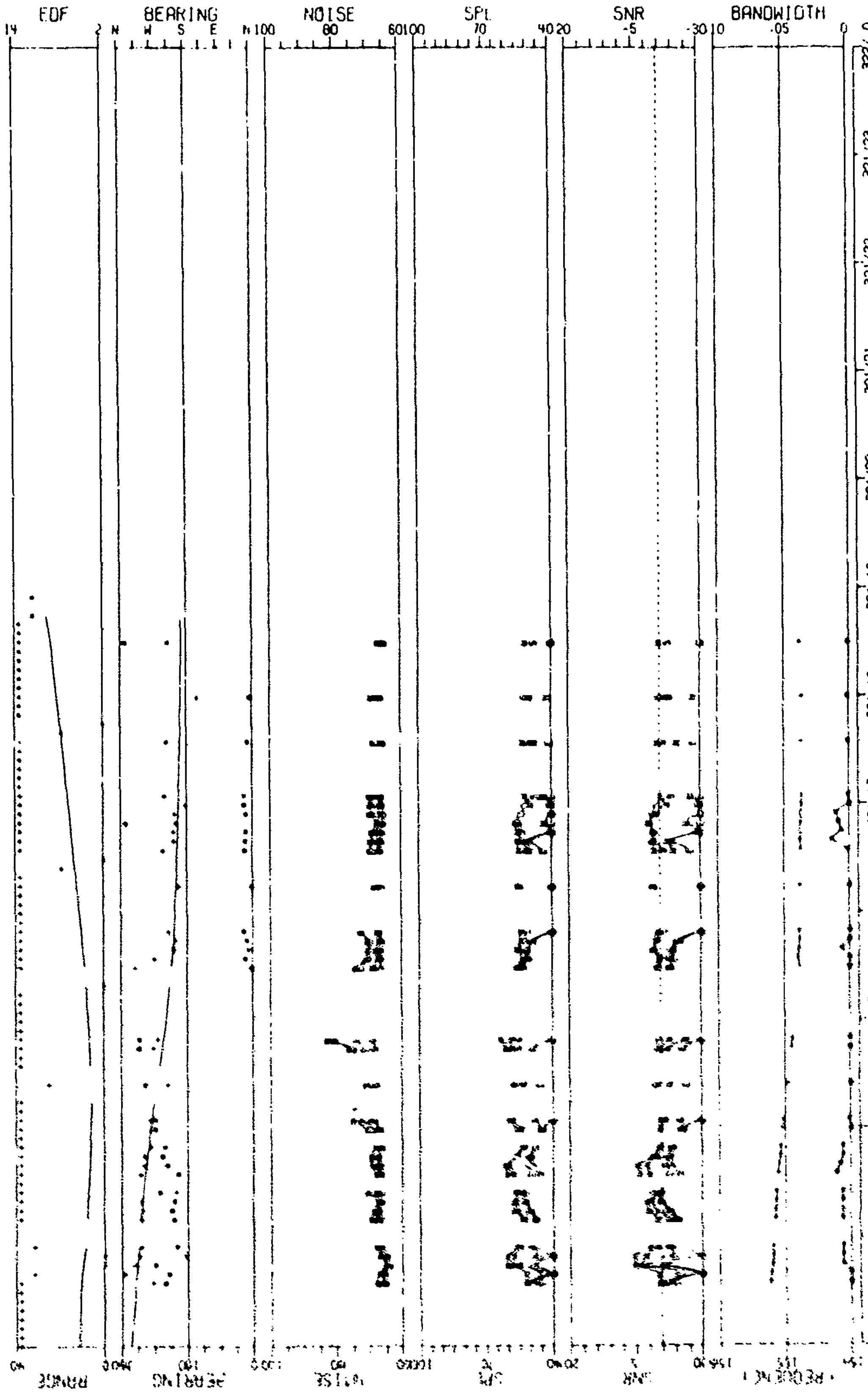

FIGURE 111
MGS-FY? 155 HZ LINE HISTORY AS OBSERVED VIA THE SINGLE CARDIOIDS SENSOR AT SITE 22 DURING THE 17 NOV FIELD EVENT WITH VERNIER RESOLUTION (U)

AS-77-2669

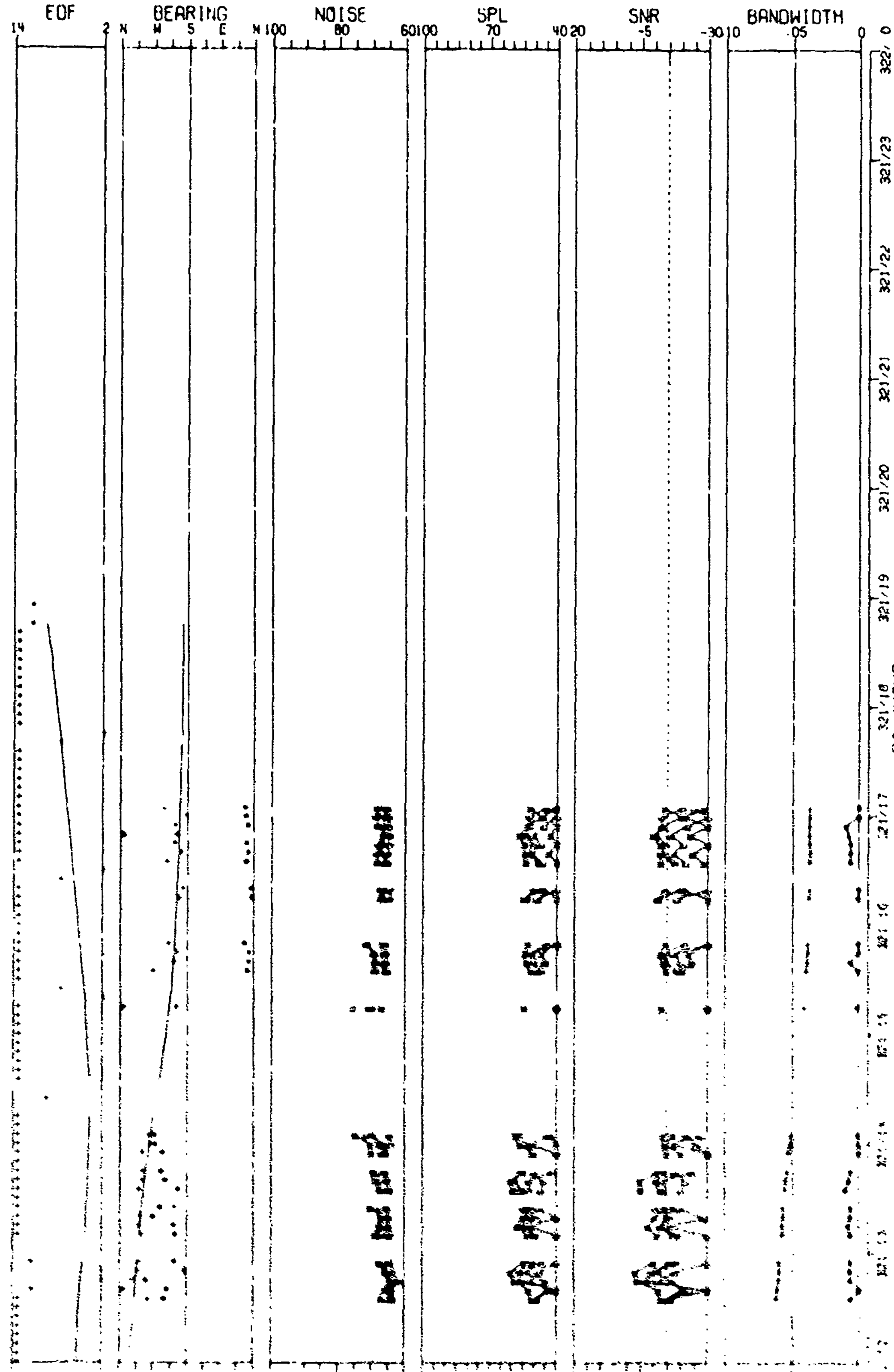

FIGURE III-66
[illegible] 155 HZ LINE HISTORY AS OBSERVED VIA THE MAX GAIN LIMACONS SENSOR
[illegible] DURING THE 17 NOV FIELD EVENT WITH VERNIER RESOLUTION (U)

AG-77-2666

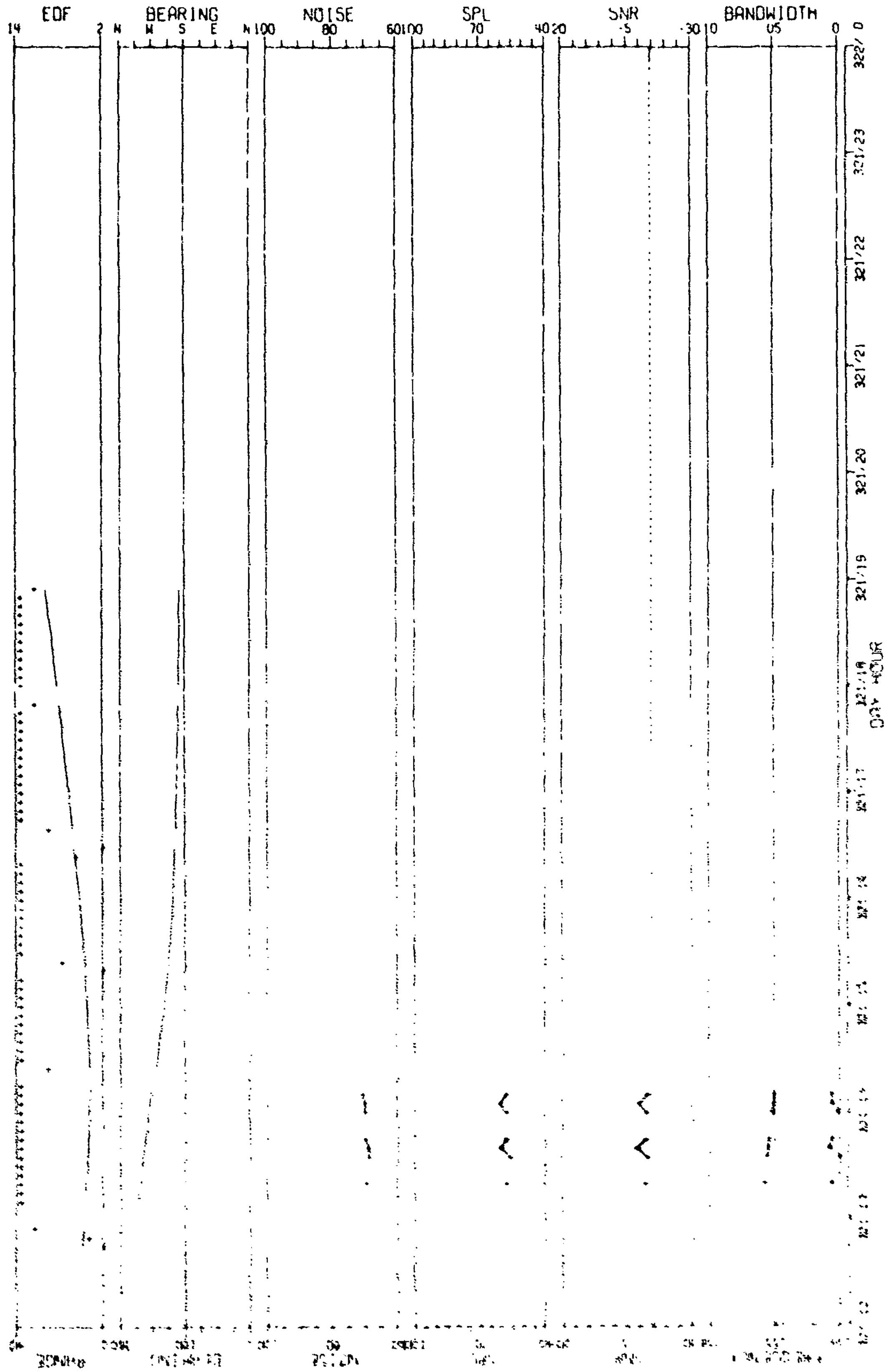

FIGURE III-67
[illegible] HISTORY AS OBSERVED VIA THE VERTICAL DIPOLE SENSOR
[illegible] DURING THE 17 NOV FIELD EVENT WITH VERNIER RESOLUTION (U)

AS-77-2667

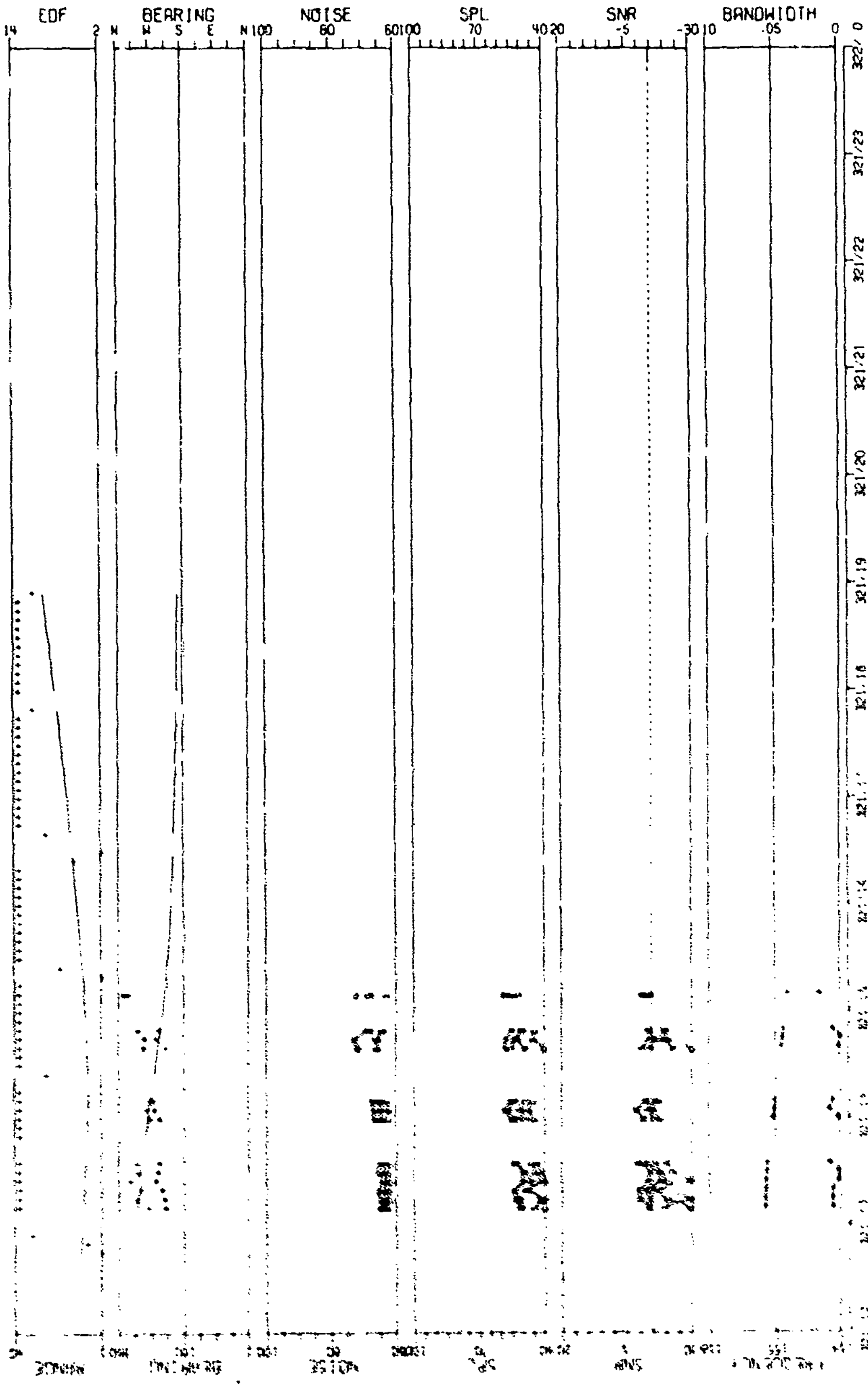

FIGURE III-68
... LINE HISTORY AS OBSERVED VIA THE DIFFERENCED CARDIOIDS SENSOR
... DURING THE 11 NOV FIELD EVENT WITH VERNIER RESOLUTION (U)

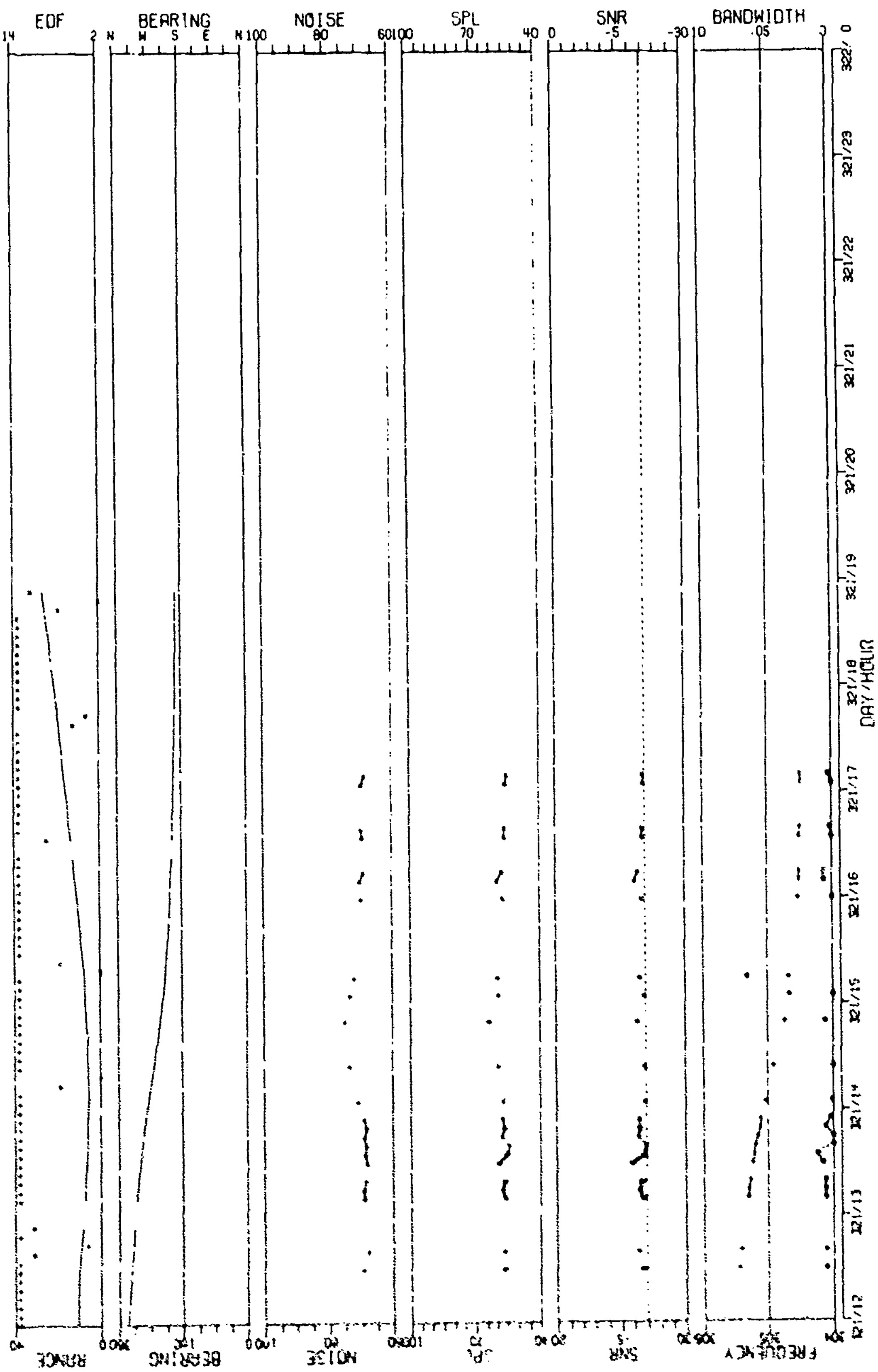

FIGURE III-69
MSS-FVT 305 HZ LINE HISTORY AS OBSERVED VIA THE OMNIDIRECTIONAL SENSOR AT SITE A2 DURING THE 17 NOV FIELD EVENT WITH VERNIER RESOLUTION (U)

AS-77-2669

FIGURE III-70
MSS-FVT 305 HZ LINE HISTORY AS OBSERVED VIA THE SINGLE CARDIOIDS SENSOR
AT SITE A2 DURING THE 17 NOV FIELD EVENT WITH VERNIER RESOLUTION (U)

AS-77-2670

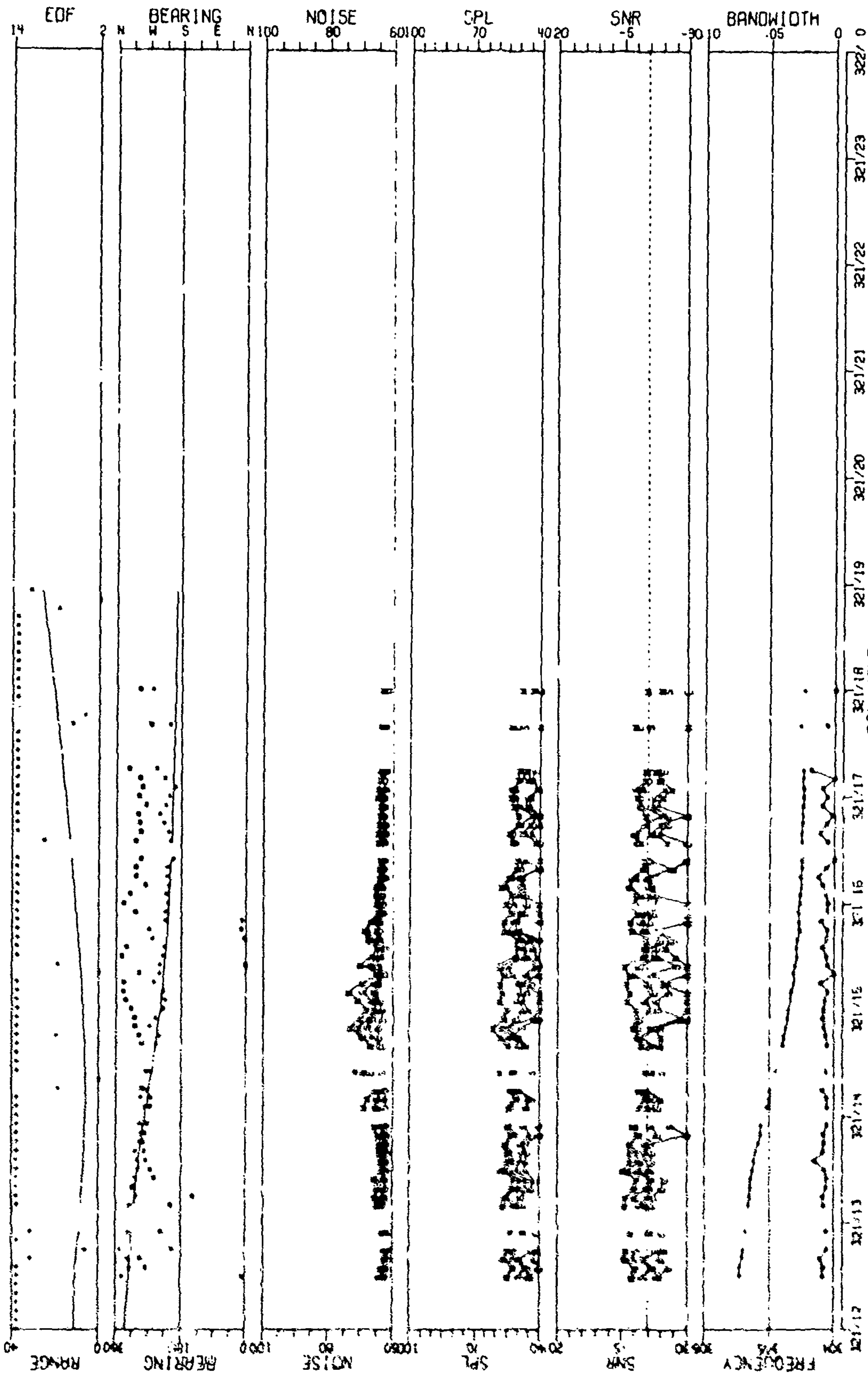

FIGURE III-71
MSS-FV1 305 HZ LINE HISTORY AS OBSERVED VIA THE MAX GAIN LIMACONS SENSOR
AT SITE A2 DURING THE 17 NOV FIELD EVENT WITH VERNIER RESOLUTION (U)

AS-77-2671

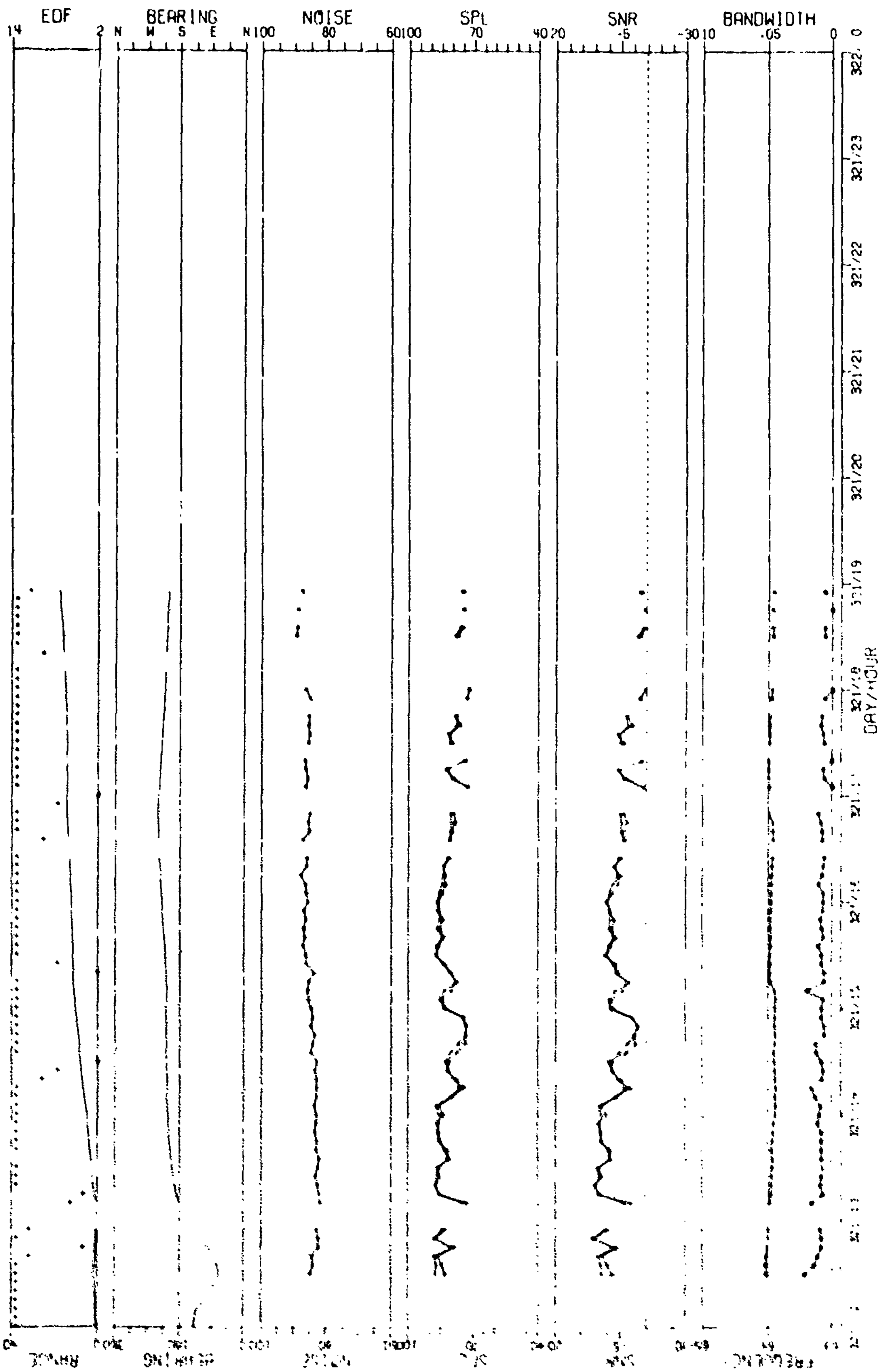

FIGURE III-72
... HISTORY AS OBSERVED VIA THE OMNIDIRECTIONAL SENSOR
... FIELD EVENT WITH VERNIER RESOLUTION (U)

AS-77-2672

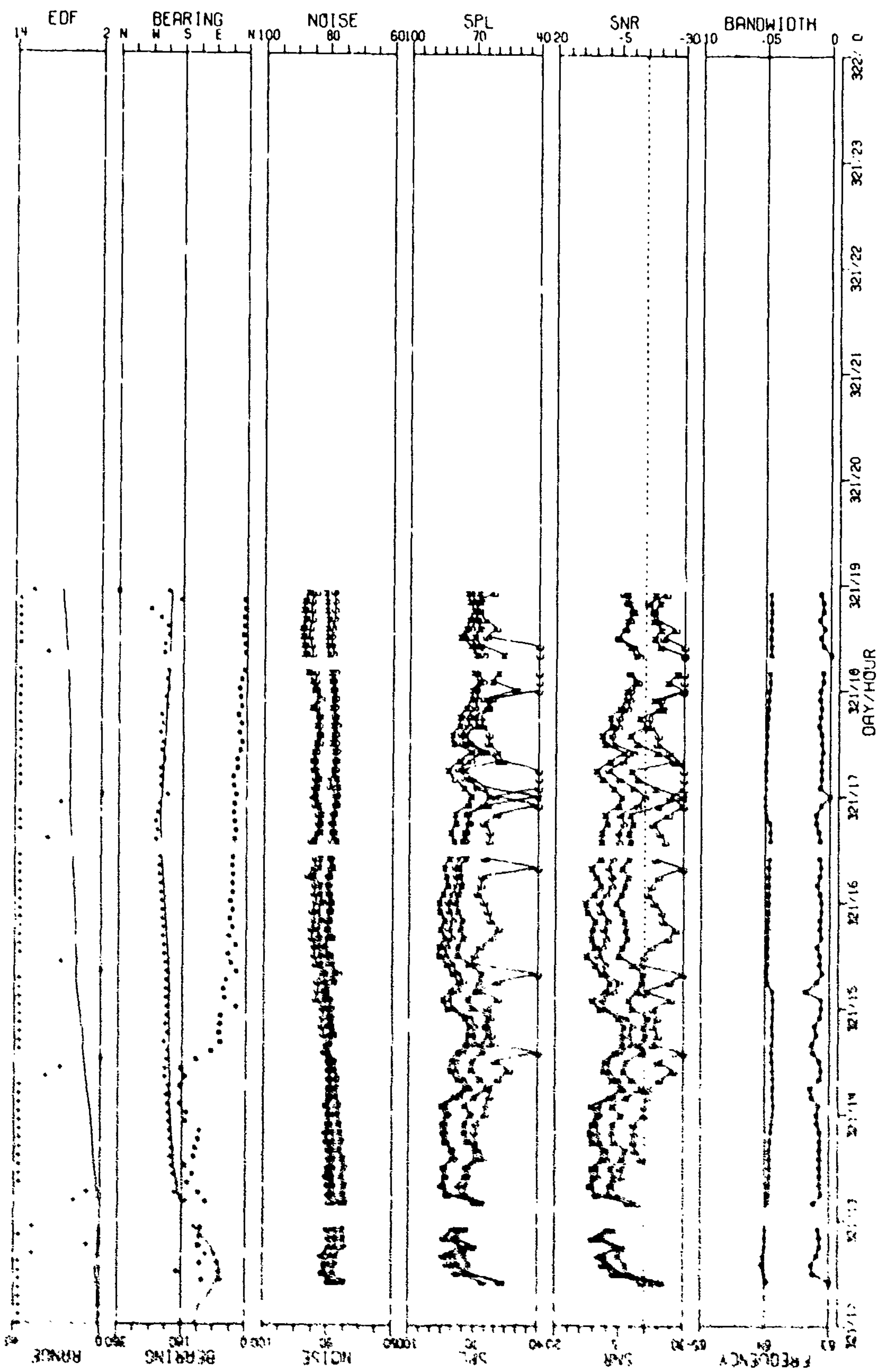

FIGURE III-73
MSS-FYT 54 HZ LINE HISTORY AS OBSERVED VIA THE SINGLE CARDIOIDS SENSOR AT SITE A2 DURING THE 17 NOV FIELD EVENT WITH VERNIER RESOLUTION (U)

AS-77-2673

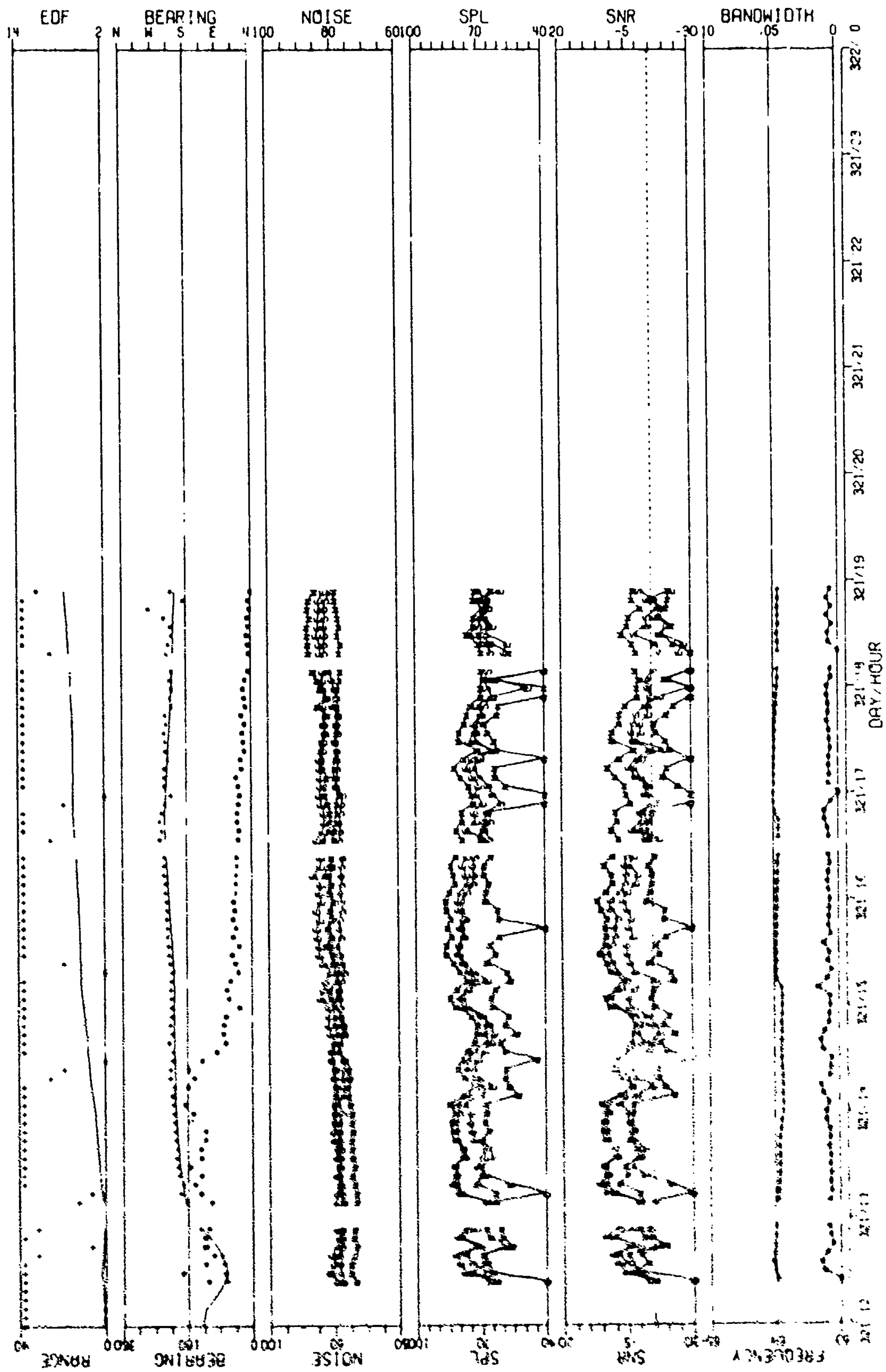

FIGURE III-74
MSS-EXT 64 HZ LINE HISTORY AS OBSERVED VIA THE MAX GAIN LIMACONS SENSOR AT SITE AC DURING THE 17 NOV FIELD EVENT WITH VERNIER RESOLUTION (U)

AS-77-2674

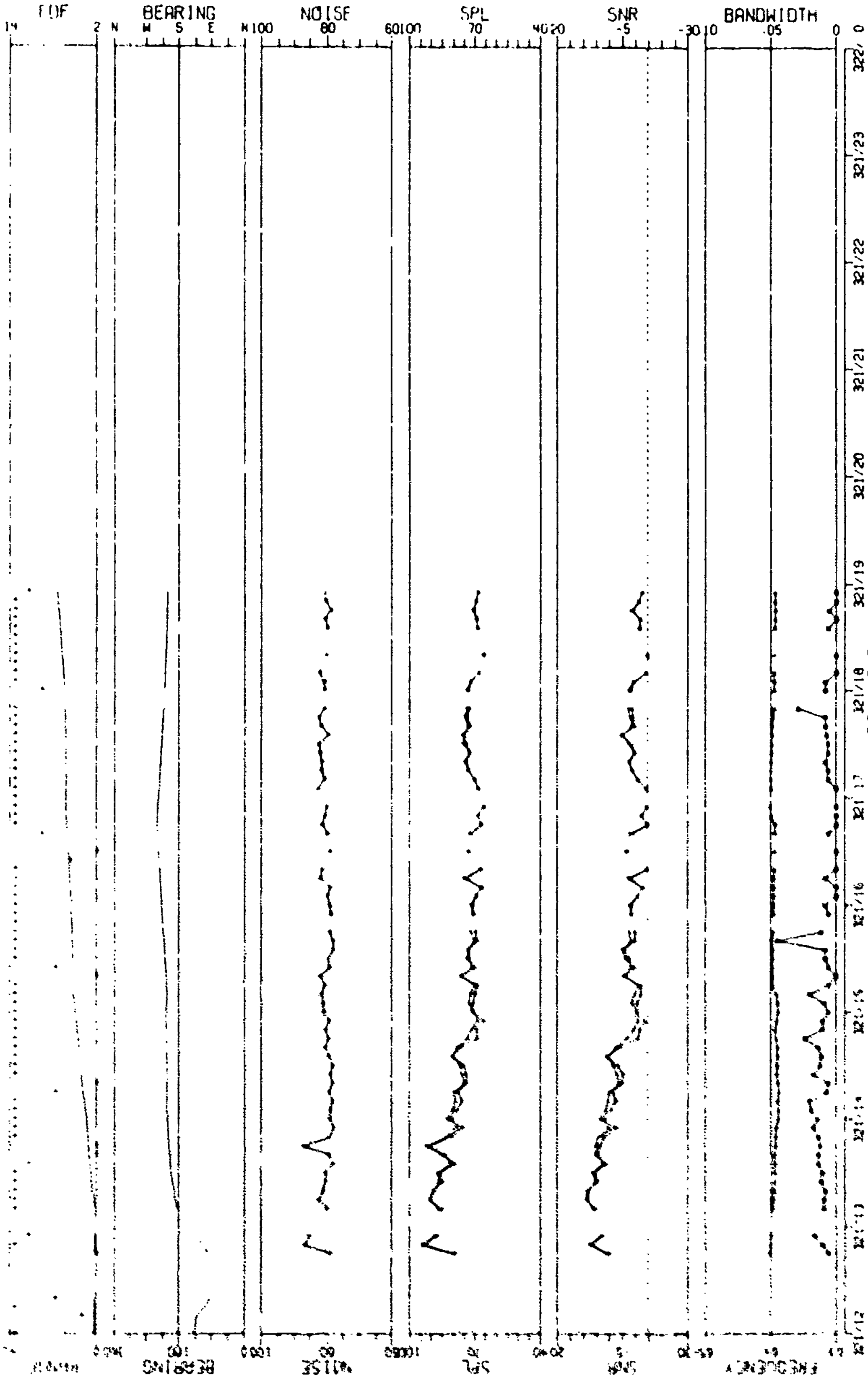

FIGURE III-75
MSS-EXT 64 HZ LINE HISTORY AS OBSERVED VIA THE VERTICAL DIPOLE SENSOR AT SITE A2 DURING THE 17 NOV FIELD EVENT WITH VERNIER RESOLUTION (U)

AS-77-2675

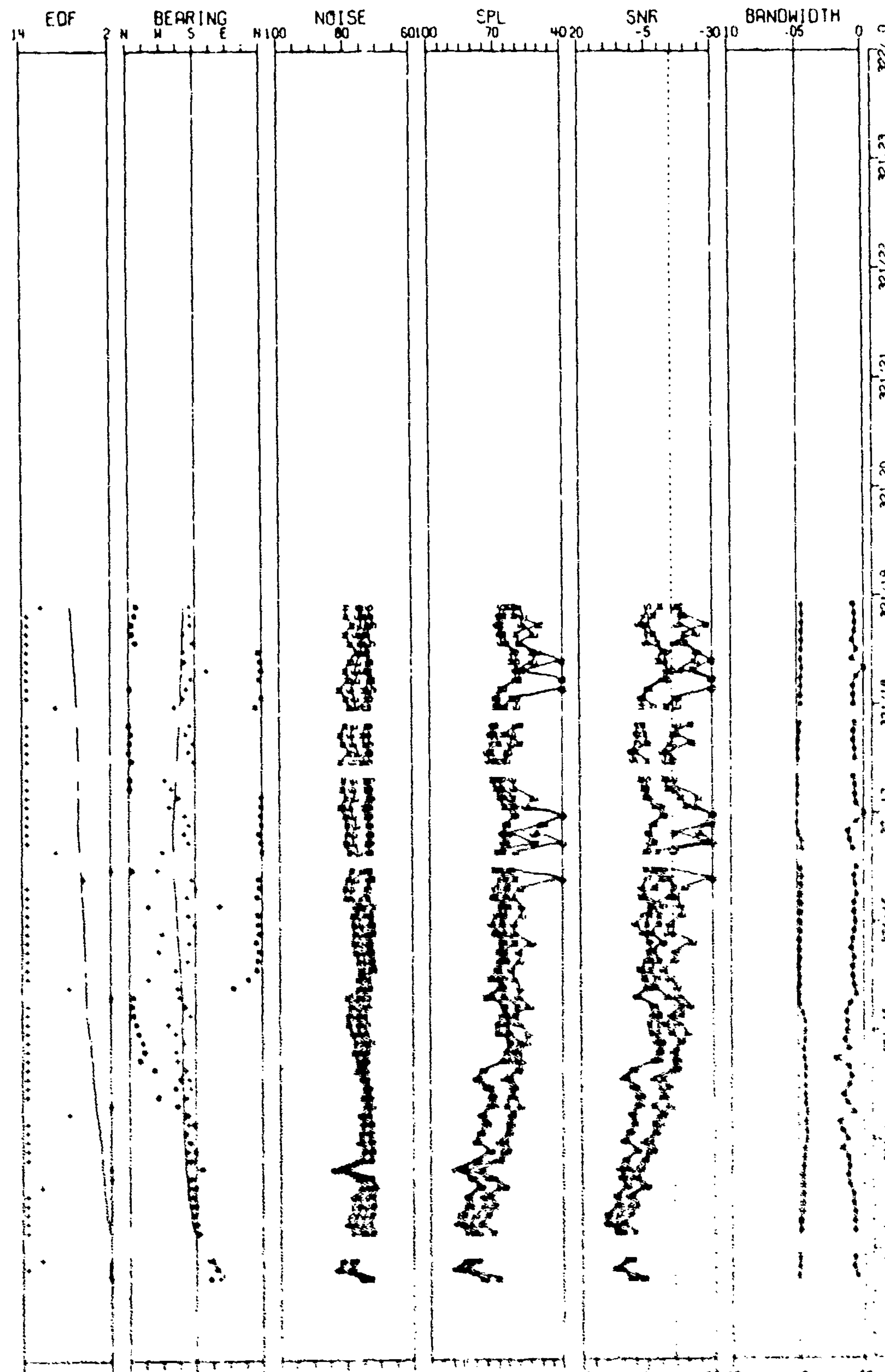

FIGURE III-76
[illegible] 54 HZ LINE HISTORY AS OBSERVED VIA THE DIFFERENCED CARDIOIDS SENSOR AT [illegible] A2 DURING THE 11 NOV FIELD EVENT WITH VERNIER RESOLUTION (U)

AS-77-2676

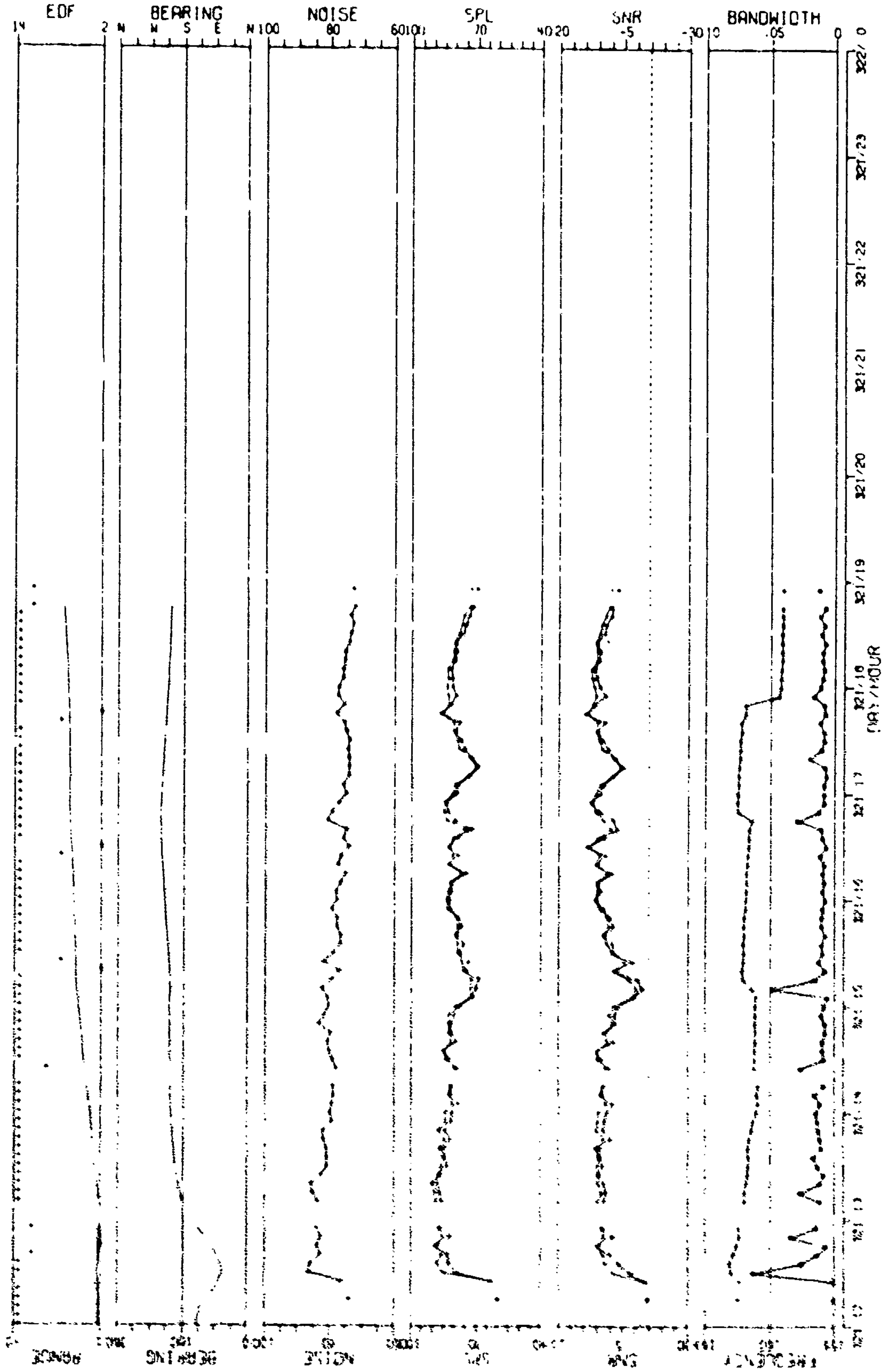

FIGURE III-77
WES-FIT 160 HZ LINE HISTORY AS OBSERVED VIA THE OMNIDIRECTIONAL SENSOR AT SITE R2 DURING THE 17 NOV FIELD EVENT WITH VERNIER RESOLUTION (U)

AS-77-2677

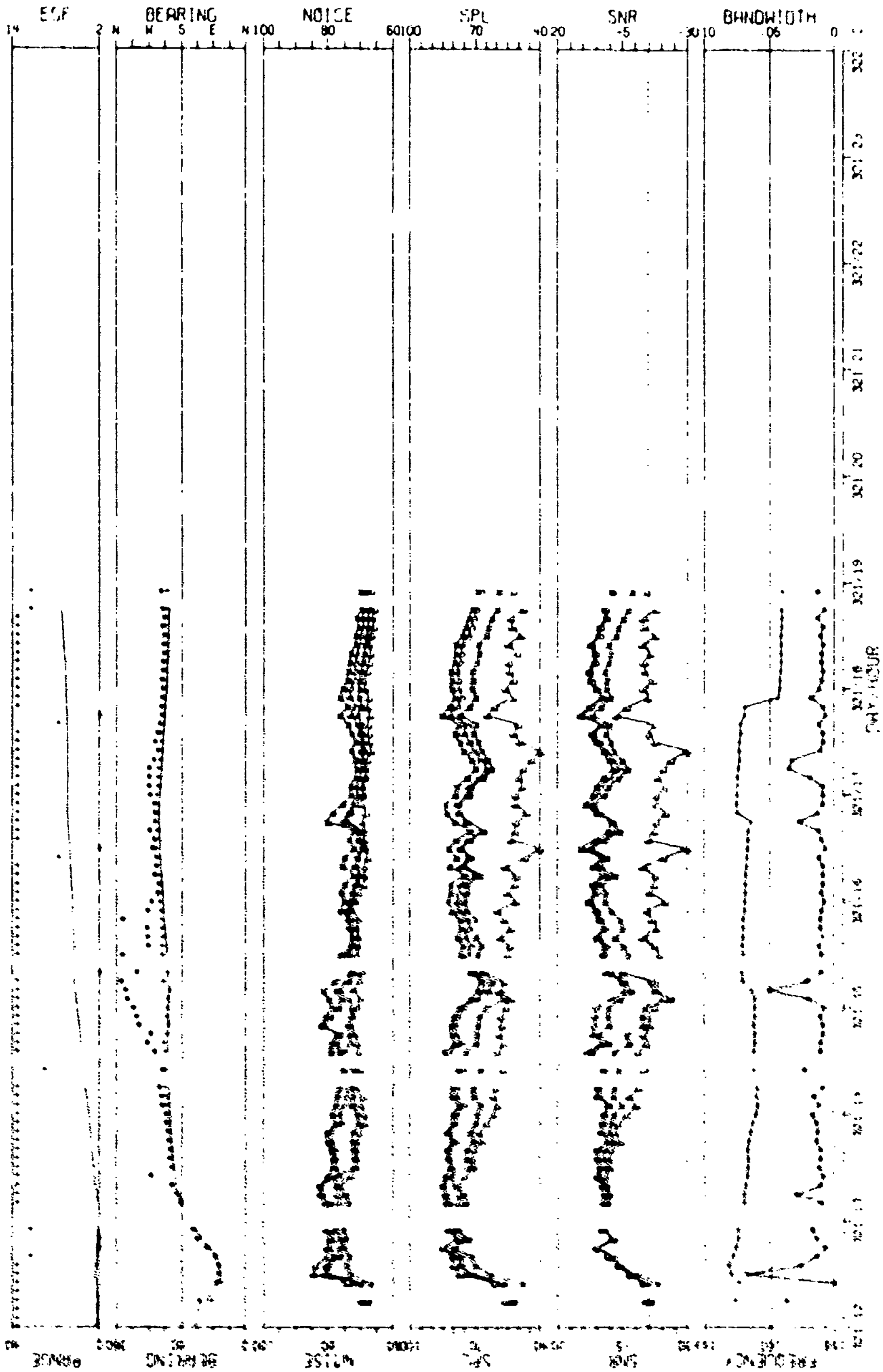

FIGURE III-18
... HZ LINE HISTORY AS OBSERVED VIA THE SINGLE CARDIOIDS SENSOR ... FIELD EVENT WITH VERNIER RESOLUTION (U)

AS-77-24[illegible]

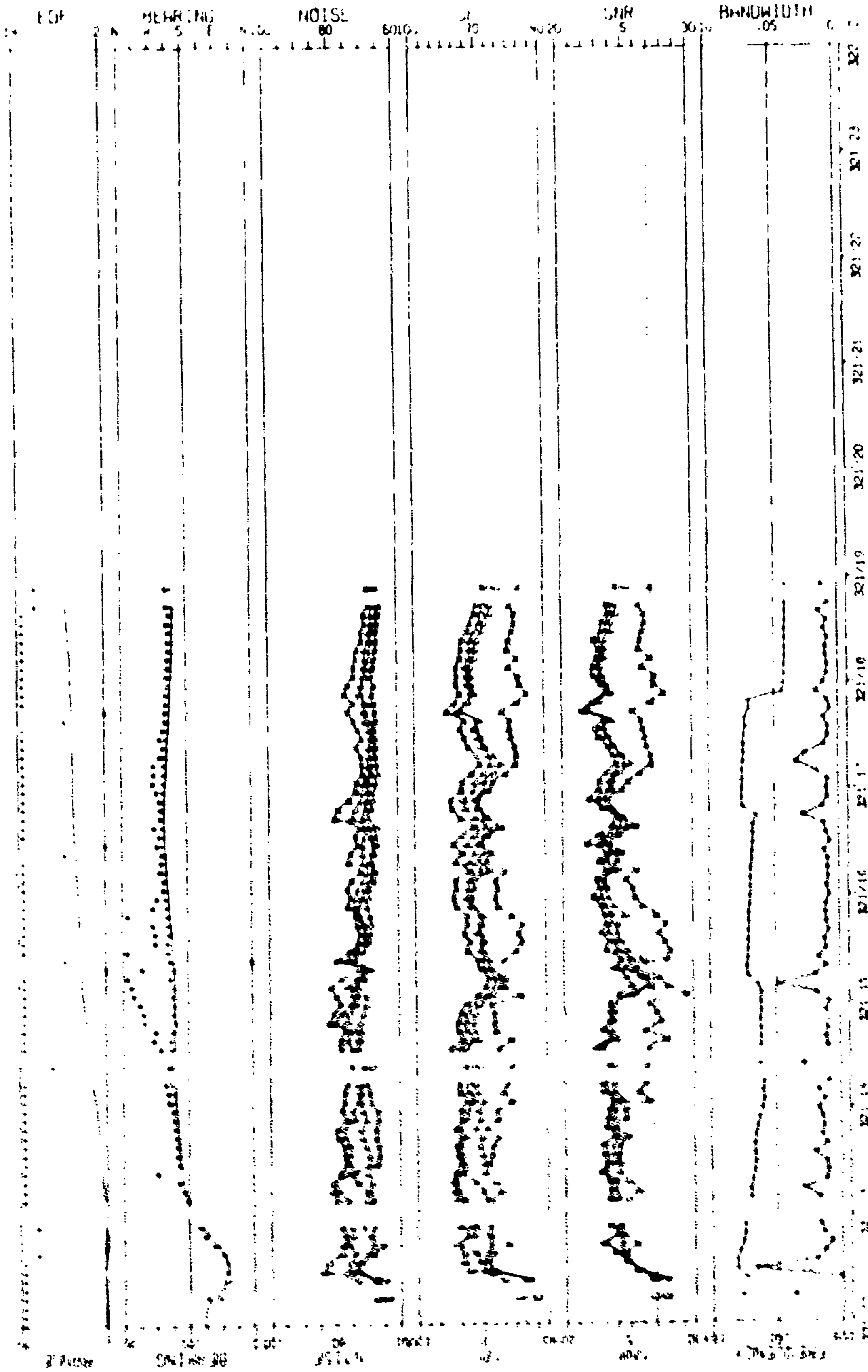

FIGURE III-73
[illegible] HZ LINE HISTORY AS OBSERVED VIA THE MAX GAIN LIMHCONS SENSOR
[illegible] DURING THE 17 NOV FIELD EVENT WITH VERNIER RESOLUTION (U)

AS-77-2679

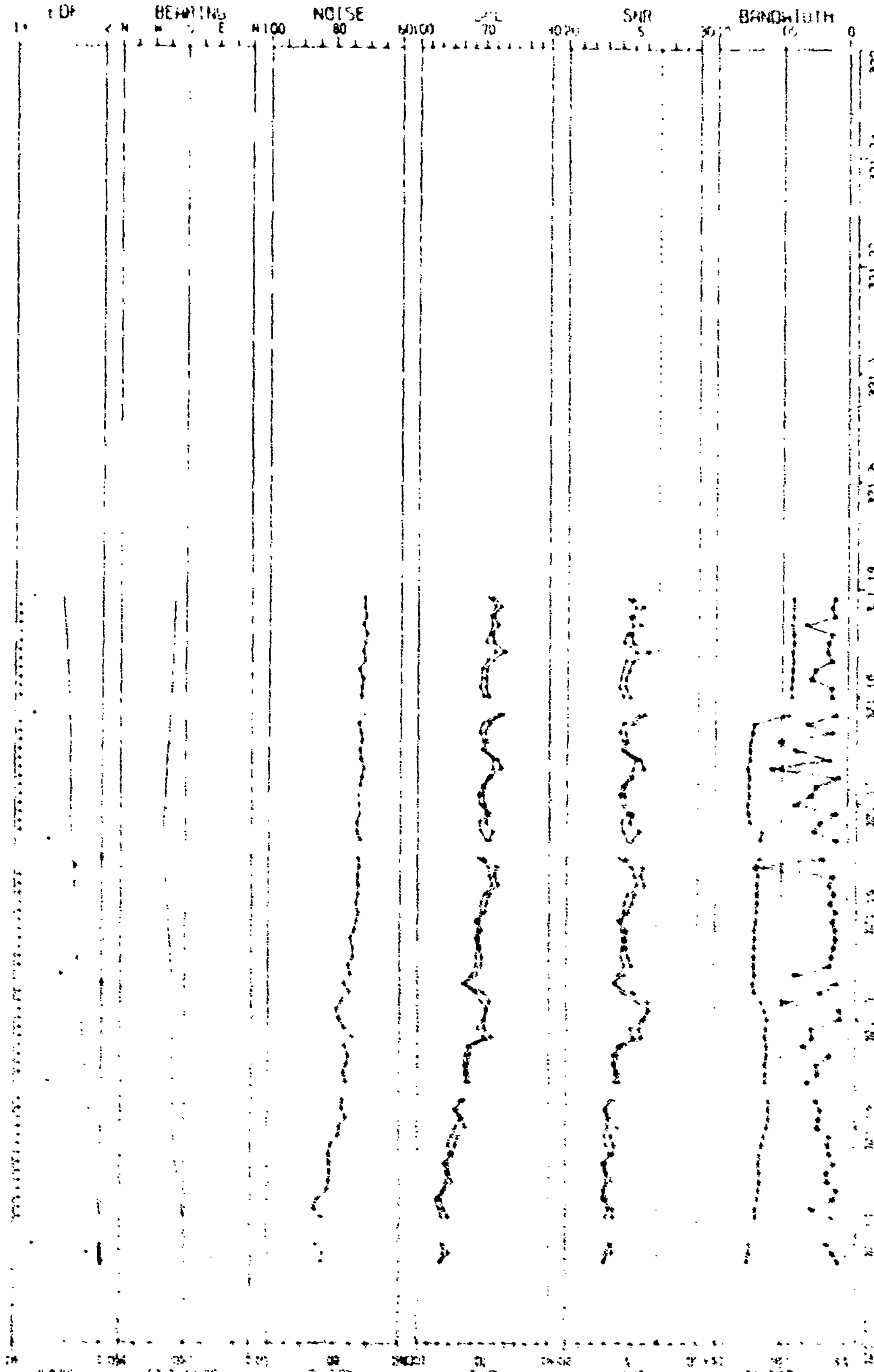

FIGURE III-80
... AS OBSERVED VIA THE VERTICAL DIPOLE SENSOR
... FIELD EVENT WITH ... RESOLUTION ...

AS-77-2659

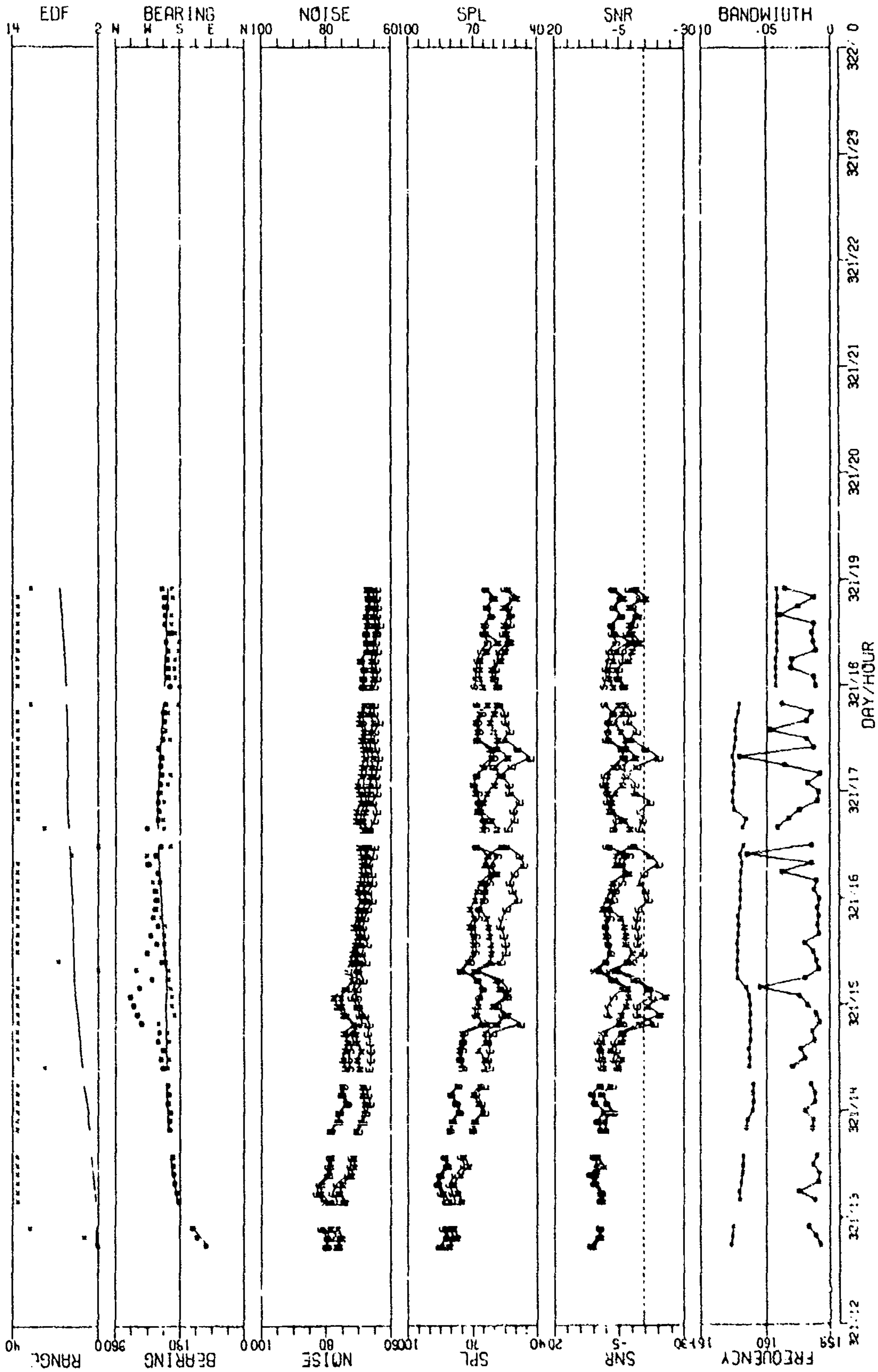

FIGURE III-81
MSS-FVT 160 HZ LINE HISTORY AS OBSERVED VIA THE DIFFERENCED CARDIOIDS SENSOR AT SITE A2 DURING THE 17 NOV FIELD EVENT WITH VERNIER RESOLUTION (U)

AS-77-2681

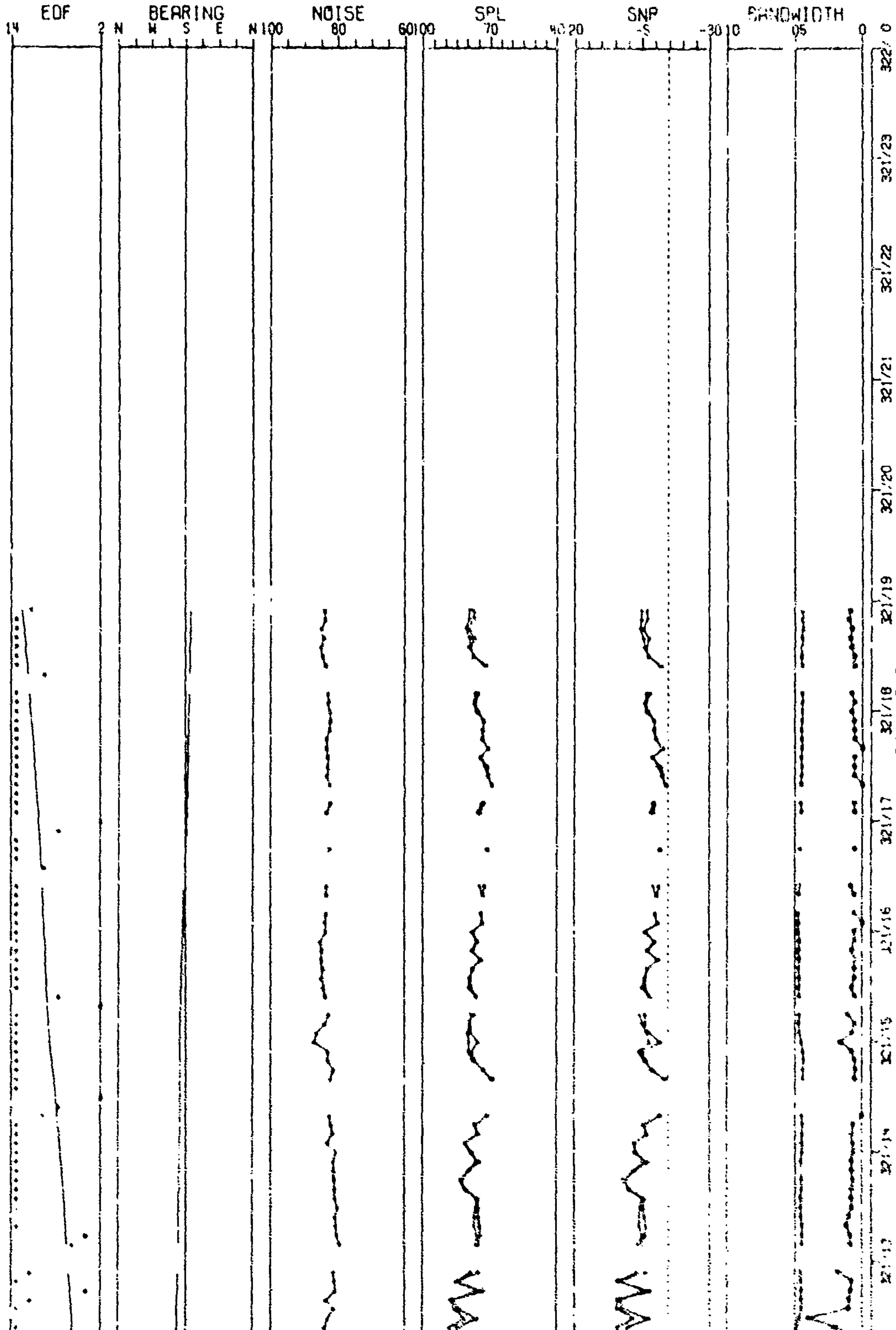

FIGURE III-82
[illegible] TO HZ LINE HISTORY AS OBSERVED VIA THE OMNIDIRECTIONAL SENSOR AT SITE A2 DURING THE 17 NOV FIELD EVENT WITH VERNIER RESOLUTION (U)

AS-77-2682

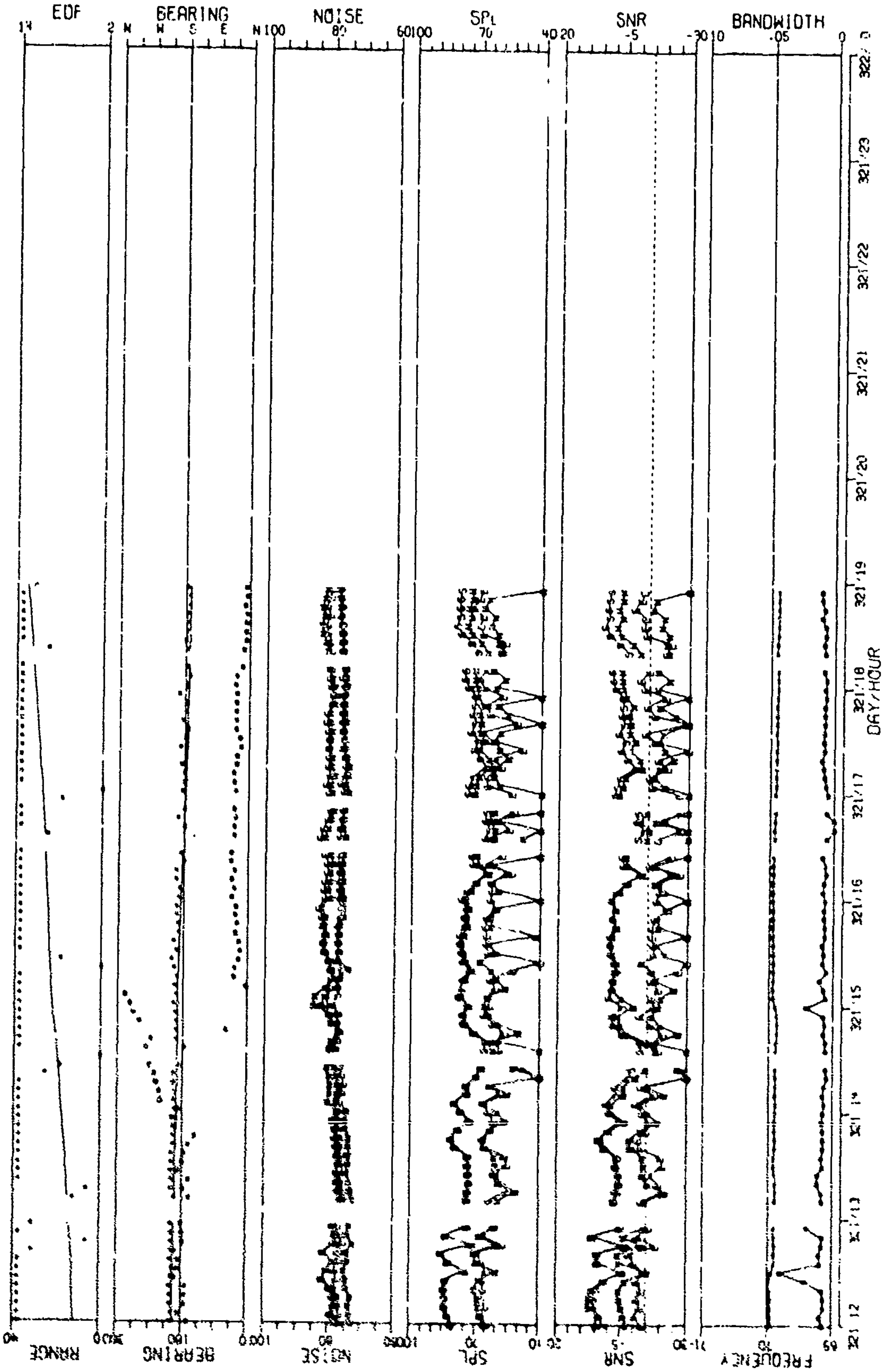

FIGURE III-83
MSS-F/T 70 HZ LINE HISTORY AS OBSERVED VIA THE SINGLE CARDIOIDS SENSOR AT SITE A2 DURING THE 17 NOV FIELD EVENT WITH VERNIER RESOLUTION (U)

AS-77-2683

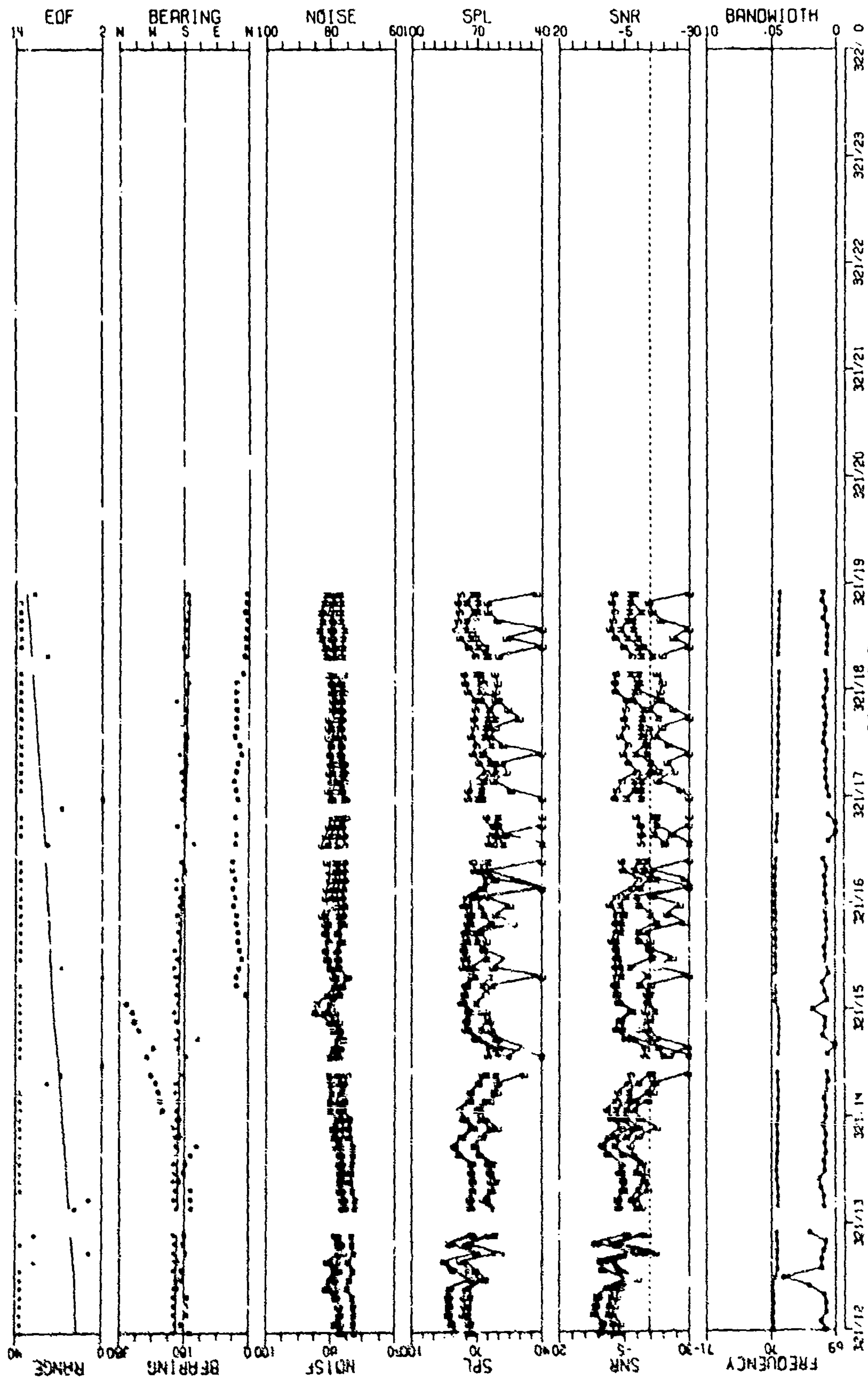

FIGURE III-84
MSS-FVT 70 HZ LINE HISTORY AS OBSERVED VIA THE MAX GAIN LIMACONS SENSOR AT SITE A2 DURING THE 17 NOV FIELD EVENT WITH VERNIER RESOLUTION (U)

AS-77-2684

FIGURE III-85
MSS-FVT 70 HZ LINE HISTORY AS OBSERVED VIA THE VERTICAL DIPOLE SENSOR
AT SITE A2 DURING THE 17 NOV FIELD EVENT WITH VERNIER RESOLUTION (U)

AS-77-2685

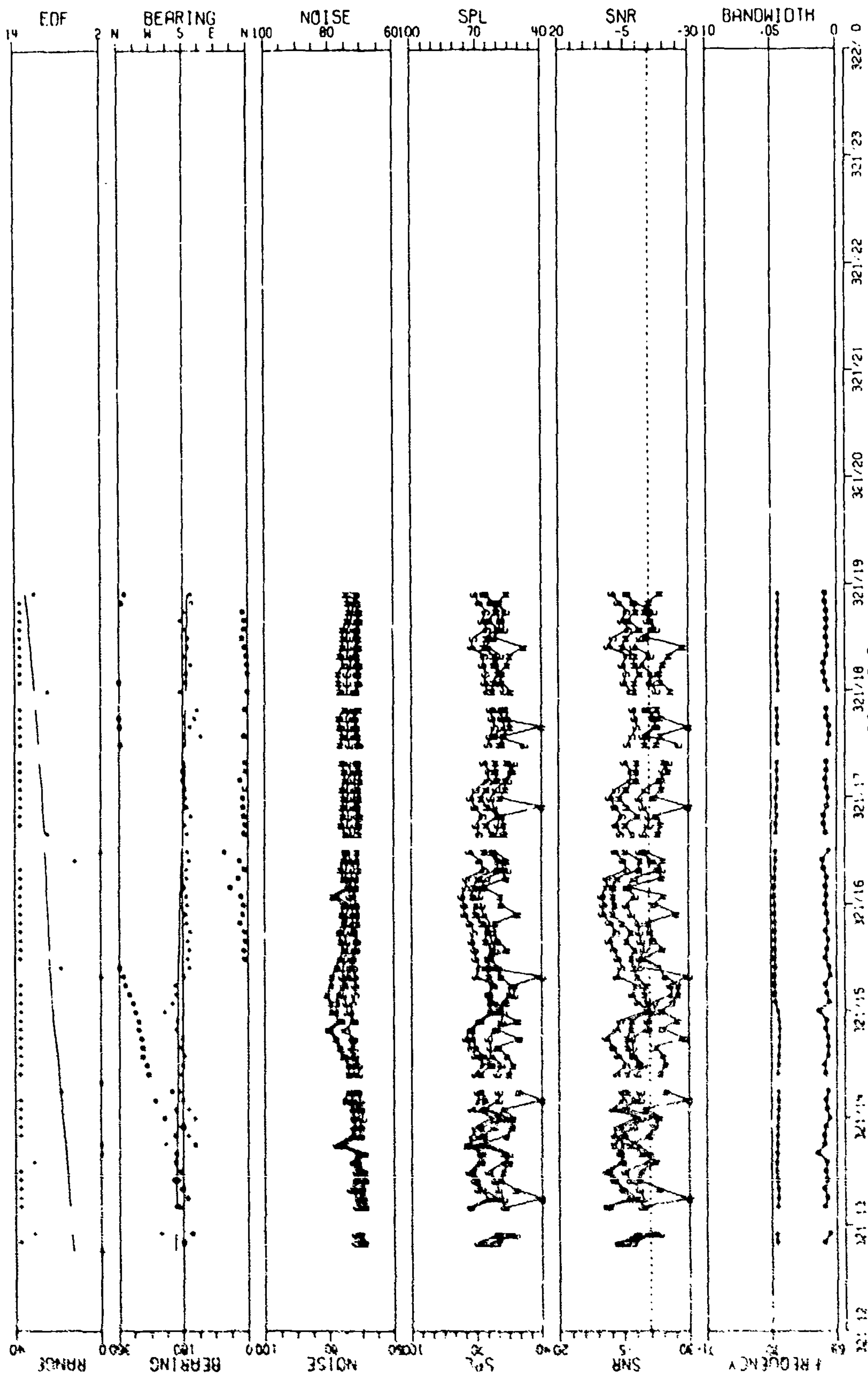

FIGURE III-86
MSS-FVT 70 HZ LINE HISTORY AS OBSERVED VIA THE DIFFERENCED CARDIOIDS SENSOR AT SITE A2 DURING THE 17 NOV FIELD EVENT WITH VERNIER RESOLUTION (U)

AS-77-2686

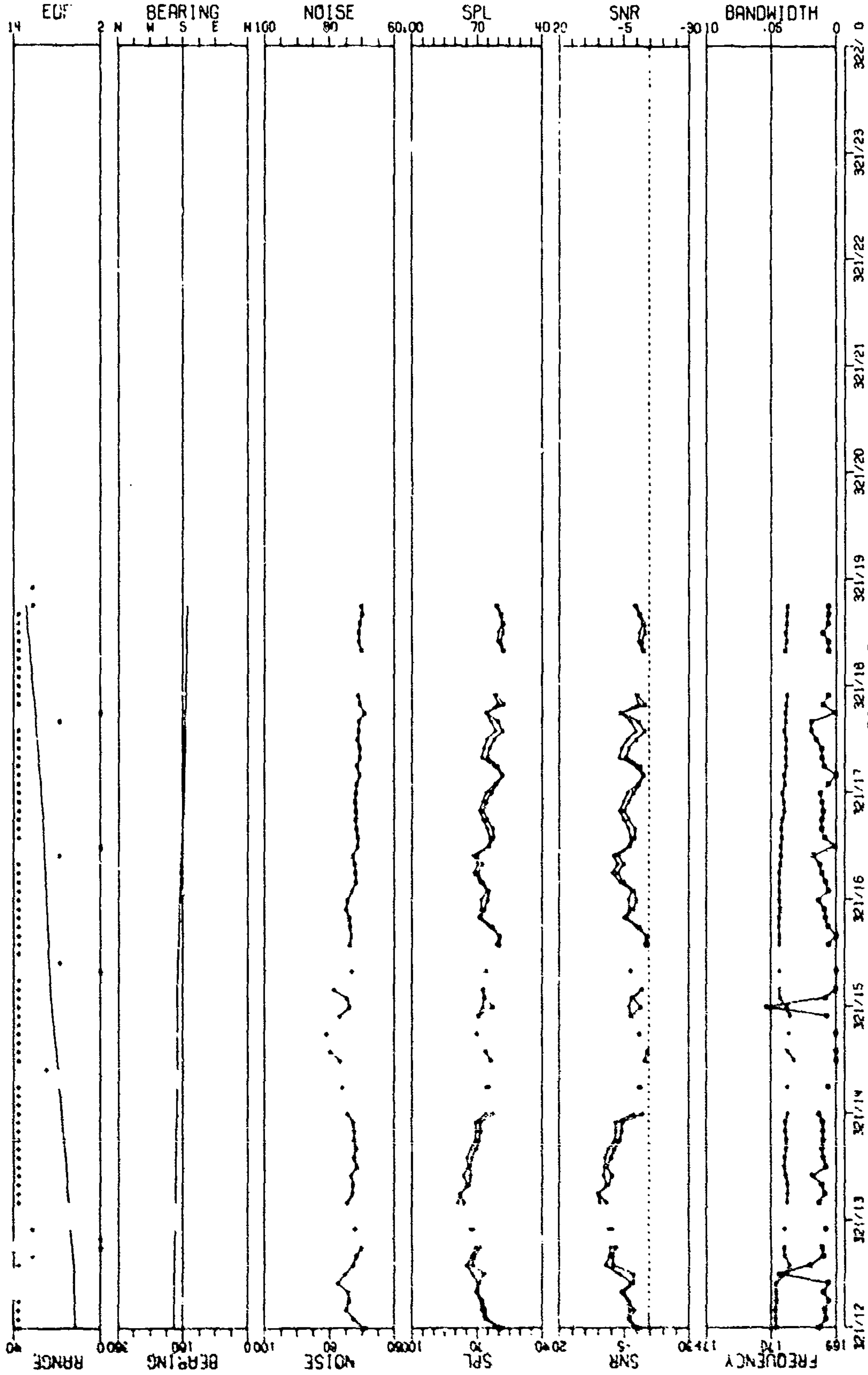

FIGURE III-87
HSS-FVT 170 HZ LINE HISTORY AS OBSERVED VIA THE OMNIDIRECTIONAL SENSOR
AT SITE A2 DURING THE 17 NOV FIELD EVENT WITH VERNIER RESOLUTION (U)

AS-77-2687

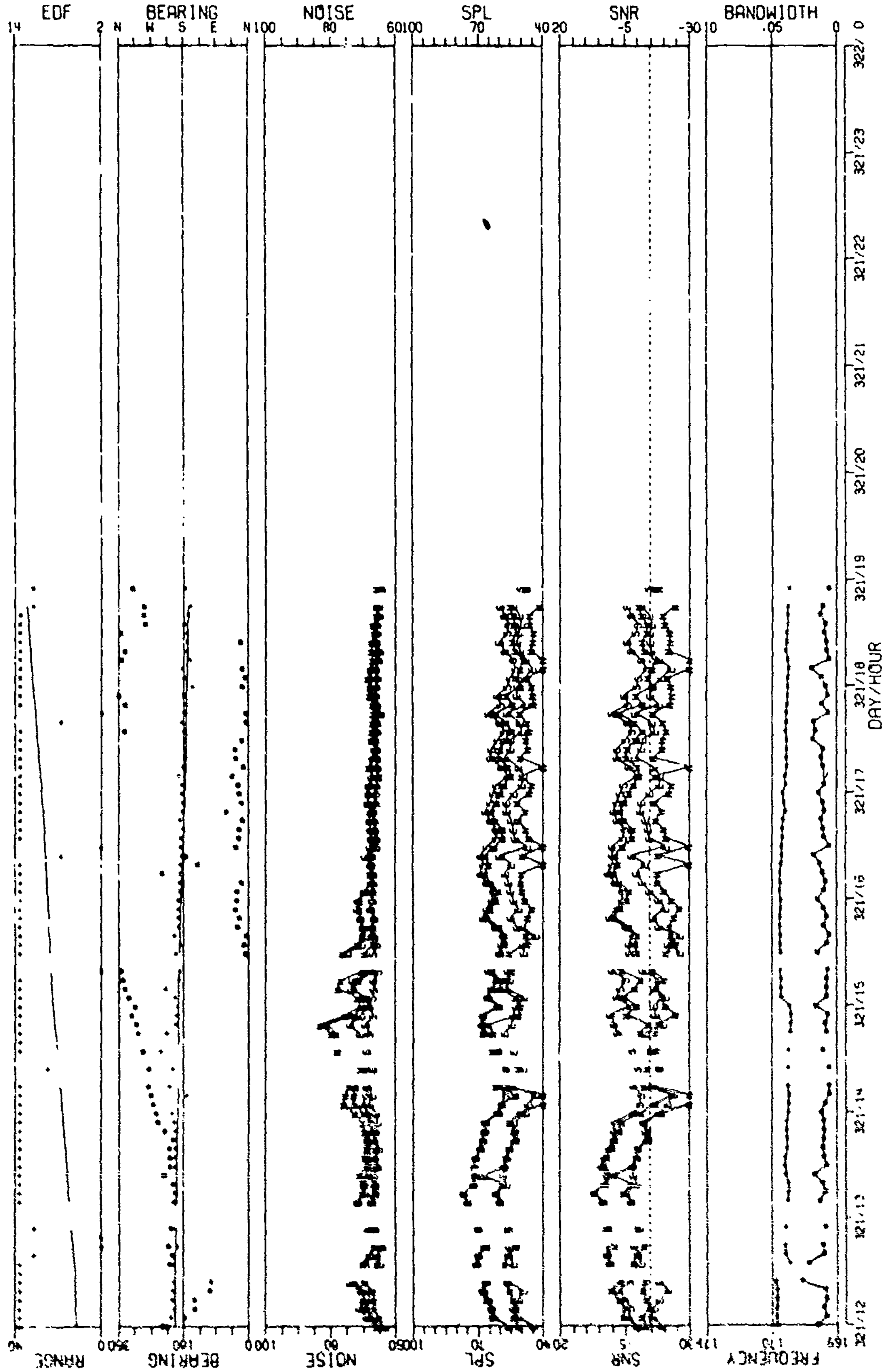

FIGURE III-88
MSS FVT 170 HZ LINE HISTORY AS OBSERVED VIA THE SINGLE CARDIOIDS SENSOR AT SITE A2 DURING THE 17 NOV FIELD EVENT WITH VERNIER RESOLUTION (U)

AS-77-2688

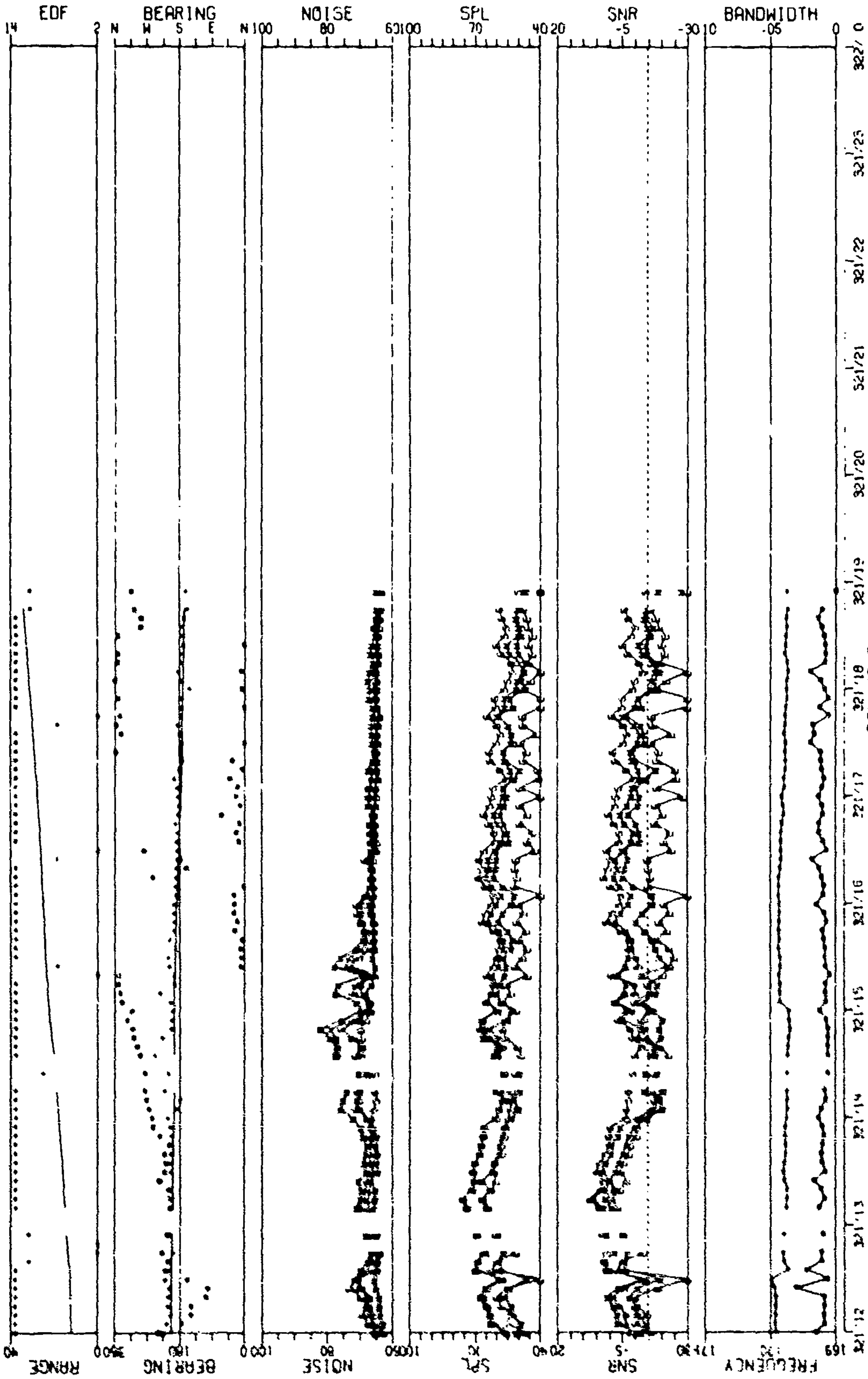

FIGURE III-89
MSS-FVT 170 HZ LINE HISTORY AS OBSERVED VIA THE MAX GAIN LIMACONS SENSOR AT SITE A2 DURING THE 17 NOV FIELD EVENT WITH VERNIER RESOLUTION (U)

AS-77-2689

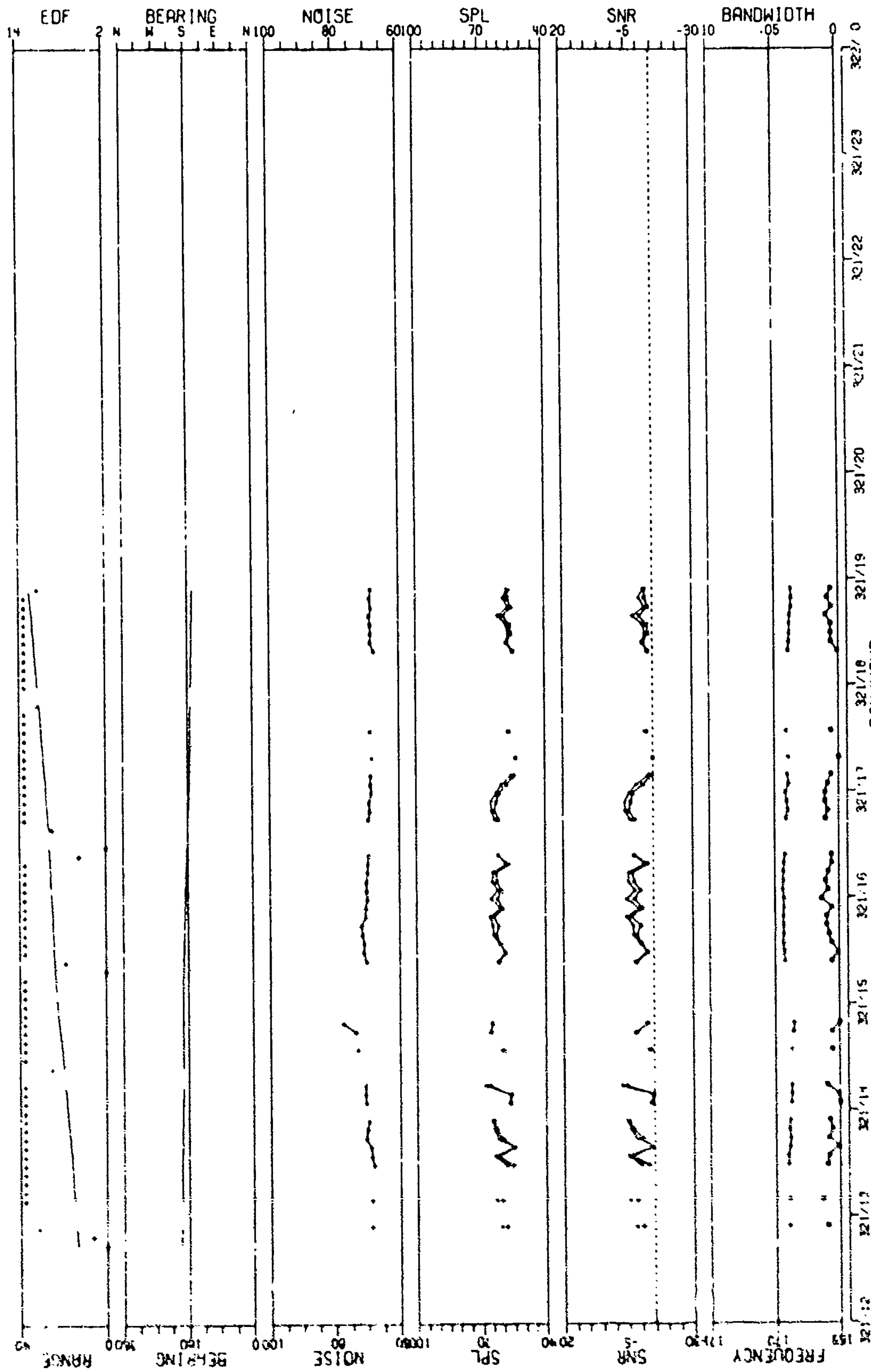

FIGURE III-90
MSS-FVT 170 HZ LINE HISTORY AS OBSERVED VIA THE VERTICAL DIPOLE SENSOR AT SITE A2 DURING THE 17 NOV FIELD EVENT WITH VERNIER RESOLUTION (U)

AS-77-2690

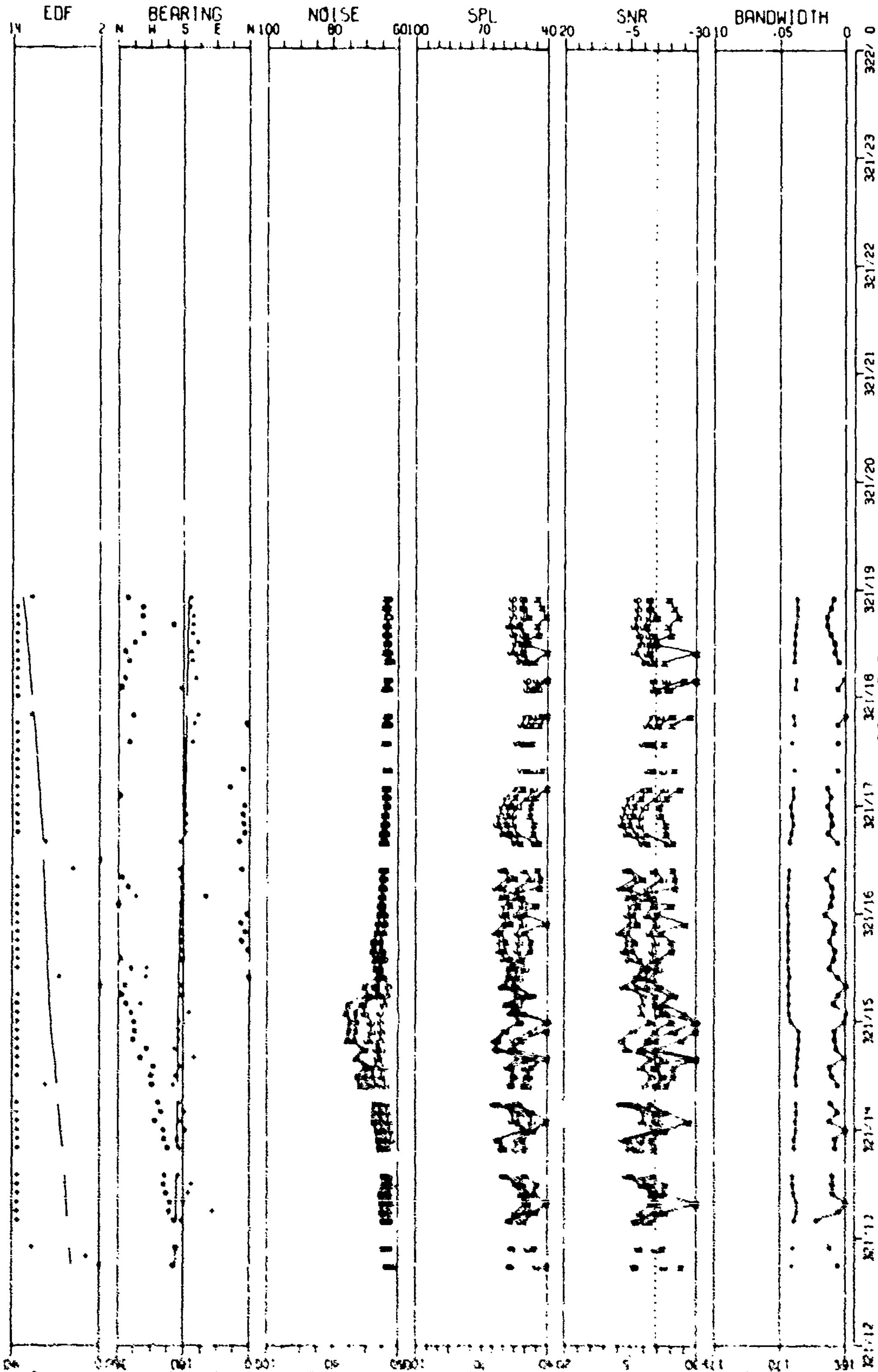

FIGURE III-91
MSS-FVT 170 HZ LINE HISTORY AS OBSERVED VIA THE DIFFERENCED CARDIOIDS SENSOR AT SITE A2 DURING THE 17 NOV FIELD EVENT WITH VERNIER RESOLUTION (U)

AS-77-2691

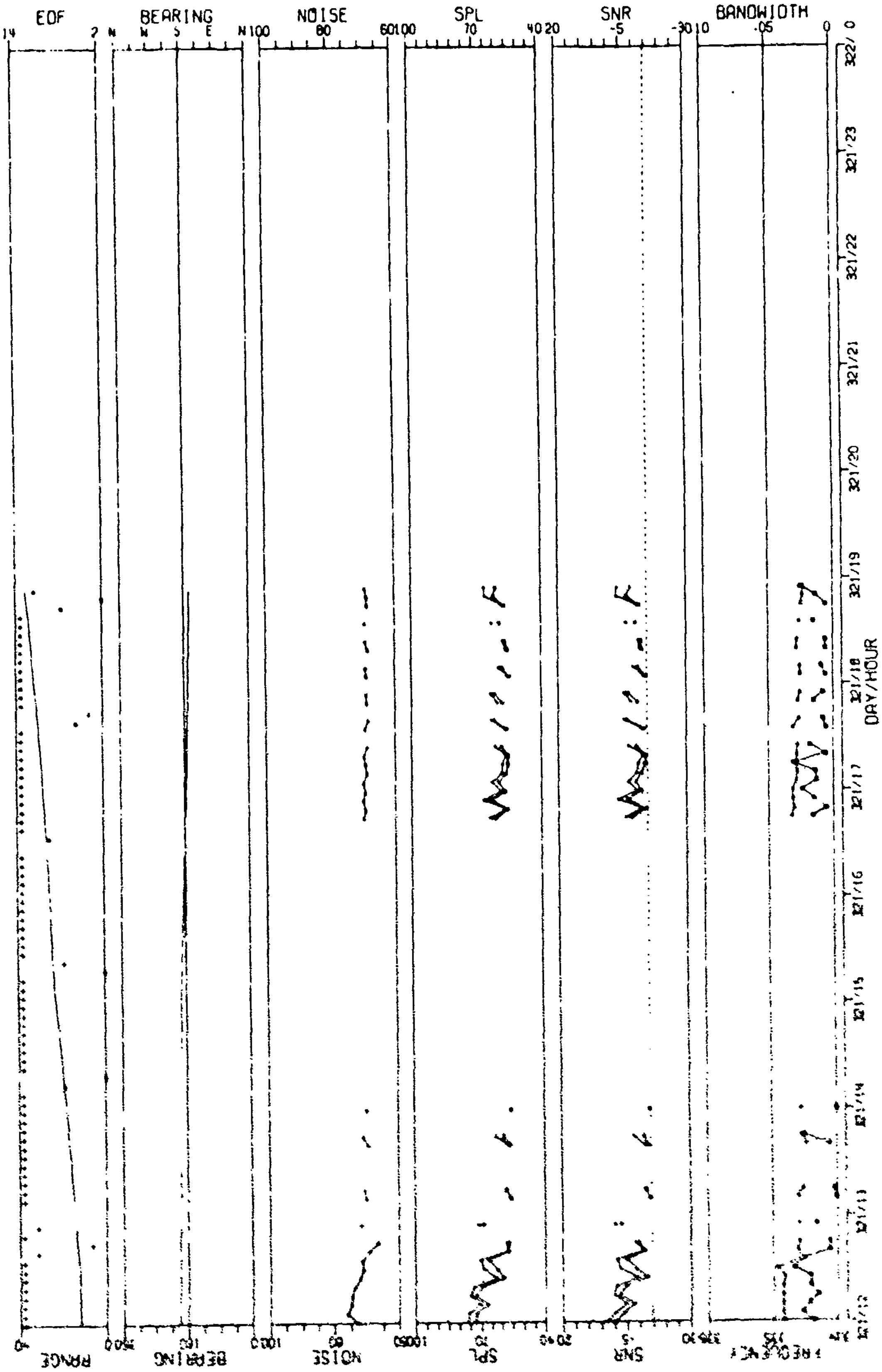

FIGURE III-92
[illegible] EVT 135 HZ LINE HISTORY AS OBSERVED VIA THE OMNIDIRECTIONAL SENSOR
AT [illegible] HZ DURING THE 1[illegible] NOV FIELD EVENT WITH VERNIER RESOLUTION (U)

AS-77-2692

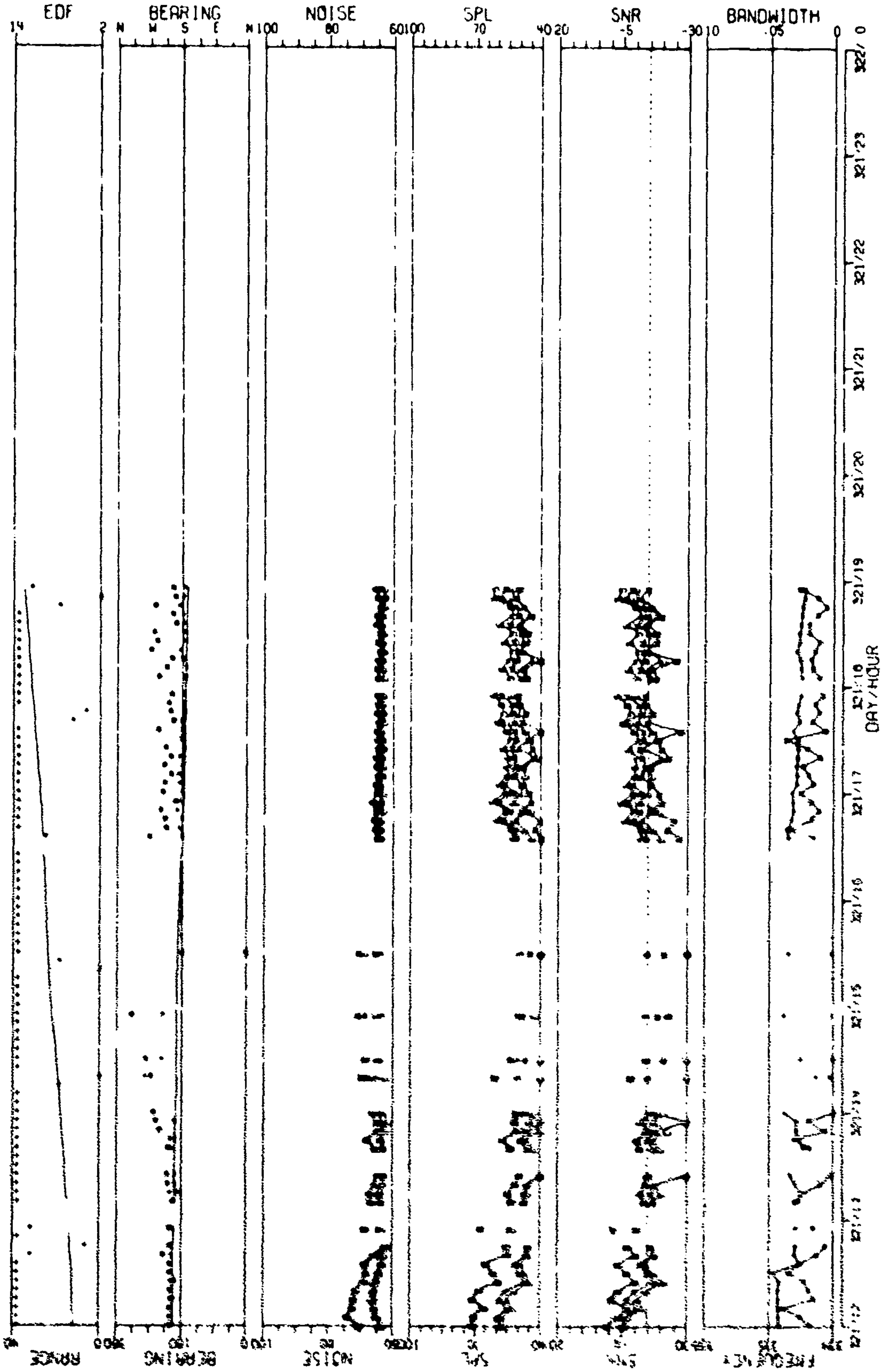

FIGURE III-93
MSS-KYT 375 HZ LINE HISTORY AS OBSERVED VIA THE SINGLE CARDIOIDS SENSOR
AT SITE A2 DURING THE 17 NOV FIELD EVENT WITH VERNIER RESOLUTION (U)

AS-77-2693

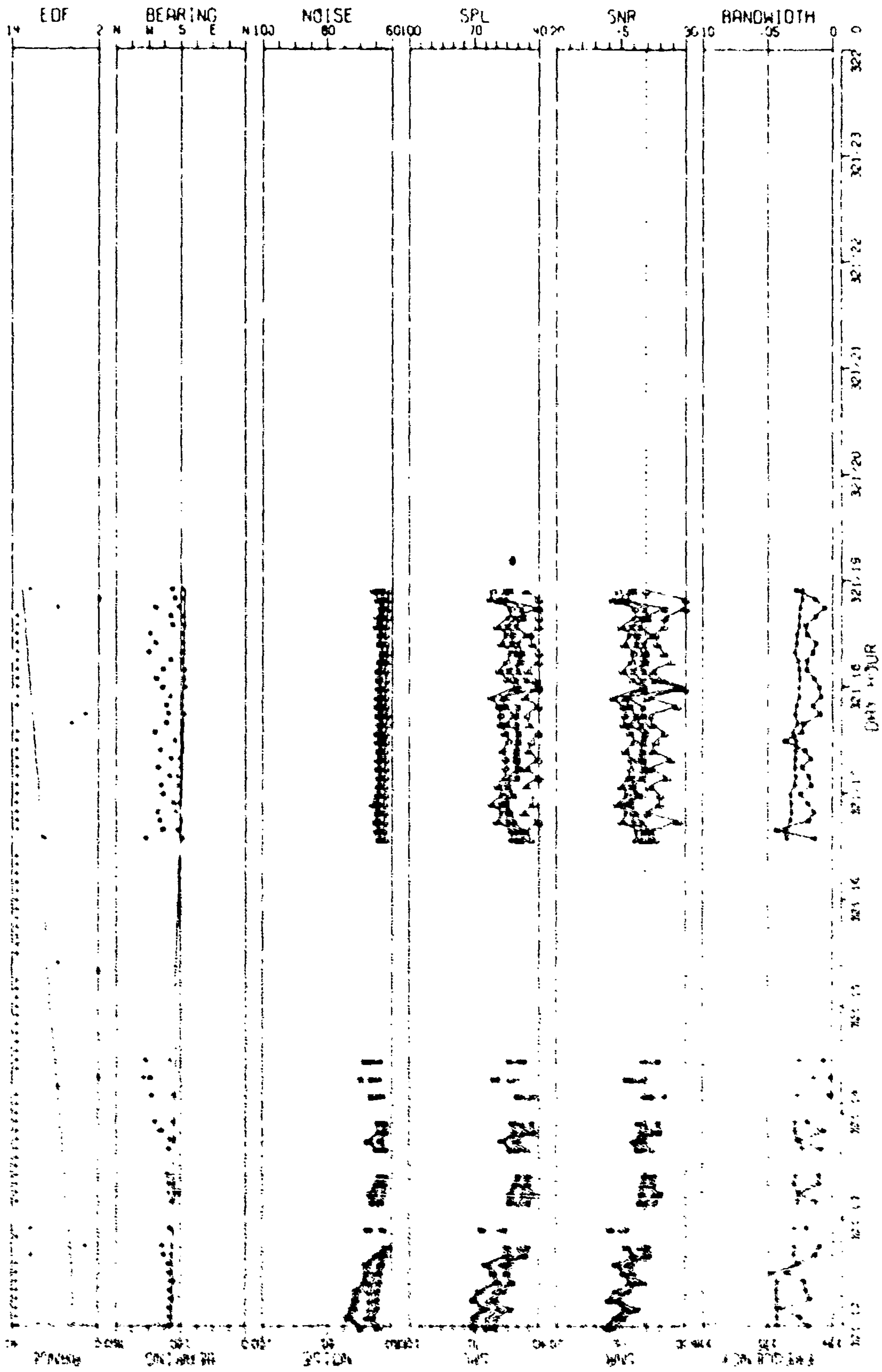

FIGURE III-94
375 HZ LINE HISTORY AS OBSERVED VIA THE MAX GAIN LIMACONS SENSOR DURING THE IT NOT FIELD EVENT WITH VERNIER RESOLUTION 'U'

AS-77-2694

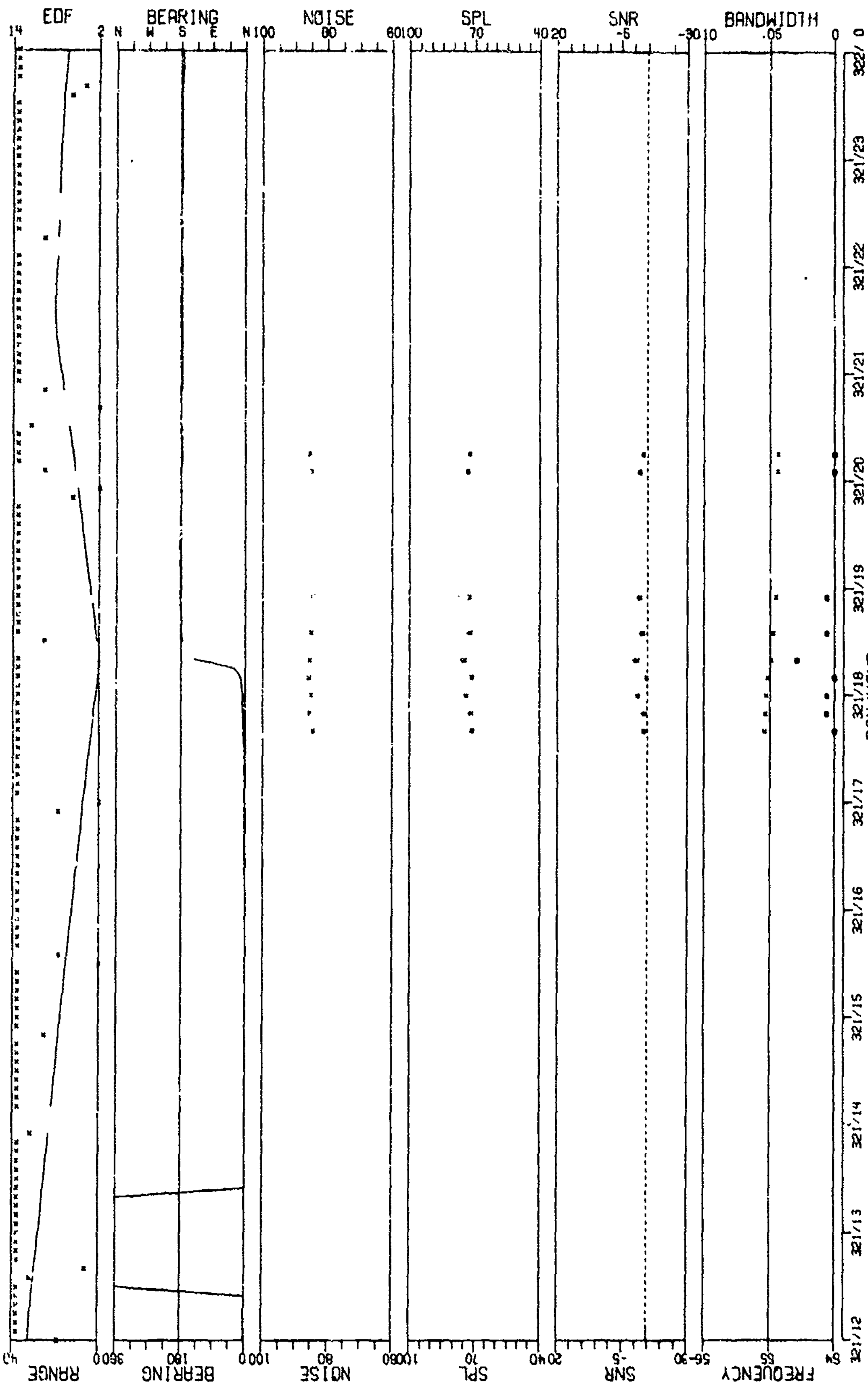

FIGURE III-95
MSS-FVT 55 HZ LINE HISTORY AS OBSERVED VIA THE OMNIDIRECTIONAL SENSOR AT SITE A3 DURING THE 17 NOV FIELD EVENT WITH VERNIER RESOLUTION (U)

AS-77-2695

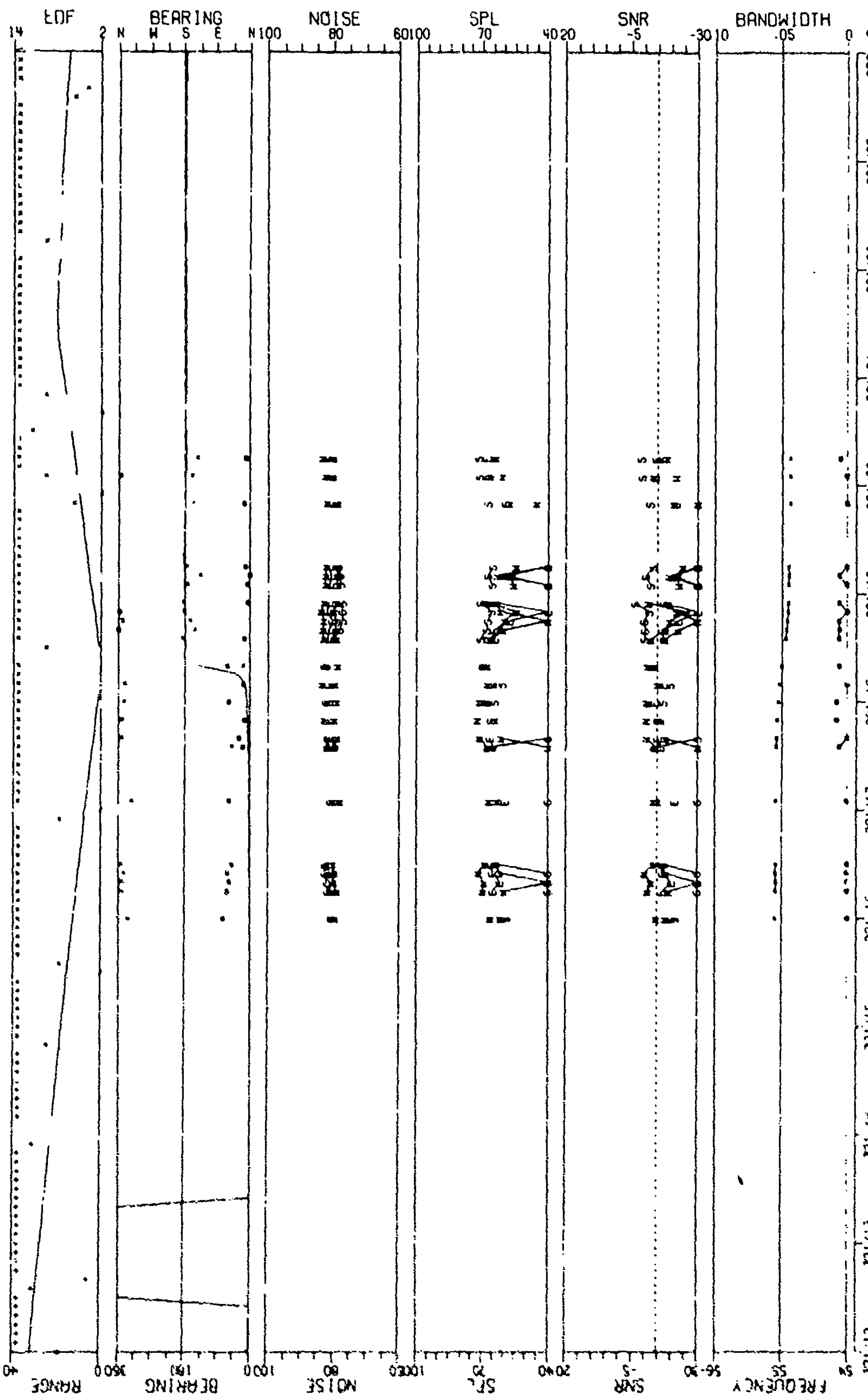

FIGURE III-96
MSS-FVT 55 HZ LINE HISTORY AS OBSERVED VIA THE SINGLE CARDIOIDS SENSOR AT SITE A3 DURING THE 17 NOV FIELD EVENT WITH VERNIER RESOLUTION (U)

AS-77-2696

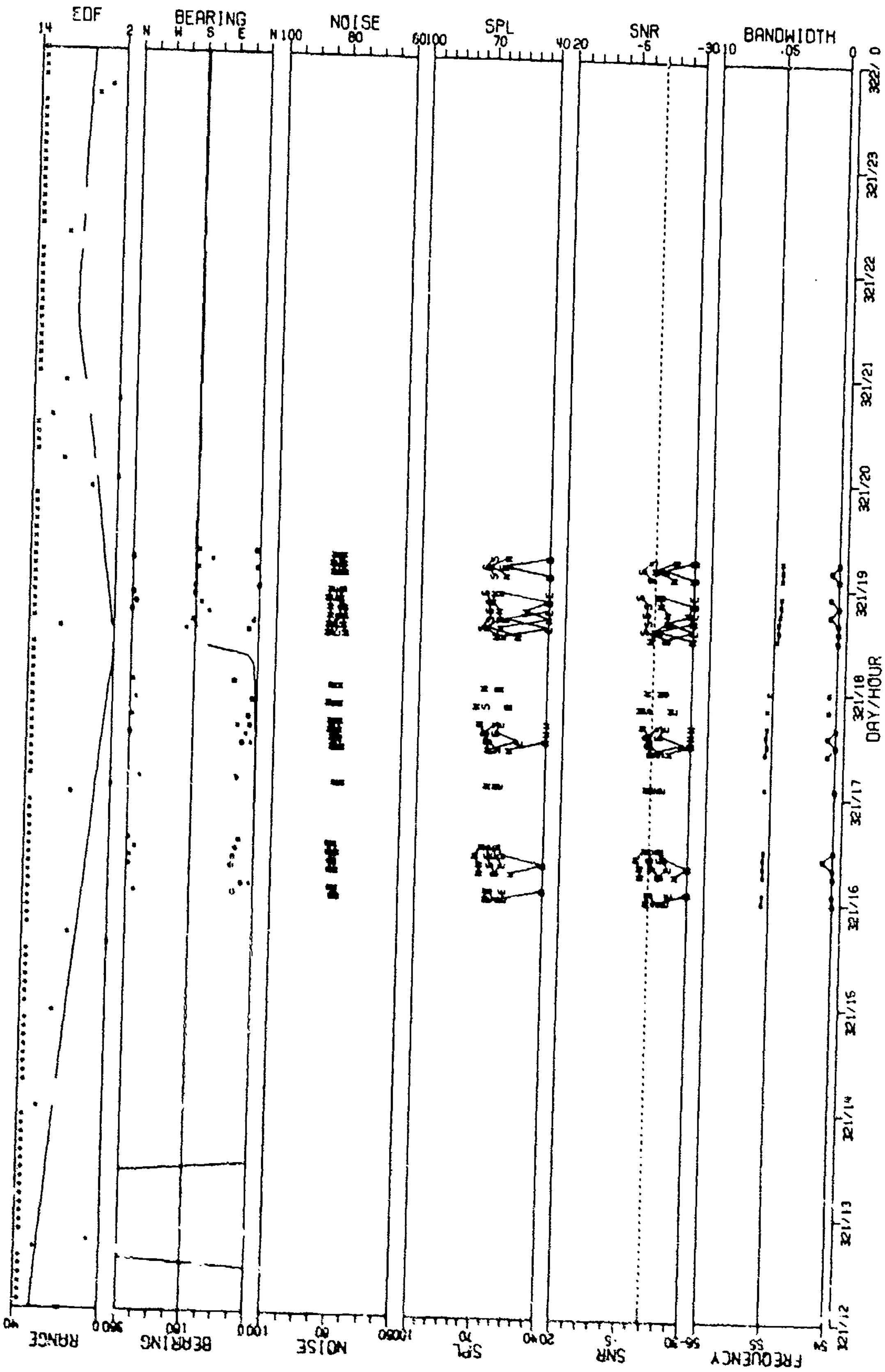

FIGURE III-97
MSS-FVT 55 HZ LINE HISTORY AS OBSERVED VIA THE MAX GAIN LIMACONS SENSOR AT SITE A3 DURING THE 17 NOV FIELD EVENT WITH VERNIER RESOLUTION (U)

AS-77-2697

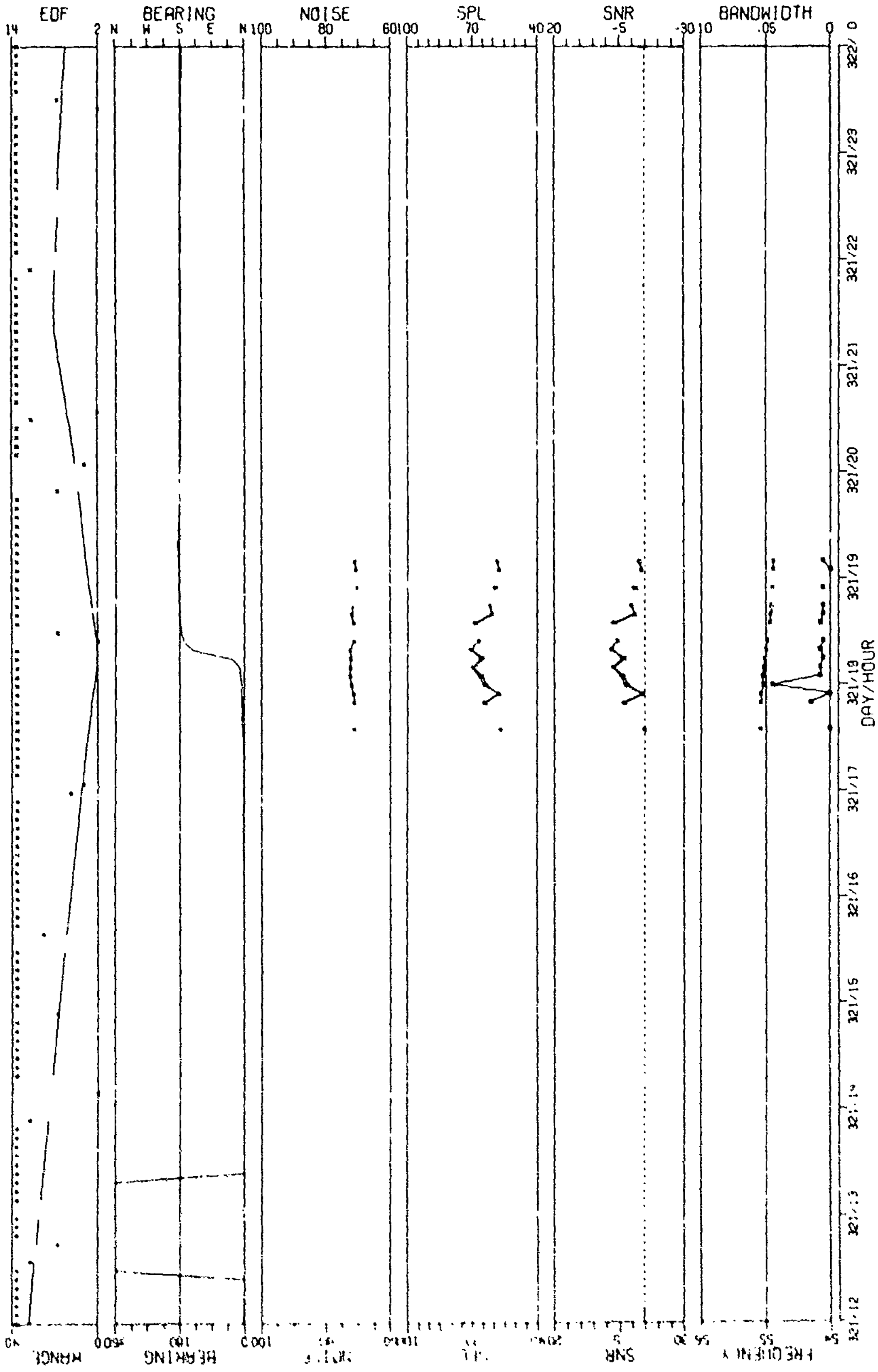

FIGURE III-98
MSS-FVT 55 HZ LINE HISTORY AS OBSERVED VIA THE VERTICAL DIPOLE SENSOR
AT SITE A3 DURING THE 17 NOV FIELD EVENT WITH VERNIER RESOLUTION (U)

AS-77-2698

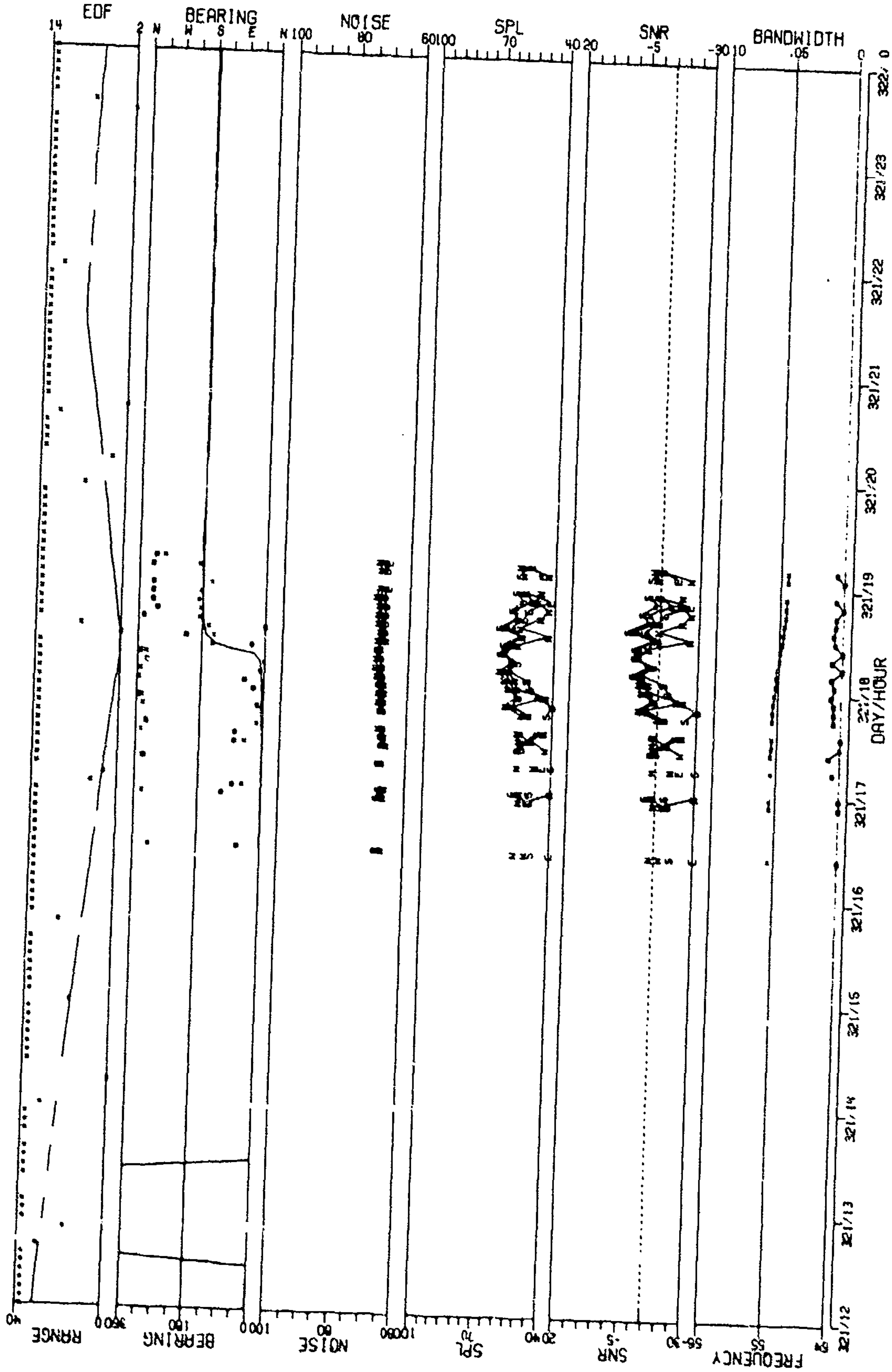

FIGURE III-99
MSS-FVT 55 HZ LINE HISTORY AS OBSERVED VIA THE DIFFERENCED CARDIOIDS SENSOR
AT SITE A3 DURING THE 17 NOV FIELD EVENT WITH VERNIER RESOLUTION (U)

AS-77-2699

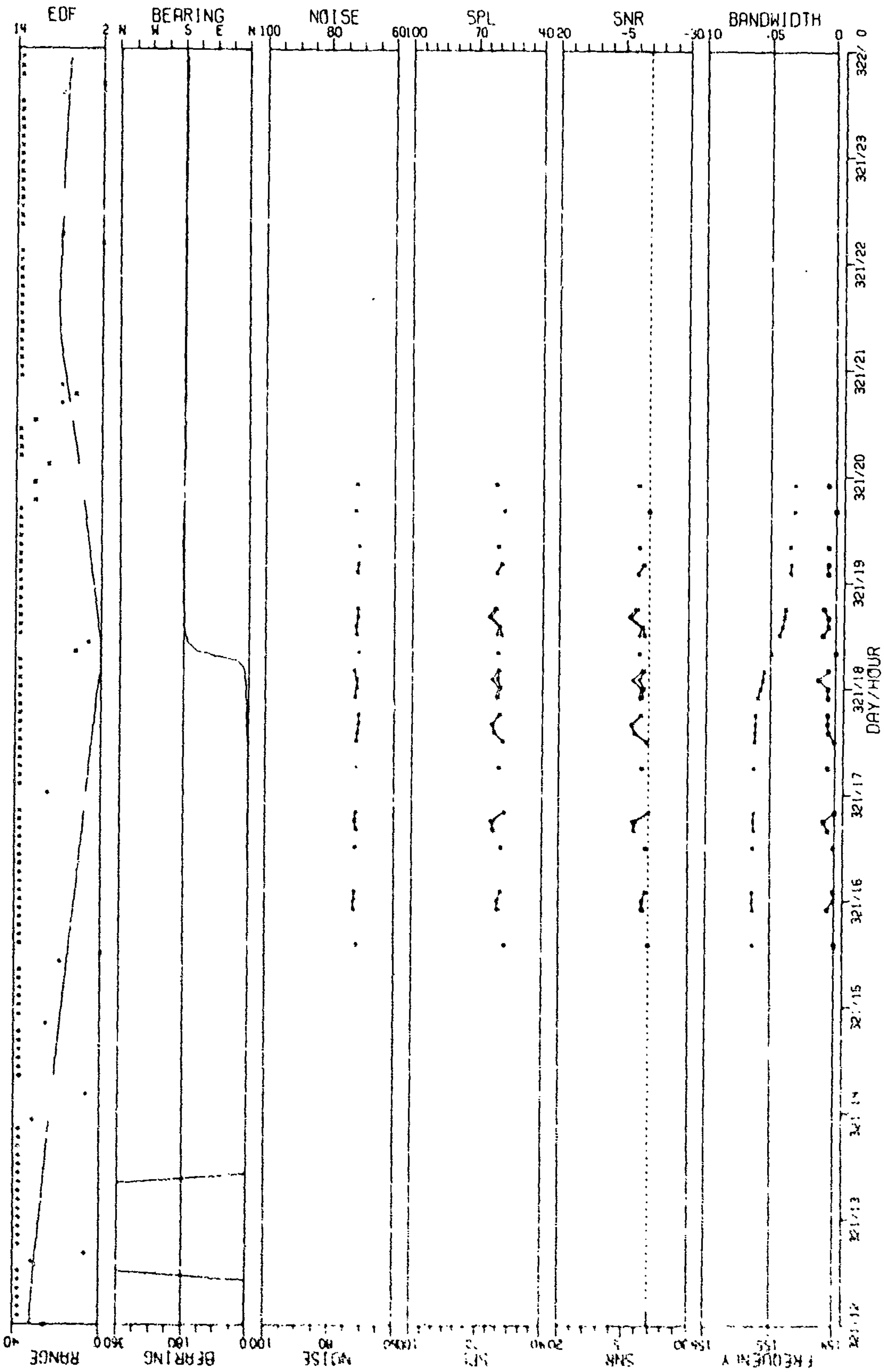

FIGURE III-100
M35-FWT 155 HZ LINE HISTORY AS OBSERVED VIA THE OMNIDIRECTIONAL SENSOR AT SITE A3 DURING THE 17 NOV FIELD EVENT WITH VERNIER RESOLUTION (U)

AS-77-2700

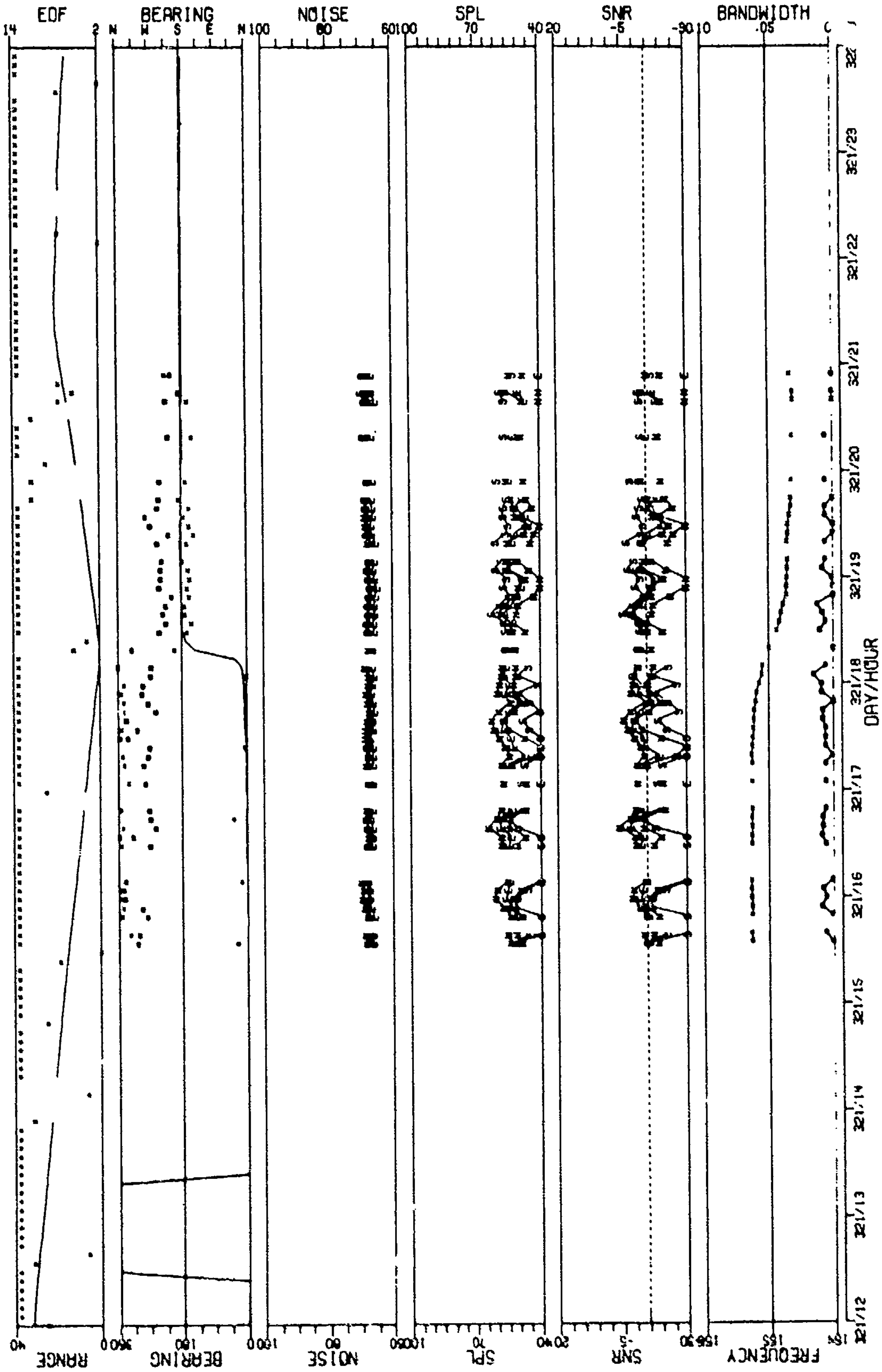

FIGURE III-101
MSS-FVT 155 HZ LINE HISTORY AS OBSERVED VIA THE SINGLE CARDIOIDS SENSOR AT SITE A3 DURING THE 17 NOV FIELD EVENT WITH VERNIER RESOLUTION (U)

AS-77-2701

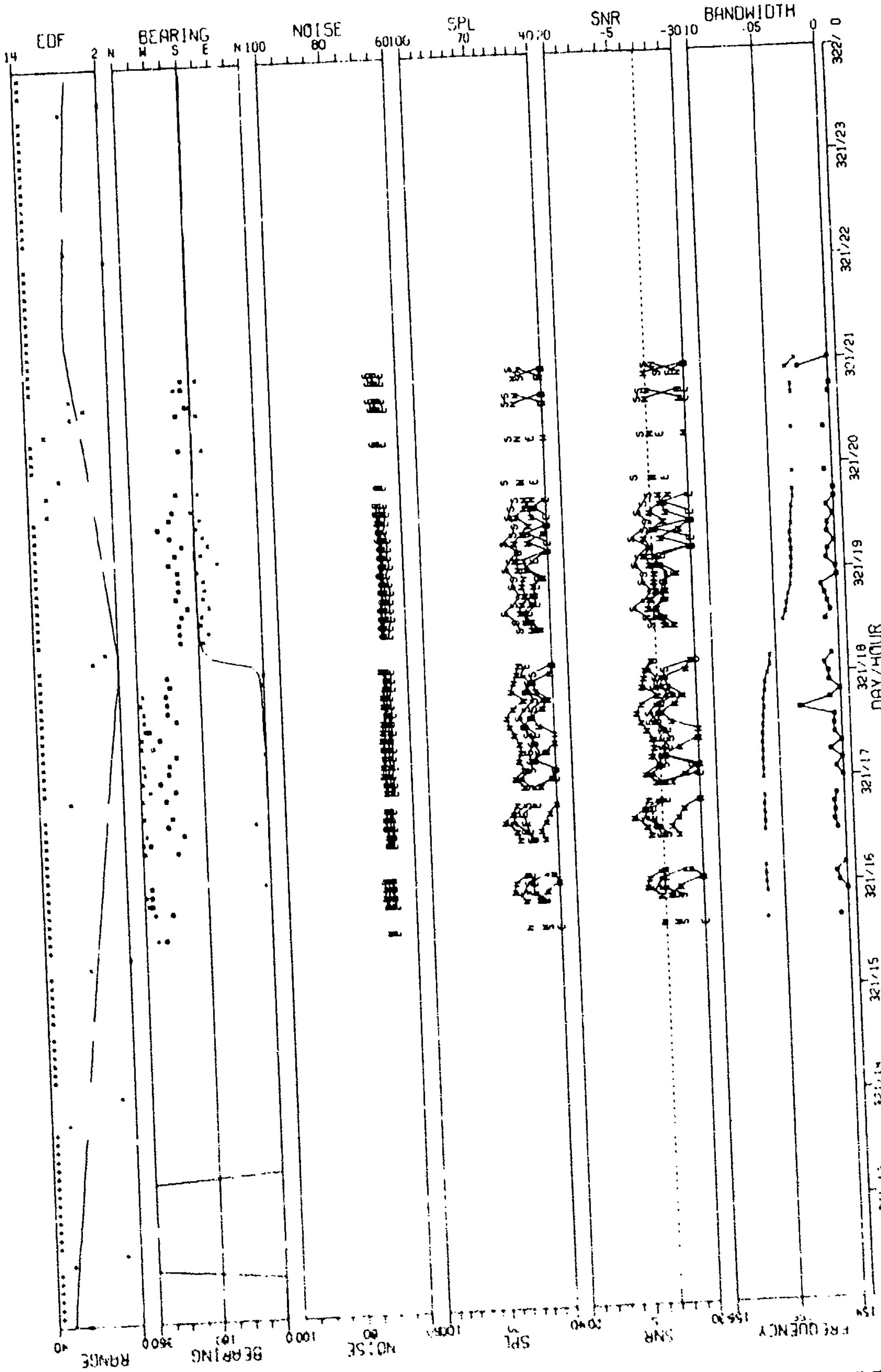

FIGURE III-102
MSS-F/T 155 HZ LINE HISTORY AS OBSERVED VIA THE MAX GAIN LIMACONS SENSOR AT SITE A3 DURING THE 17 NOV FIELD EVENT WITH VERNIER RESOLUTION (U)

AS-77-2702

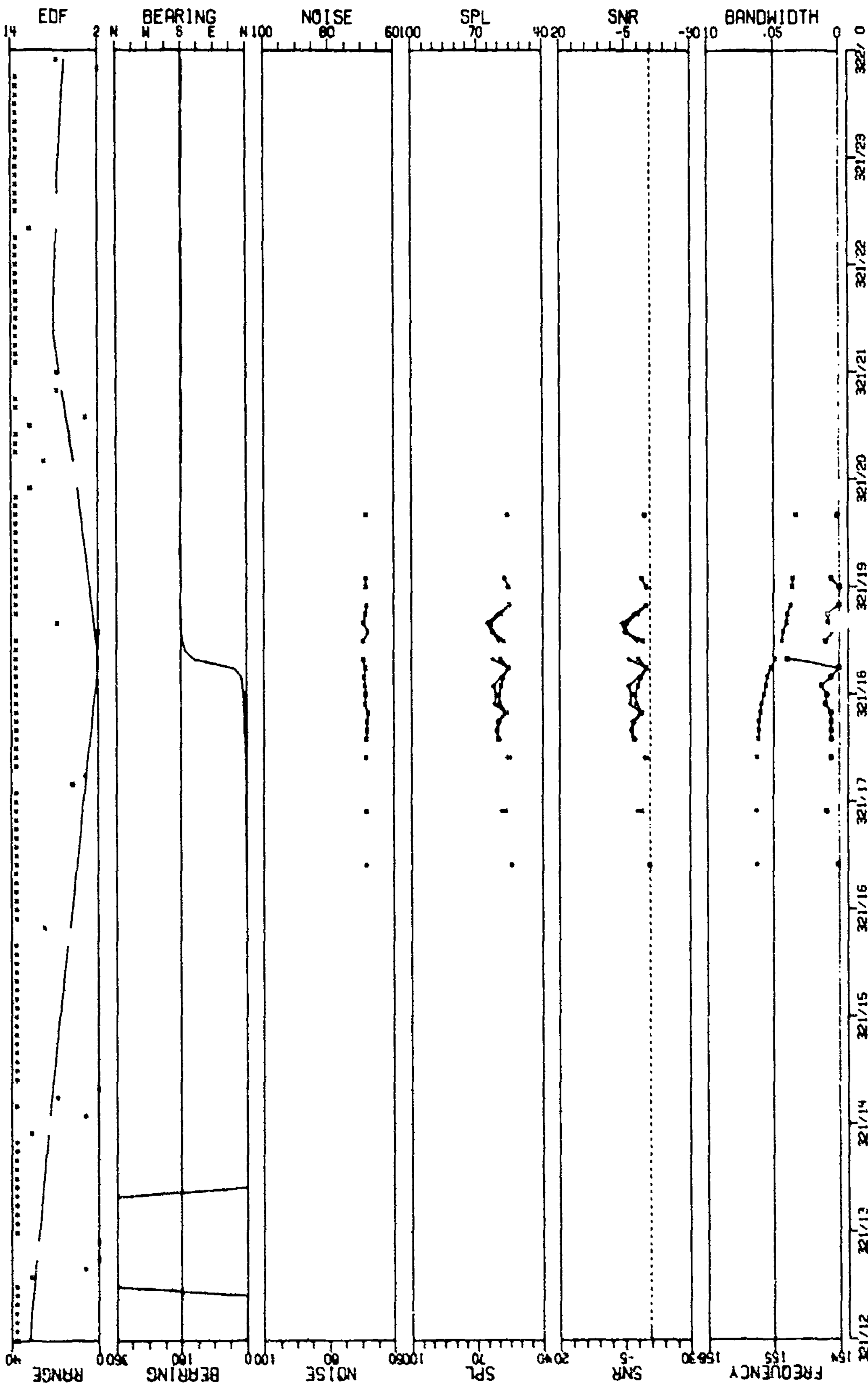

FIGURE III-103
MSS-FVT 155 HZ LINE HISTORY AS OBSERVED VIA THE VERTICAL DIPOLE SENSOR AT SITE A3 DURING THE 17 NOV FIELD EVENT WITH VERNIER RESOLUTION (U)

AS-77-2703

FIGURE III-104
MSS-FVT 155 HZ LINE HISTORY AS OBSERVED VIA THE DIFFERENCED CARDIOIDS SENSOR AT SITE A3 DURING THE 17 NOV FIELD EVENT WITH VERNIER RESOLUTION (U)

AS-77-2704

FIGURE III-105
MSS-FVT 305 HZ LINE HISTORY AS OBSERVED VIA THE OMNIDIRECTIONAL SENSOR AT SITE A3 DURING THE 17 NOV FIELD EVENT WITH VERNIER RESOLUTION (U)

AS-77-2705

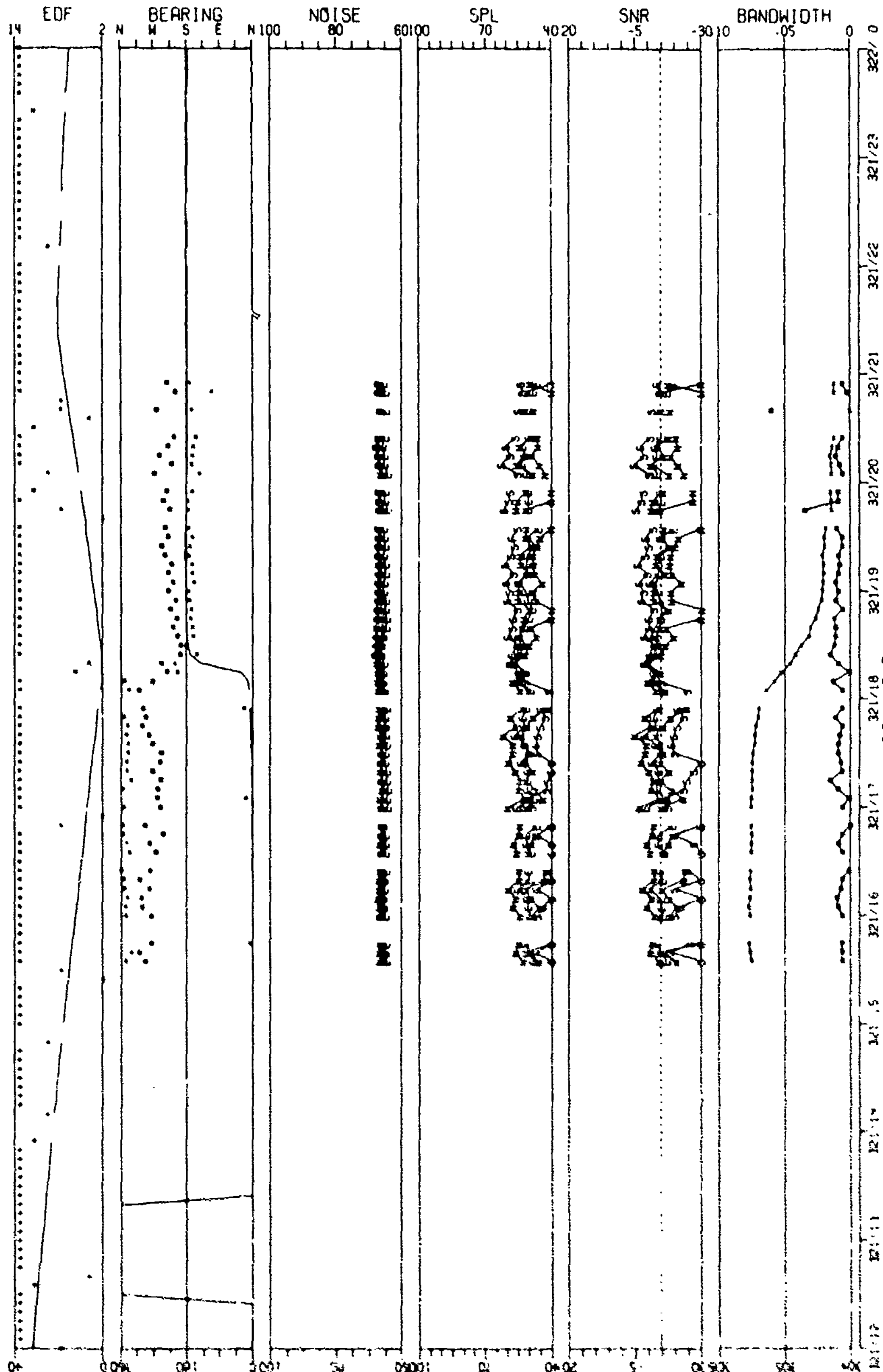

FIGURE III-106
MSS-FVT 305 HZ LINE HISTORY AS OBSERVED VIA THE SINGLE CARDIOIDS SENSOR AT SITE A3 DURING THE 17 NOV FIELD EVENT WITH VERNIER RESOLUTION (U)

AS-77-2706

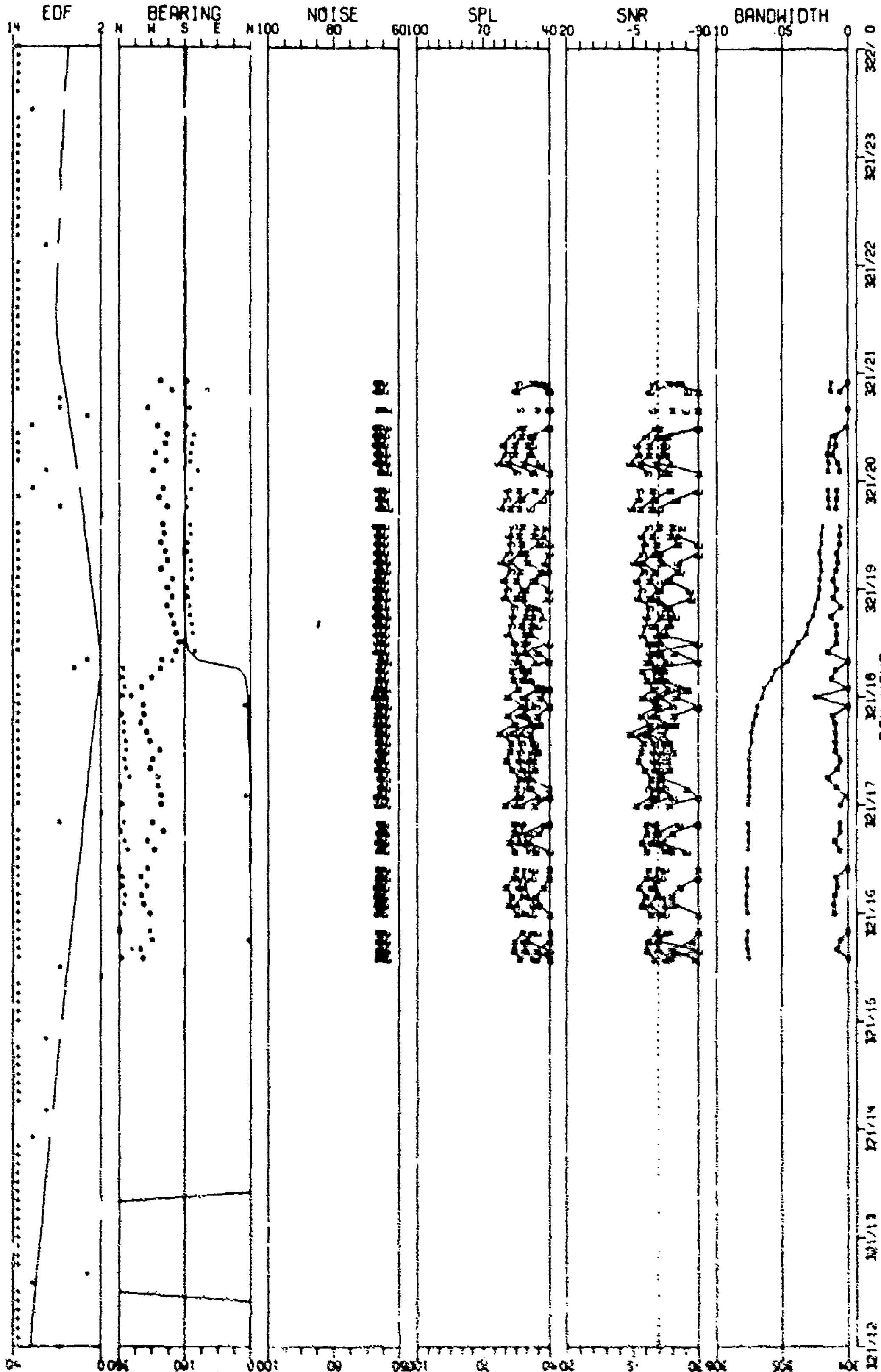

FIGURE III-107
M3S-FVT 305 HZ LINE HISTORY AS OBSERVED VIA THE MAX GAIN LIMACONS SENSOR AT SITE A3 DURING THE 17 NOV FIELD EVENT WITH VERNIER RESOLUTION (U)

AS-77-2707

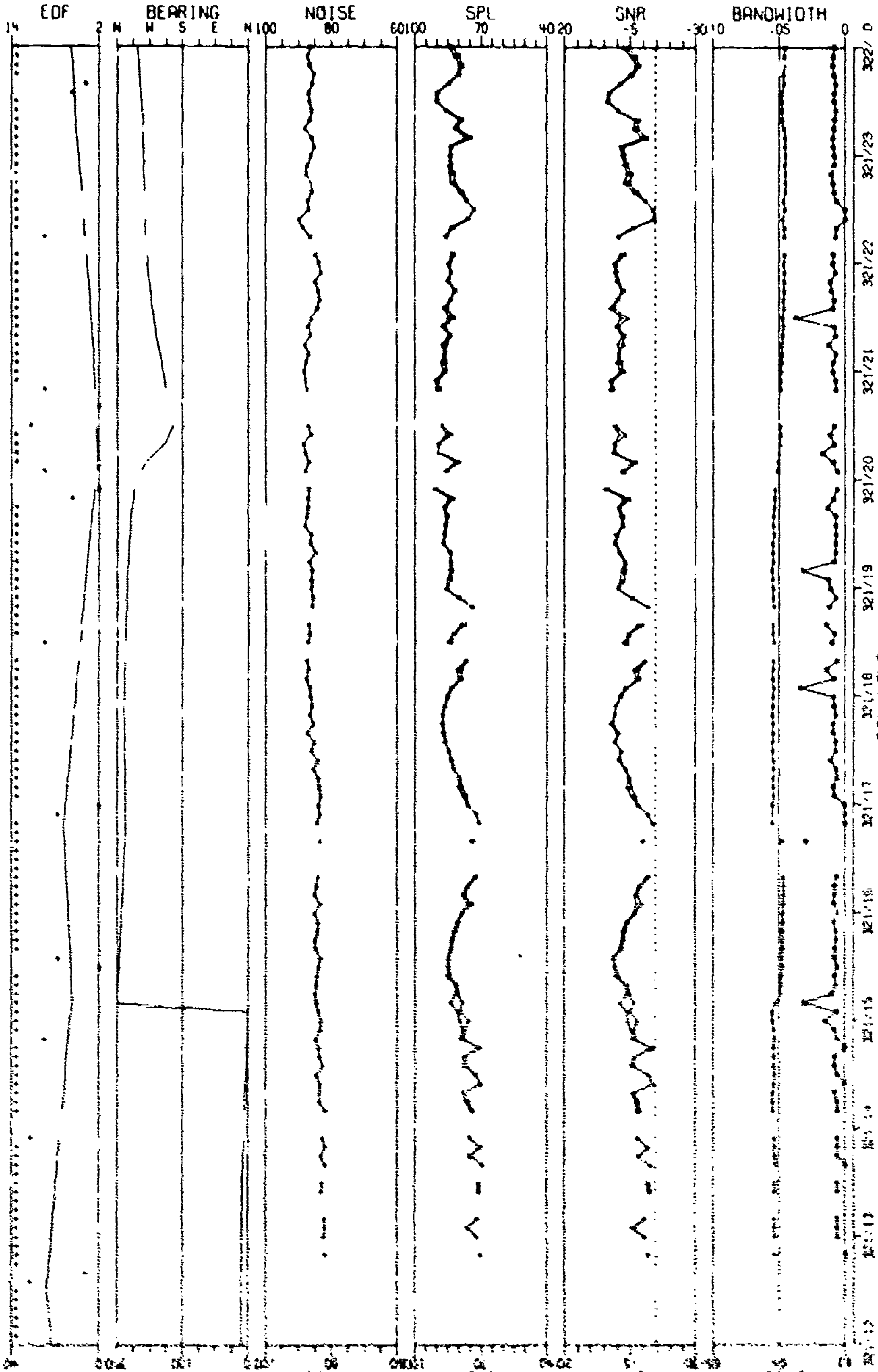

FIGURE III-108
MSS-FYT 64 HZ LINE HISTORY AS OBSERVED VIA THE OMNIDIRECTIONAL SENSOR AT SITE #3 DURING THE 17 NOV FIELD EVENT WITH VERNIER RESOLUTION (U)

AS-77-2708

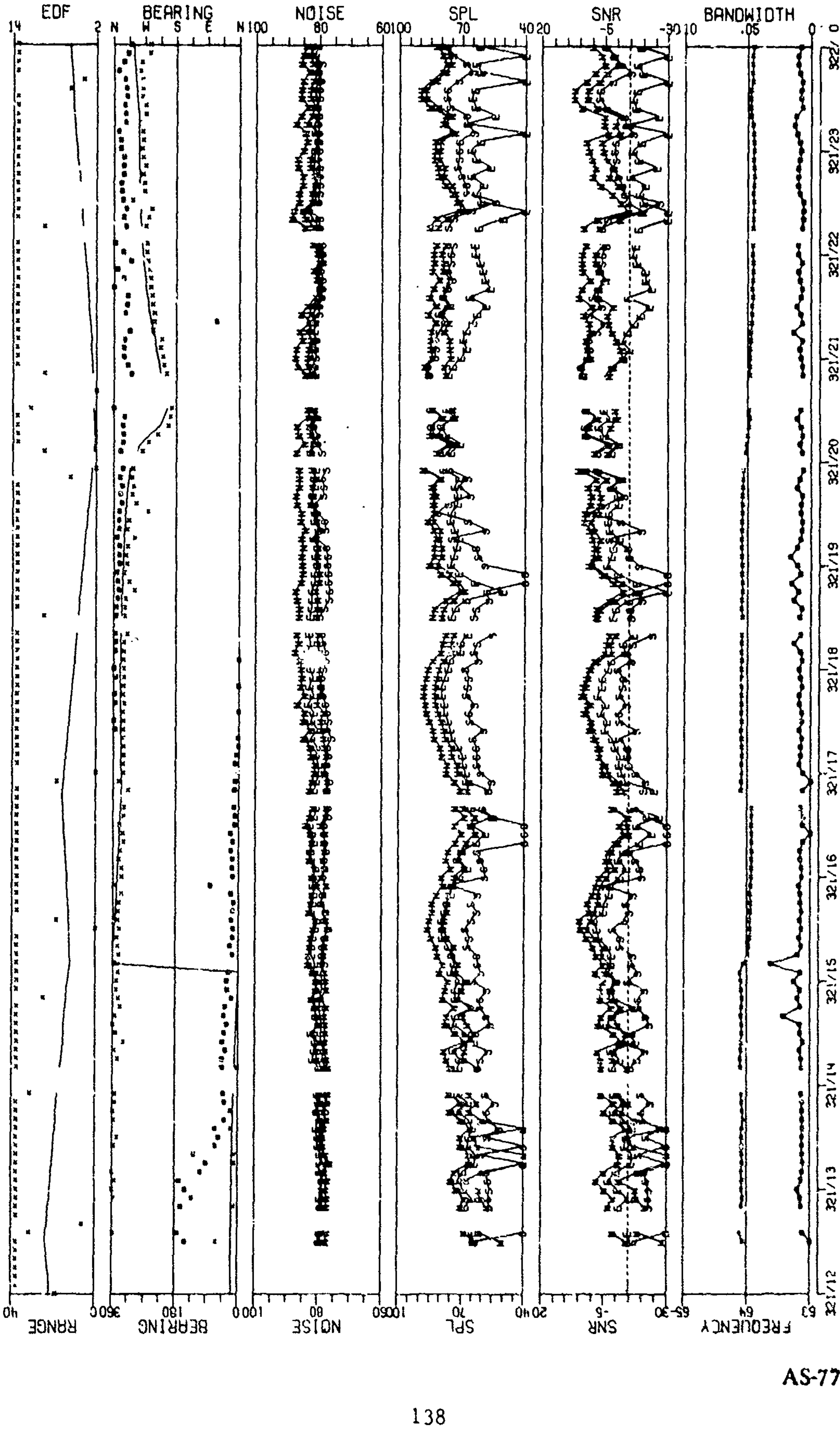

FIGURE III-109
MSS-FVI 64 HZ LINE HISTORY AS OBSERVED VIA THE SINGLE CARDIOIDS SENSOR
AT SITE A3 DURING THE 17 NOV FIELD EVENT WITH VERNIER RESOLUTION (U)

AS-77-2709

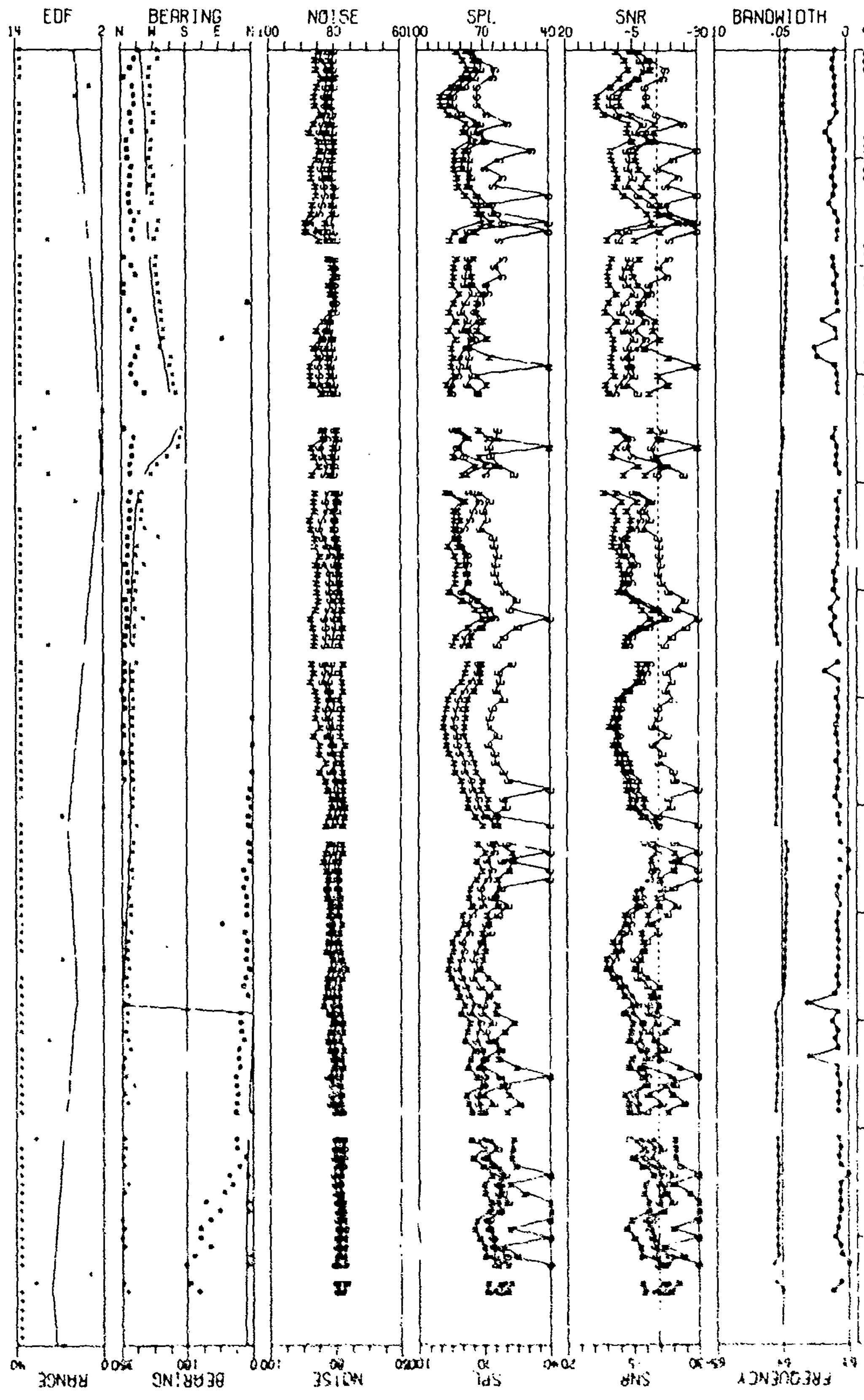

FIGURE III-110
MSS-FVT 64 HZ LINE HISTORY AS OBSERVED VIA THE MAX GAIN LIMACONS SENSOR
AT SITE A3 DURING THE 17 NOV FIELD EVENT WITH VERNIER RESOLUTION (U)

AS-77-2710

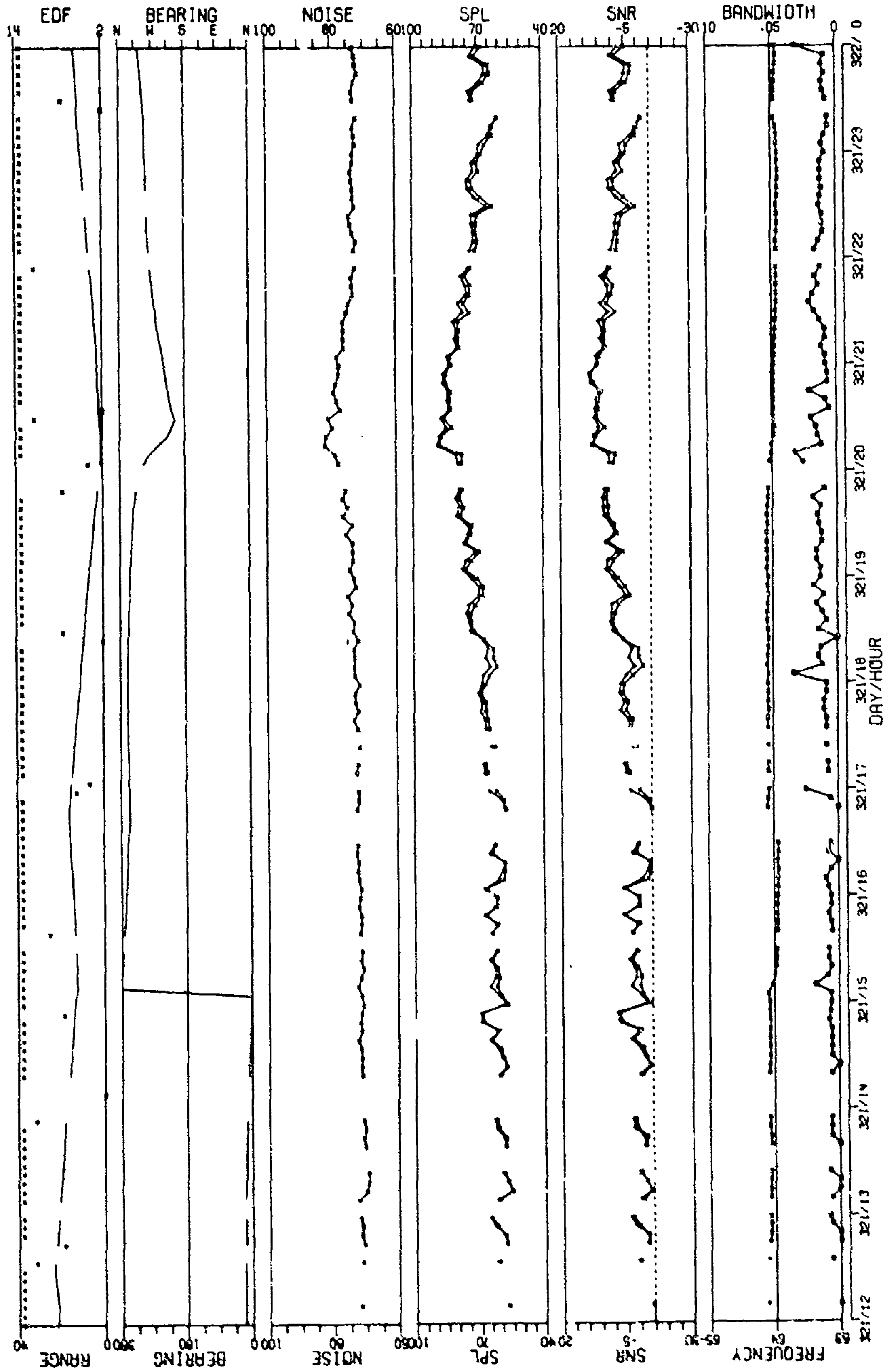

FIGURE III-111
MSS-FVT 64 HZ LINE HISTORY AS OBSERVED VIA THE VERTICAL DIPOLE SENSOR AT SITE A3 DURING THE 17 NOV FIELD EVENT WITH VERNIER RESOLUTION (U)

AS-77-2711

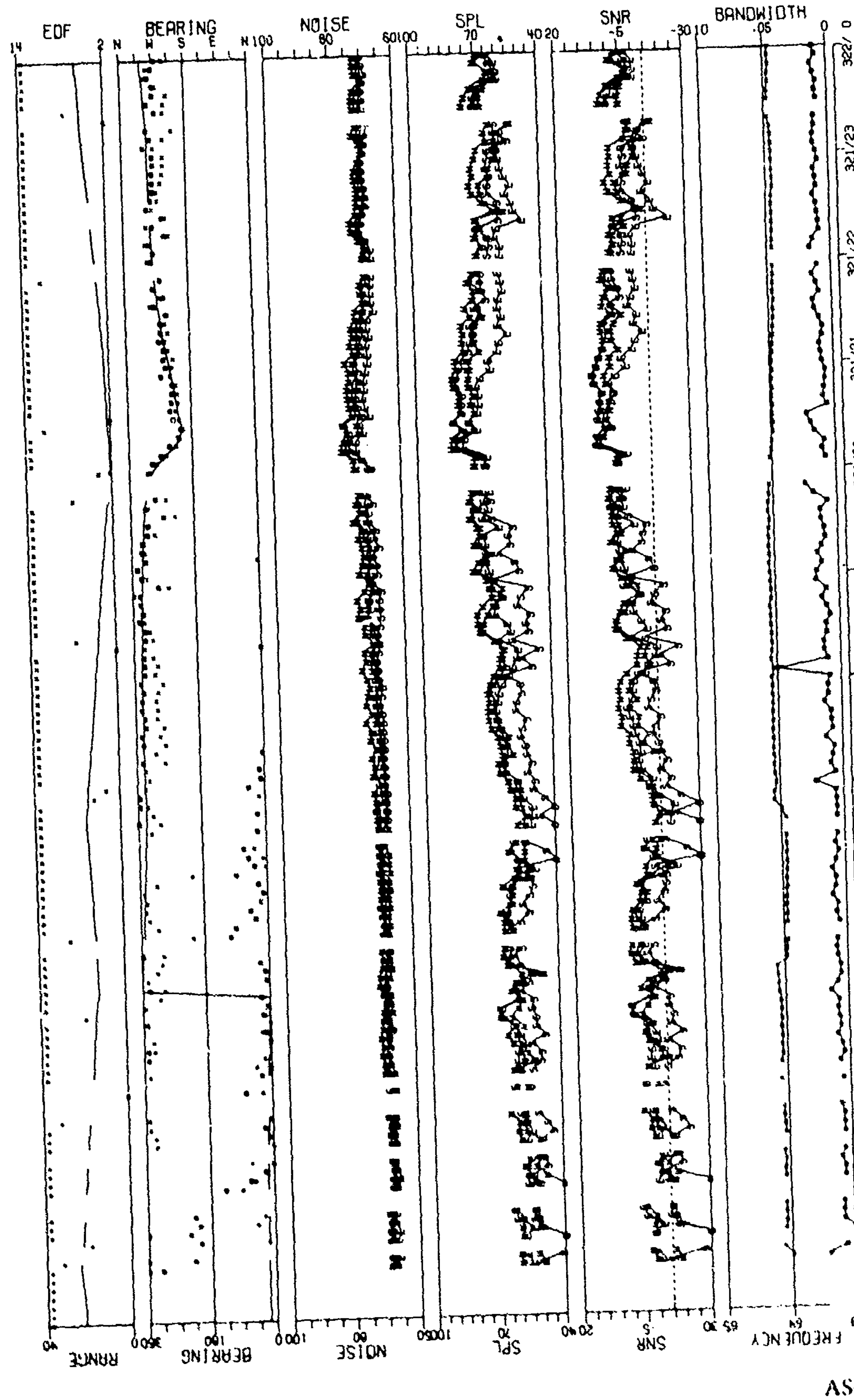

FIGURE III-112
MSS-FVT 64 HZ LINE HISTORY AS OBSERVED VIA THE DIFFERENCED CARDIOIDS SENSOR AT SITE A3 DURING THE 17 NOV FIELD EVENT WITH VERNIER RESOLUTION (U)

AS-77-2712

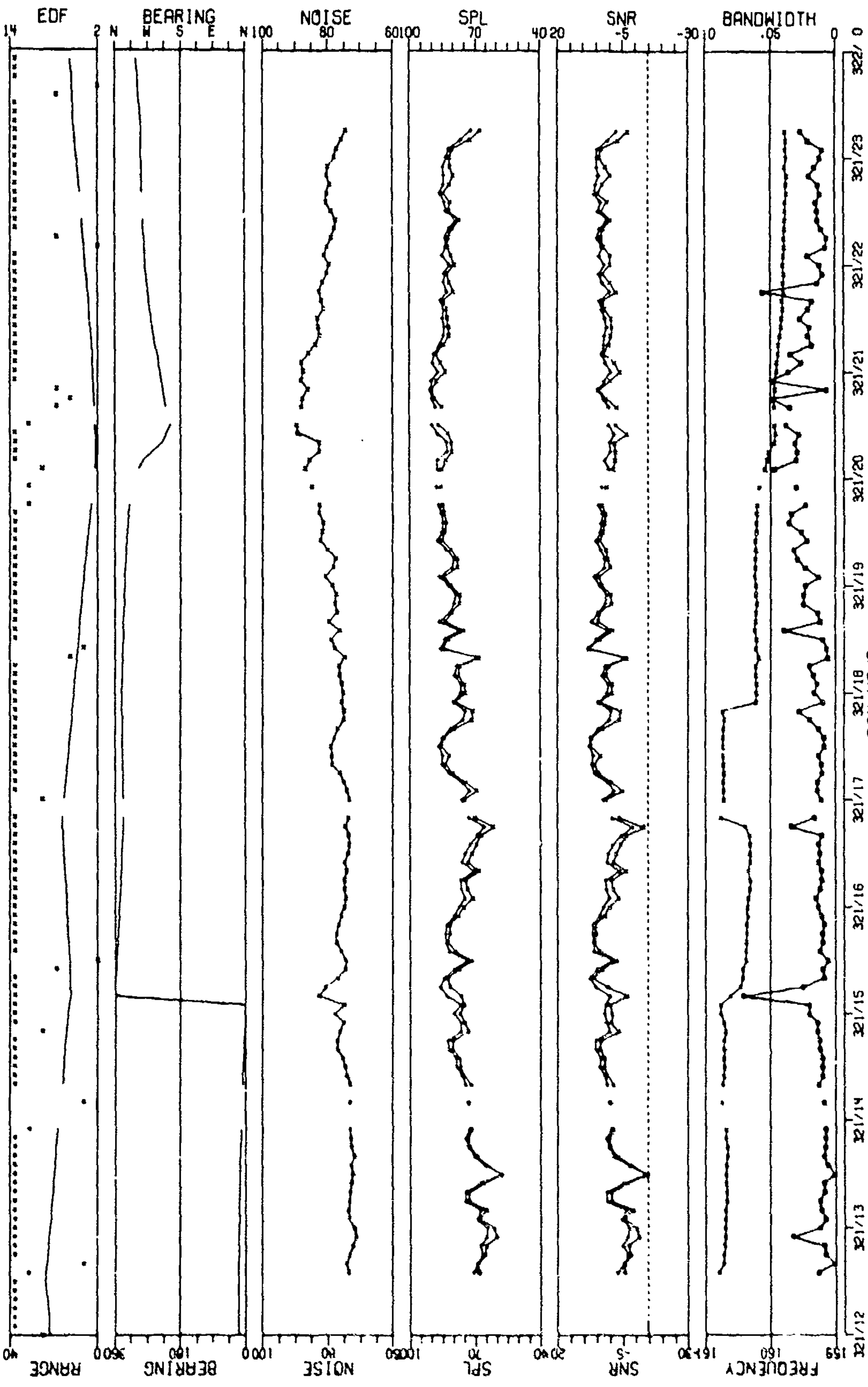

FIGURE III-113
MSS-FVT 160 HZ LINE HISTORY AS OBSERVED VIA THE OMNIDIRECTIONAL SENSOR AT SITE A3 DURING THE 17 NOV FIELD EVENT WITH VERNIER RESOLUTION (U)

AS-77-2713

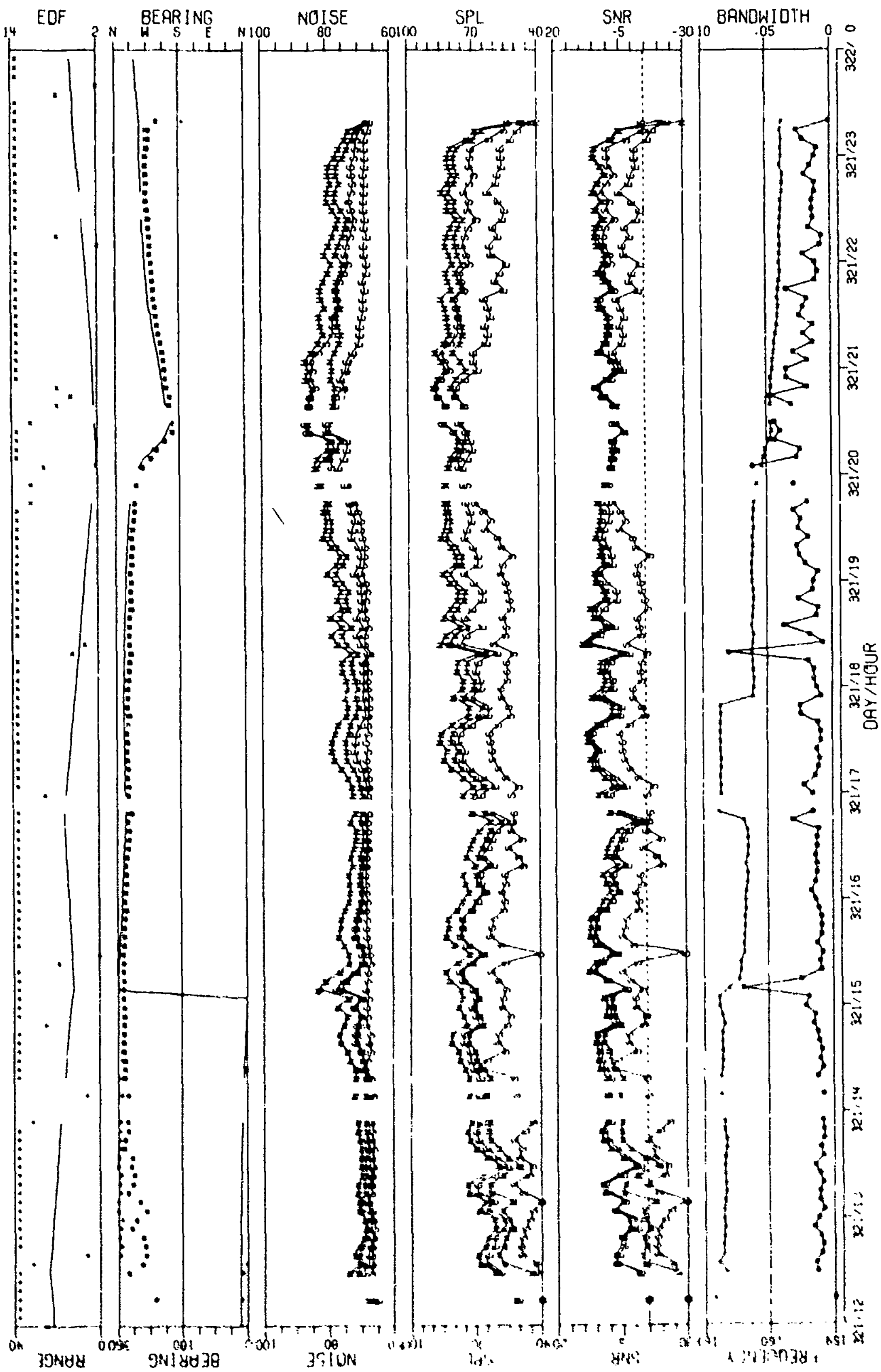

FIGURE III-114
MSS-F/T 160 HZ LINE HISTORY AS OBSERVED VIA THE SINGLE CARDIOIDS SENSOR
AT SITE A3 DURING THE 17 NOV FIELD EVENT WITH VERNIER RESOLUTION (U)

AS-77-2714

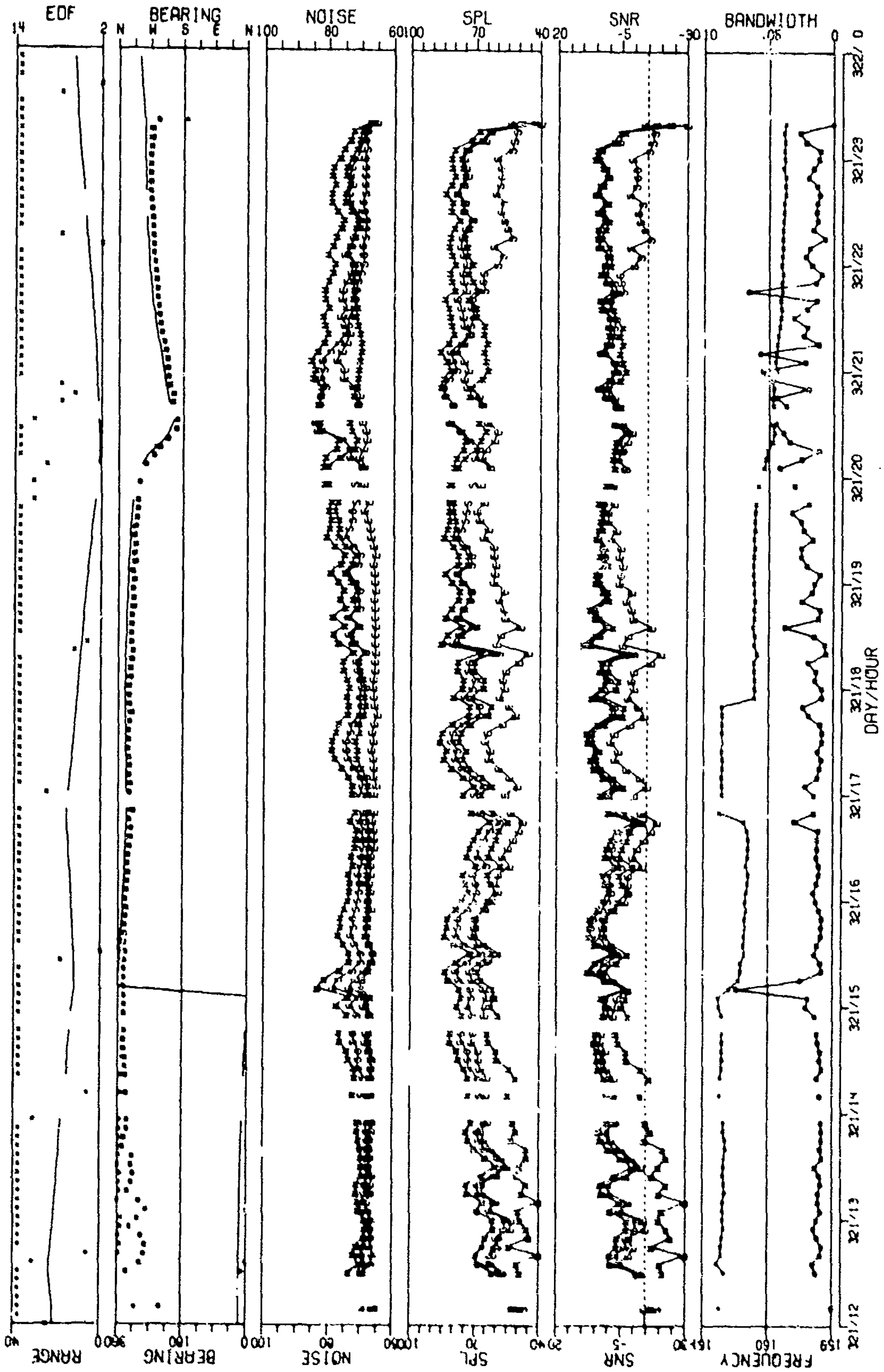

FIGURE III-115
MSS-FVT 160 HZ LINE HISTORY AS OBSERVED VIA THE MAX GAIN LIMACONS SENSOR
AT SITE A3 DURING THE 17 NOV FIELD EVENT WITH VERNIER RESOLUTION (U)

AS-77-2715

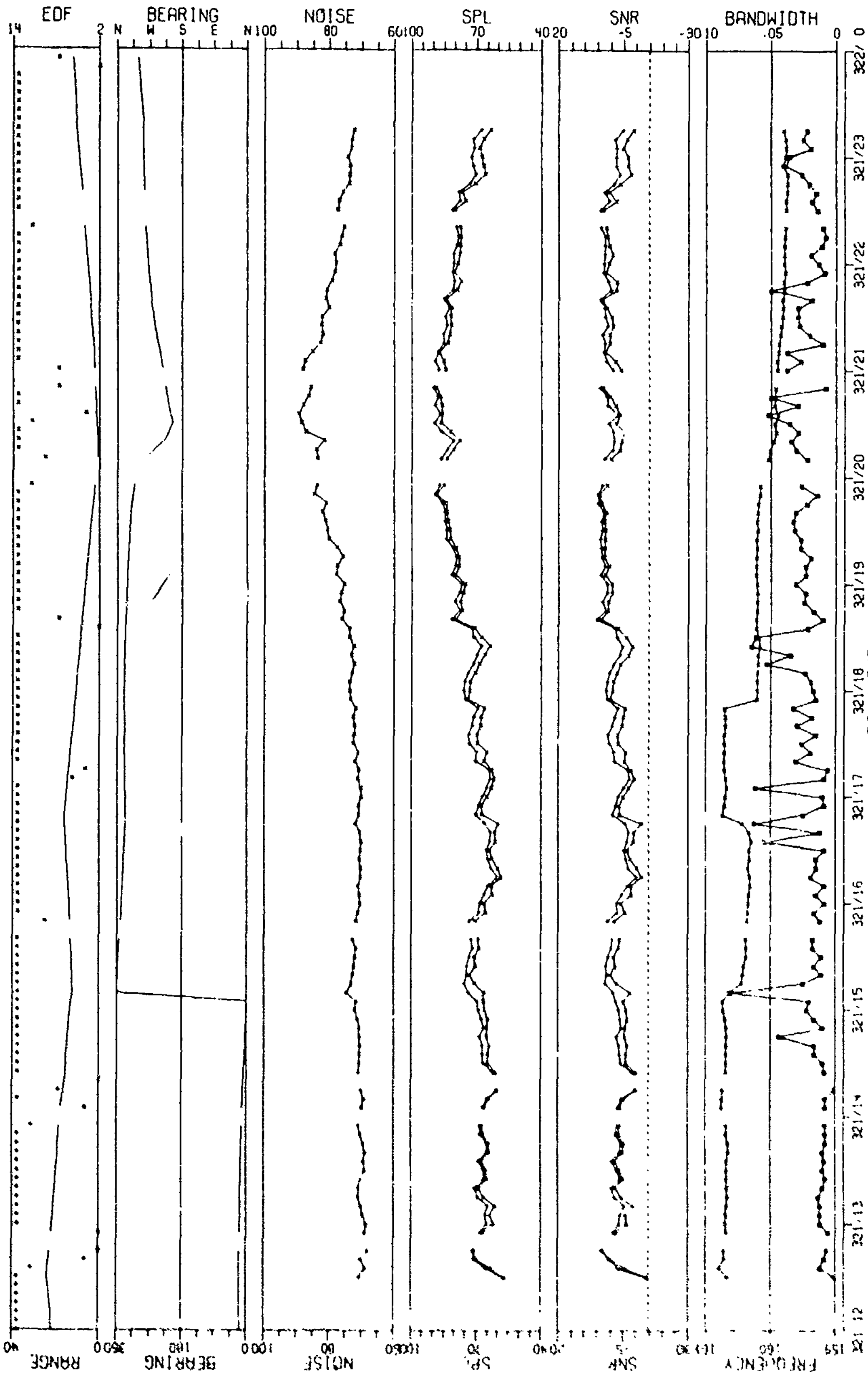

FIGURE III-116
MSS-FVT 160 HZ LINE HISTORY AS OBSERVED VIA THE VERTICAL DIPOLE SENSOR AT SITE A3 DURING THE 17 NOV FIELD EVENT WITH VERNIER RESOLUTION (U)

AS-77-2716

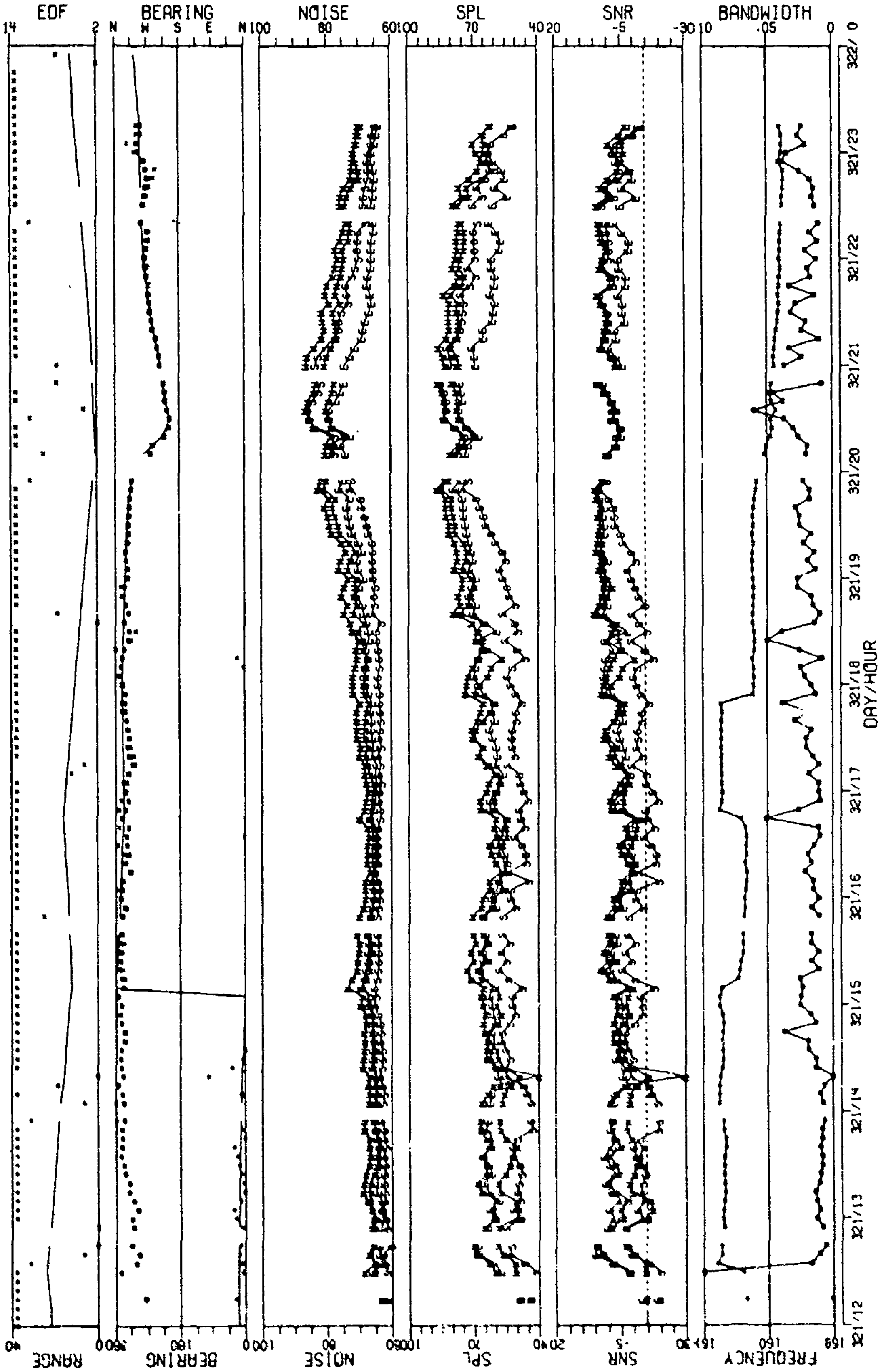

FIGURE III-117
MSS-FVT 160 HZ LINE HISTORY AS OBSERVED VIA THE DIFFERENCED CARDIOIDS SENSOR
AT SITE A3 DURING THE 17 NOV FIELD EVENT WITH VERNIER RESOLUTION (U)

AS-77-2717

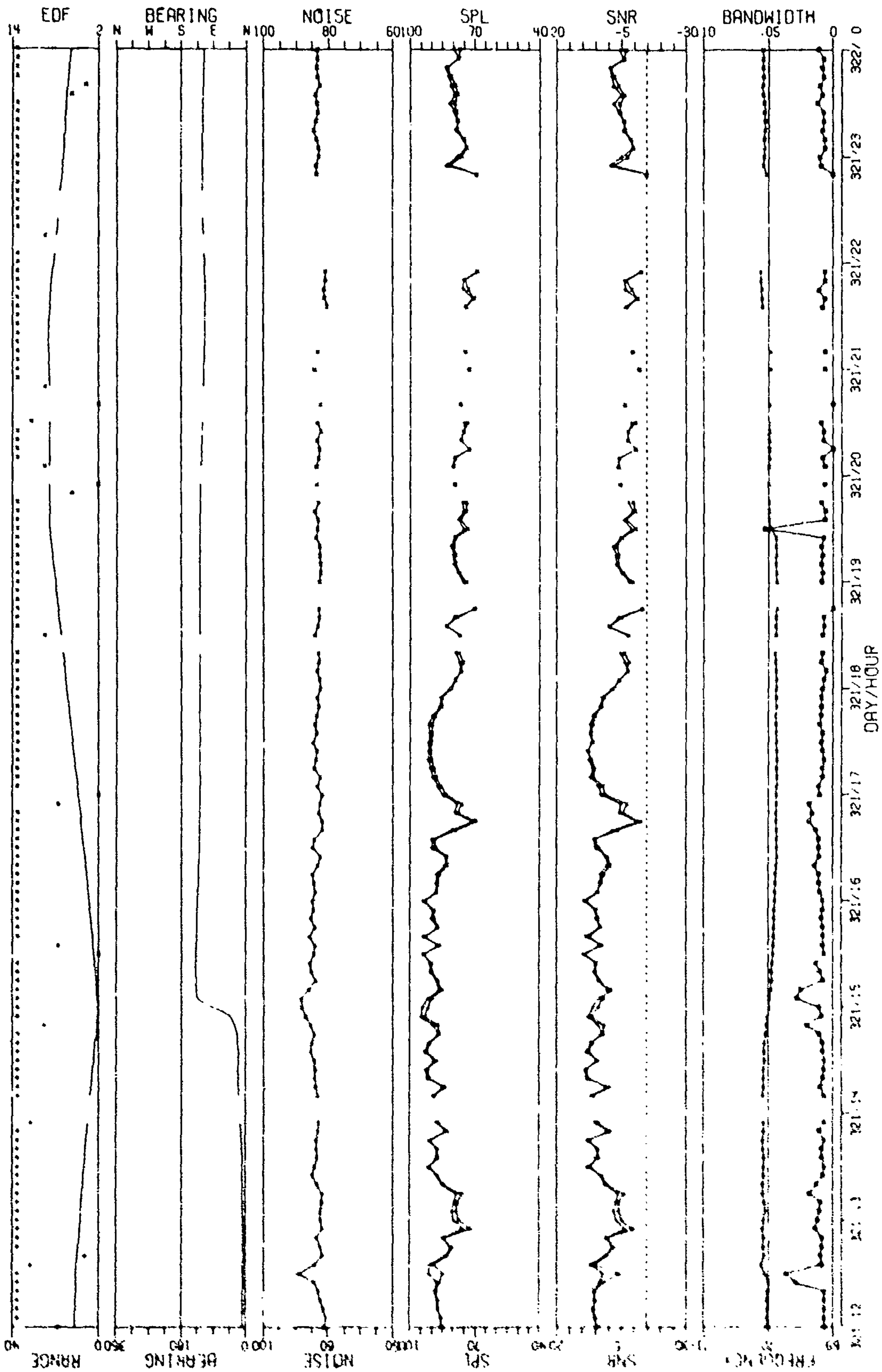

FIGURE III-118
MSS-FAT 70 HZ LINE HISTORY AS OBSERVED VIA THE OMNIDIRECTIONAL SENSOR AT SITE A3 DURING THE 17 NOV FIELD EVENT WITH VERNIER RESOLUTION (U)

AS-77-2718

FIGURE III-119
MSS-FVT 70 HZ LINE HISTORY AS OBSERVED VIA THE SINGLE CARDIOIDS SENSOR AT SITE A3 DURING THE 17 NOV FIELD EVENT WITH VERNIER RESOLUTION (U)

AS-77-2719

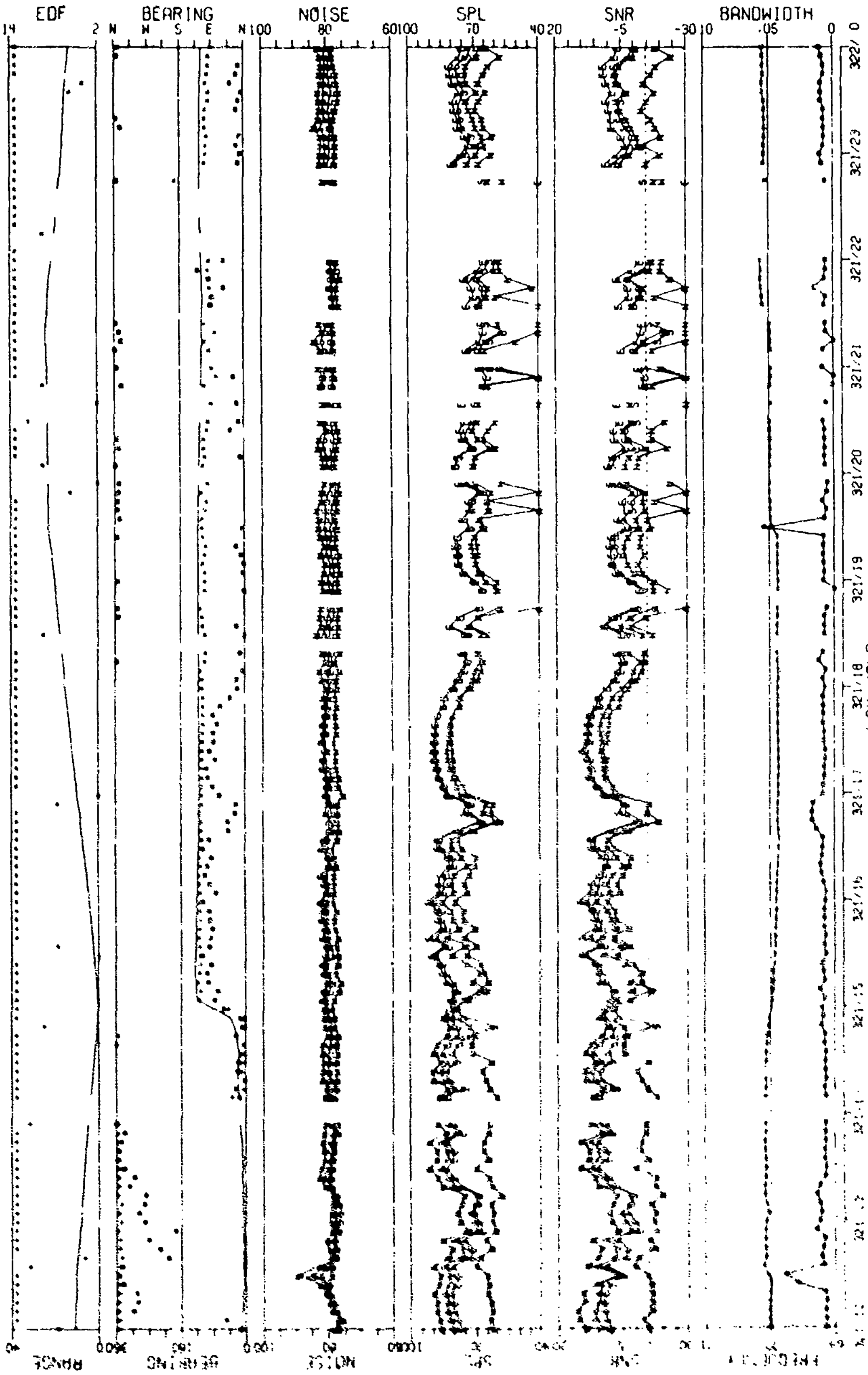

FIGURE III-120
[illegible] HZ LINE HISTORY AS OBSERVED VIA THE MAX GAIN LIMACONS SENSOR
[illegible] DURING THE 17 NOV FIELD EVENT WITH VERNIER RESOLUTION (U)

AS-77-2720

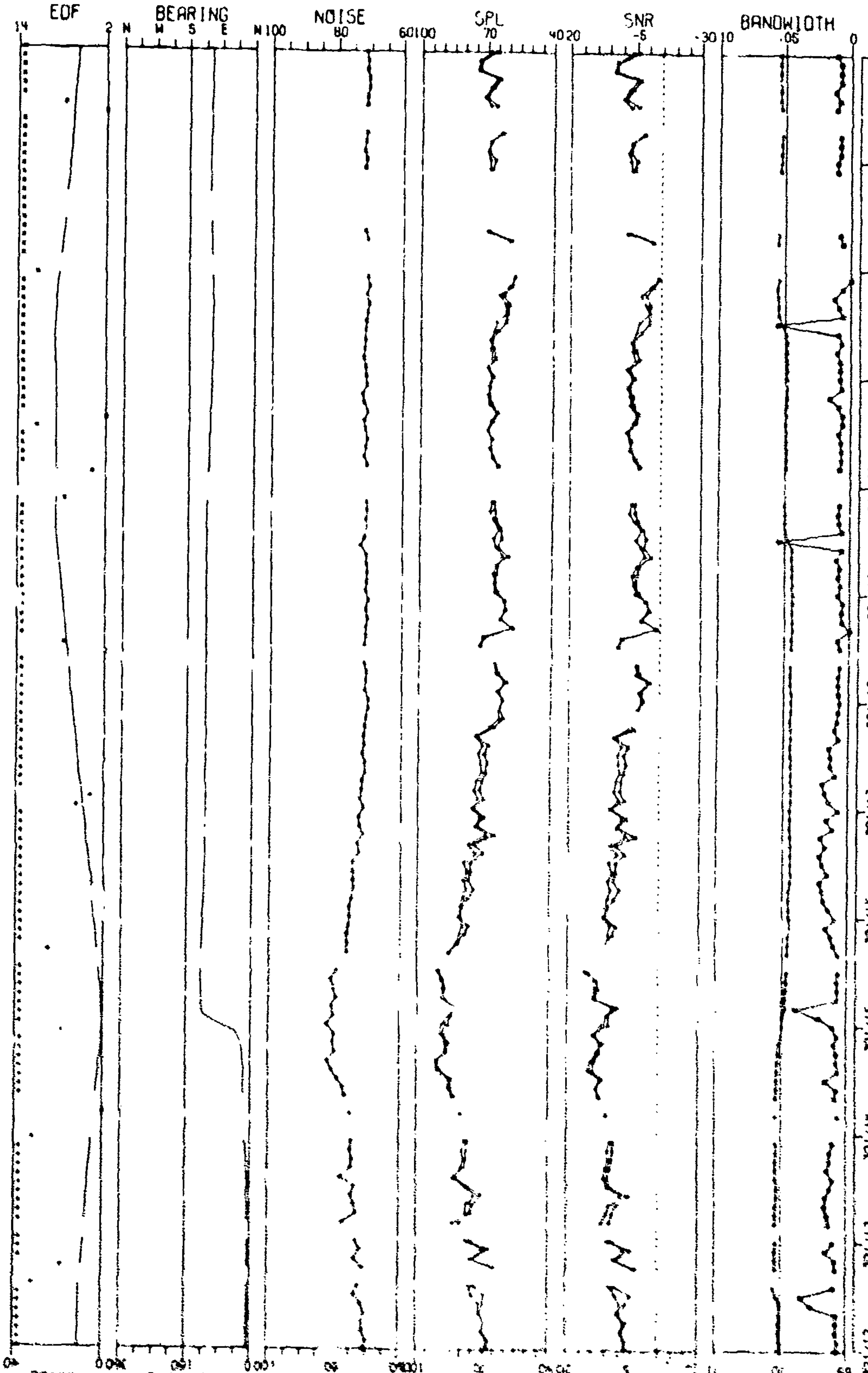

FIGURE III-121
MSS-FYT 70 HZ LINE HISTORY AS OBSERVED VIA THE VERTICAL DIPOLE SENSOR AT SITE A3 DURING THE 17 NOV FIELD EVENT WITH VERNIER RESOLUTION (U)

AS-77-2721

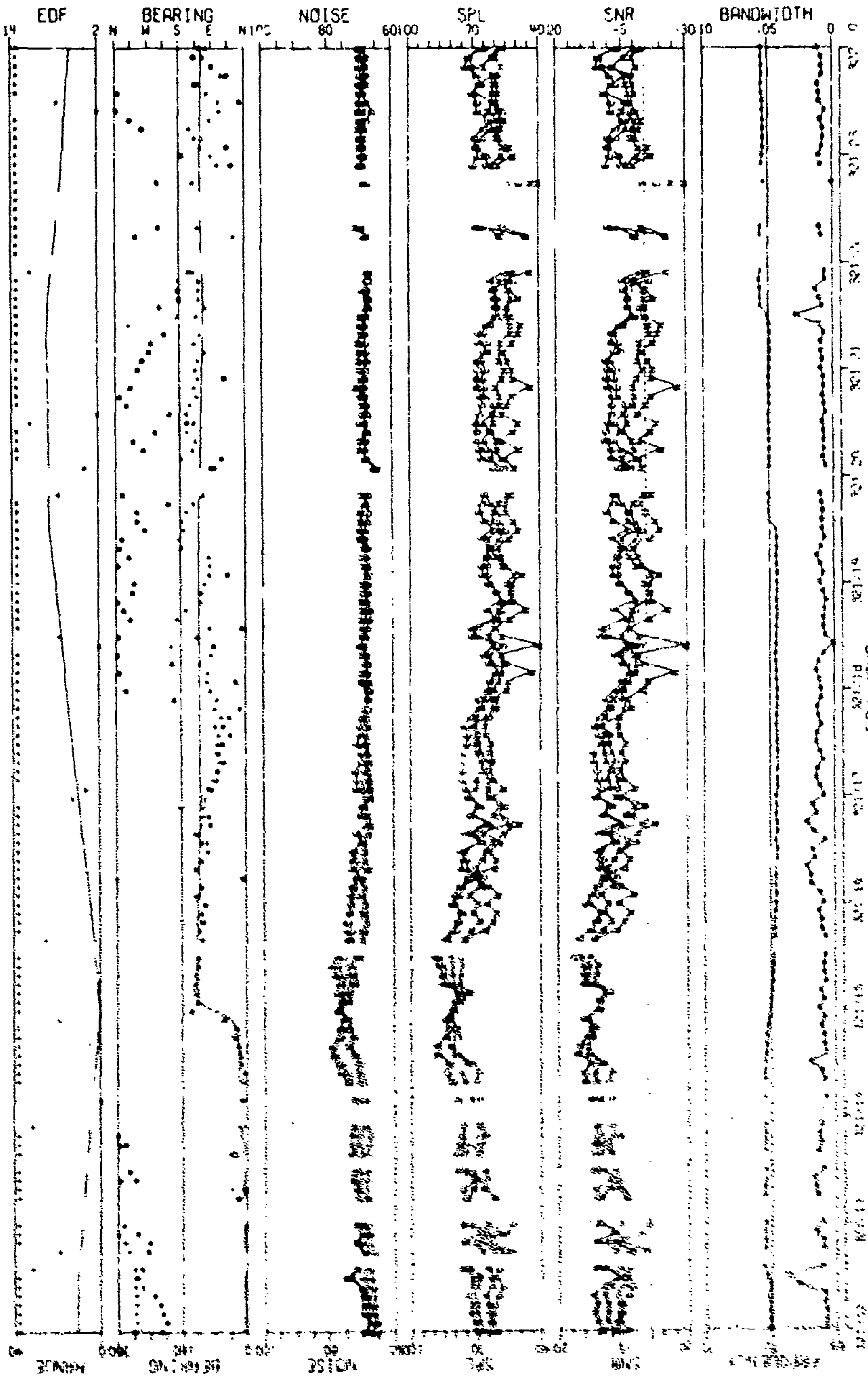

FIGURE III-122
[illegible] AS OBSERVED VIA THE DIFFERENCED CARDIOIDS SENSOR
[illegible] DURING THE 17 NOV FIELD EVENT WITH VERNIER RESOLUTION (U)

AS-77-2722

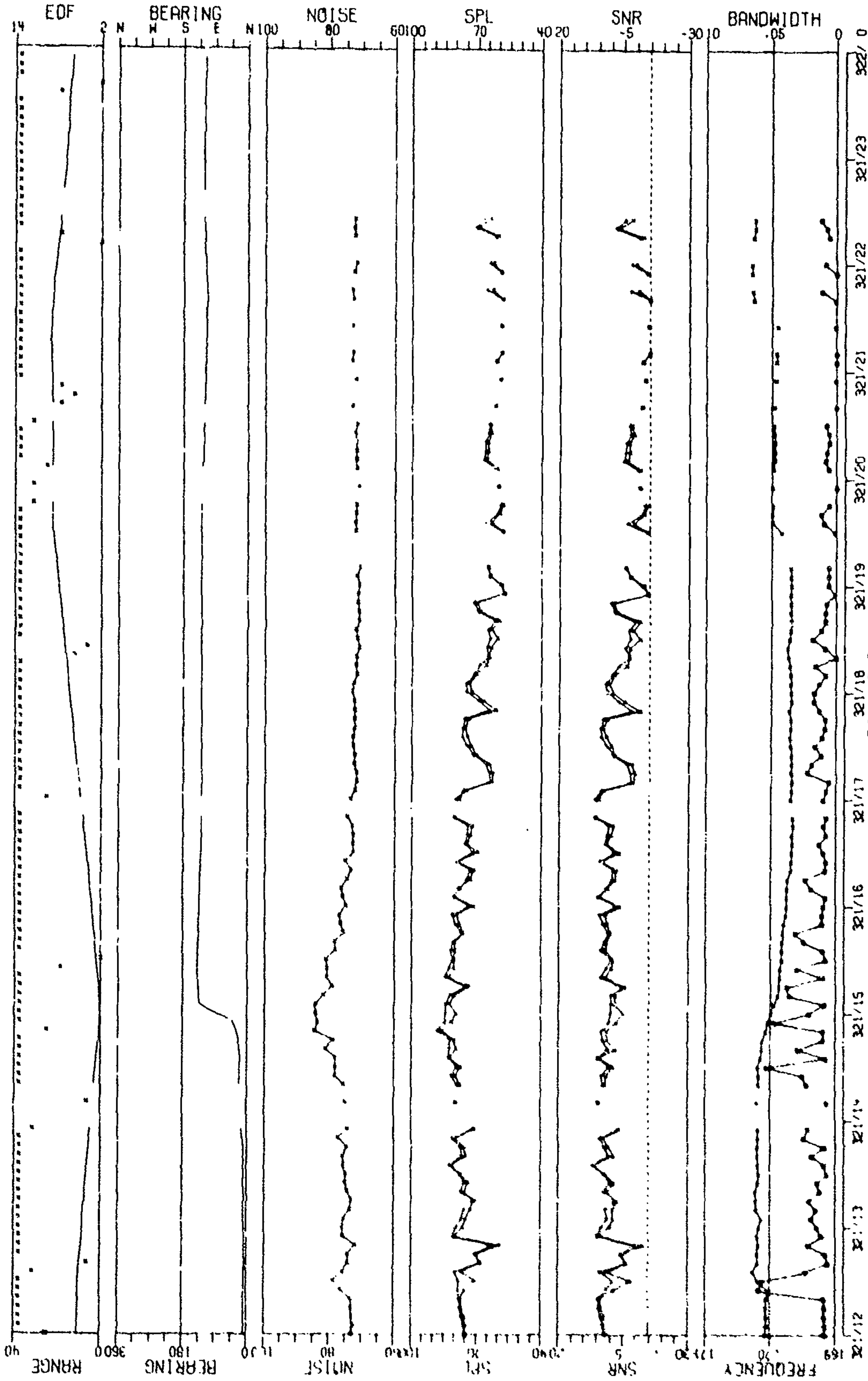

FIGURE III-123
MSS-F/T 170 HZ LINE HISTORY AS OBSERVED VIA THE OMNIDIRECTIONAL SENSOR AT SITE A3 DURING THE 17 NOV FIELD EVENT WITH VERNIER RESOLUTION (U)

AS-77-2723

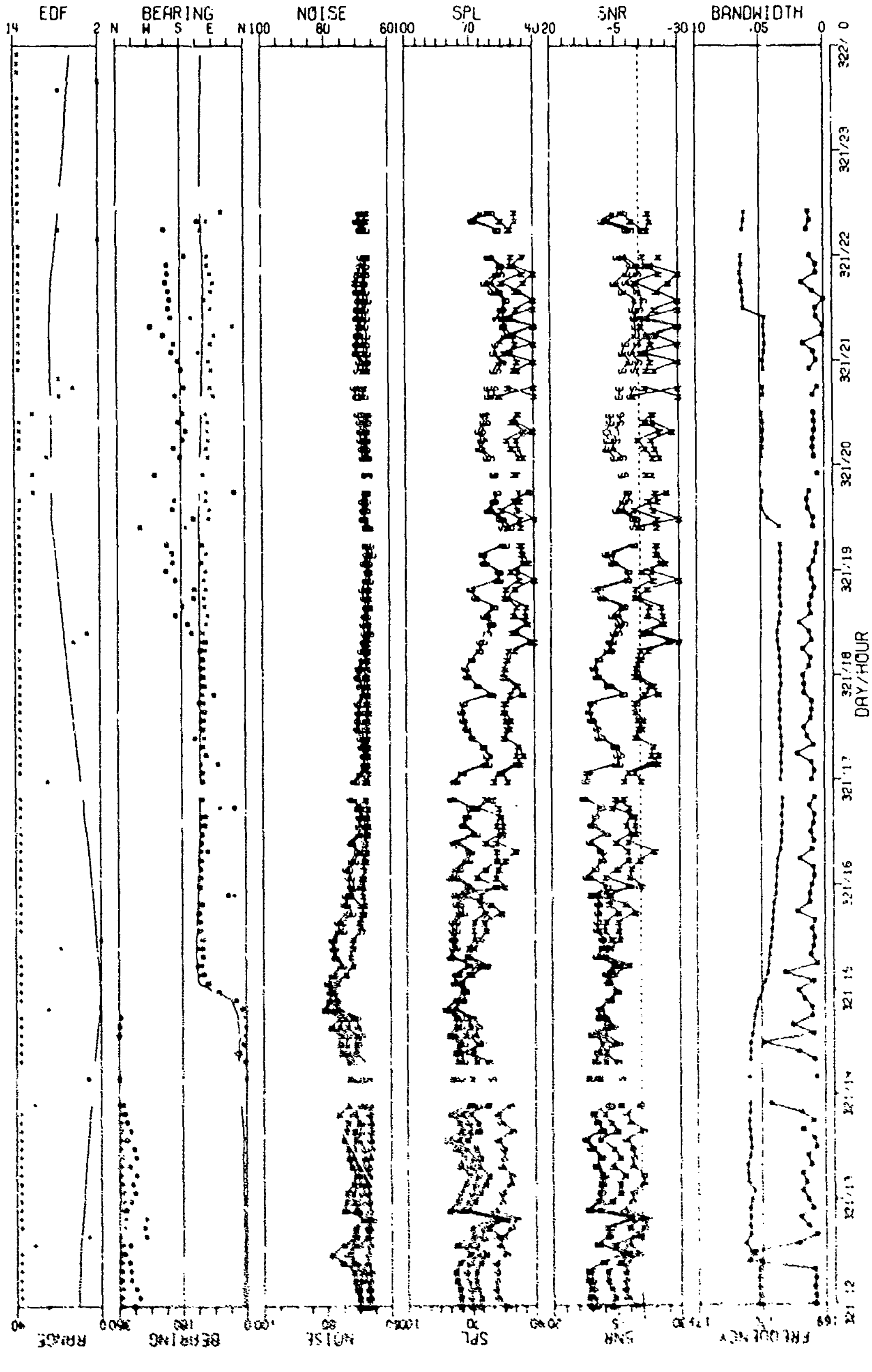

FIGURE III-124
MSS-FVT [illegible] HZ LINE HISTORY AS OBSERVED VIA THE SINGLE CARDIOIDS SENSOR AT SITE A3 DURING THE 17 NOV FIELD EVENT WITH VERNIER RESOLUTION (U)

AS-77-2724

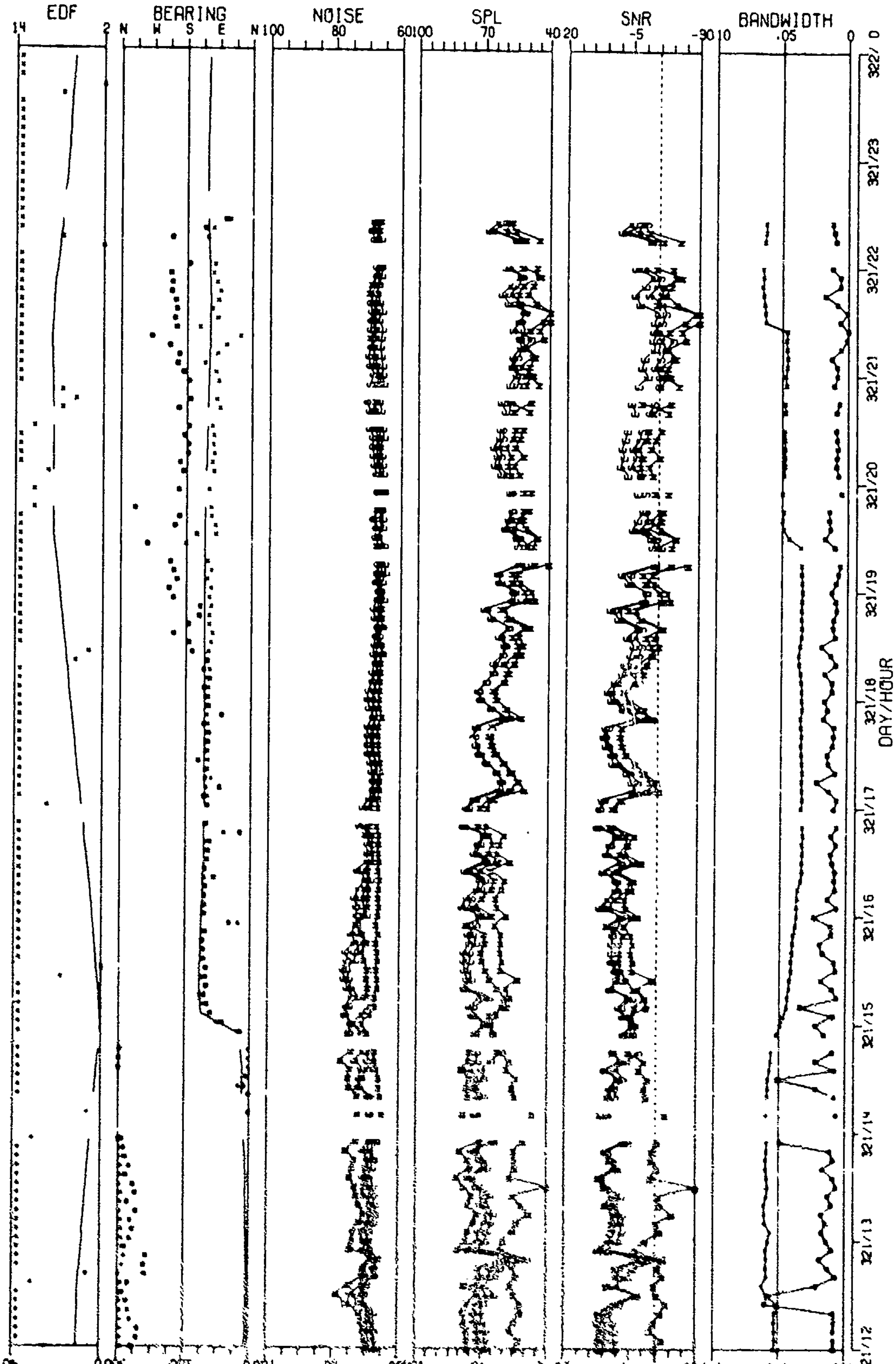

FIGURE III-125
MSS-FVT 170 HZ LINE HISTORY AS OBSERVED VIA THE MAX GAIN LIMACONS SENSOR AT SITE A3 DURING THE 17 NOV FIELD EVENT WITH VERNIER RESOLUTION (U)

AS-77-2725

FIGURE III-126
MSS-FVT 170 HZ LINE HISTORY AS OBSERVED VIA THE VERTICAL DIPOLE SENSOR AT SITE A3 DURING THE 17 NOV FIELD EVENT WITH VERNIER RESOLUTION (U)

AS-77-2726

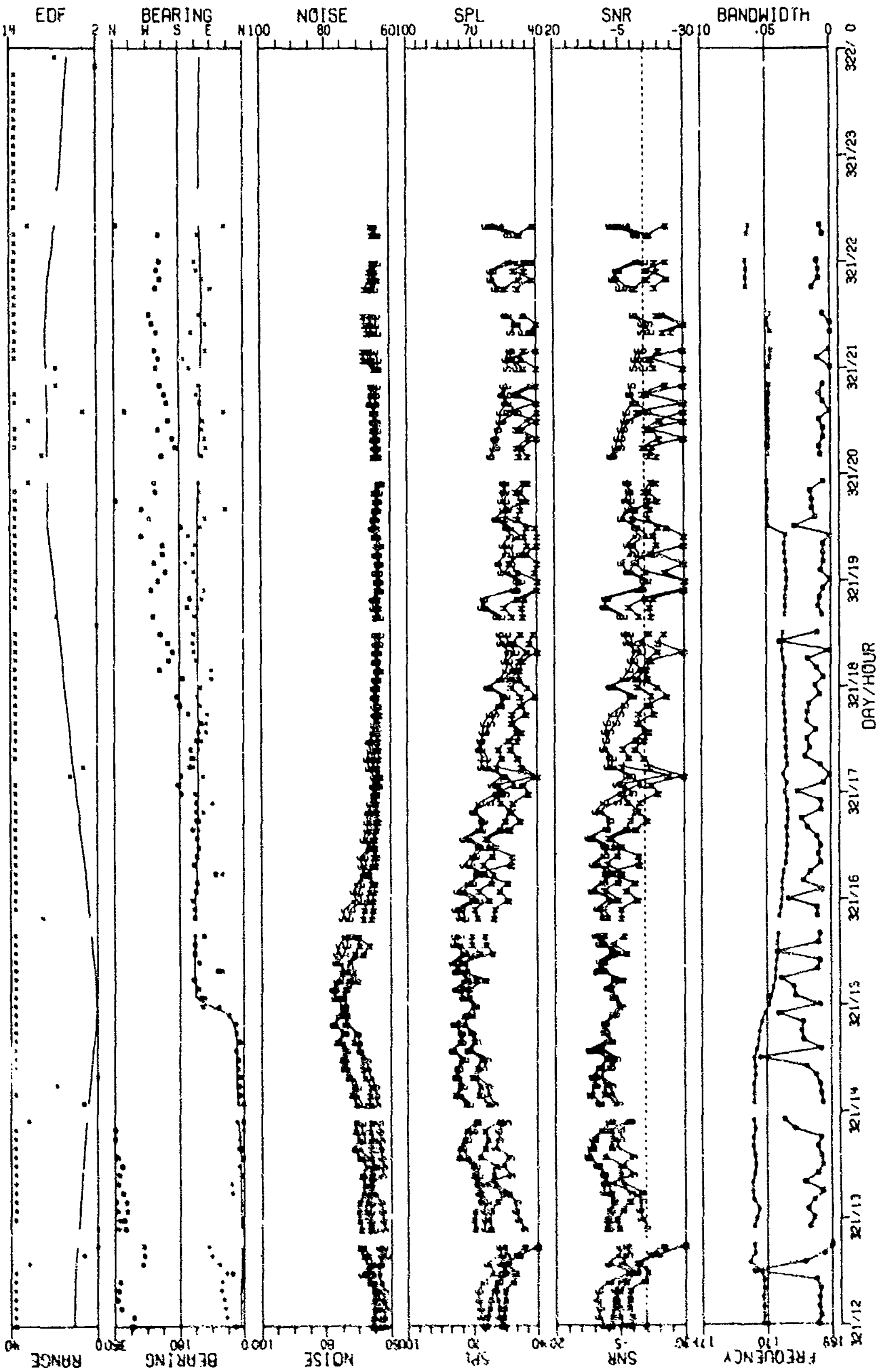

FIGURE III-127
MSS-FVT 170 HZ LINE HISTORY AS OBSERVED VIA THE DIFFERENCED CARDIOIDS SENSOR AT SITE A3 DURING THE 17 NOV FIELD EVENT WITH VERNIER RESOLUTION (U)

AS-77-2727

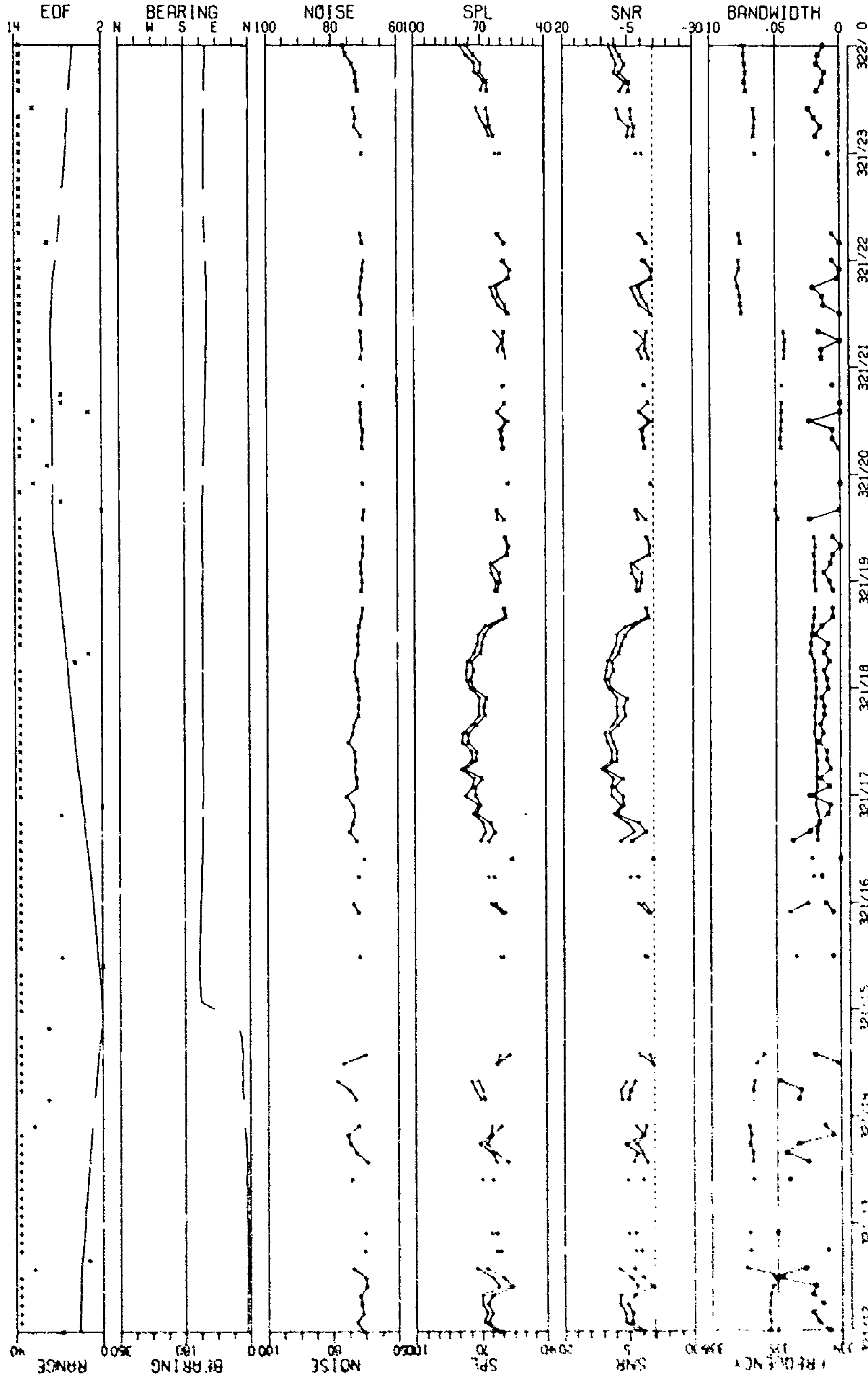

FIGURE III-128
MSS-EVT 325 HZ LINE HISTORY AS OBSERVED VIA THE OMNIDIRECTIONAL SENSOR AT SITE H3 DURING THE 17 NOV FIELD EVENT WITH VERNIER RESOLUTION (U)

AS-77-2728

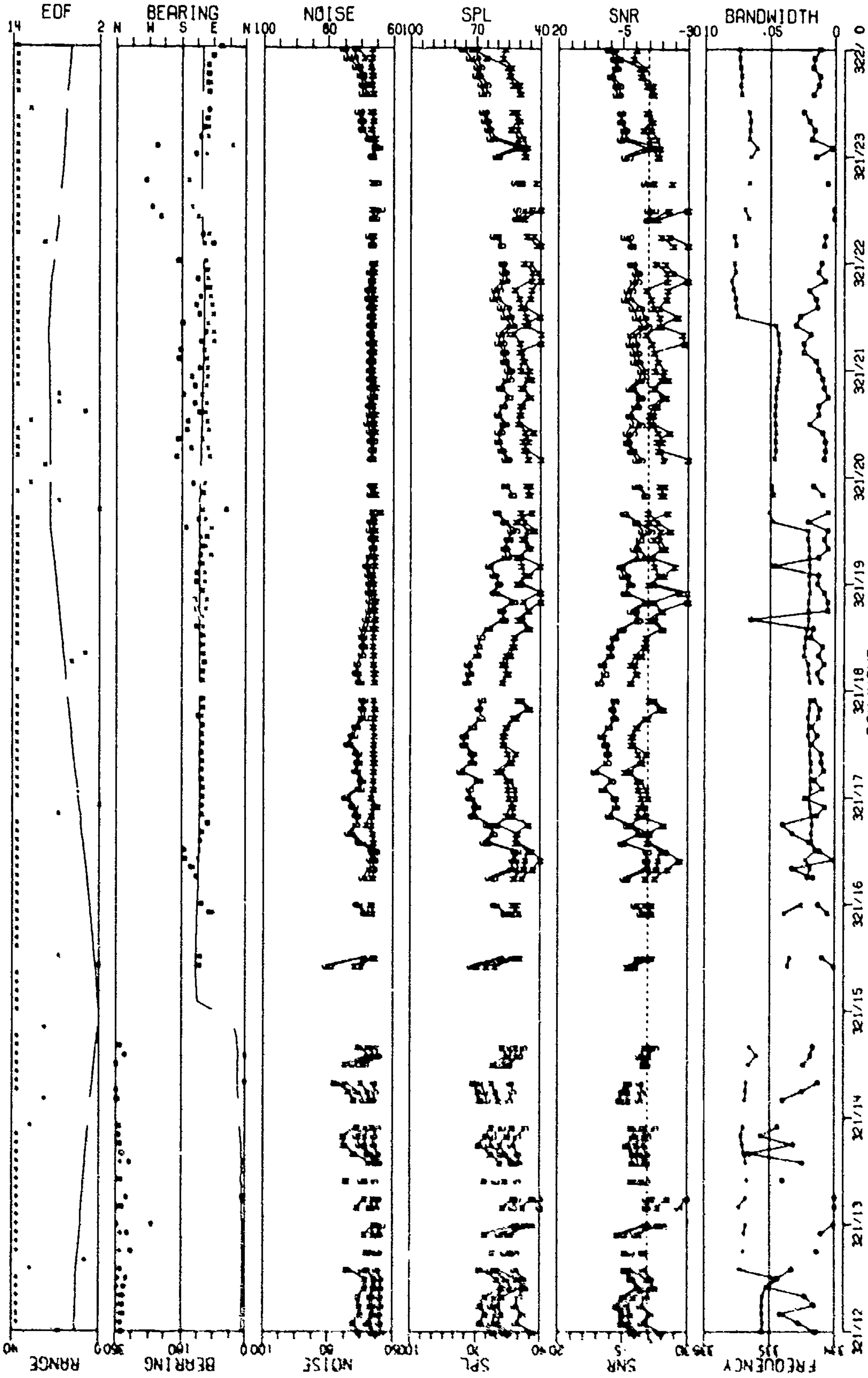

FIGURE III-129
MSS-FVT 335 HZ LINE HISTORY AS OBSERVED VIA THE SINGLE CARDIOIDS SENSOR
AT SITE A3 DURING THE 17 NOV FIELD EVENT WITH VERNIER RESOLUTION (U)

AS-77-2729

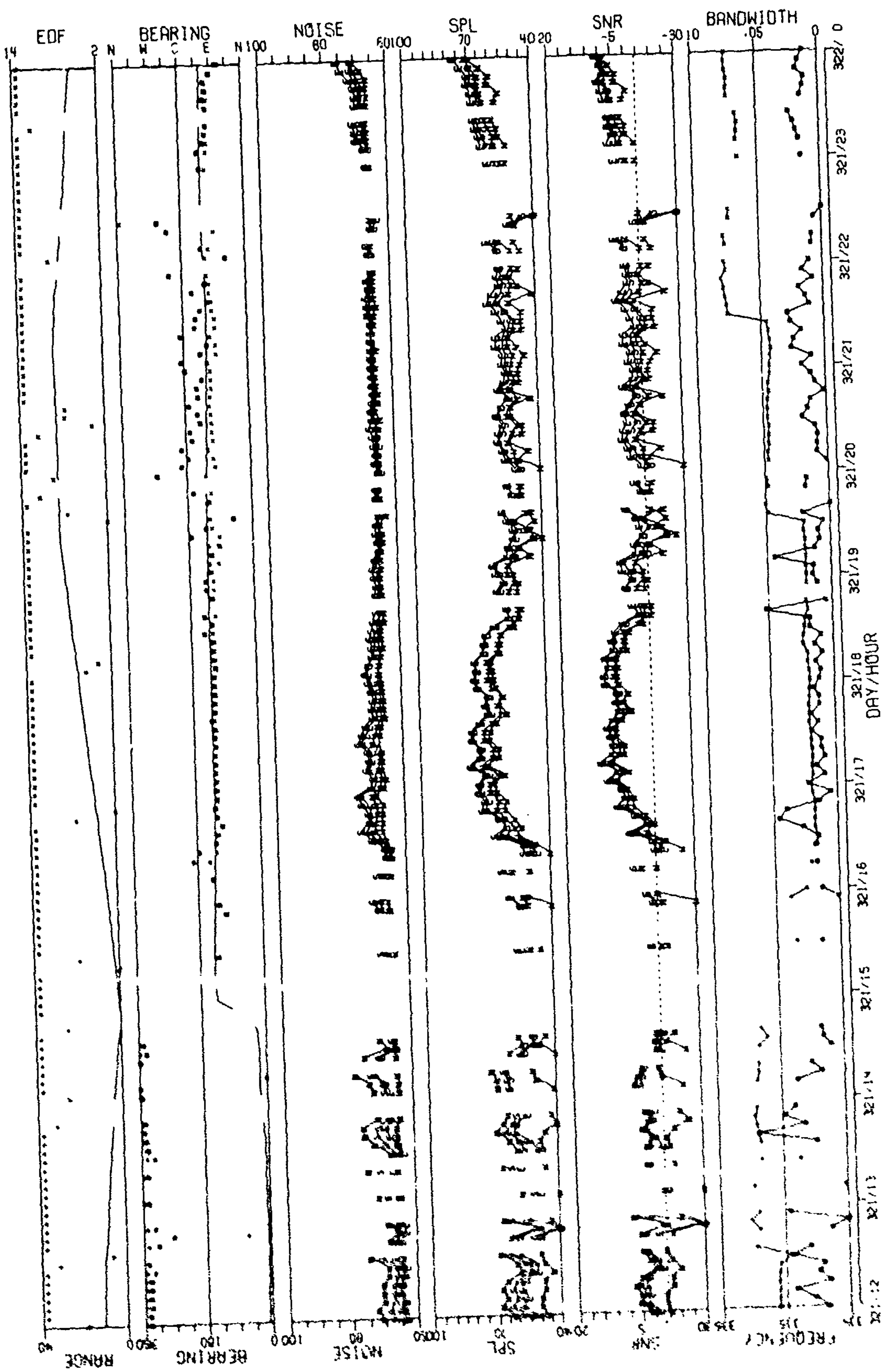

FIGURE III-130
MSS-FVT 335 HZ LINE HISTORY AS OBSERVED VIA THE MAX GAIN LIMACONS SENSOR
AT SITE A3 DURING THE 17 NOV FIELD EVENT WITH VERNIER RESOLUTION (U)

AS-77-2730

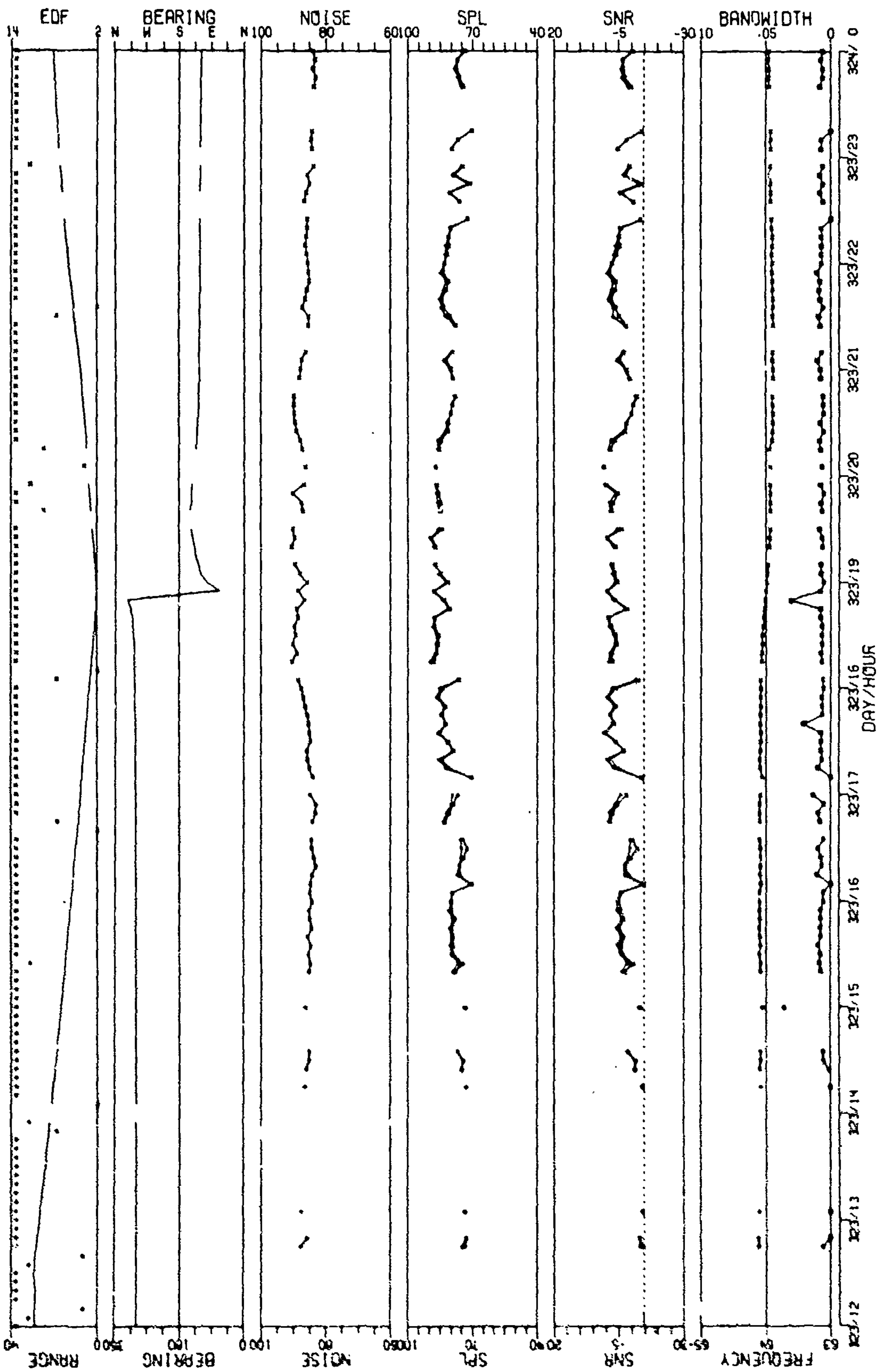

FIGURE III-131
MSS-FVT 64 HZ LINE HISTORY AS OBSERVED VIA THE OMNIDIRECTIONAL SENSOR AT SITE A3 DURING THE 19 NOV FIELD EVENT WITH VERNIER RESOLUTION (U)

AS-77-2731

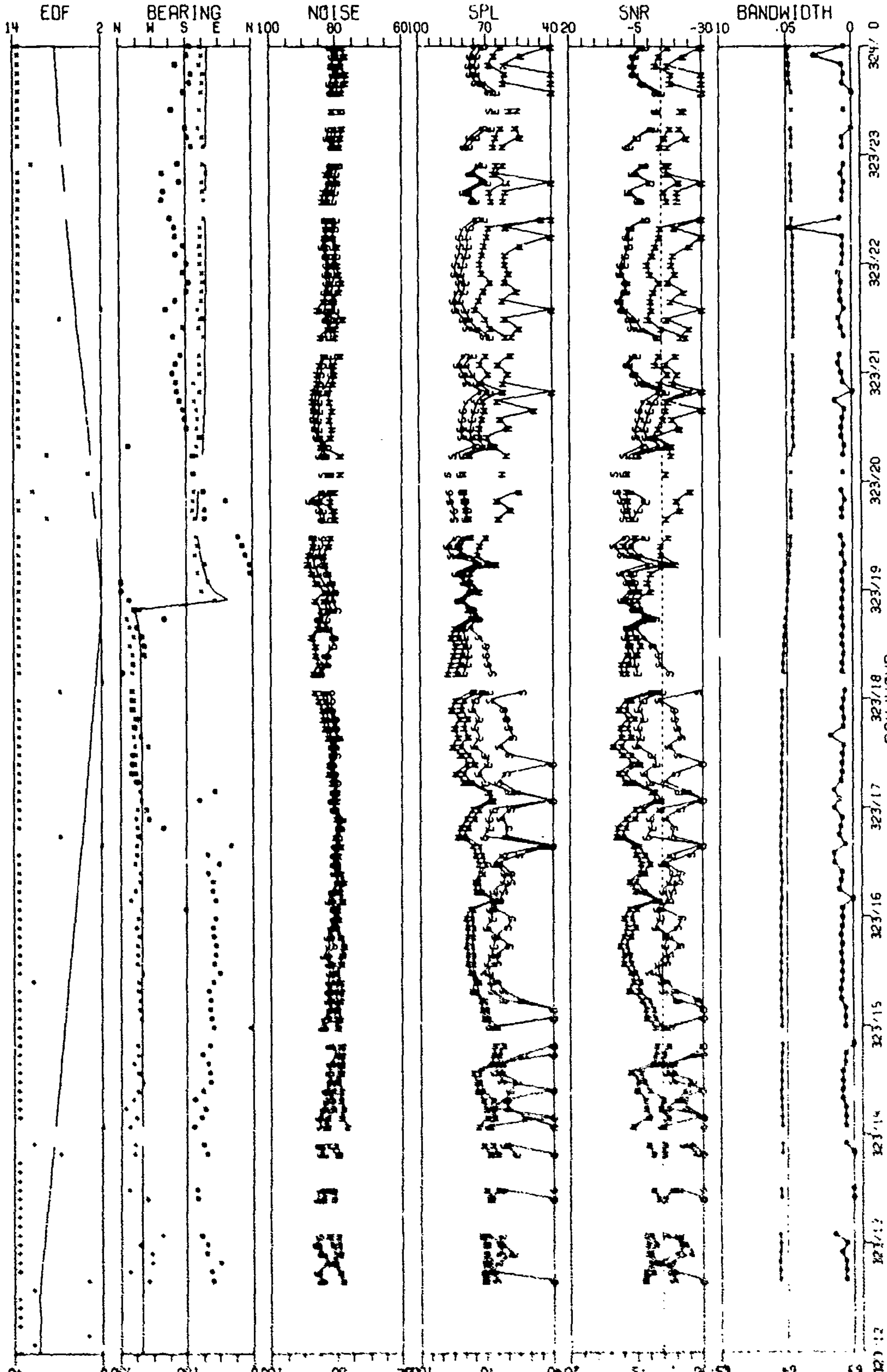

FIGURE III-132
MSS-FV* 64 HZ LINE HISTORY AS OBSERVED VIA THE SINGLE CARDIOIDS SENSOR
AT SITE A3 DURING THE 19 NOV FIELD EVENT WITH VERNIER RESOLUTION (U)

AS-77-2732

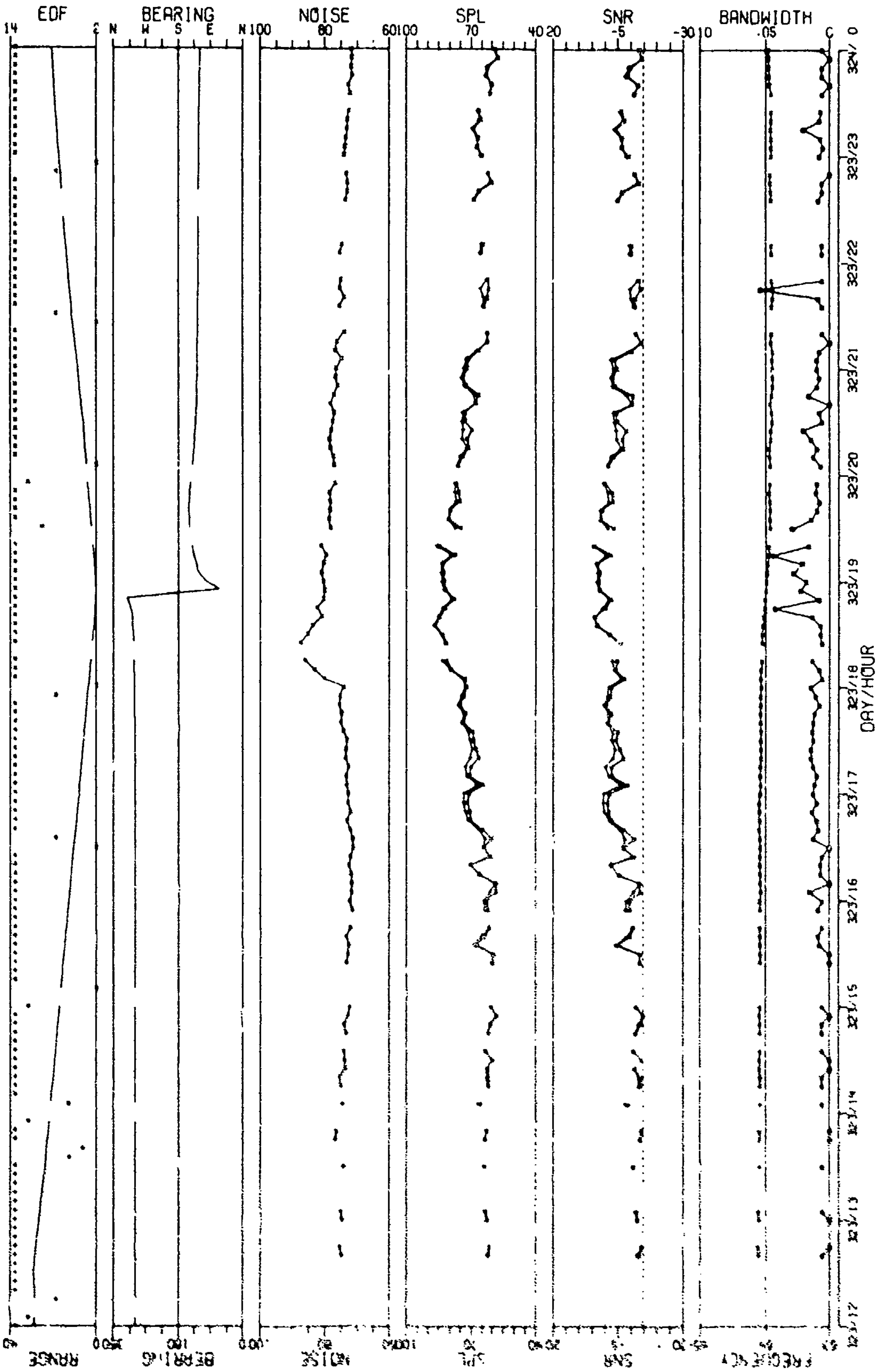

FIGURE III-133
MSS-FVT 64 HZ LINE HISTORY AS OBSERVED VIA THE VERTICAL DIPOLE SENSOR AT SITE A3 DURING THE 19 NOV FIELD EVENT WITH VERNIER RESOLUTION (U)

AS-77-2733

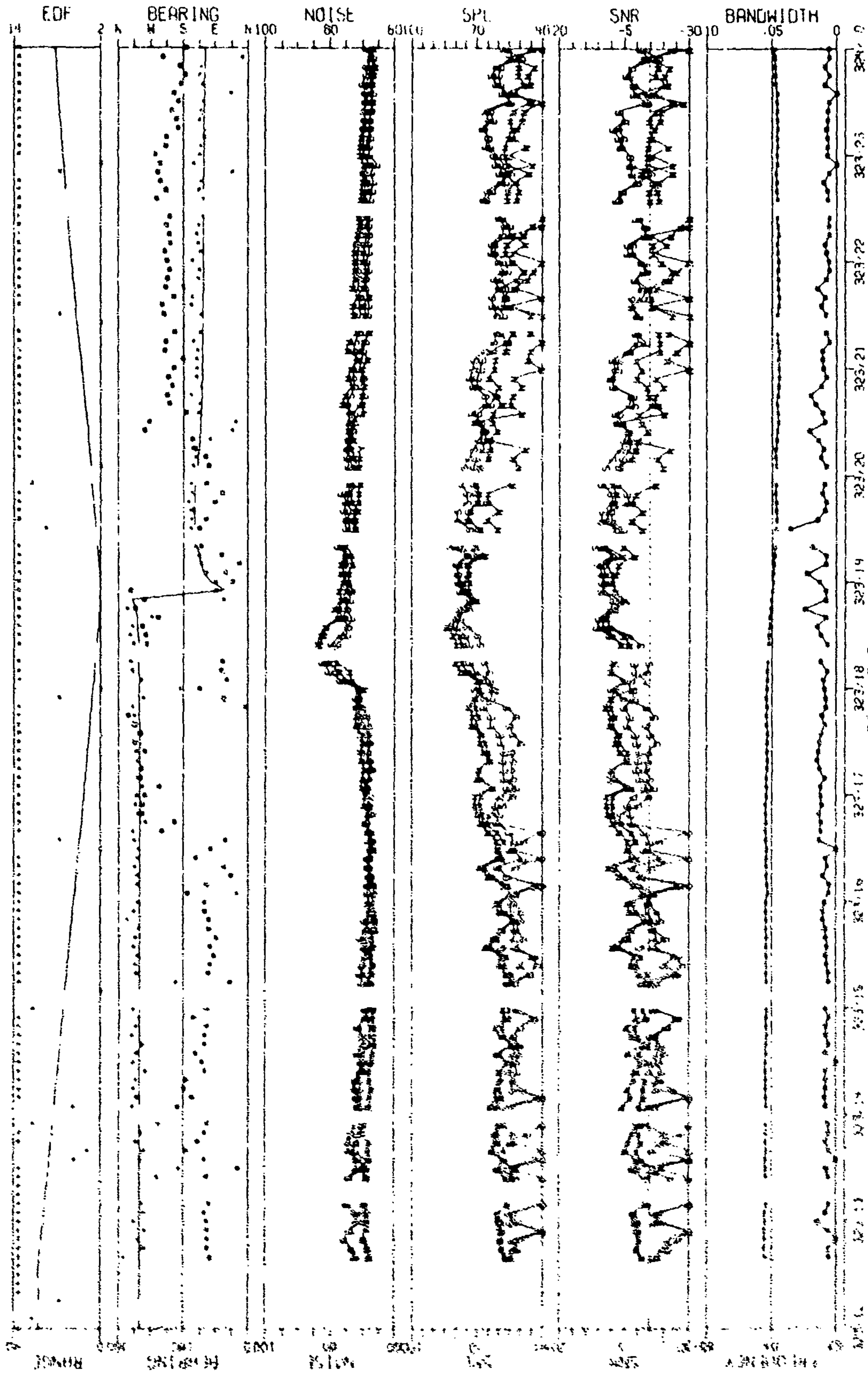

FIGURE III-134
MSS-FFT 64 HZ LINE HISTORY AS OBSERVED VIA THE DIFFERENCED CARDIOIDS SENSOR AT SITE A2 DURING THE 19 NOV FIELD EVENT WITH VERNIER RESOLUTION (U)

AS-77-2734

CONFIDENTIAL

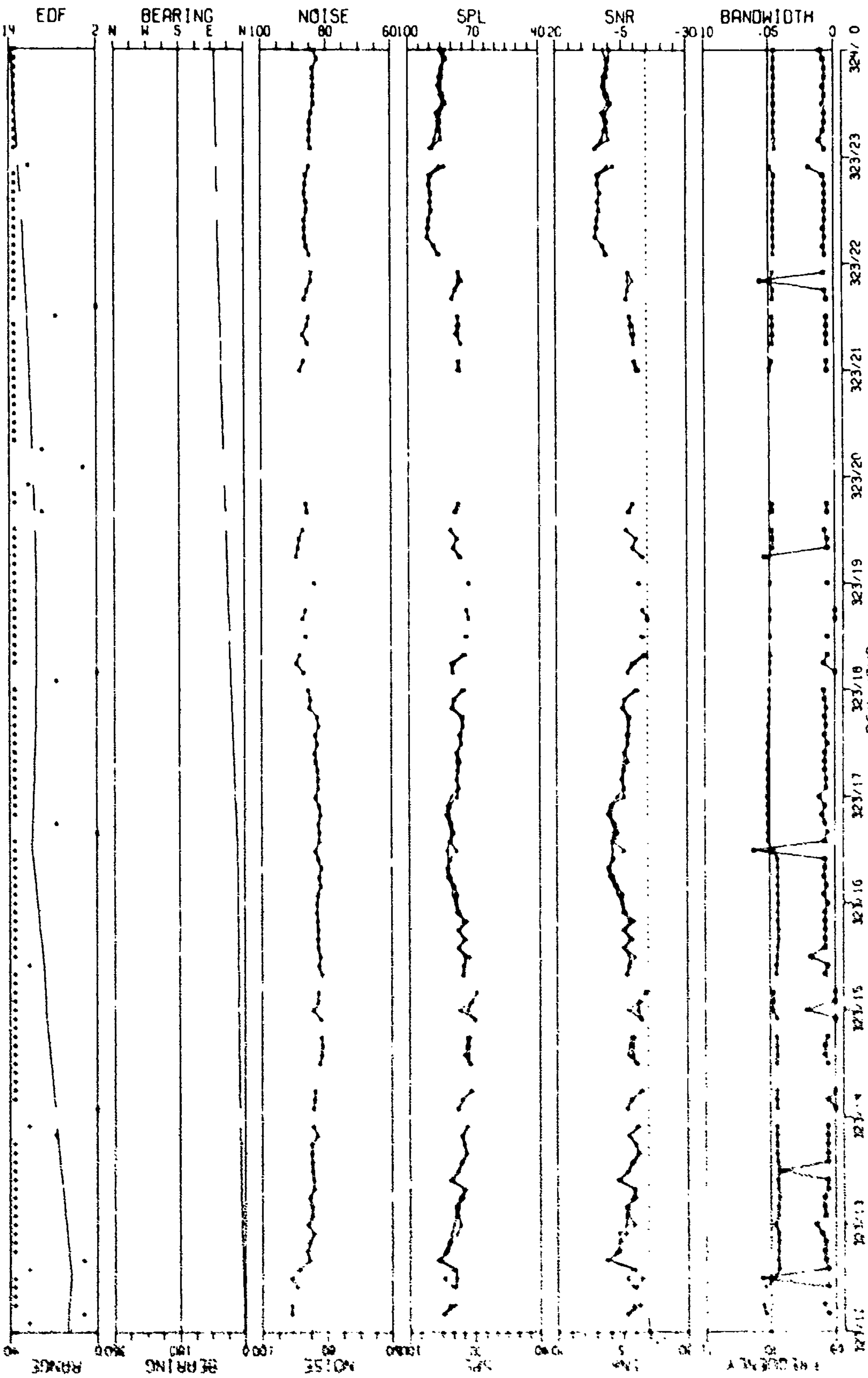

FIGURE III-135
MSS-EVT 70 HZ LINE HISTORY AS OBSERVED VIA THE OMNIDIRECTIONAL SENSOR AT SITE A3 DURING THE 13 NOV FIELD EVENT WITH VERNIER RESOLUTION (U)

AS-77-2735

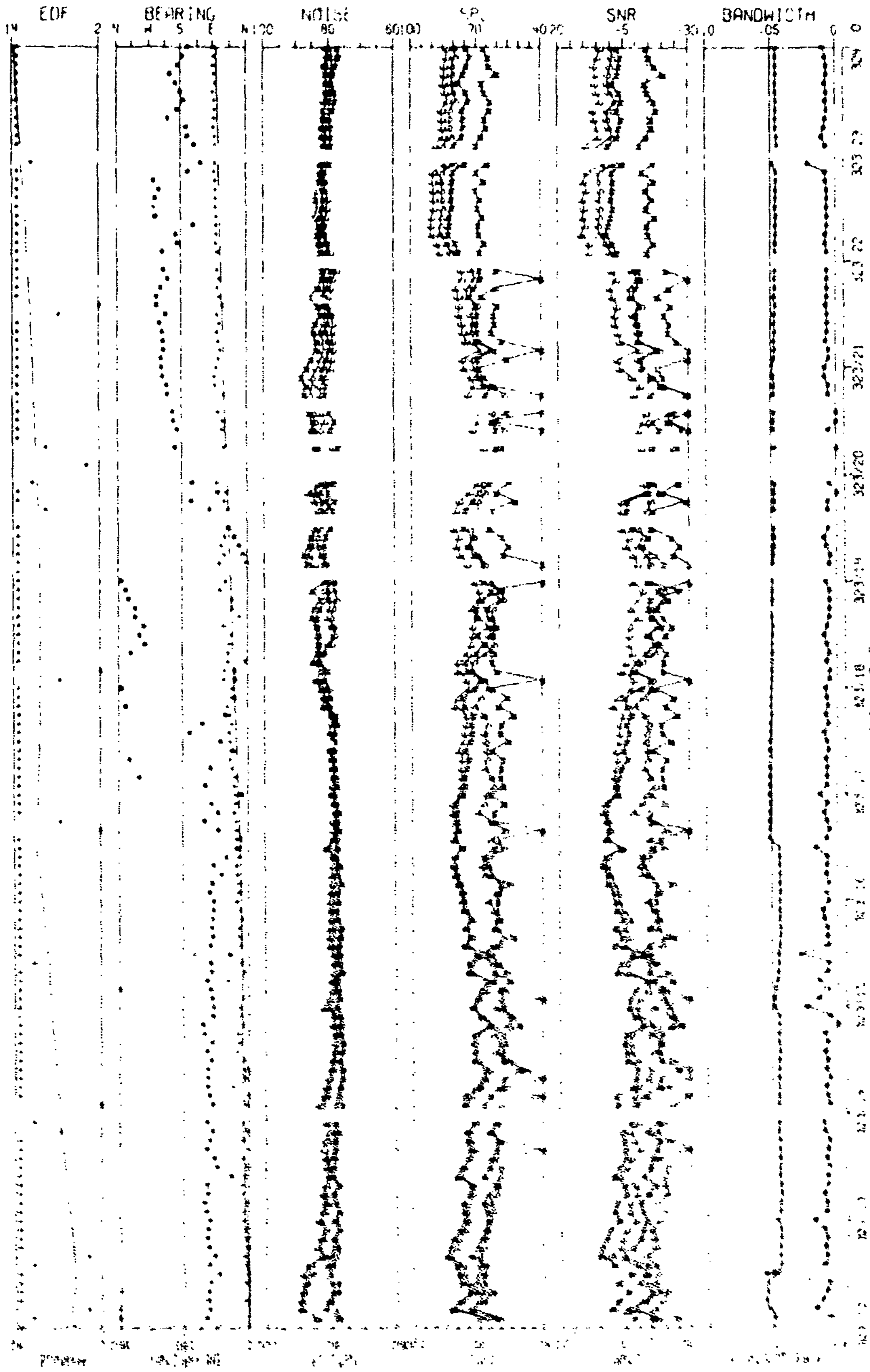

FIGURE III 136
... LINE HISTORY AS OBSERVED VIA THE SINGLE CARDIOIDS SENSOR
... FIXED EVENT WITH VERNIER RESOLUTION ...

AS-77-2736

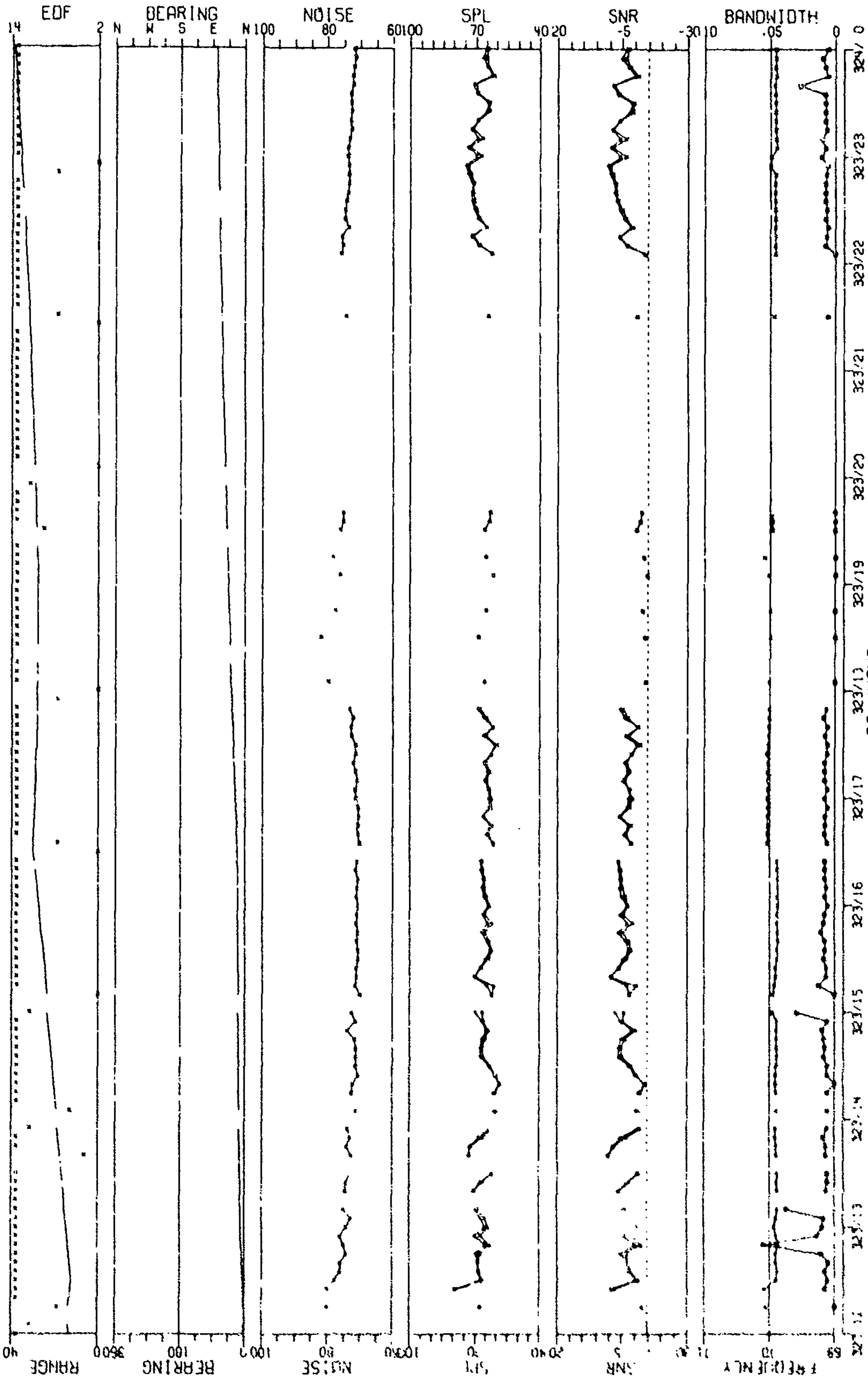

FIGURE III-137
MSS-FVT 70 HZ LINE HISTORY AS OBSERVED VIA THE VERTICAL DIPOLE SENSOR AT SITE A3 DURING THE 19 NOV FIELD EVENT WITH VERNIER RESOLUTION (U)

AS-77-2?37

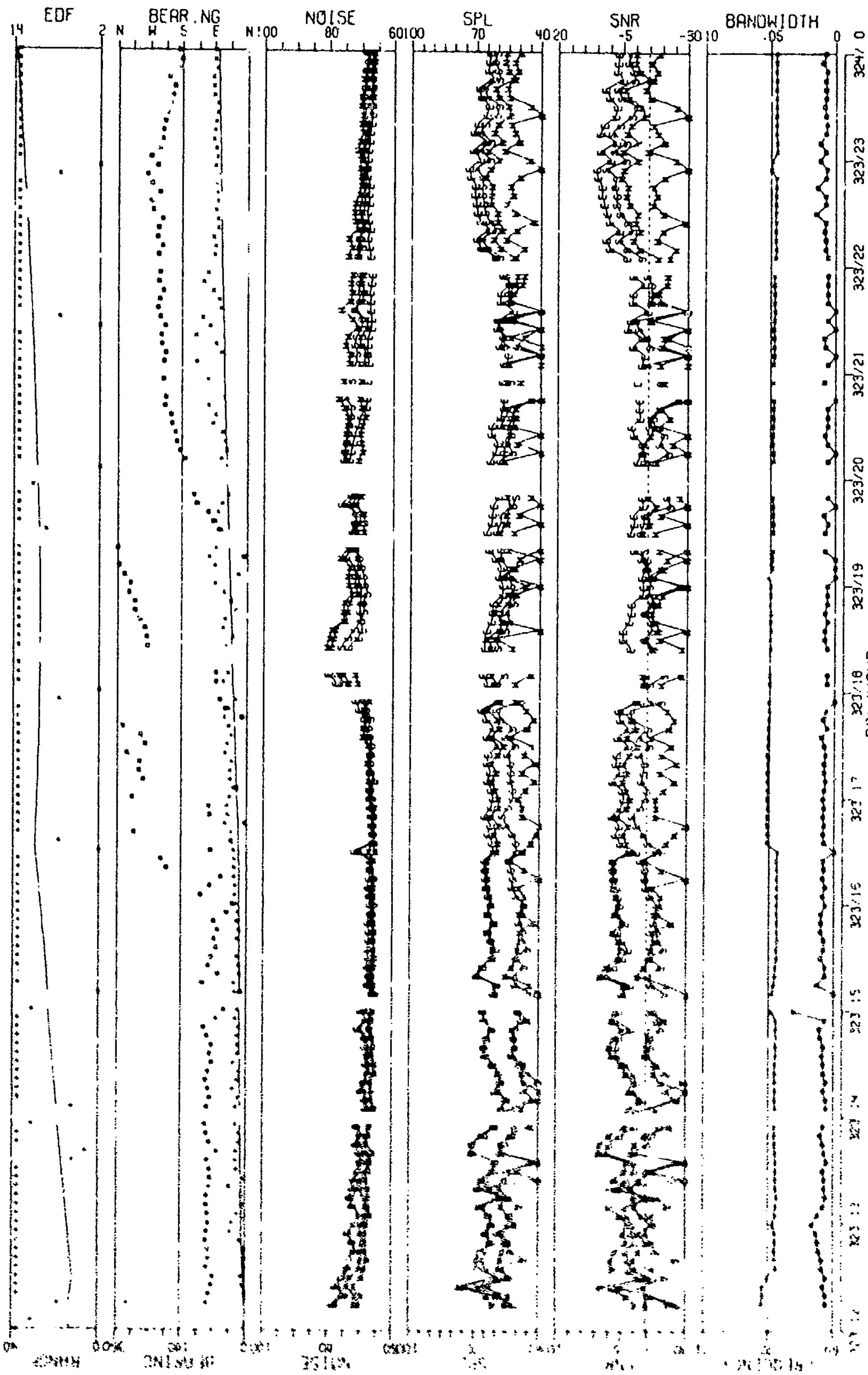

FIGURE III-138
MISS-E ... 70 HZ LINE HISTORY AS OBSERVED VIA THE DIFFERENCED CARDIOIDS SENSOR AT SITE A3 DURING THE 19 NOV FIELD EVENT WITH VERNIER RESOLUTION (U)

AS-77-2738

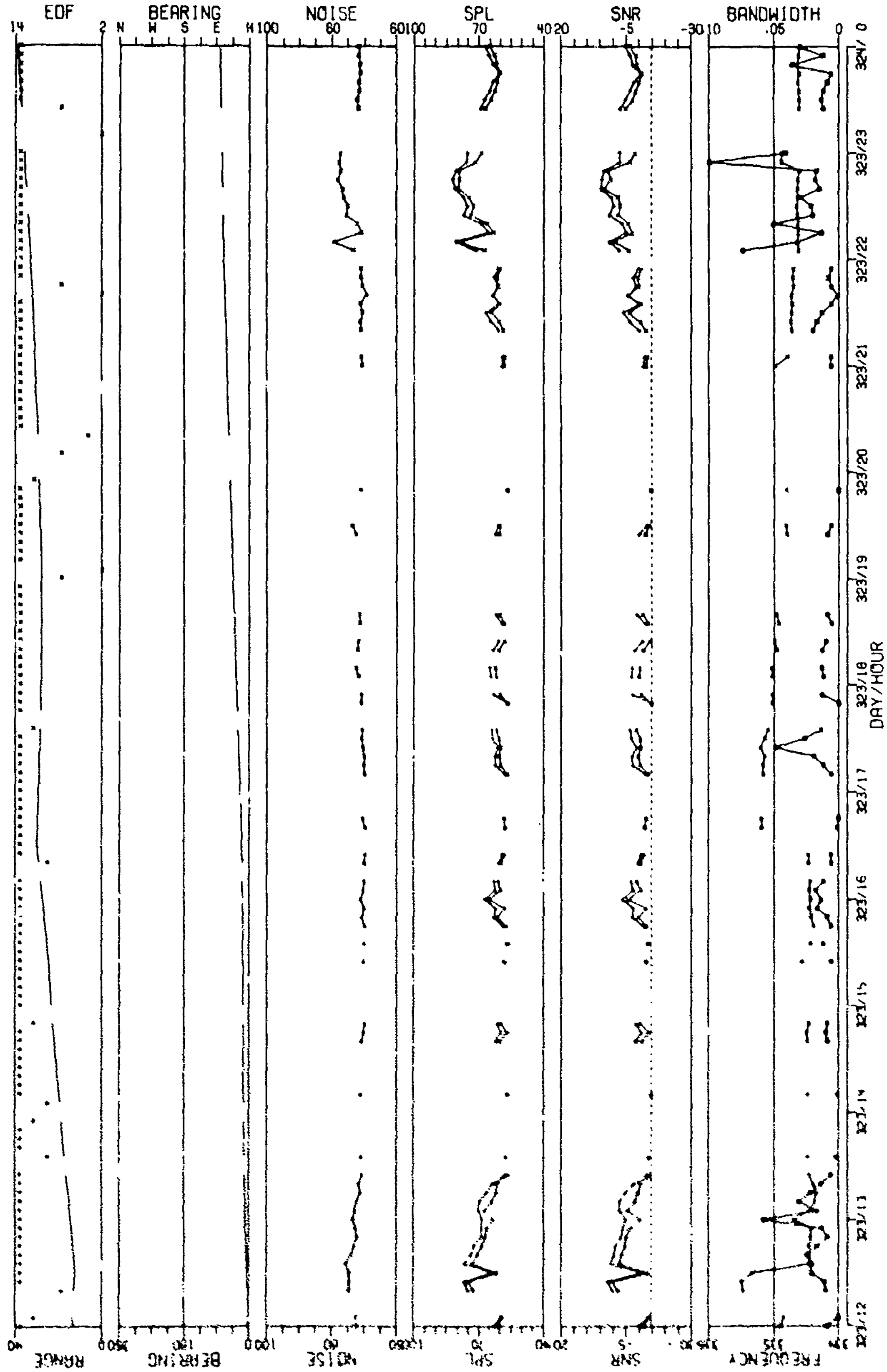

FIGURE III-139
MSS-FVT 335 HZ LINE HISTORY AS OBSERVED VIA THE OMNIDIRECTIONAL SENSOR AT SITE A3 DURING THE 19 NOV FIELD EVENT WITH VERNIER RESOLUTION (U)

AS-77-2739

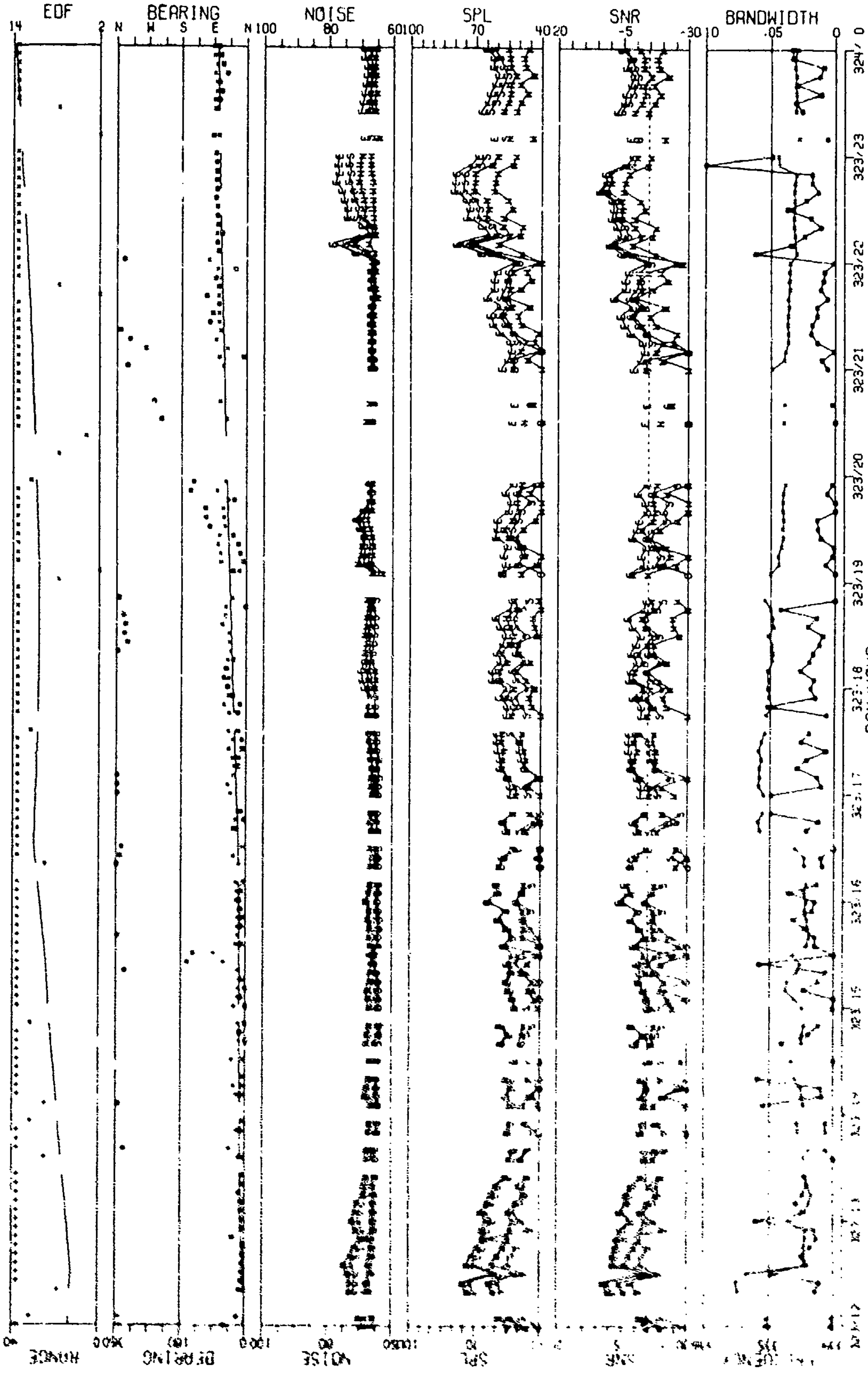

FIGURE III-140
[illegible] 25 HZ LINE HISTORY AS OBSERVED VIA THE SINGLE CARDIOIDS SENSOR
[illegible] DURING THE 19 NOV FIELD EVENT WITH VERNIER RESOLUTION (U)

AS-77-2740

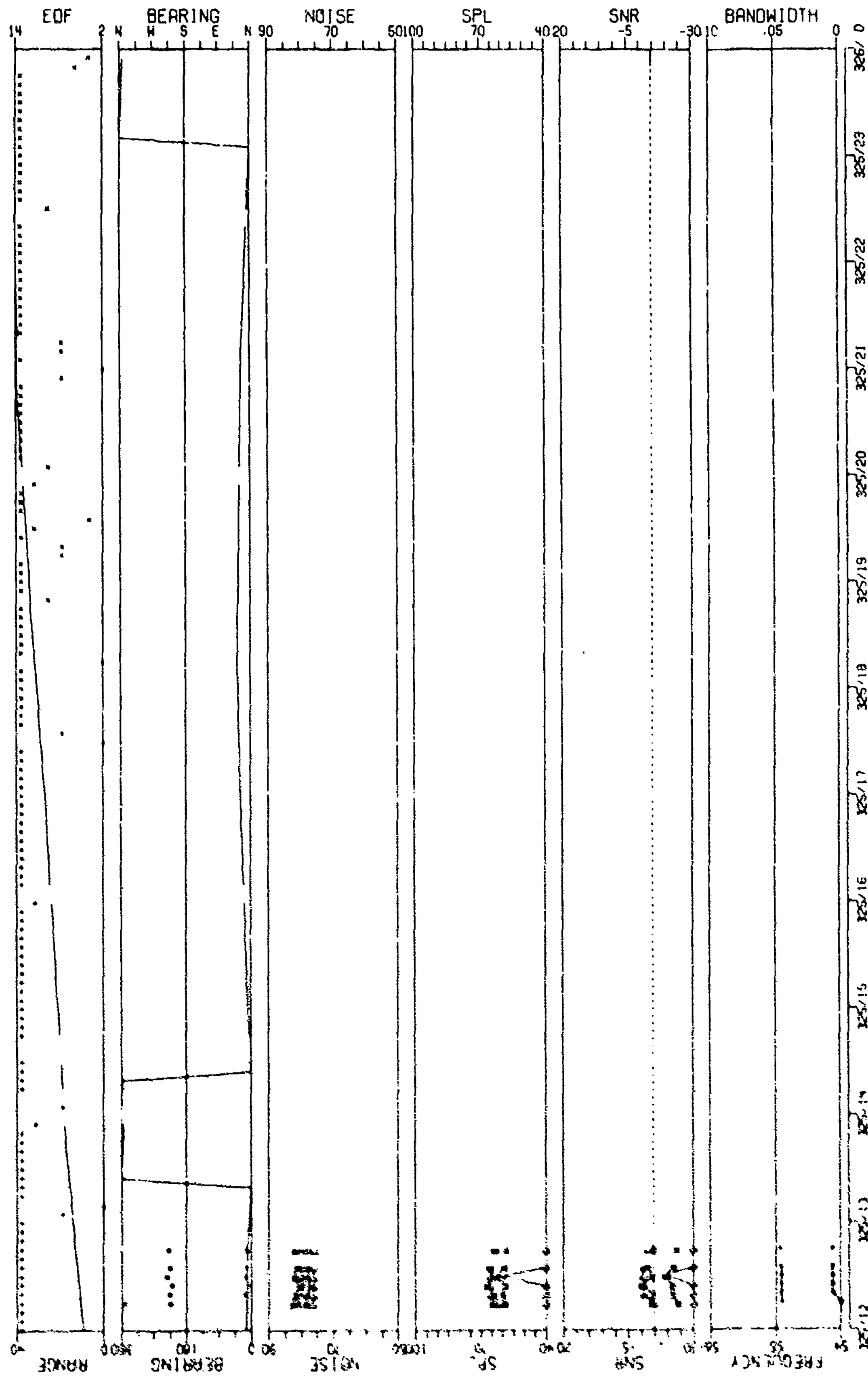

FIGURE III-141
MSS-FVT 55 HZ LINE HISTORY AS OBSERVED VIA THE SINGLE CARDIOIDS SENSOR AT SITE A3 DURING THE 21 NOV FIELD EVENT WITH VERNIER RESOLUTION (U)

AS-77-2741

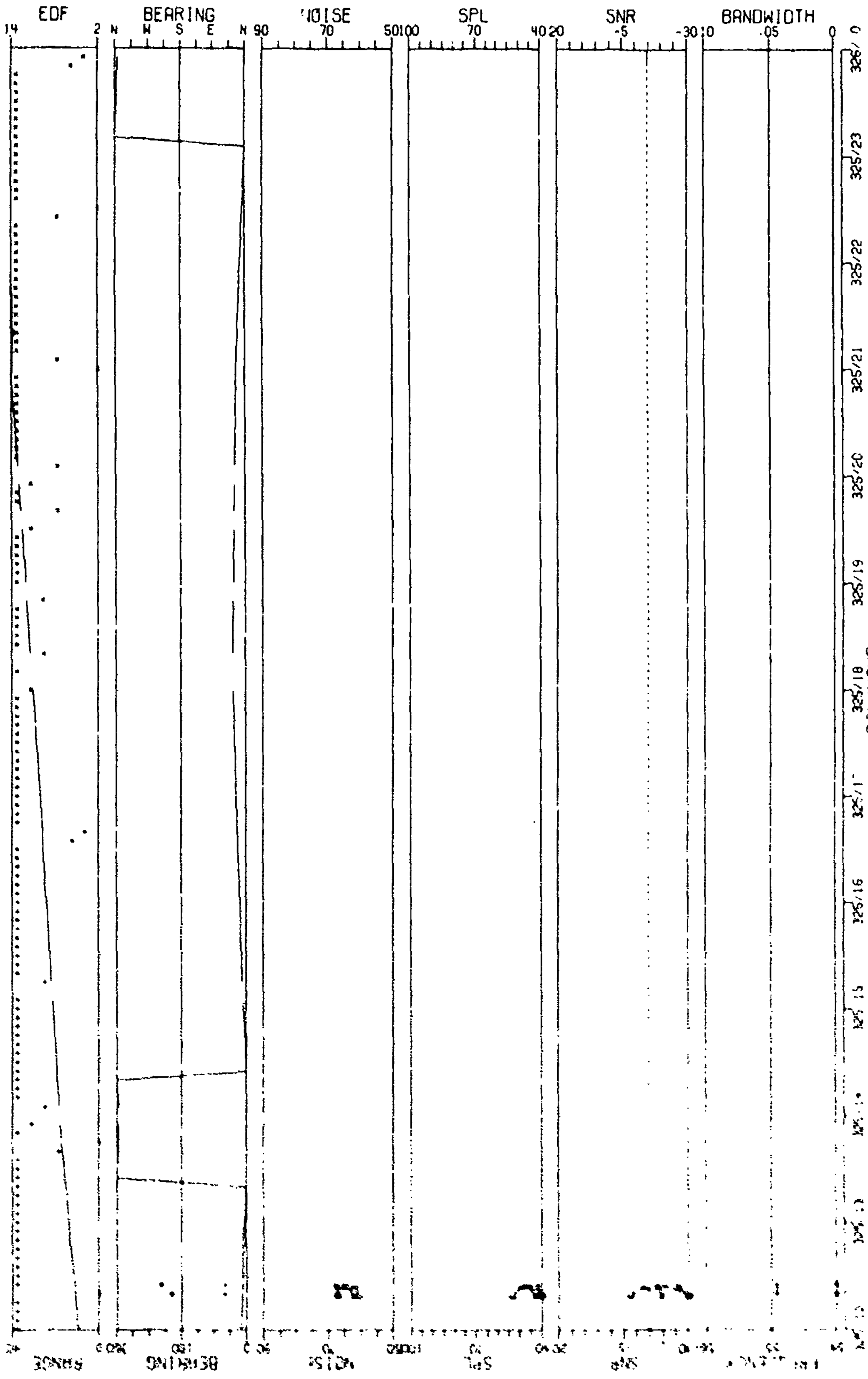

FIGURE III-142
MSS-F,T 55 HZ LINE HISTORY AS OBSERVED VIA THE DIFFERENCED CARDIOIDS SENSOR AT SITE A3 DURING THE 21 NOV FIELD EVENT WITH VERNIER RESOLUTION (U)

AS-77-2742

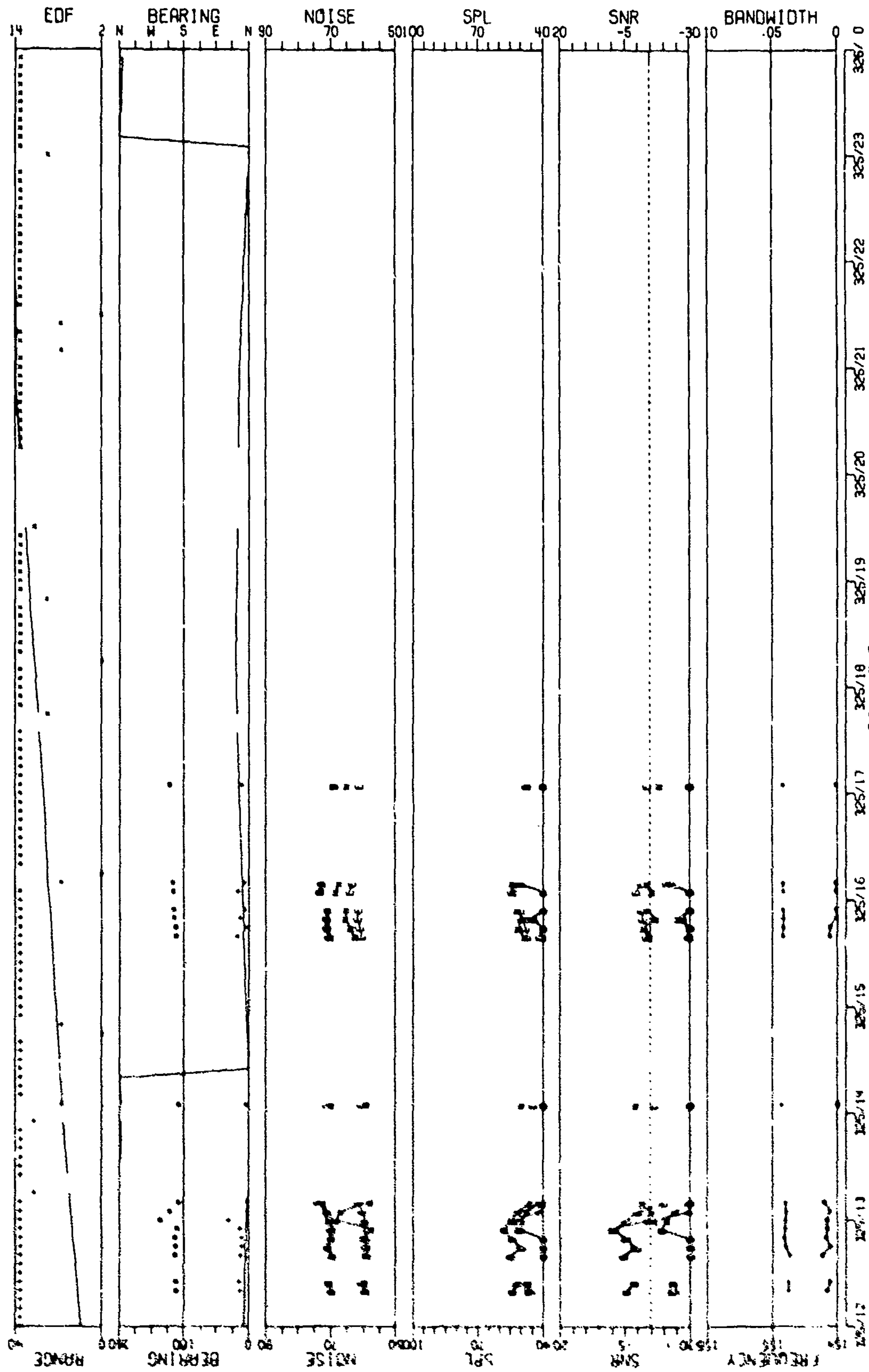

FIGURE III-143
MSS-FVT 155 HZ LINE HISTORY AS OBSERVED VIA THE SINGLE CARDIOIDS SENSOR
AT SITE A3 DURING THE 21 NOV FIELD EVENT WITH VERNIER RESOLUTION (U)

AS-77-2743

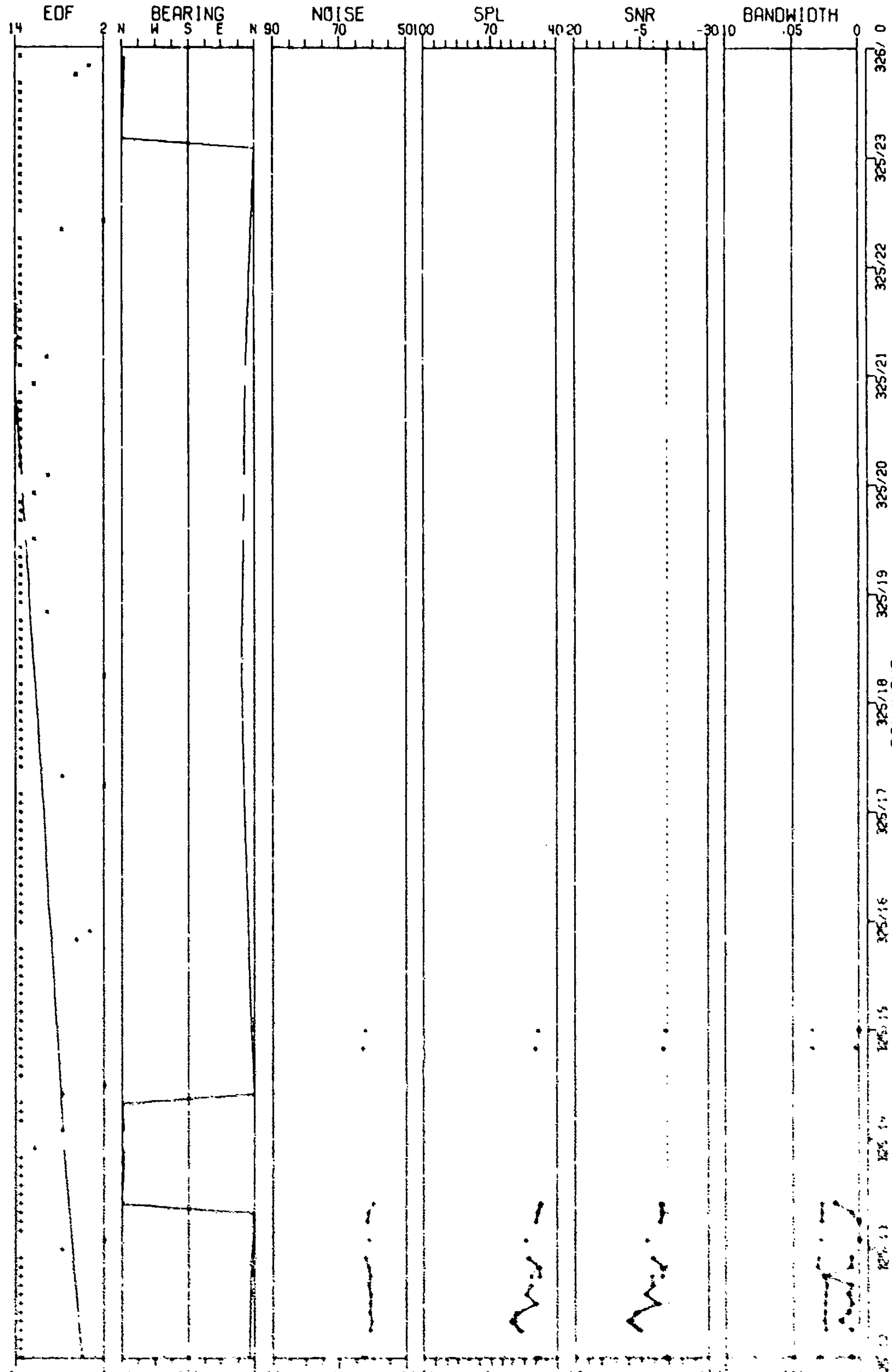

FIGURE III-144
...-FIT 305 HZ LINE HISTORY AS OBSERVED VIA THE OMNIDIRECTIONAL SENSOR AT SITE A3 DURING THE 21 NOV FIELD EVENT WITH VERNIER RESOLUTION (U)

AS-77-2744

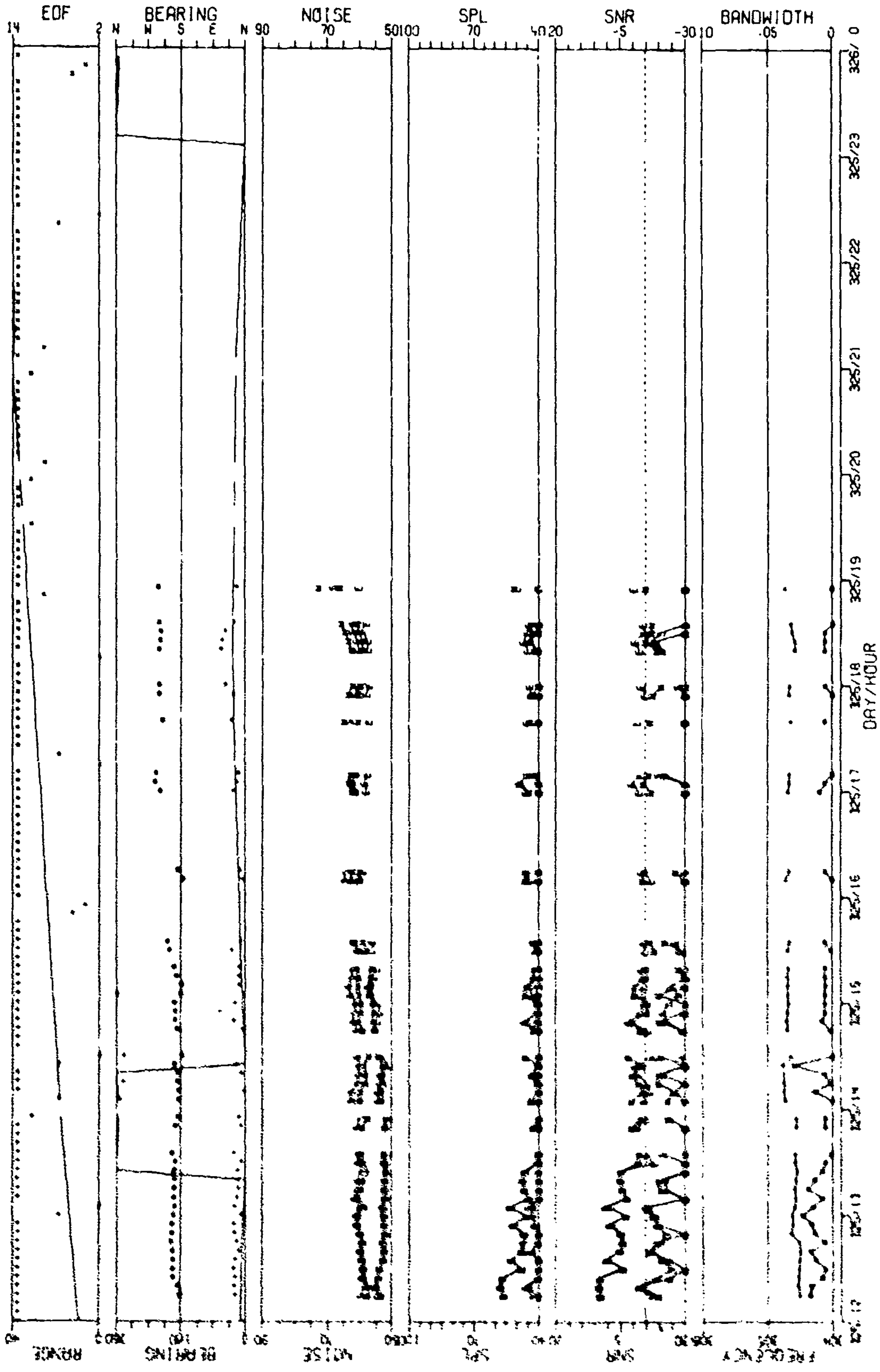

FIGURE III-145
MSS-FVT 305 HZ LINE HISTORY AS OBSERVED VIA THE SINGLE CARDIOIDS SENSOR AT SITE A3 DURING THE 21 NOV FIELD EVENT WITH VERNIER RESOLUTION (U)

AS-77-2745

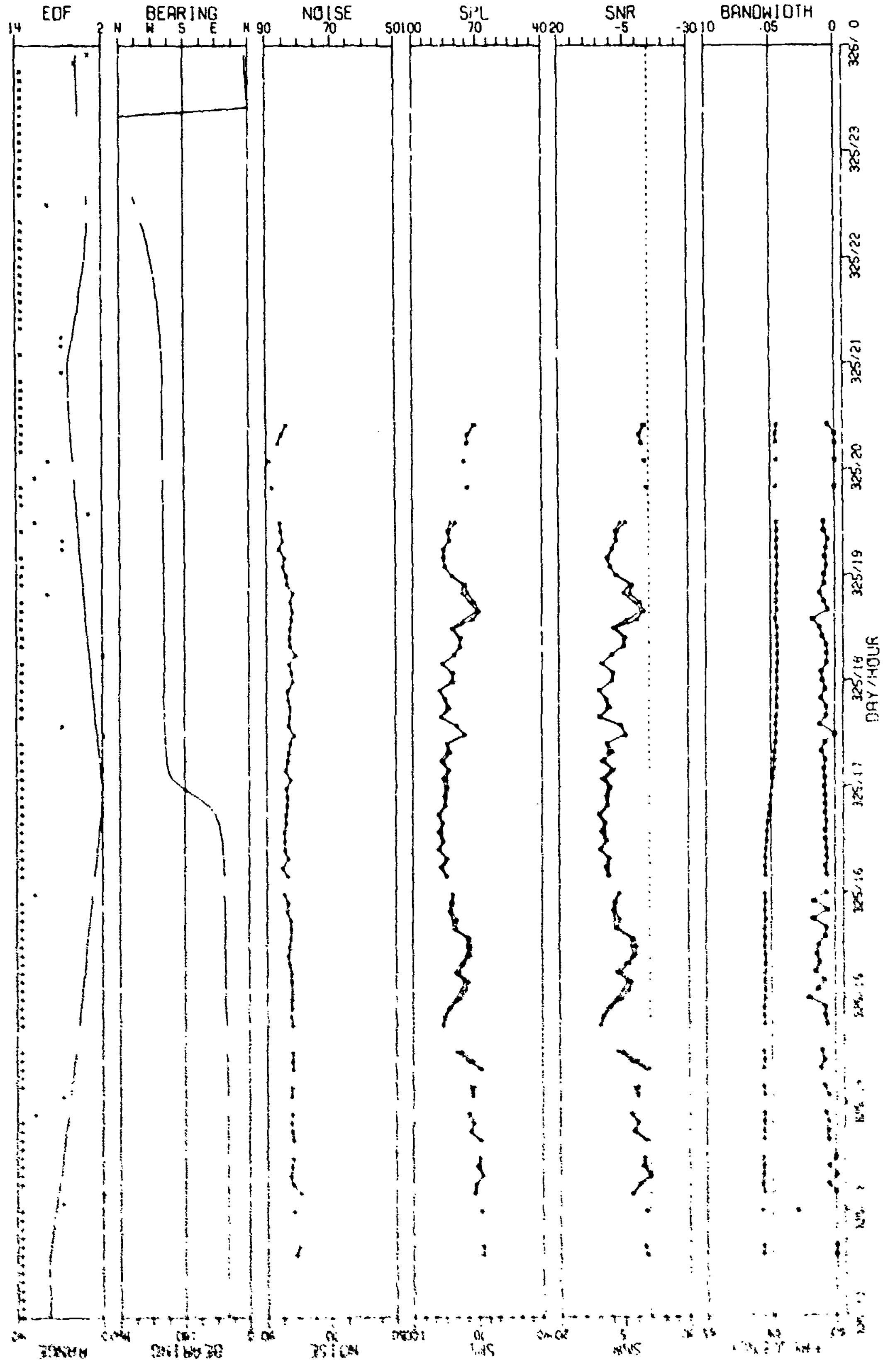

FIGURE III-146
[illegible] 64 HZ LINE HISTORY AS OBSERVED VIA THE OMNIDIRECTIONAL SENSOR [illegible] SITE A3 DURING THE 21 NOV FIELD EVENT WITH VERNIER RESOLUTION (U)

AS-77-2746

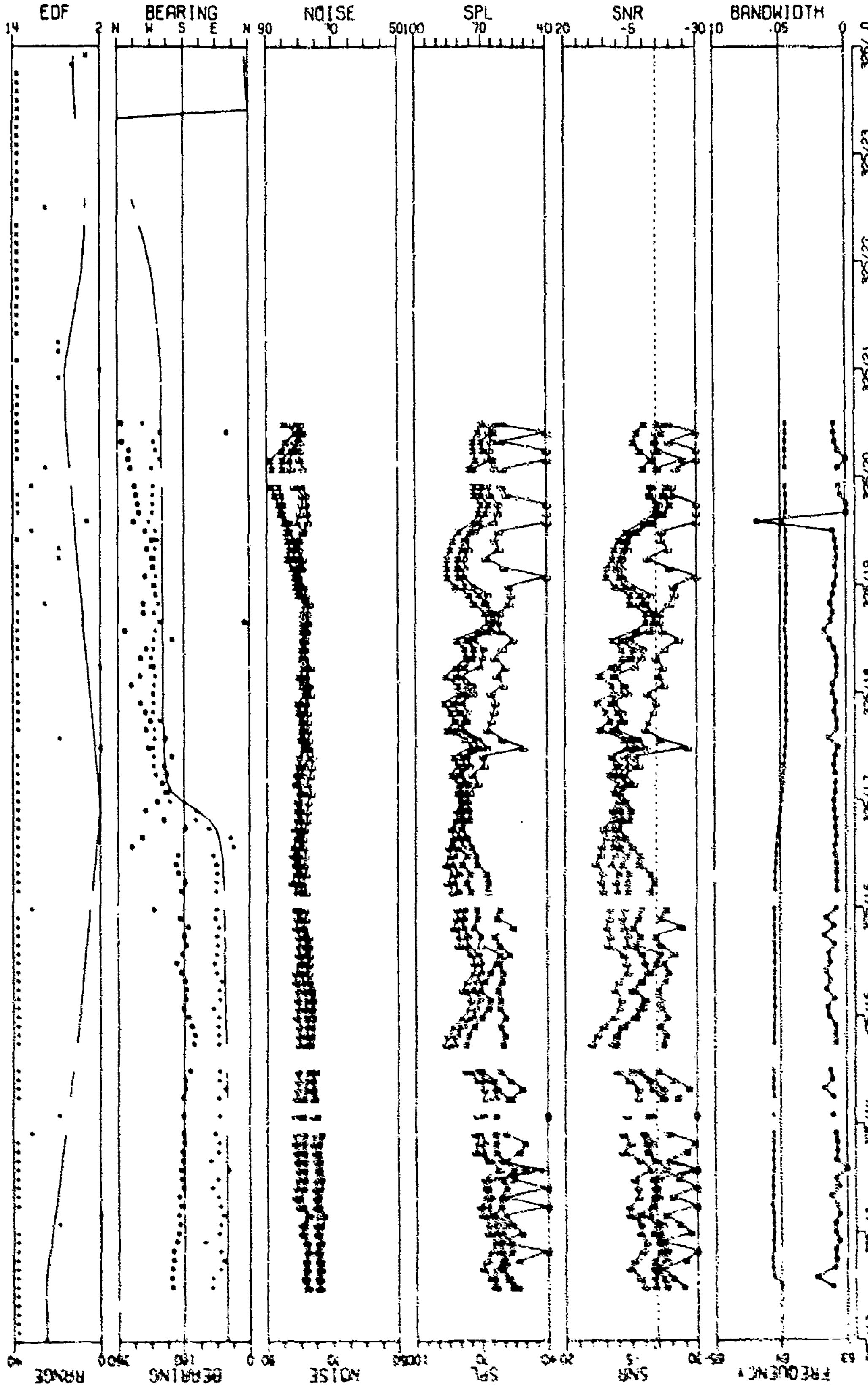

FIGURE III-147
MSS-FVI 64 HZ LINE HISTORY AS OBSERVED VIA THE SINGLE CARDIOIDS SENSOR AT SITE A3 DURING THE 21 NOV FIELD EVENT WITH VERNIER RESOLUTION (U)

AS-77-2747

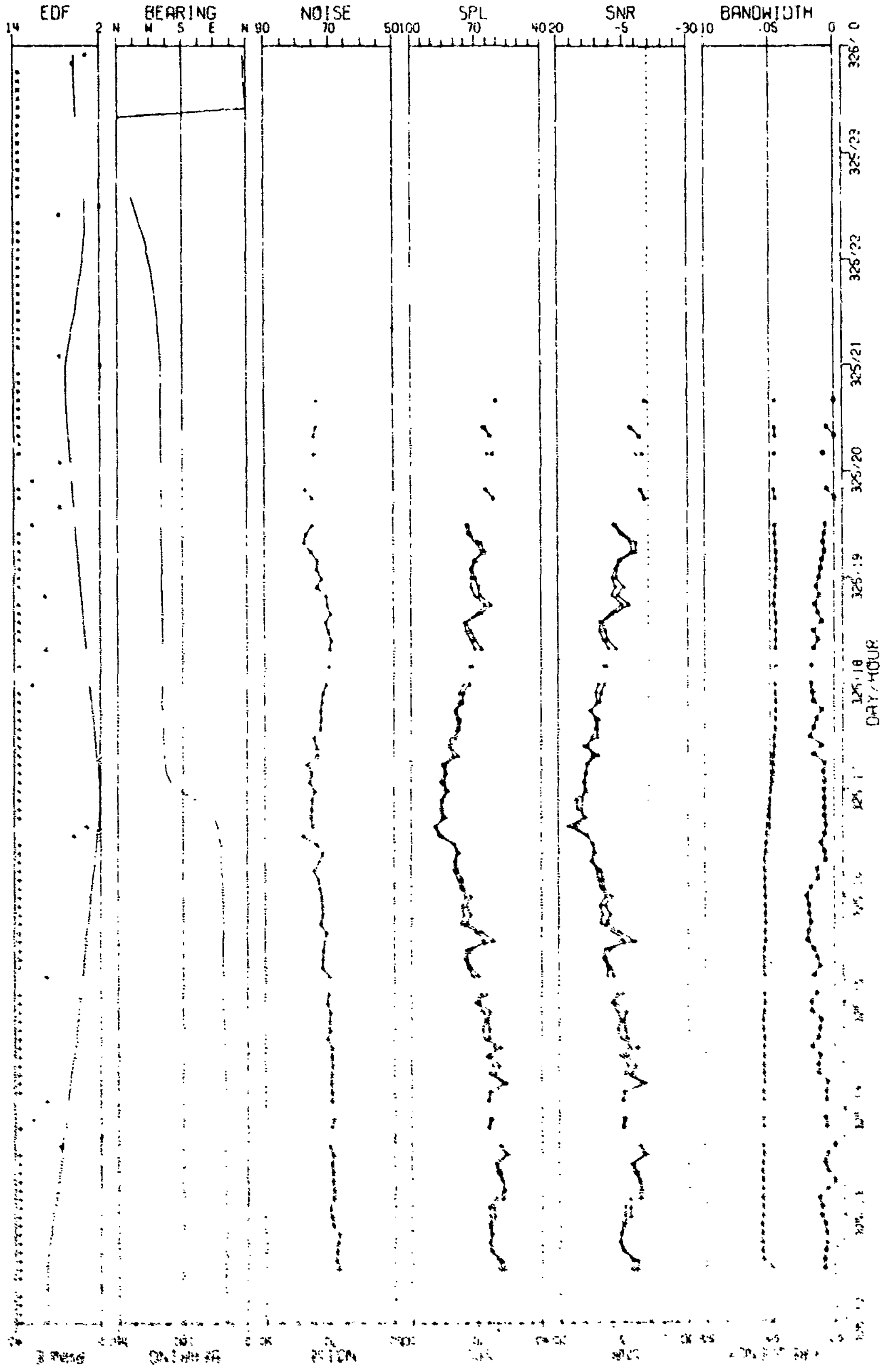

FIGURE III-148
[illegible] LINE HISTORY AS OBSERVED VIA THE VERTICAL DIPOLE SENSOR
[illegible] THE 21 NOV FIELD EVENT WITH VERNIER RESOLUTION (U)

AS-77-2748

FIGURE III-149
ASS-FVT AN H2 LINE HISTORY AS OBSERVED VIA THE DIFFERENCED CARDIOIDS SENSOR AT SITE A3 DURING THE 2. NO. FIELD EVENT WITH VERNIER RESOLUTION (U)

AS-77-2749

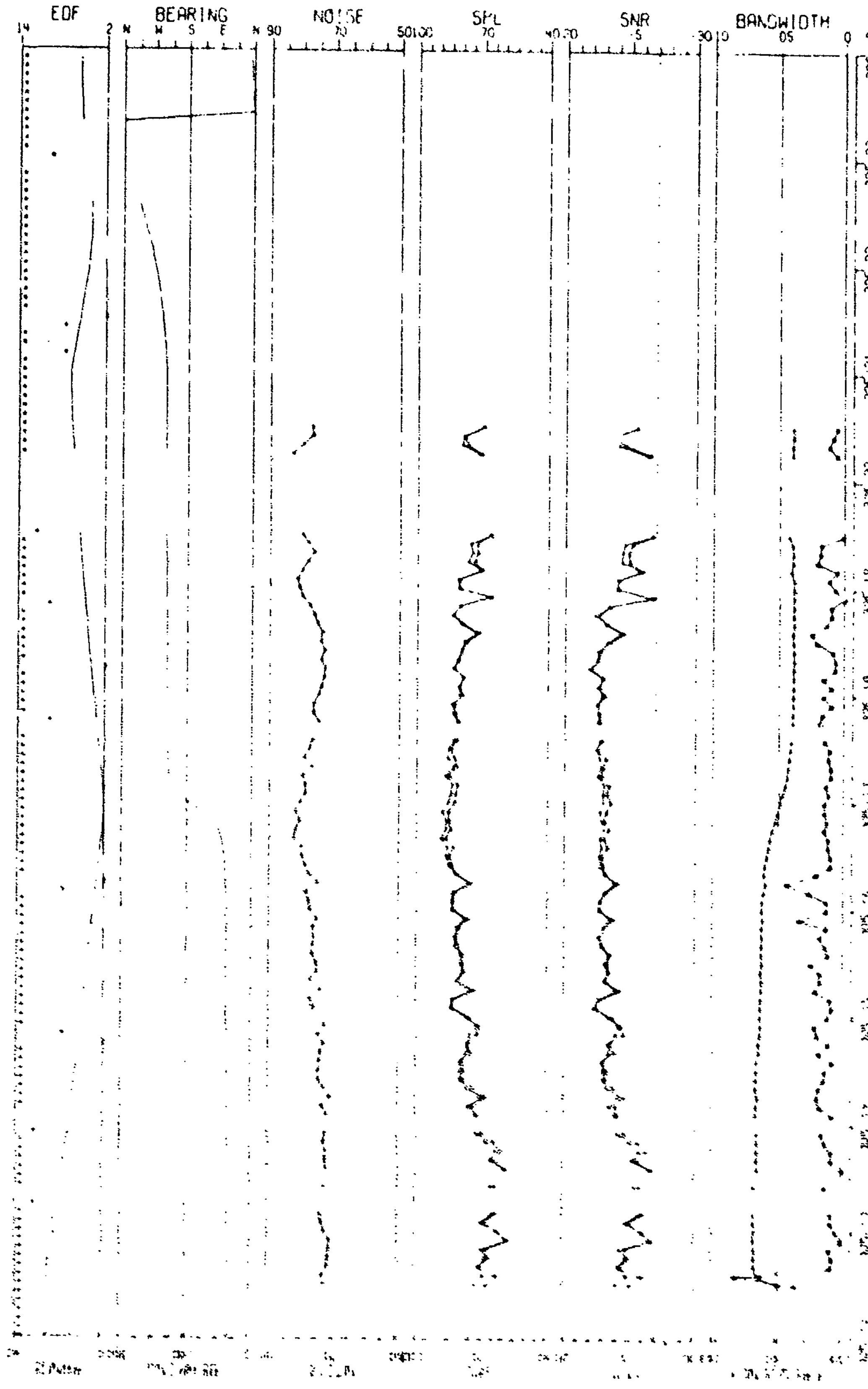

FIGURE III-150
OBSERVED VIA THE OMNIDIRECTIONAL SENSOR
RESOLUTION (U)

AS-77-2750

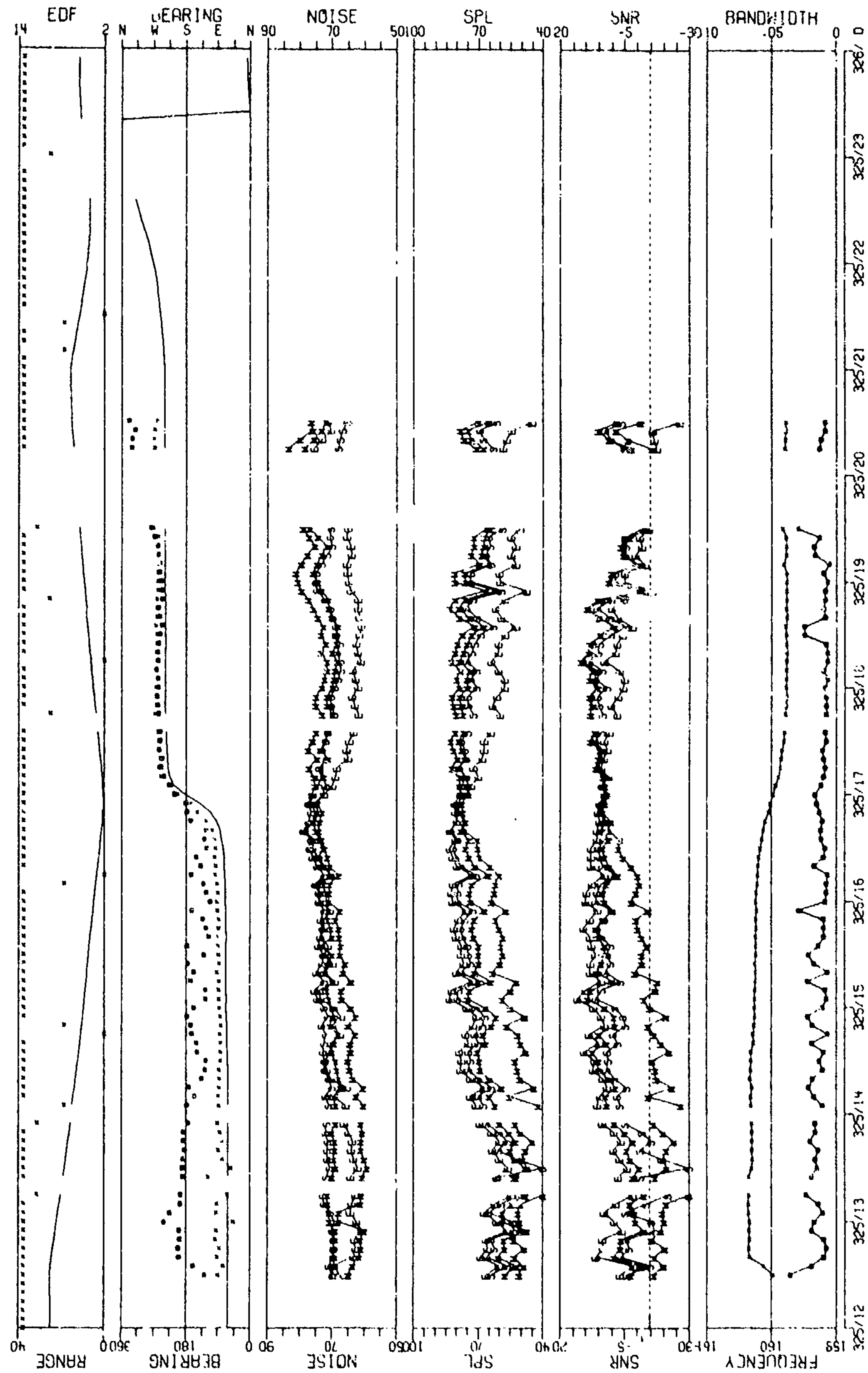

FIGURE III-151
MSS-FVT 160 HZ LINE HISTORY AS OBSERVED VIA THE SINGLE CARDIOIDS SENSOR AT SITE A3 DURING THE 21 NOV FIELD EVENT WITH VERNIER RESOLUTION (U)

AS-77-2751

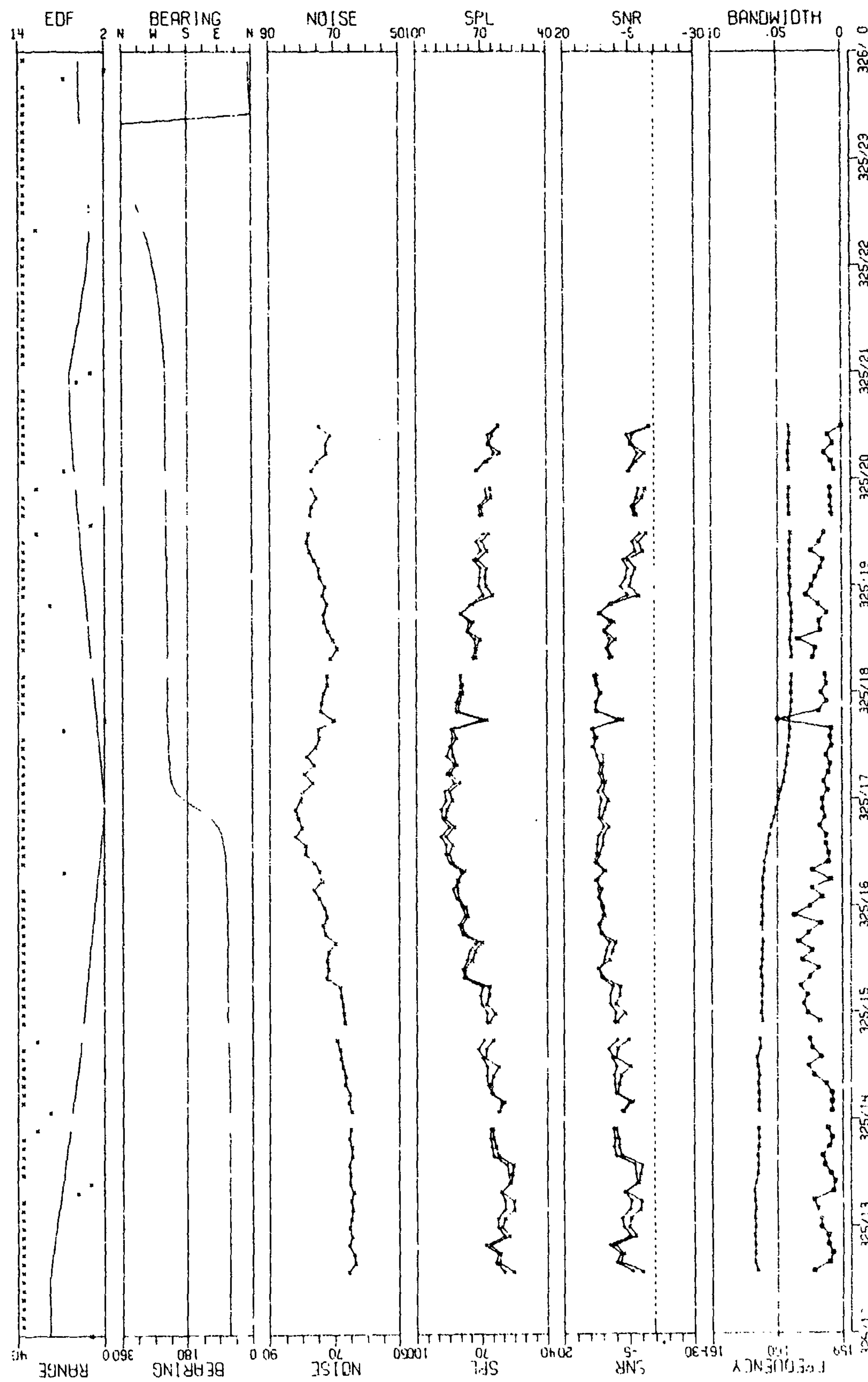

FIGURE III-152
MSS-FVI 160 HZ LINE HISTORY AS OBSERVED VIA THE VERTICAL DIPOLE SENSOR AT SITE A3 DURING THE 21 NOV FIELD EVENT WITH VERNIER RESOLUTION (U)

AS-77-2752

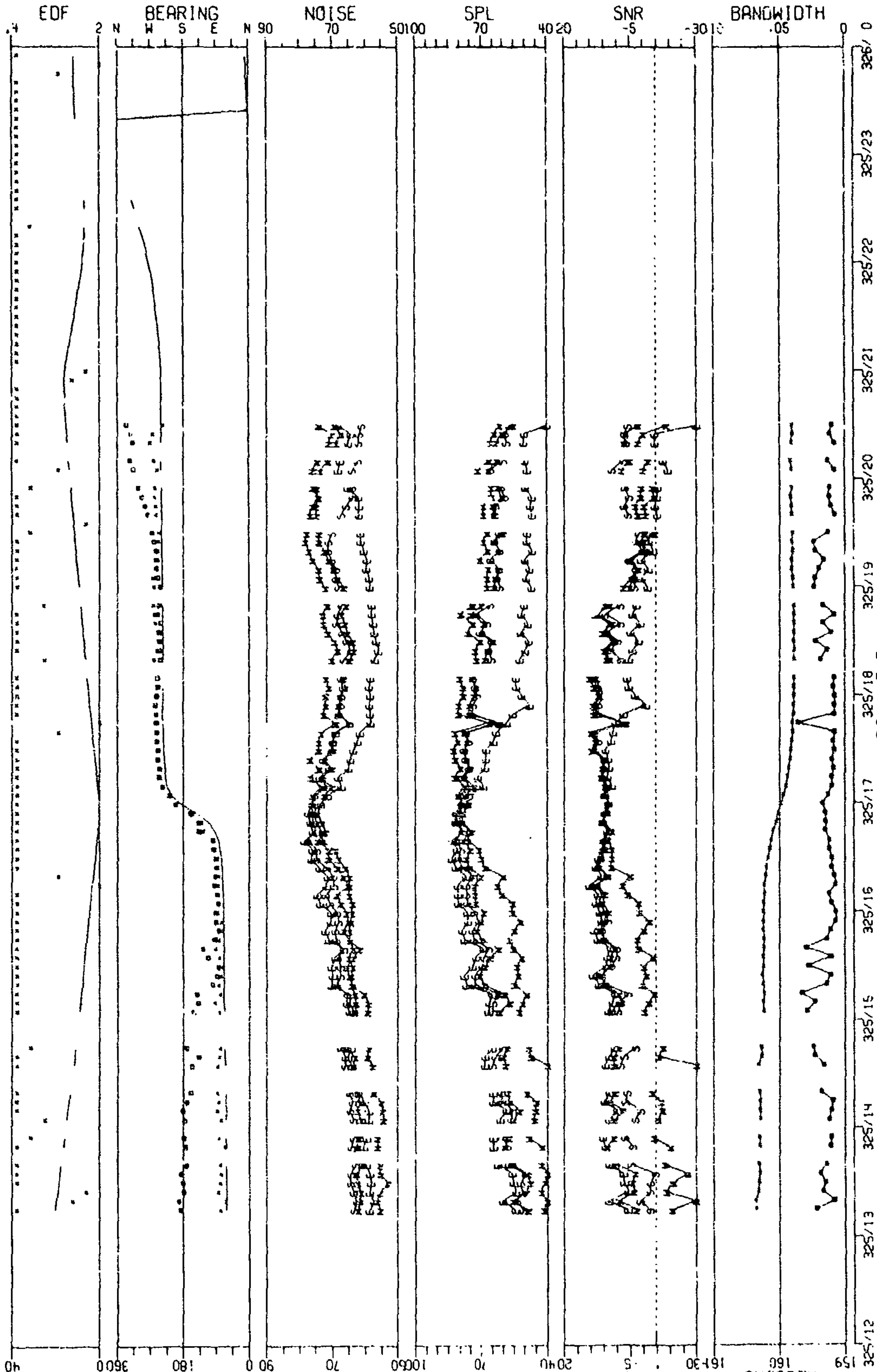

FIGURE III-153
MSS-FVT 160 HZ LINE HISTORY AS OBSERVED VIA THE DIFFERENCED CARDIOIDS SENSOR
AT SITE A3 DURING THE 21 NOV FIELD EVENT WITH VERNIER RESOLUTION (U)

AS-77-2753

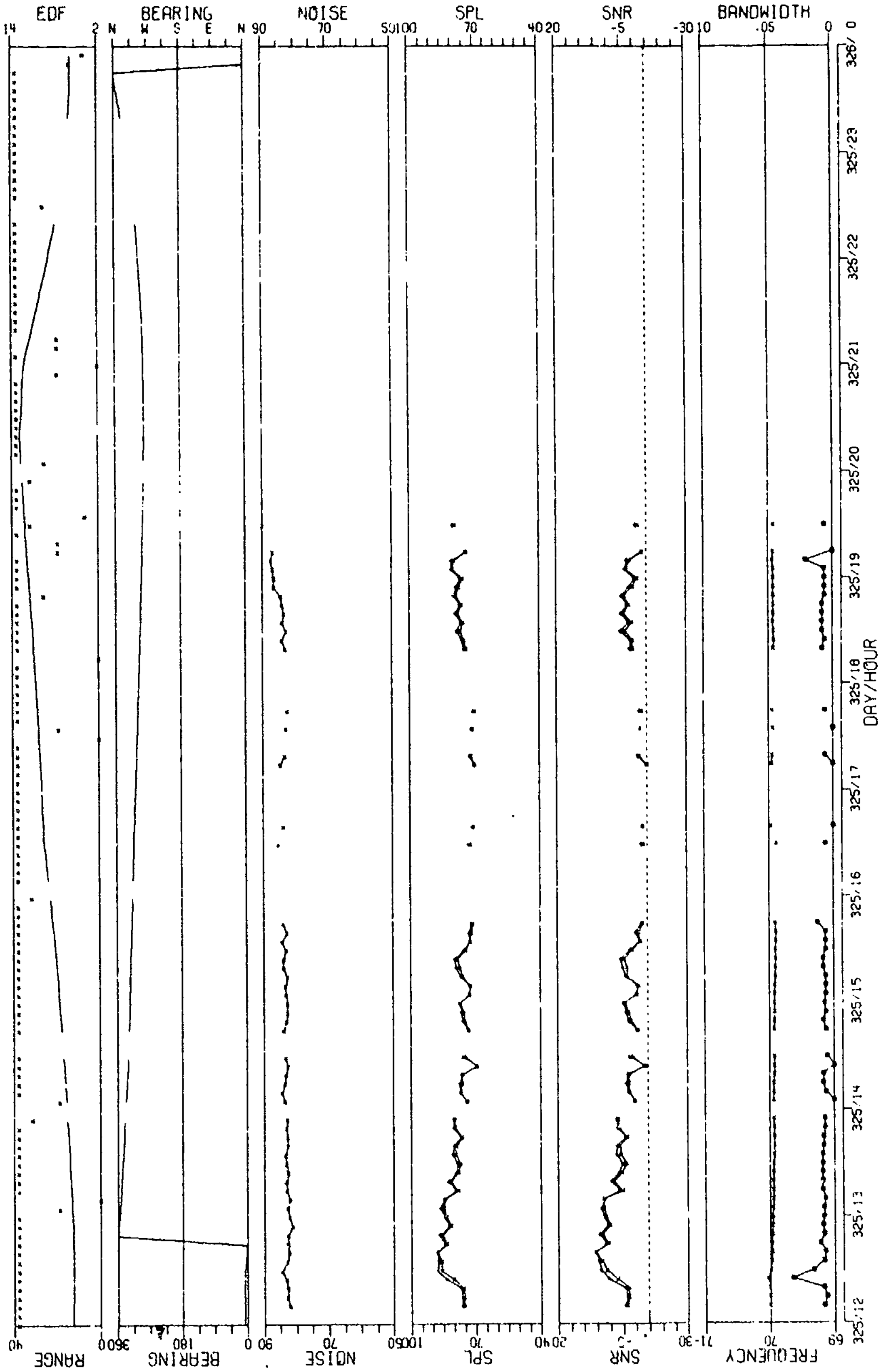

FIGURE III-154
MSS-FVT 70 HZ LINE HISTORY AS OBSERVED VIA THE OMNIDIRECTIONAL SENSOR
AT SITE A3 DURING THE 21 NOV FIELD EVENT WITH VERNIER RESOLUTION (U)

AS-77-2754

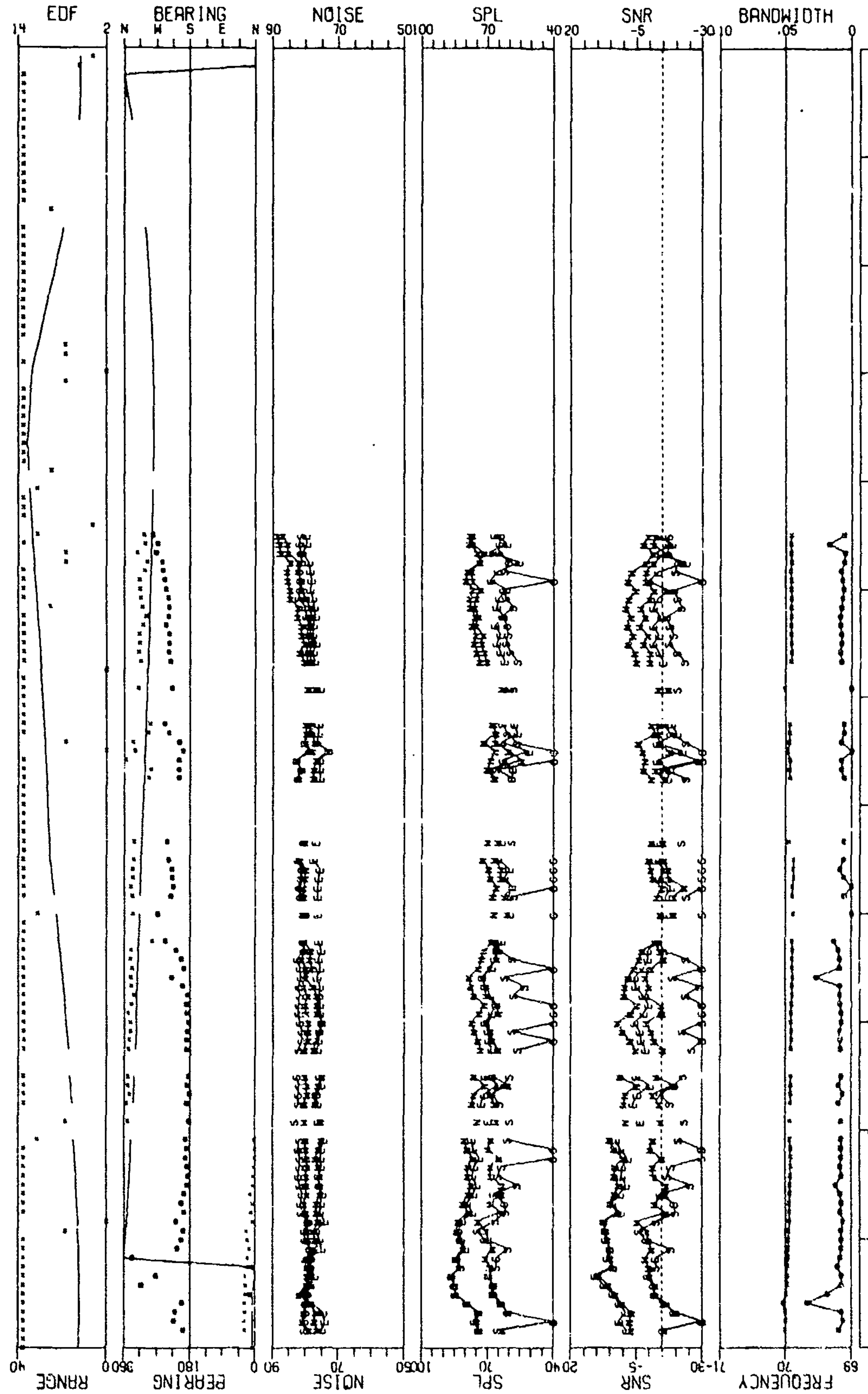

FIGURE III-155
MSS-FVT 70 HZ LINE HISTORY AS OBSERVED VIA THE SINGLE CARDIOIDS SENSOR AT SITE A3 DURING THE 21 NOV FIELD EVENT WITH VERNIER RESOLUTION (U)

AS-77-2755

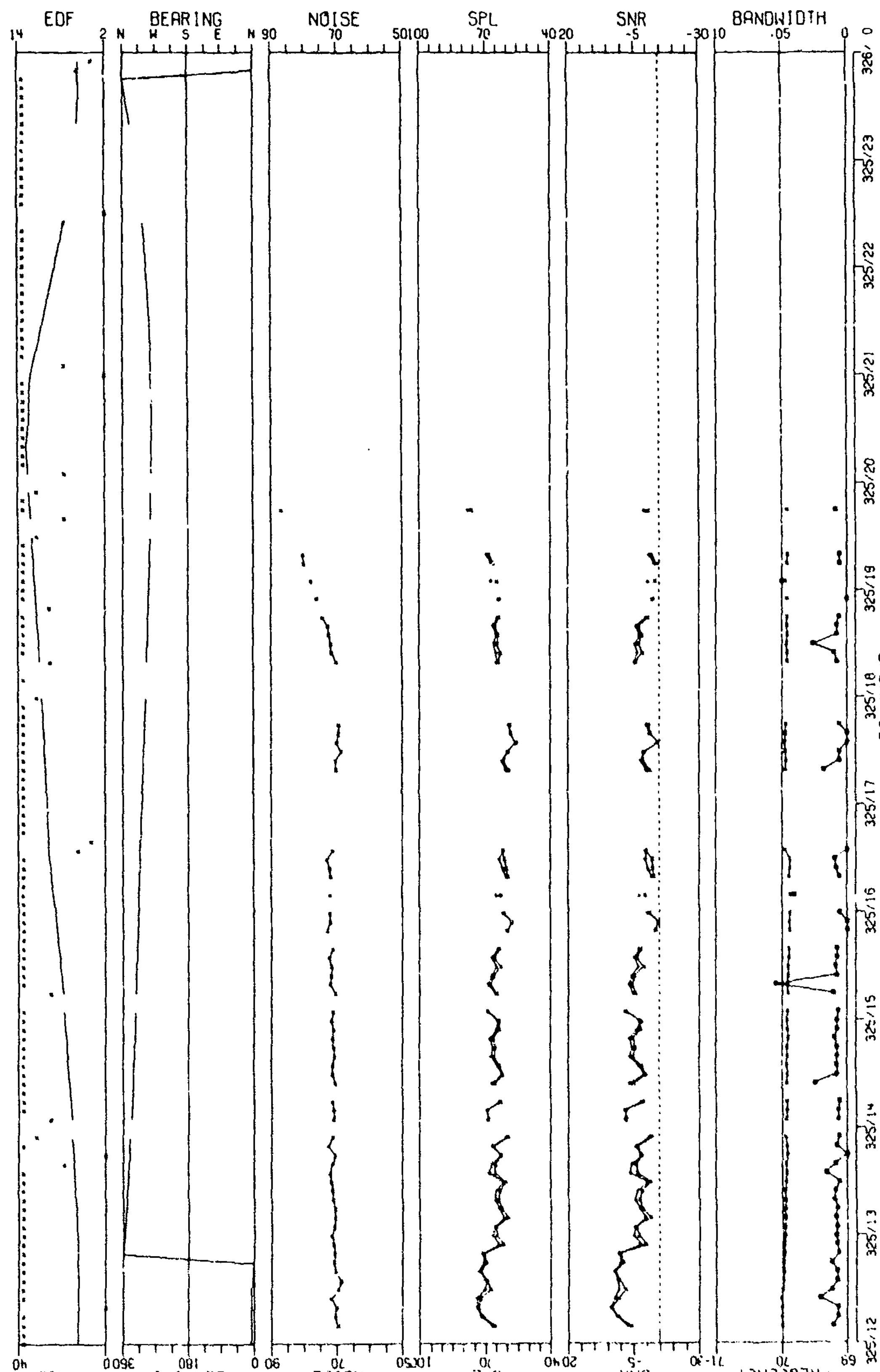

FIGURE III-156
MSS-FVT 70 HZ LINE HISTORY AS OBSERVED VIA THE VERTICAL DIPOLE SENSOR AT SITE A3 DURING THE 21 NOV FIELD EVENT WITH VERNIER RESOLUTION (U)

AS-77-2756

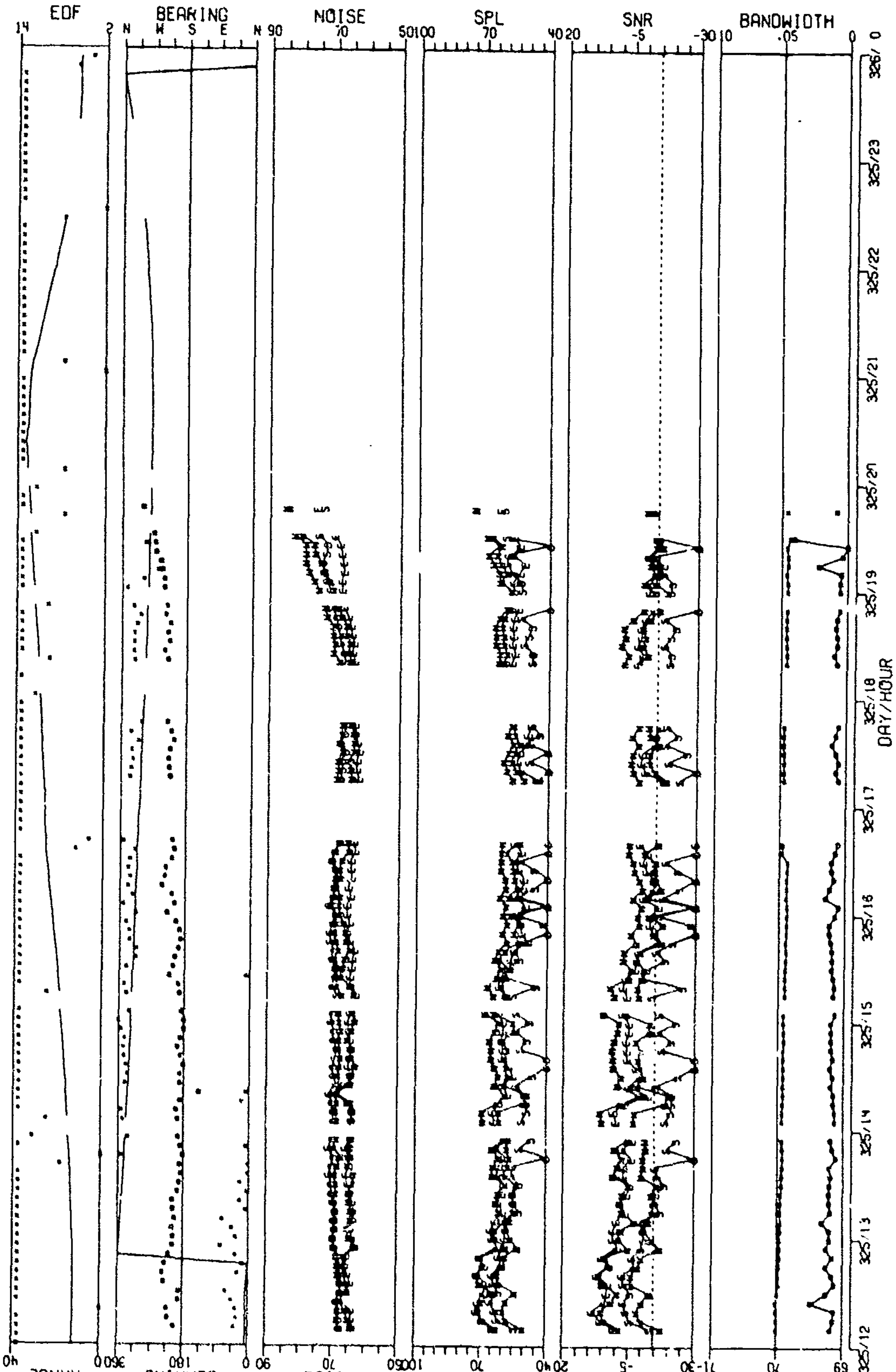

FIGURE III-157
MSS-FVT 70 HZ LINE HISTORY AS OBSERVED VIA THE DIFFERENCED CARDIOIDS SENSOR AT SITE A3 DURING THE 21 NOV FIELD EVENT WITH VERNIER RESOLUTION (U)

AS-77-2757

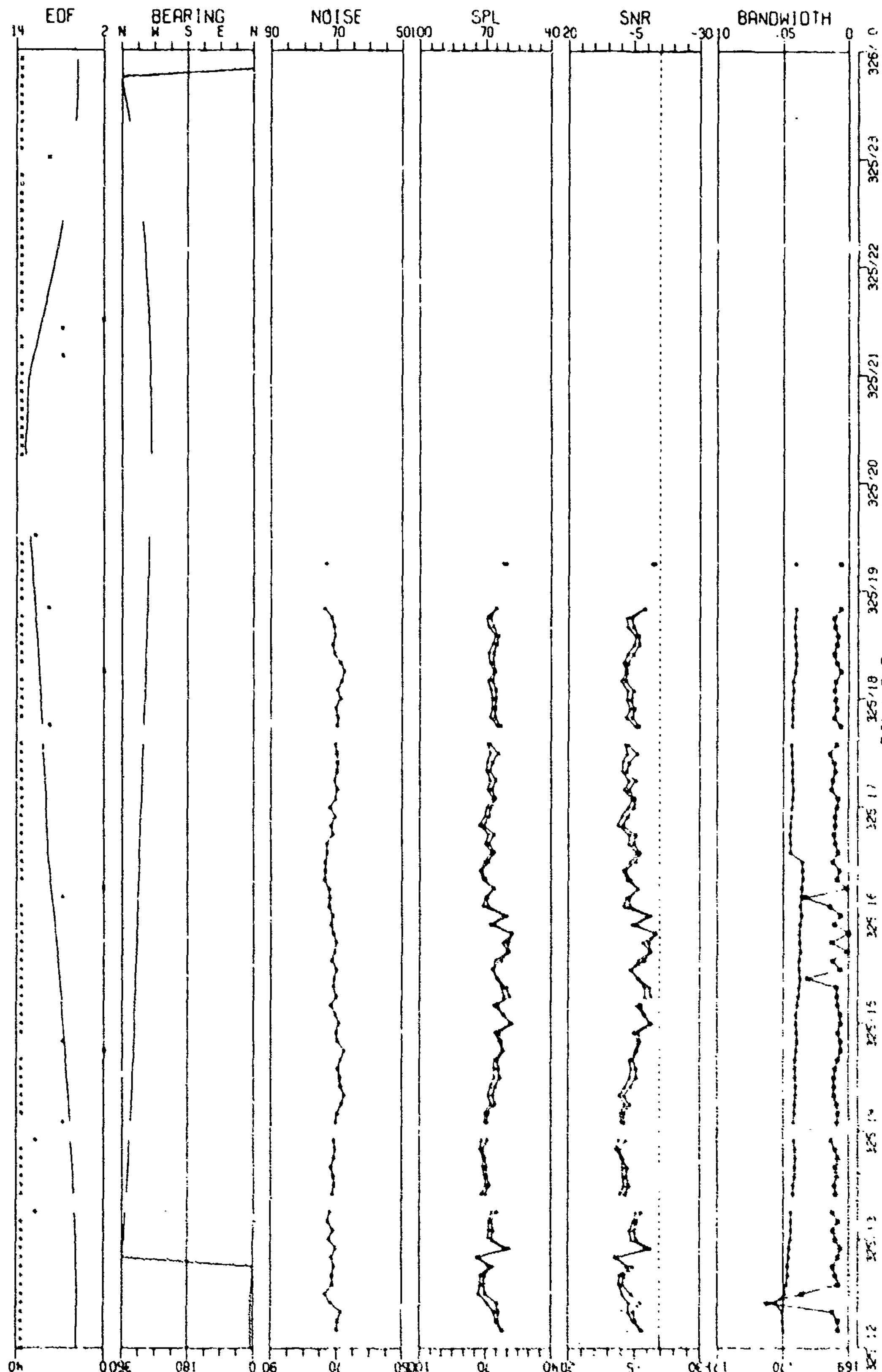

FIGURE III-158
[illegible] LINE HISTORY AS OBSERVED VIA THE OMNIDIRECTIONAL SENSOR [illegible] THE 21 [illegible] FIELD EVENT WITH VERNIER RESOLUTION (U)

AS-77-2758

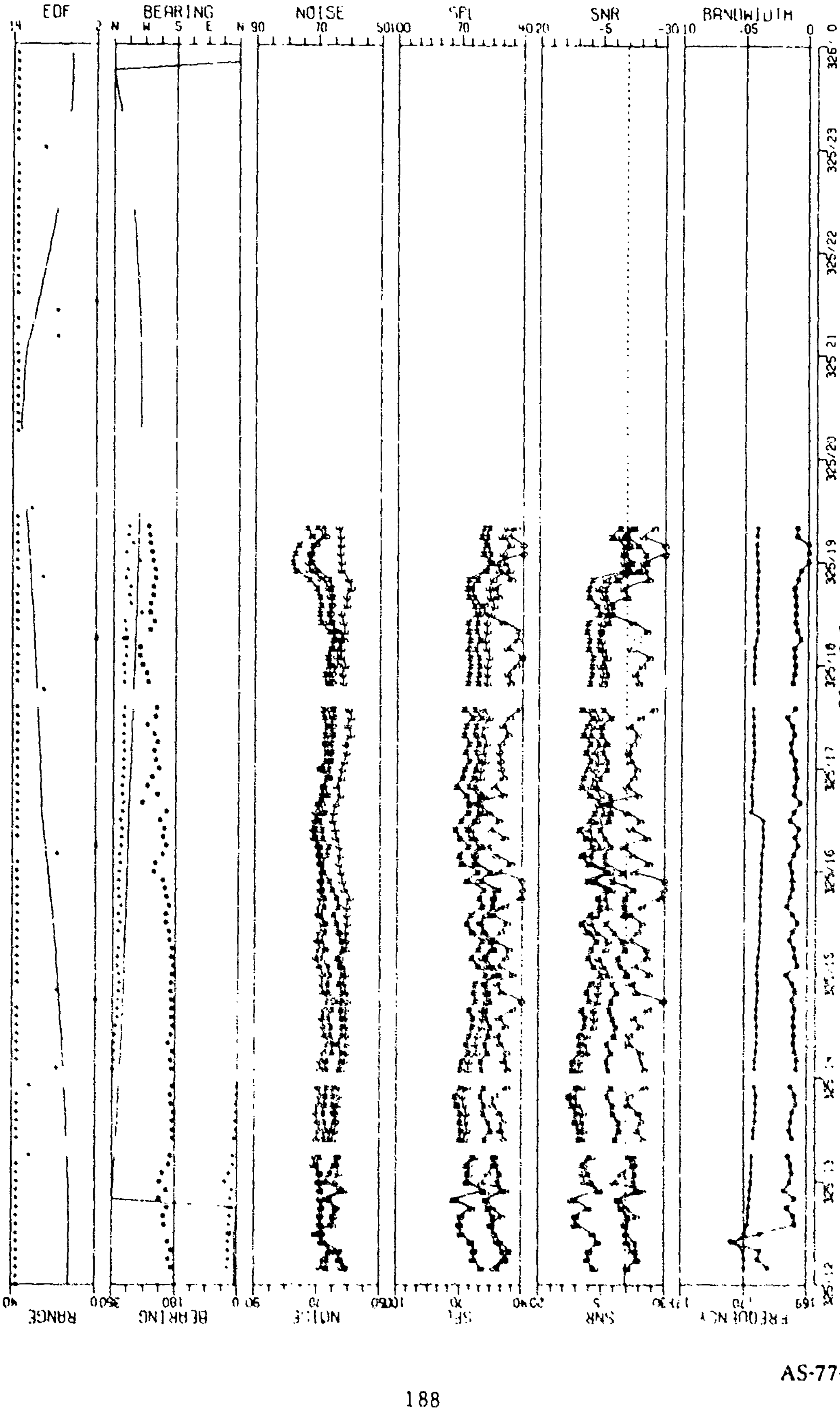

FIGURE III-159
[illegible] HZ LINE HISTORY AS OBSERVED VIA THE SINGLE CARDI[illegible] SENSOR
[illegible] DURING THE 21 NOV FIELD EVENT WITH VERNIER RESOLUTION (U)

AS-77-2759

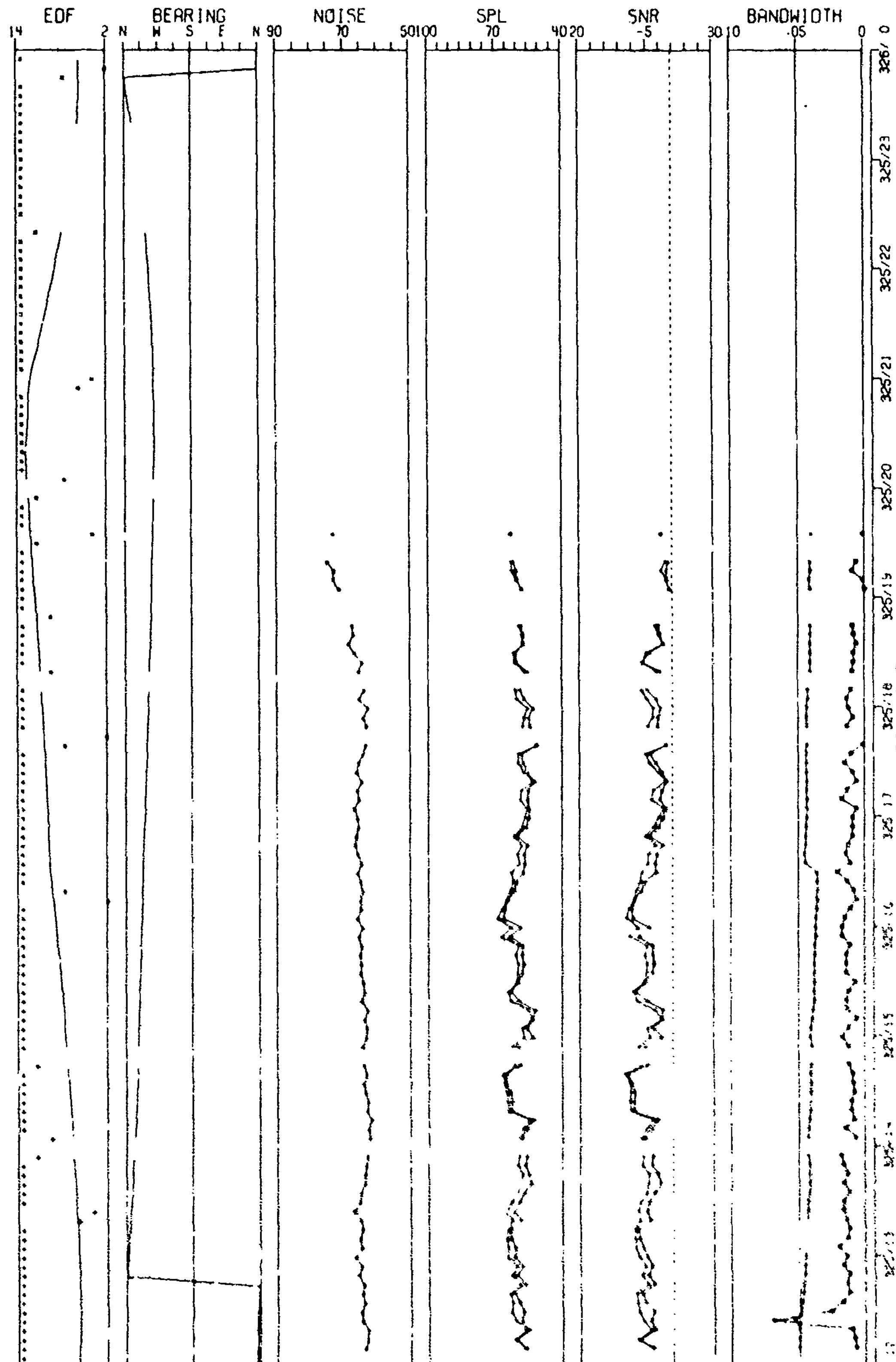

FIGURE III-160
MSS-F[illegible] HZ LINE HISTORY AS OBSERVED VIA THE VERTICAL DIPOLE SENSOR
[illegible] DURING THE 21 NOV. FIELD EVENT WITH VERNIER RESOLUTION (U)

AS-77-2760

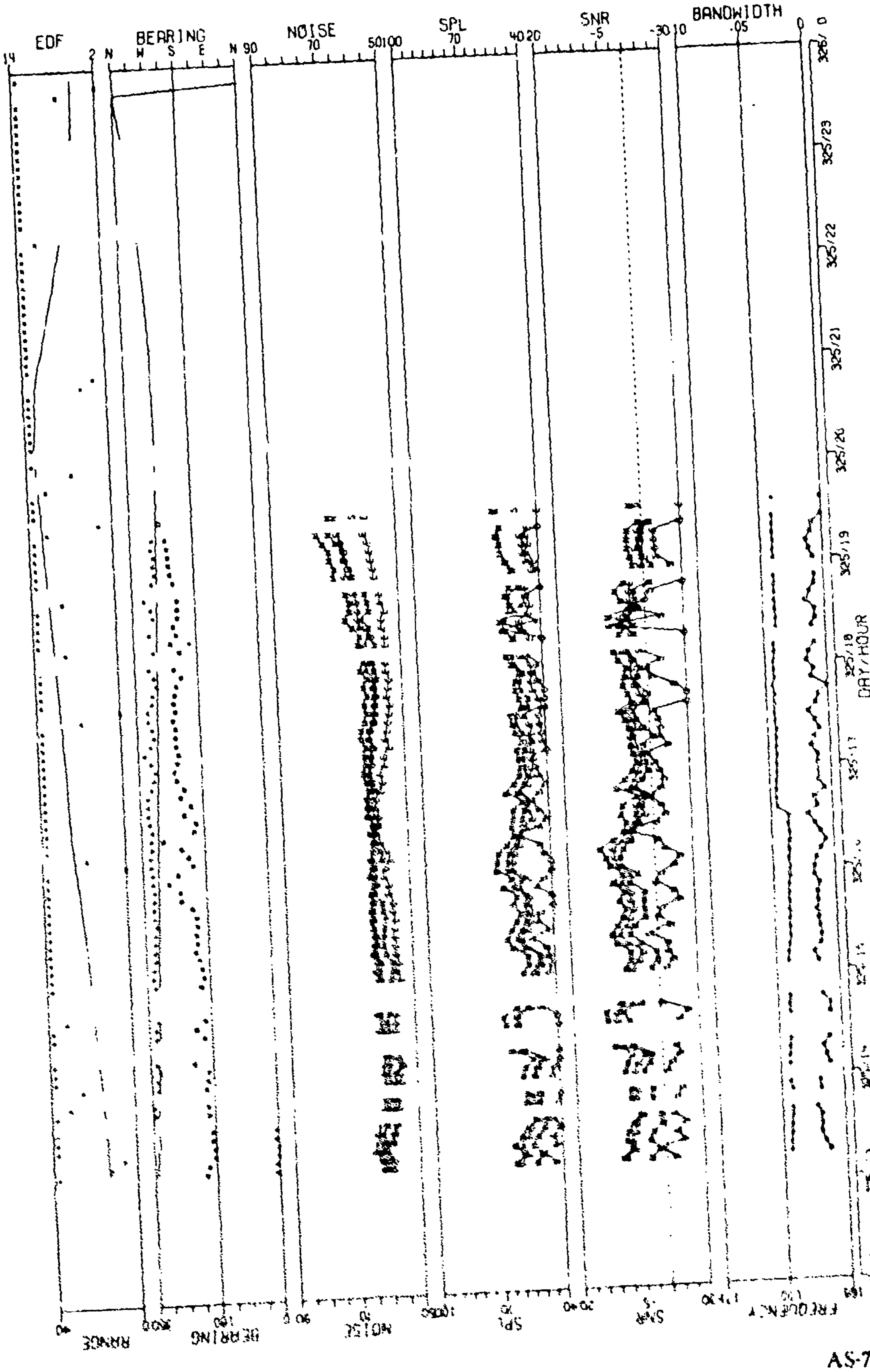

FIGURE III-161
MSS FY1 170 HZ LINE HISTORY AS OBSERVED VIA THE DIFFERENCED CARDIOIDS SENSOR AT SITE 33 DURING THE 21 NOV FIELD EVENT WITH VERNIER RESOLUTION (U)

AS-77-2761

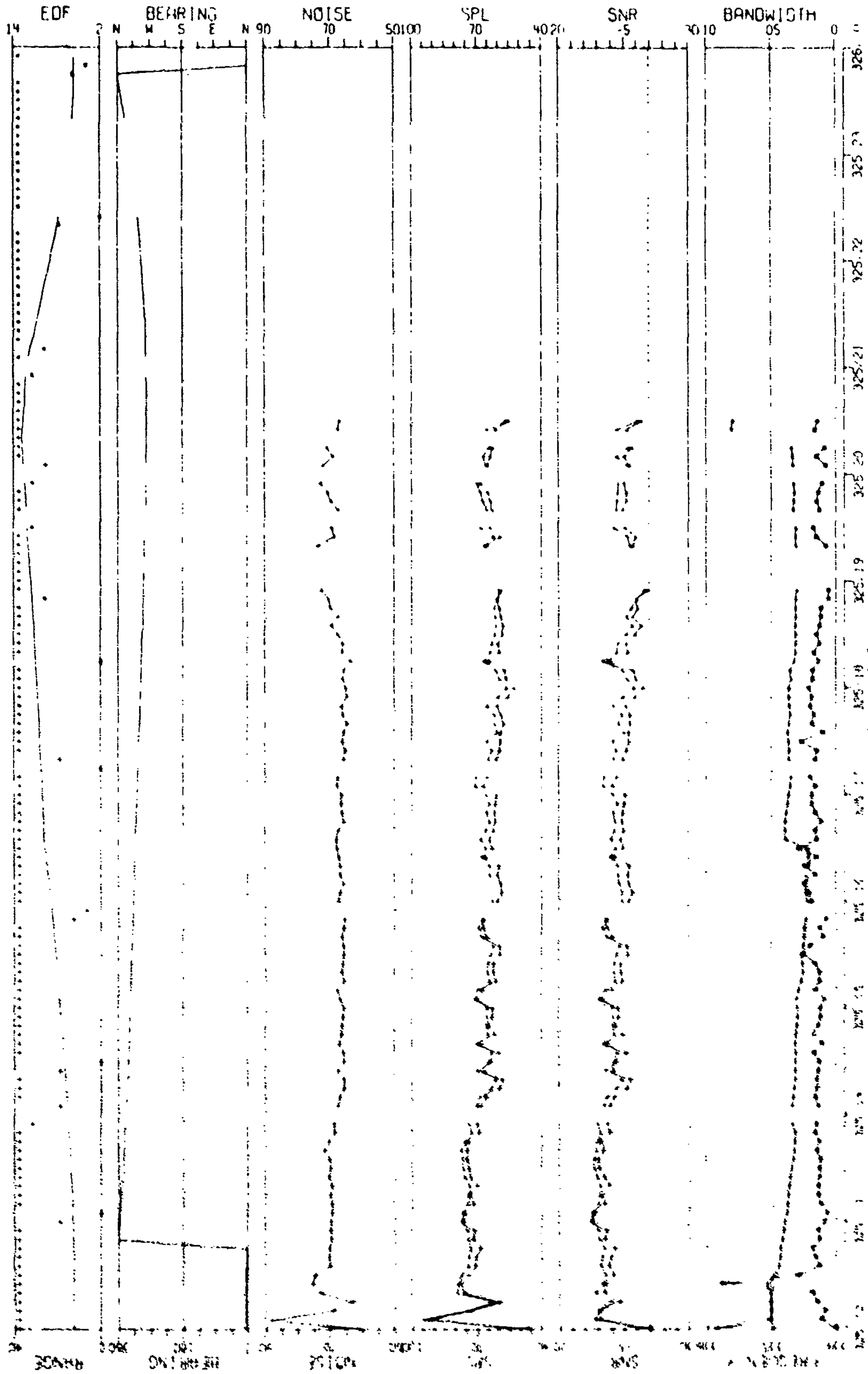

FIGURE III-102
... RECORDED WITH THE OMNIDIRECTIONAL SENSOR
... FIELD EVENT WITH VERNIER RESOLUTION (U)

AS-77-2762

FIGURE III-163
MOSS FVT 335 HZ LINE HISTORY AS OBSERVED VIA THE SINGLE CARDIOIDS SENSOR AT SITE A3 DURING THE 21 NOV FIELD EVENT WITH VERNIER RESOLUTION (U)

AS-77-2763

APPENDIX C

PROPAGATION LOSS versus RANGE CURVES (U)

(FIGURES III-164 - III-171)

CONFIDENTIAL

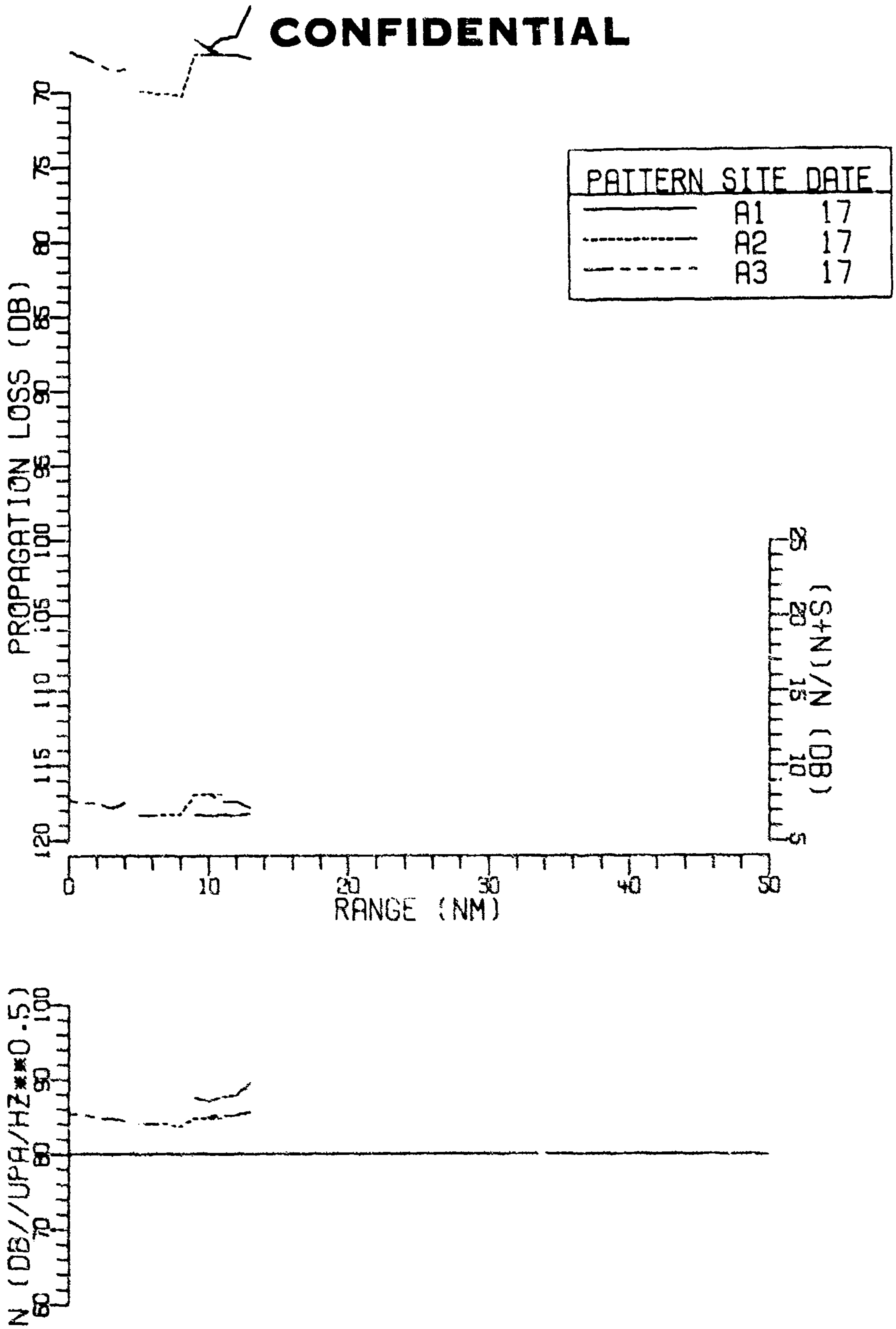

FIGURE III-164
MSS-FVT NEAR BOTTOM OMNIDIRECTIONAL SENSOR
PROPAGATION LOSS RESULTS FOR 55HZ AT 141DB (U)

AS-77-2764

CONFIDENTIAL

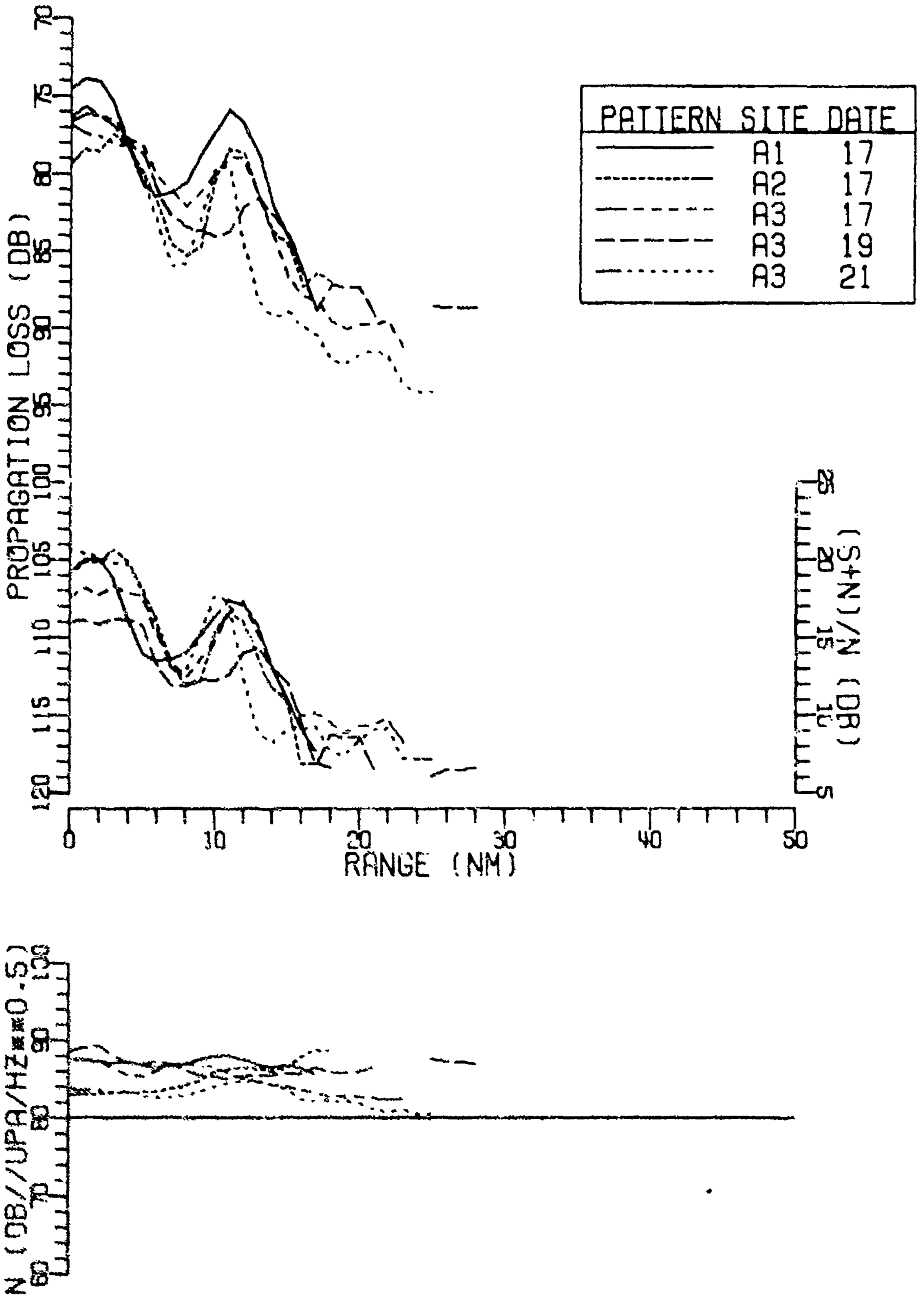

FIGURE III-165
MSS-FVT NEAR BOTTOM OMNIDIRECTIONAL SENSOR
PROPAGATION LOSS RESULTS FOR 64HZ AT 162DB (U)

AS-77-2765

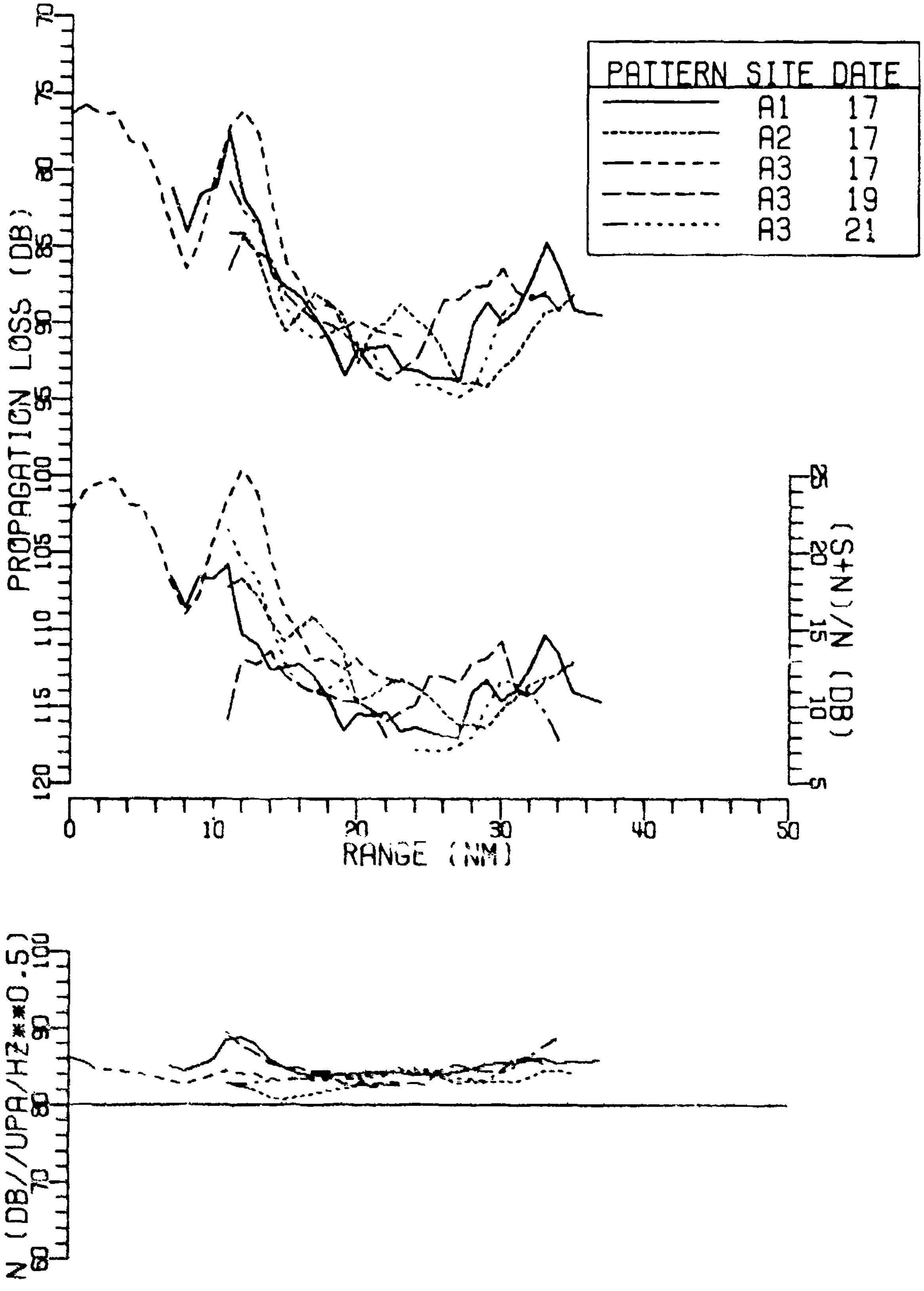

FIGURE III-166
MSS-FVT NEAR BOTTOM OMNIDIRECTIONAL SENSOR
PROPAGATION LOSS RESULTS FOR 70HZ AT 166DB (U)

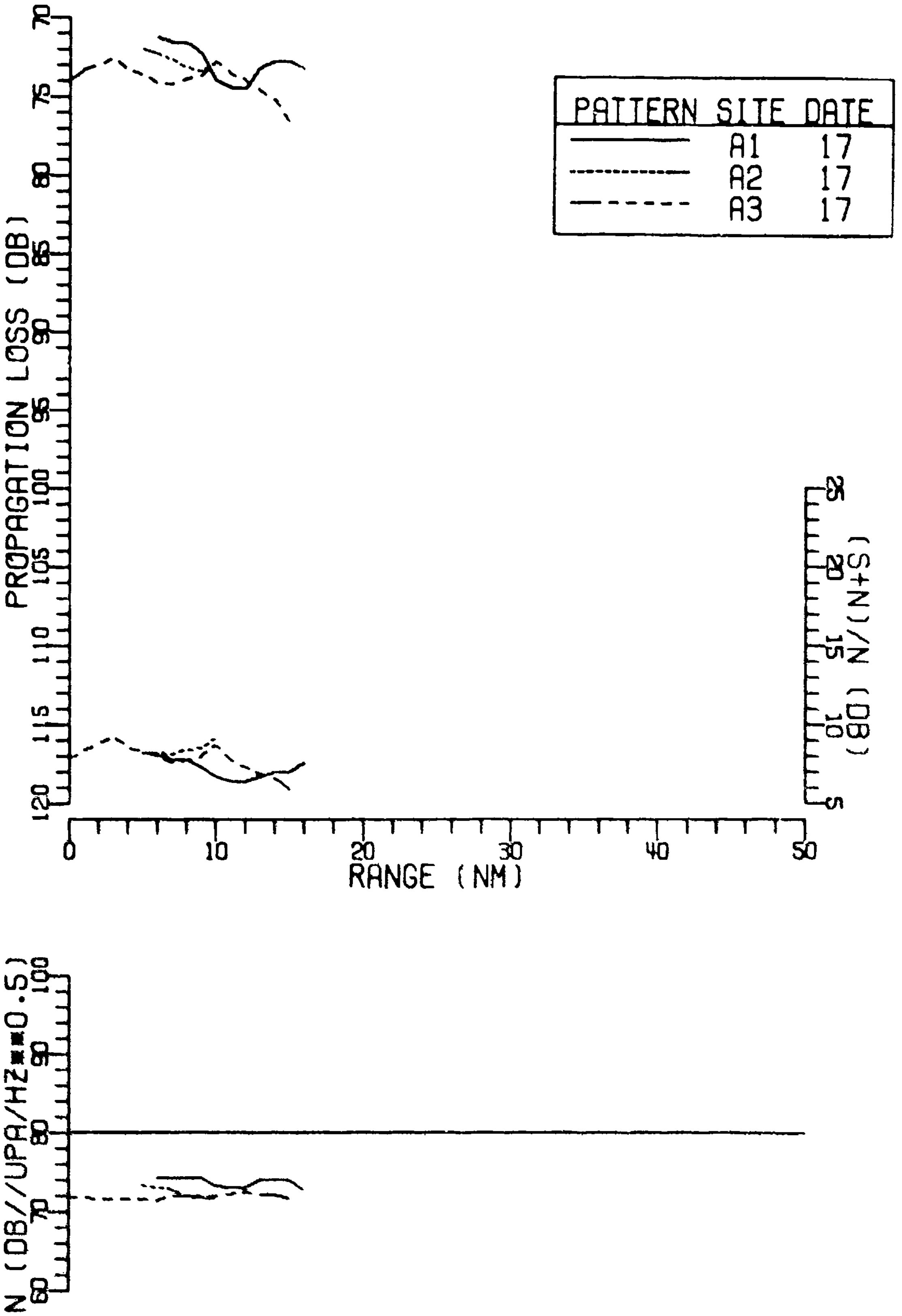

FIGURE III-167
MSS-FVT NEAR BOTTOM OMNIDIRECTIONAL SENSOR
PROPAGATION LOSS RESULTS FOR 155HZ AT 134DB (U)

AS-77-2767

CONFIDENTIAL

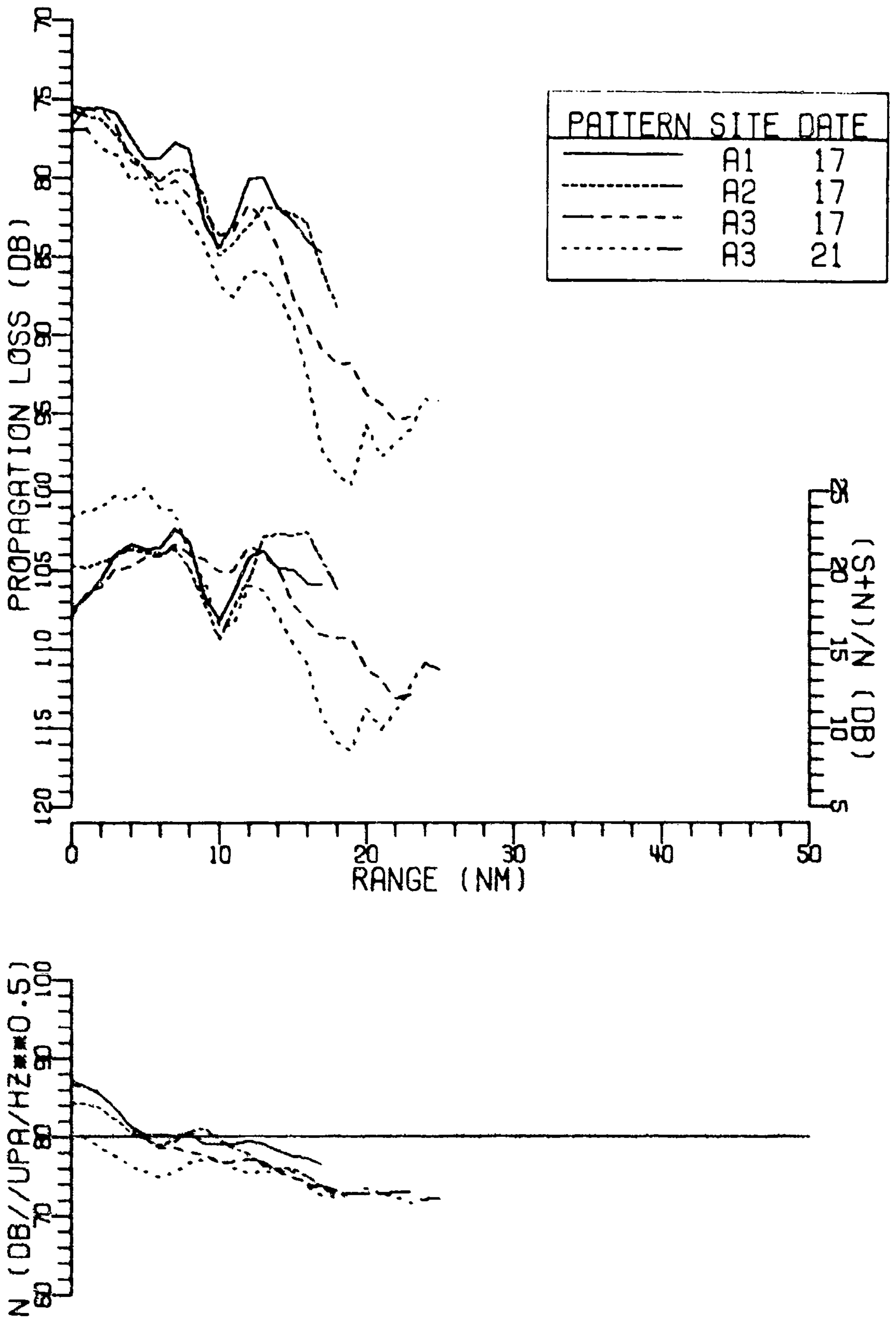

FIGURE III-168
MSS-FVT NEAR BOTTOM OMNIDIRECTIONAL SENSOR
PROPAGATION LOSS RESULTS FOR 160HZ AT 161DB (U)

AS-77-2768

CONFIDENTIAL

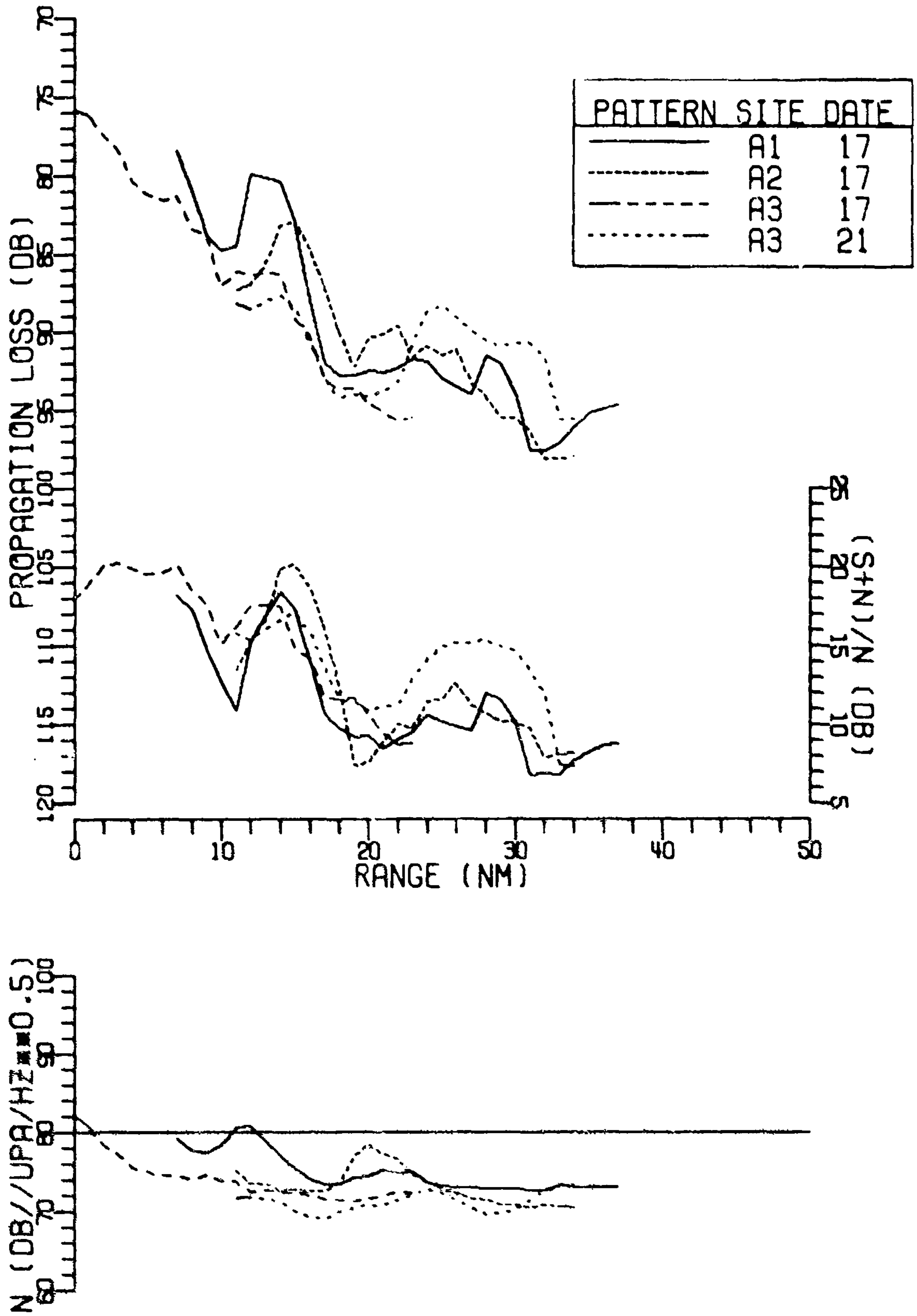

FIGURE III-169
MSS-FVT NEAR BOTTOM OMNIDIRECTIONAL SENSOR
PROPAGATION LOSS RESULTS FOR 170HZ AT 156DB (U)

CONFIDENTIAL

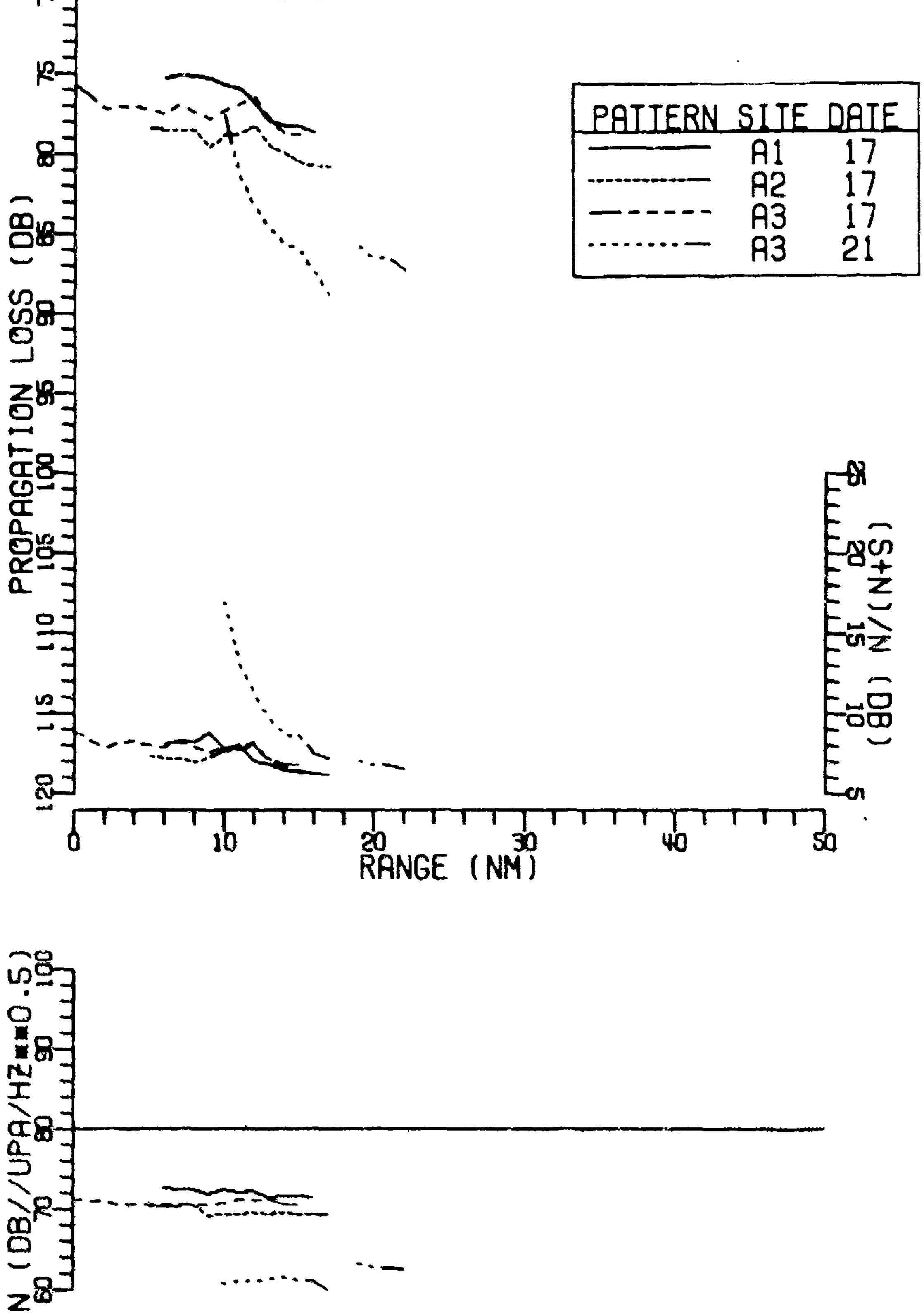

FIGURE III-170
MSS-FVT NEAR BOTTOM OMNIDIRECTIONAL SENSOR
PROPAGATION LOSS RESULTS FOR 305HZ AT 136DB (U)

AS-77-2770

CONFIDENTIAL

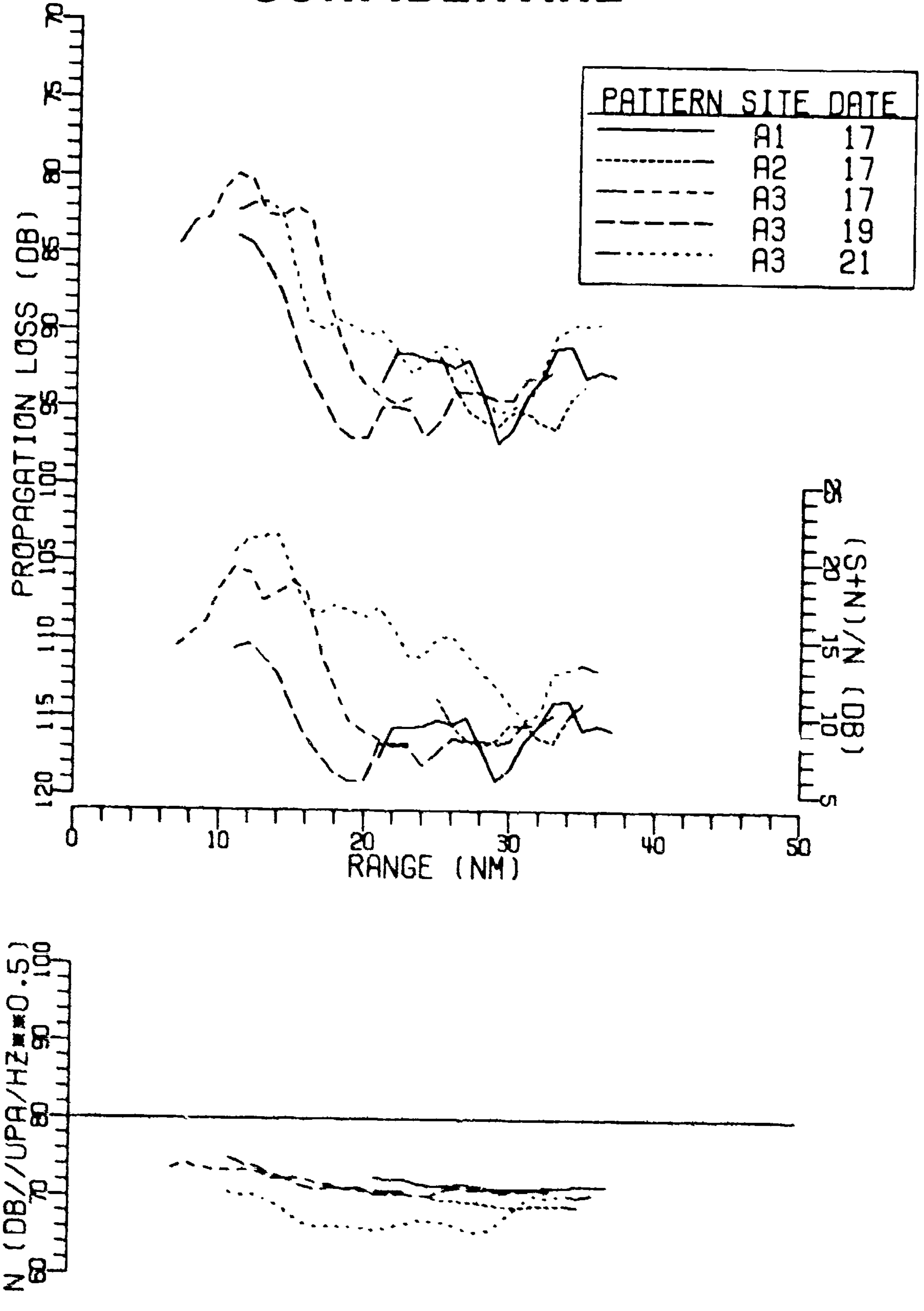

FIGURE III-171
MSS-FVT NEAR BOTTOM OMNIDIRECTIONAL SENSOR
PROPAGATION LOSS RESULTS FOR 335HZ AT 154DB (U)

AS-77-2771

APPENDIX D

ARRAY GAIN versus RANGE CURVES (U)

(FIGURES III-172 - III-199)

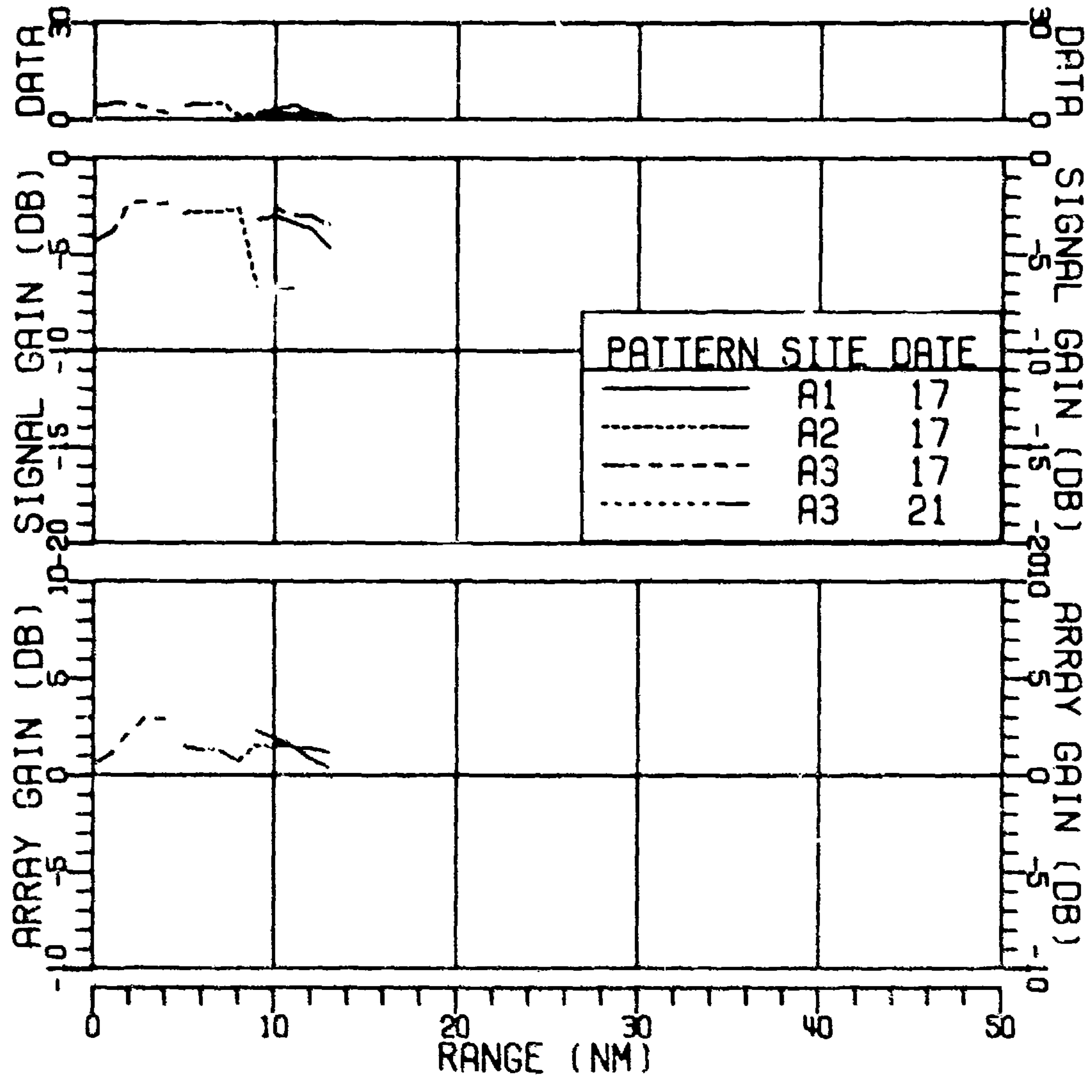

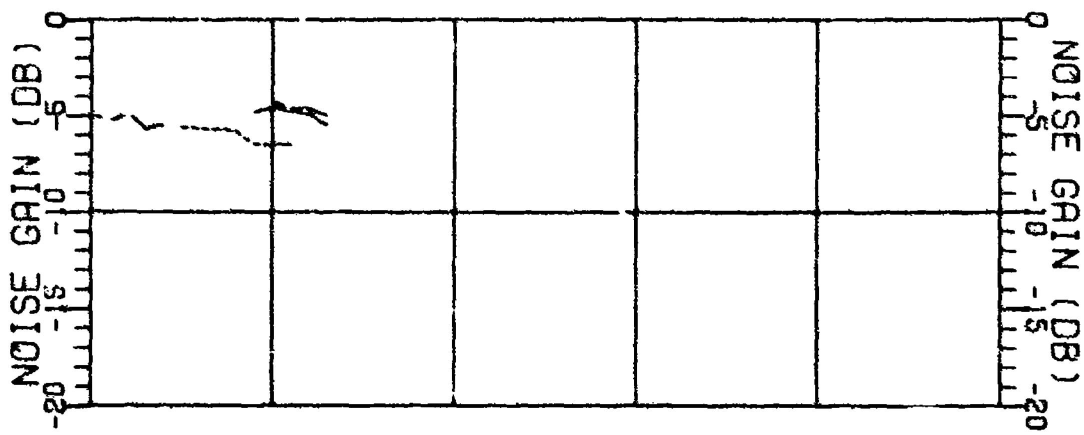

FIGURE III-172
MSS-FVT NEAR BOTTOM SINGLE CARDIOIDS SENSOR
ARRAY GAIN RESULTS FOR 55HZ AT 141DB (U)

AS-77-2772

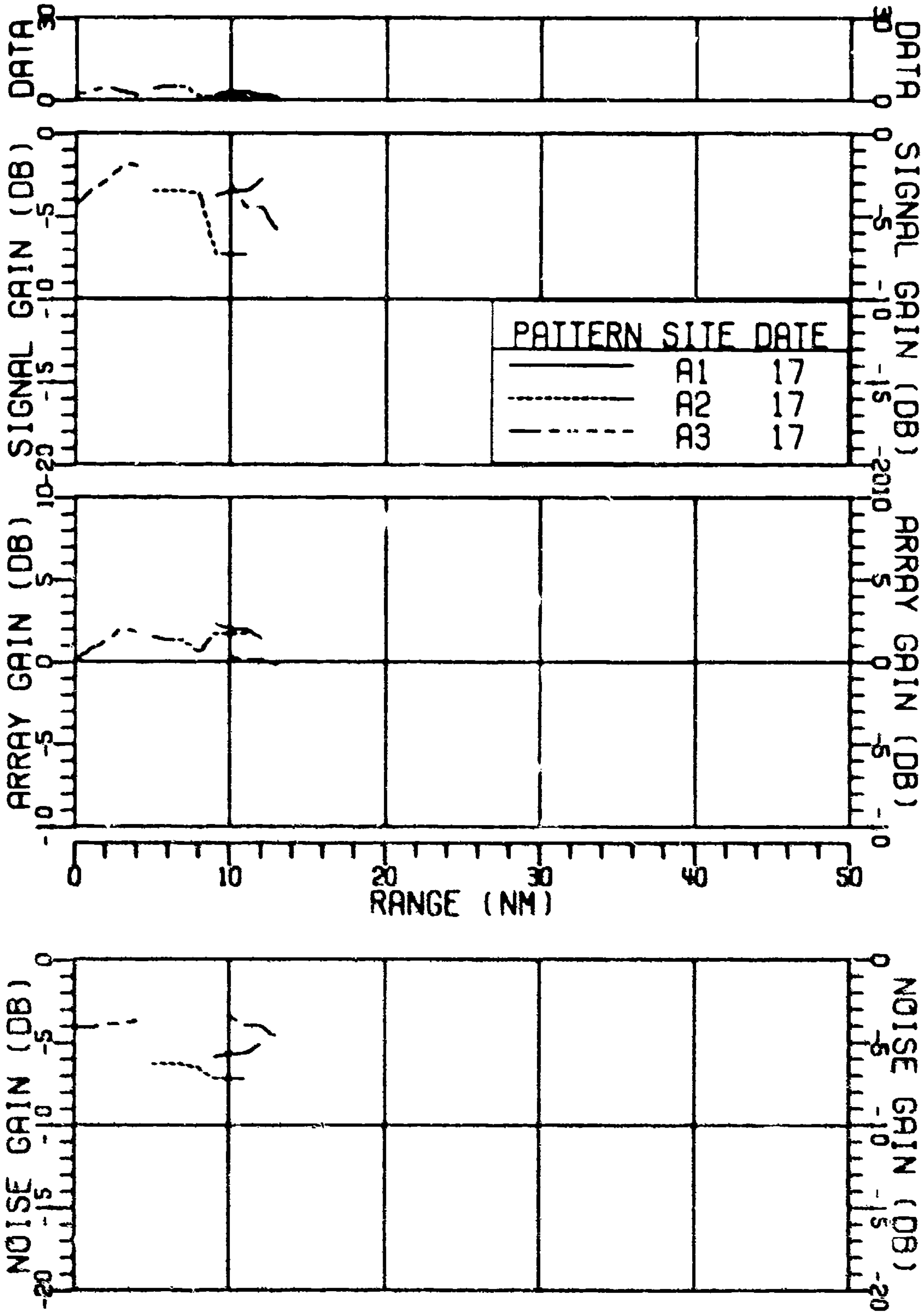

FIGURE III-173
MSS-FVT NEAR BOTTOM MAX GAIN LIMACONS SENSOR
ARRAY GAIN RESULTS FOR 55HZ AT 141DB (U)

AS-77-2773

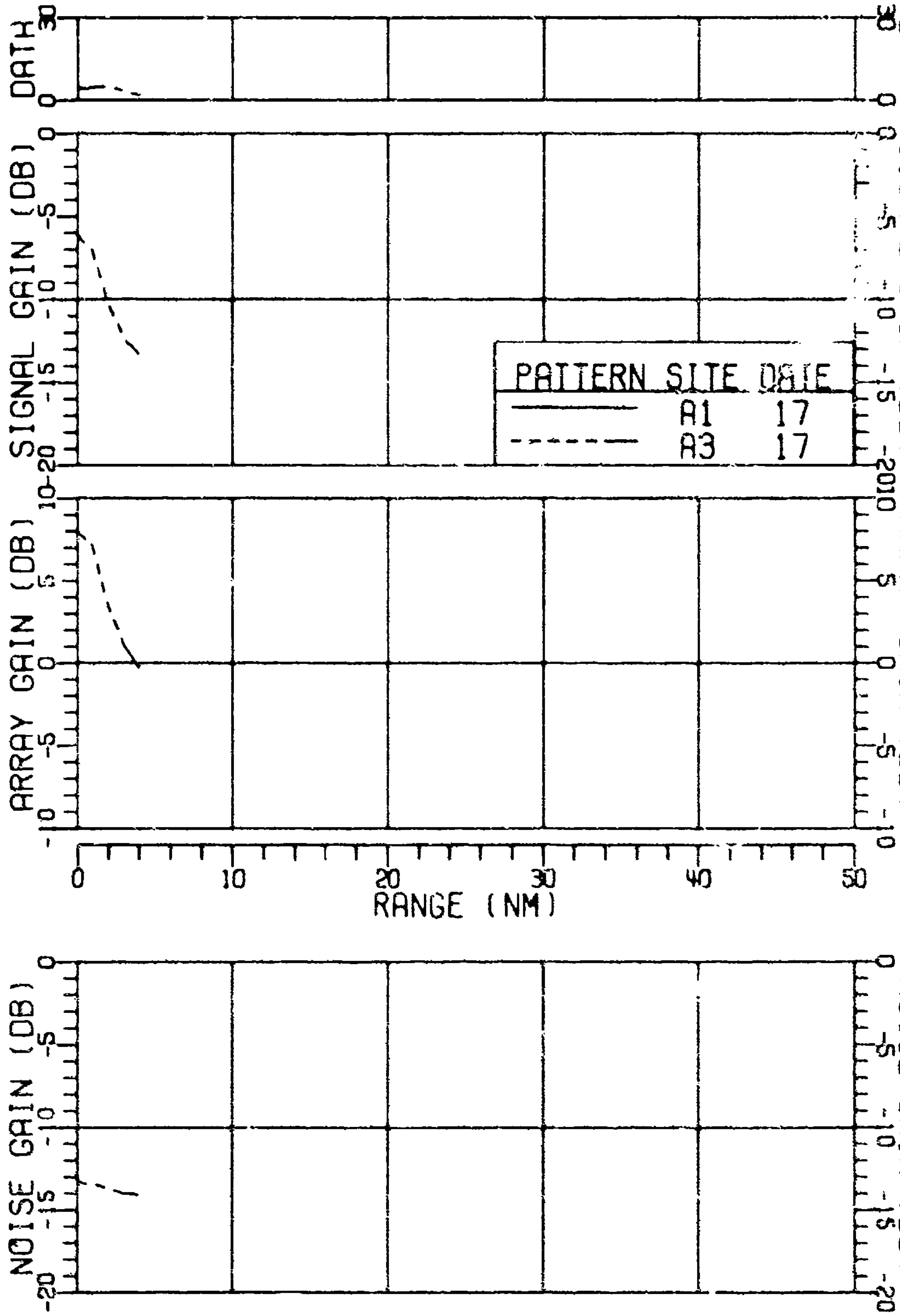

FIGURE III-174
MSS-FVT NEAR BOTTOM VERTICAL DIPOLE SENSOR
ARRAY GAIN RESULTS FOR 55HZ AT 141DB (U)

AS-77-2774

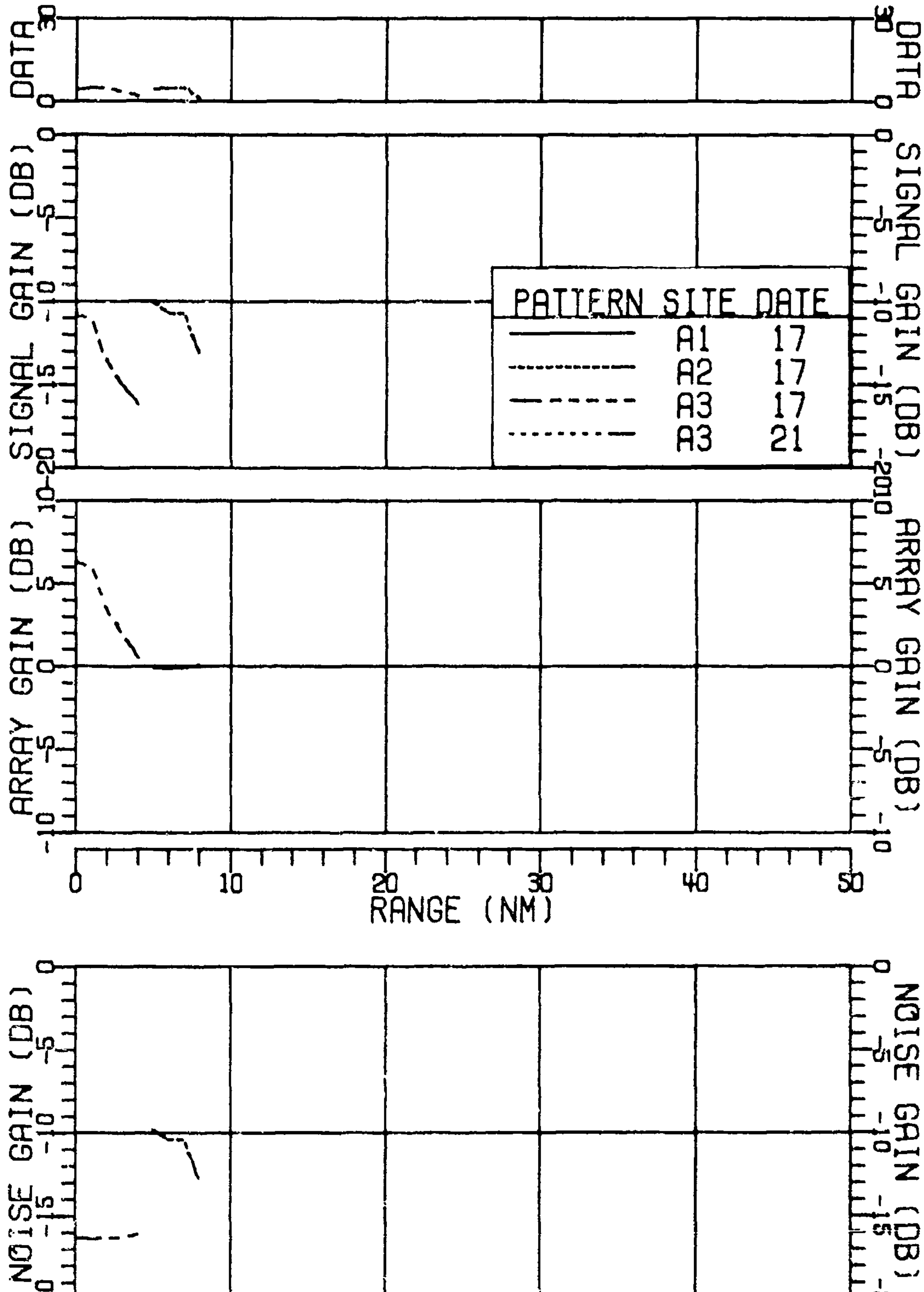

FIGURE III-175
MSS-FVT NEAR BOTTOM DIFFERENCED CARDIOIDS SENSOR ARRAY GAIN RESULTS FOR 55HZ AT 141DB (U)

AS-77-2775

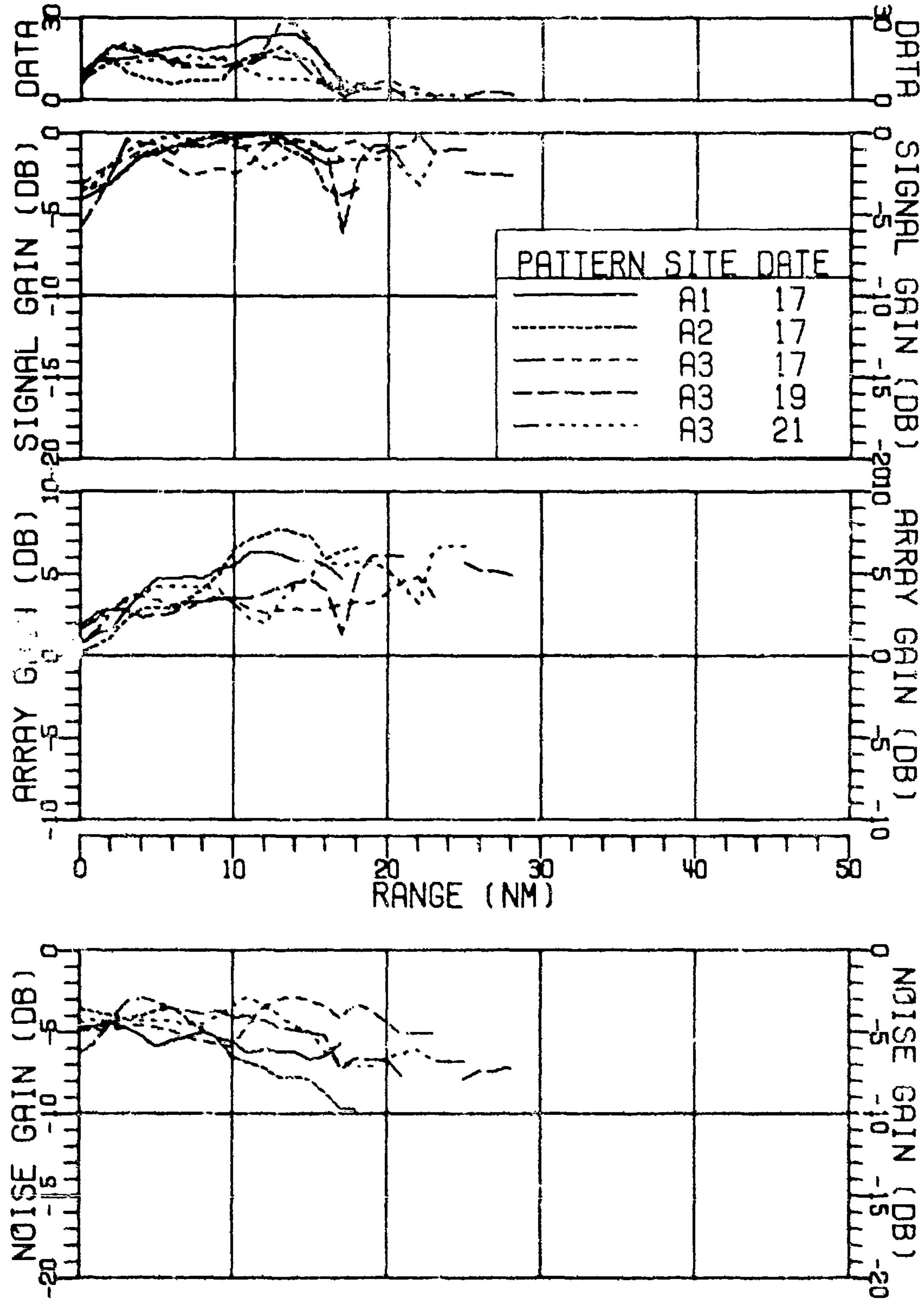

FIGURE III-176
MSS-FVT NEAR BOTTOM SINGLE CARDIOIDS SENSOR
ARRAY GAIN RESULTS FOR 64HZ AT 162DB (U)

AS-77-2776

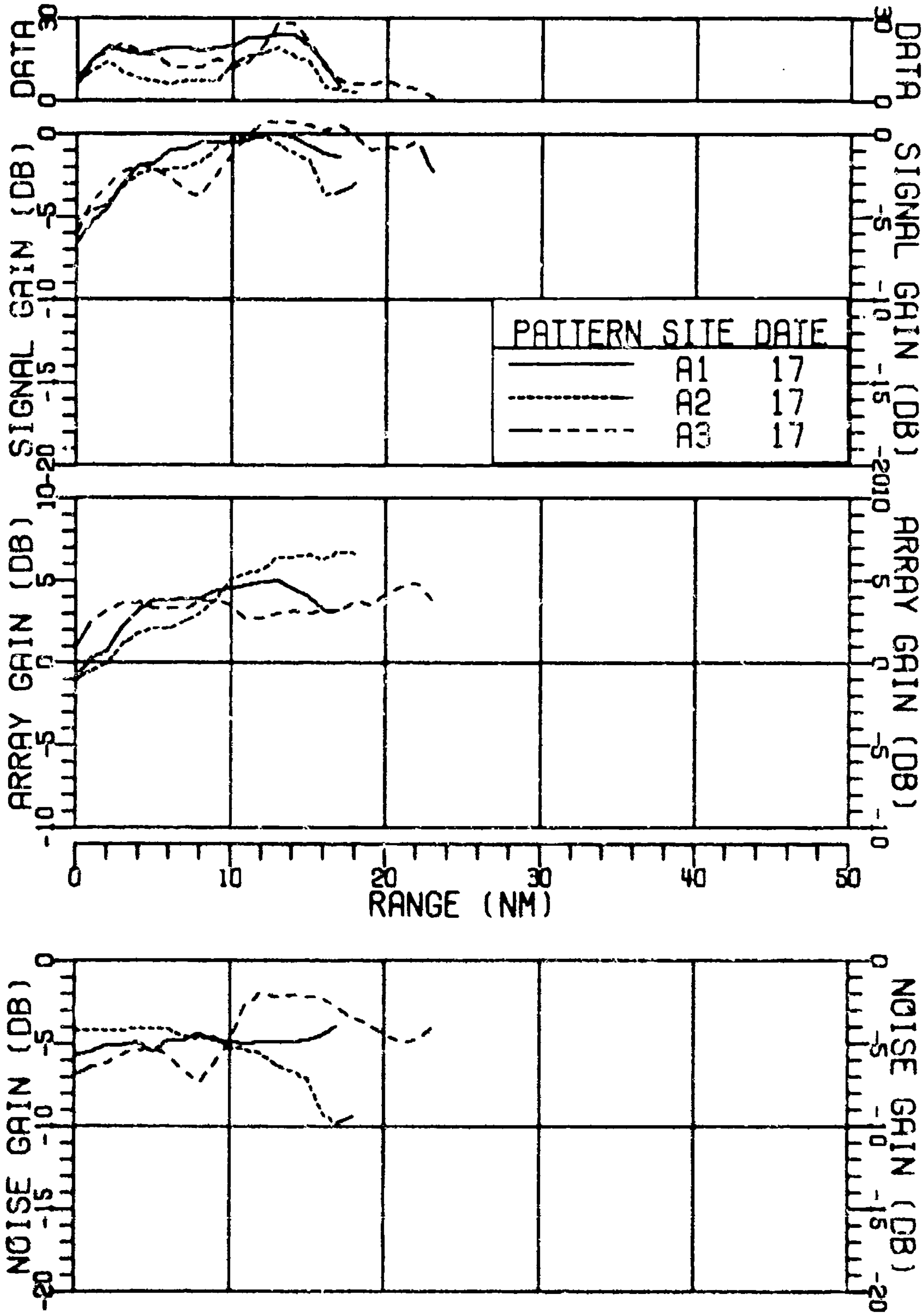

FIGURE III-177
MSS-FVT NEAR BOTTOM MAX GAIN LIMACONS SENSOR
ARRAY GAIN RESULTS FOR 64HZ AT 162DB (U)

AS-77-2777

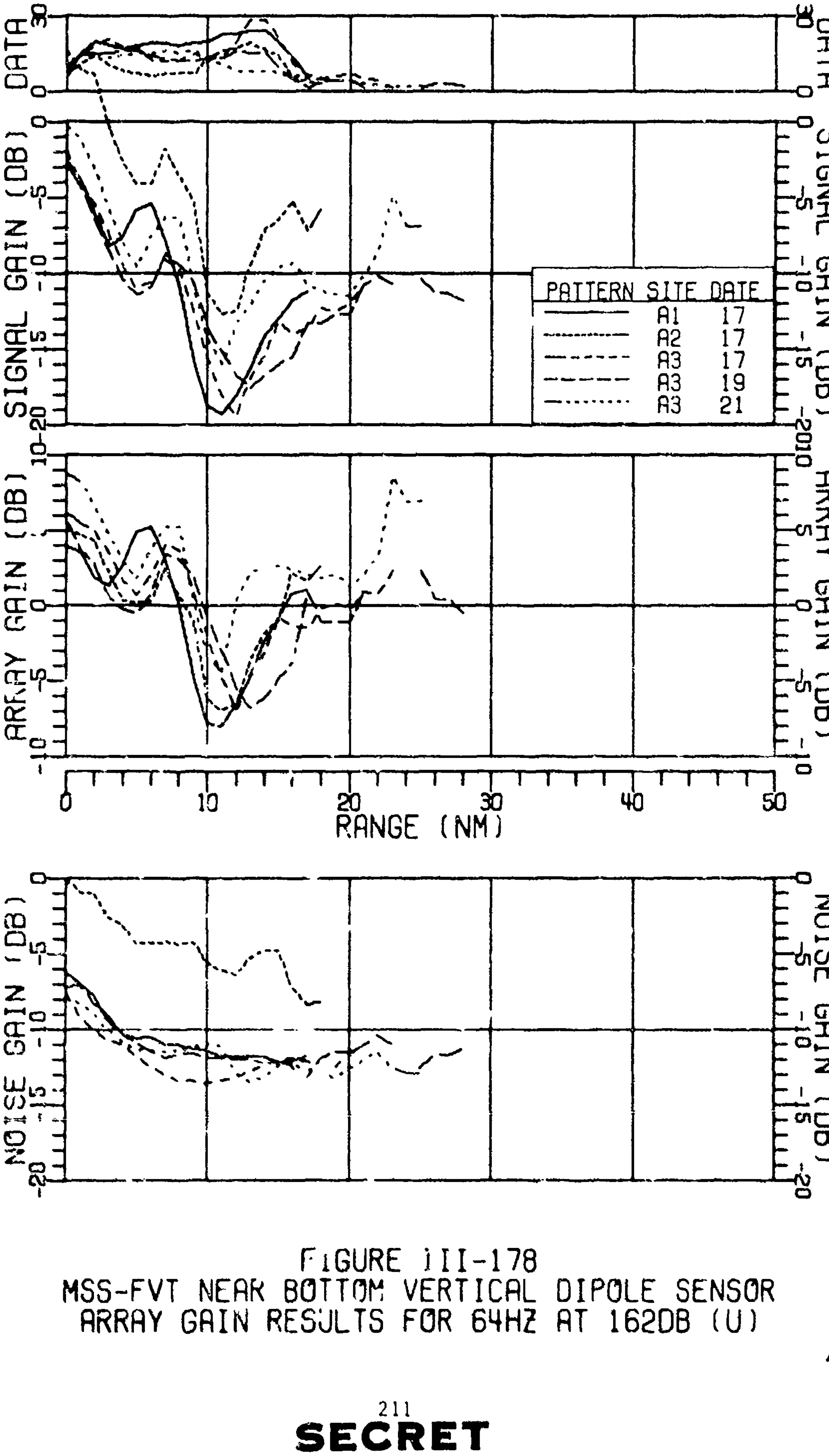

FIGURE III-178
MSS-FVT NEAR BOTTOM VERTICAL DIPOLE SENSOR
ARRAY GAIN RESULTS FOR 64HZ AT 162DB (U)

AS-77-2778

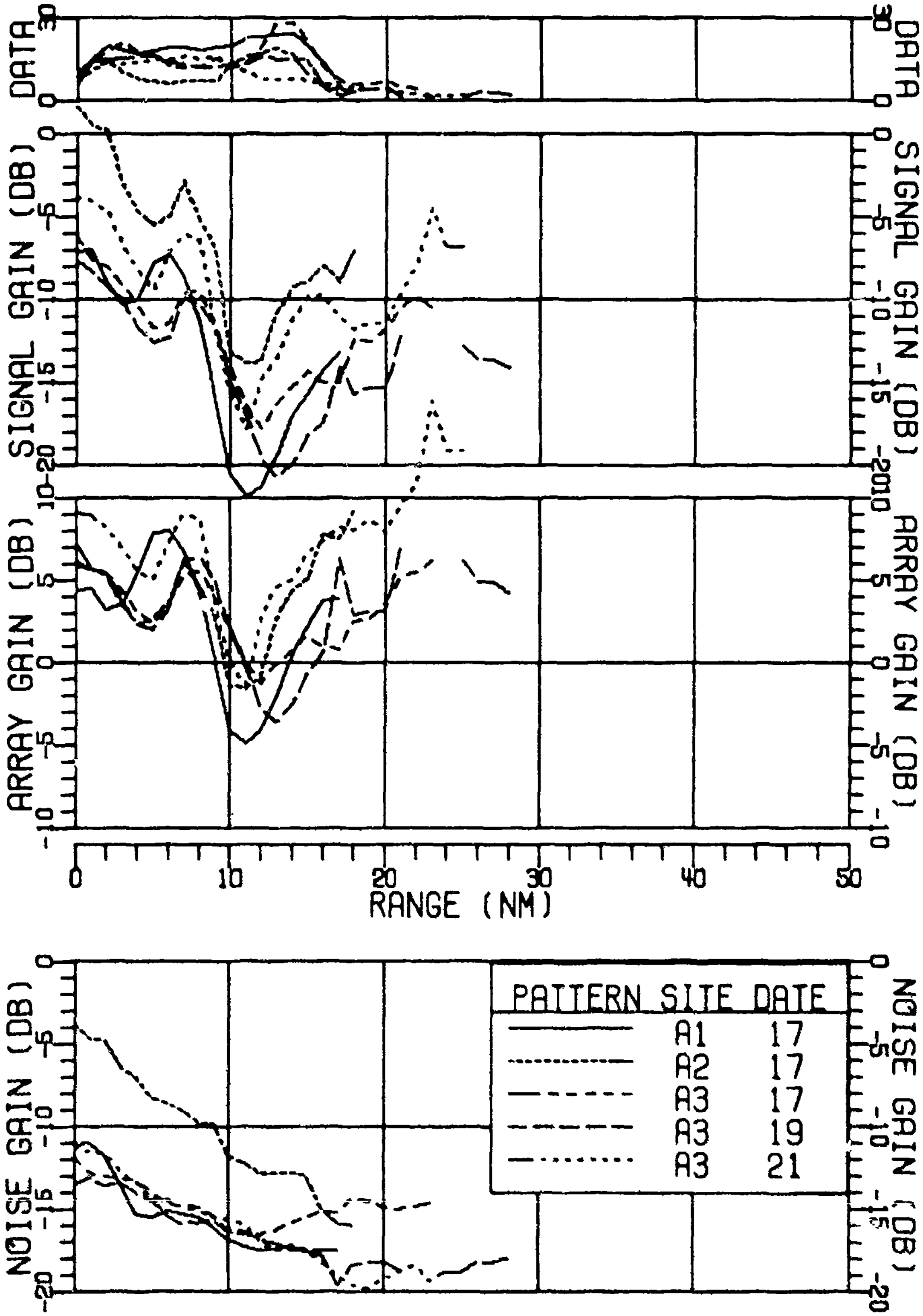

FIGURE III-179
MSS-FVT NEAR BOTTOM DIFFERENCED CARDIOIDS SENSOR
ARRAY GAIN RESULTS FOR 64HZ AT 162DB (U)

AS-77-2779

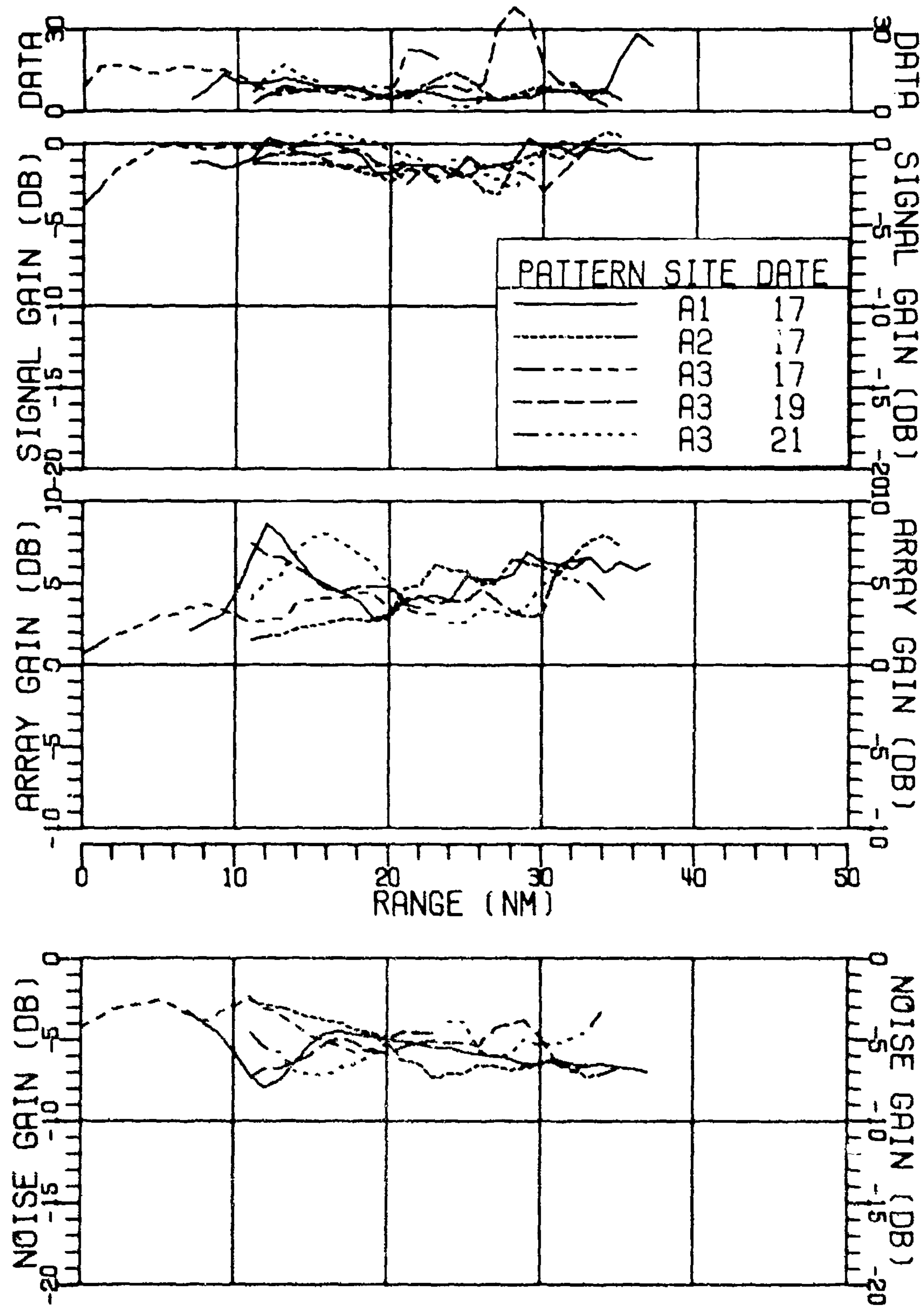

FIGURE III-180
MSS-FVT NEAR BOTTOM SINGLE CARDIOIDS SENSOR
ARRAY GAIN RESULTS FOR 70HZ AT 166DB (U)

AS-77-2780

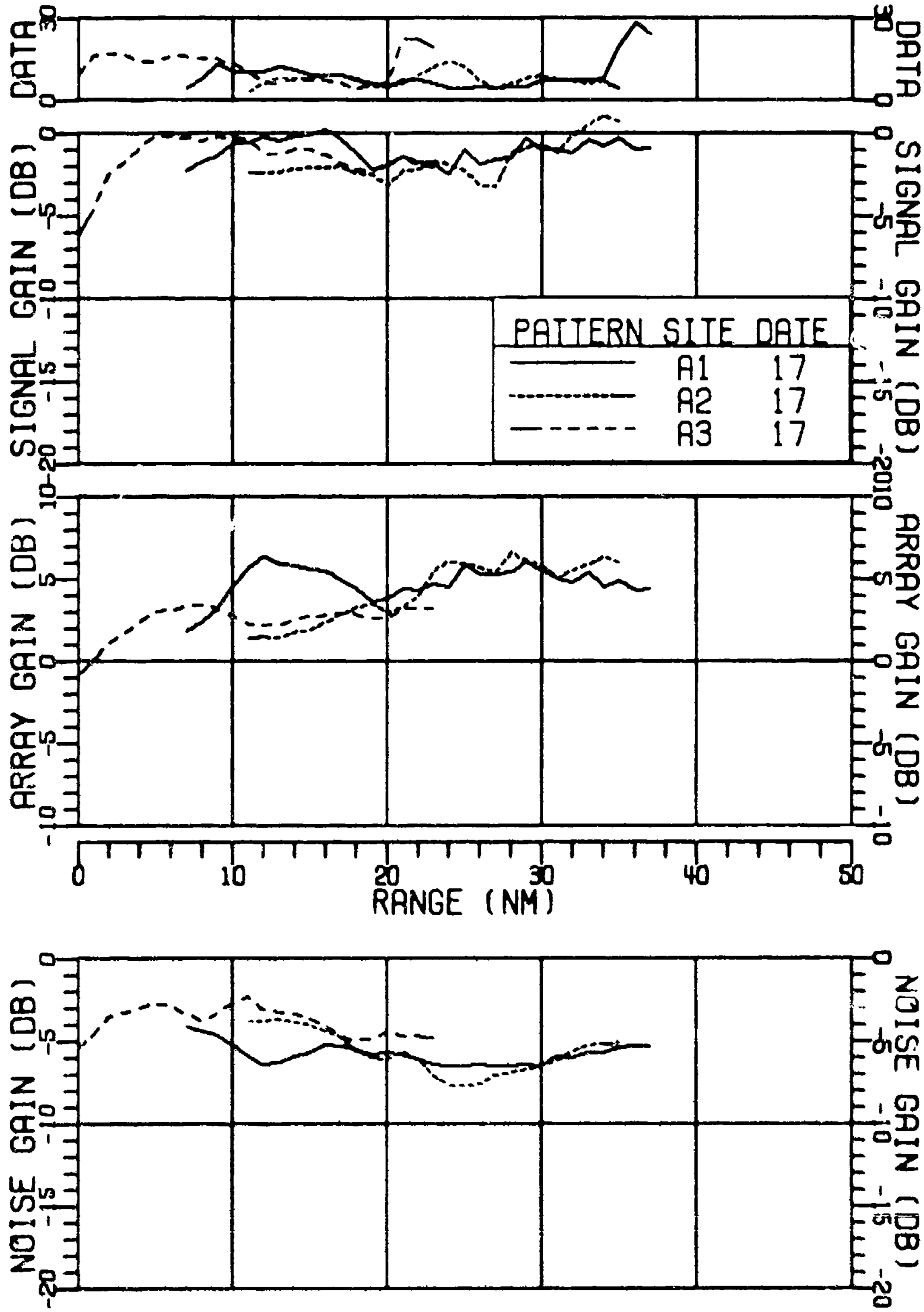

FIGURE III-181
MSS-FVT NEAR BOTTOM MAX GAIN LIMACONS SENSOR
ARRAY GAIN RESULTS FOR 70HZ AT 166DB (U)

AS-77-2781

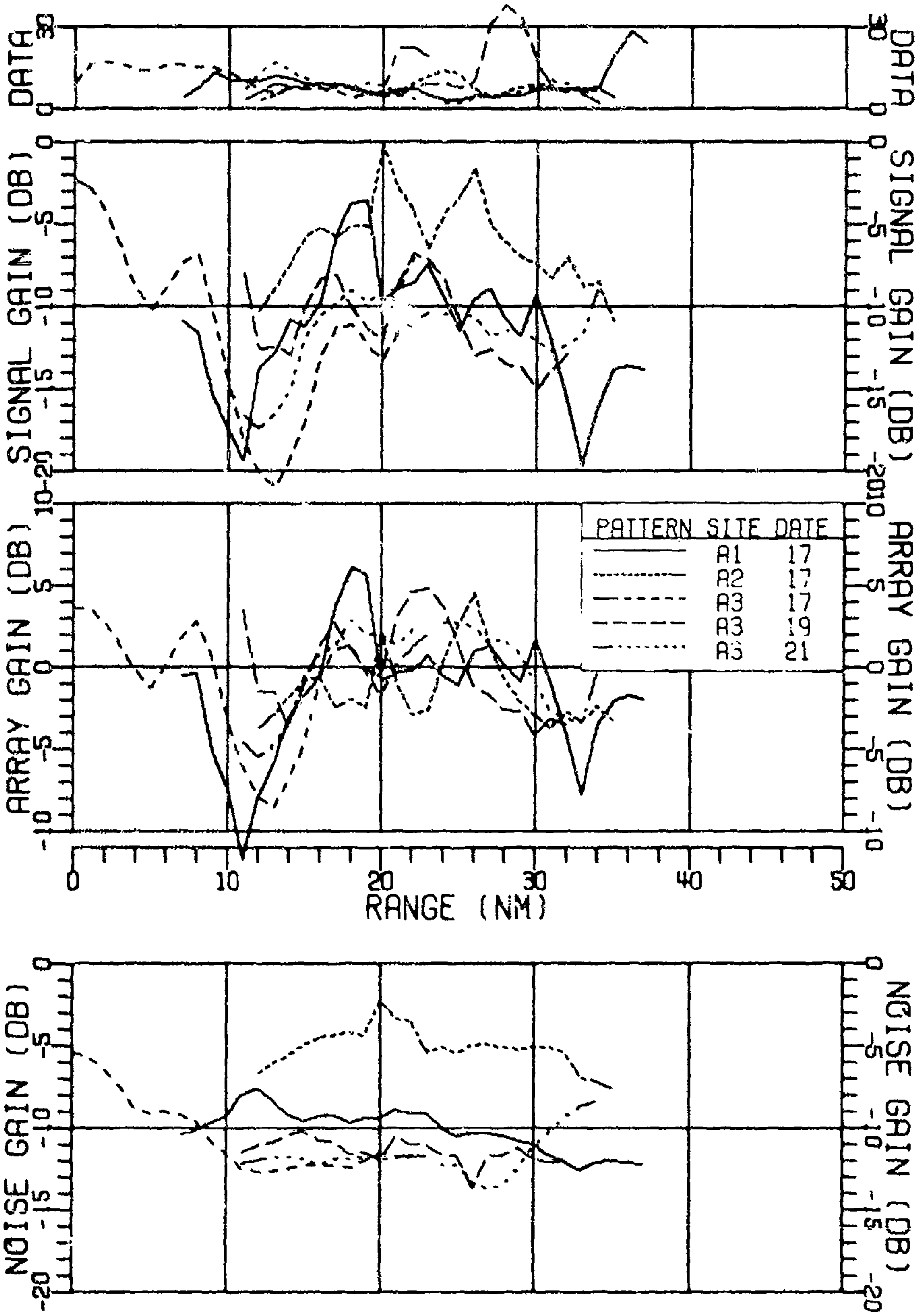

FIGURE III-182
MSS-FVT NEAR BOTTOM VERTICAL DIPOLE SENSOR
ARRAY GAIN RESULTS FOR 70HZ AT 166DB (U)

AS-77-2782

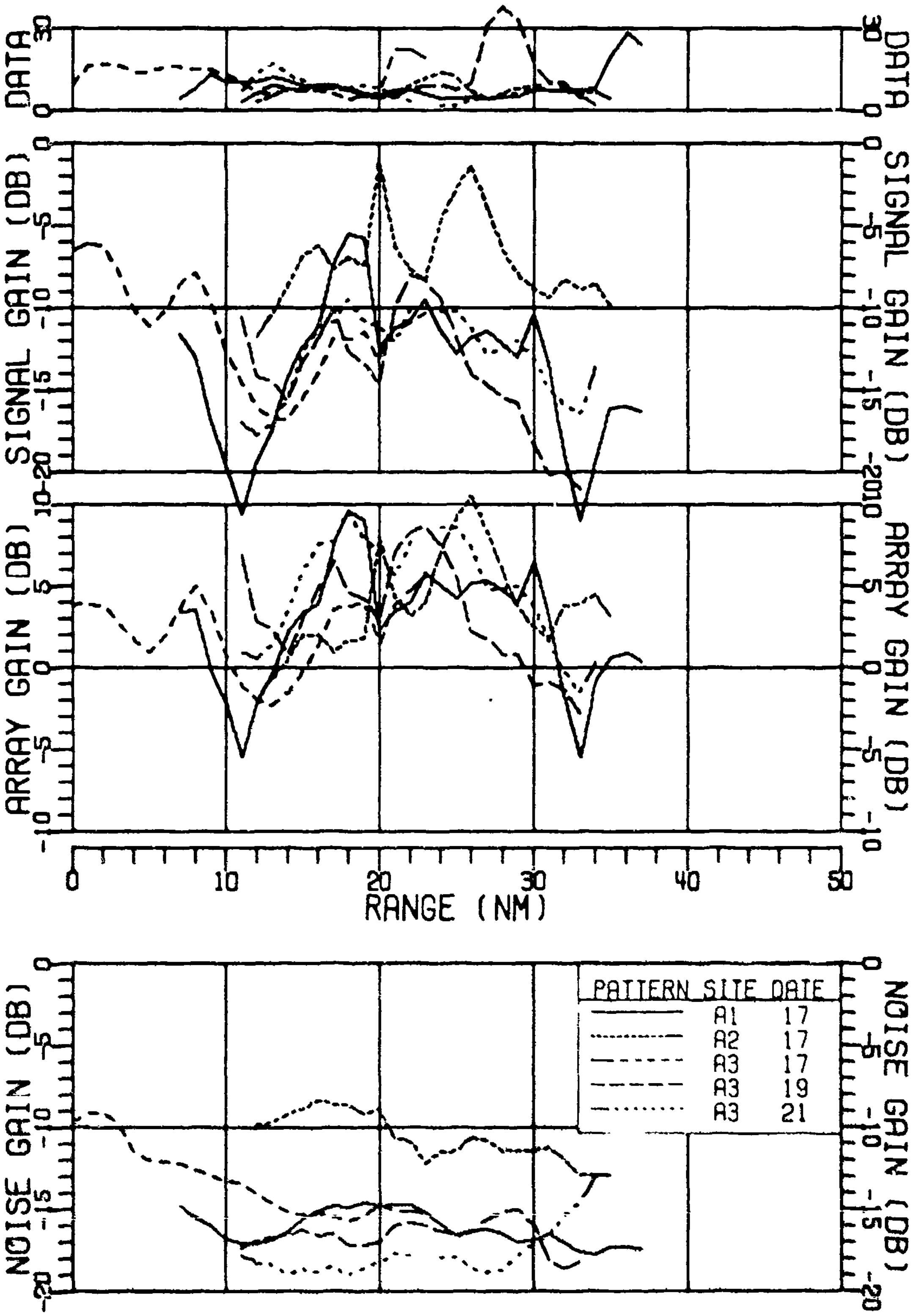

FIGURE III-183
MSS-FVT NEAR BOTTOM DIFFERENCED CARDIOIDS SENSOR
ARRAY GAIN RESULTS FOR 70HZ AT 166DB (U)

AS-77-2783

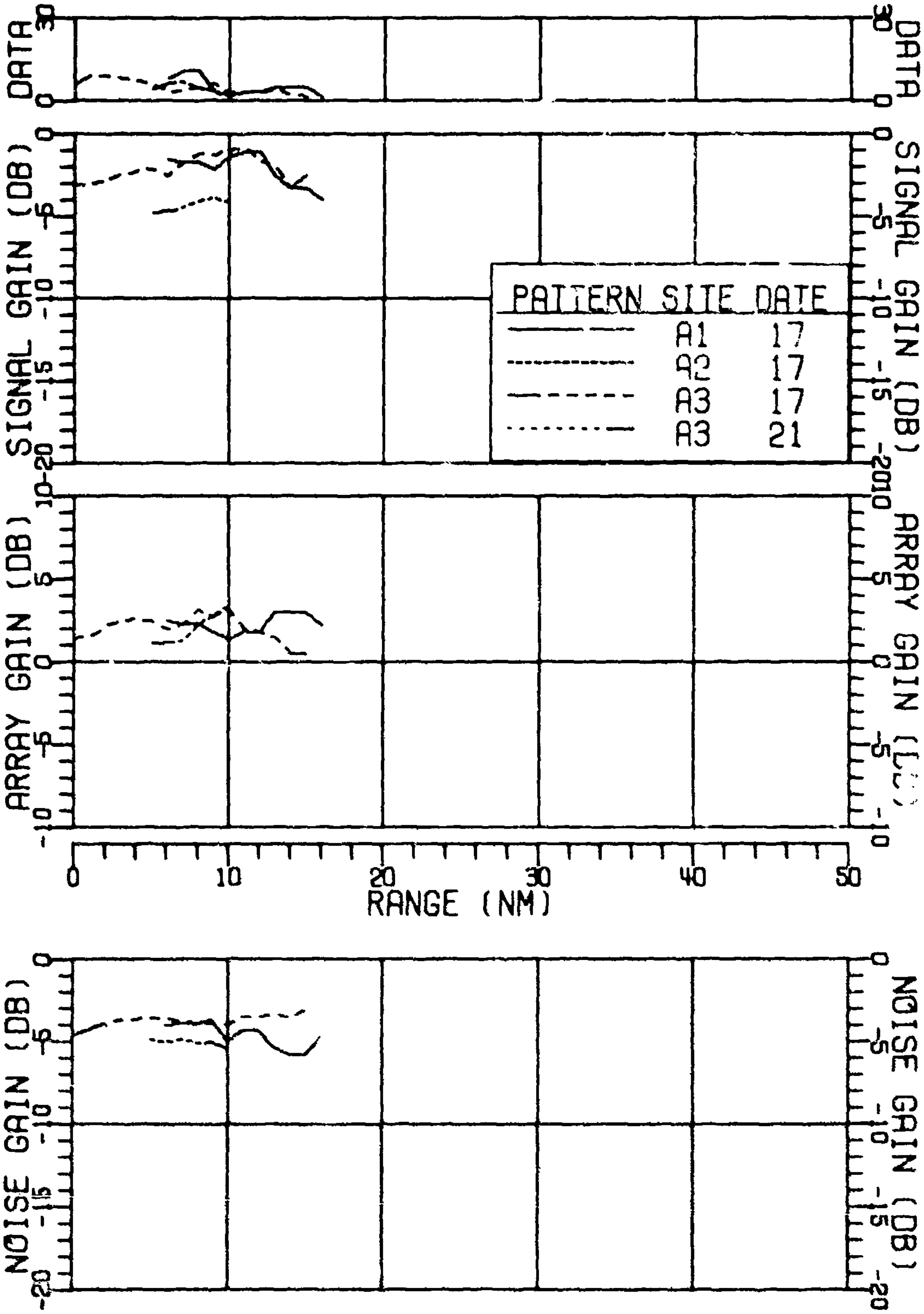

FIGURE III-184
MSS-FVT NEAR BOTTOM SINGLE CARDIOIDS SENSOR
ARRAY GAIN RESULTS FOR 155HZ AT 134DB (U)

AS 77-2784

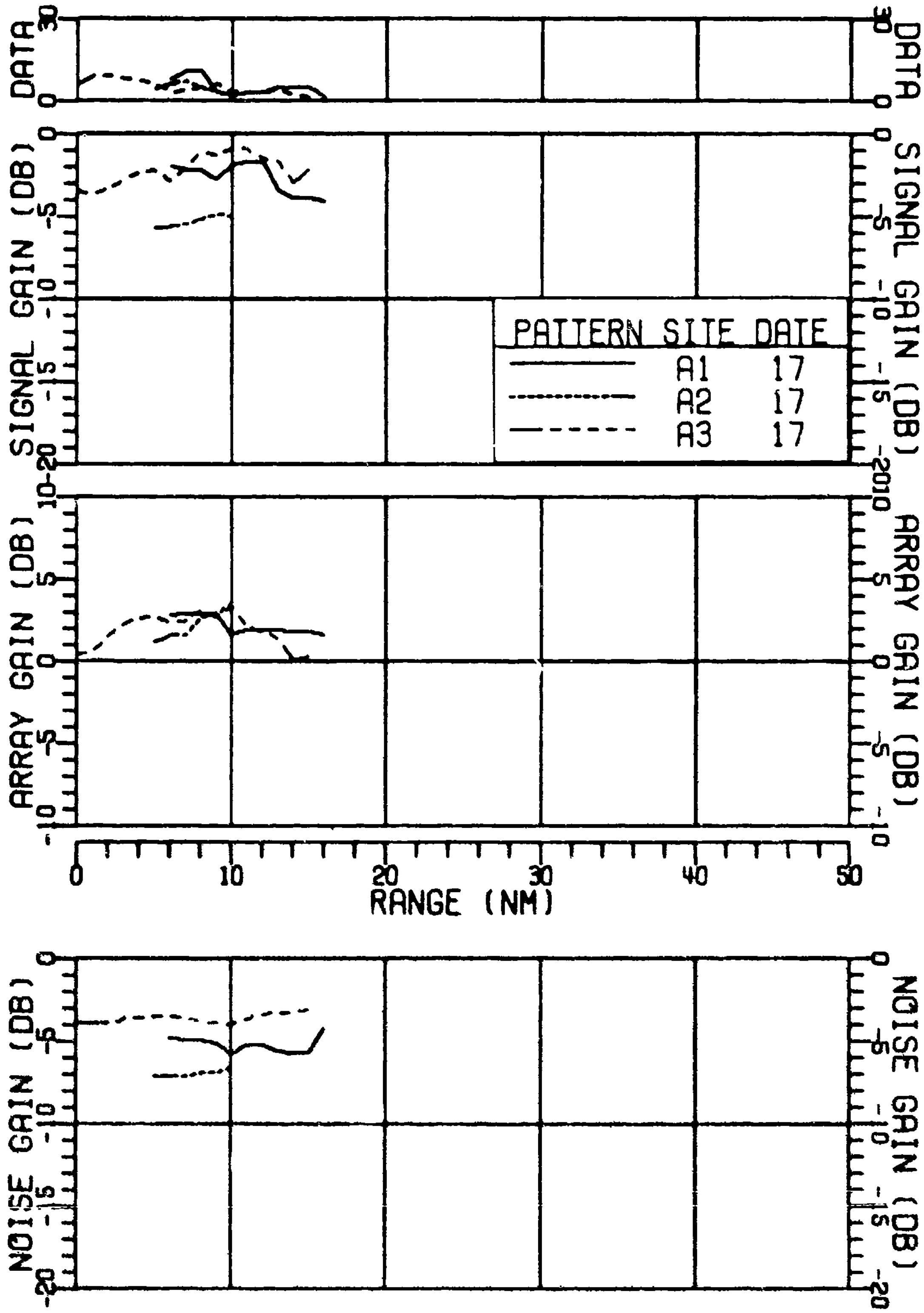

FIGURE III-185
MSS-FVT NEAR BOTTOM MAX GAIN LIMACONS SENSOR
ARRAY GAIN RESULTS FOR 155HZ AT 134DB (U)

AS-77-2785

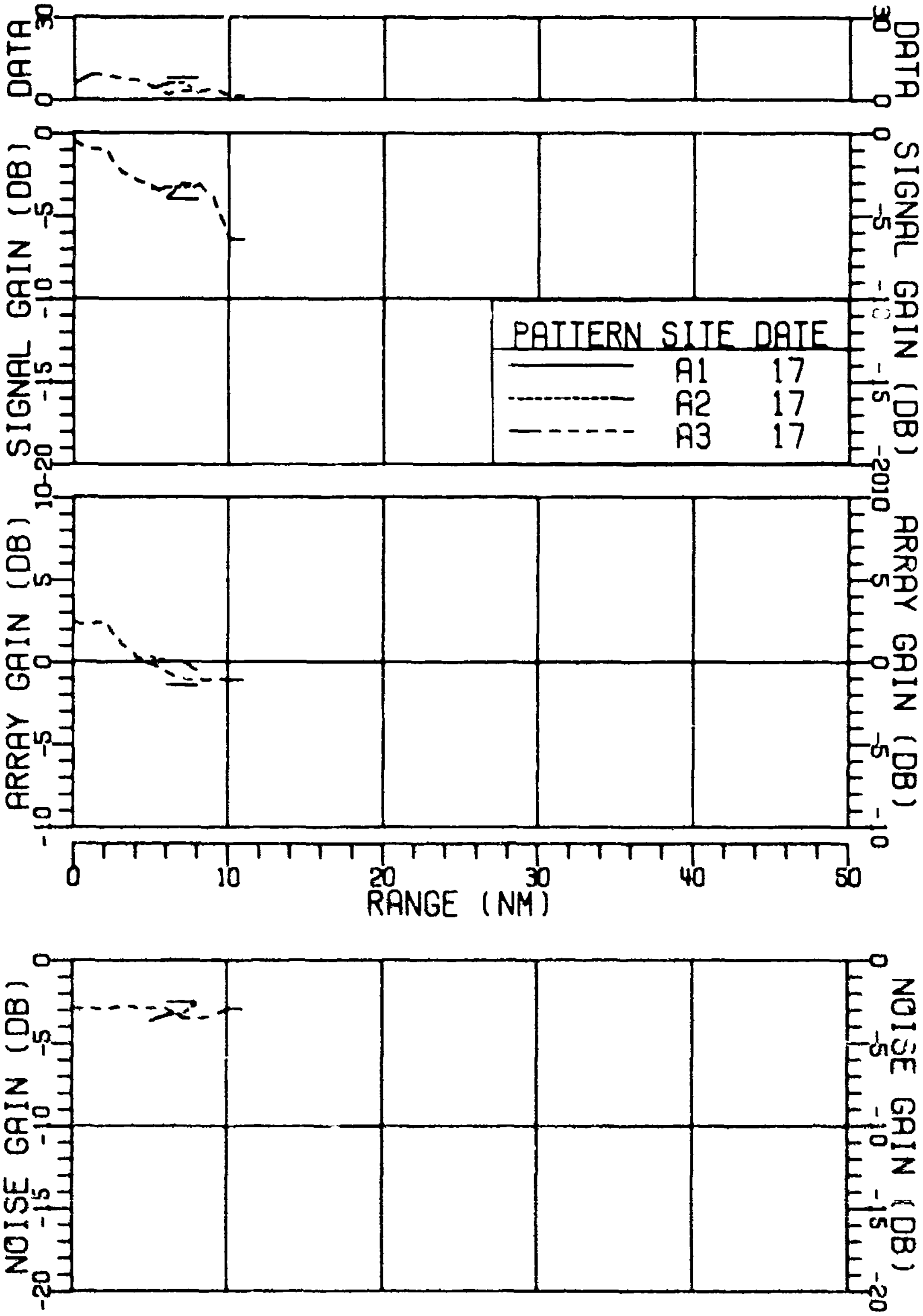

FIGURE III-186
MSS-FVT NEAR BOTTOM VERTICAL DIPOLE SENSOR
ARRAY GAIN RESULTS FOR 155HZ AT 134DB (U)

AS-77-2786

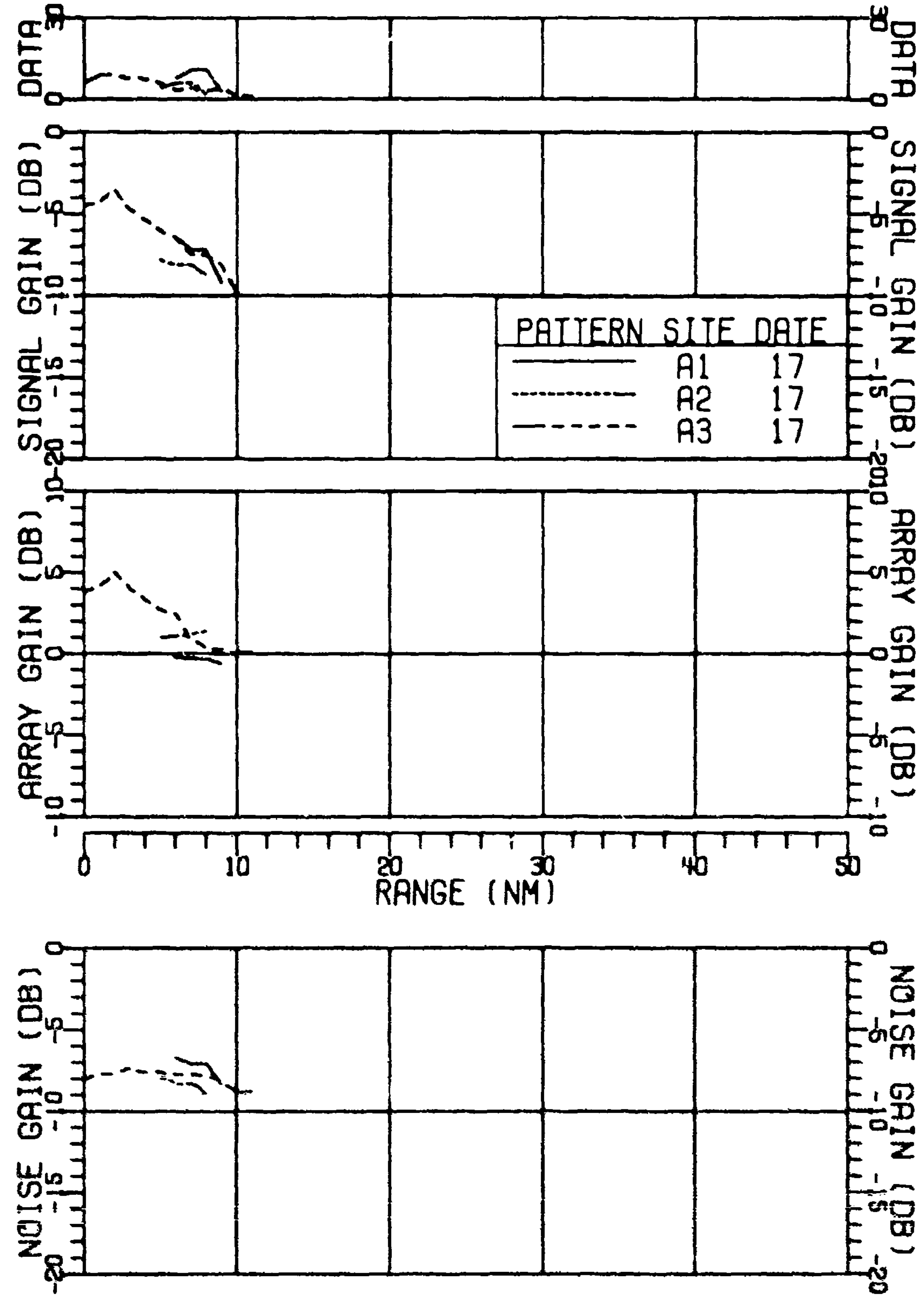

FIGURE III-187
MSS-FVT NEAR BOTTOM DIFFERENCED CARDIOIDS SENSOR
ARRAY GAIN RESULTS FOR 155HZ AT 134DB (U)

AS-77-2767

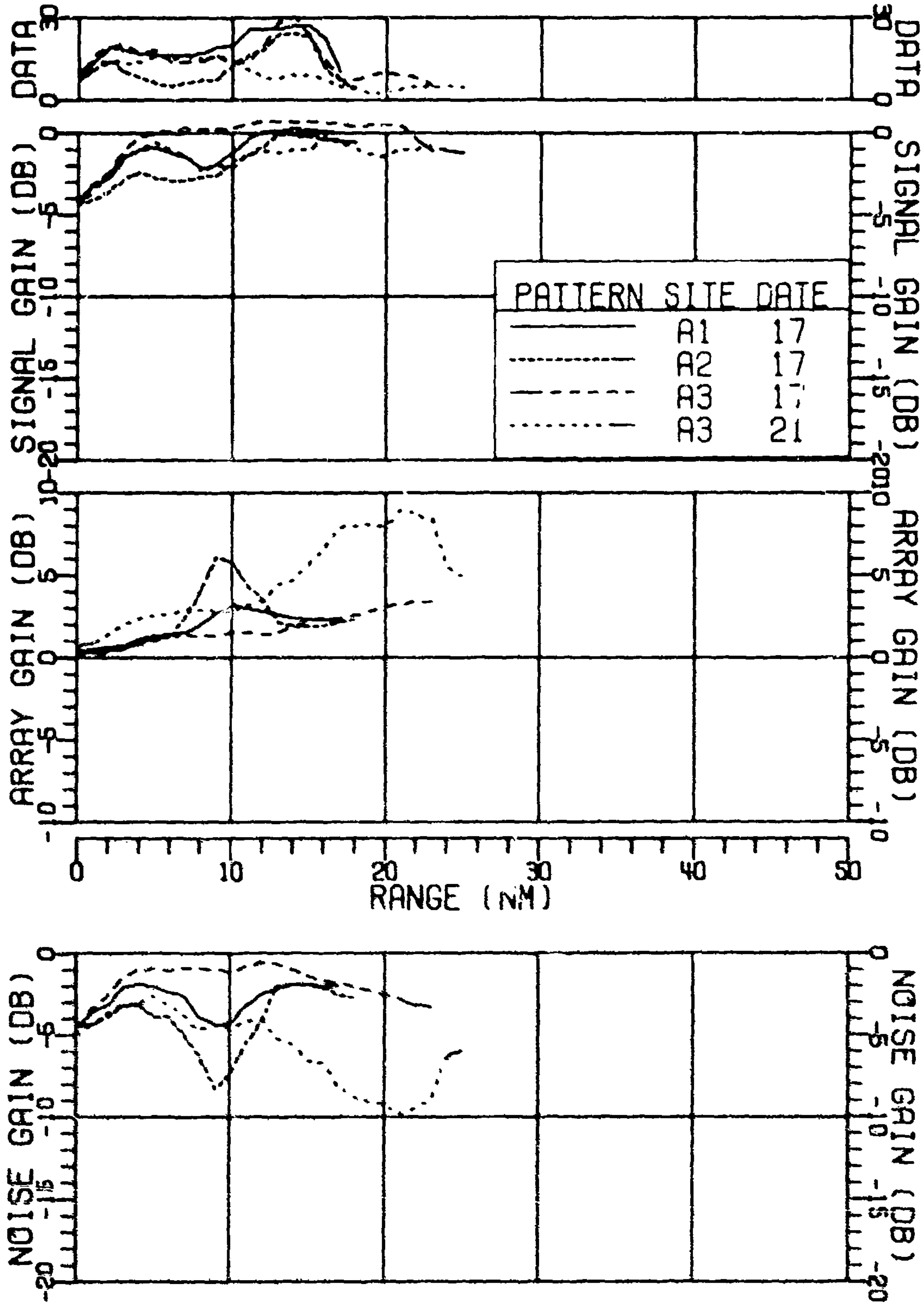

FIGURE III-188
MSS-FVT NEAR BOTTOM SINGLE CARDIOIDS SENSOR
ARRAY GAIN RESULTS FOR 160HZ AT 161DB (U)

AS-77-2788

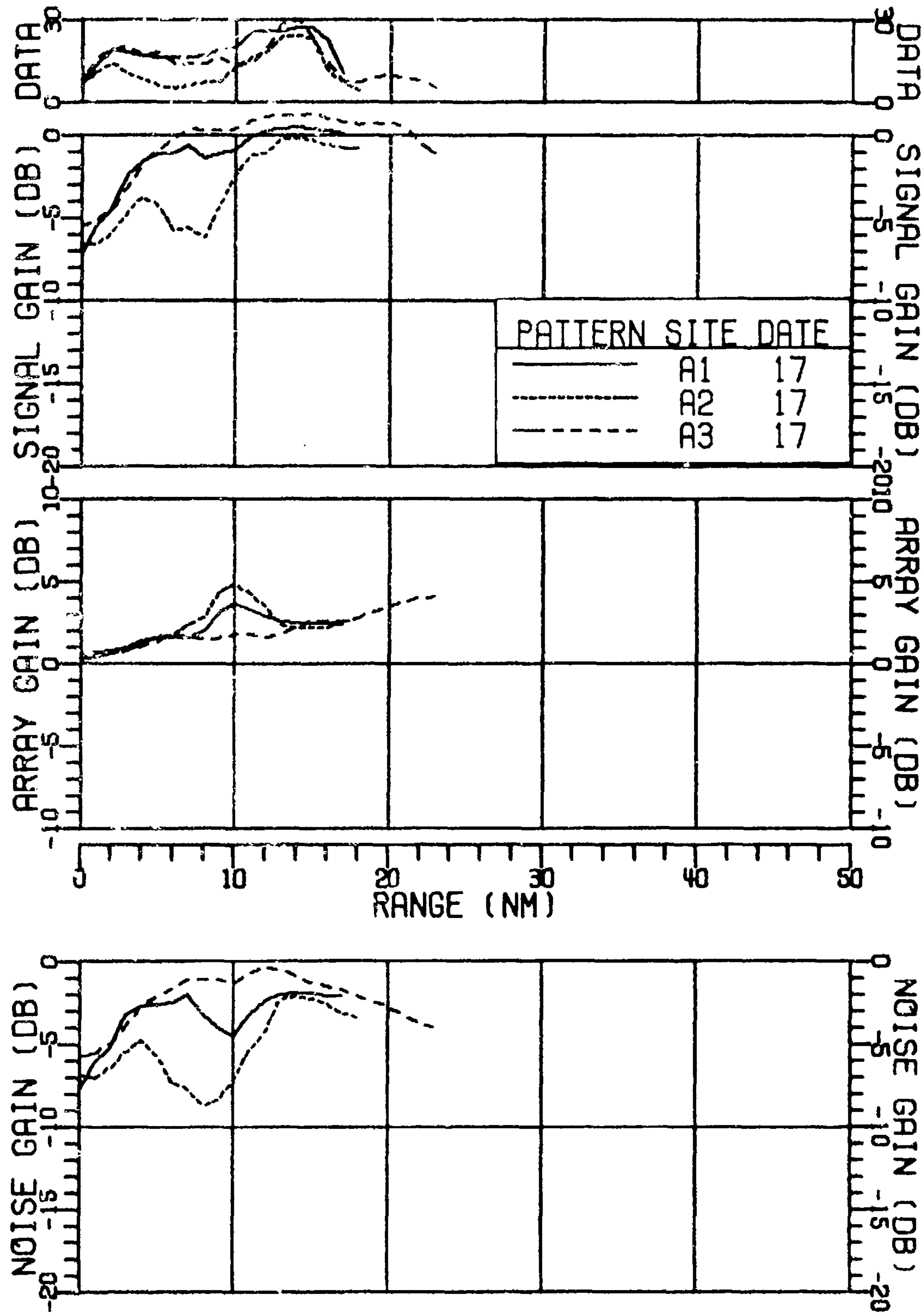

FIGURE III-189
MSS-FVT NEAR BOTTOM MAX GAIN LIMACONS SENSOR
ARRAY GAIN RESULTS FOR 160HZ AT 161DB (U)

AS-77-2789

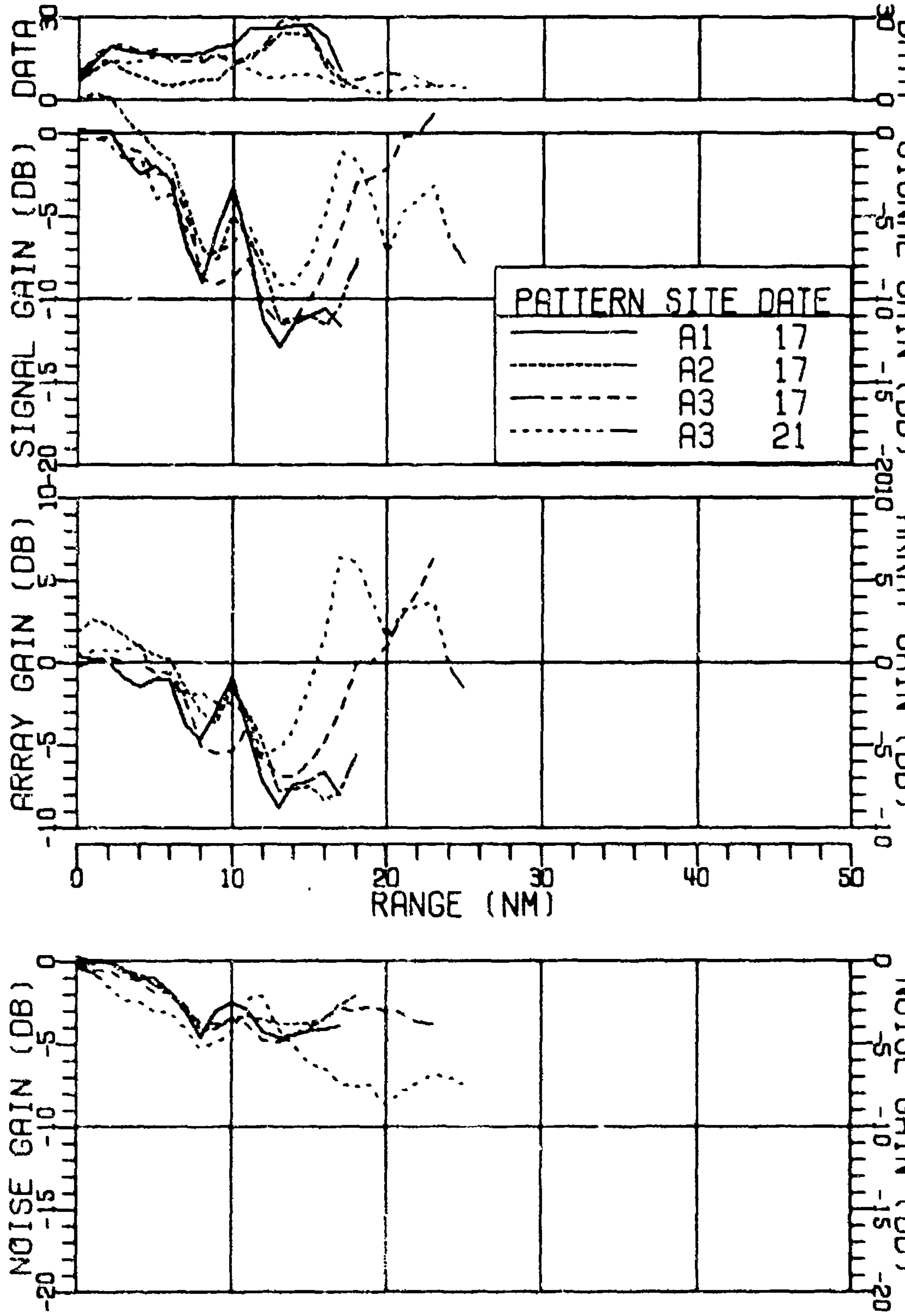

FIGURE III-190
MSS-FVT NEAR BOTTOM VERTICAL DIPOLE SENSOR
ARRAY GAIN RESULTS FOR 160HZ AT 161DB (U)

AS-77-2790

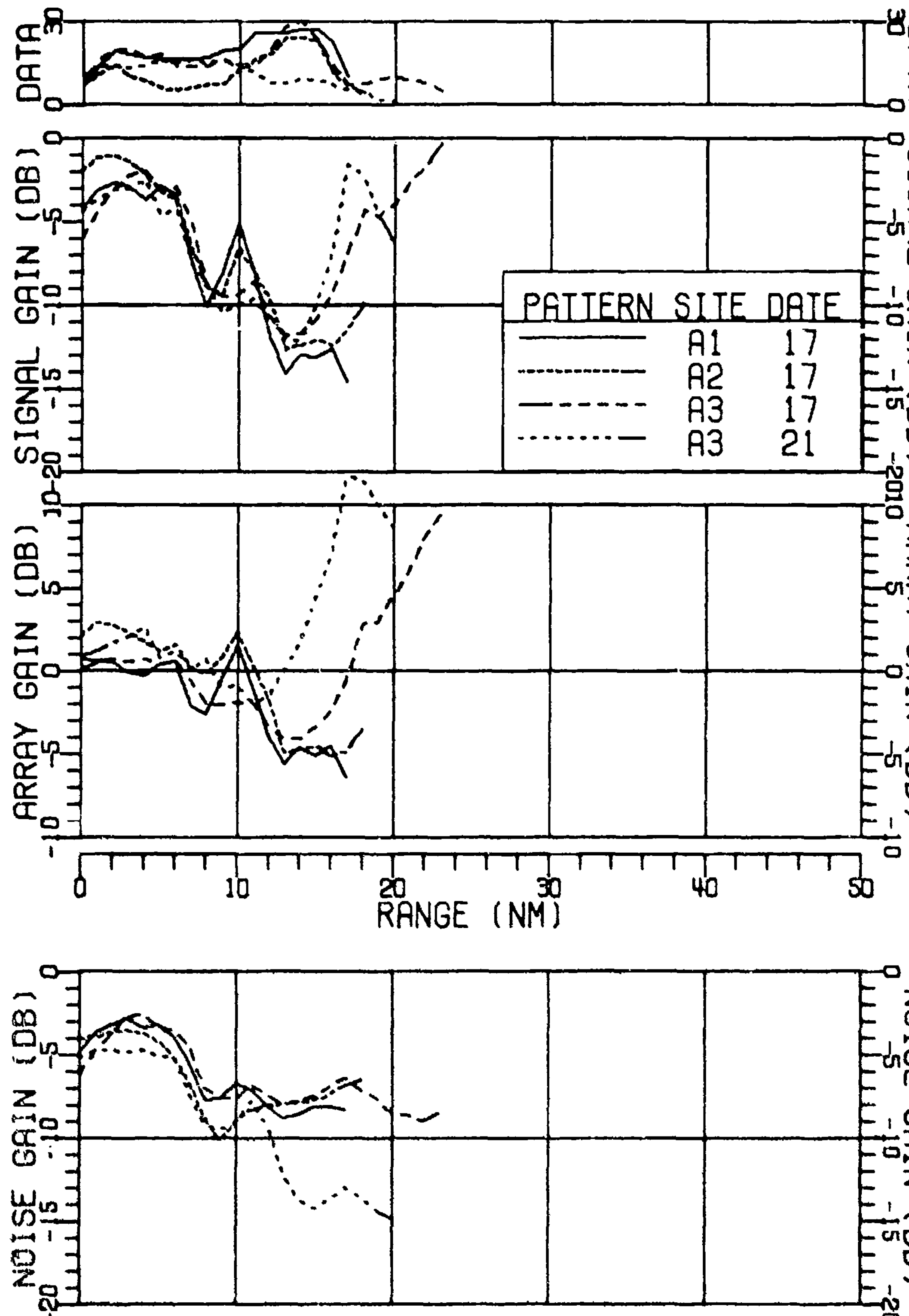

FIGURE III-191
MSS-FVT NEAR BOTTOM DIFFERENCED CARDIOIDS SENSOR
ARRAY GAIN RESULTS FOR 160HZ AT 161DB (U)

AS-77-2791

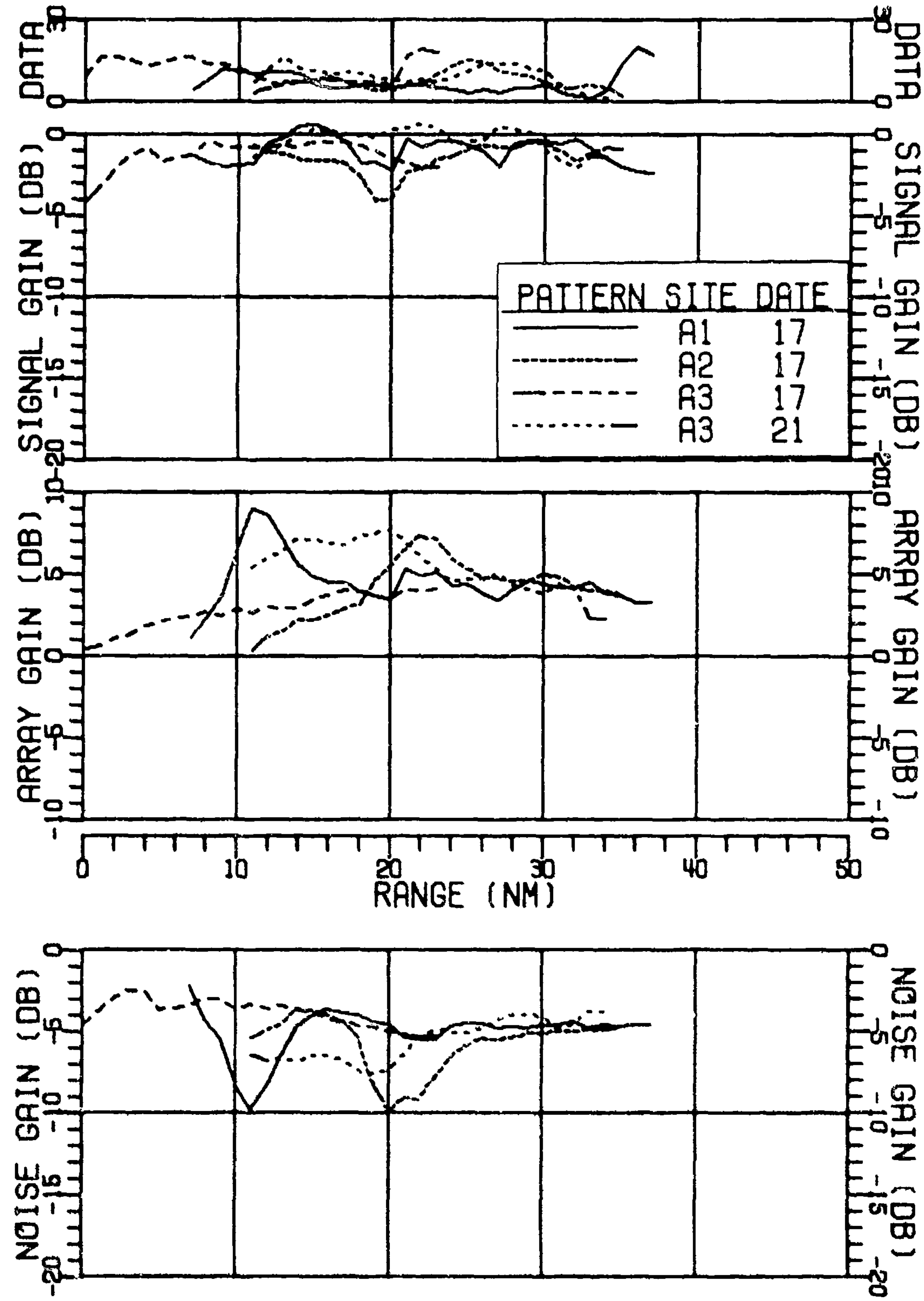

FIGURE III-192
MSS-FVT NEAR BOTTOM SINGLE CARDIOIDS SENSOR
ARRAY GAIN RESULTS FOR 170HZ AT 156DB (U)

AS-77-2792

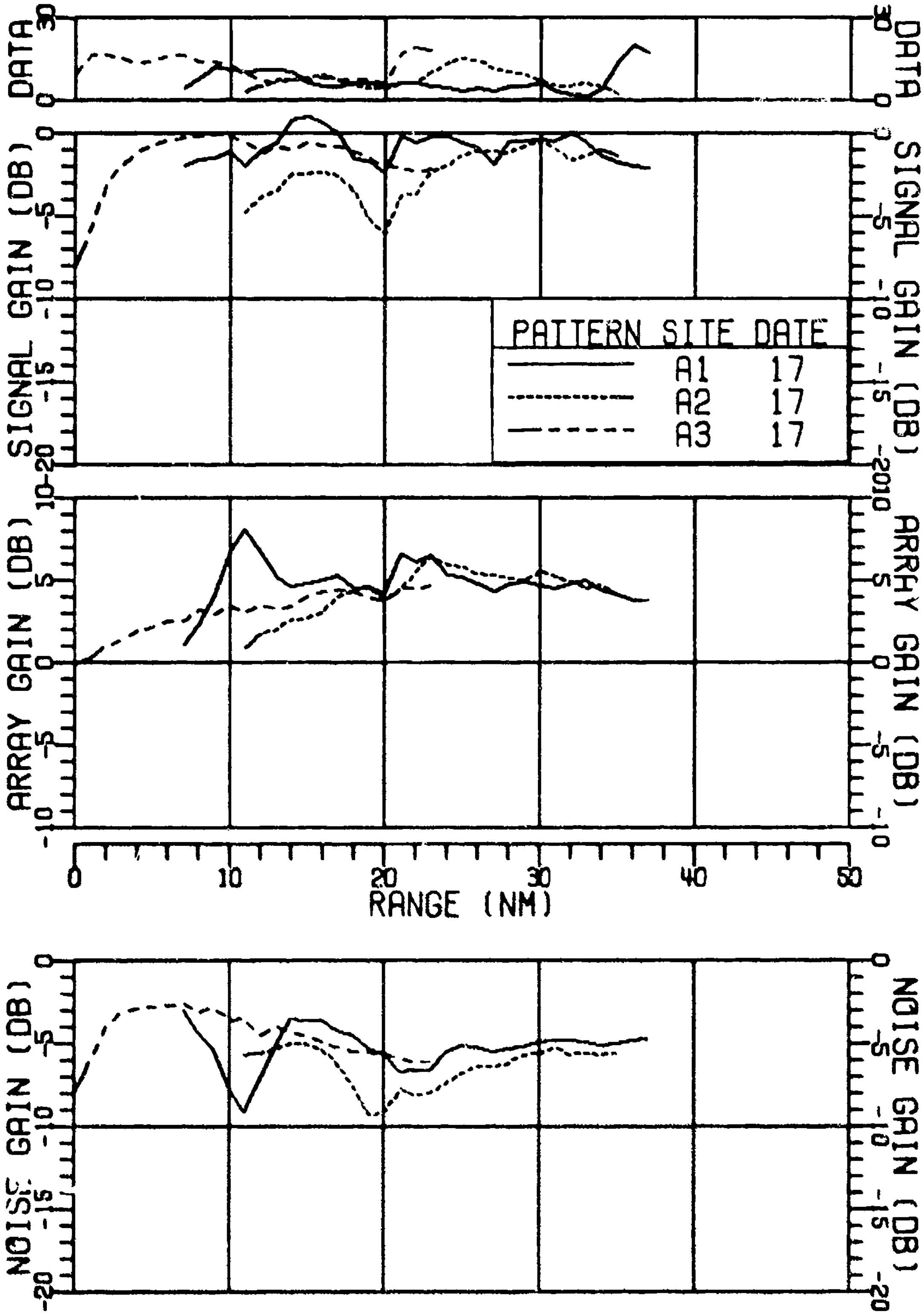

FIGURE III-193
MSS-FVT NEAR BOTTOM MAX GAIN LIMACONS SENSOR
ARRAY GAIN RESULTS FOR 170HZ AT 156DB (U)

AS-77-2793

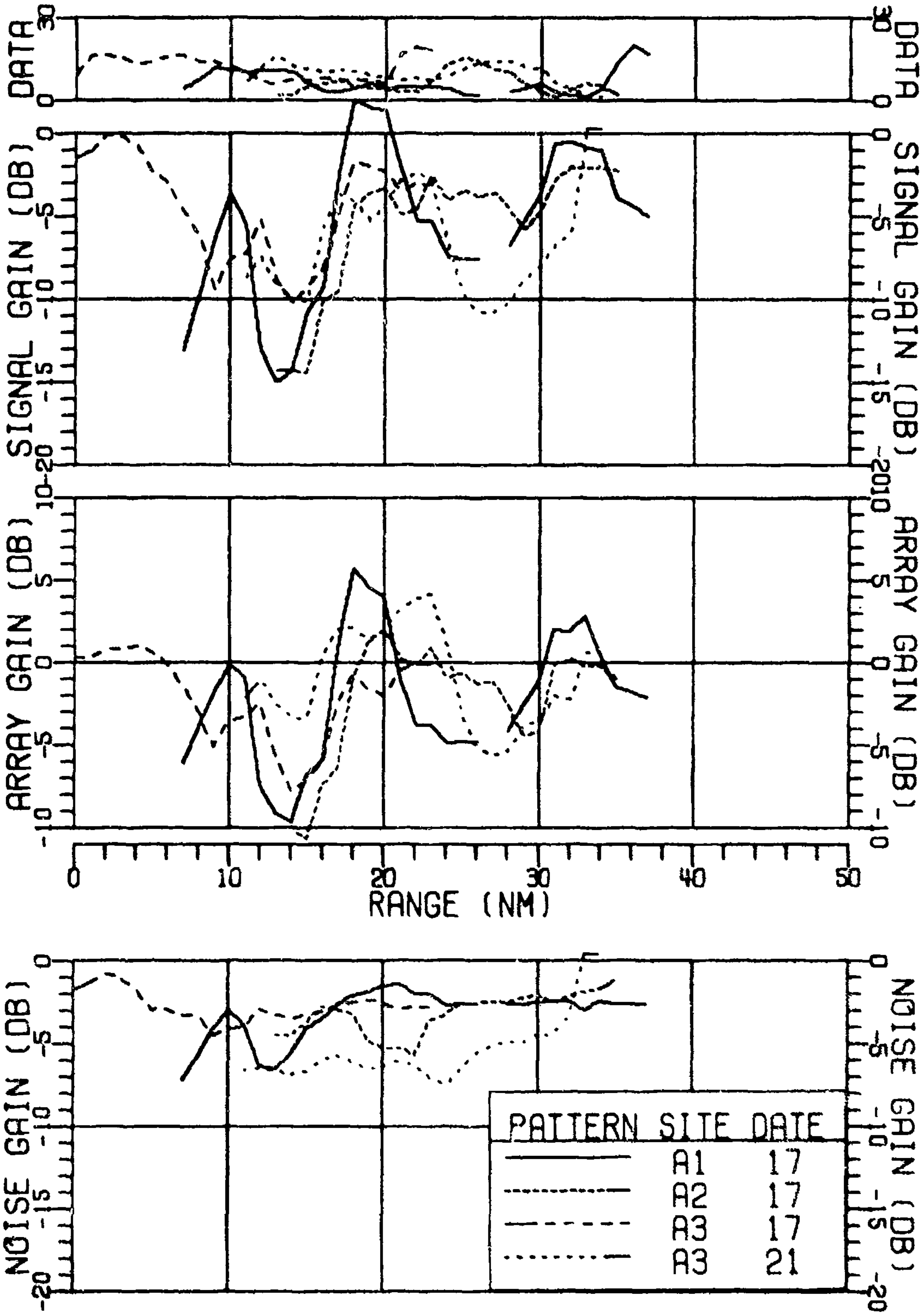

FIGURE III-194
MSS-FVT NEAR BOTTOM VERTICAL DIPOLE SENSOR
ARRAY GAIN RESULTS FOR 170HZ AT 156DB (U)

AS-77-2794

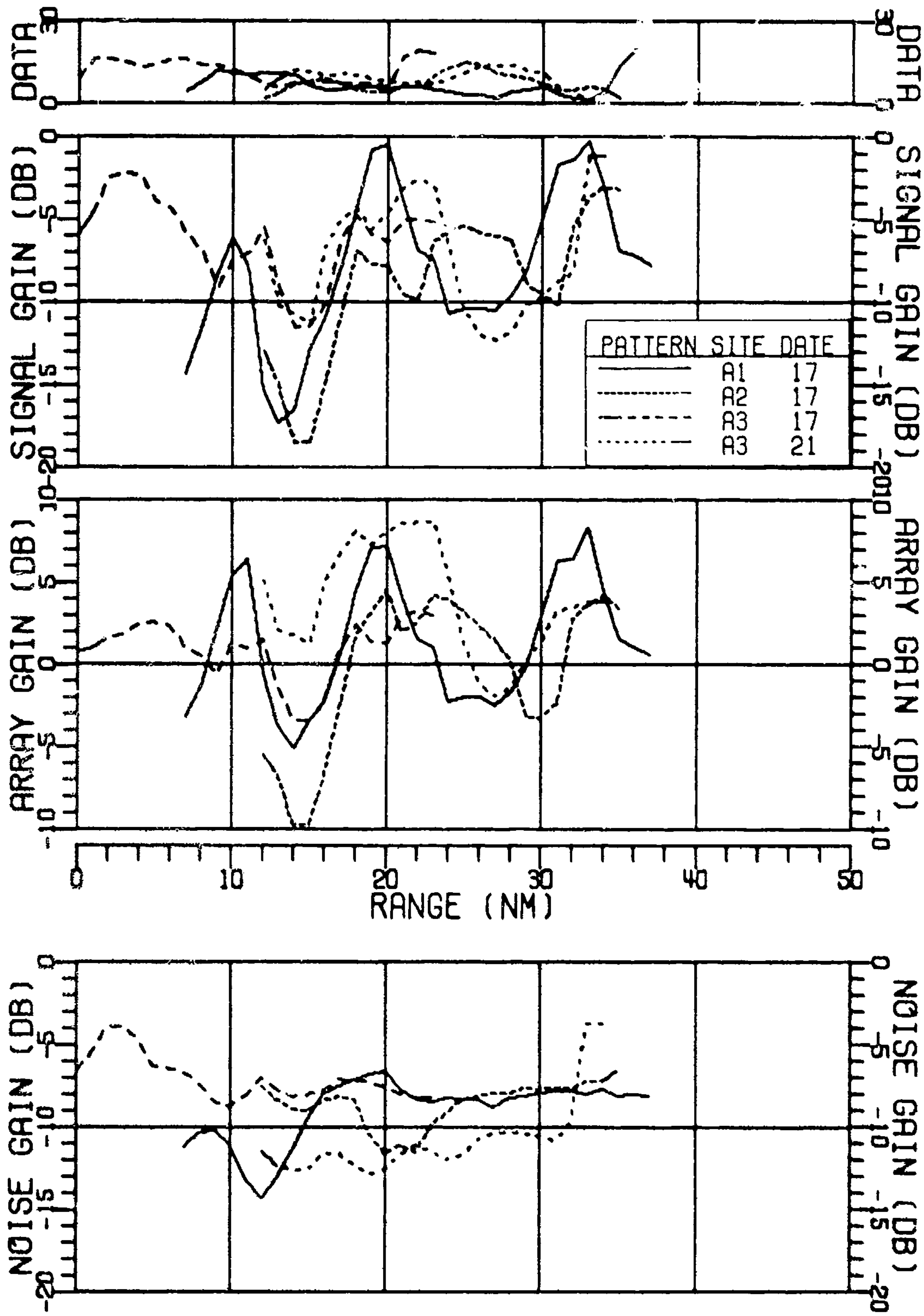

FIGURE III-195
MSS-FVT NEAR BOTTOM DIFFERENCED CARDIOIDS SENSOR
ARRAY GAIN RESULTS FOR 170HZ AT 156DB (U)

AS-77-2795

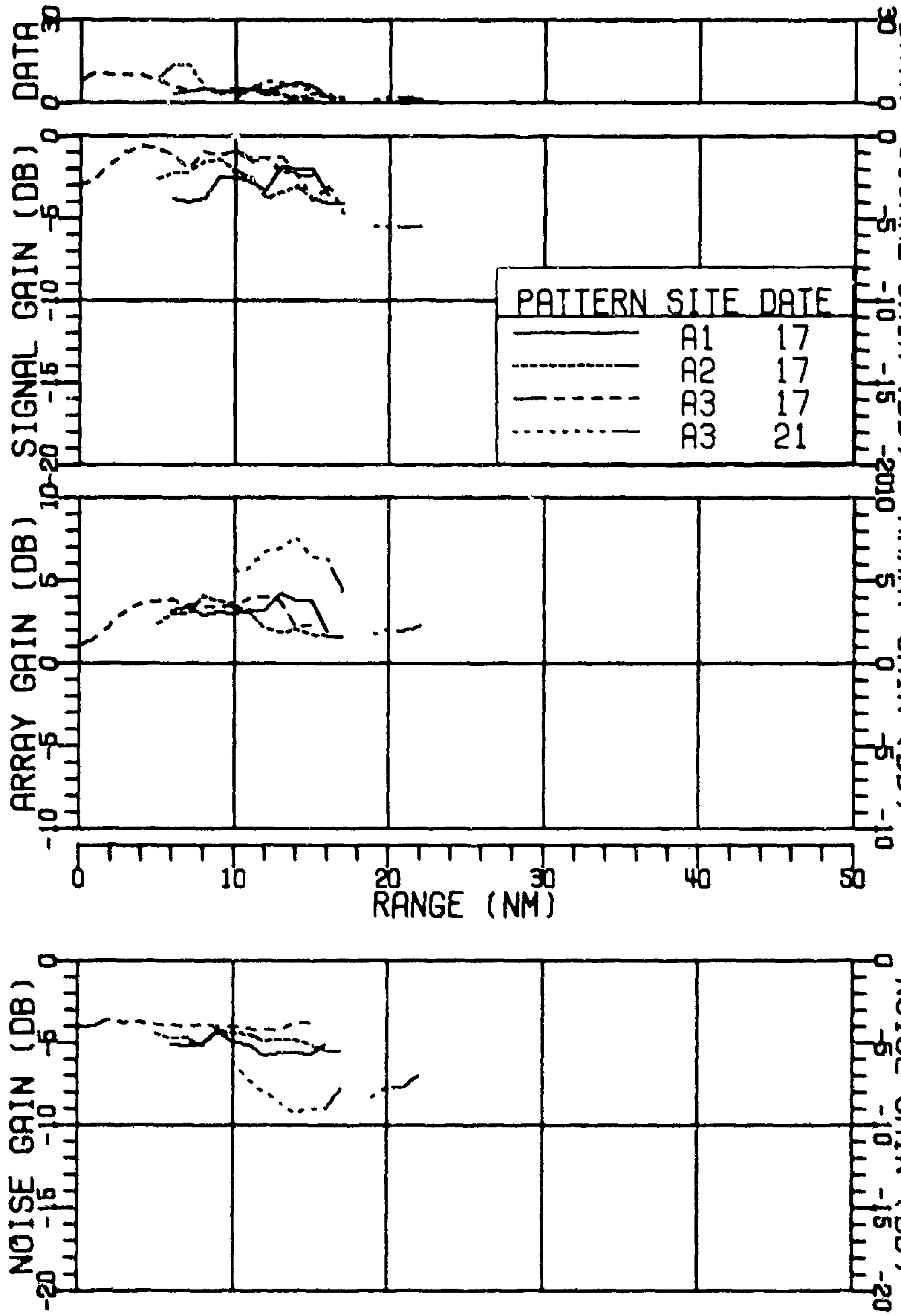

FIGURE III-196
MSS-FVT NEAR BOTTOM SINGLE CARDIOIDS SENSOR
ARRAY GAIN RESULTS FOR 305HZ AT 136DB (U)

AS-77-2796

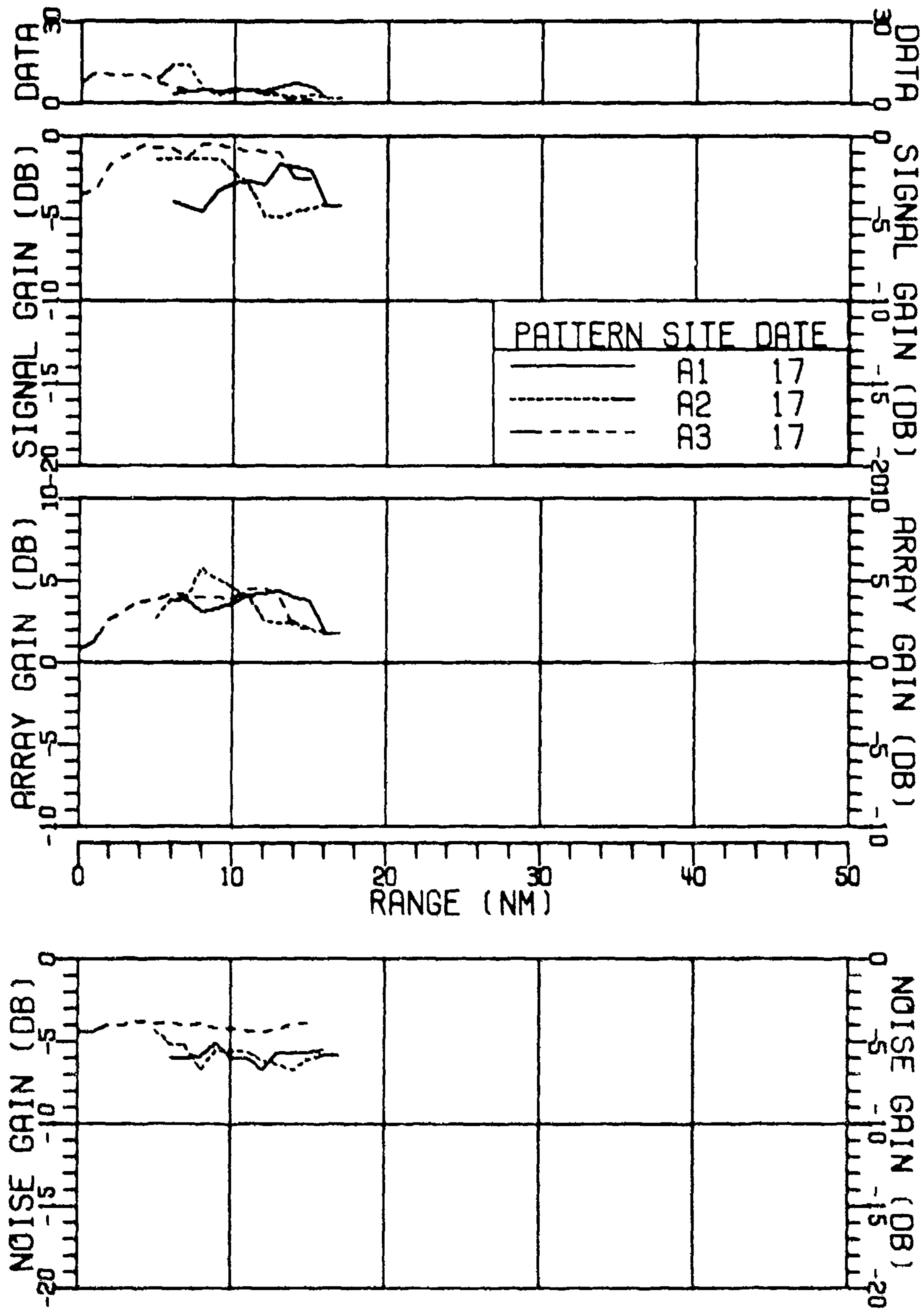

FIGURE III-197
MSS-FVT NEAR BOTTOM MAX GAIN LIMACONS SENSOR
ARRAY GAIN RESULTS FOR 305HZ AT 136DB (U)

AS-77-2797

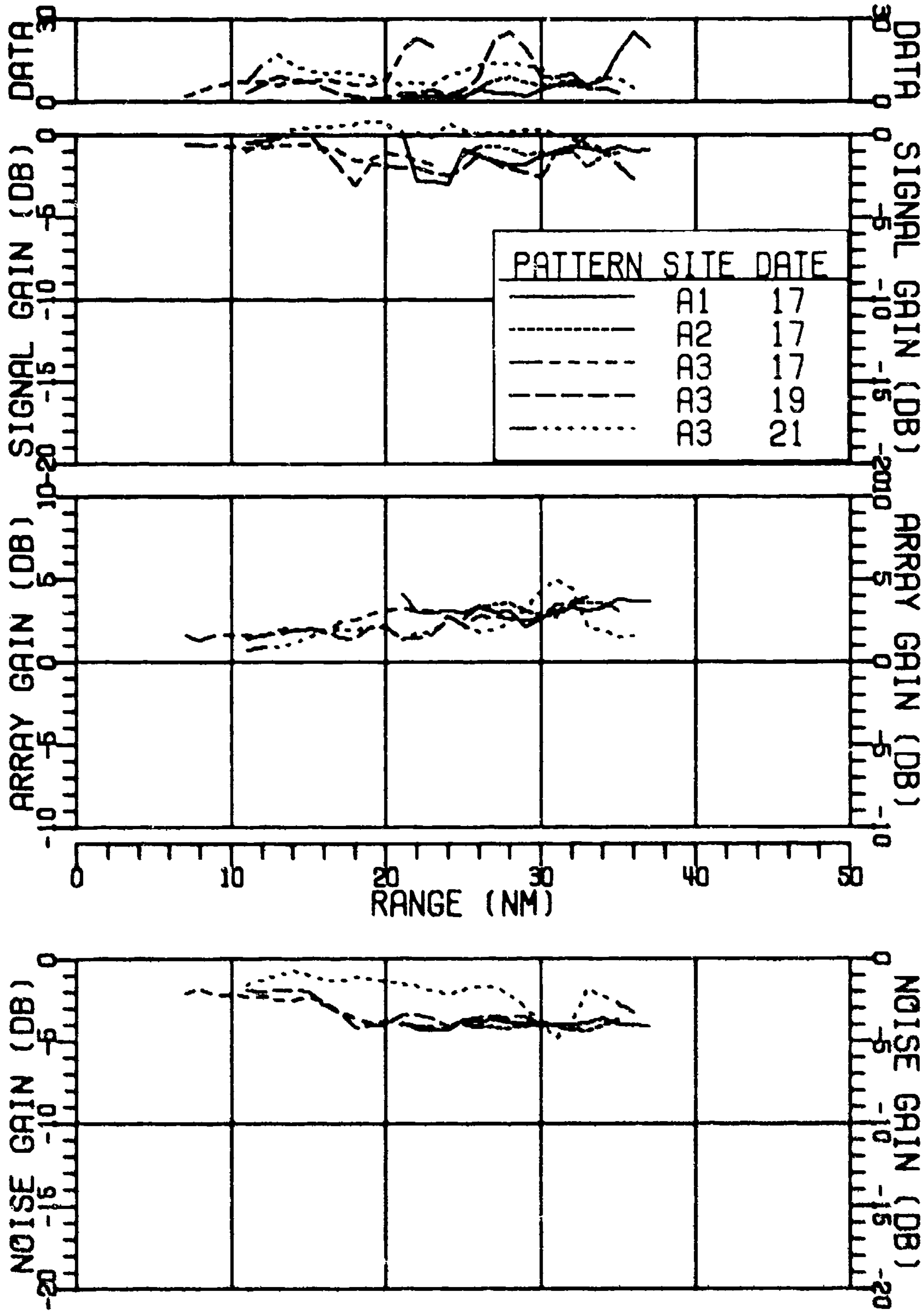

FIGURE III-198
MSS-FVT NEAR BOTTOM SINGLE CARDIOIDS SENSOR
ARRAY GAIN RESULTS FOR 335HZ AT 154DB (U)

AS-77-2798

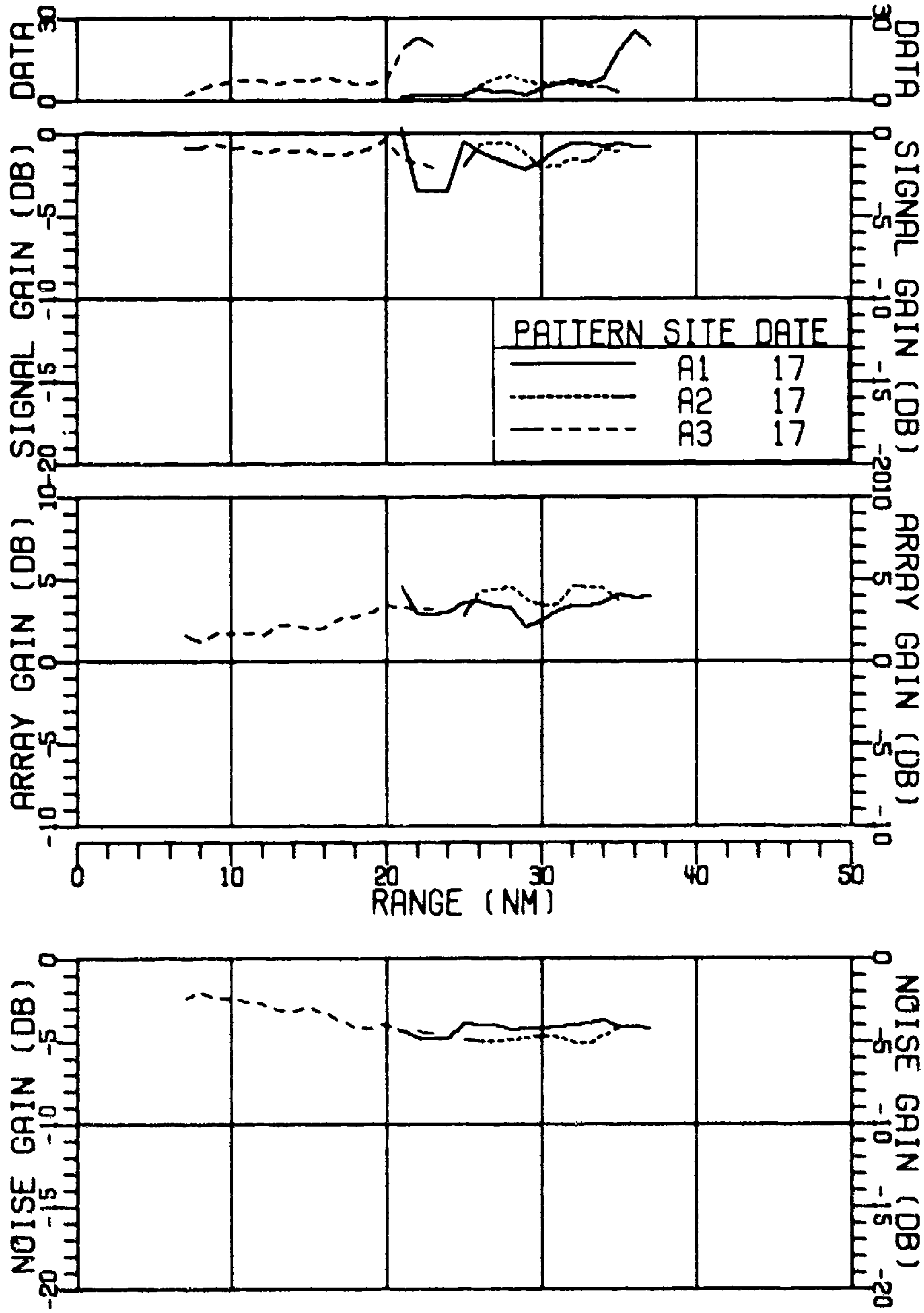

FIGURE III-199
MSS-FVT NEAR BOTTOM MAX GAIN LIMACONS SENSOR
ARRAY GAIN RESULTS FOR 335HZ AT 154DB (U)

AS-77-2799

APPENDIX E

PERCENTAGE DETECTION versus RANGE CURVES (U)

(FIGURES III-200 - III-235)

(The reverse of this page is blank.)

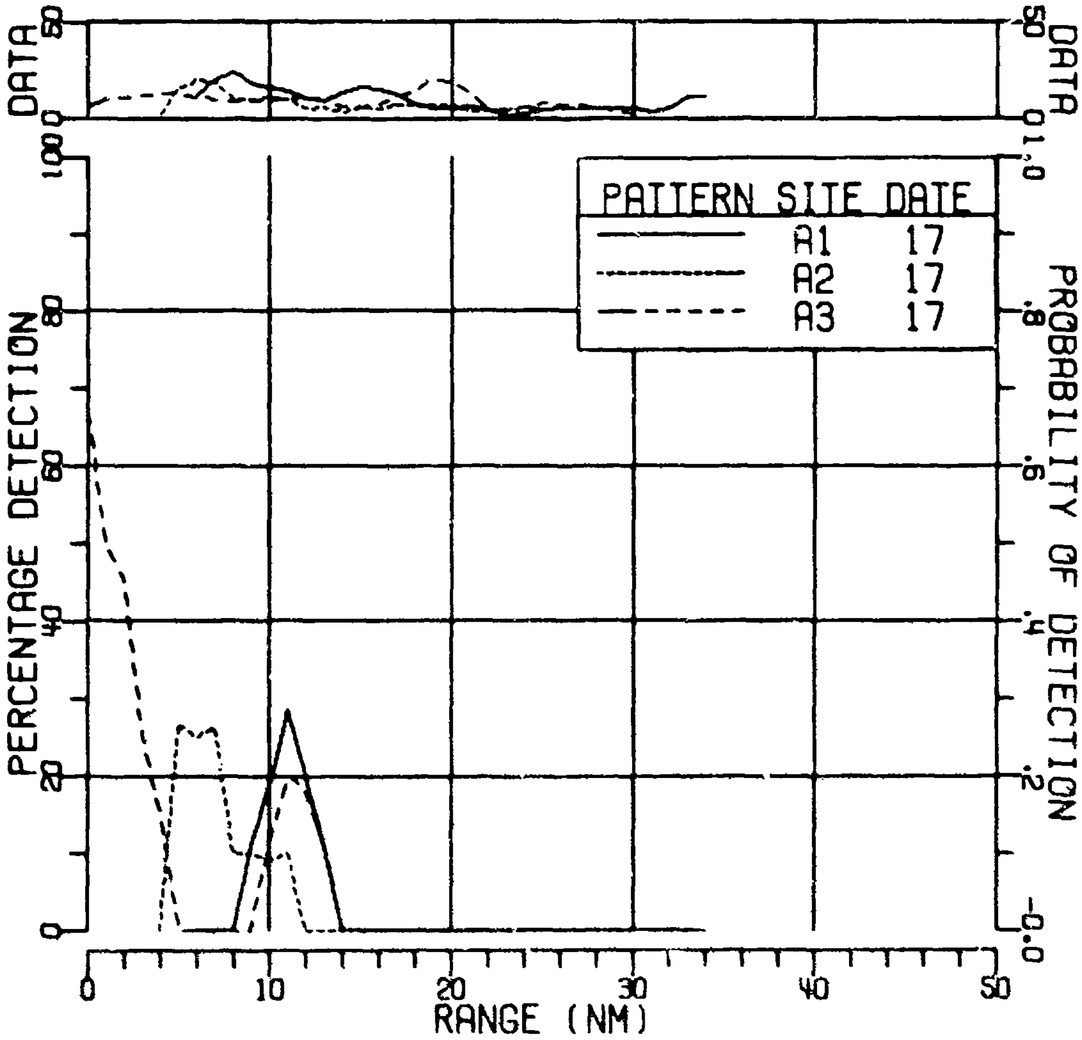

FIGURE III-200
MSS-FVT NEAR BOTTOM OMNIDIRECTIONAL SENSOR
DETECTION RESULTS FOR 55HZ AT 141DB (U)

AS-77-2800

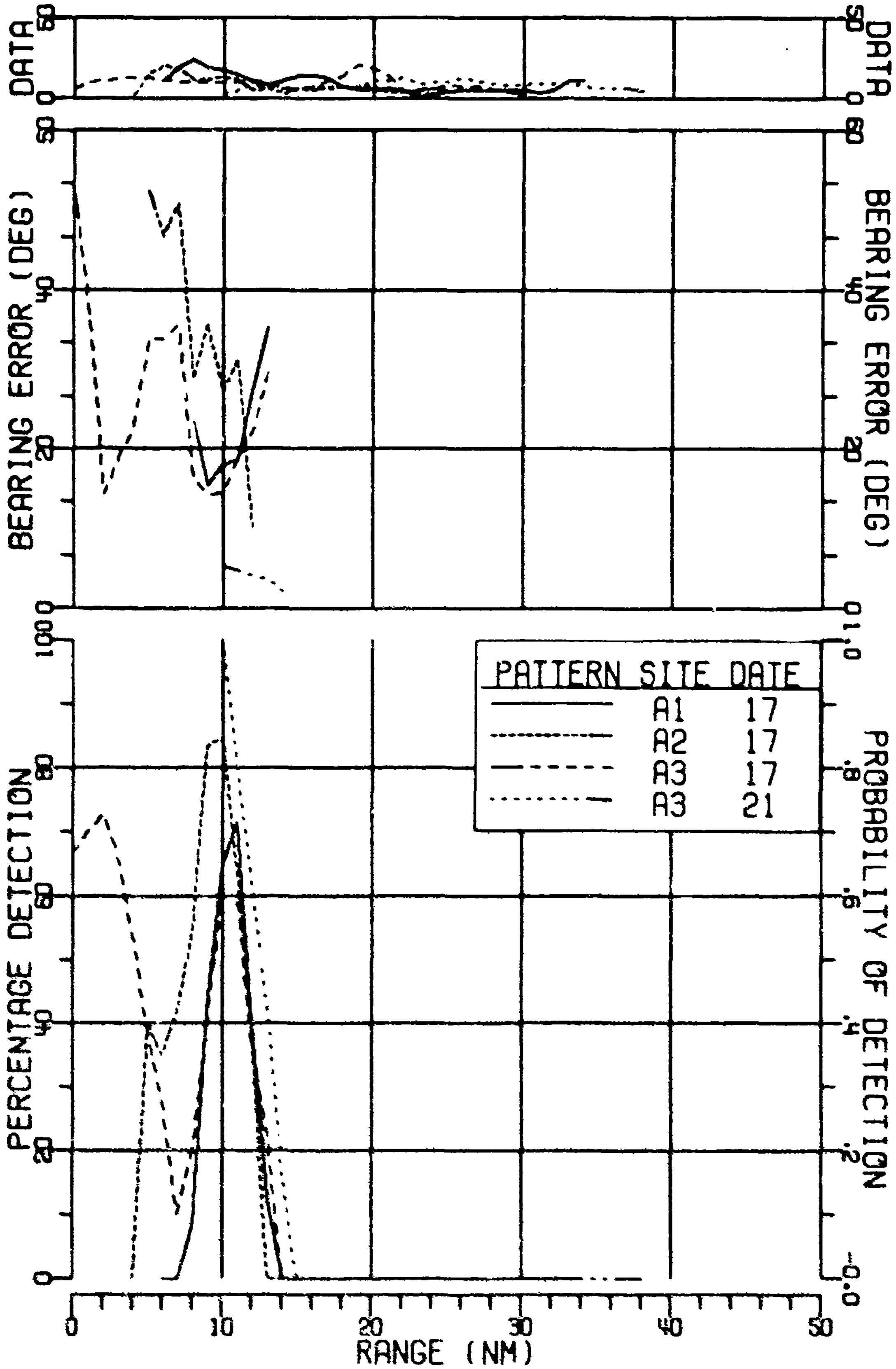

FIGURE III-201
MSS-FVT NEAR BOTTOM SINGLE CARDIOIDS SENSOR DETECTION RESULTS FOR 55HZ AT 141DB (U)

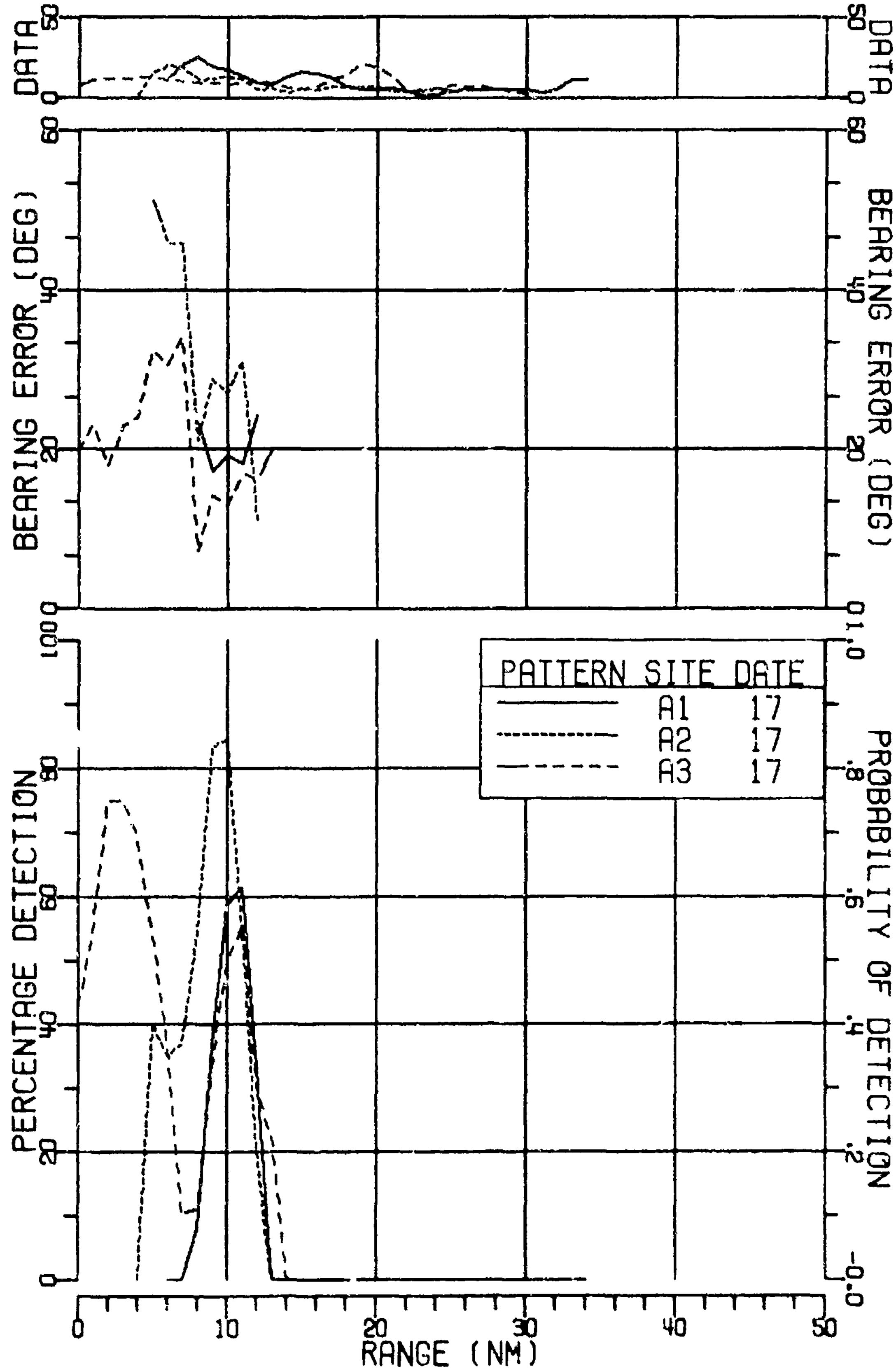

FIGURE III-202
MSS-FVT NEAR BOTTOM MAX GAIN LIMACONS SENSOR
DETECTION RESULTS FOR 55HZ AT 141DB (U)

AS-77-2802

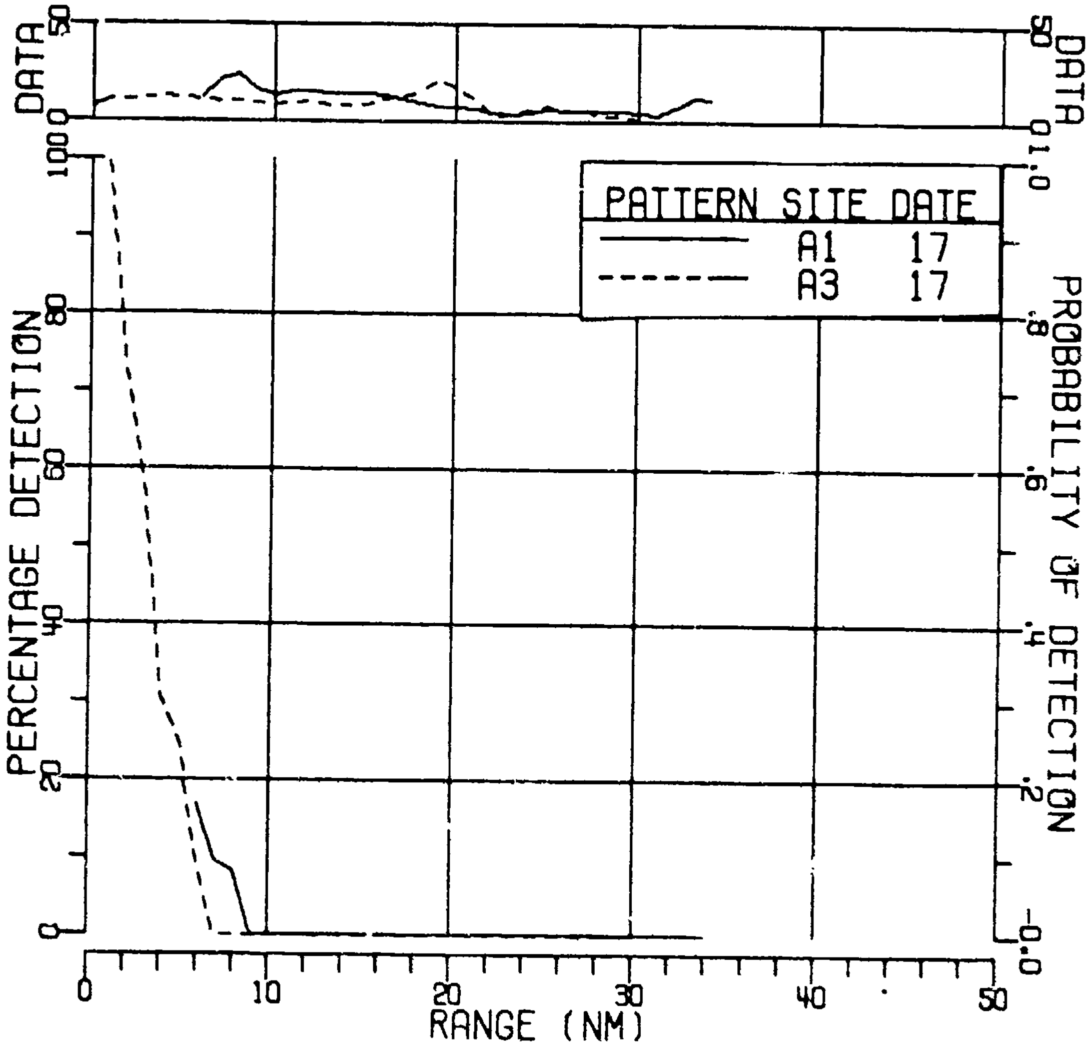

FIGURE III-203
MSS-FVT NEAR BOTTOM VERTICAL DIPOLE SENSOR
DETECTION RESULTS FOR 55HZ AT 141DB (U)

AS-77-2803

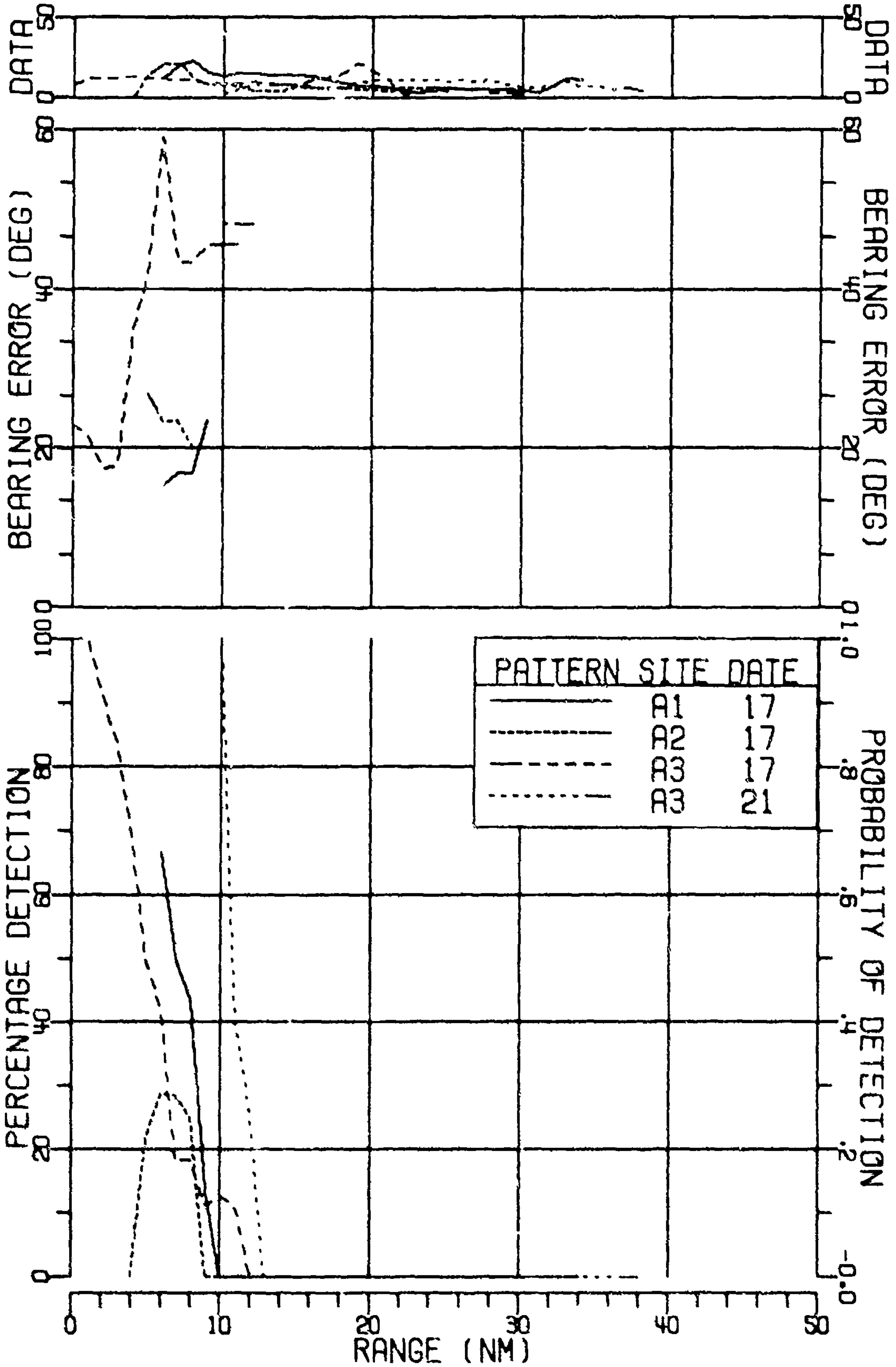

FIGURE III-204
MSS-FVT NEAR BOTTOM DIFFERENCED CARDIOIDS SENSOR
DETECTION RESULTS FOR 55HZ AT 141DB (U)

AS-77-2804

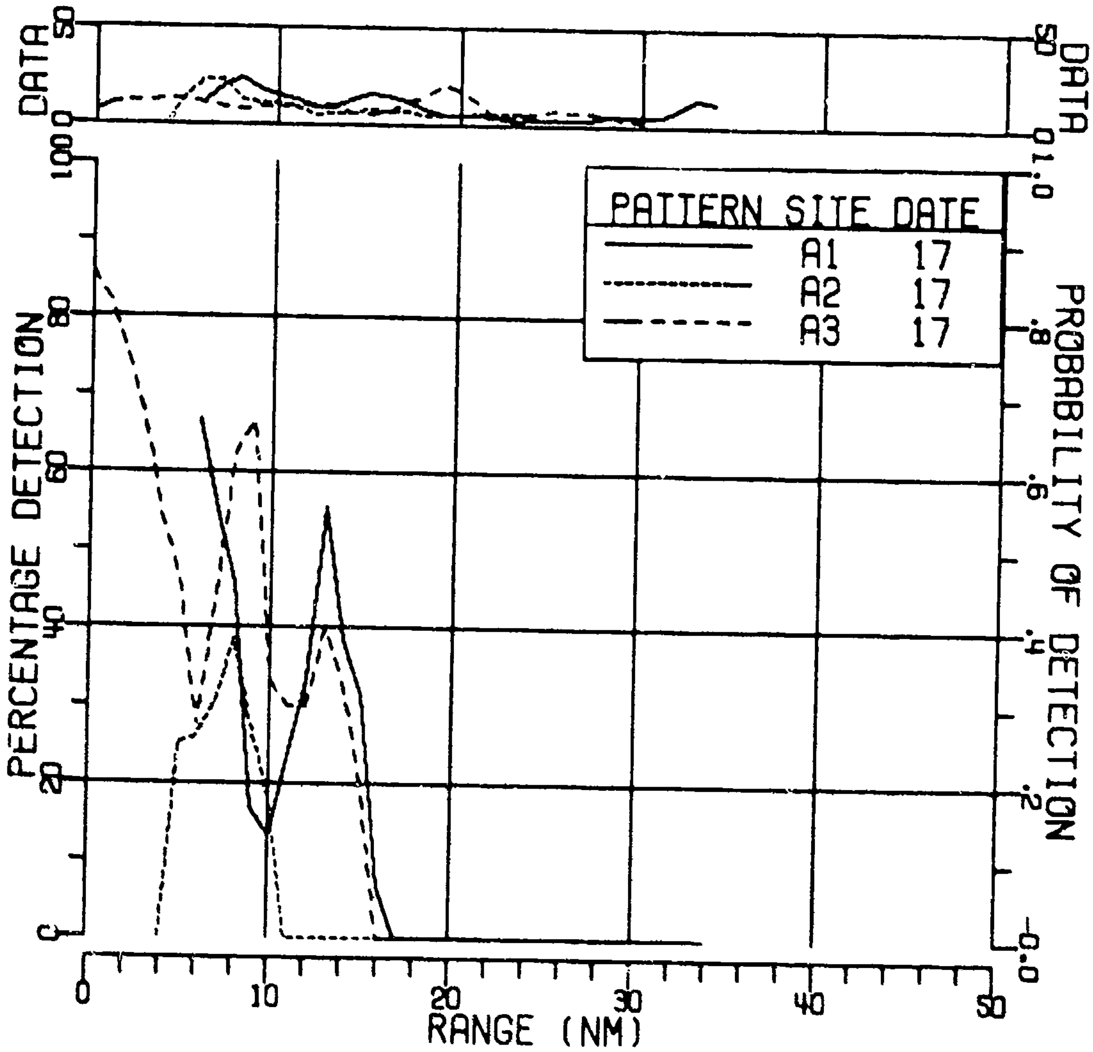

FIGURE III-205
MSS-FVT NEAR BOTTOM OMNIDIRECTIONAL SENSOR DETECTION RESULTS FOR 155HZ AT 134DB (U)

AS-77-2805

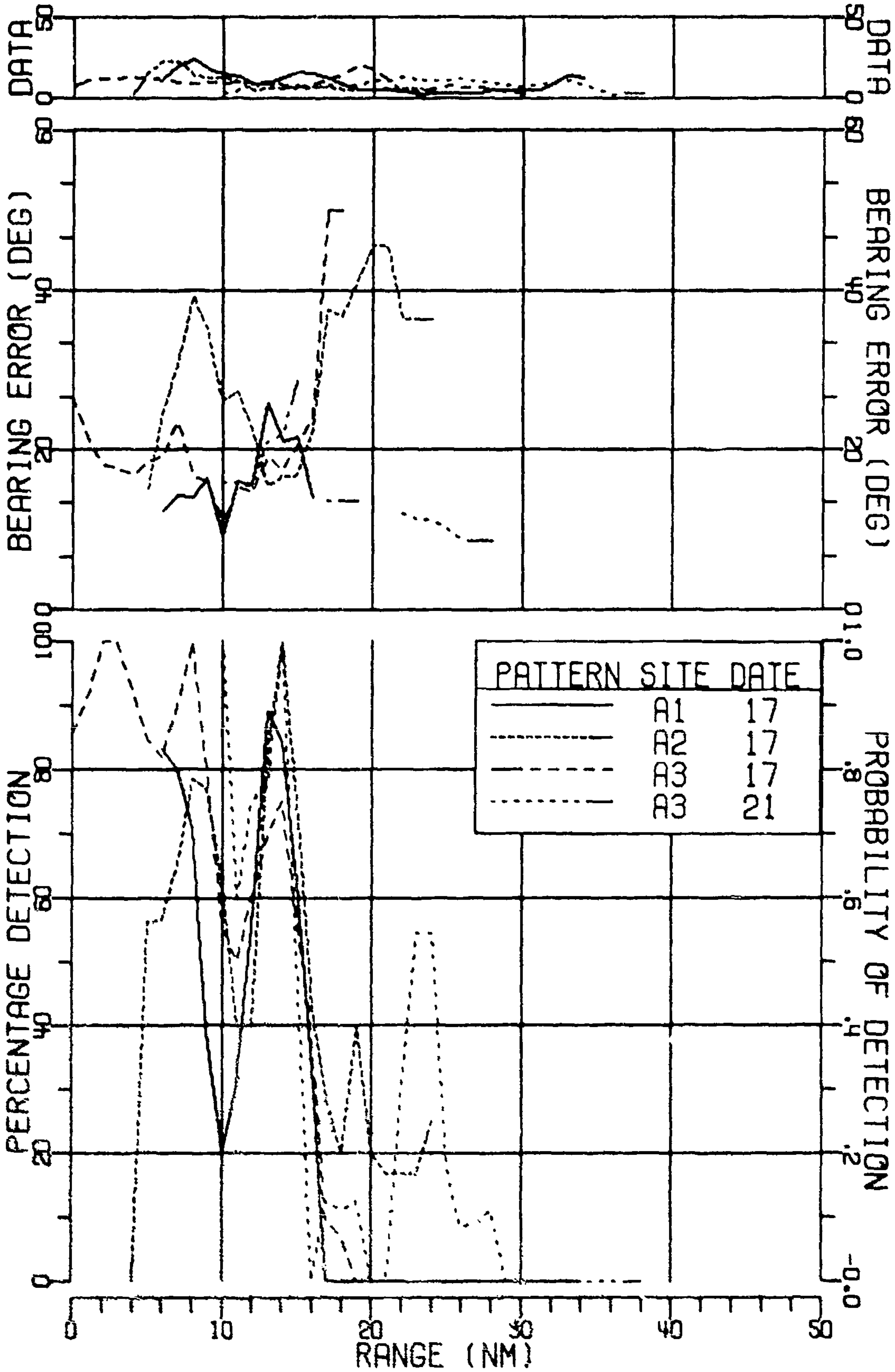

FIGURE III-206
MSS-FVT NEAR BOTTOM SINGLE CARDIOIDS SENSOR DETECTION RESULTS FOR 155HZ AT 134DB (U)

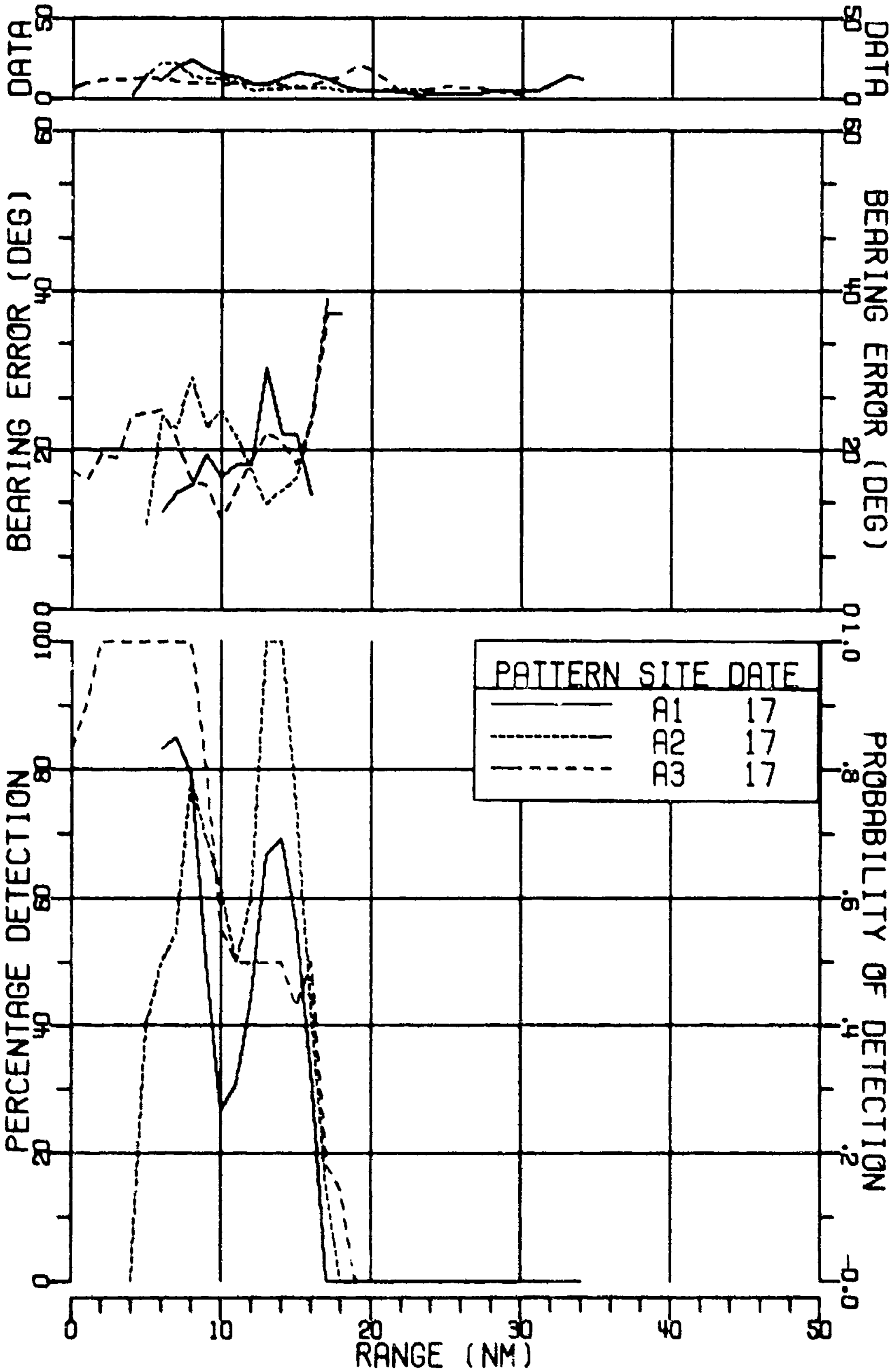

FIGURE III-207
MSS-FVT NEAR BOTTOM MAX GAIN LIMACONS SENSOR
DETECTION RESULTS FOR 155HZ AT 134DB (U)

AS-77-2807

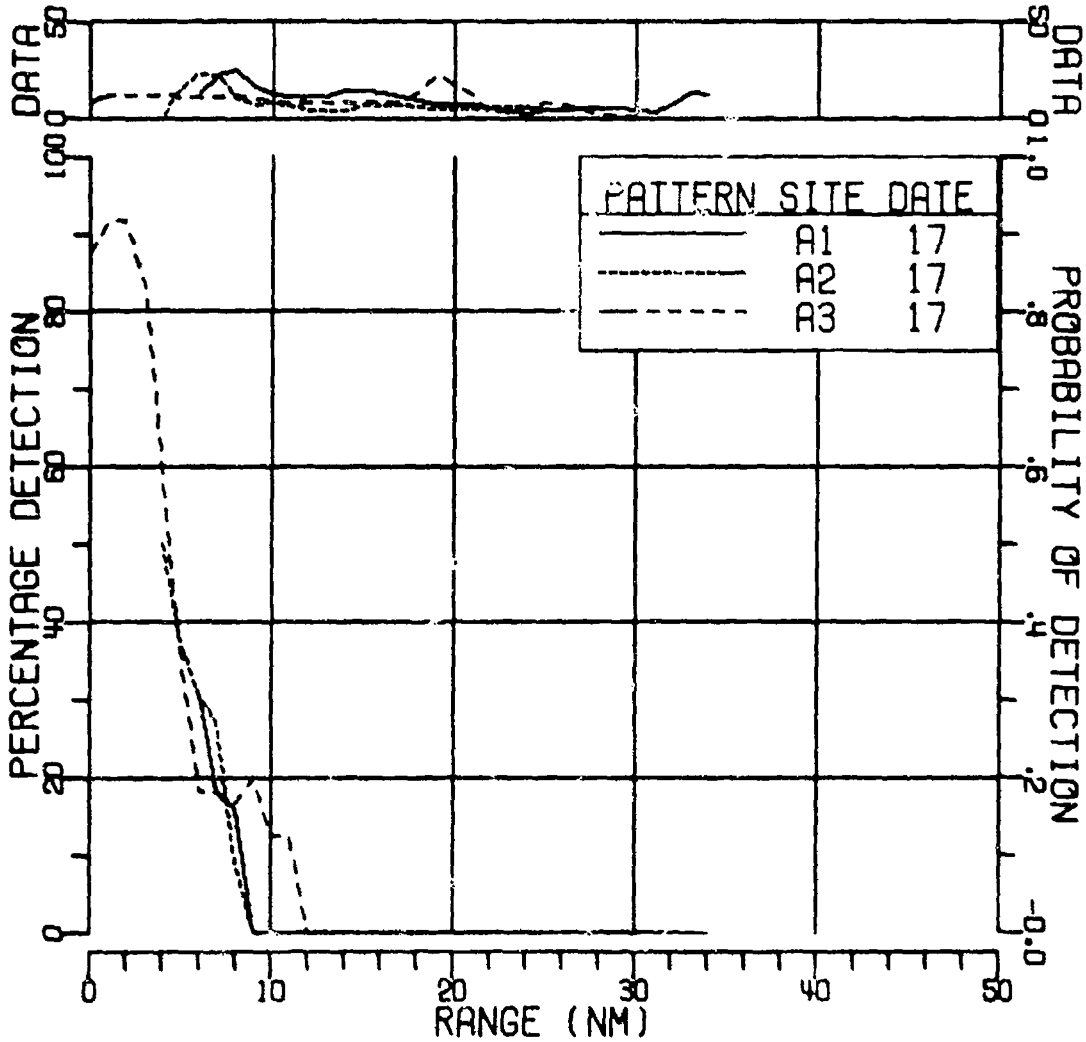

FIGURE III-208
MSS-FVT NEAR BOTTOM VERTICAL DIPOLE SENSOR
DETECTION RESULTS FOR 155HZ AT 134DB (U)

AS-77-2808

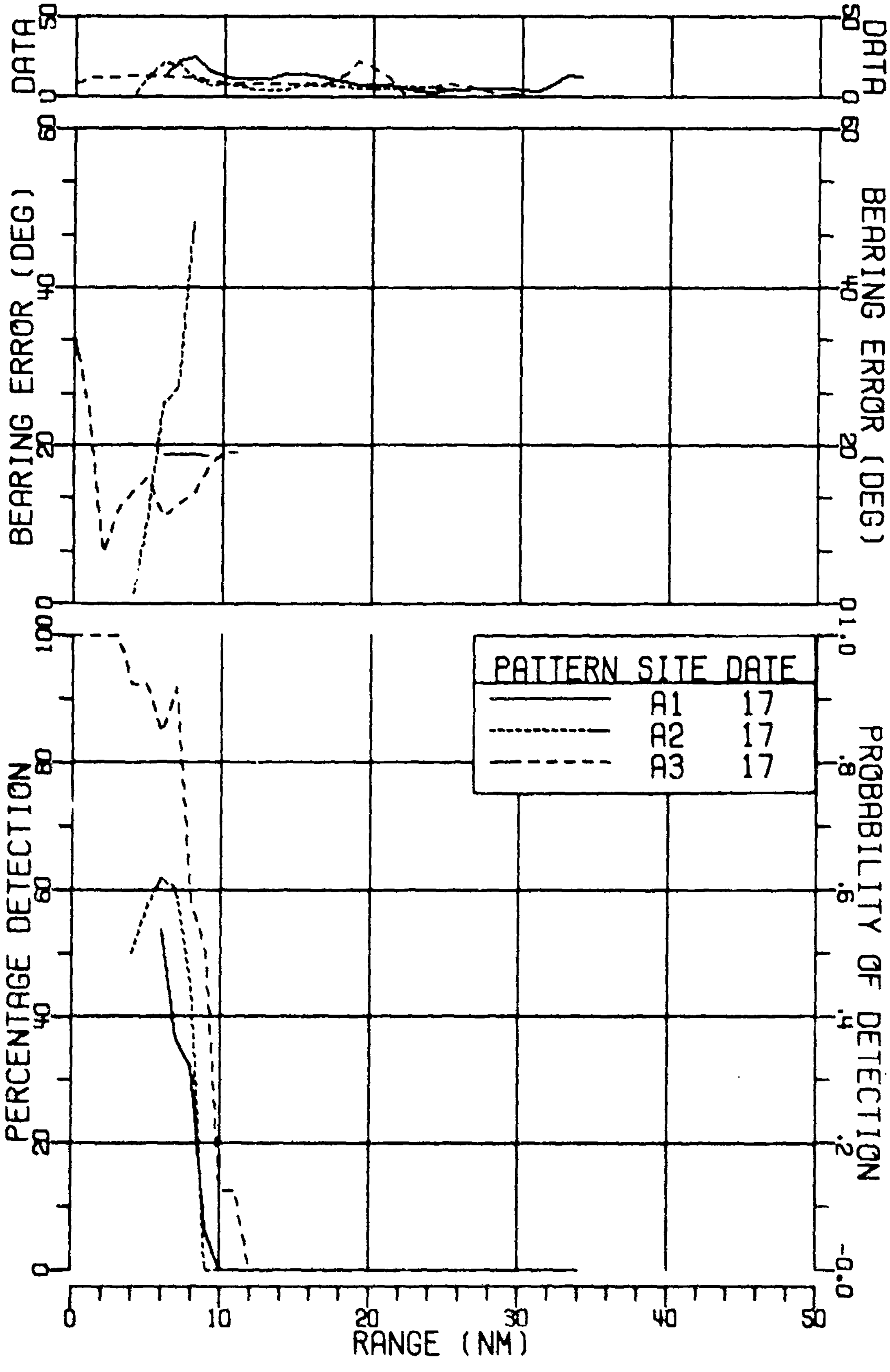

FIGURE III-209
MSS-FVT NEAR BOTTOM DIFFERENCED CARDIOIDS SENSOI
DETECTION RESULTS FOR 155HZ AT 134DB (U)

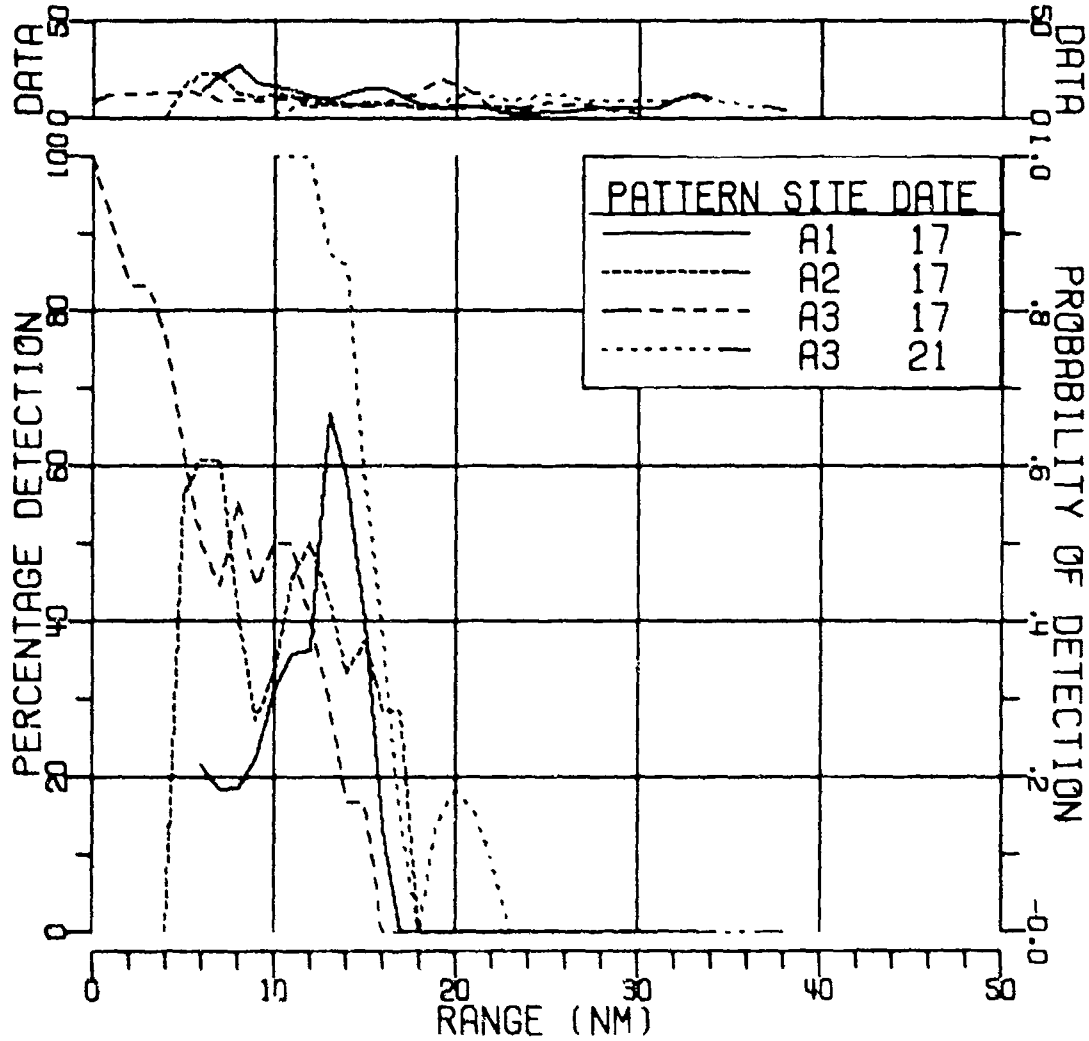

FIGURE III-210
MSS-FVT NEAR BOTTOM OMNIDIRECTIONAL SENSOR
DETECTION RESULTS FOR 305HZ AT 136DB (U)

AS-77-2810

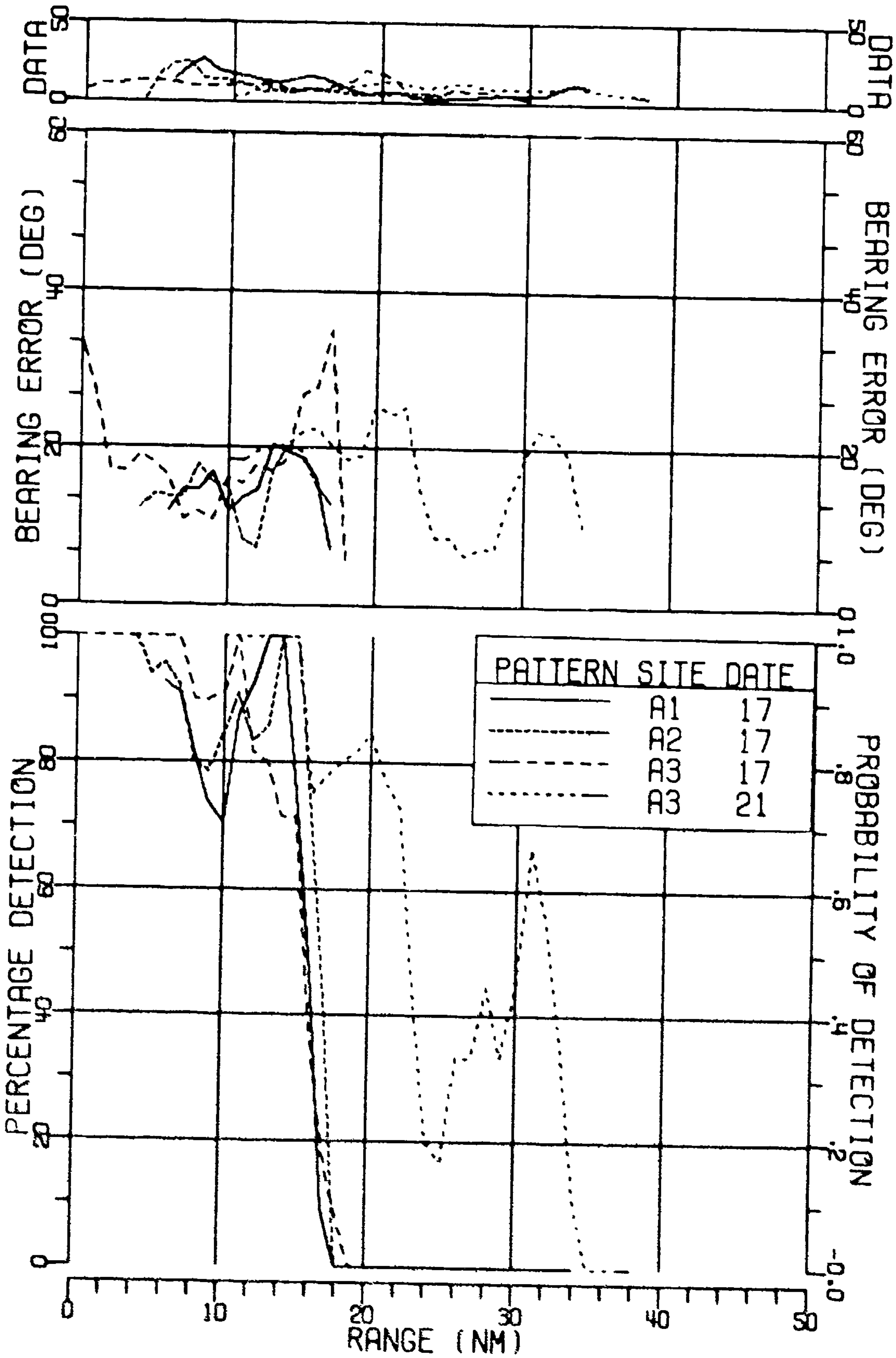

FIGURE III-211
MSS-FVT NEAR BOTTOM SINGLE CARDIOIDS SENSOR DETECTION RESULTS FOR 305HZ AT 136DB (U)

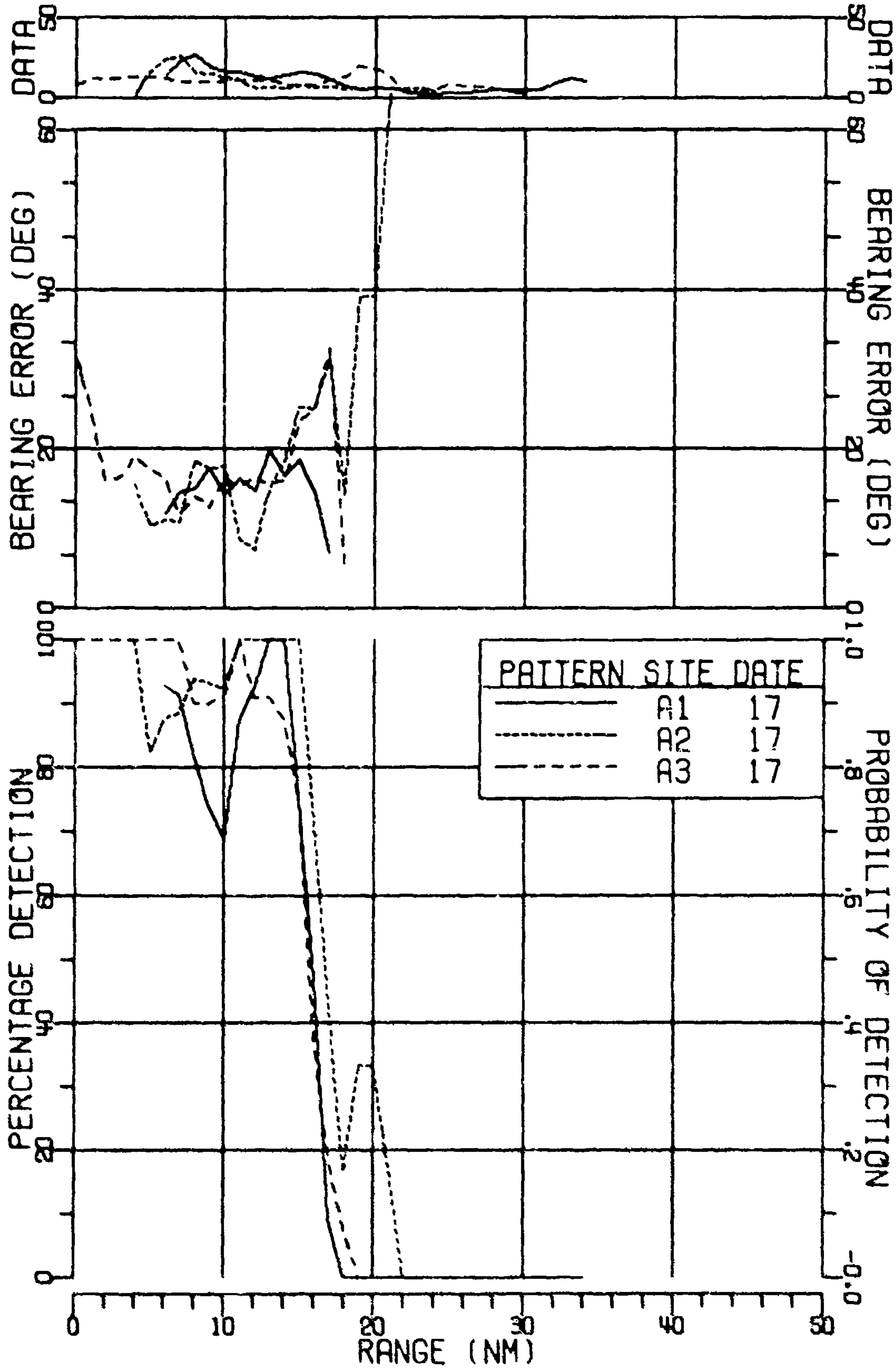

FIGURE III-212
MSS-FVT NEAR BOTTOM MAX GAIN LIMACONS SENSOR DETECTION RESULTS FOR 305HZ AT 136DB (U)

AS-77-281

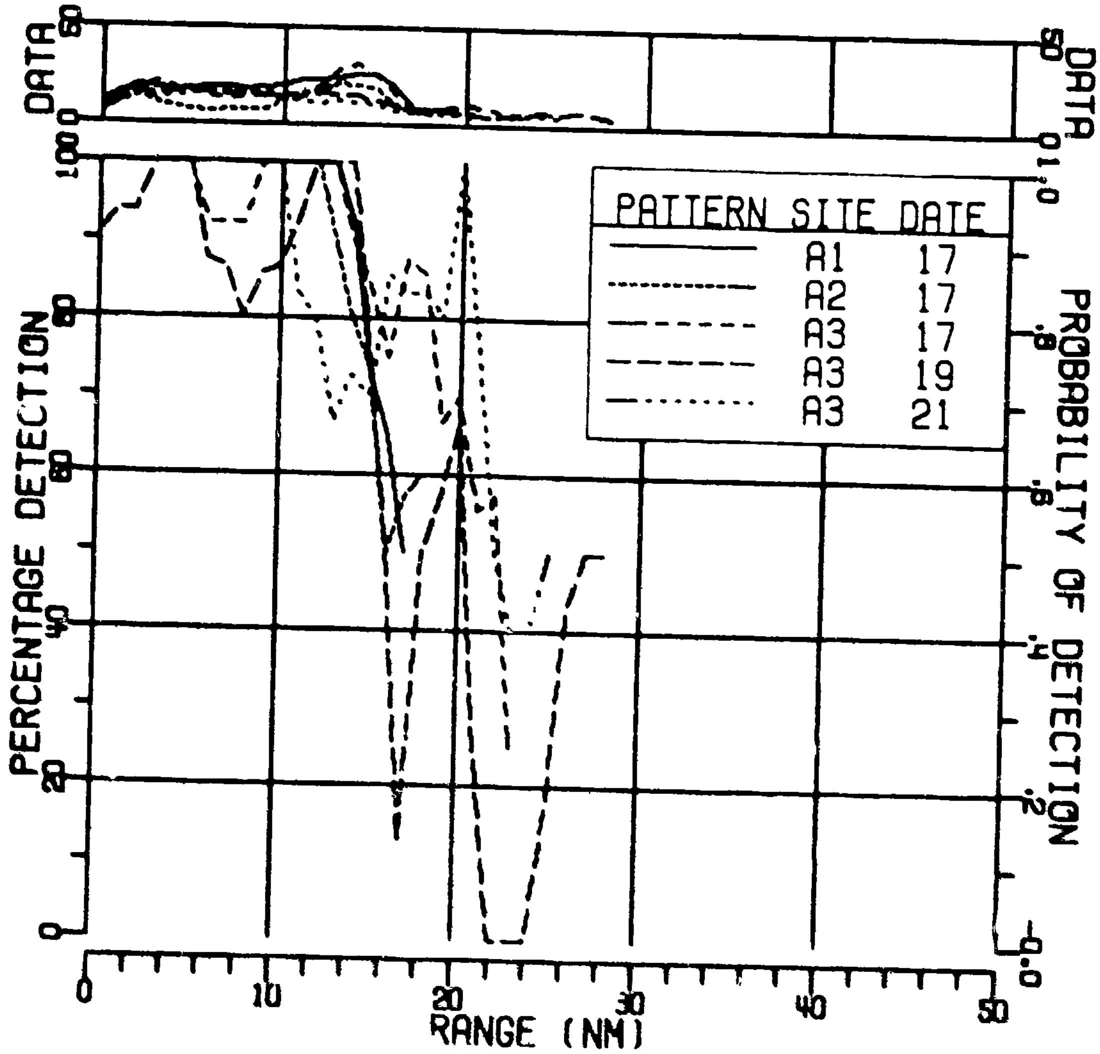

FIGURE III-213
MSS-FVT NEAR BOTTOM OMNIDIRECTIONAL SENSOR
DETECTION RESULTS FOR 64HZ AT 162DB (U)

AS-77-2813

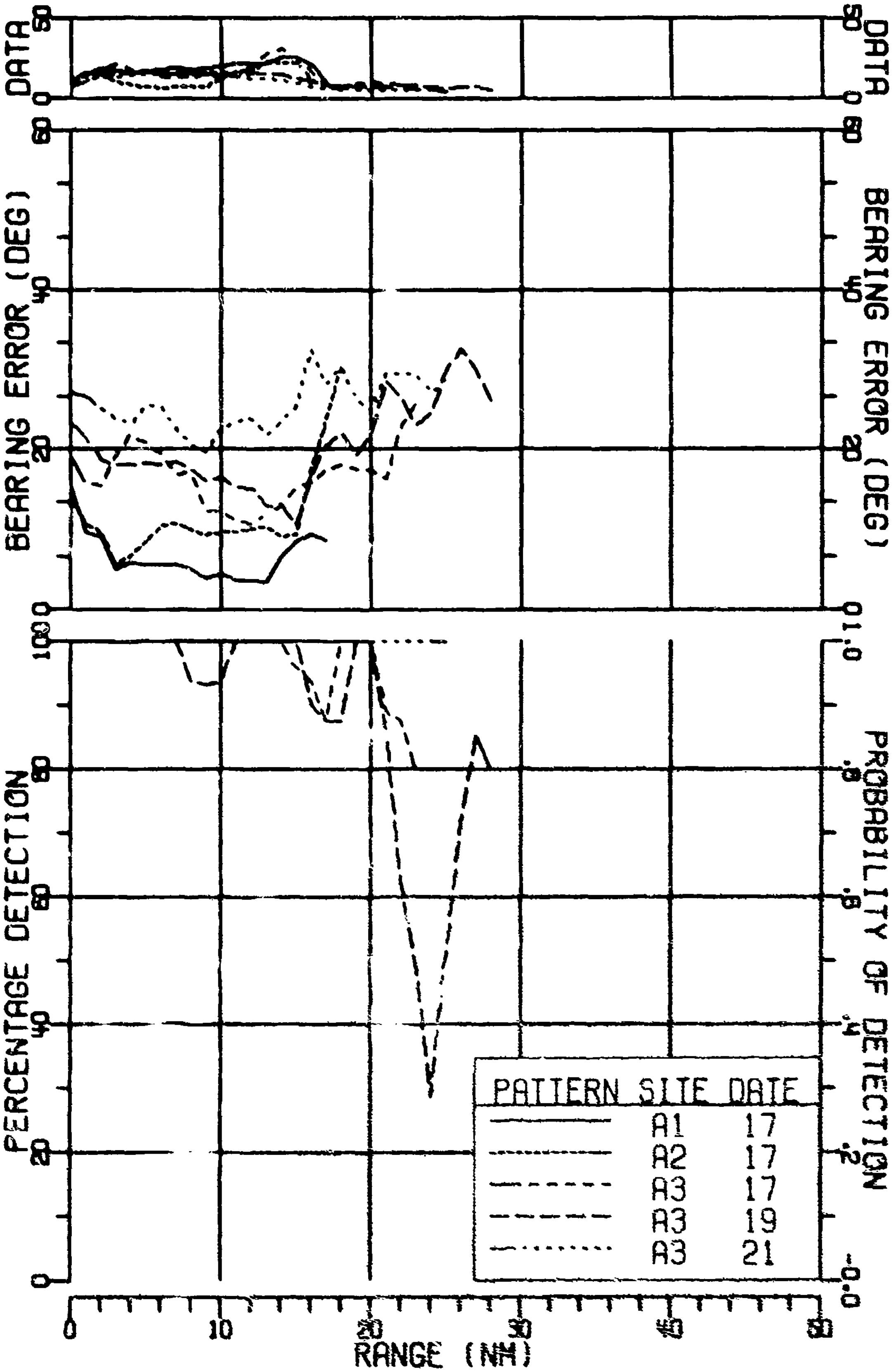

FIGURE III-214
MSS-FVT NEAR BOTTOM SINGLE CARDIOIDS SENSOR
DETECTION RESULTS FOR 64HZ AT 162DB (U)

AP-77-281

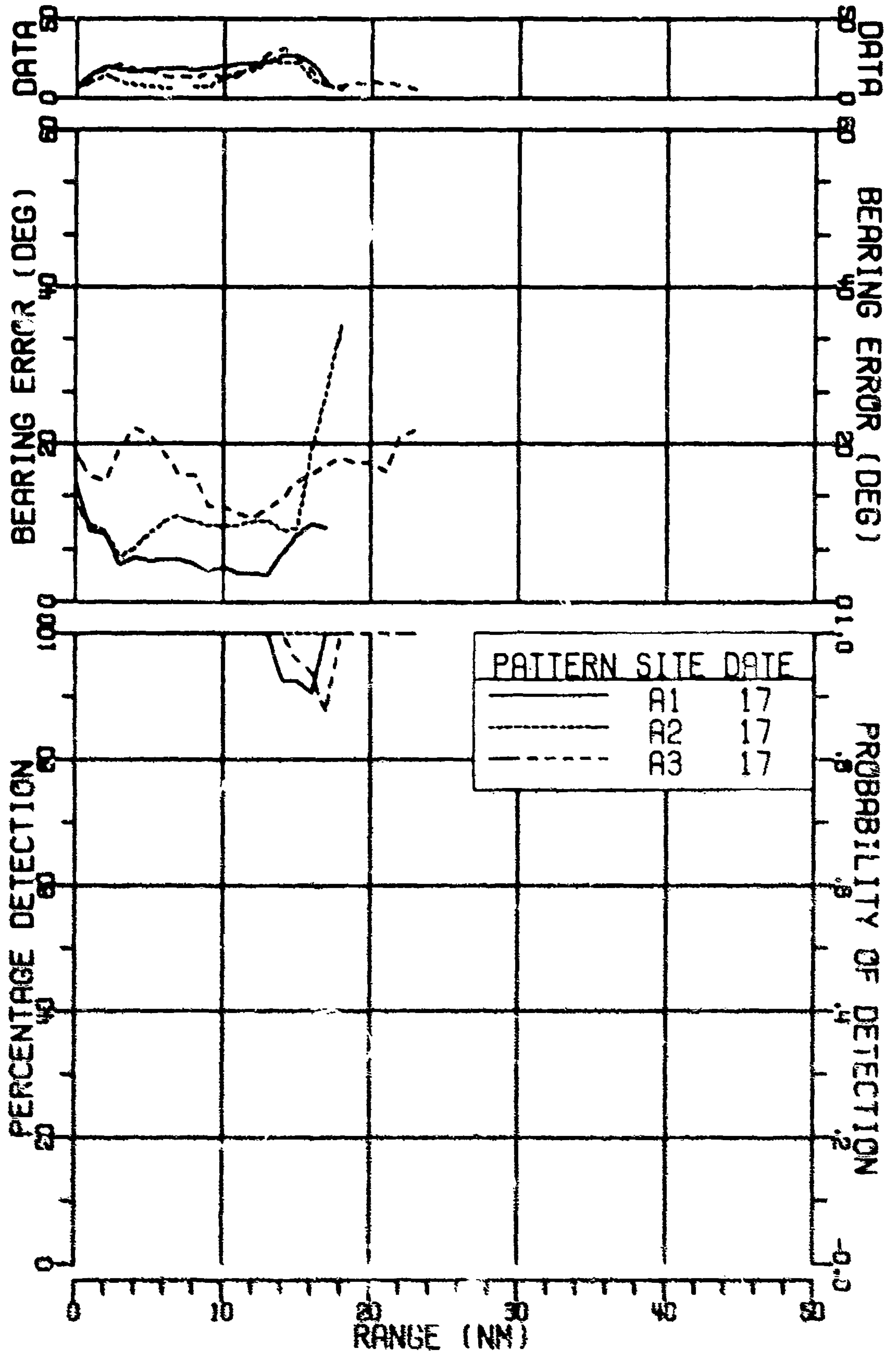

FIGURE III-215
NSS-FVT NEAR BOTTOM MAX GAIN LIMACONS SENSOR
DETECTION RESULTS FOR 64HZ AT 162DB (U)

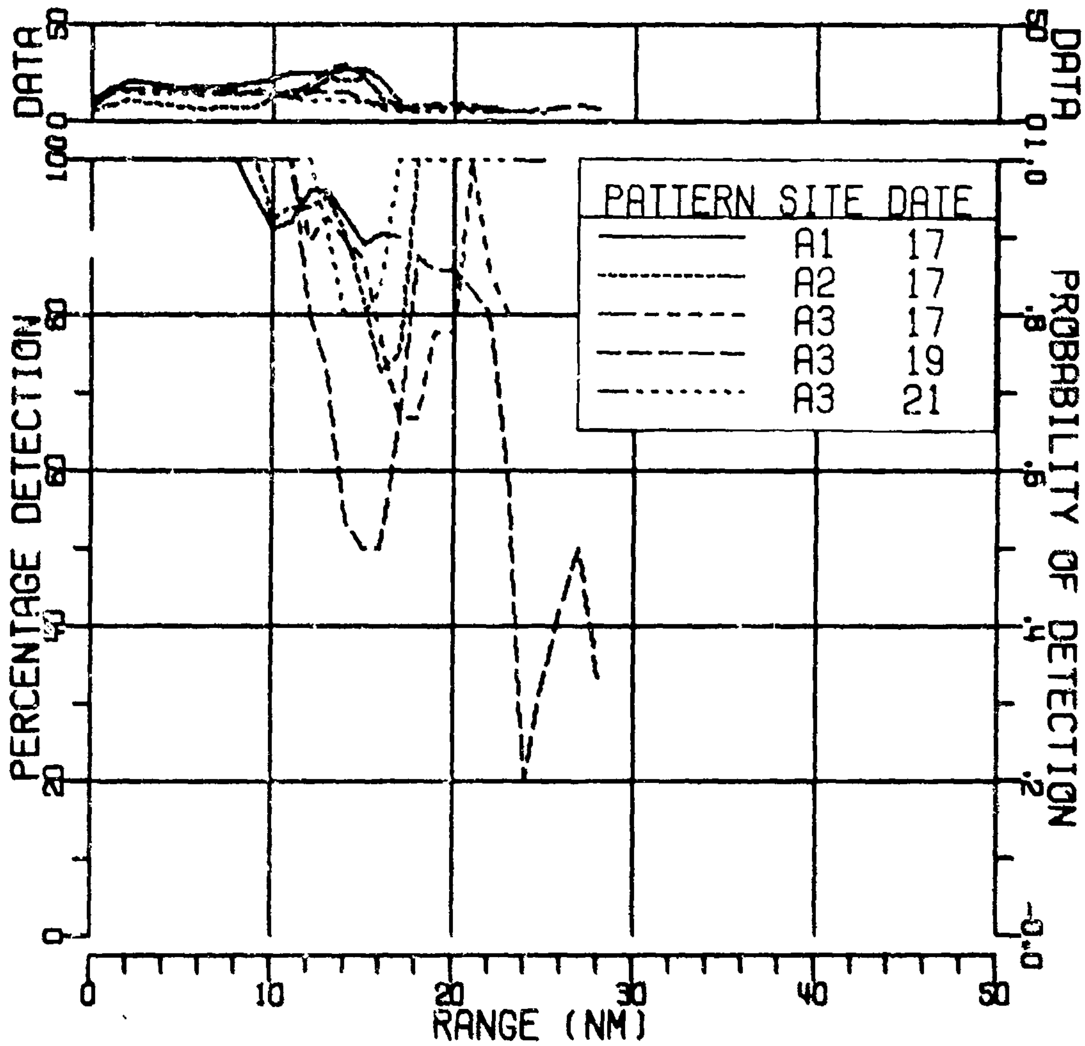

FIGURE III-216
MSS-FVT NEAR BOTTOM VERTICAL DIPOLE SENSOR
DETECTION RESULTS FOR 64HZ AT 162DB (U)

AS-77-?8

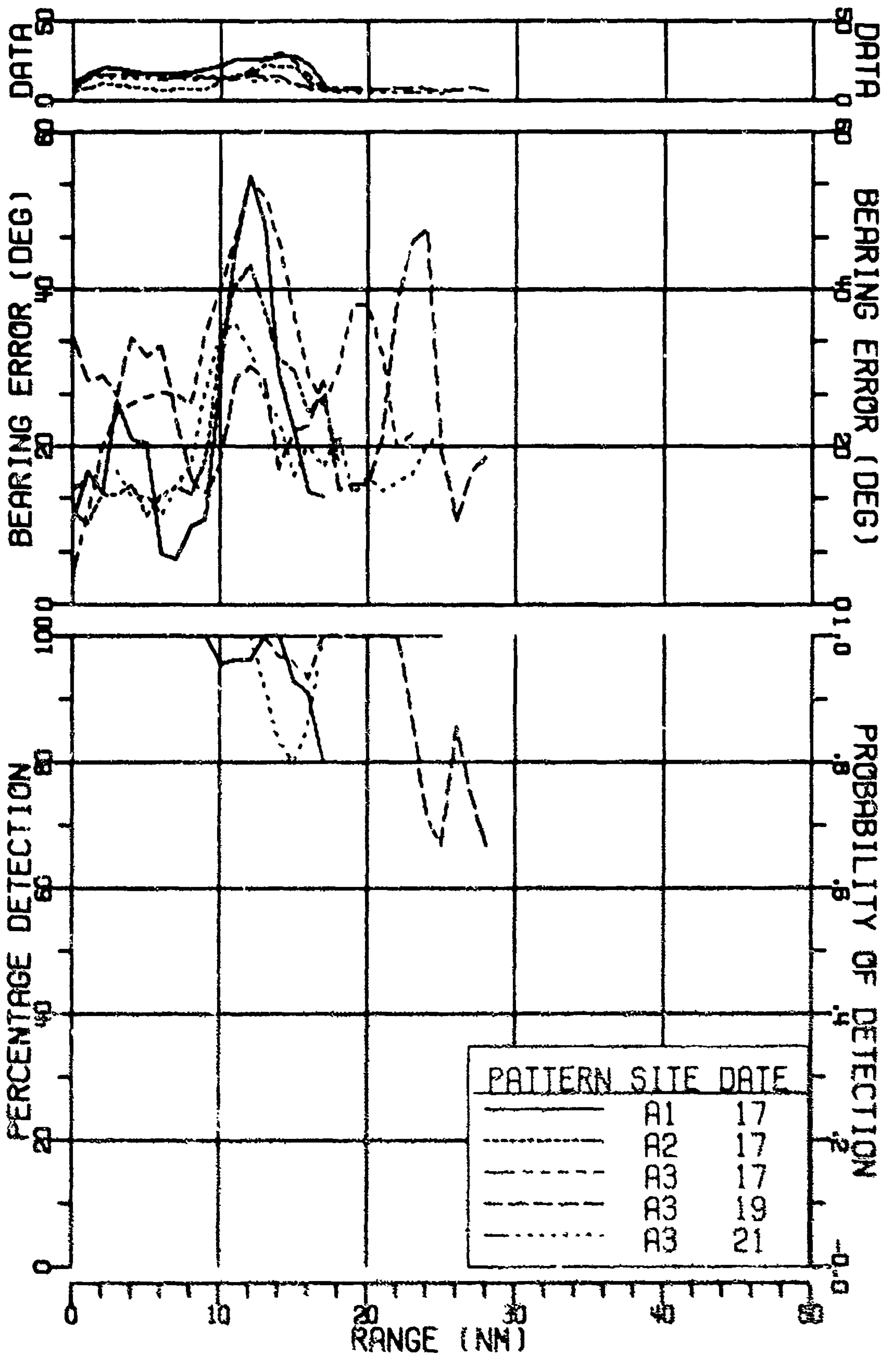

FIGURE III-217
MSS-FV1 NEAR BOTTOM DIFFERENCED CARDIOIDS SENSOR DETECTION RESULTS FOR 64HZ AT 162DB (U)

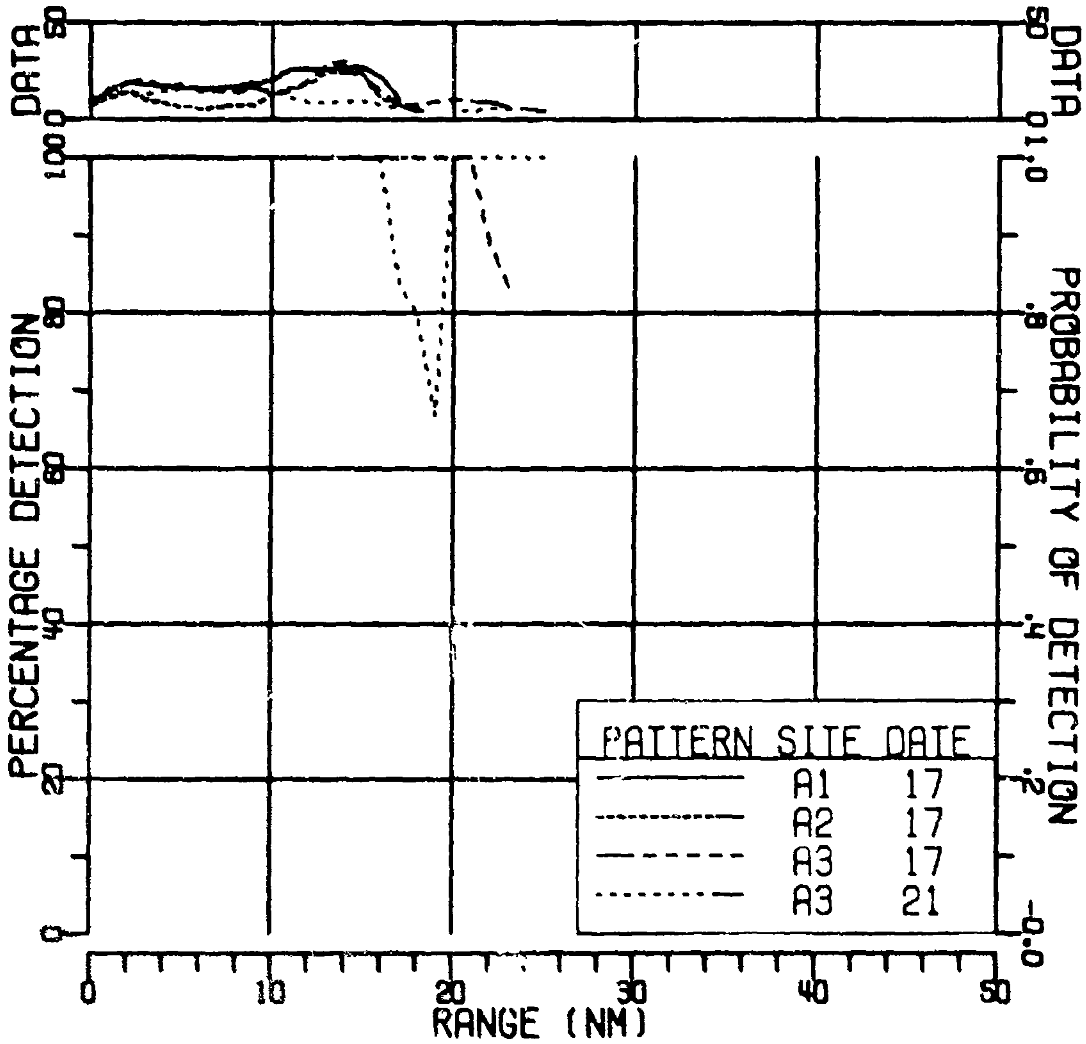

FIGURE III-218
MSS-FVT NEAR BOTTOM OMNIDIRECTIONAL SENSOR
DETECTION RESULTS FOR 160HZ AT 161DB (U)

AS-77-2818

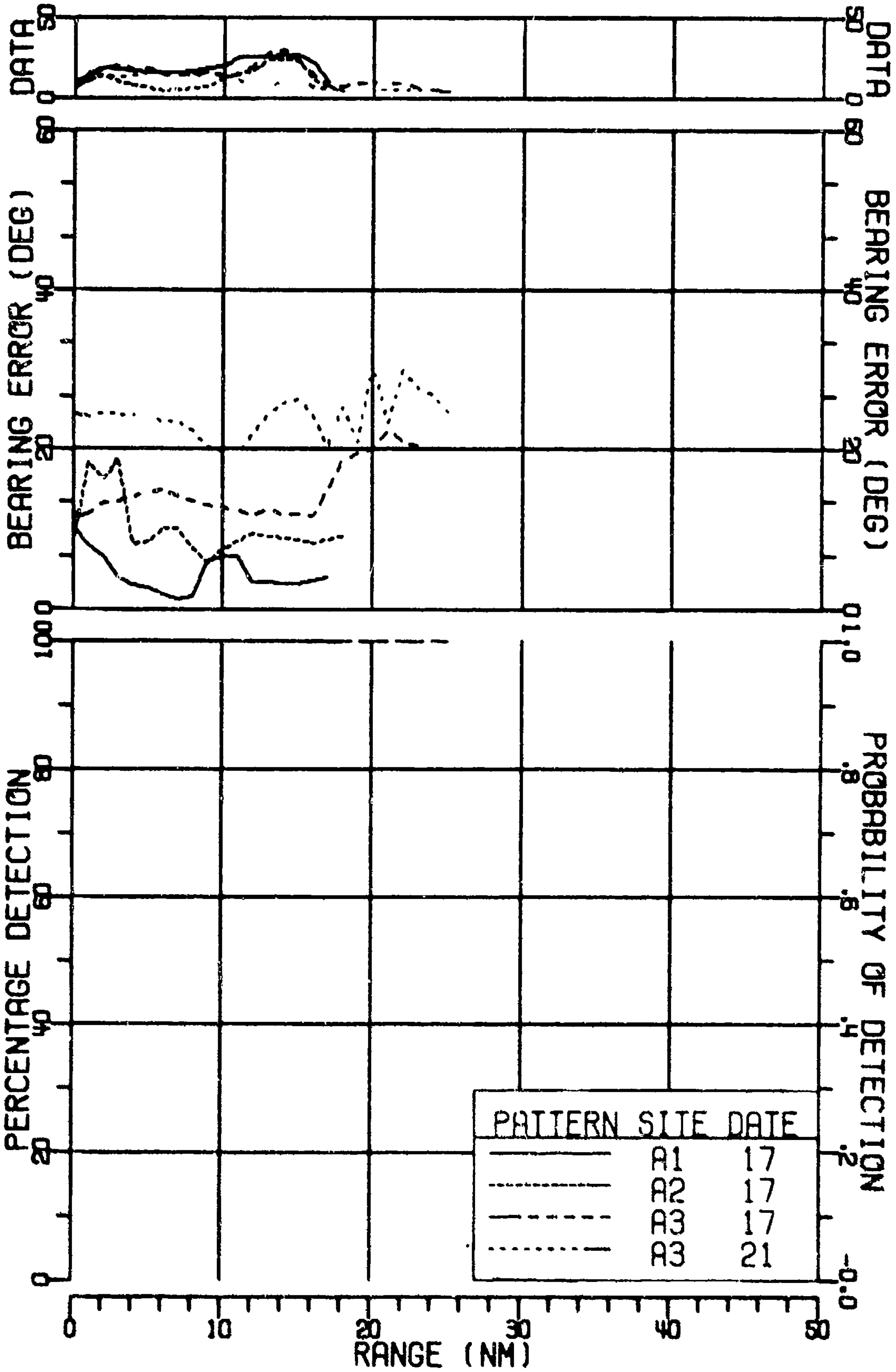

FIGURE III-219
MSS-FVT NEAR BOTTOM SINGLE CARDIOIDS SENSOR
DETECTION RESULTS FOR 160HZ AT 161DB (U)

AS-77-2819

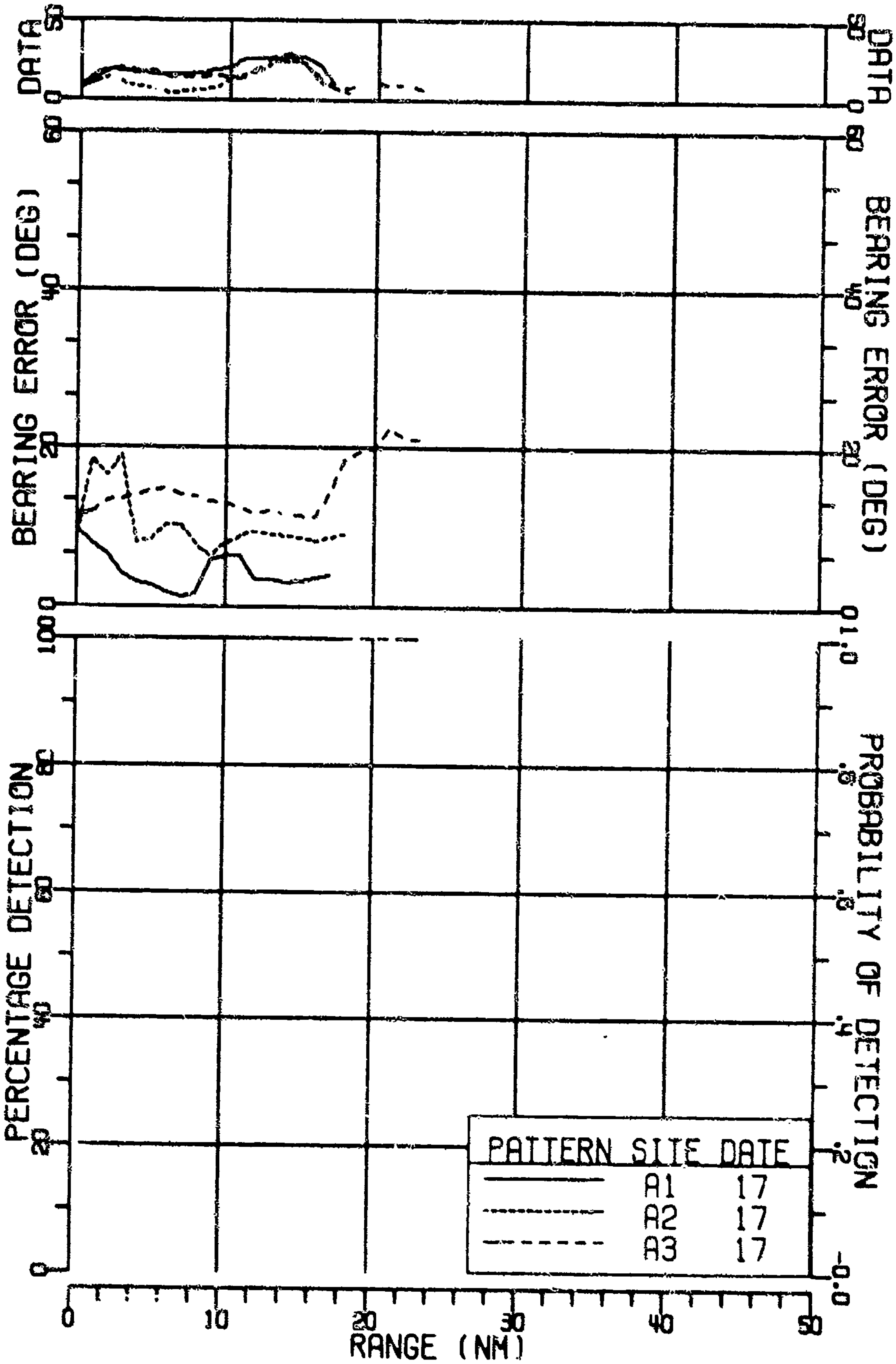

FIGURE III-220
MSS-FVT NEAR BOTTOM MAX GAIN LIMACONS SENSOR
DETECTION RESULTS FOR 160HZ AT 161DB (U)

AS-77-2820

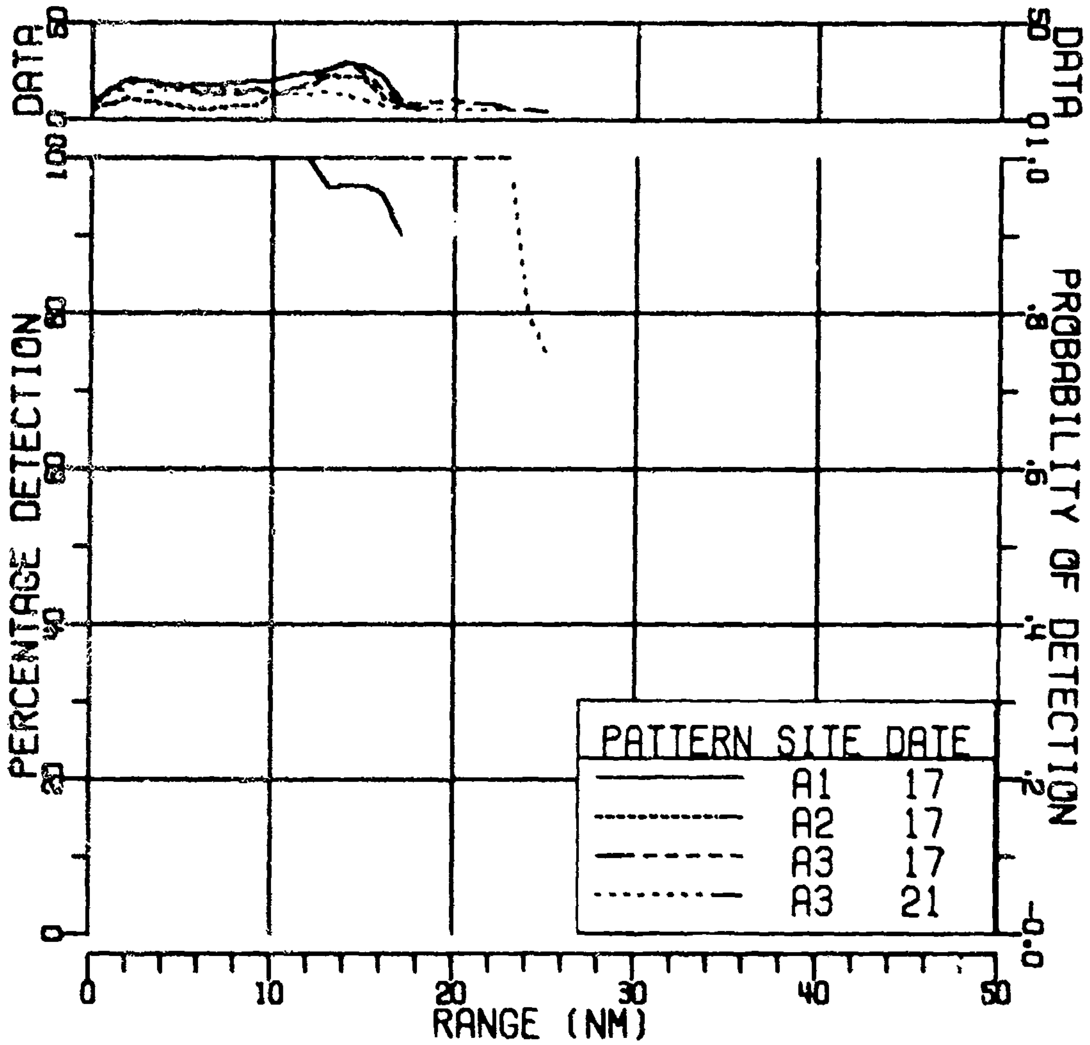

FIGURE III-221
MSS-FVT NEAR BOTTOM VERTICAL DIPOLE SENSOR
DETECTION RESULTS FOR 160HZ AT 161DB (U)

AS-77-2821

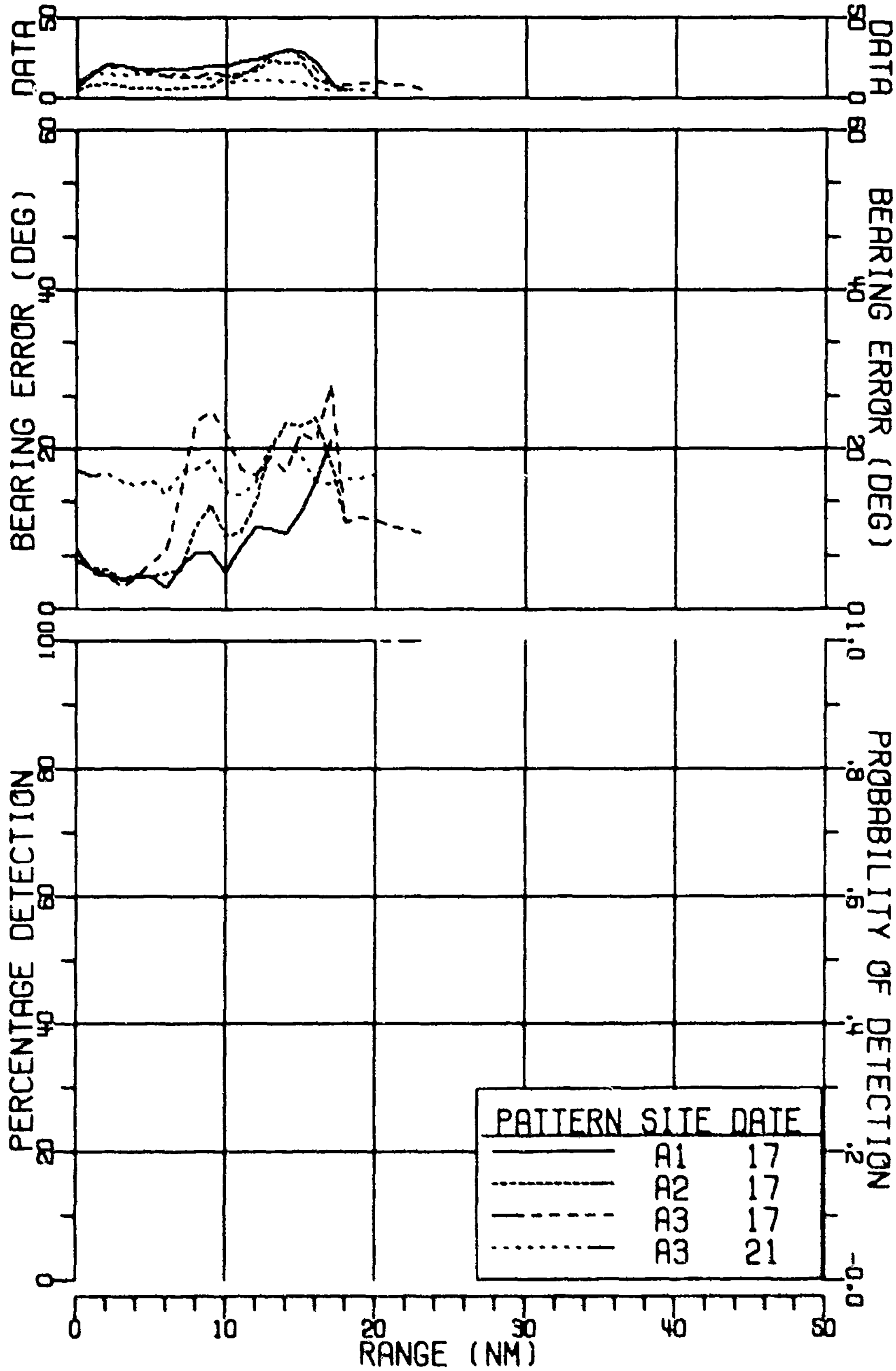

FIGURE III-222
MSS-FVT NEAR BOTTOM DIFFERENCED CARDIOIDS SENSOR DETECTION RESULTS FOR 160HZ AT 161DB (U)

AS-77-2

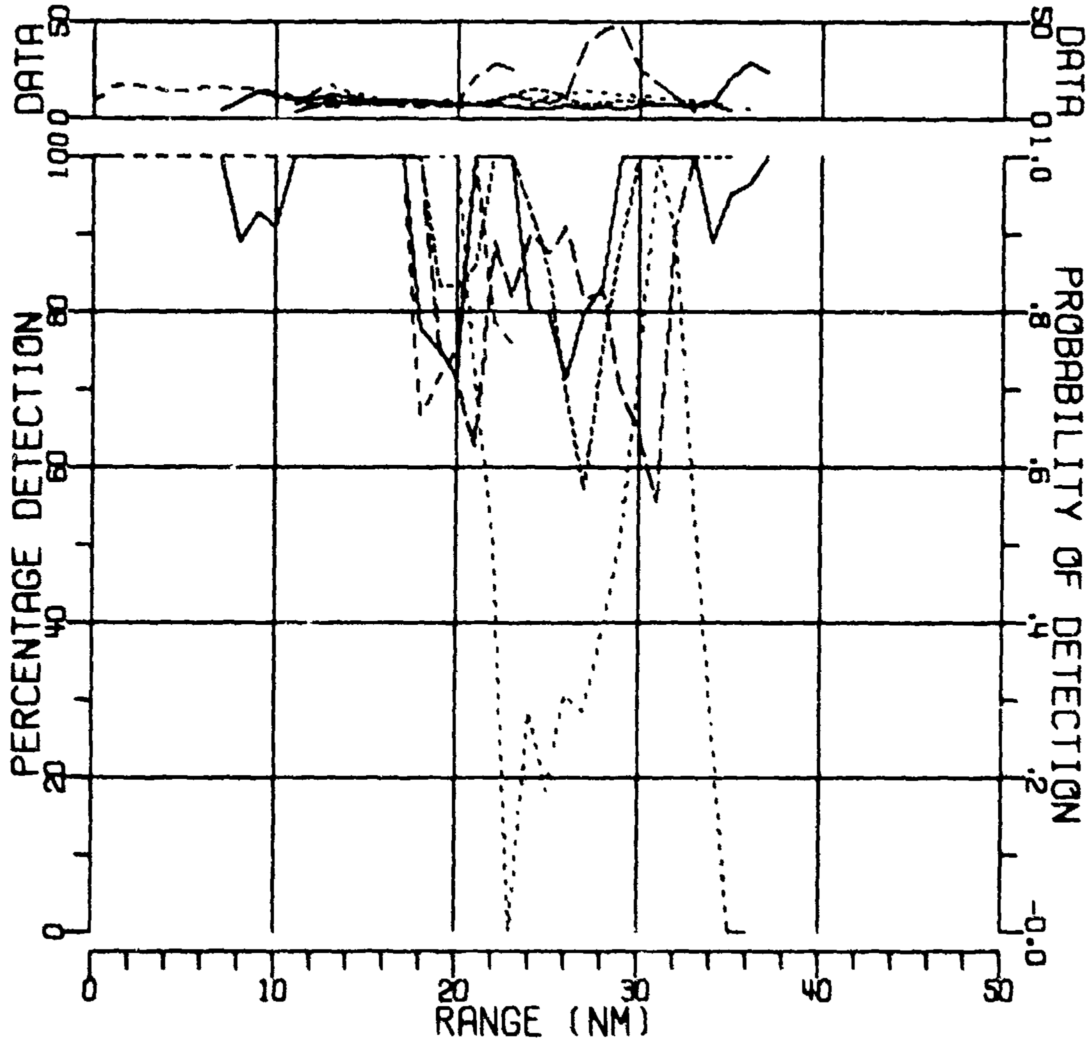

FIGURE III-223
MSS-FVT NEAR BOTTOM OMNIDIRECTIONAL SENSOR
DETECTION RESULTS FOR 70HZ AT 166DB (U)

PATTERN	SITE	DATE
	A1	17
	A2	17
	A3	17
	A3	19
	A3	21

AS-77-2823

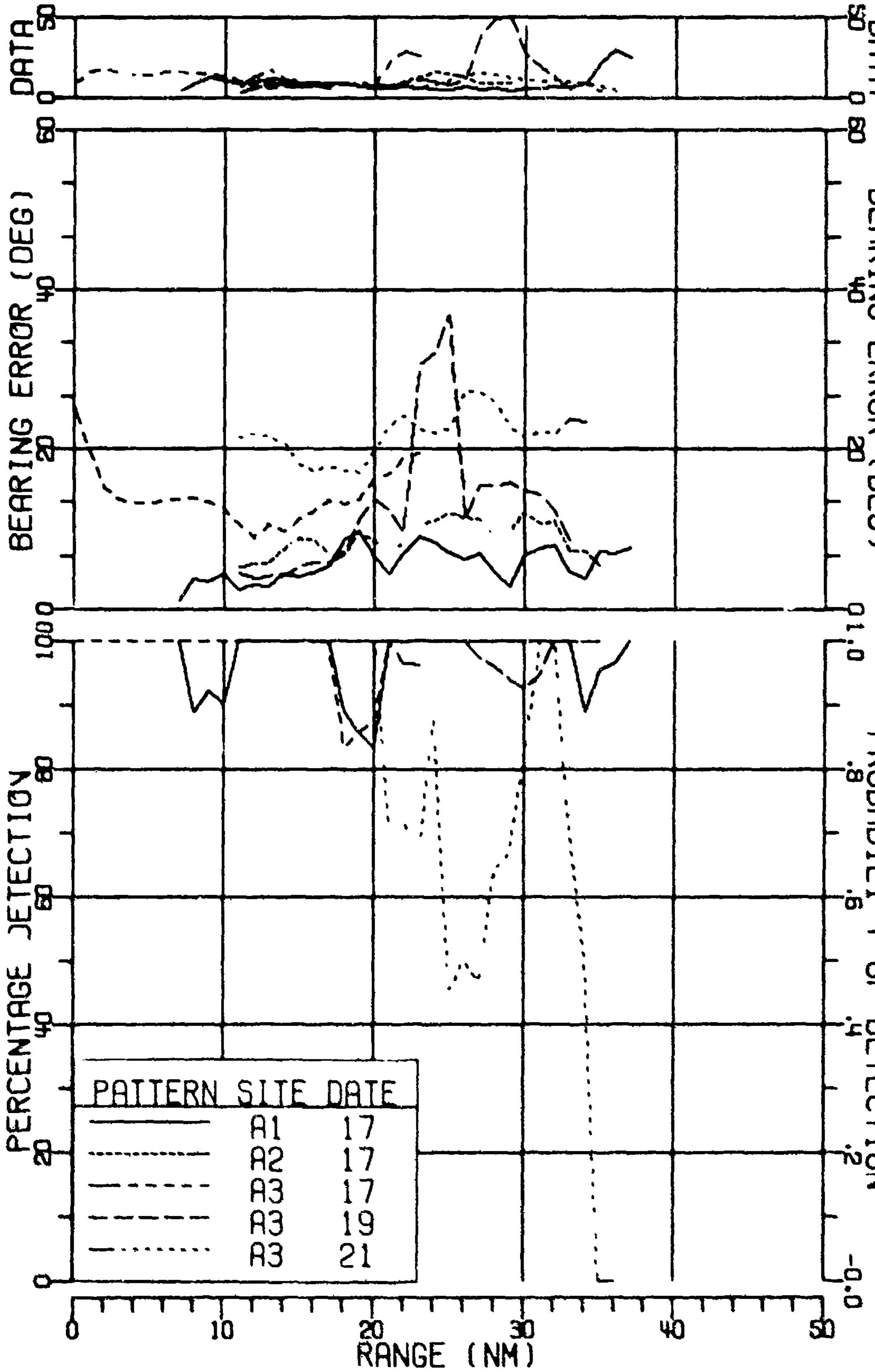

FIGURE III-224
MSS-FVT NEAR BOTTOM SINGLE CARDIOIDS SENSOR
DETECTION RESULTS FOR 70HZ AT 166DB (U)

AS-77-28

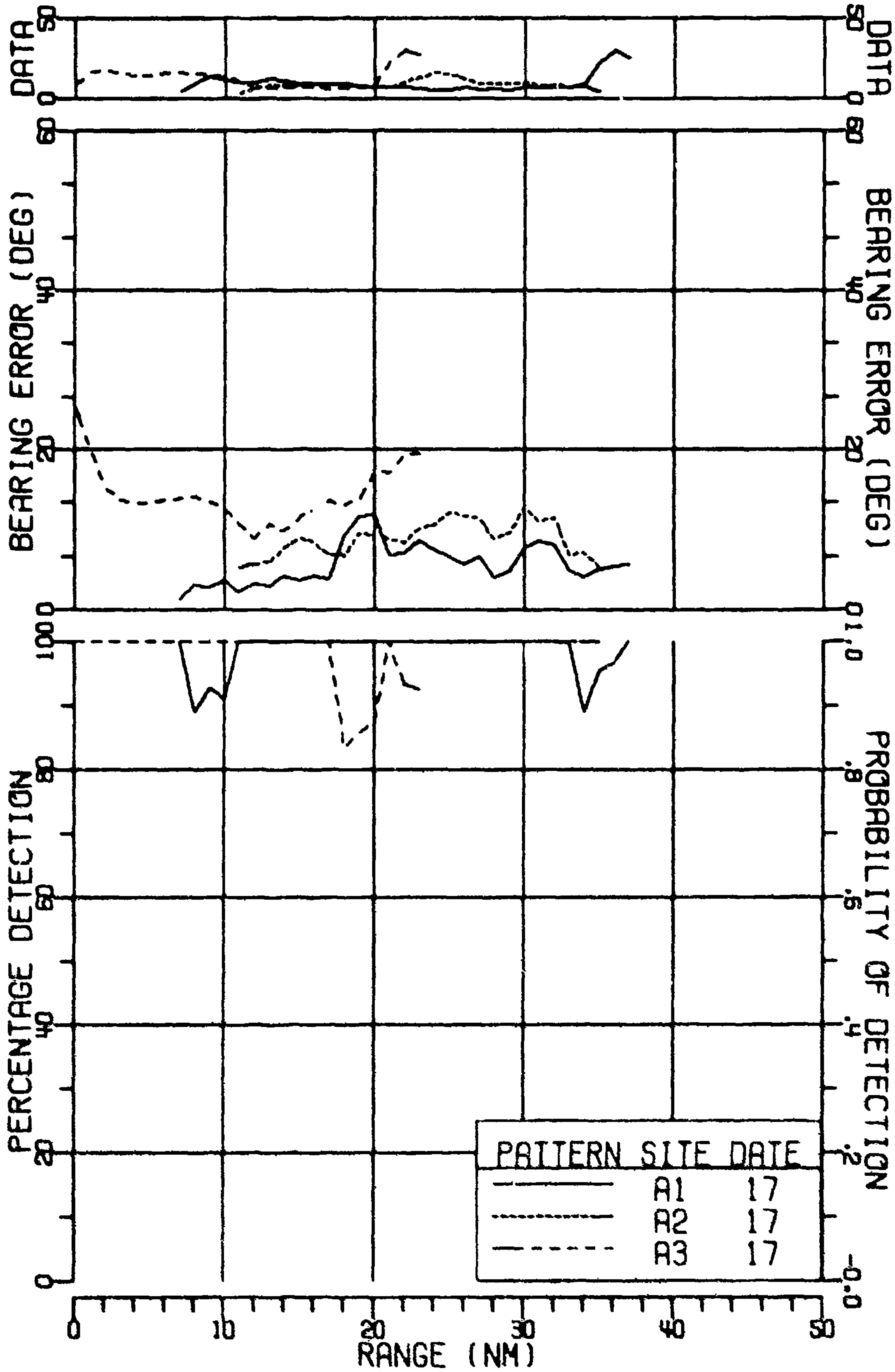

FIGURE III-225
MSS-FVT NEAR BOTTOM MAX GAIN LIMACONS SENSOR
DETECTION RESULTS FOR 70HZ AT 166DB (U)

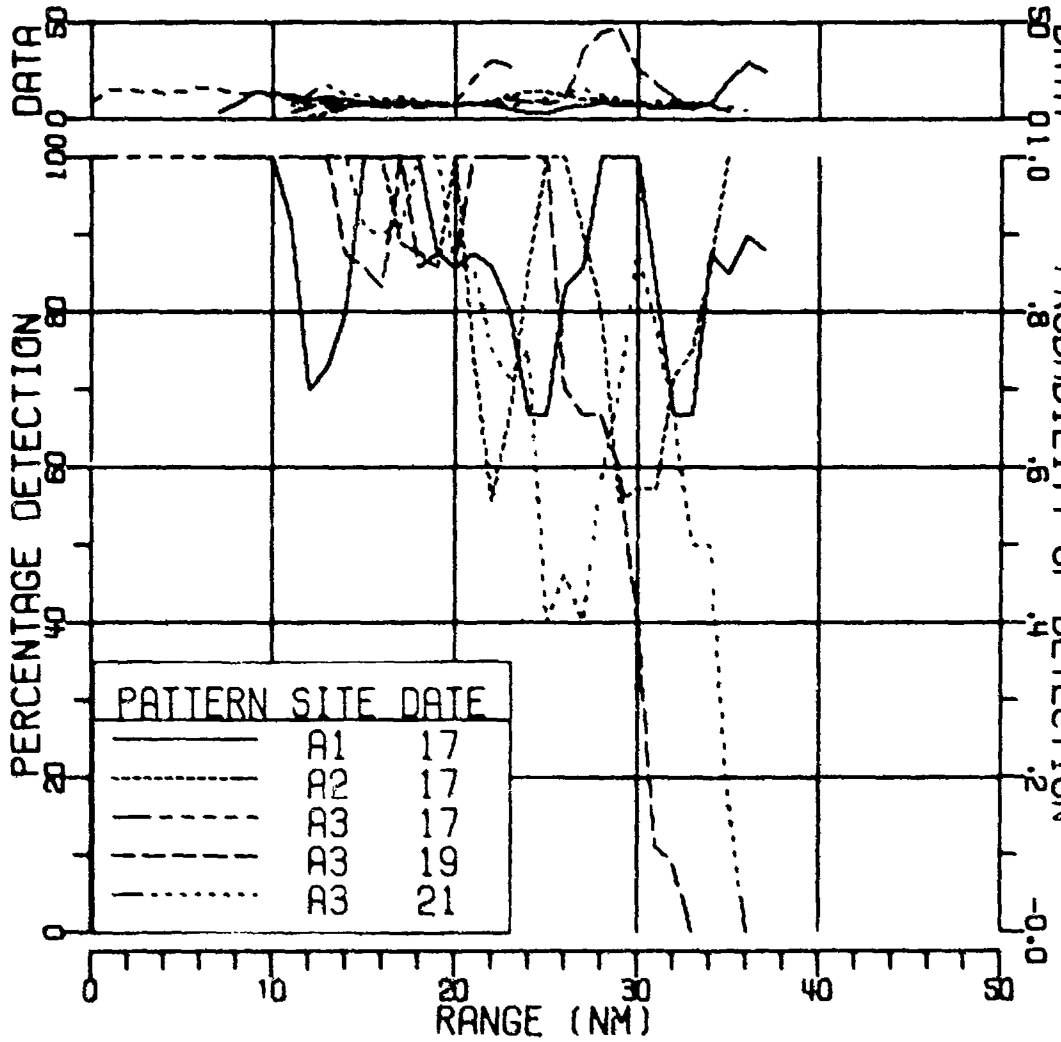

FIGURE III-226
MSS-FVT NEAR BOTTOM VERTICAL DIPOLE SENSOR
DETECTION RESULTS FOR 70HZ AT 166DB (U)

AS-77-2826

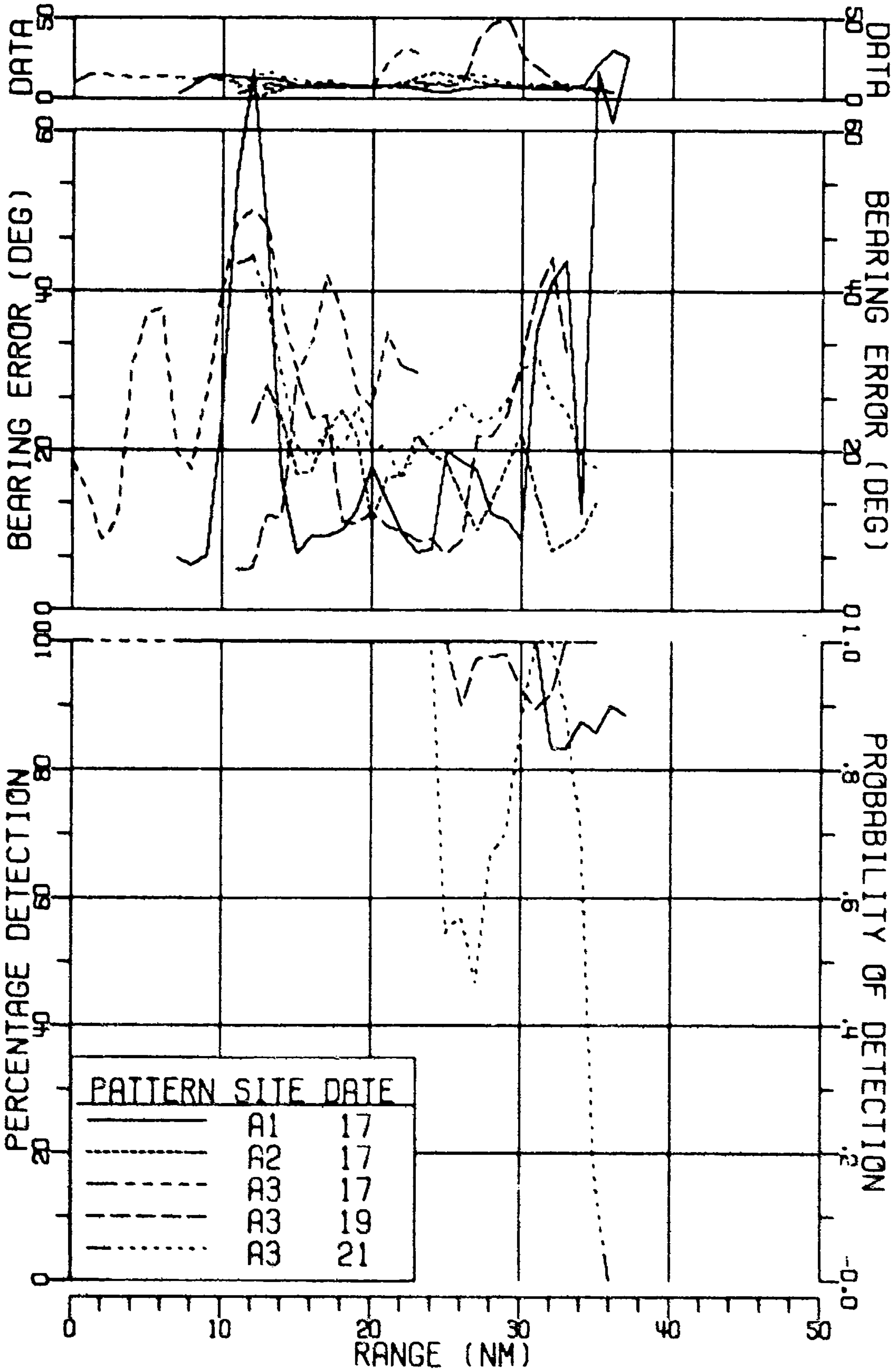

FIGURE III-227
MSS-FVT NEAR BOTTOM DIFFERENCED CARDIOIDS SENSOR
DETECTION RESULTS FOR 70HZ AT 166DB (U)

AS-77-2827

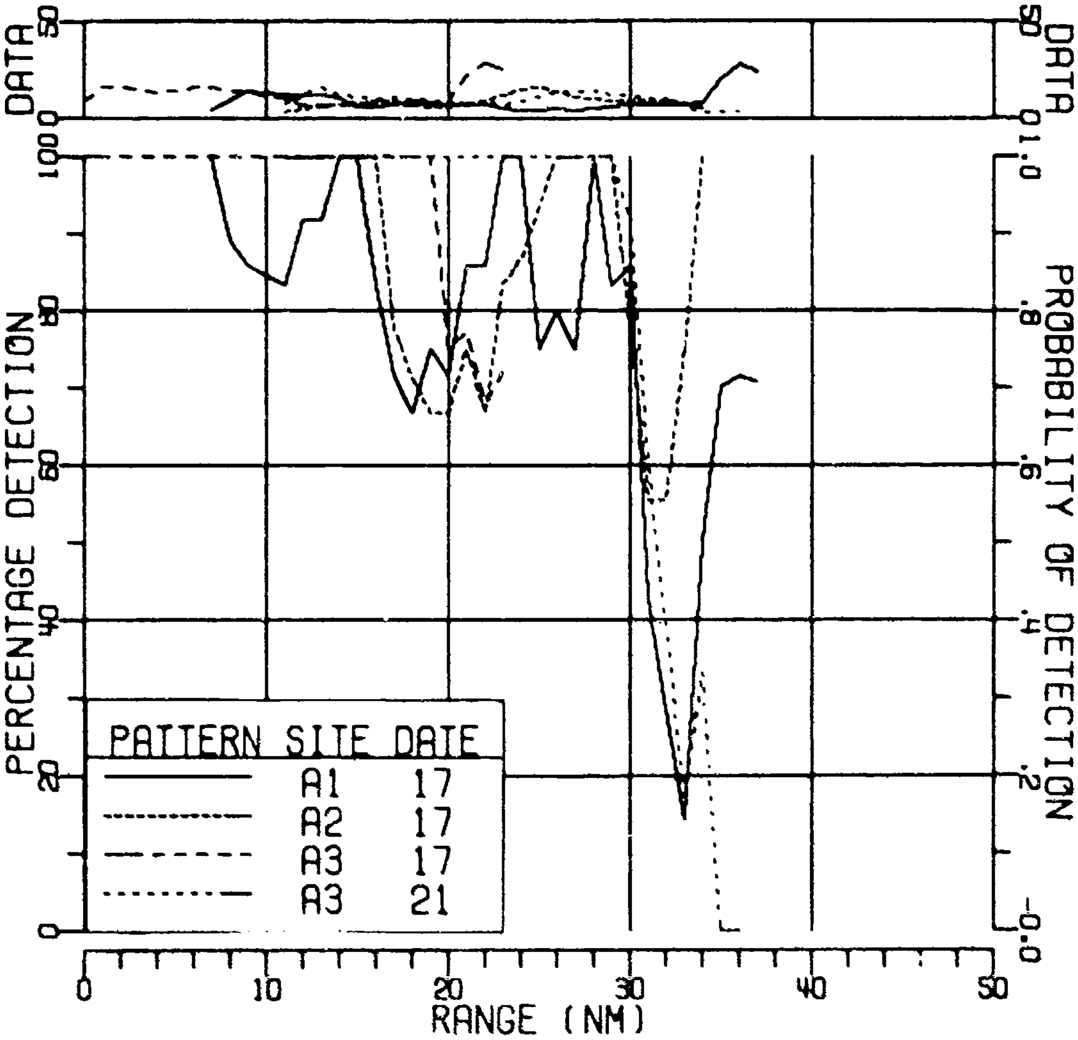

FIGURE III-228
MSS-FVT NEAR BOTTOM OMNIDIRECTIONAL SENSOR
DETECTION RESULTS FOR 170HZ AT 156DB (U)

AS-77-2828

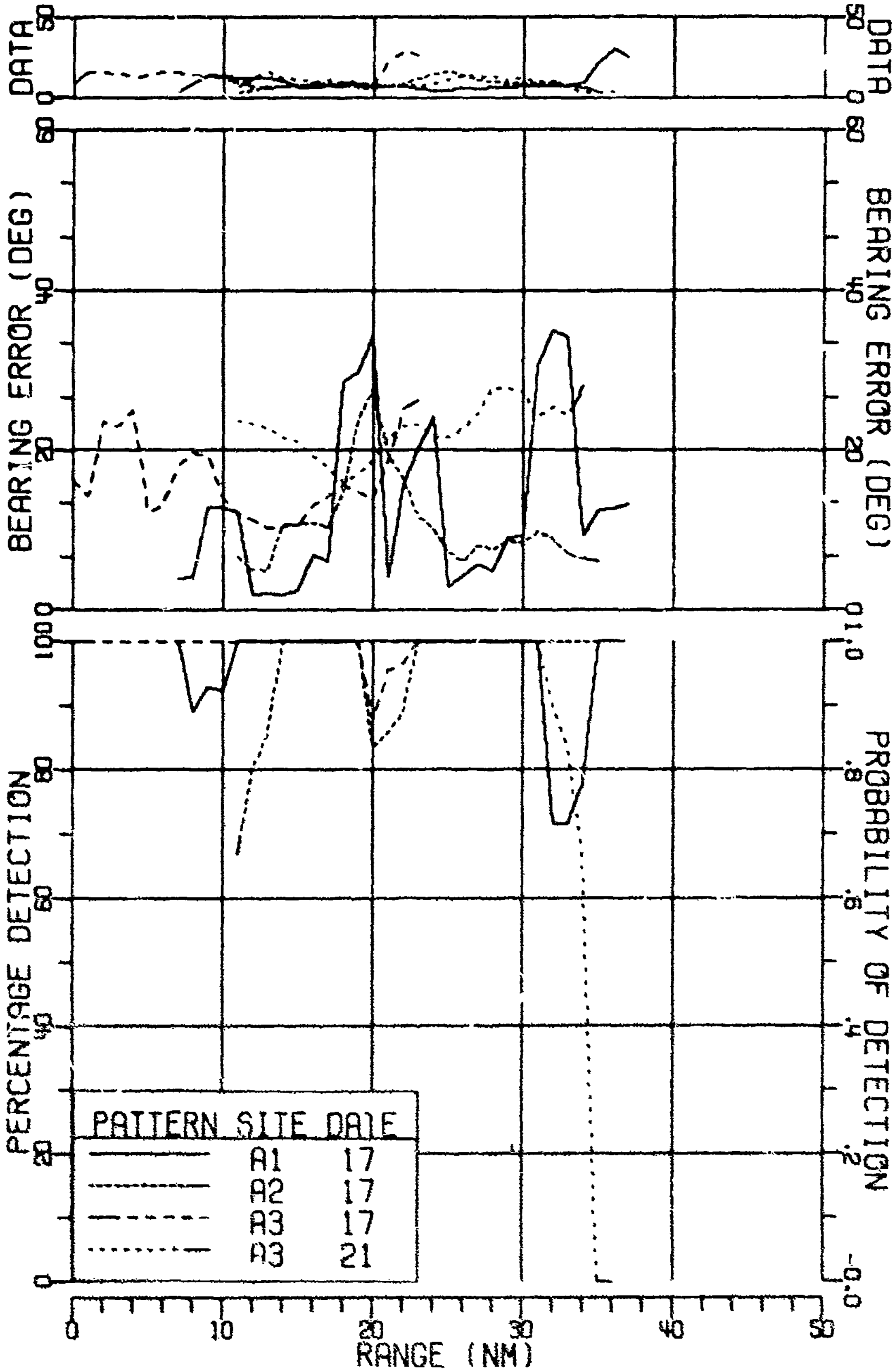

FIGURE III-229
MSS-FVT NEAR BOTTOM SINGLE CARDIOIDS SENSOR DETECTION RESULTS FOR 170HZ AT 156DB (U)

AS-77-2629

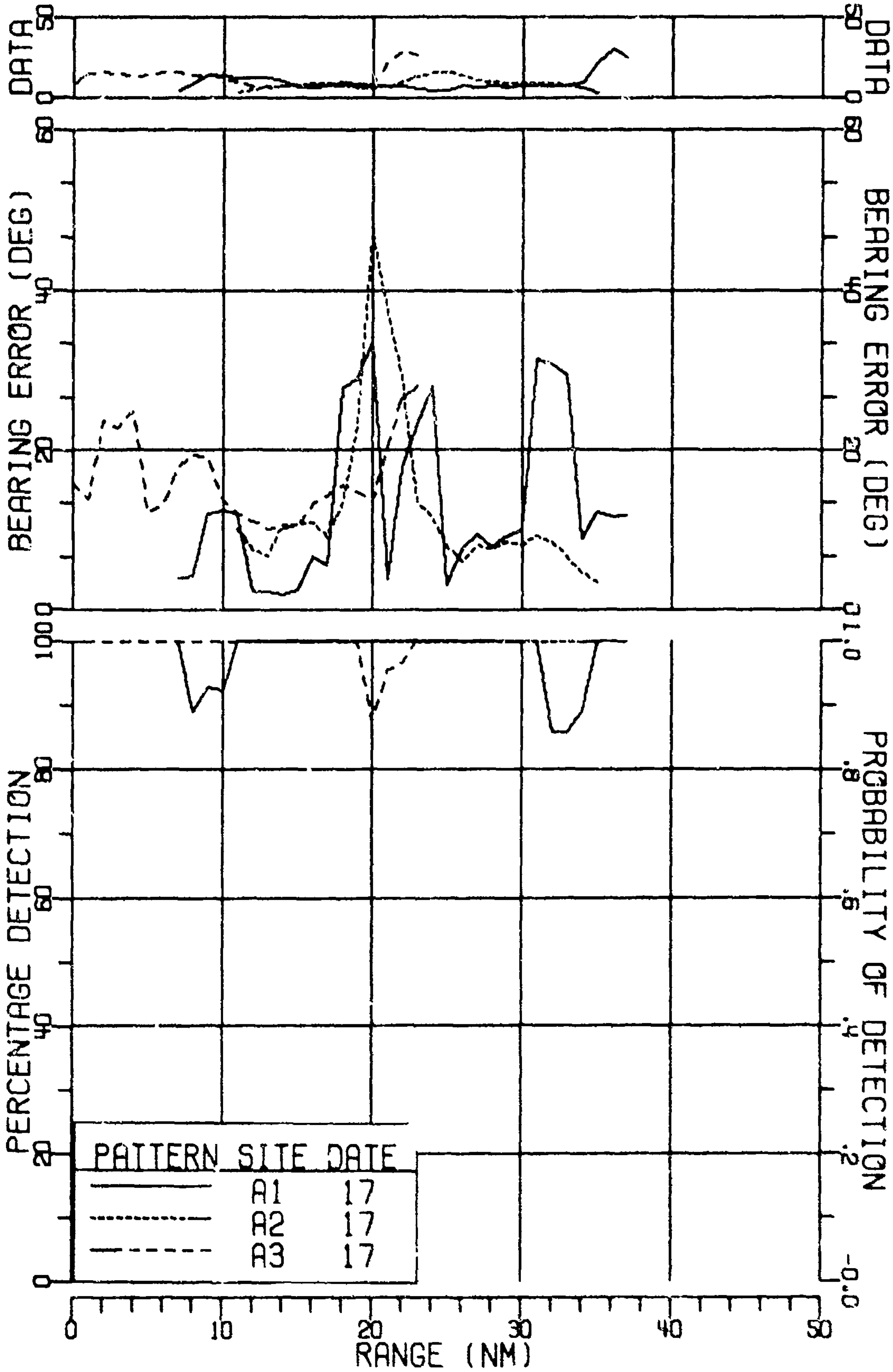

FIGURE III-230
MSS-FVT NEAR BOTTOM MAX GAIN LIMACONS SENSOR
DETECTION RESULTS FOR 170HZ A1 156DB (U)

AS-77-283

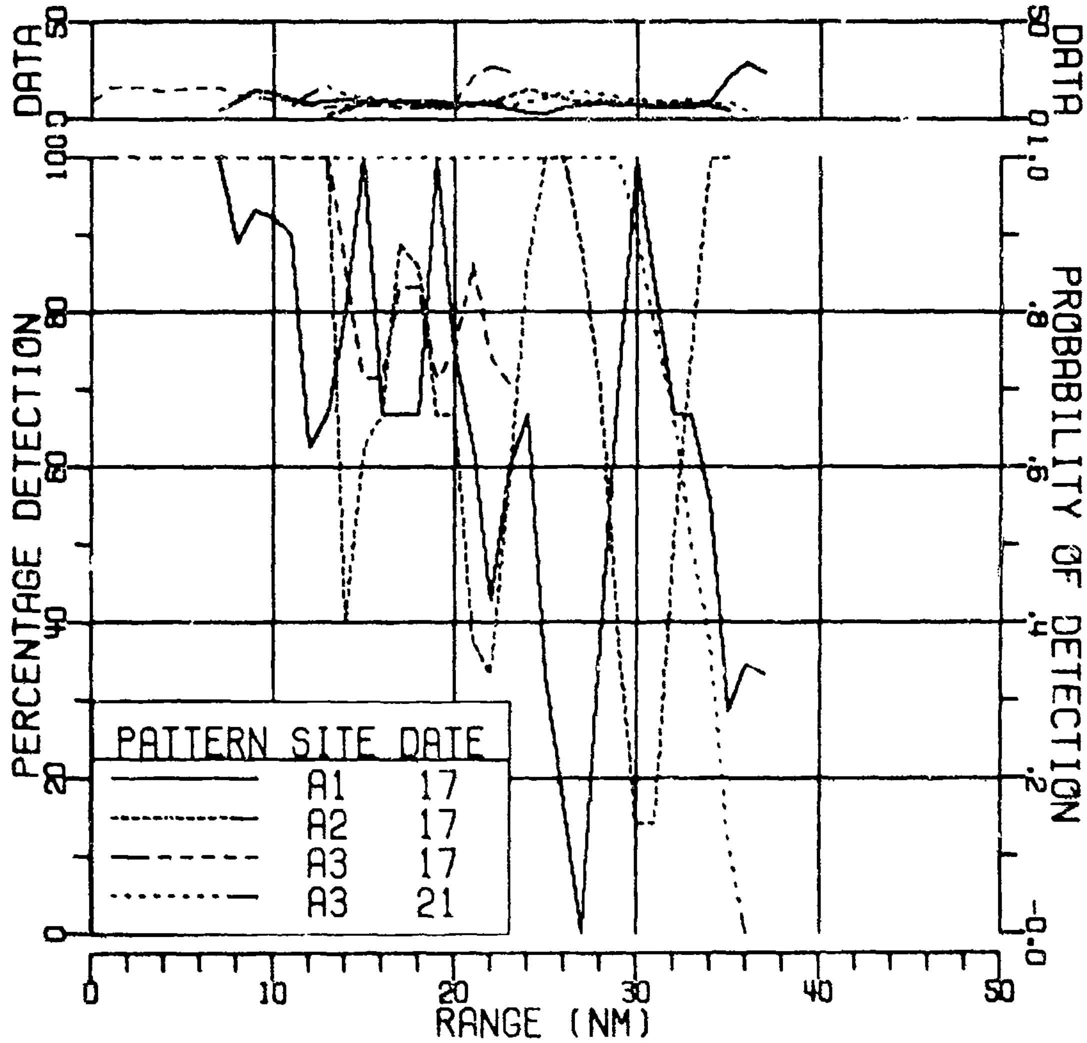

FIGURE III-231
MSS-FVT NEAR BOTTOM VERTICAL DIPOLE SENSOR
DETECTION RESULTS FOR 170HZ AT 156DB (U)

AS-77-2831

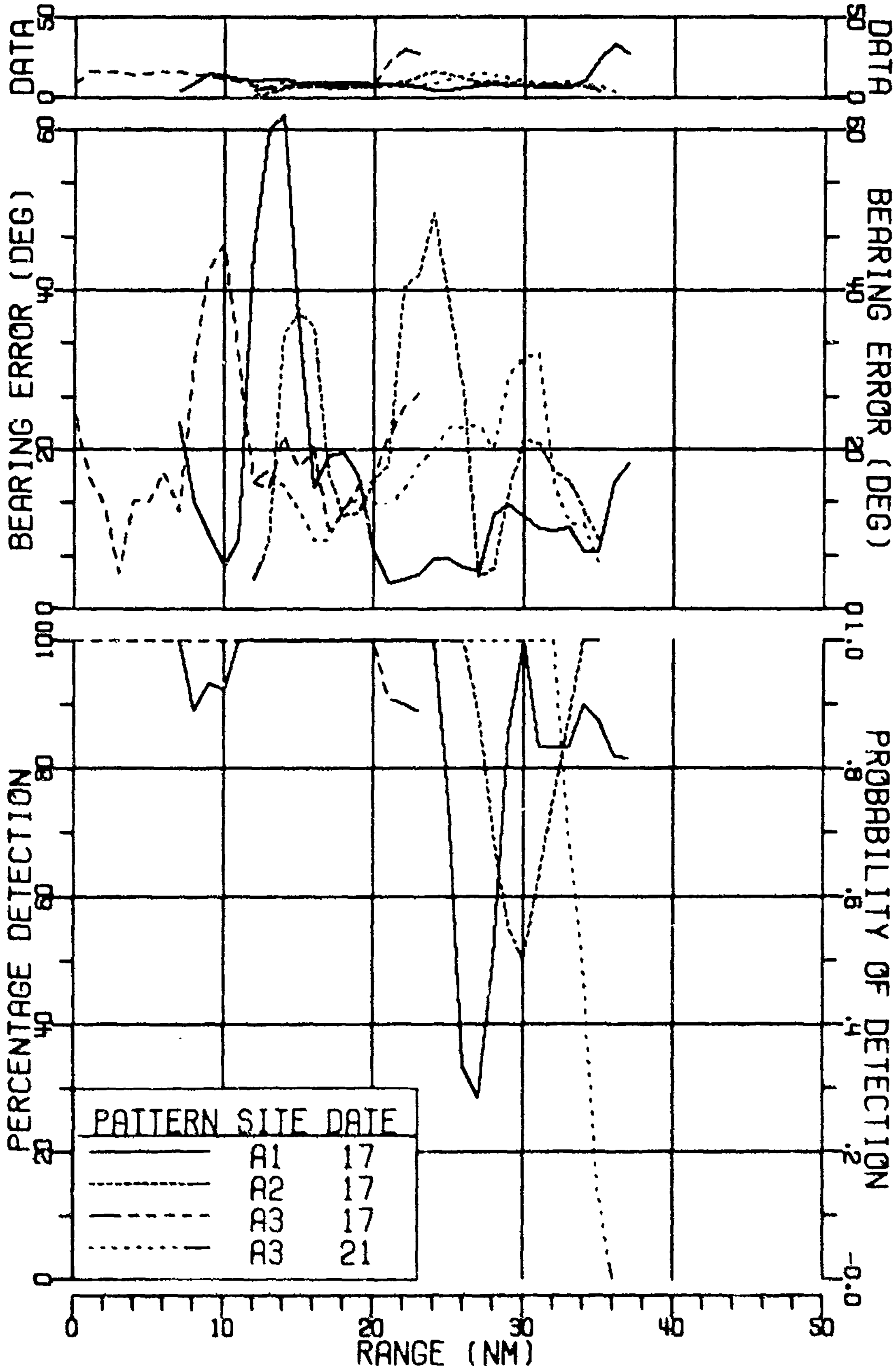

FIGURE III-232
MSS-FVT NEAR BOTTOM DIFFERENCED CARDIOIDS SENSOR
DETECTION RESULTS FOR 170HZ AT 156DB (U)

AS-77-2

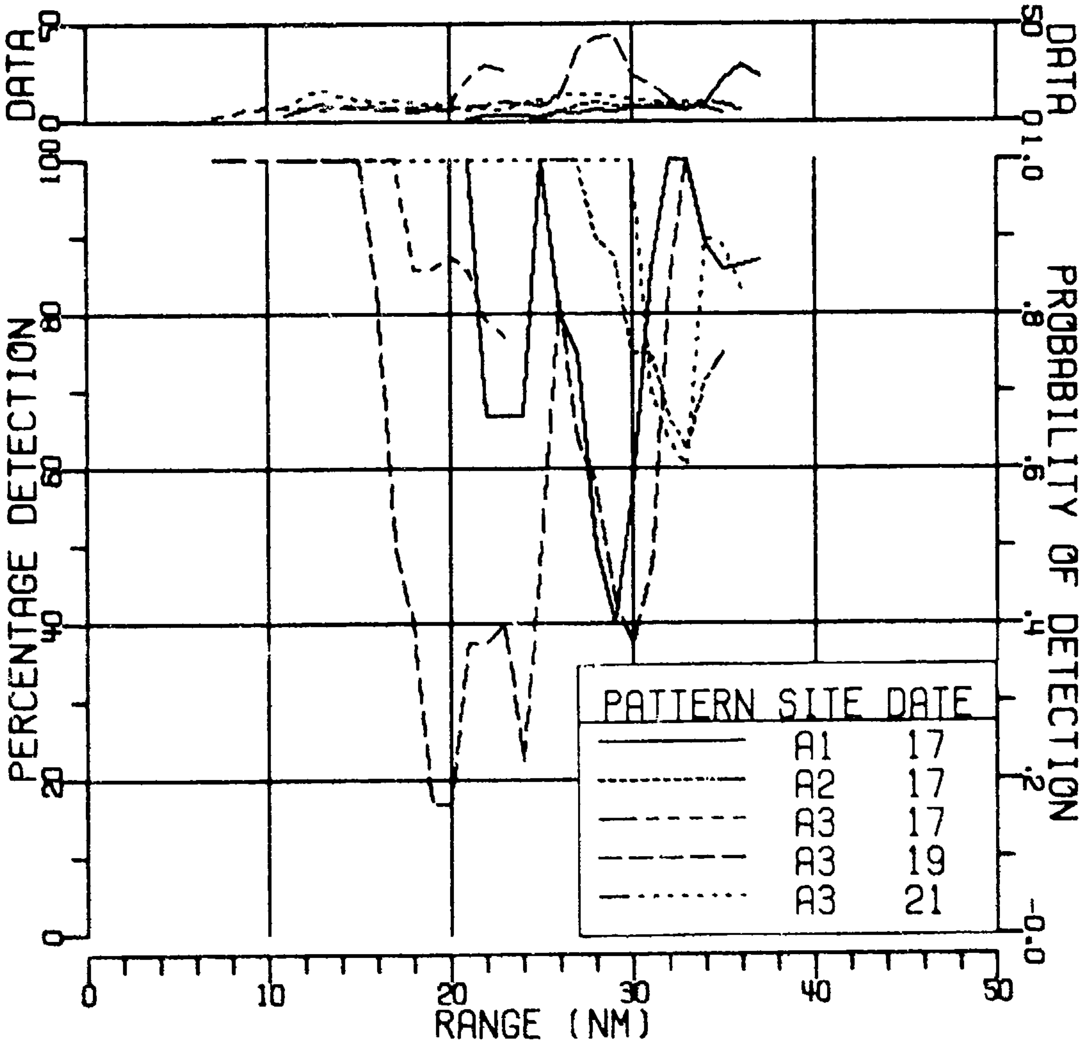

FIGURE III-233
MSS-FVT NEAR BOTTOM OMNIDIRECTIONAL SENSOR
DETECTION RESULTS FOR 335HZ AT 154DB (U)

AS-77-2833

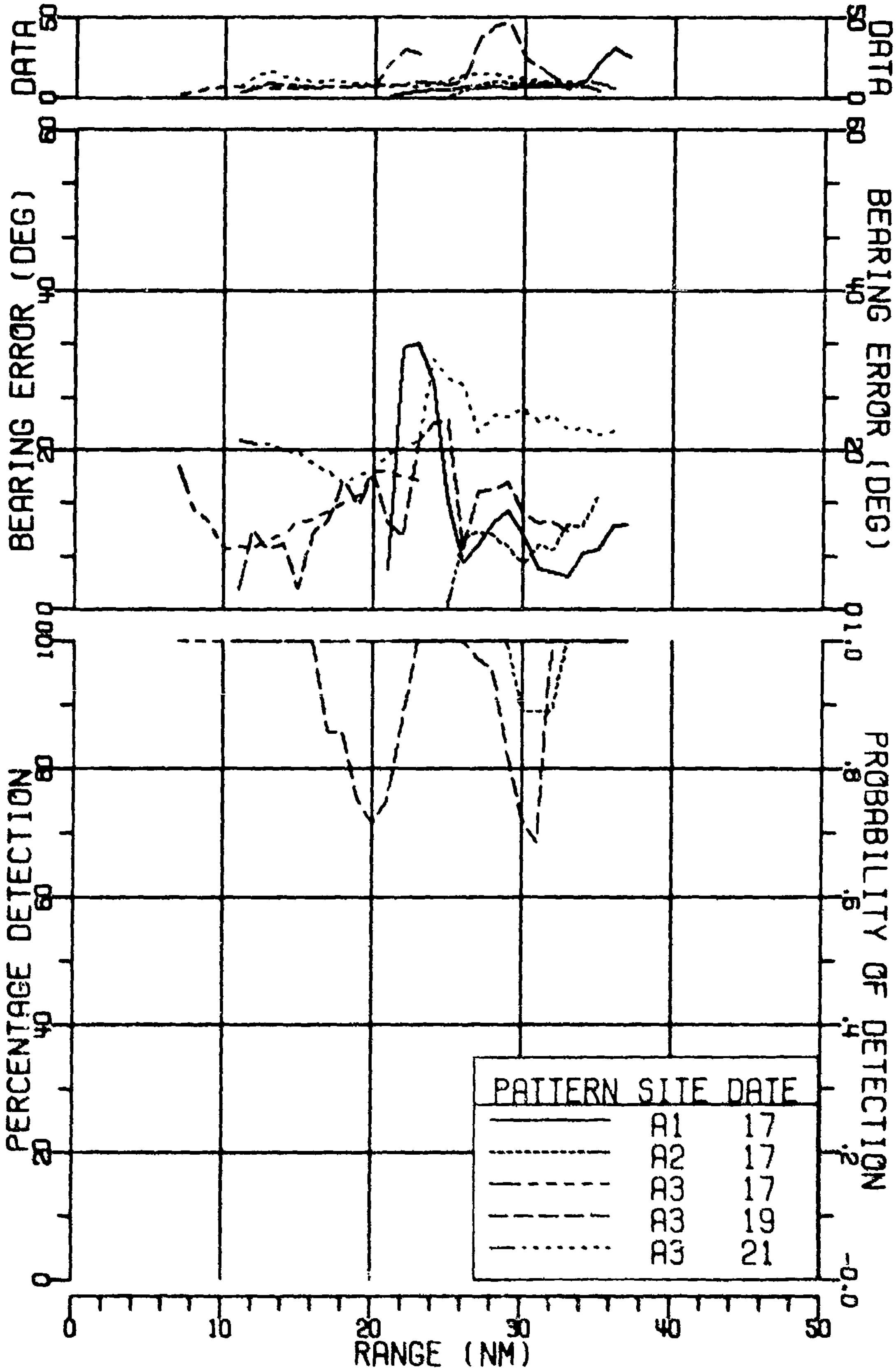

FIGURE III-234
MSS-FVT NEAR BOTTOM SINGLE CARDIOIDS SENSOR
DETECTION RESULTS FOR 335HZ AT 154DB (U)

AS-77-2834

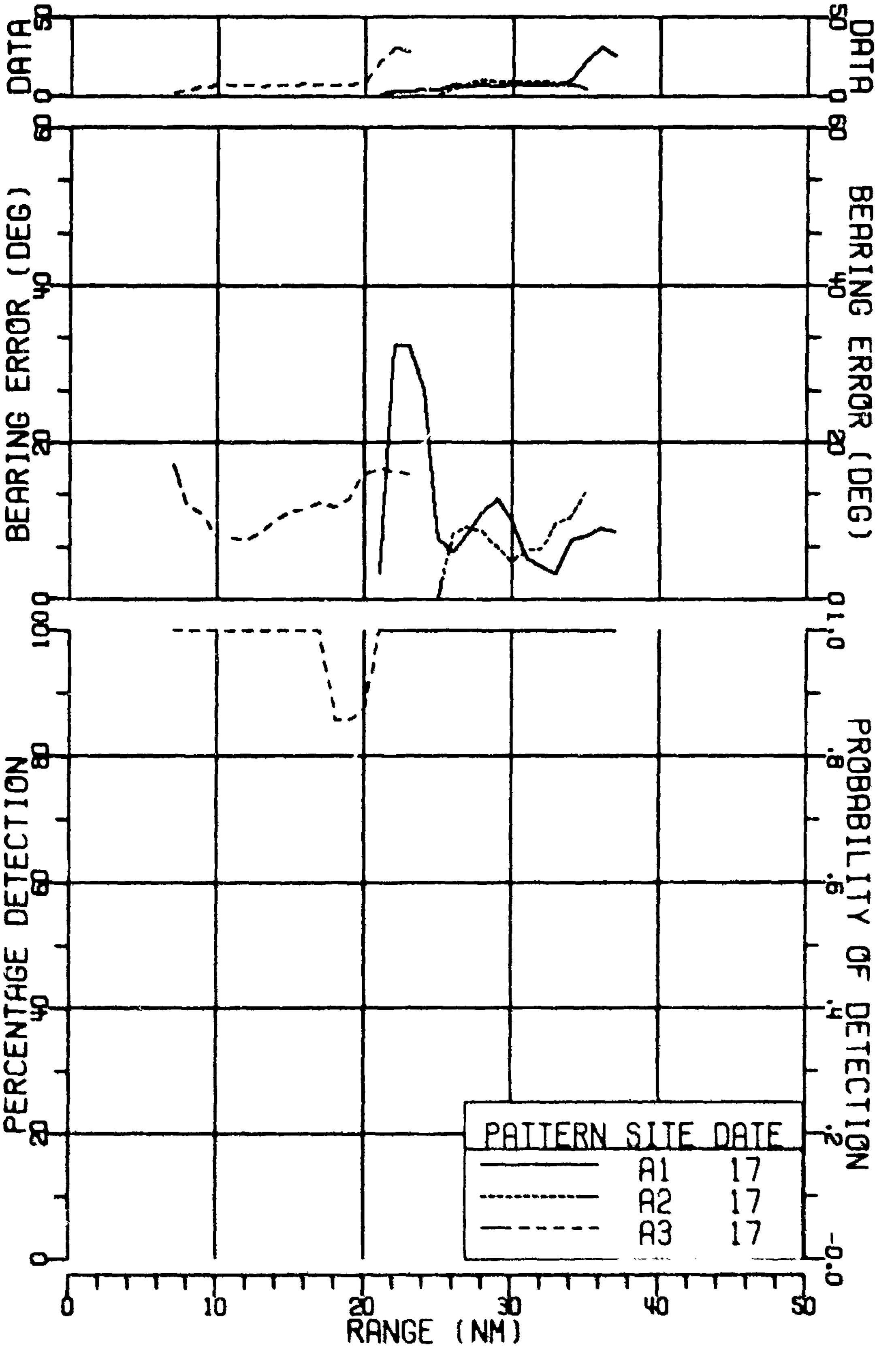

FIGURE III-235
MSS-FVT NEAR BOTTOM MAX GAIN LIMACONS SENSOR
DETECTION RESULTS FOR 335HZ AT 154DB (U)

AS-77-2835

APPENDIX F

BEARING ERROR versus SIGNAL-TO-NOISE RATIO CURVES (U)

(FIGURES III-236 - III-257)

(The reverse of this page is blank.)

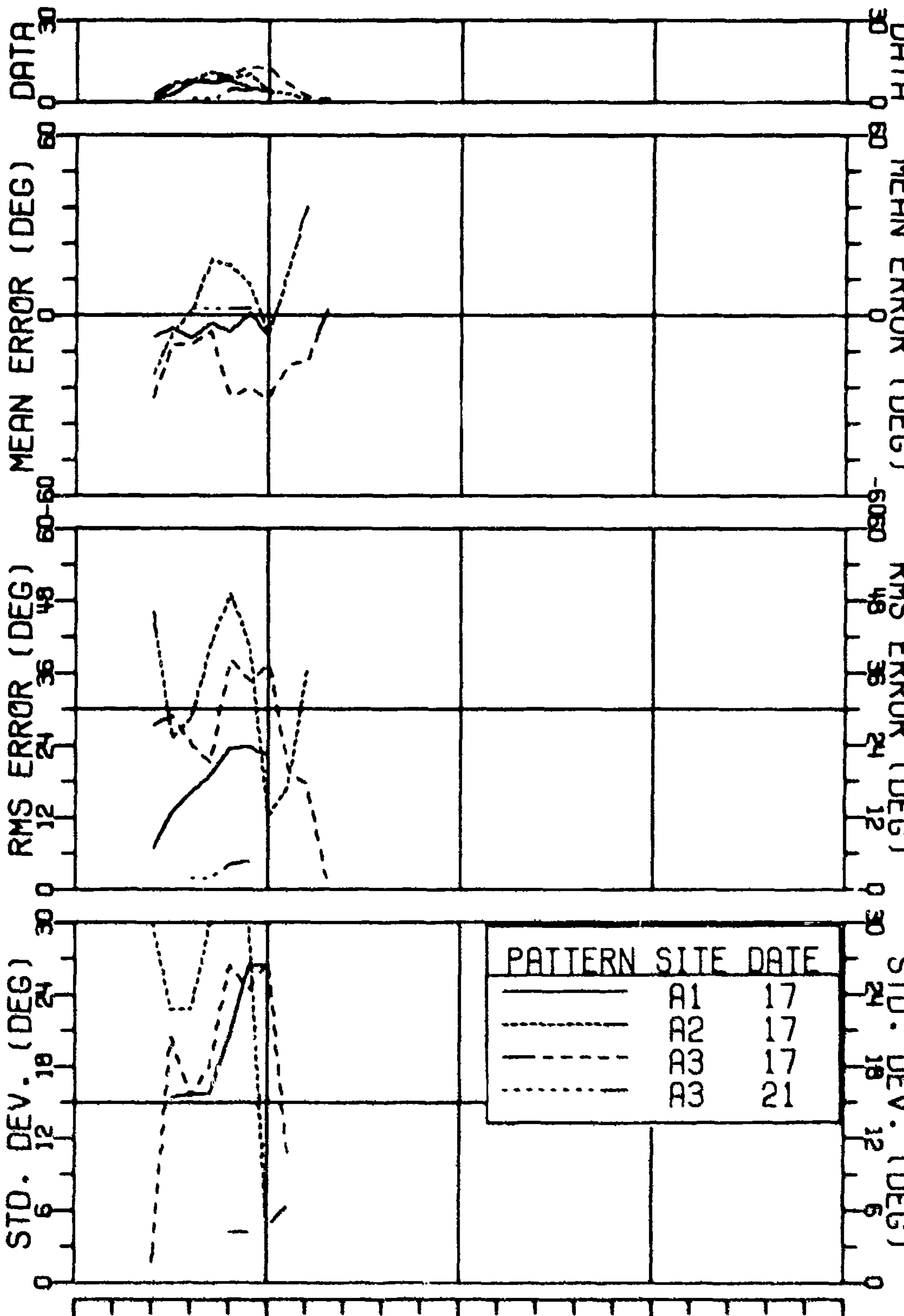

FIGURE III-236
MSS-FVT NEAR BOTTOM SINGLE CARDIOIDS SENSOR
BEARING ERROR RESULTS FOR 55HZ AT 141DB (U)

AS-77-28?

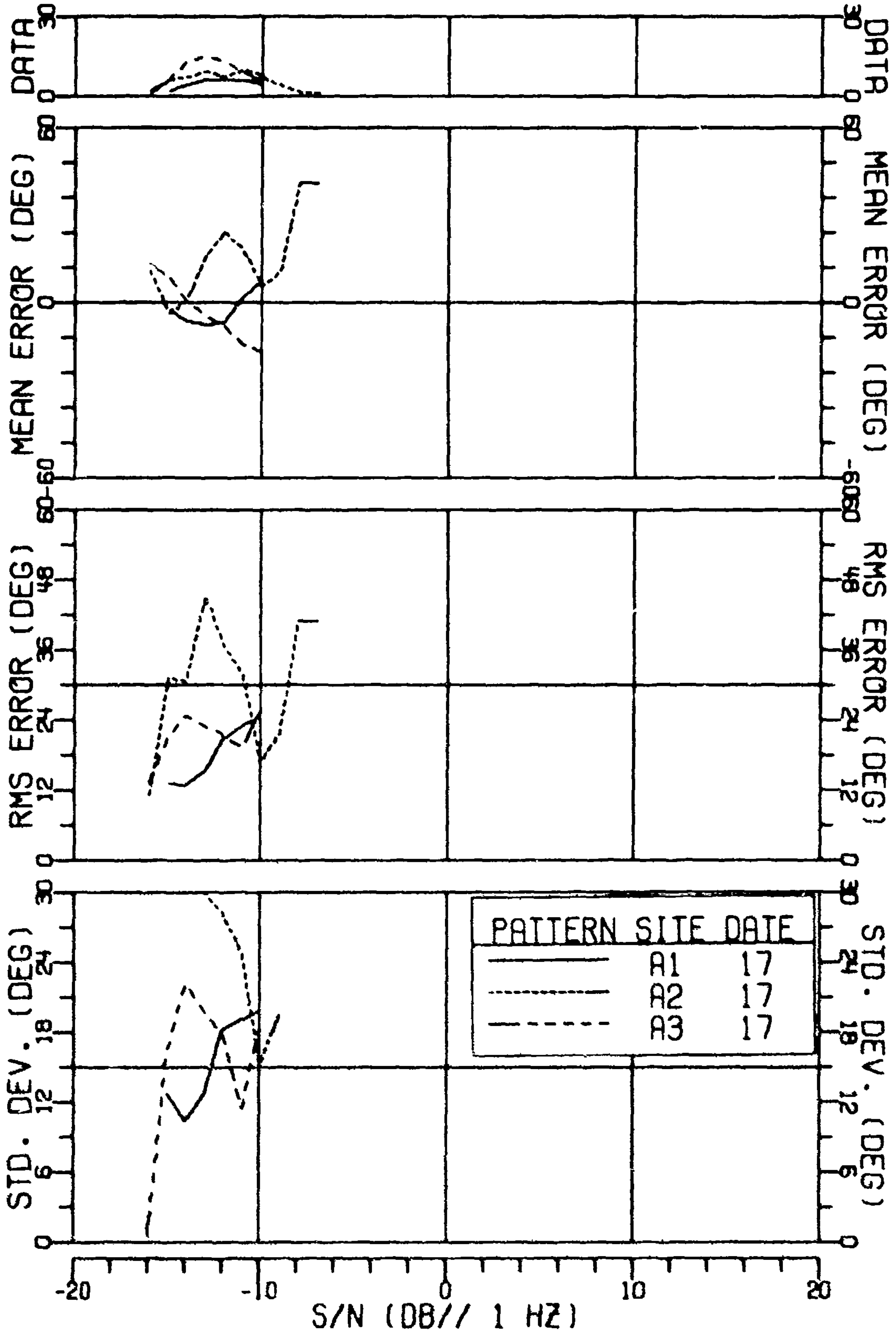

FIGURE III-237
MSS-FVT NEAR BOTTOM MAX GAIN LIMACONS SENSOR
BEARING ERROR RESULTS FOR 55HZ AT 141DB (U)

AS-77-2837

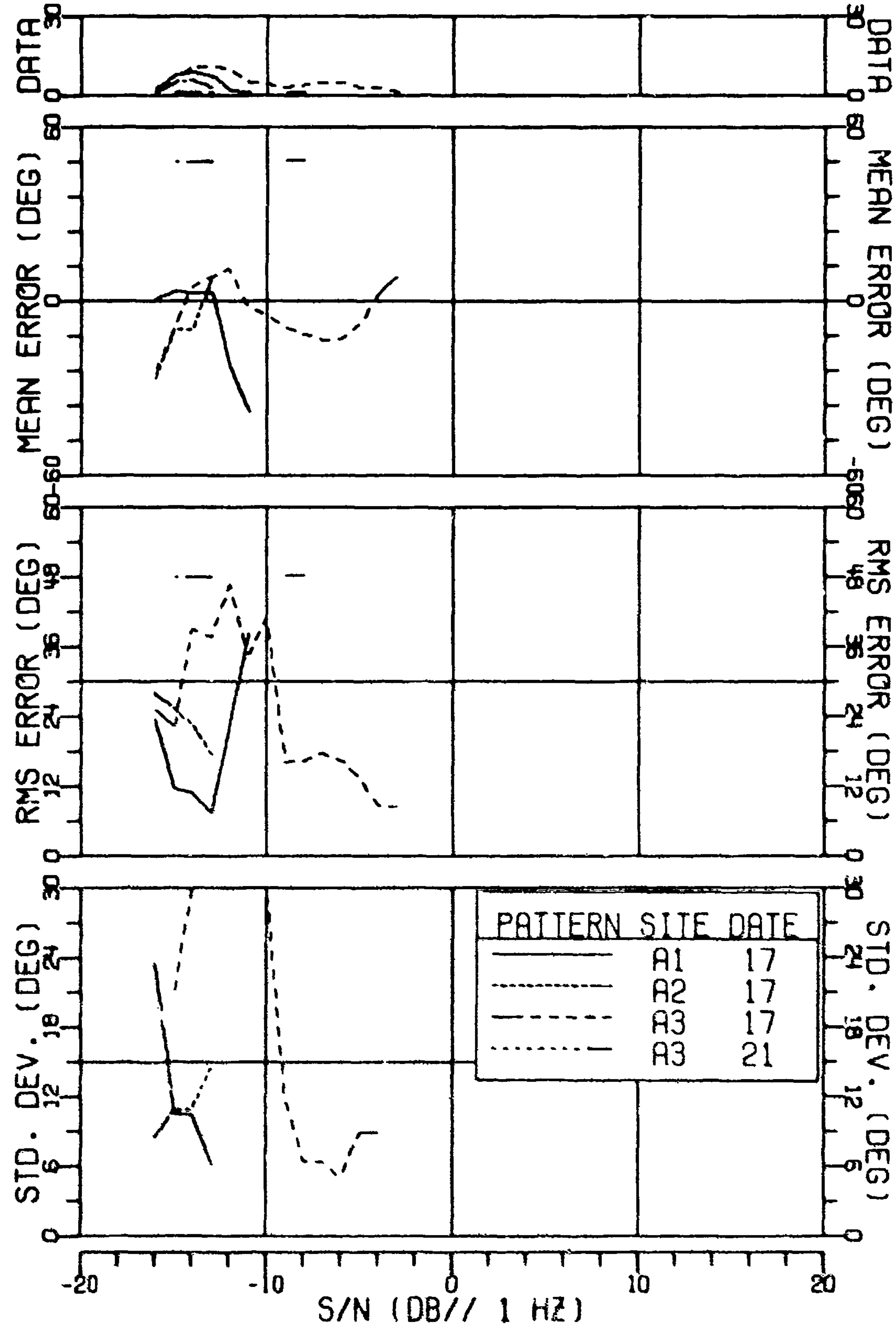

FIGURE III-238
MSS-FVT NEAR BOTTOM DIFFERENCED CARDIOIDS SENSOR
BEARING ERROR RESULTS FOR 55HZ AT 141DB (U)

AS-77-2838

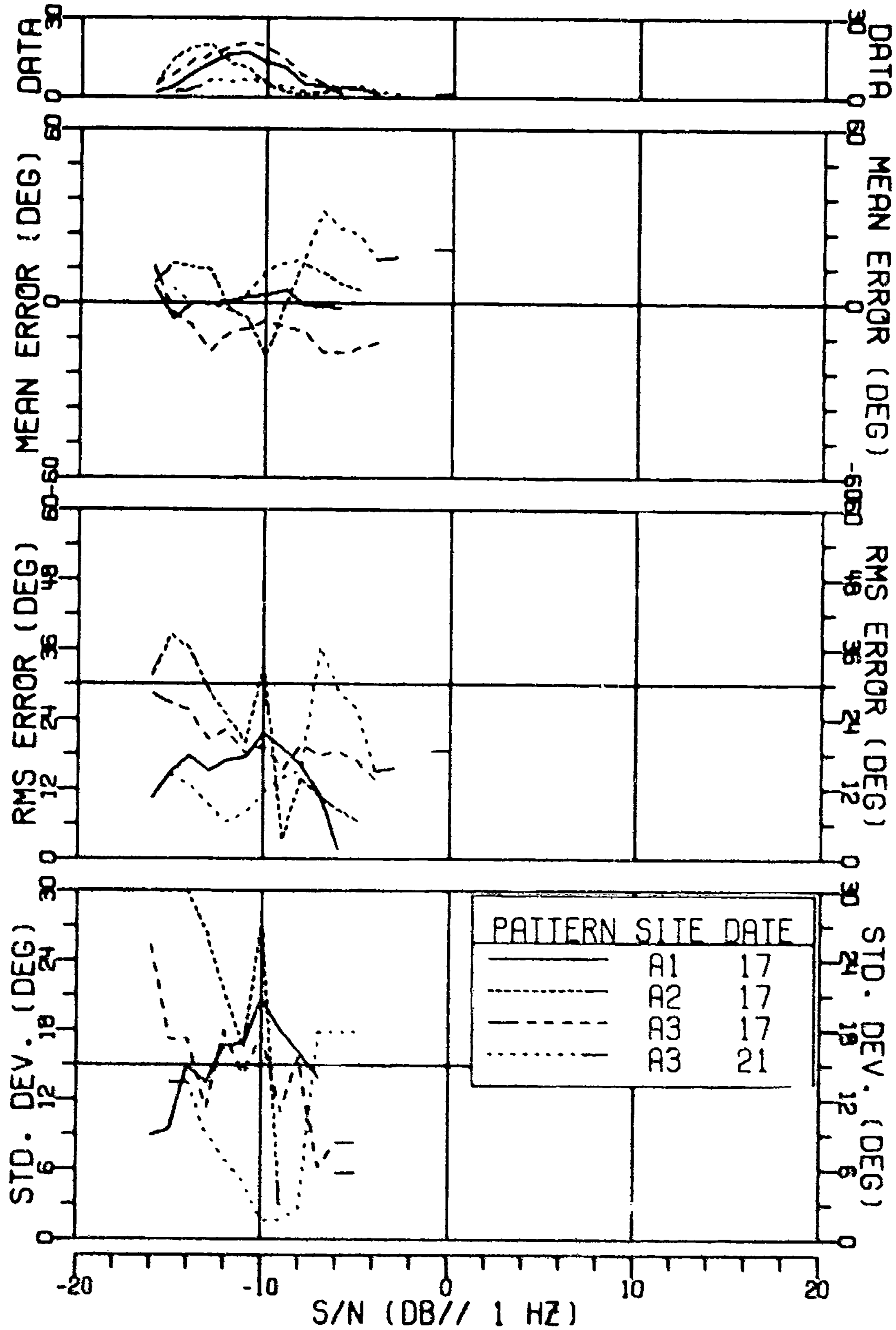

FIGURE III-239
MSS-FVT NEAR BOTTOM SINGLE CARDIOIDS SENSOR
BEARING ERROR RESULTS FOR 155HZ AT 134DB (U)

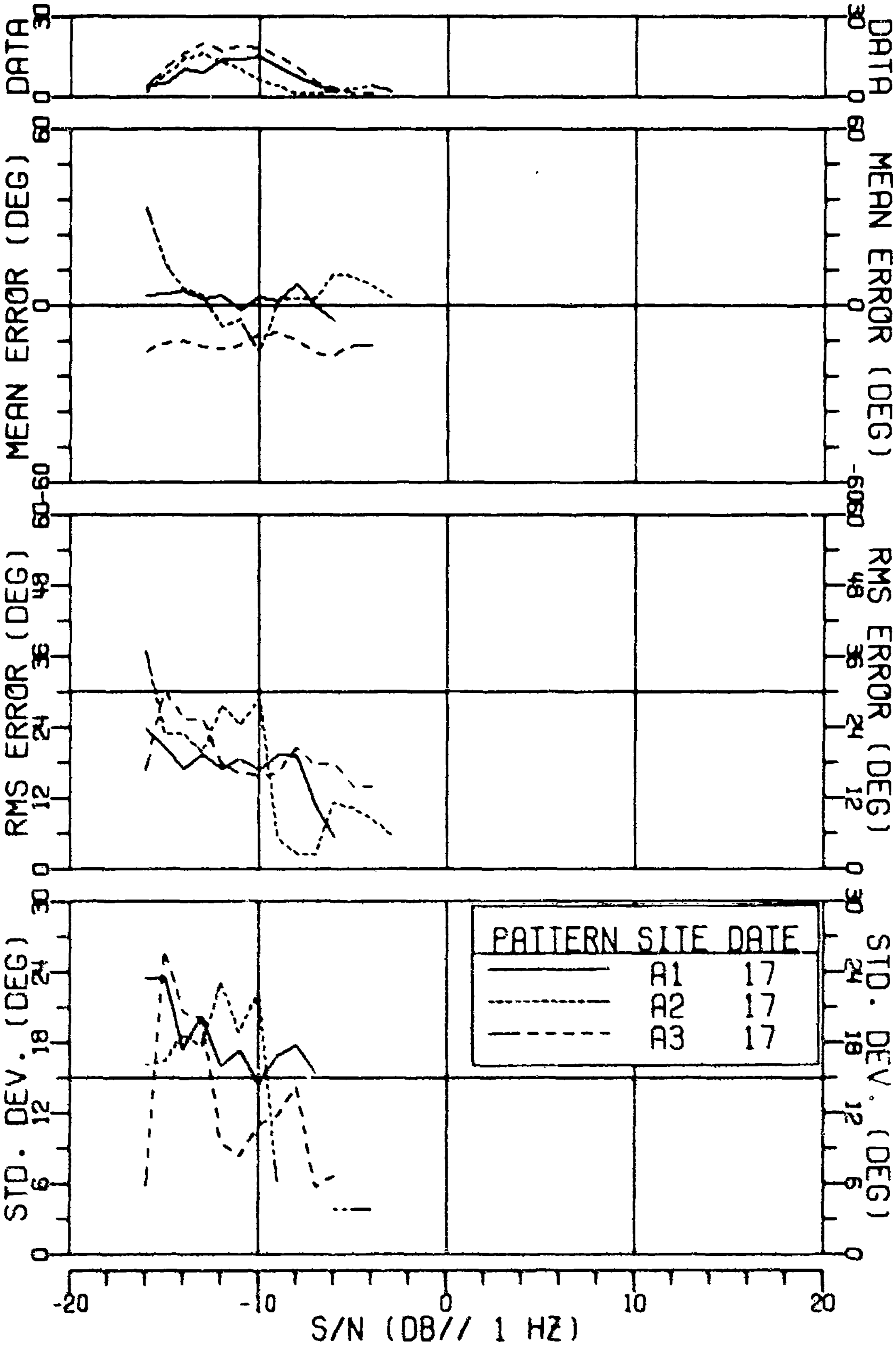

FIGURE III-240
MSS-FVT NEAR BOTTOM MAX GAIN LIMACONS SENSOR
BEARING ERROR RESULTS FOR 155HZ AT 134DB (U)

AS-77-28

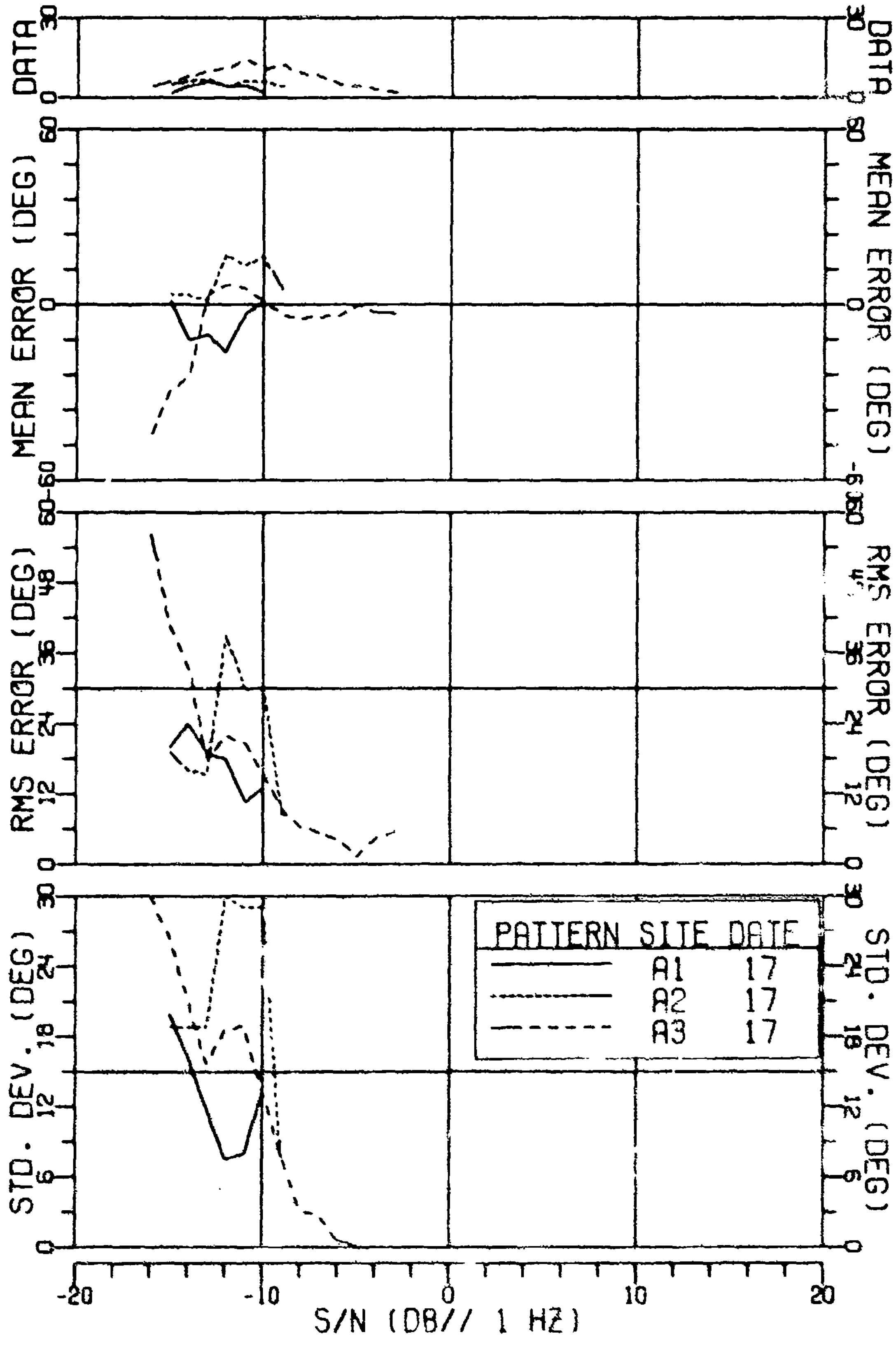

FIGURE III-241
MSS-FVT NEAR BOTTOM DIFFERENCED CARDIOIDS SENSOR
BEARING ERROR RESULTS FOR 155HZ AT 134DB (U)

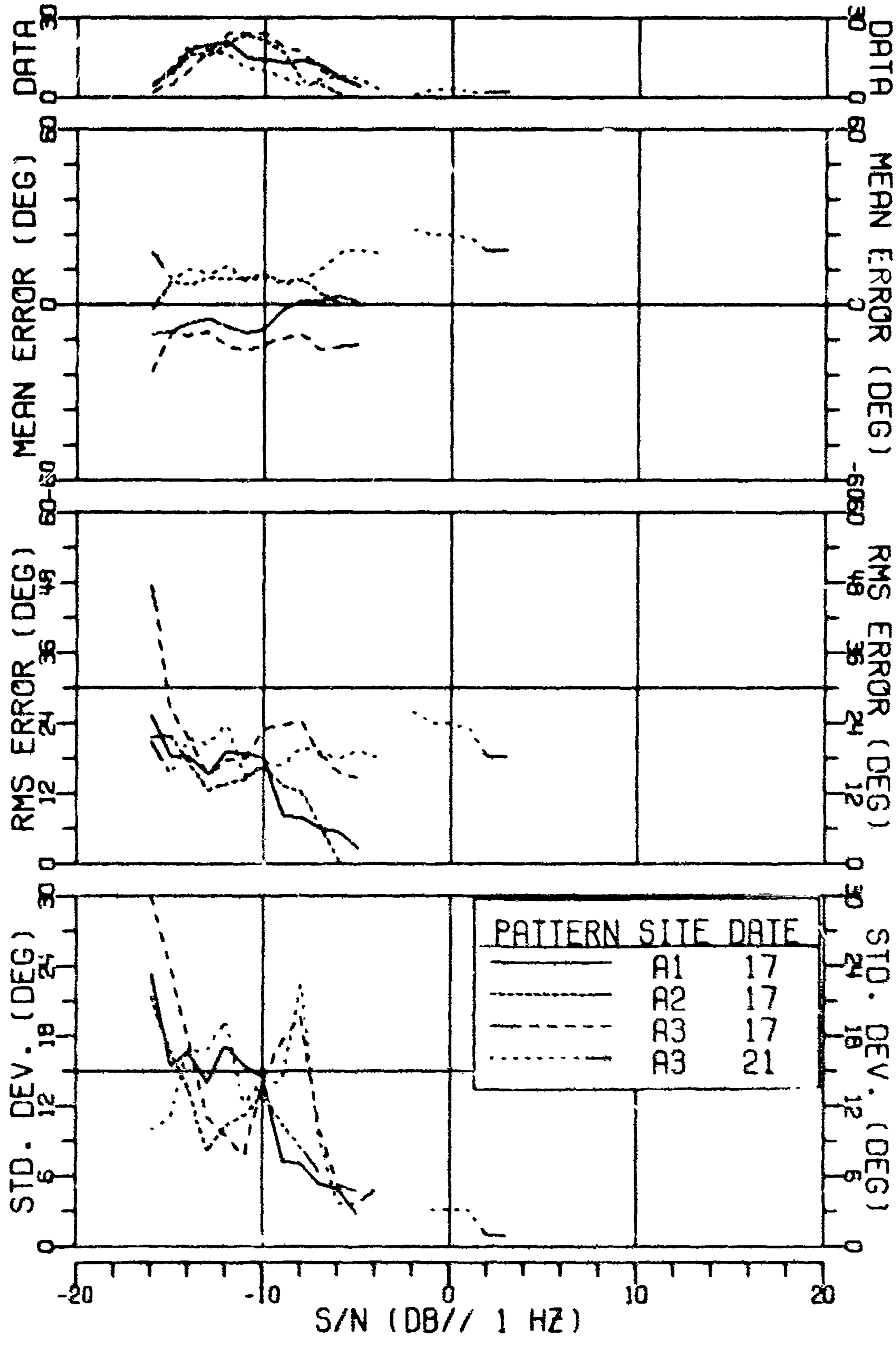

FIGURE III-242
MSS-FVT NEAR BOTTOM SINGLE CARDIOIDS SENSOR
BEARING ERROR RESULTS FOR 305 HZ AT 136DB (U)

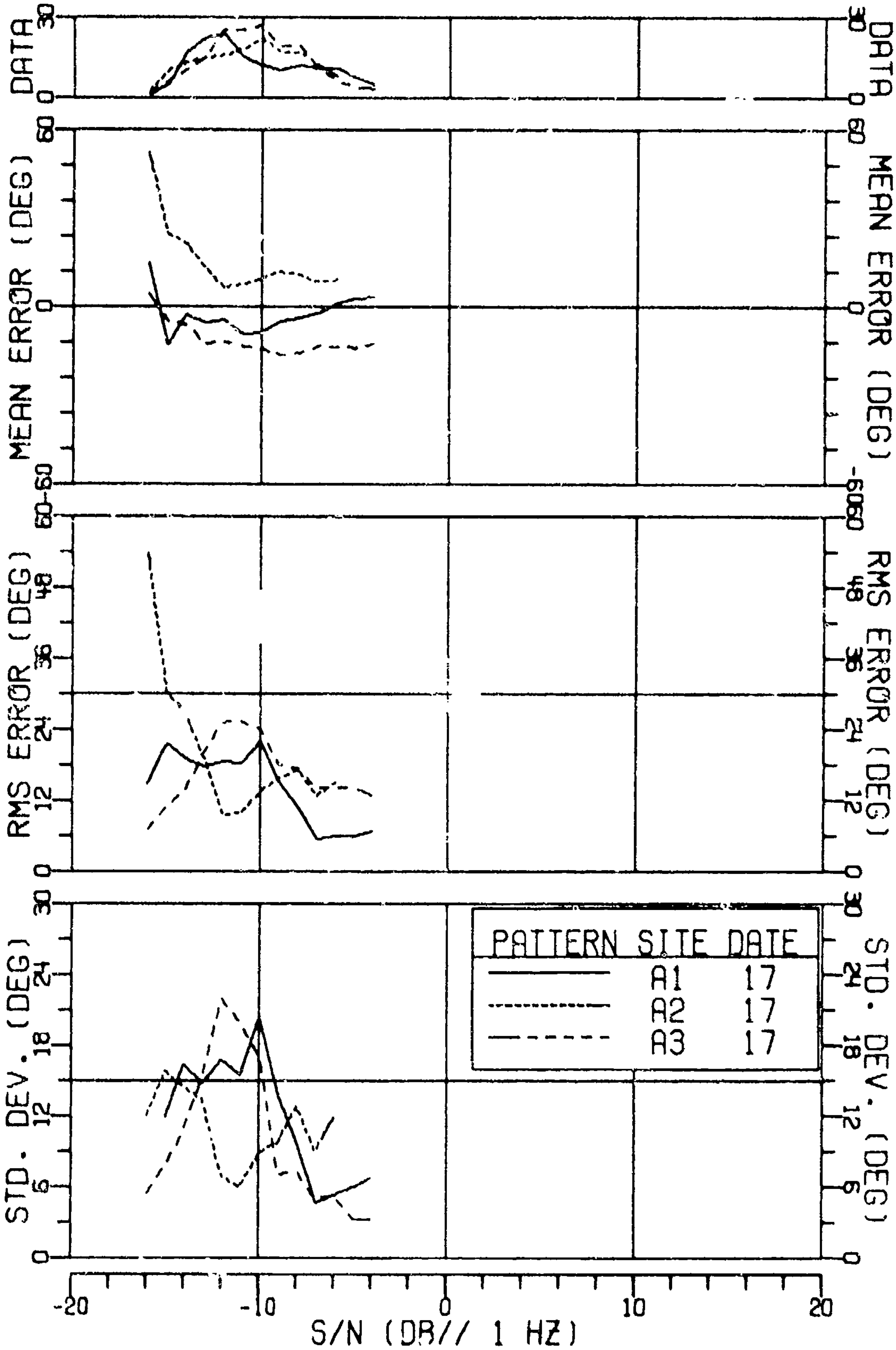

FIGURE III-243
MSS-FVT NEAR BOTTOM MAX GAIN LIMACONS SENSOR
BEARING ERROR RESULTS FOR 305 HZ AT 136DB (U)

AS-77-2843

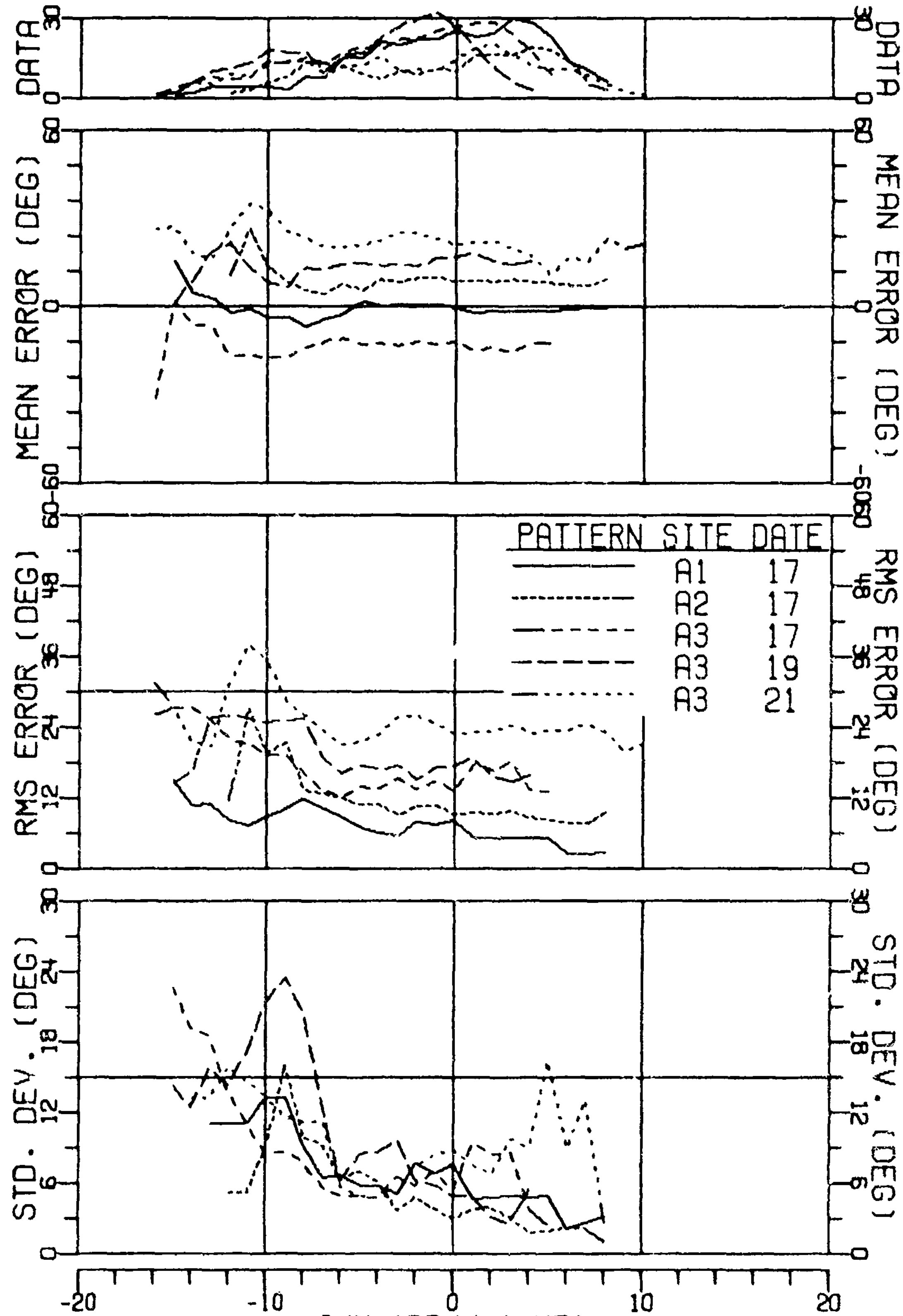

FIGURE III-244
MSS-FVT NEAR BOTTOM SINGLE CARDIOIDS SENSOR
BEARING ERROR RESULTS FOR 64HZ AT 162DB (U)

AS-77-2844

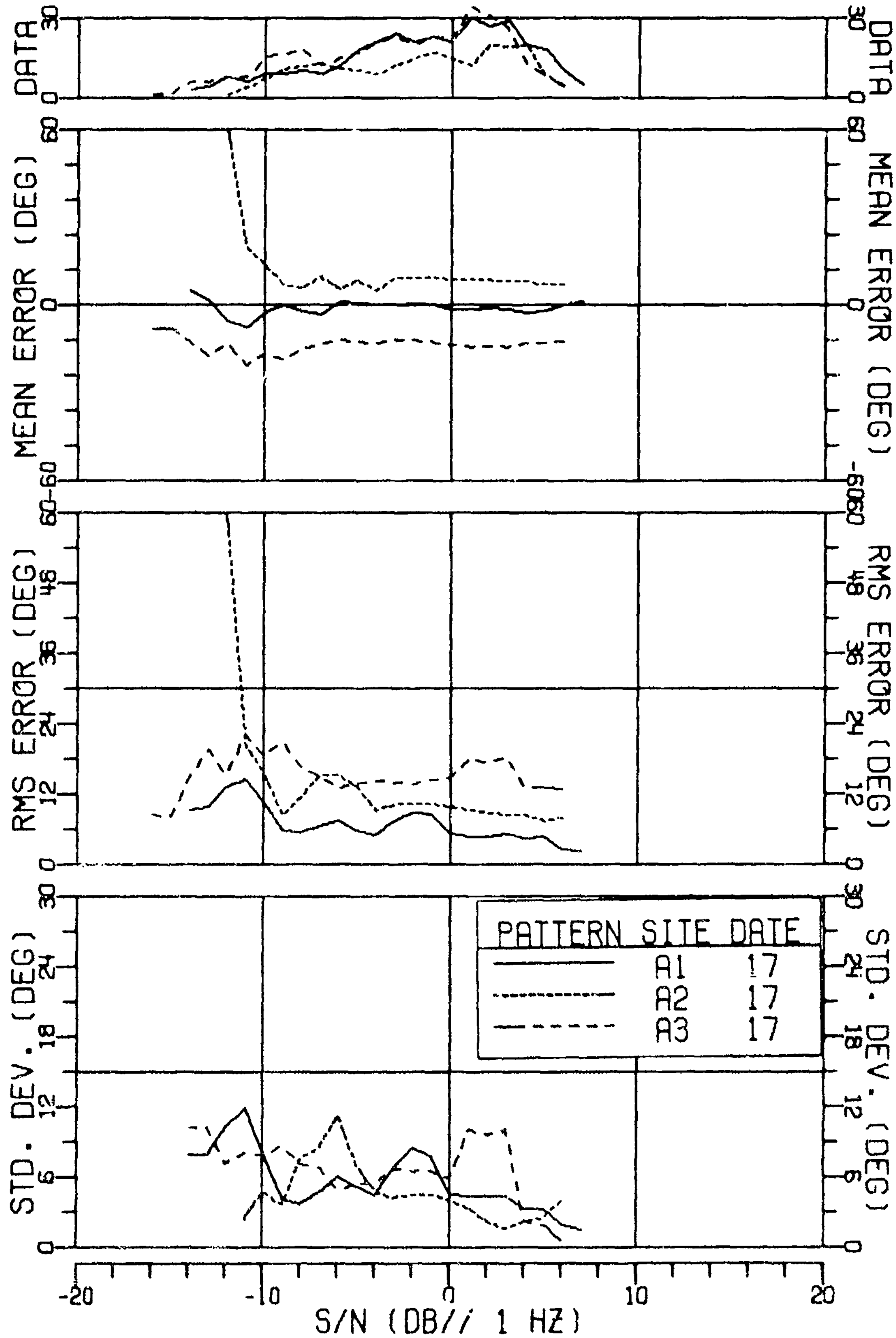

FIGURE III-245
MSS-FVT NEAR BOTTOM MAX GAIN LIMACONS SENSOR
BEARING ERROR RESULTS FOR 64HZ AT 162DB (U)

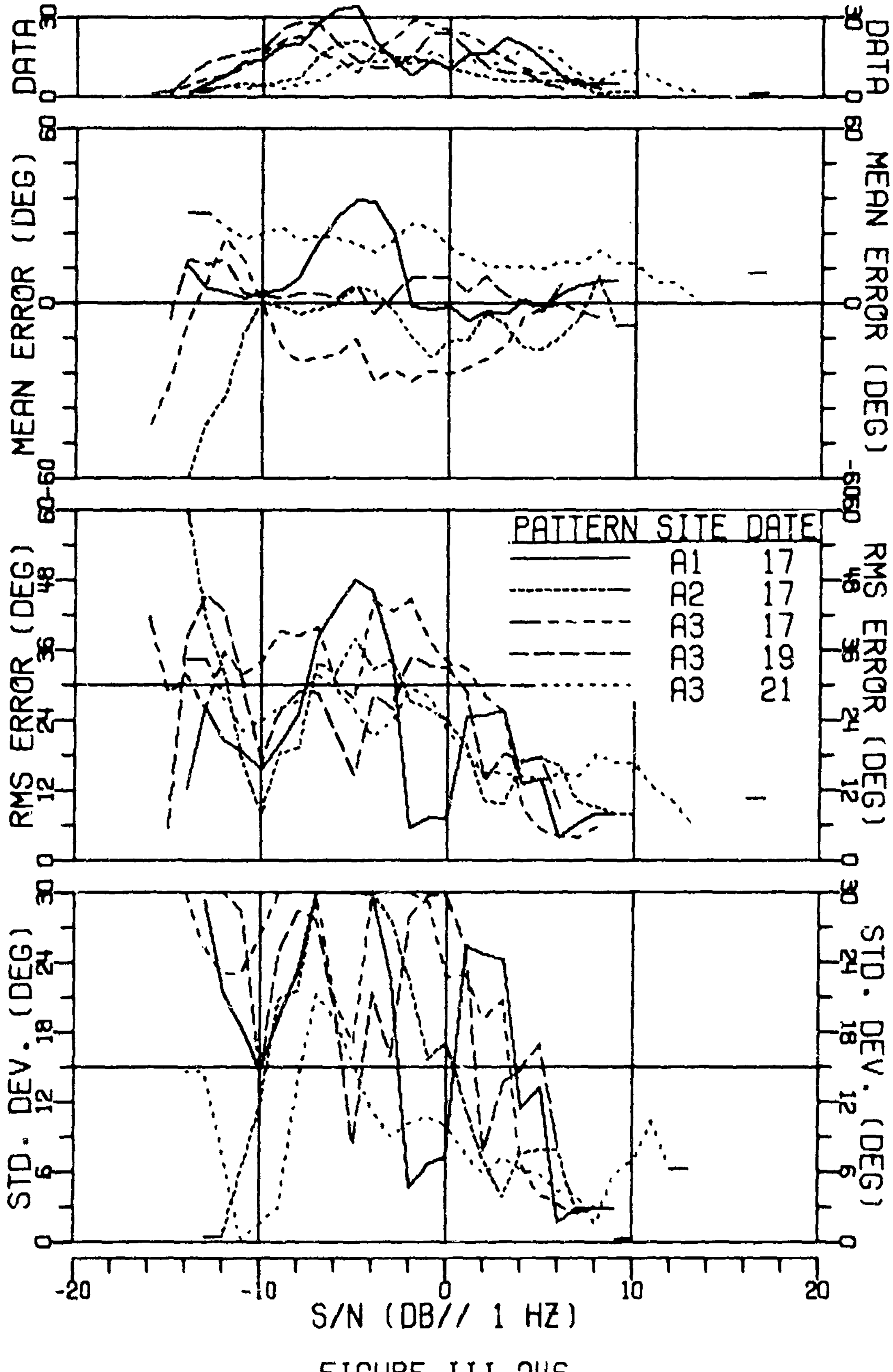

FIGURE III-246
MSS-FVT NEAR BOTTOM DIFFERENCED CARDIOIDS SENSOR
BEARING ERROR RESULTS FOR 64HZ AT 162DB (U)

AS-77-2846

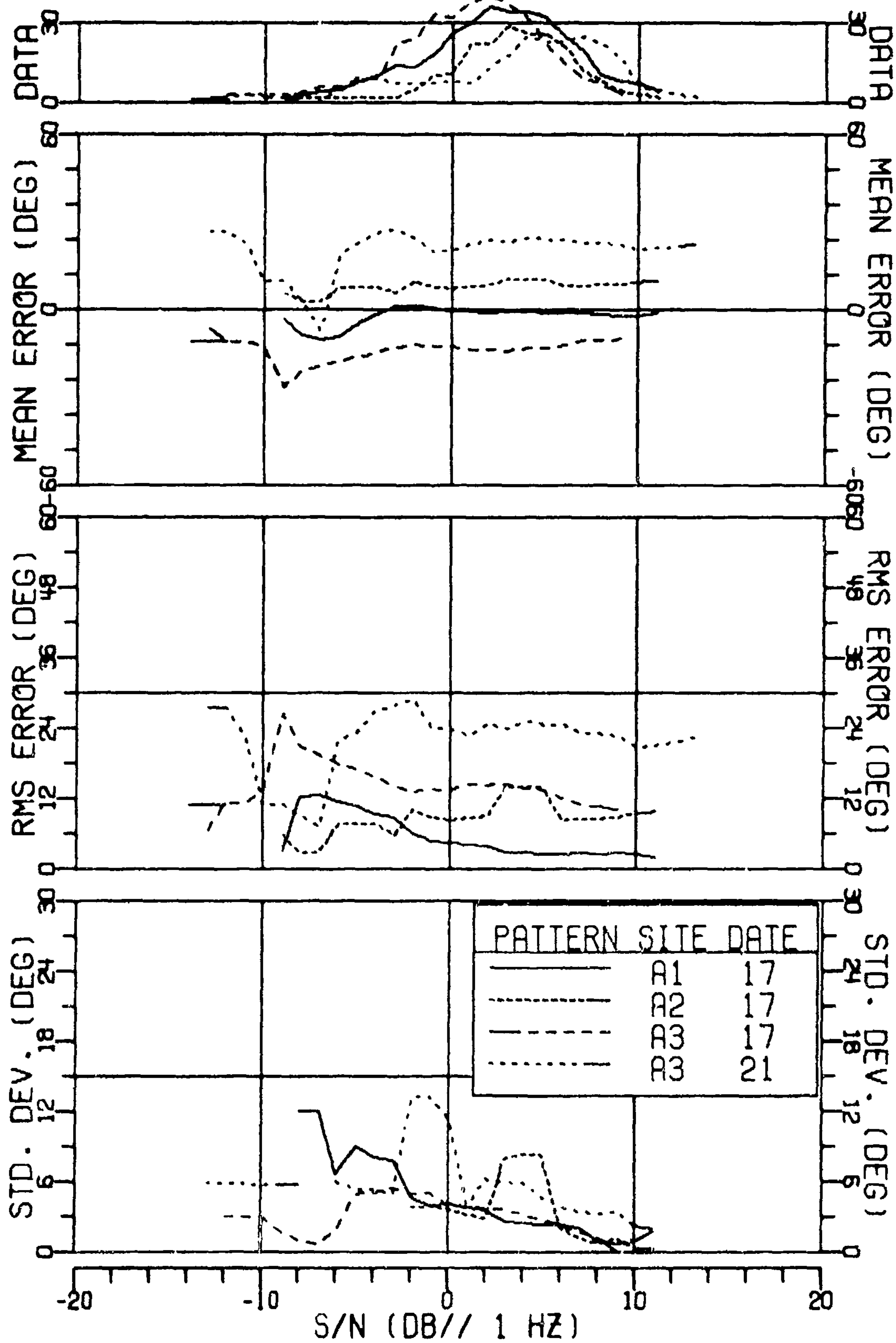

FIGURE III-247
MSS-FVT NEAR BOTTOM SINGLE CARDIOIDS SENSOR
BEARING ERROR RESULTS FOR 160HZ AT 161DB (U)

AS-77-2847

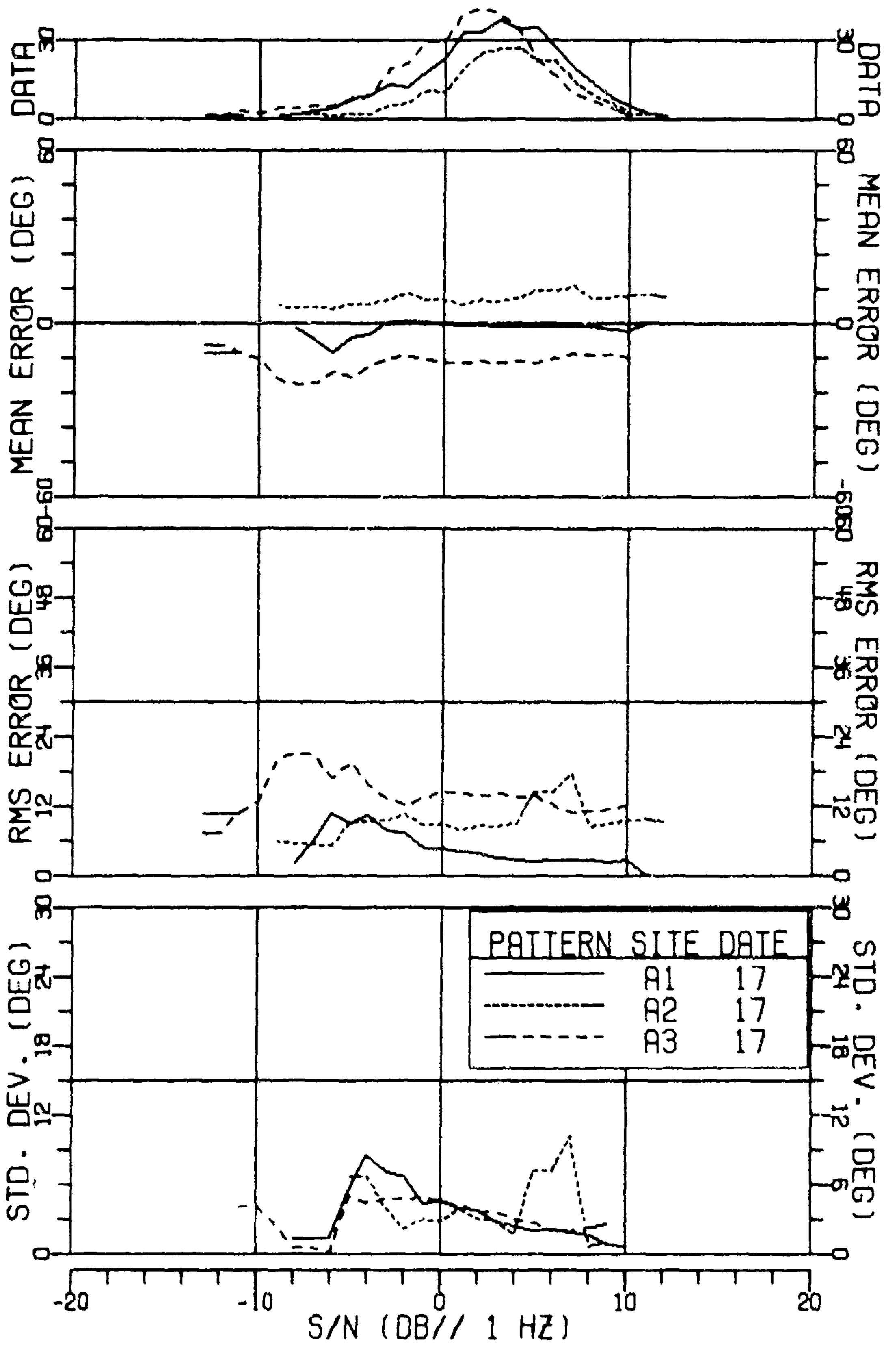

FIGURE III-248
MSS-FVT NEAR BOTTOM MAX GAIN LIMACONS SENSOR BEARING ERROR RESULTS FOR 160HZ AT 161DB (U)

AS-77-28

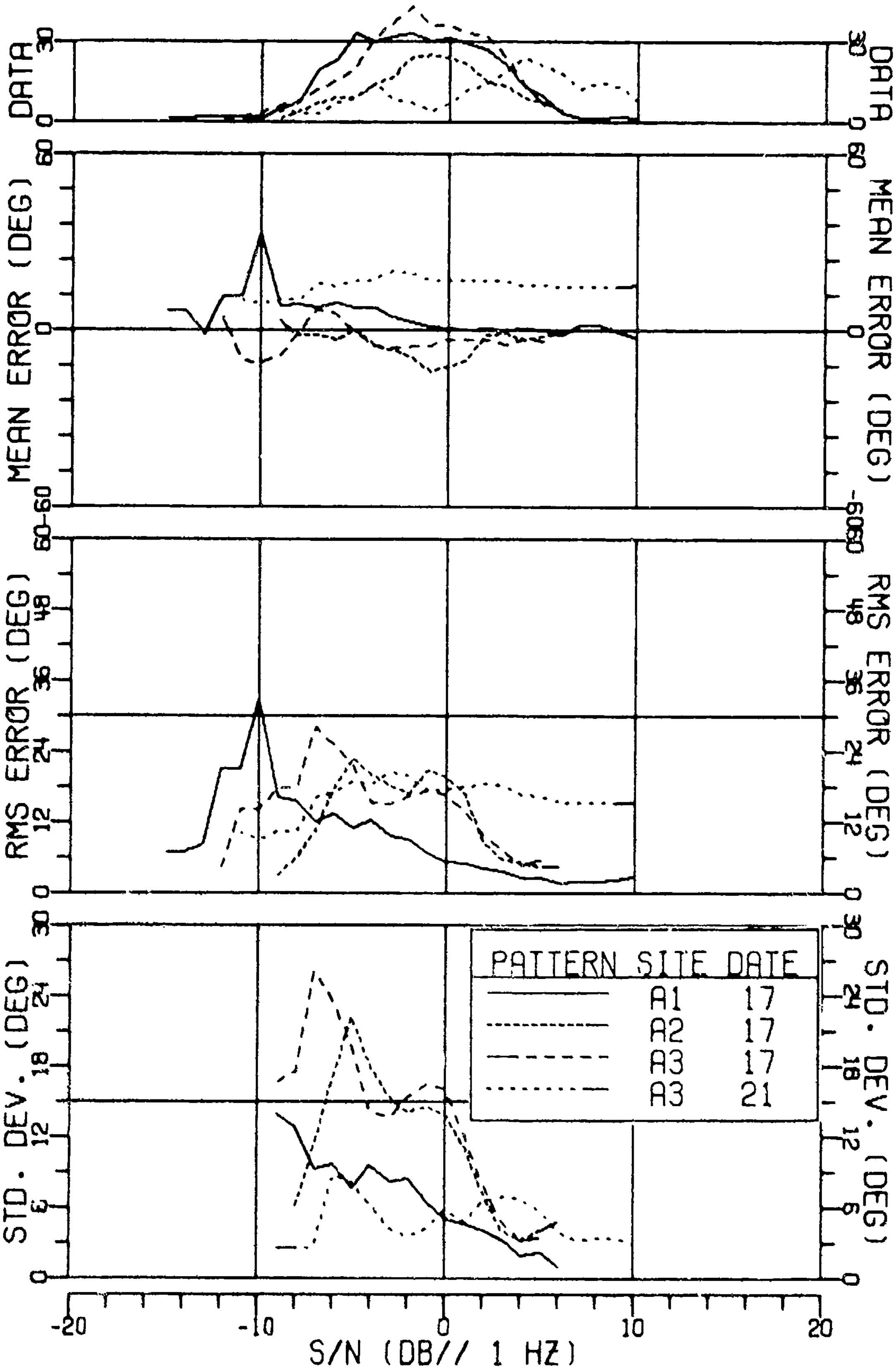

FIGURE III-249
MSS-FVT NEAR BOTTOM DIFFERENCED CARDIOIDS SENSOR
BEARING ERROR RESULTS FOR 160HZ AT 161DB (U)

A?-77-2849

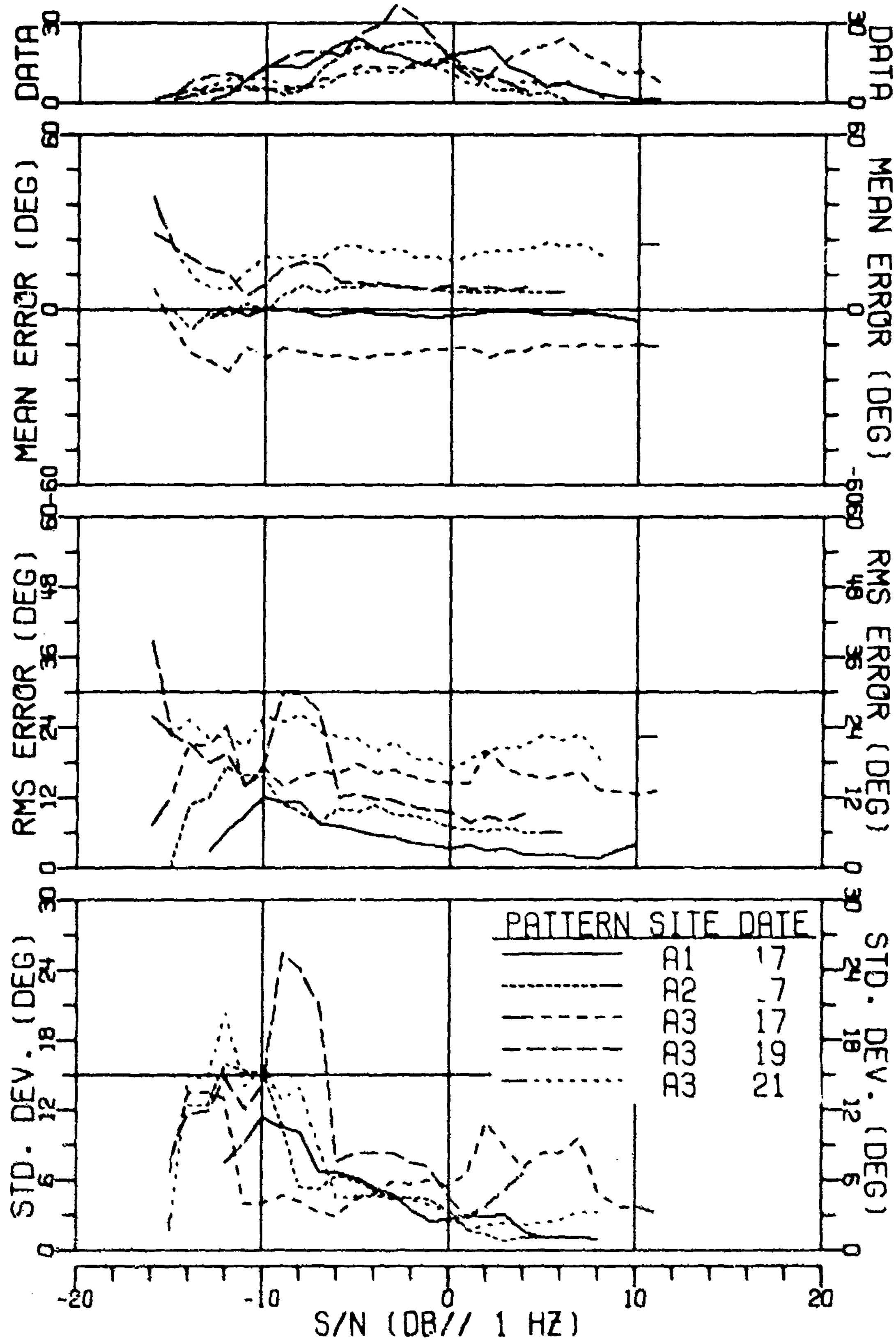

FIGURE III-250
MSS-FVT NEAR BOTTOM SINGLE CARDIOIDS SENSOR
BEARING ERROR RESULTS FOR 70HZ AT 166DB (U)

AS-77-

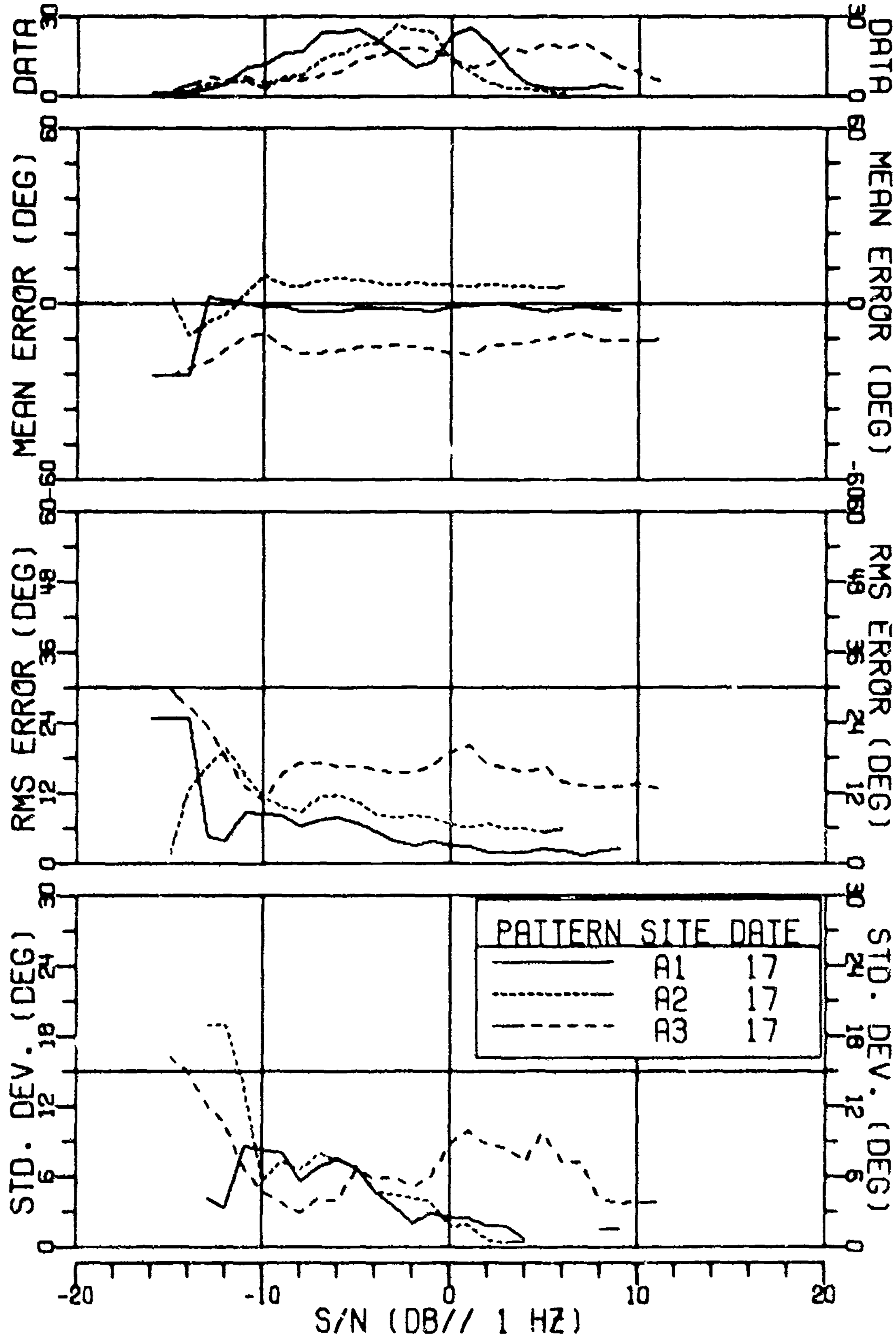

FIGURE III-251
MSS-FVT NEAR BOTTOM MAX GAIN LIMACONS SENSOR
BEARING ERROR RESULTS FOR 70HZ AT 166DB (U)

AS-77-2851

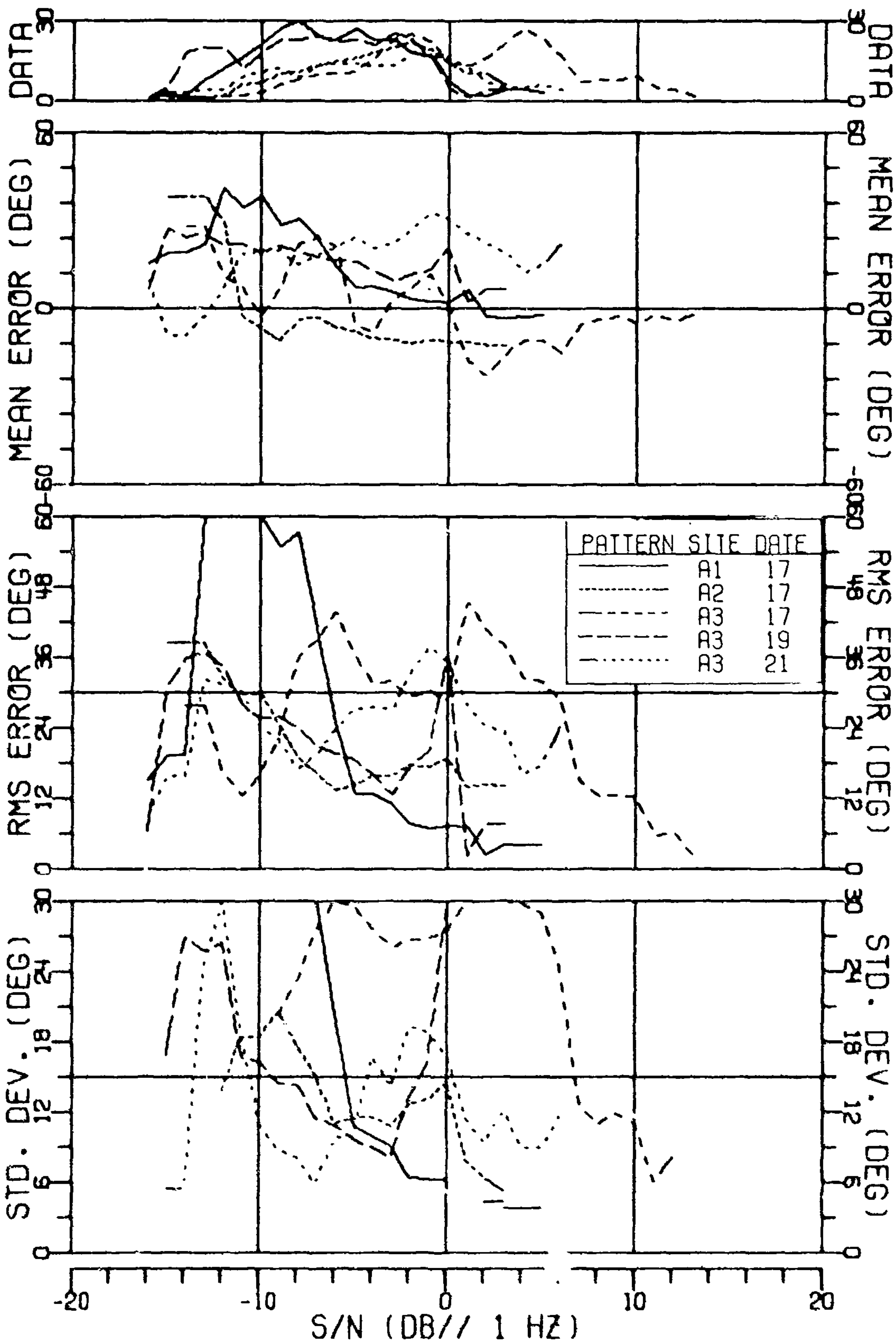

FIGURE III-252
MSS-FVT NEAR BOTTOM DIFFERENCED CARDIOIDS SENSOR
BEARING ERROR RESULTS FOR 70HZ AT 166DB (U)

AS-77-285

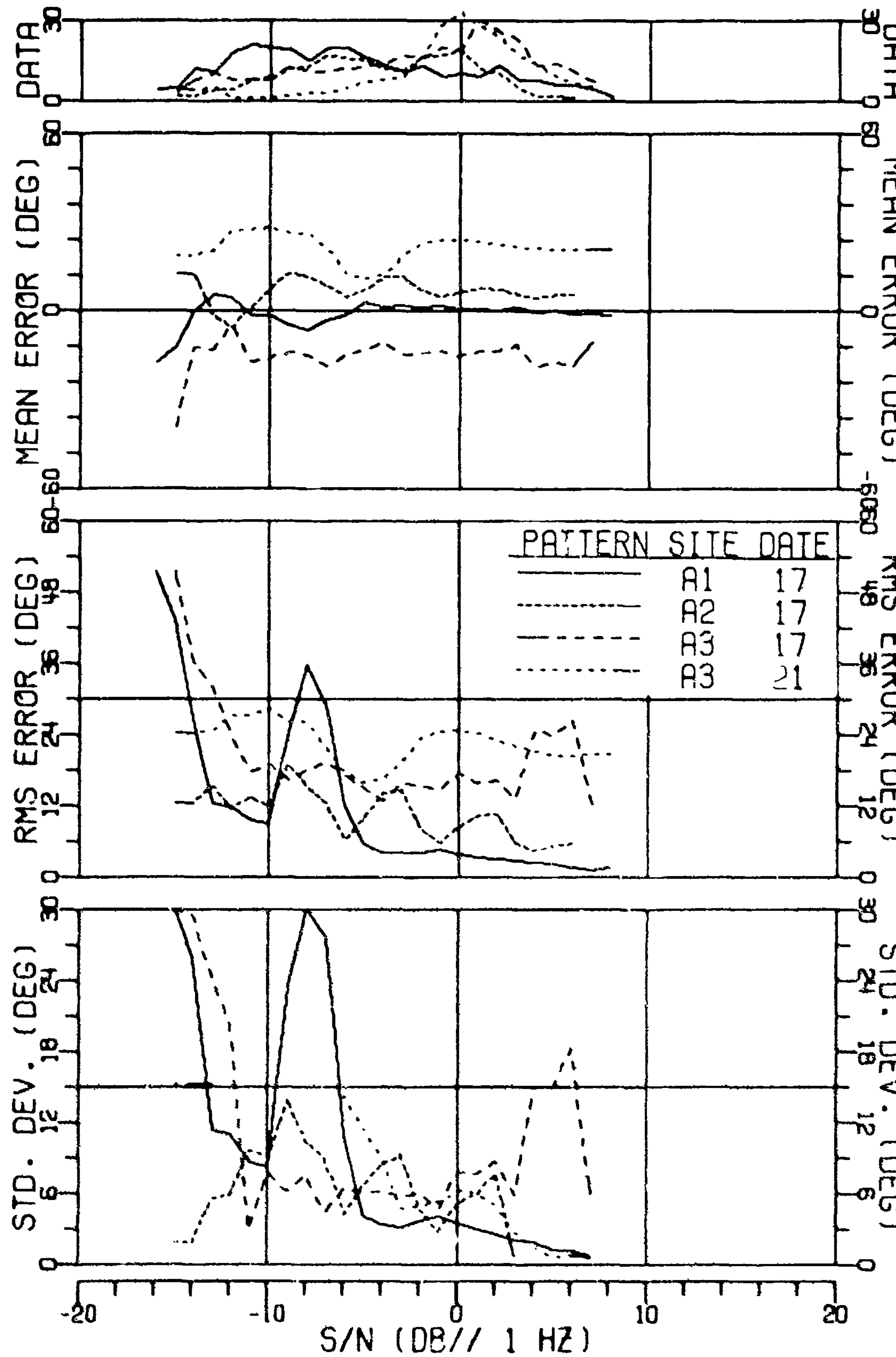

FIGURE III-253
MSS-FVT NEAR BOTTOM SINGLE CARDIOIDS SENSOR
BEARING ERROR RESULTS FOR 170HZ AT 156DB (U)

AS-77-2853

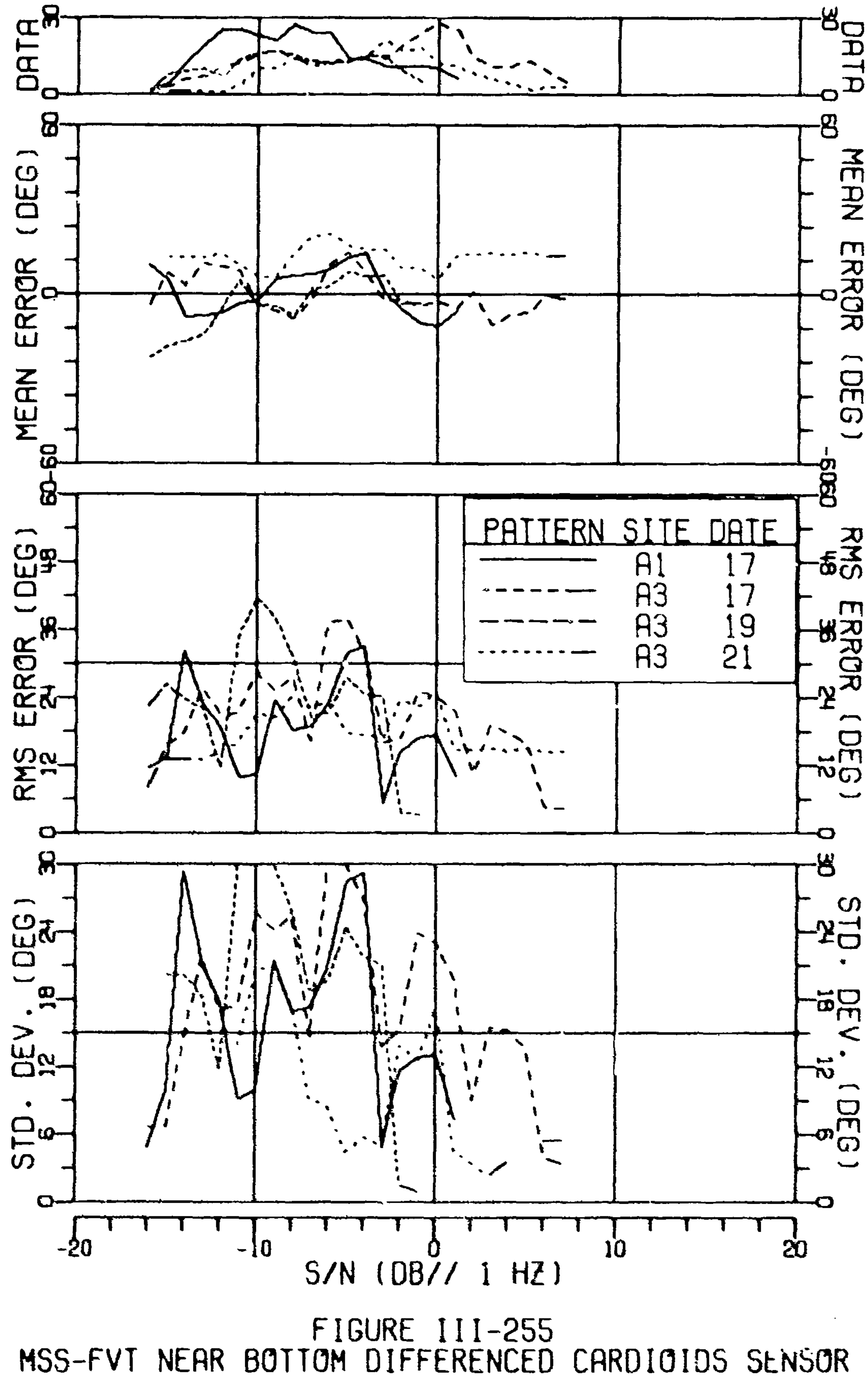

FIGURE III-255
MSS-FVT NEAR BOTTOM DIFFERENCED CARDIOIDS SENSOR
BEARING ERROR RESULTS FOR 170HZ AT 156DB (U)

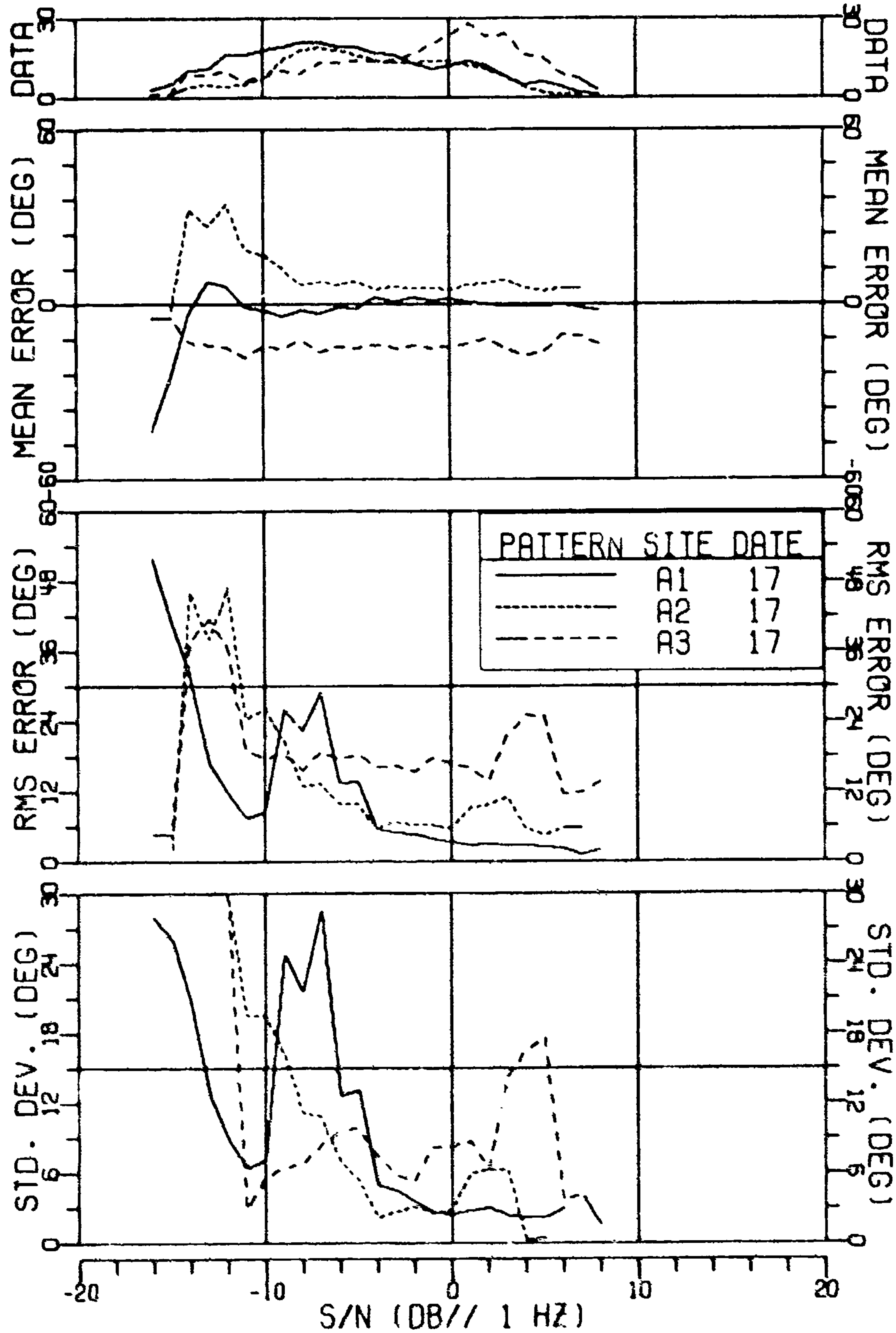

FIGURE III-254
MSS-FVT NEAR BOTTOM MAX GAIN LIMACONS SENSOR
BEARING ERROR RESULTS FOR 170HZ AT 156DB (U)

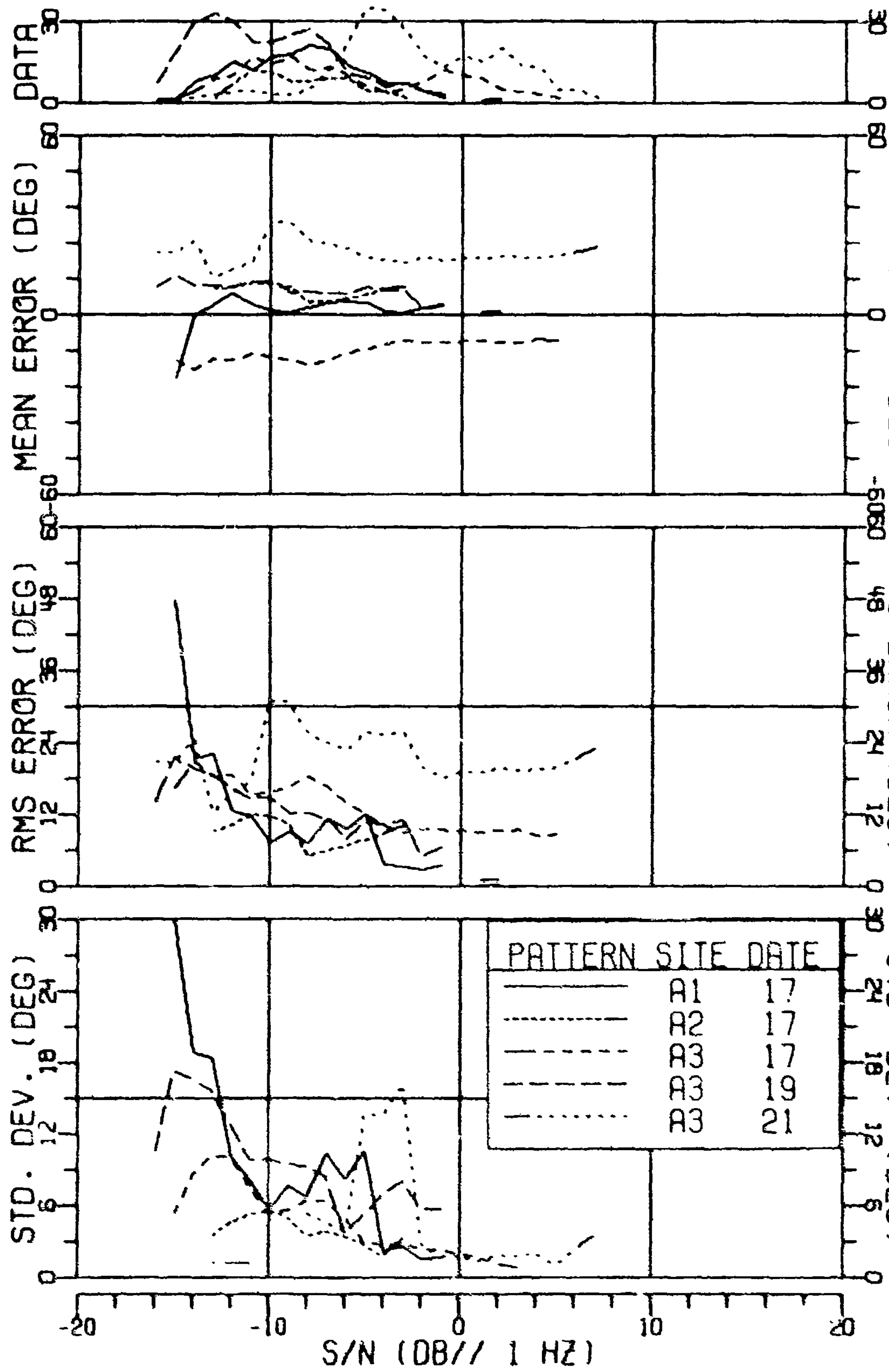

FIGURE III-256
MSS-FVT NEAR BOTTOM SINGLE CARDIOIDS SENSOR
BEARING ERROR RESULTS FOR 335HZ AT 154DB (U)

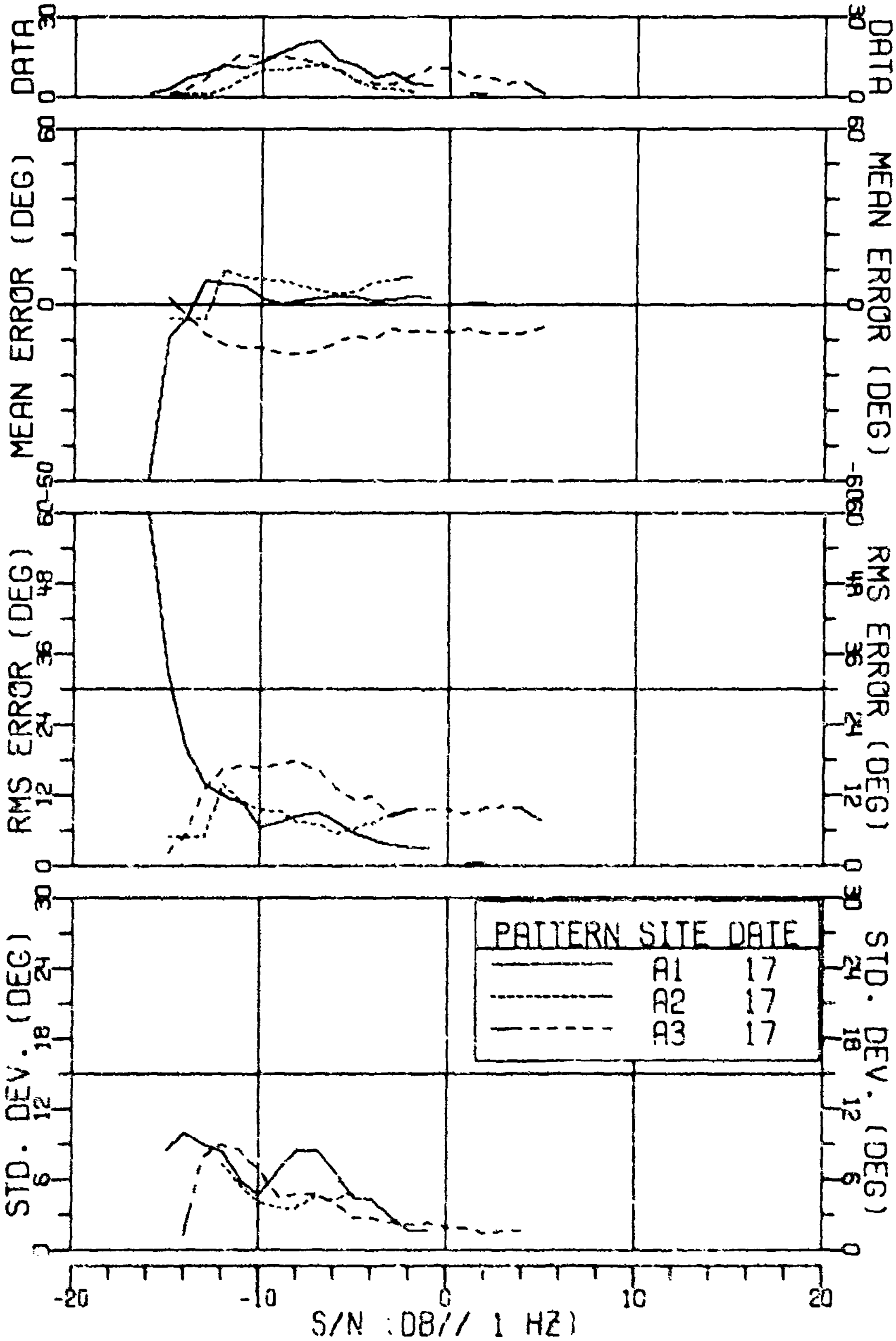

FIGURE III-257
MSS-FVT NEAR BOTTOM MAX GAIN LIMACONS SENSOR
BEARING ERROR RESULTS FOR 335HZ AT 154DB (U)

AS-77-2857

APPENDIX G

SIGNAL-TO-NOISE RATIO versus RANGE CURVES (U)

(FIGURES III-258 - III 293)

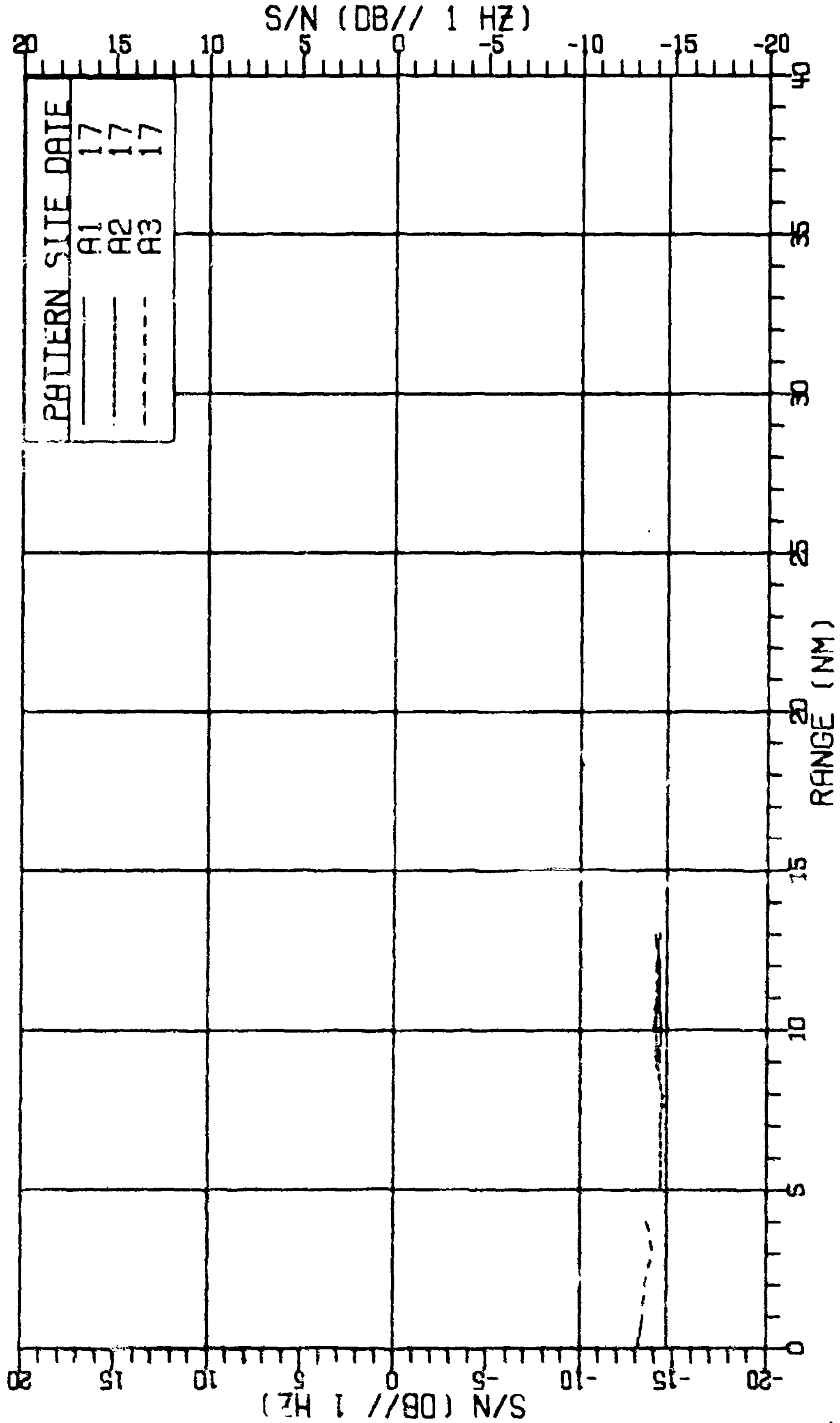

FIGURE III-258
MSS-FVT NEAR BOTTOM OMNIDIRECTIONAL SENSOR
SIGNAL-TO-NOISE RESULTS FOR 55HZ AT 141DB (U)

AS-77-2858

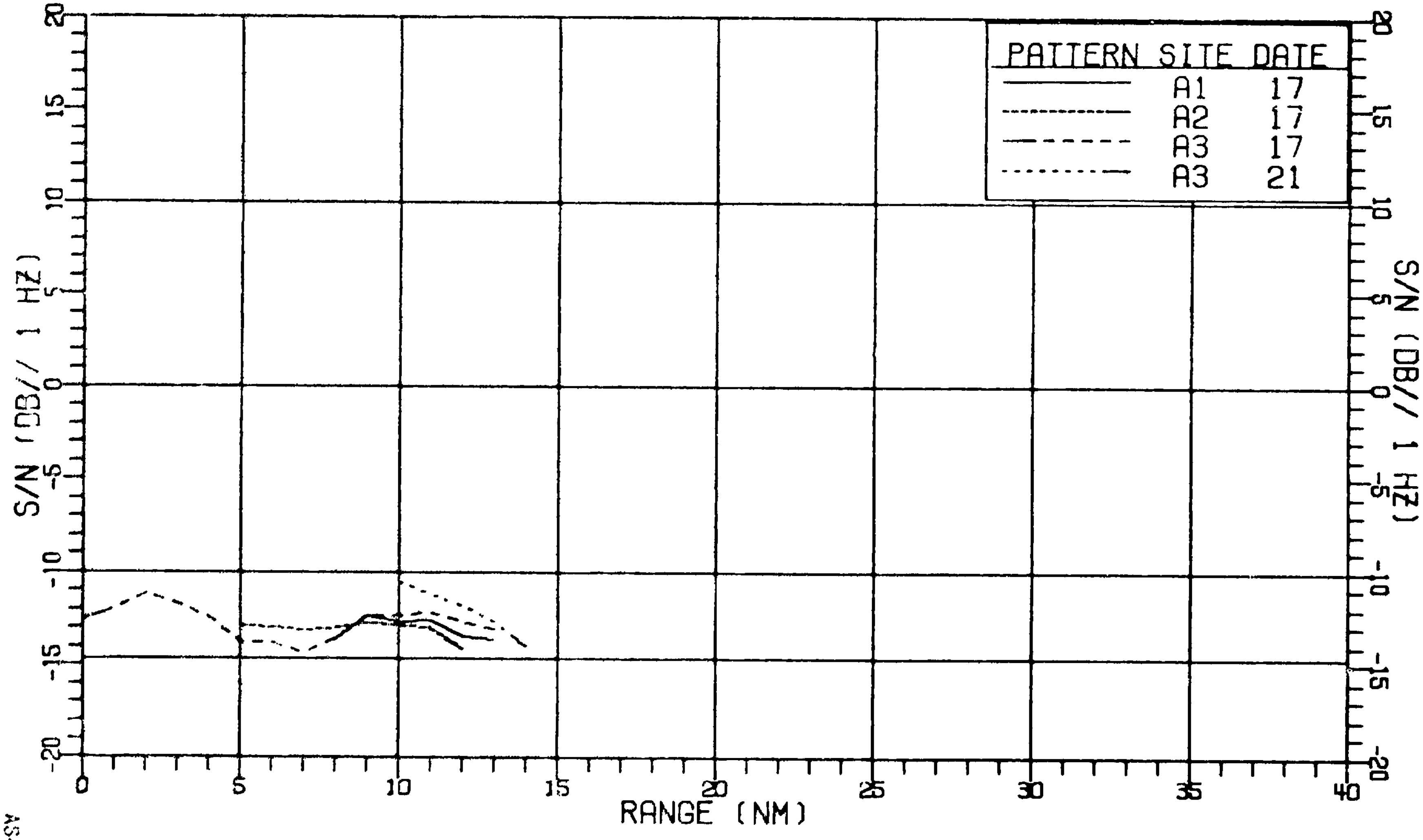

FIGURE III-259
MSS-FVT NEAR BOTTOM SINGLE CARDIOIDS SENSOR
SIGNAL-TO-NOISE RESULTS FOR 55HZ AT 141DB (U)

AS-77-2859

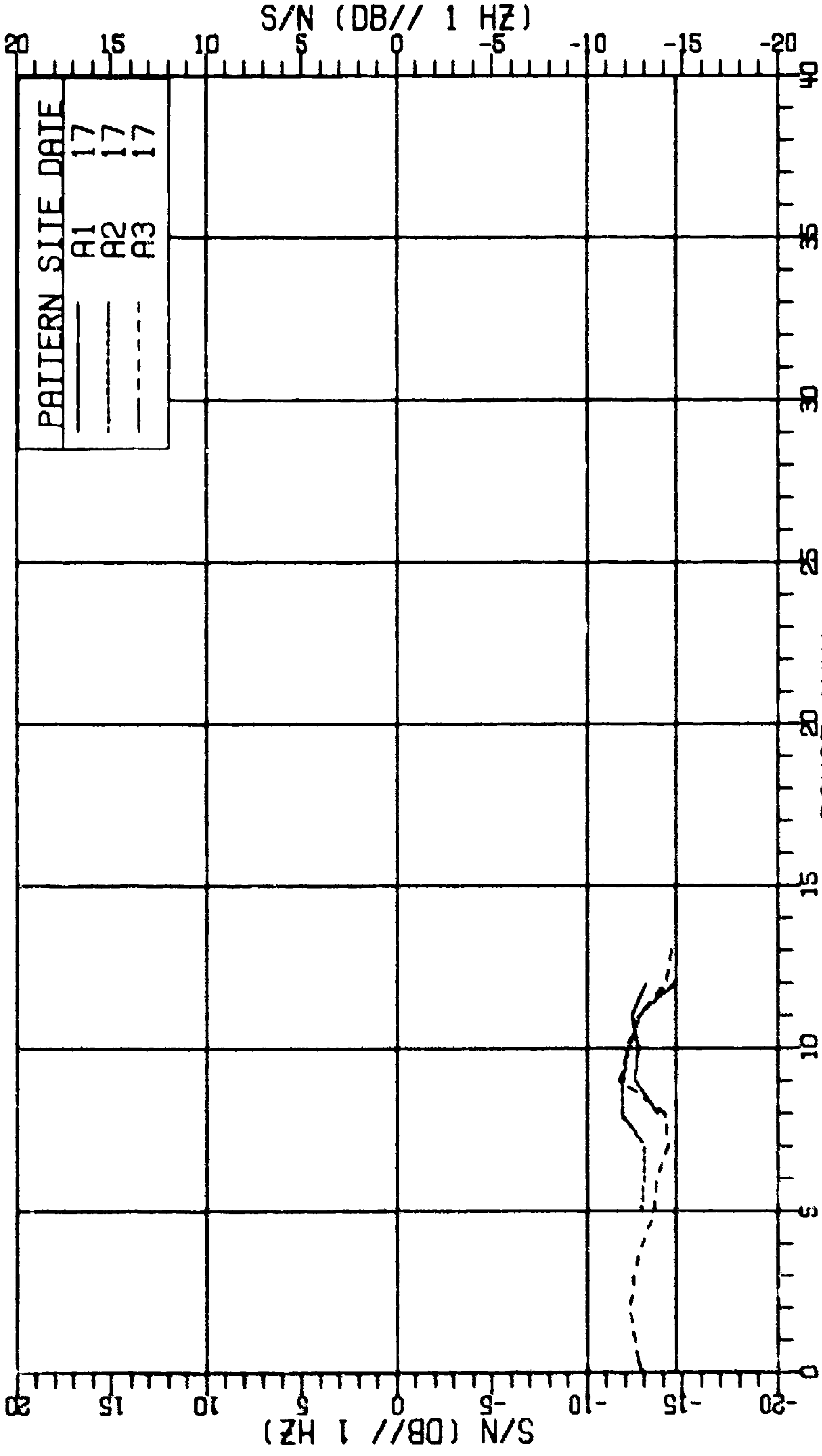

FIGURE III-260
MSS-FVT NEAR BOTTOM MAX GAIN LIMACONS SENSOR
SIGNAL-TO-NOISE RESULTS FOR 55HZ AT 141DB (U)

AS-77-2560

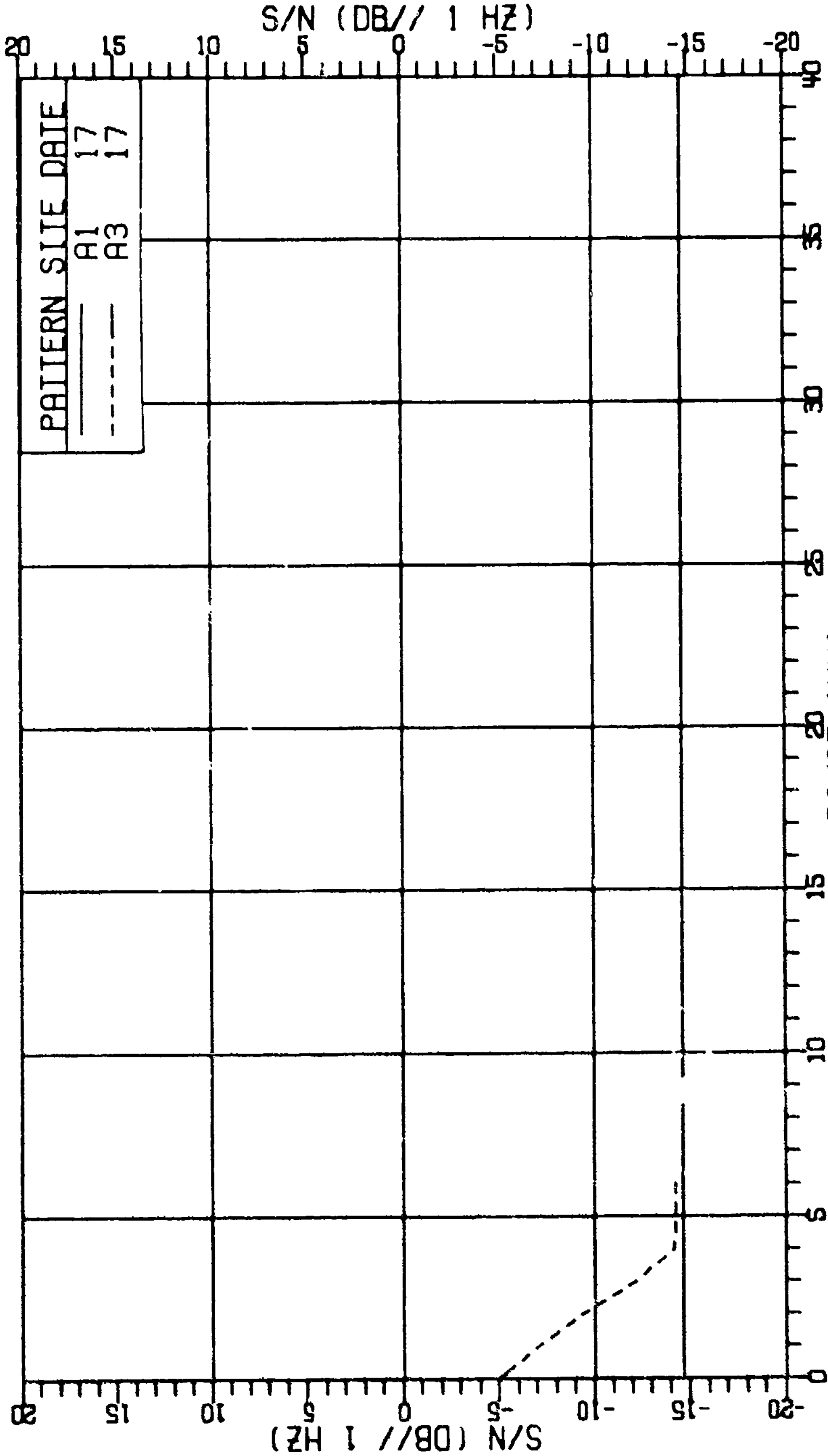

FIGURE III-261
MSS-FVT NEAR BOTTOM VERTICAL DIPOLE SENSOR
SIGNAL-TO-NOISE RESULTS FOR 55HZ AT 141DB (U)

AS-77-2861

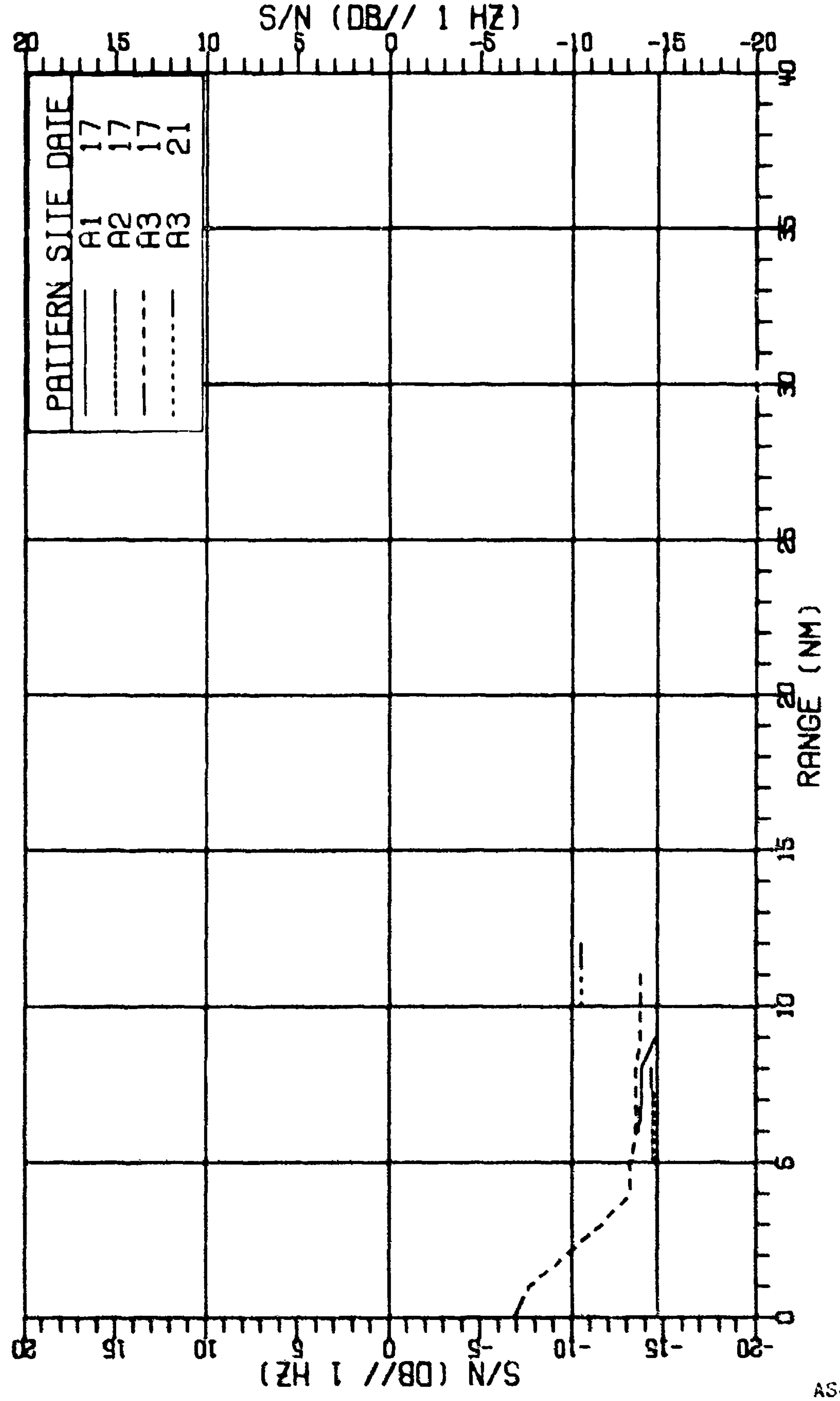

FIGURE III-262
MSS-FVT NEAR BOTTOM DIFFERENCED CARDIOIDS SENSOR
SIGNAL-TO-NOISE RESULTS FOR 55HZ AT 141DB (U)

AS-77-2860

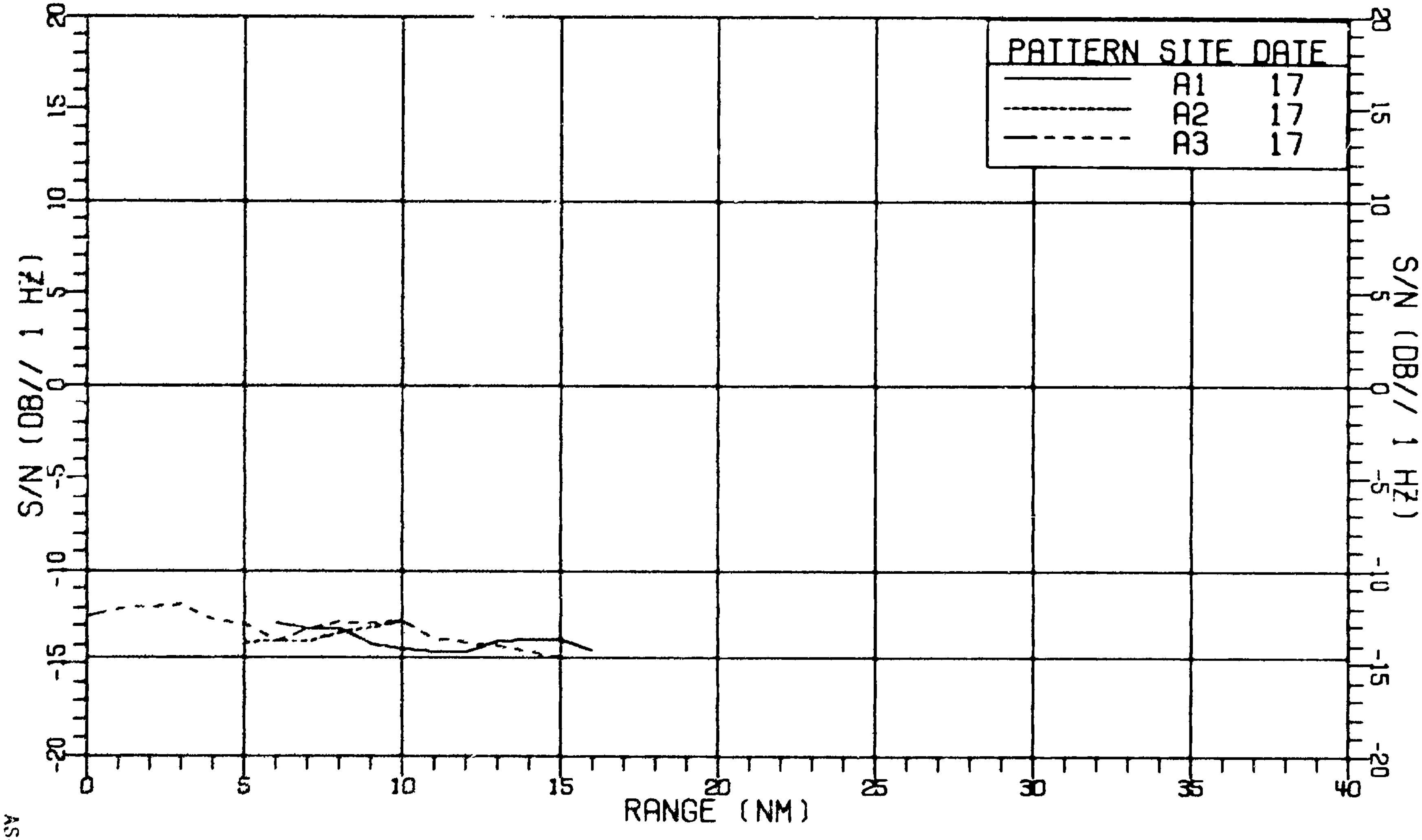

FIGURE III-263
MSS-FVT NEAR BOTTOM OMNIDIRECTIONAL SENSOR
SIGNAL-TO-NOISE RESULTS FOR 155HZ AT 134DB (U)

AS-77-2863

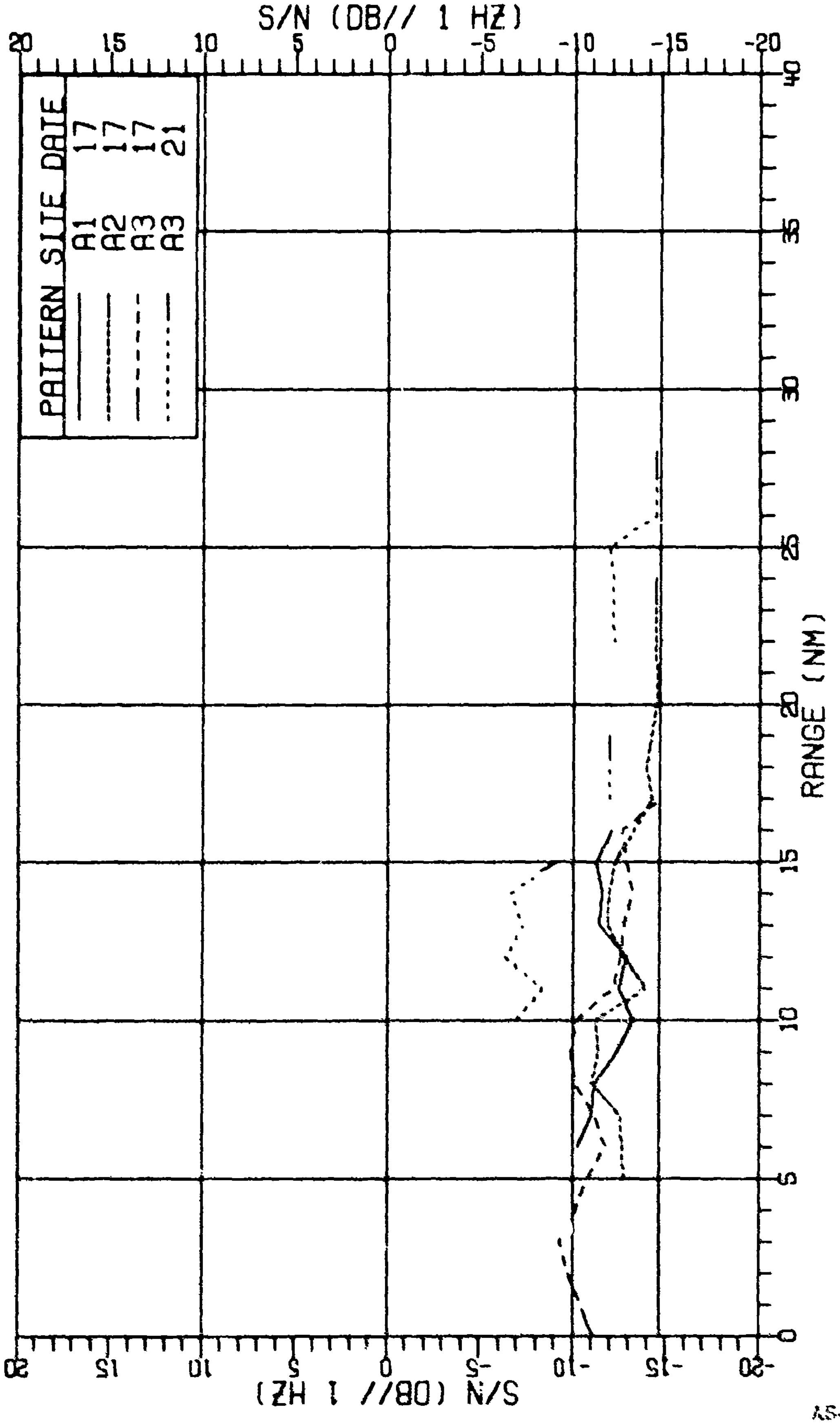

FIGURE III-264
MSS-FVT NEAR BOTTOM SINGLE CARDIOIDS SENSOR
SIGNAL-TO-NOISE RESULTS FOR 155HZ AT 134DB (U)

AS-77-2864

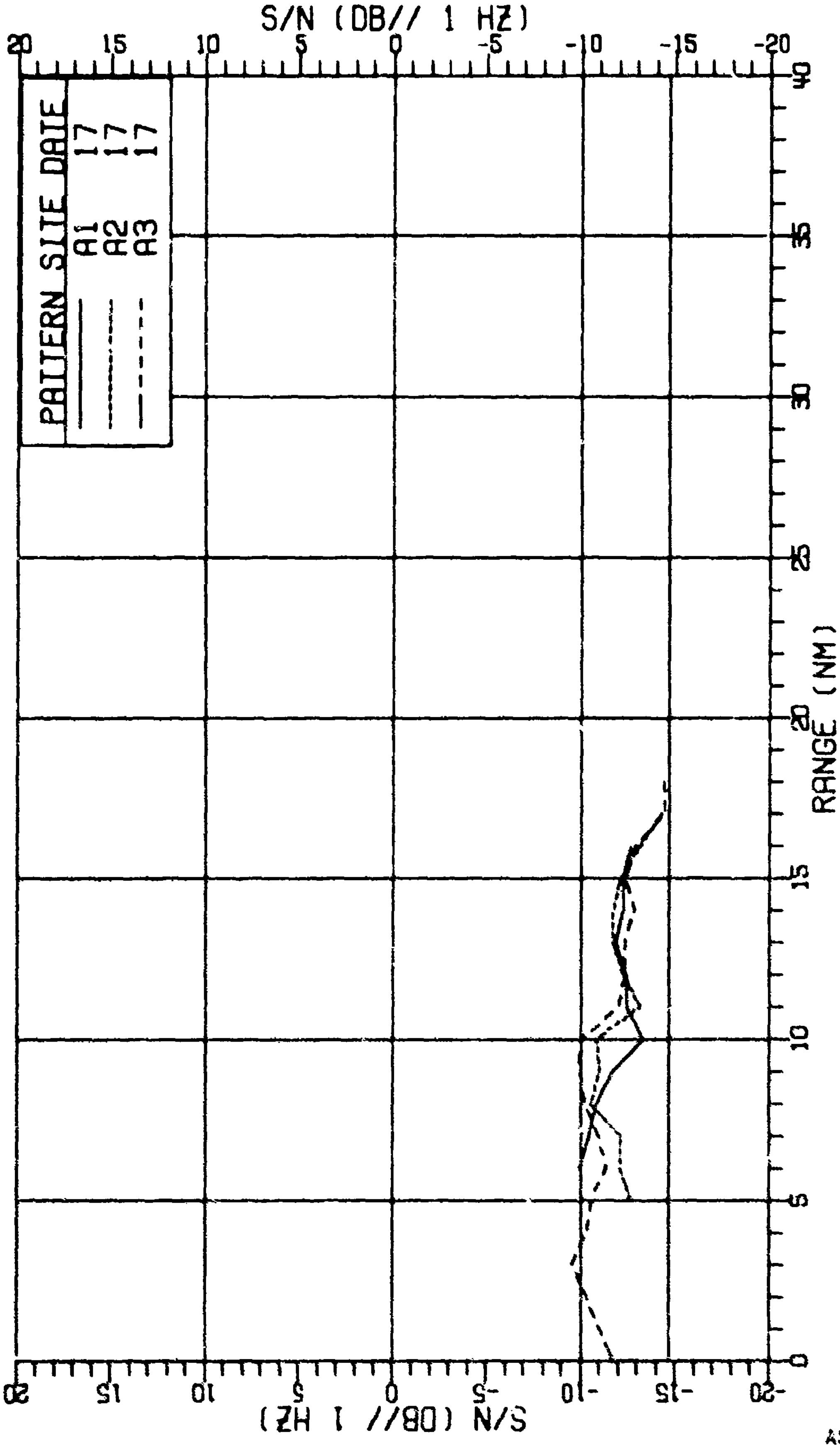

FIGURE III-265
MSS-FVT NEAR BOTTOM MAX GAIN LIMACONS SENSOR
SIGNAL-TO-NOISE RESULTS FOR 155HZ AT 134DB (U)

AS-77-2865

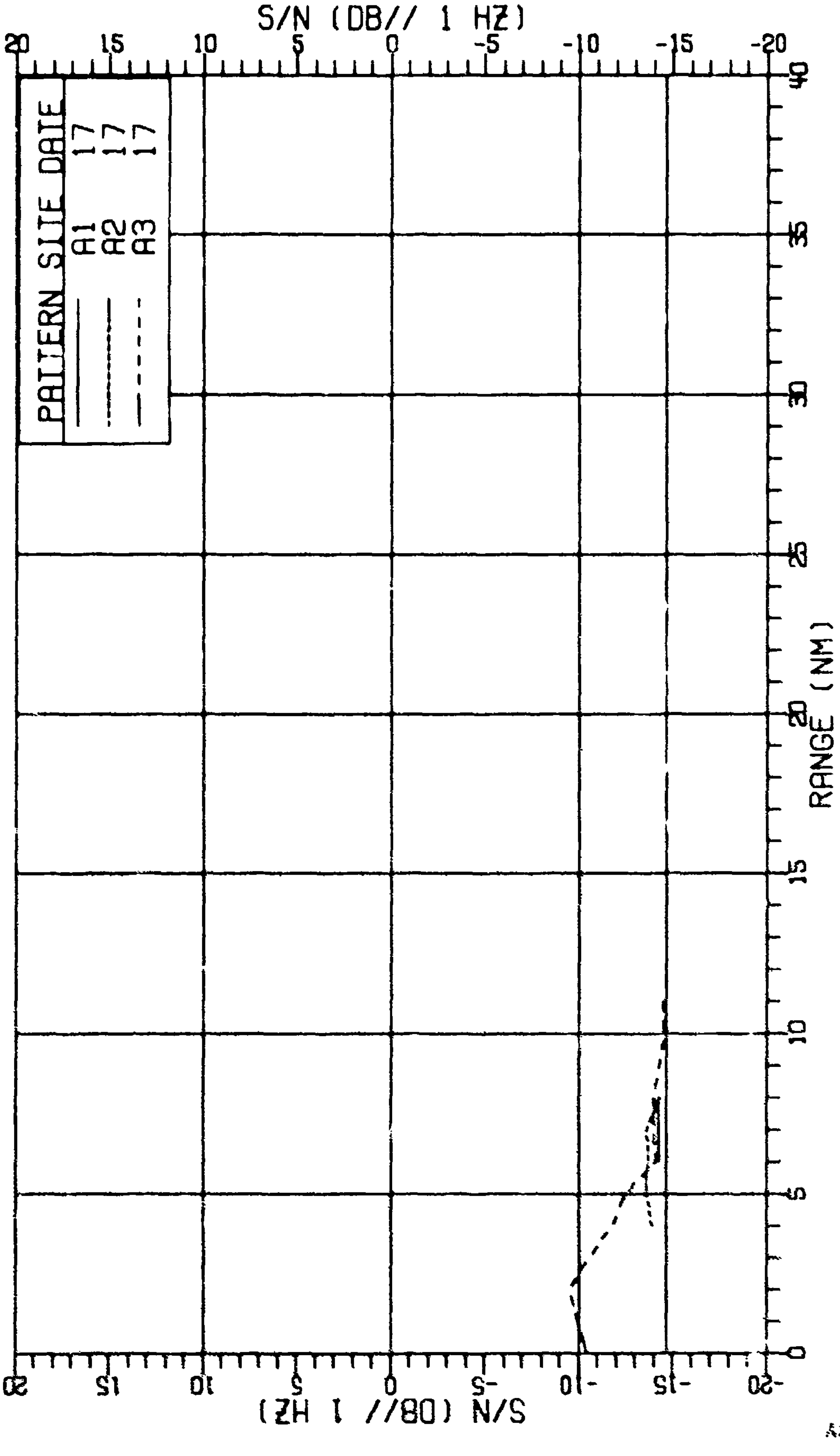

FIGURE III-266
MSS-FVT NEAR BOTTOM VERTICAL DIPOLE SENSOR
SIGNAL-TO-NOISE RESULTS FOR 155HZ AT 134DB (U)

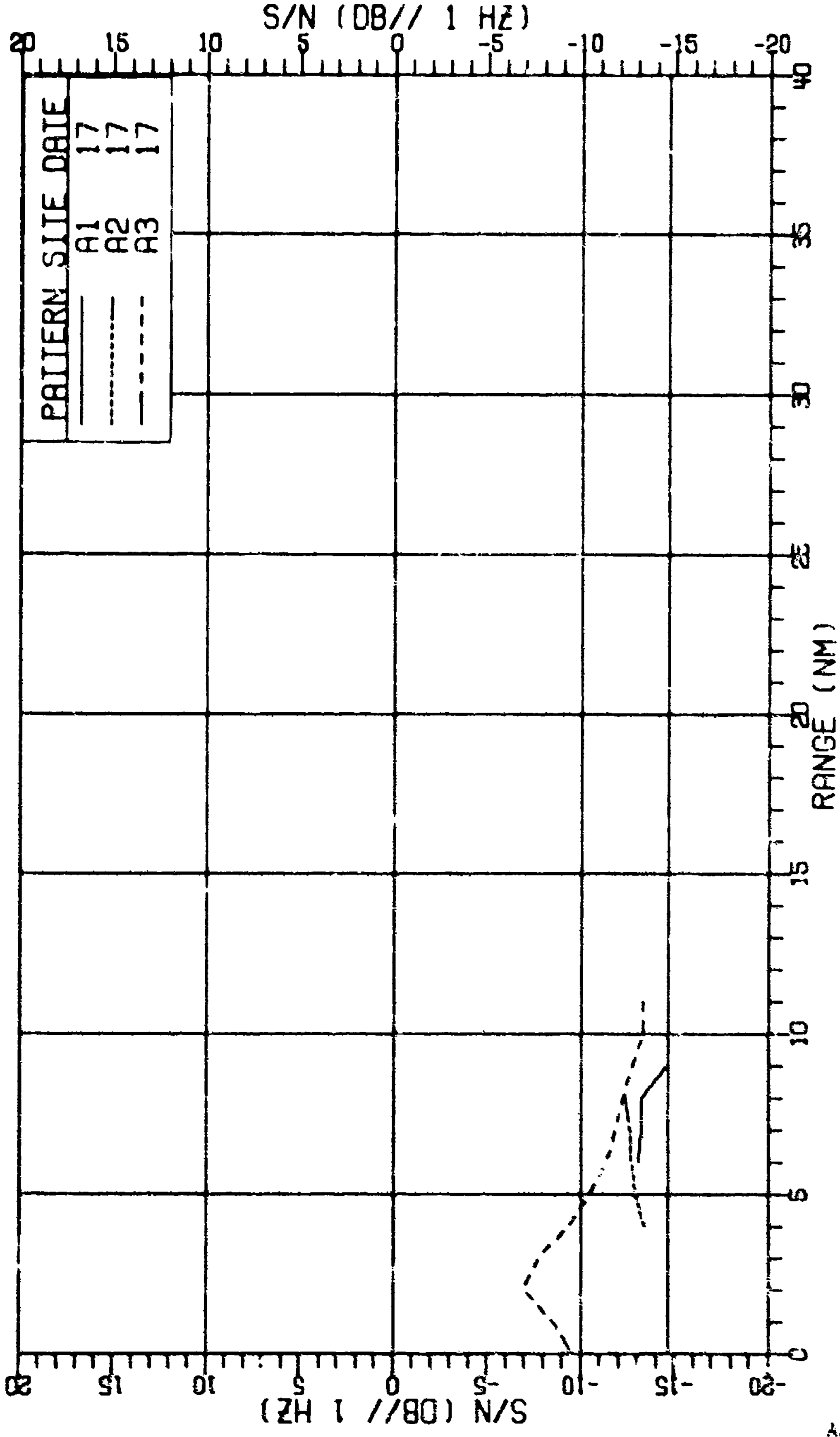

FIGURE III-267
MSS-FVT NEAR BOTTOM DIFFERENCED CARDIOIDS SENSOR
SIGNAL-TO-NOISE RESULTS FOR 155HZ AT 134DB (U)

AS-77-2867

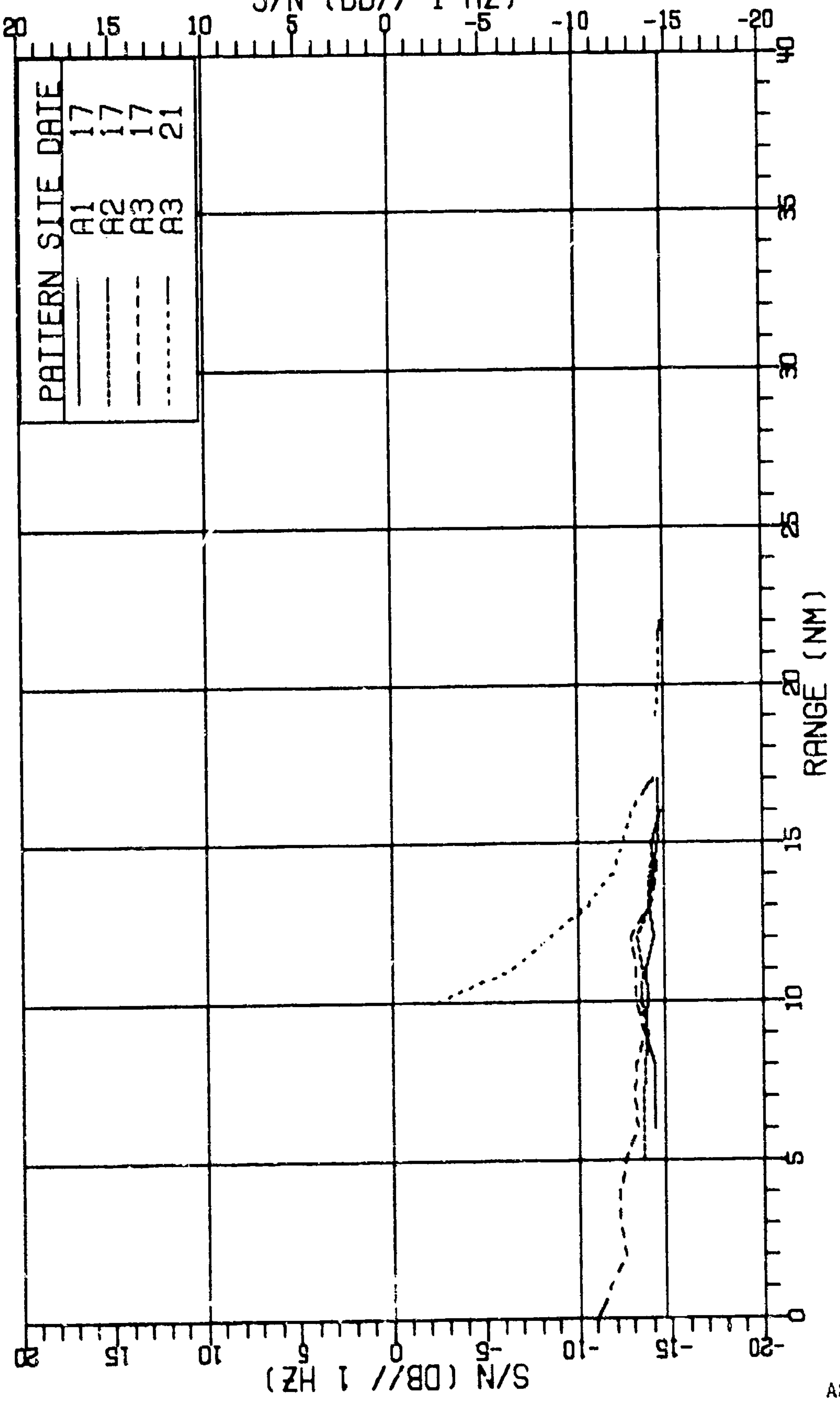

FIGURE III-268
MSS-FVT NEAR BOTTOM OMNIDIRECTIONAL SENSOR
SIGNAL-TO-NOISE RESULTS FOR 305HZ AT 136DB (U)

AS-77-2868

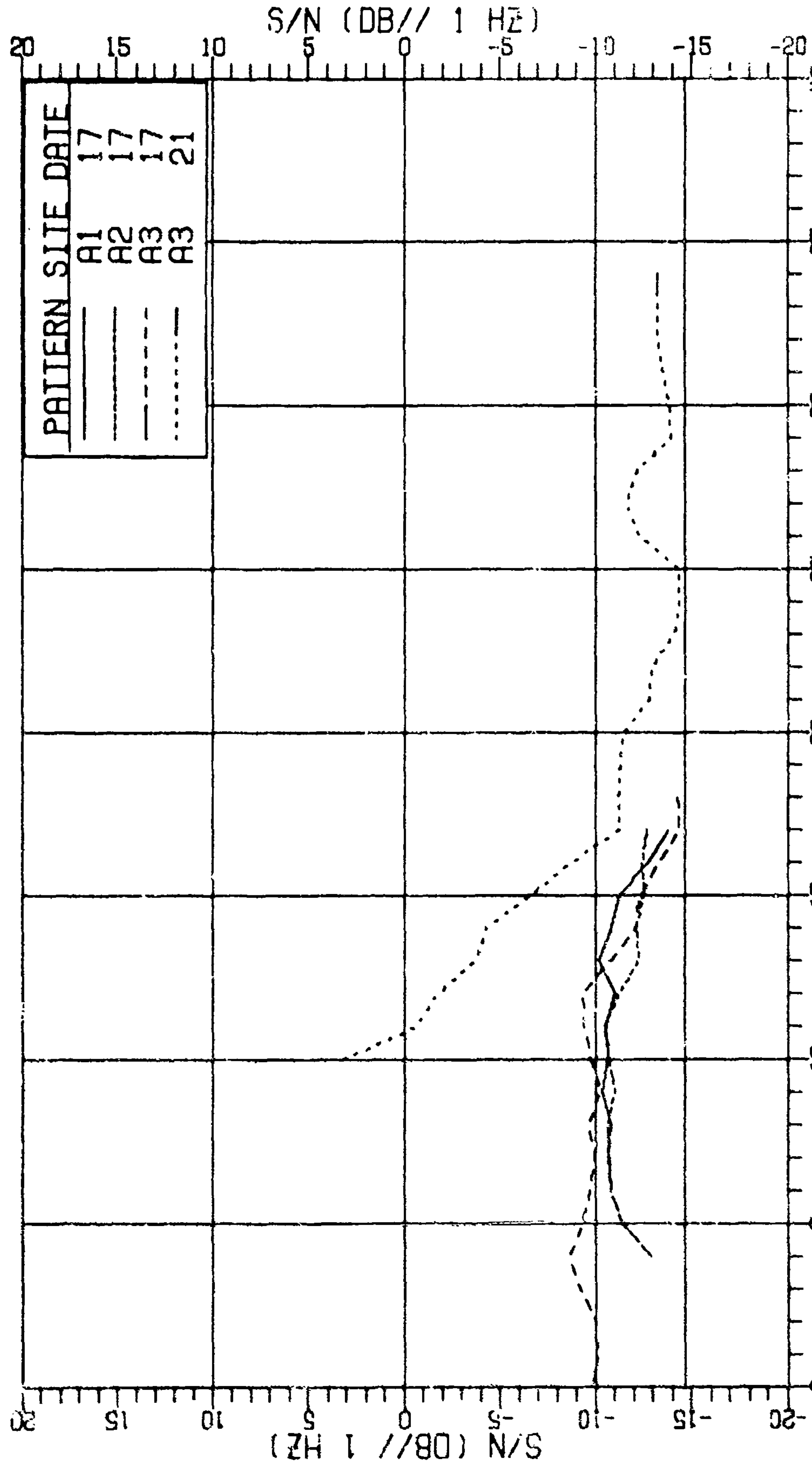

FIGURE III-269
MSS-FVT NEAR BOTTOM SINGLE CARDIOIDS SENSOR
SIGNAL-TO-NOISE RESULTS FOR 305HZ AT 136DB (U)

AS-77-2869

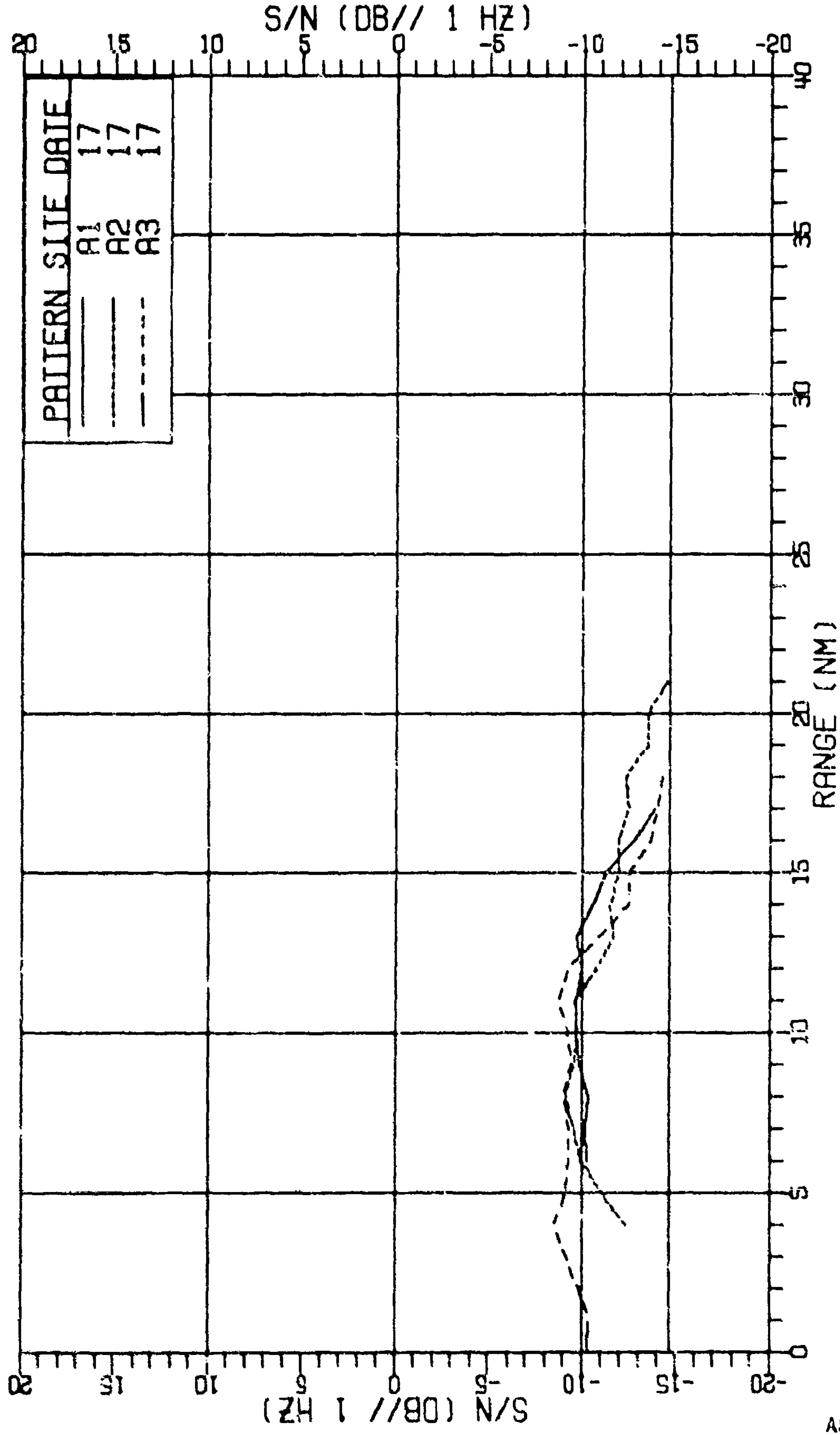

FIGURE III-270
MSS-FVT NEAR BOTTOM MAX GAIN LIMACONS SENSOR
SIGNAL-TO-NOISE RESULTS FOR 305HZ AT 136DB (U)

AS-77-2870

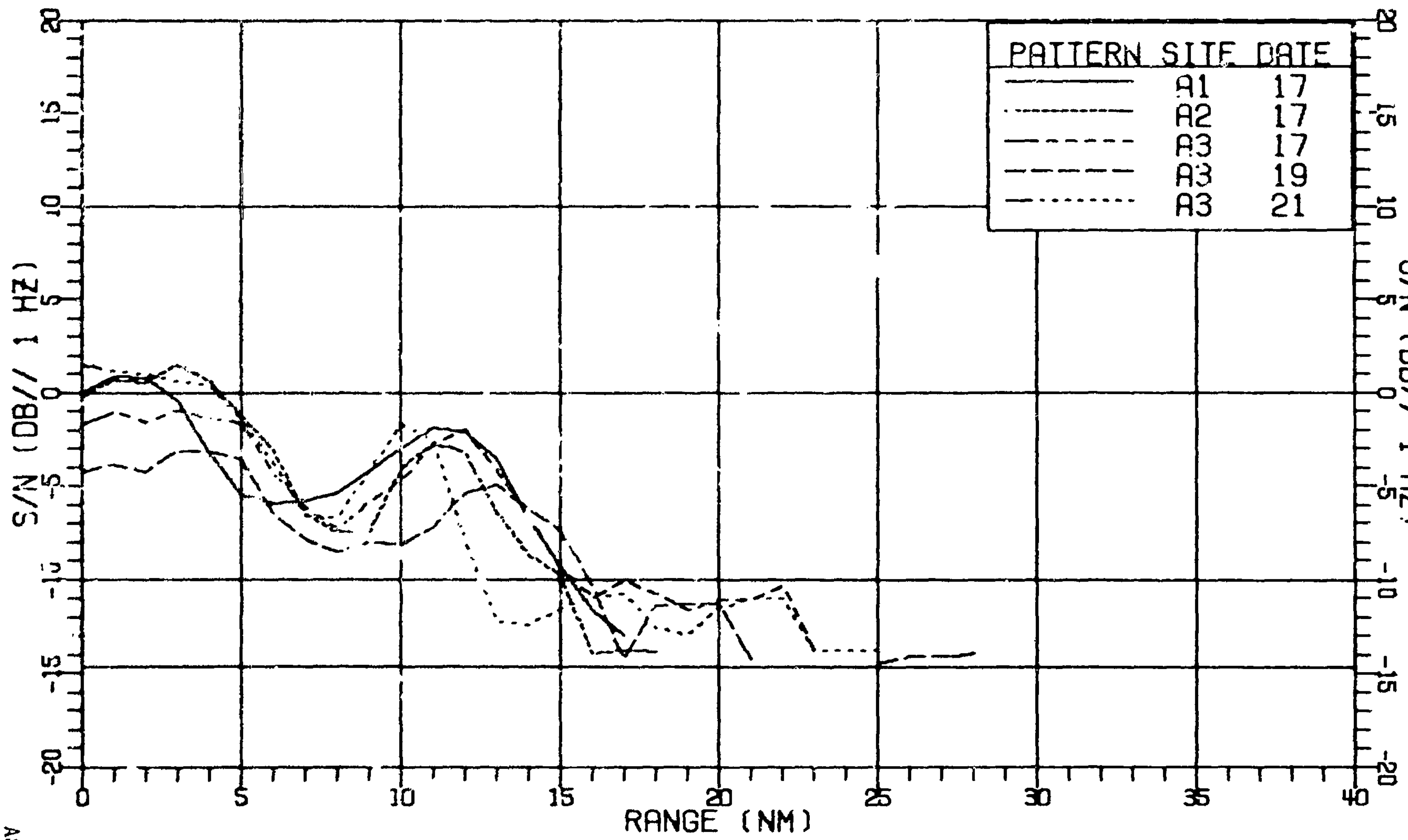

FIGURE III-271
MSS-FVT NEAR BOTTOM OMNIDIRECTIONAL SENSOR
SIGNAL-TO-NOISE RESULTS FOR 64HZ AT 162DB (U)

AS-77-2871

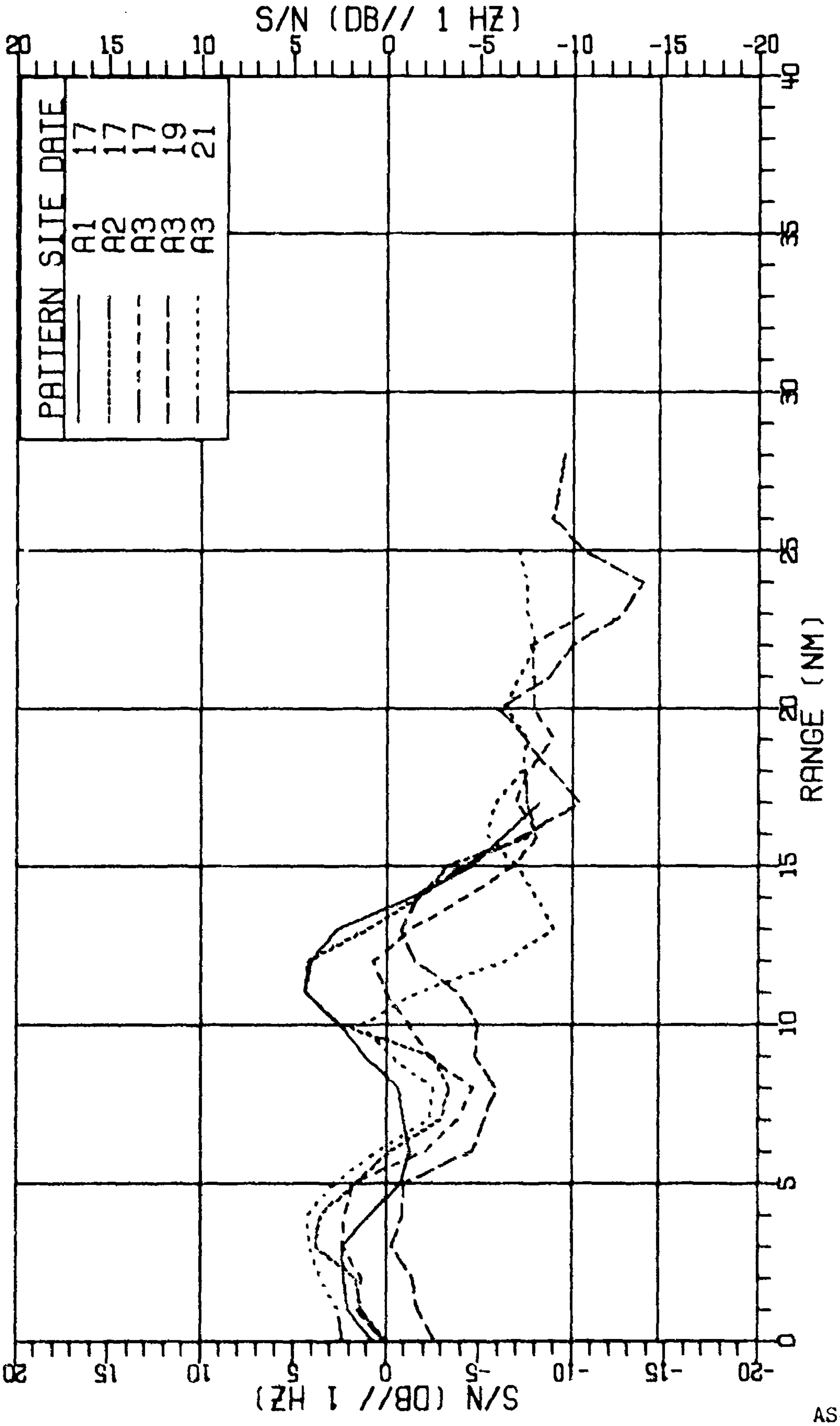

FIGURE III-272
MSS-FVT NEAR BOTTOM SINGLE CARDIOIDS SENSOR
SIGNAL-TO-NOISE RESULTS FOR 64HZ AT 162DB (U)

AS-77-2872

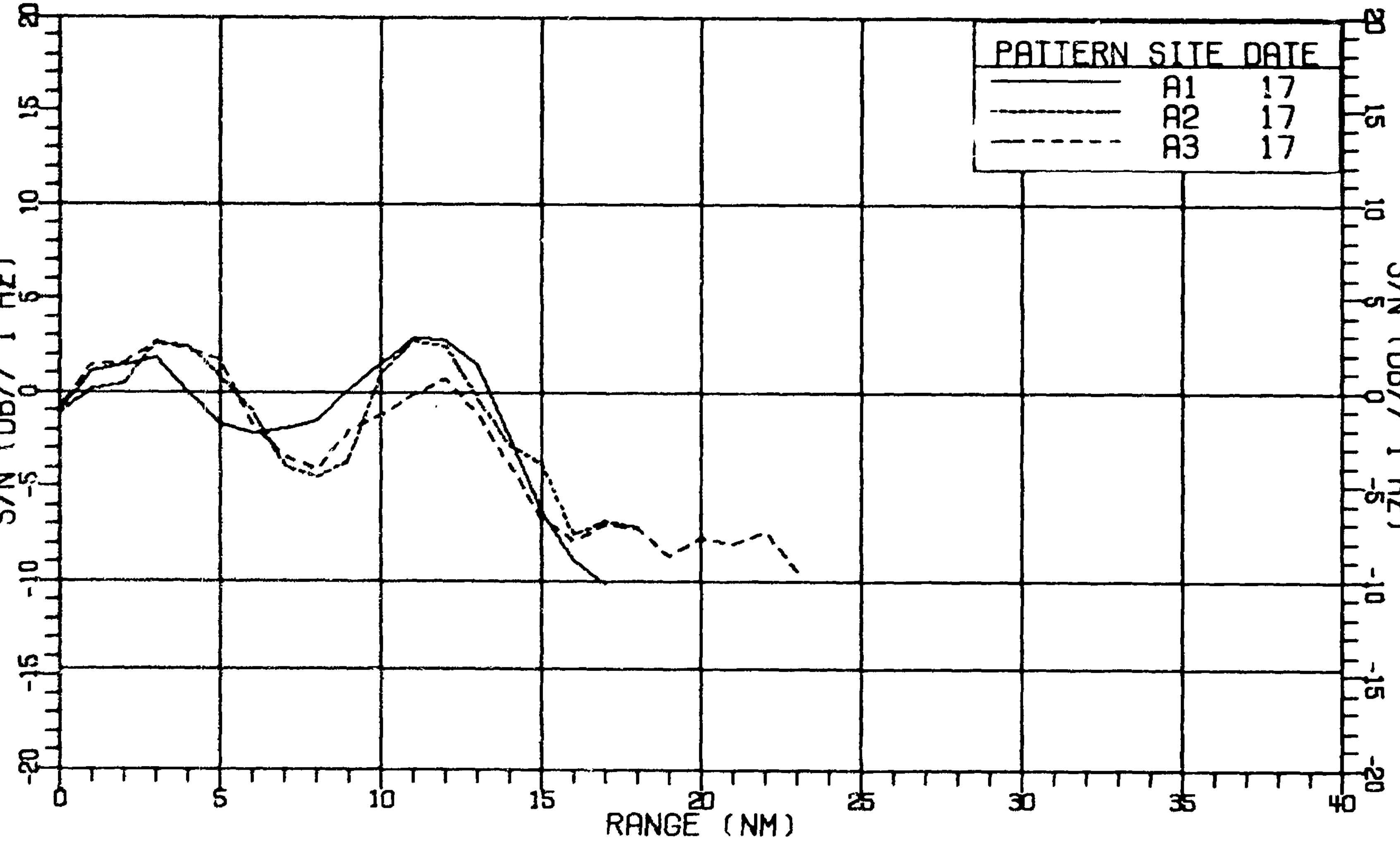

FIGURE III-273
MSS-FVT NEAR BOTTOM MAX GAIN LIMACONS SENSOR
SIGNAL-TO-NOISE RESULTS FOR 64HZ AT 162DB (U)

AS-77-2873

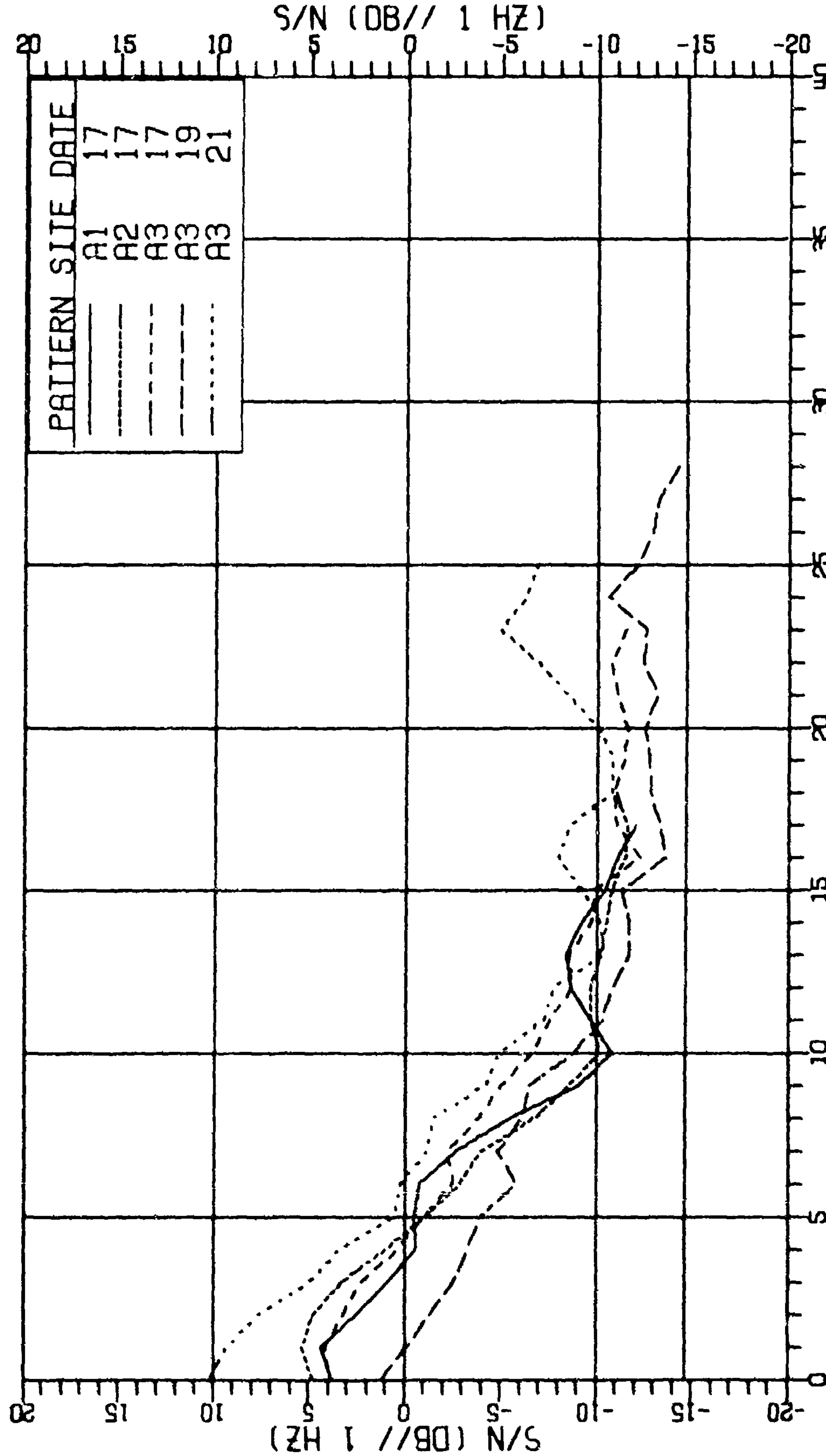

FIGURE III-274
MSS-FVT NEAR BOTTOM VERTICAL DIPOLE SENSOR
SIGNAL-TO-NOISE RESULTS FOR 64HZ AT 162DB (U)

AS-77-2874

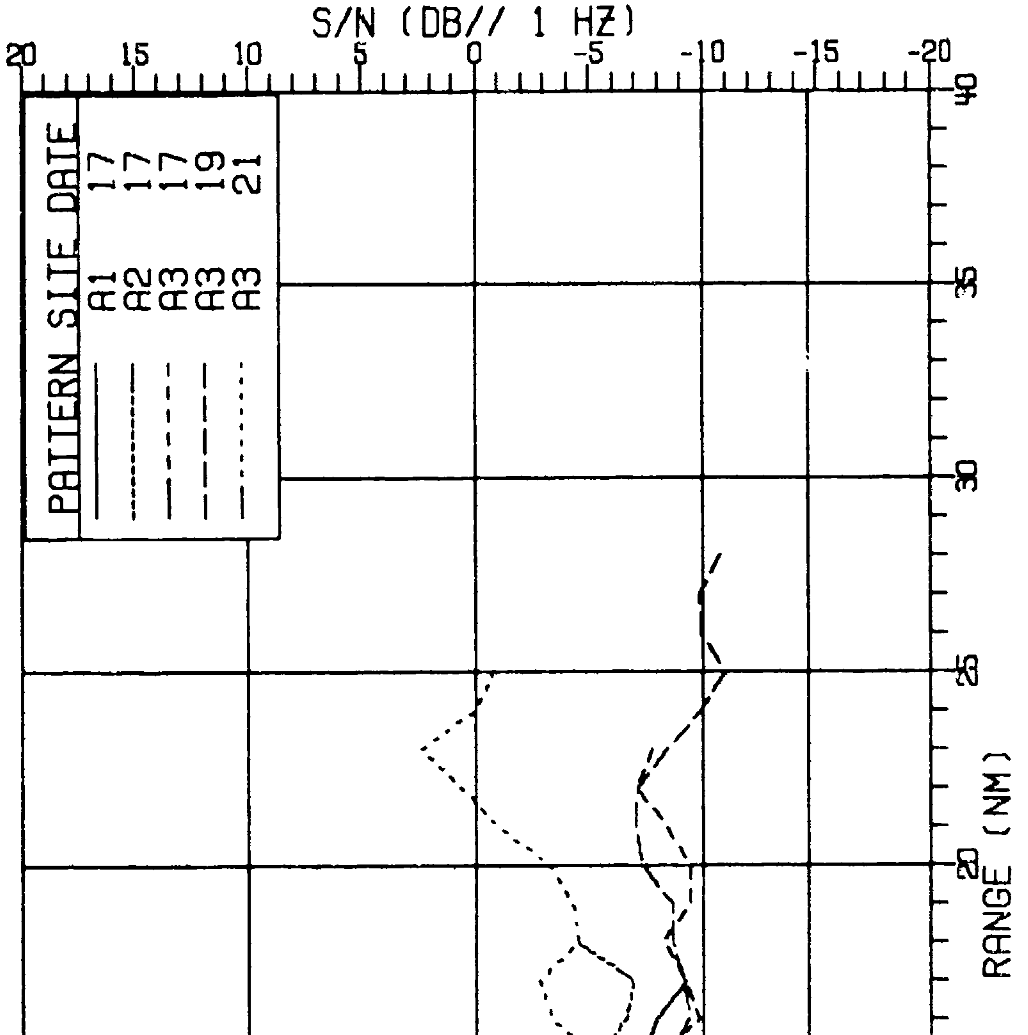

FIGURE III-275
MSS-FVT NEAR BOTTOM DIFFERENCED CARDIOIDS SENSOR
SIGNAL-TO-NOISE RESULTS FOR 64HZ AT 162DB (U)

AS-77-2875

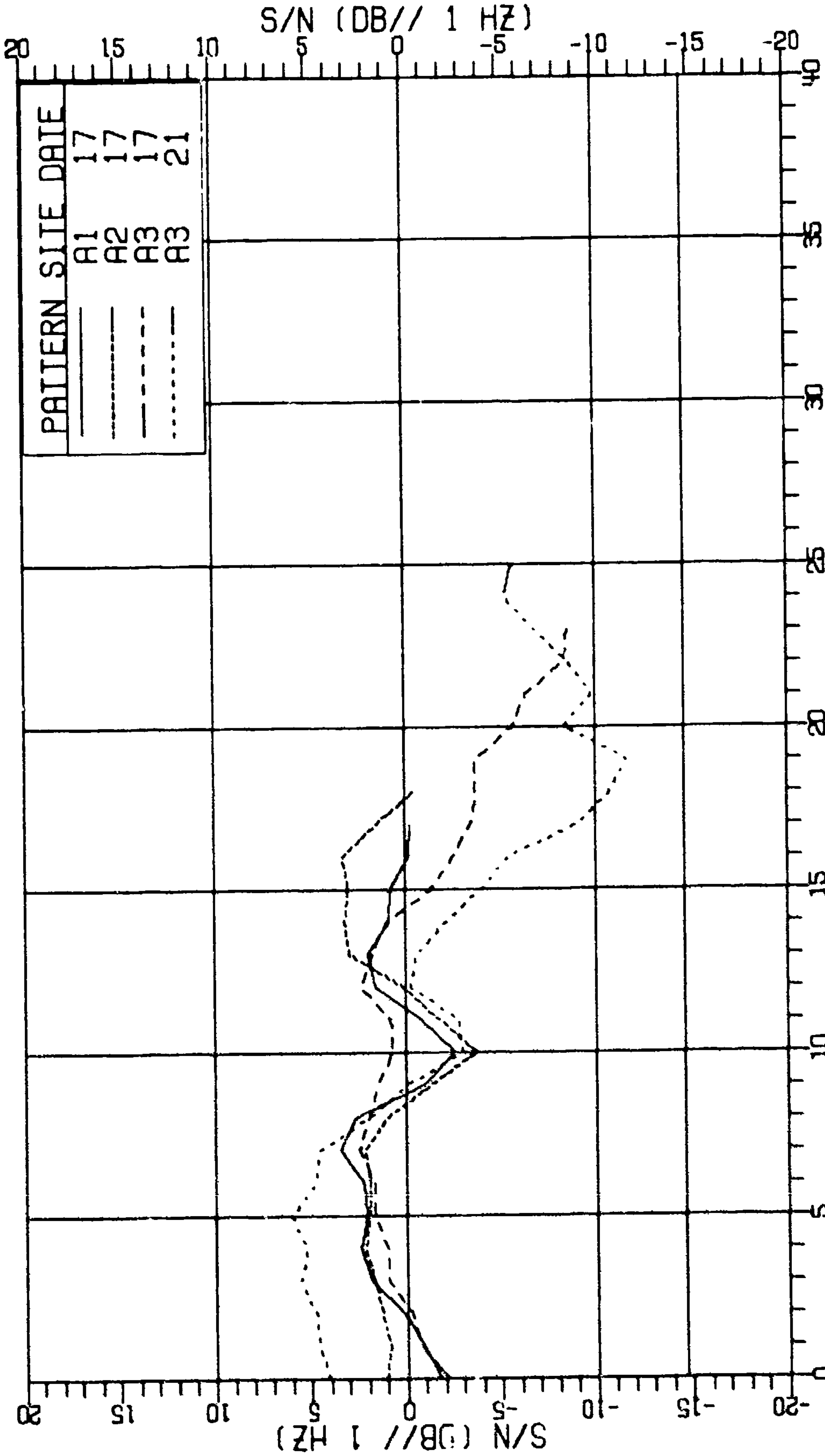

FIGURE III-276
MSS-FVT NEAR BOTTOM OMNIDIRECTIONAL SENSOR
SIGNAL-TO-NOISE RESULTS FOR 160HZ AT 161DB (U)

AS-77-2876

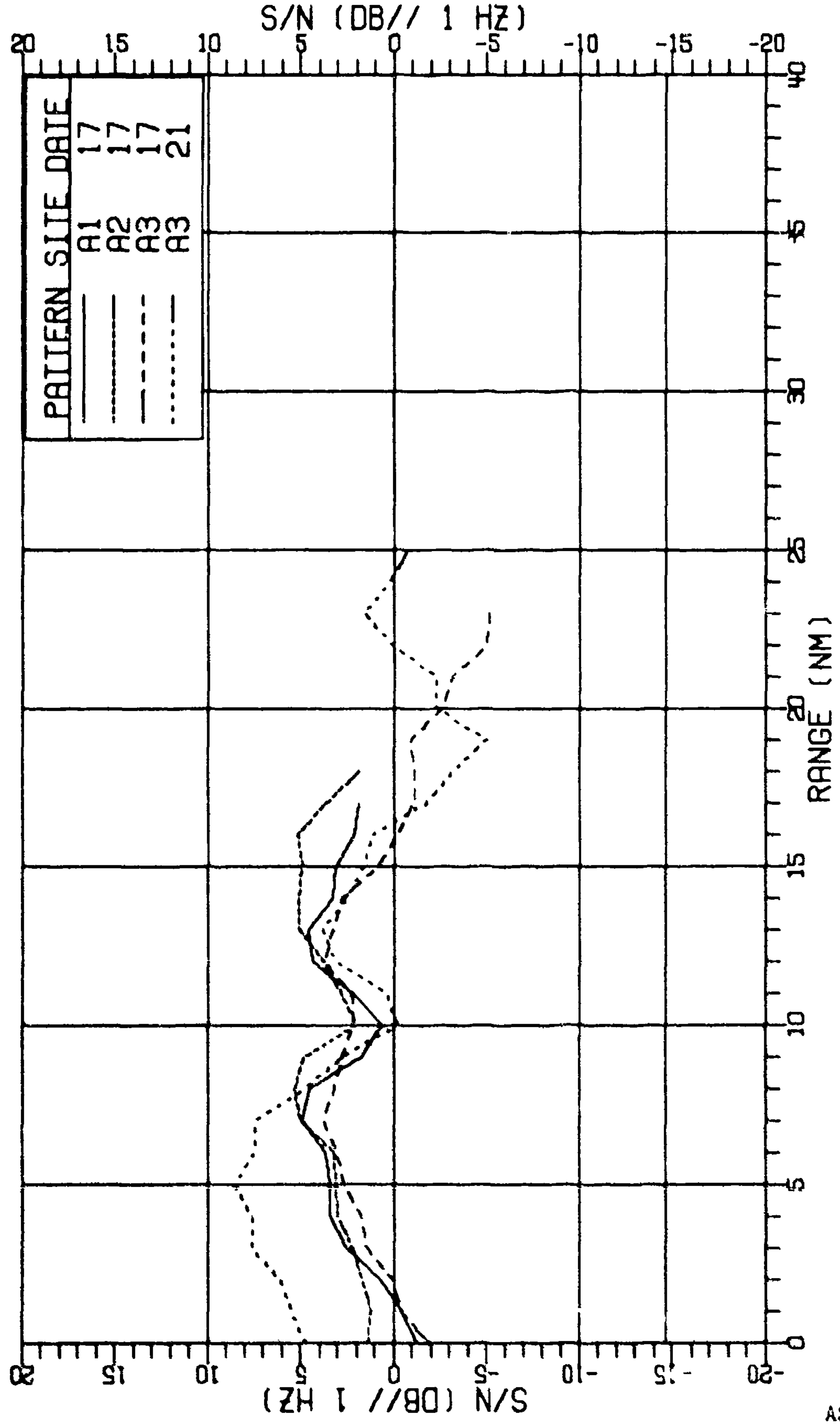

FIGURE III-277
MSS-FVT NEAR BOTTOM SINGLE CARDIOIDS SENSOR
SIGNAL-TO-NOISE RESULTS FOR 160HZ AT 161DB (U)

AS-77-2877

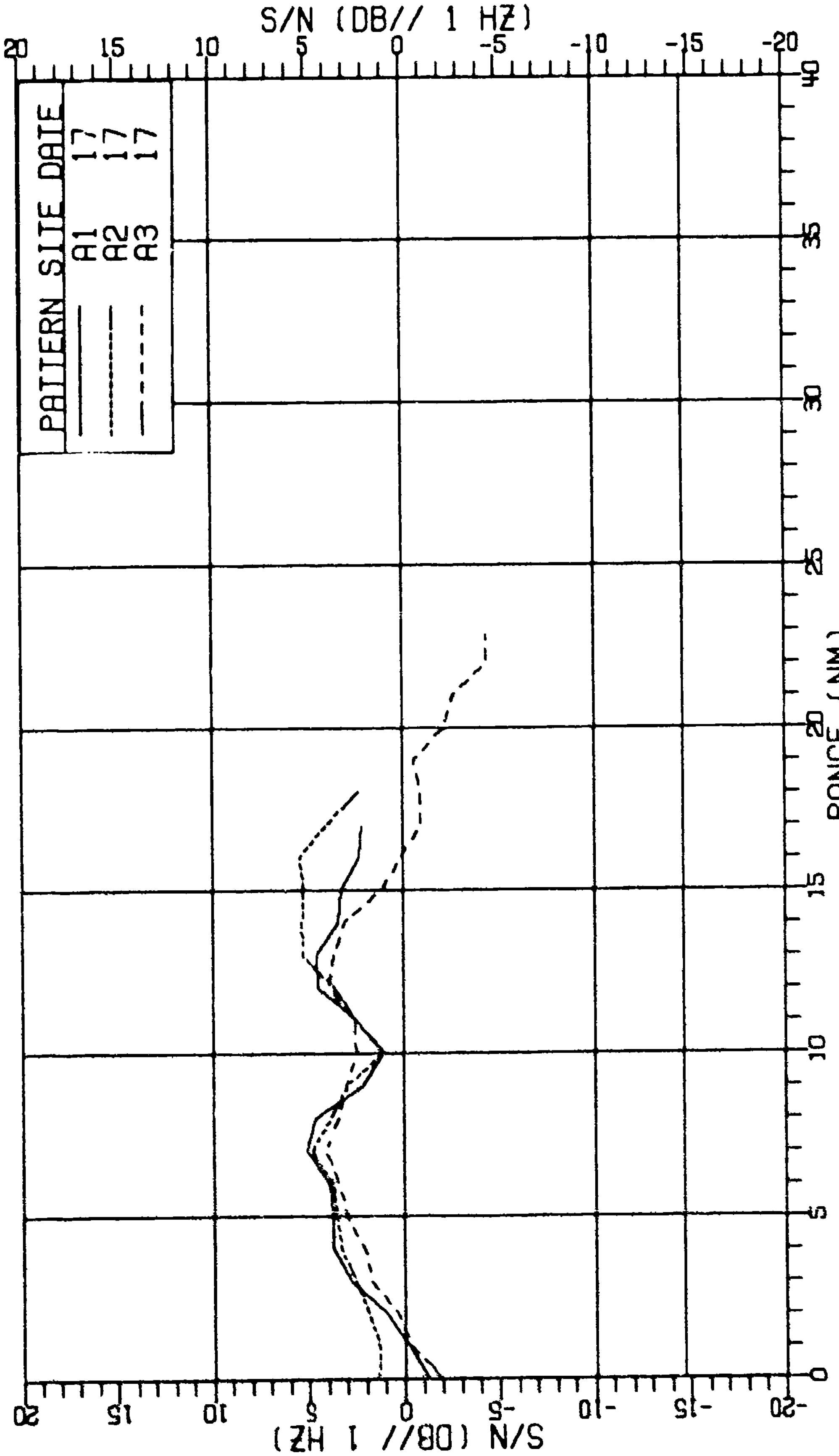

FIGURE III-278
MSS-FVT NEAR BOTTOM MAX GAIN LIMACONS SENSOR
SIGNAL-TO-NOISE RESULTS FOR 160HZ AT 161DB (U)

AS-77-2878

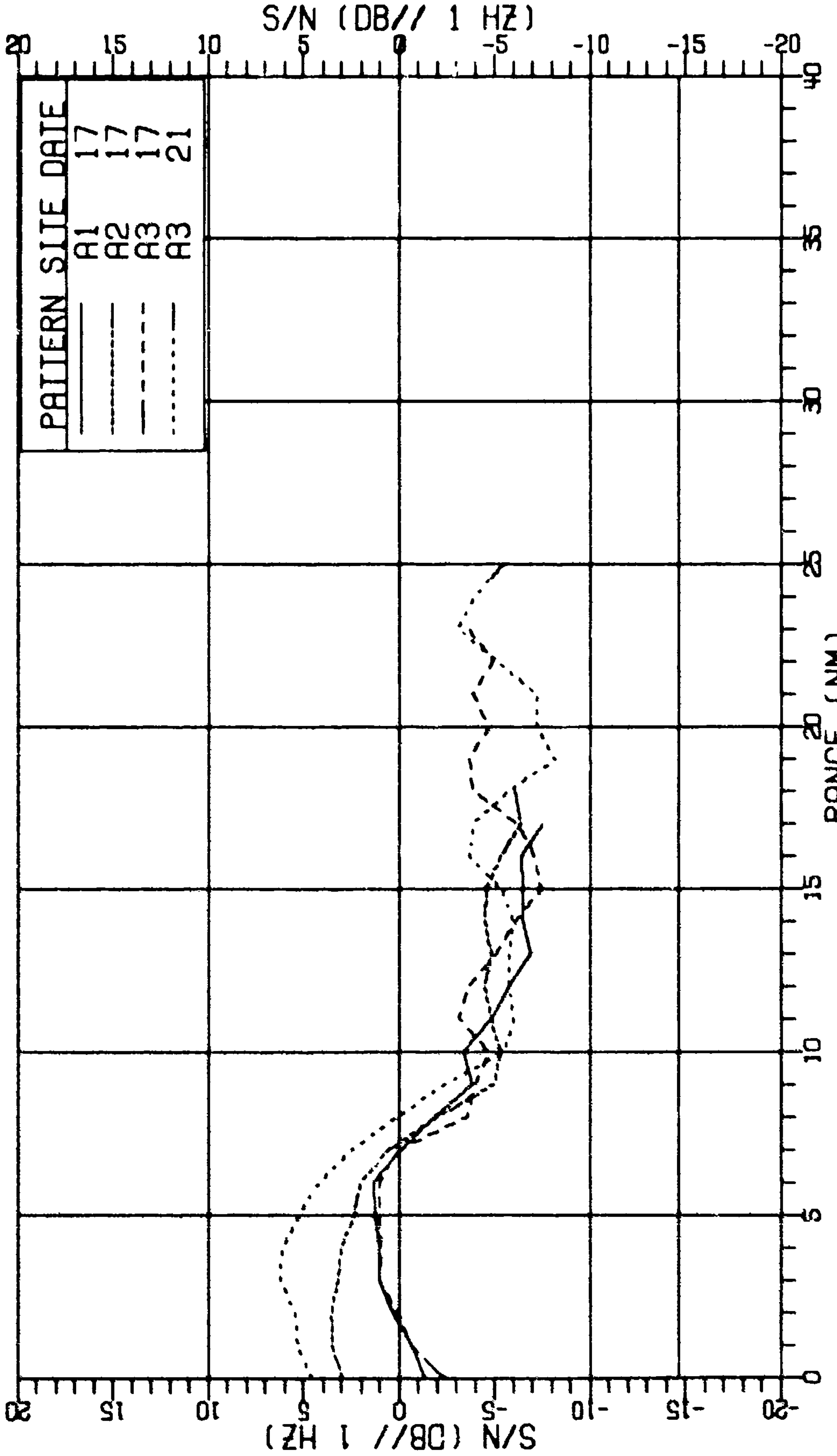

FIGURE III-279
MSS-FVT NEAR BOTTOM VERTICAL DIPOLE SENSOR
SIGNAL-TO-NOISE RESULTS FOR 160HZ AT 161DB (U)

AS-77-2879

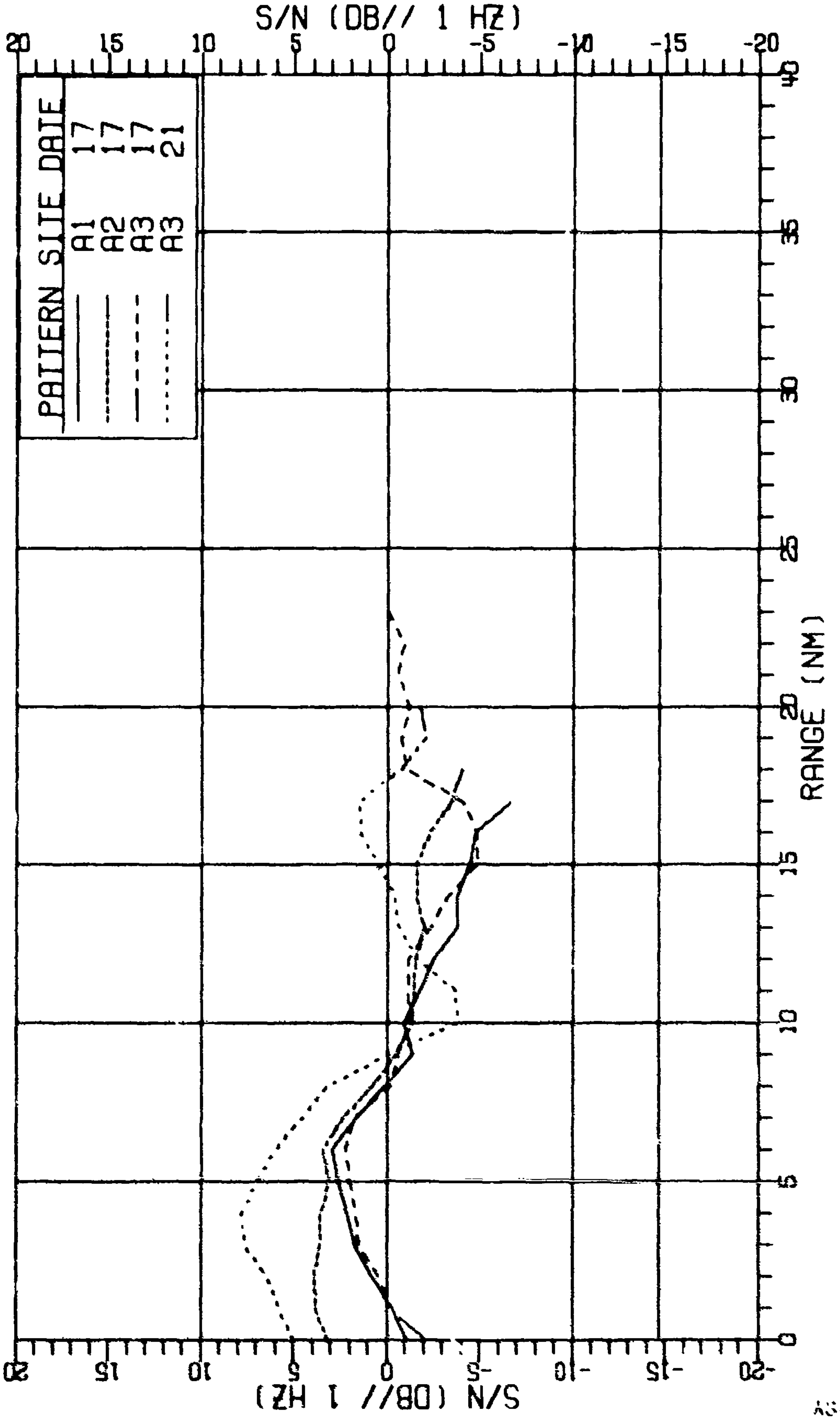

FIGURE III-280
MSS-FVT NEAR BOTTOM DIFFERENCED CARDIOIDS SENSOR
SIGNAL-TO-NOISE RESULTS FOR 160HZ AT 161DB (U)

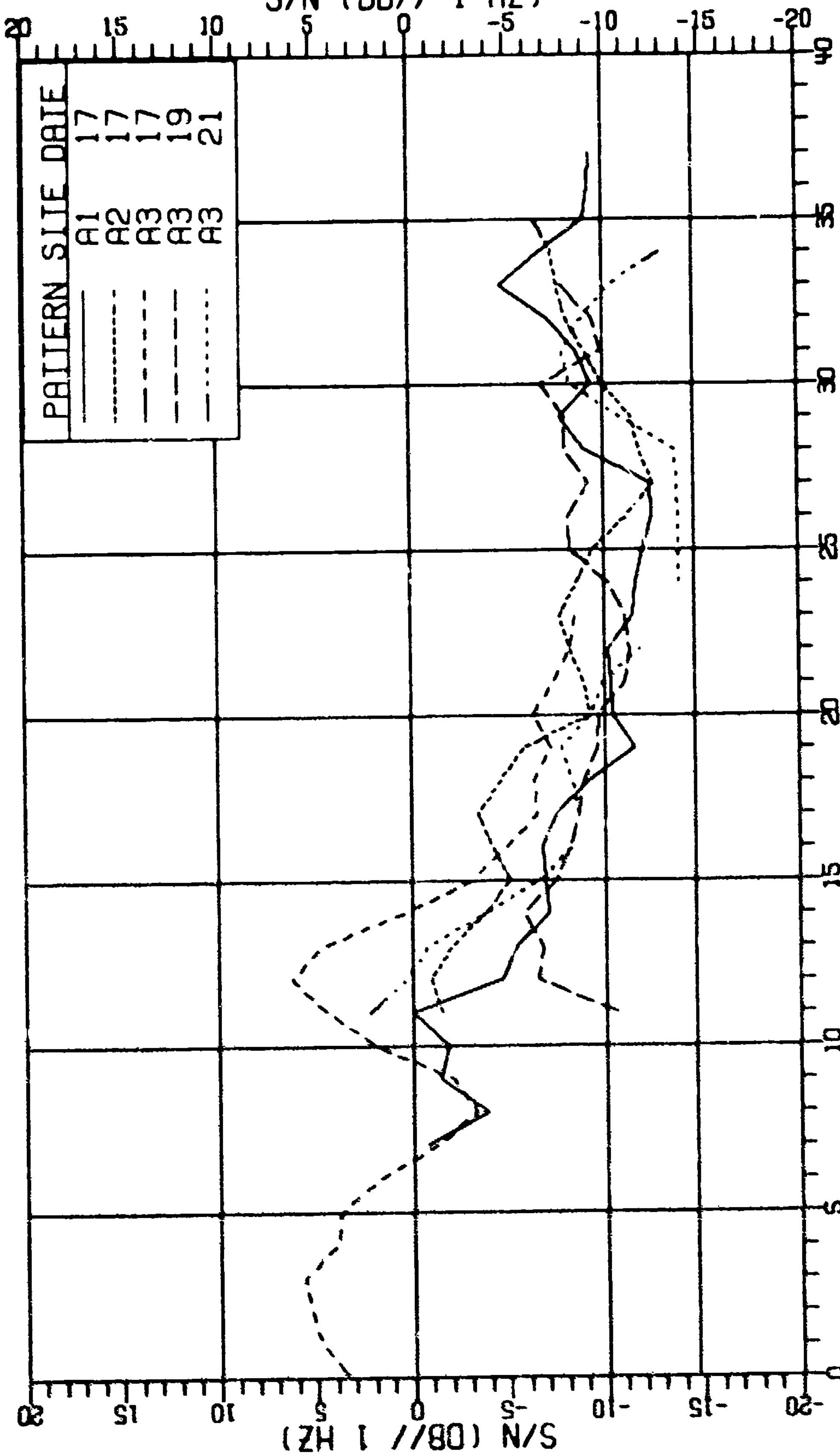

FIGURE III-281
MSS-FVT NEAR BOTTOM OMNIDIRECTIONAL SENSOR
SIGNAL-TO-NOISE RESULTS FOR 70HZ AT 166DB (U)

AS-77-2881

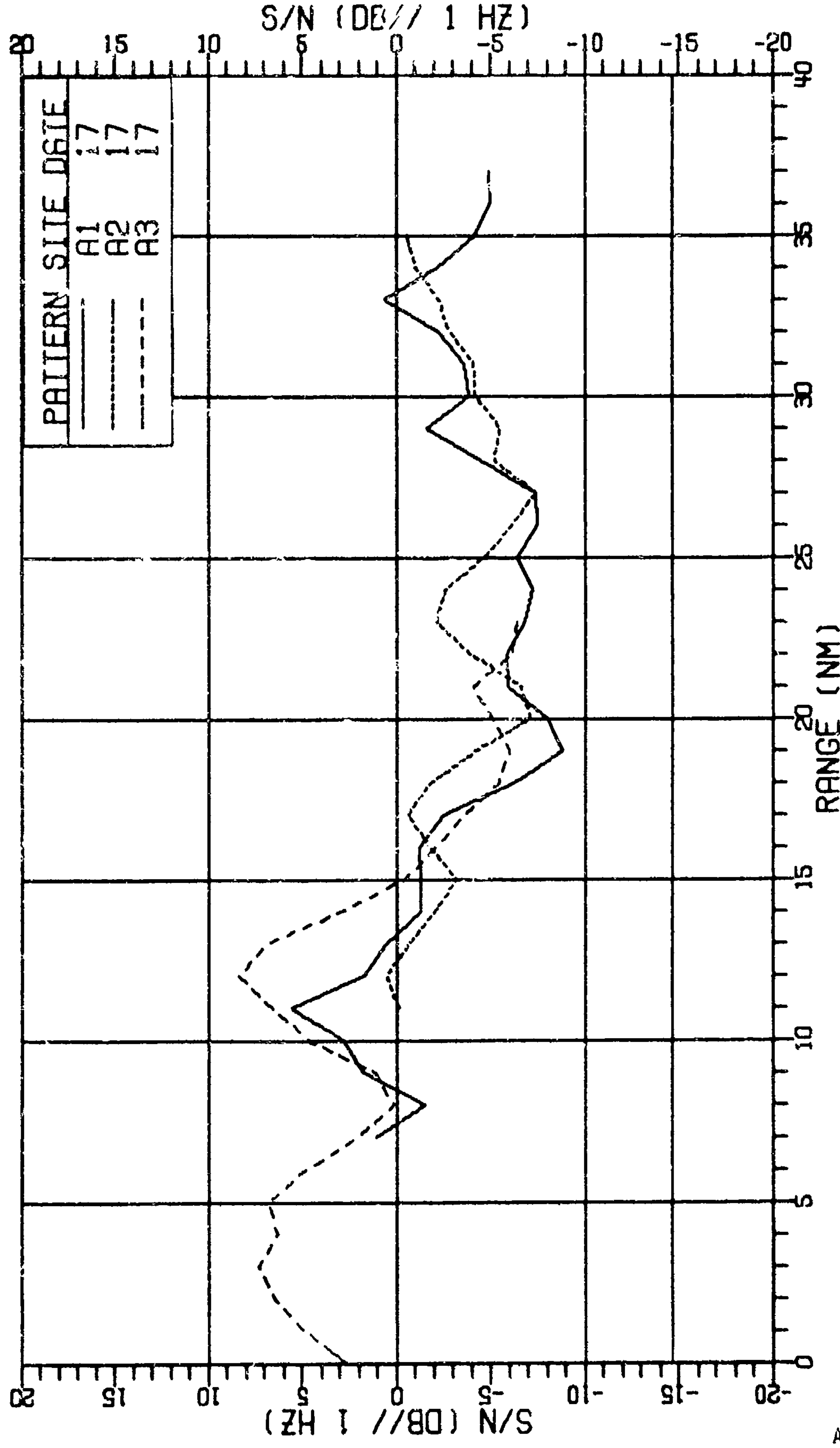

FIGURE III-283
MSS-FVT NEAR BOTTOM MAX GAIN LIMACONS SENSOR
SIGNAL-TO-NOISE RESULTS FOR 70HZ AT 166DB (U)

AS-77-2883

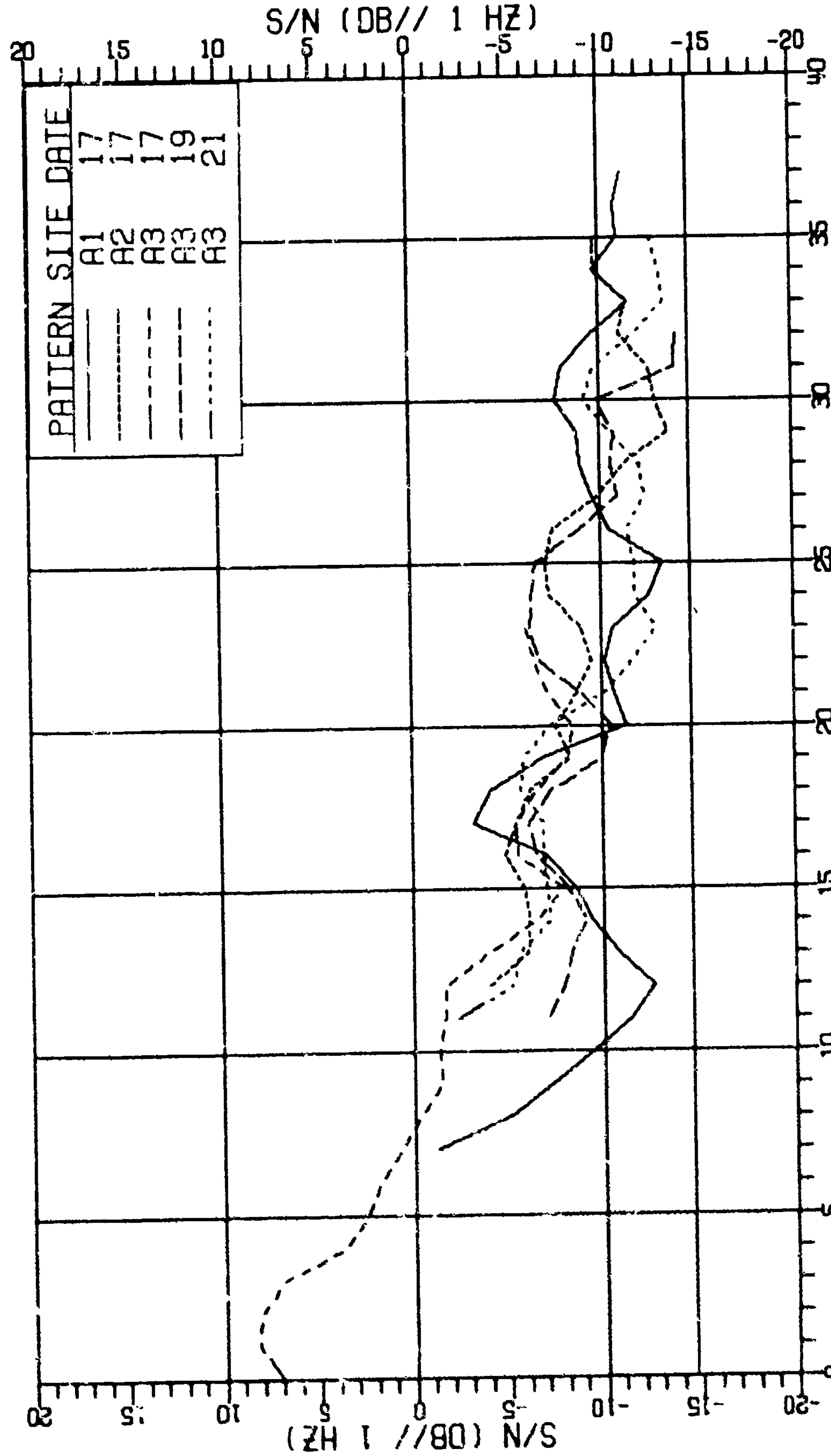

FIGURE III-284
MSS-FVT NEAR BOTTOM VERTICAL DIPOLE SENSOR
SIGNAL-TO-NOISE RESULTS FOR 70HZ AT 166DB (U)

AS-77-2884

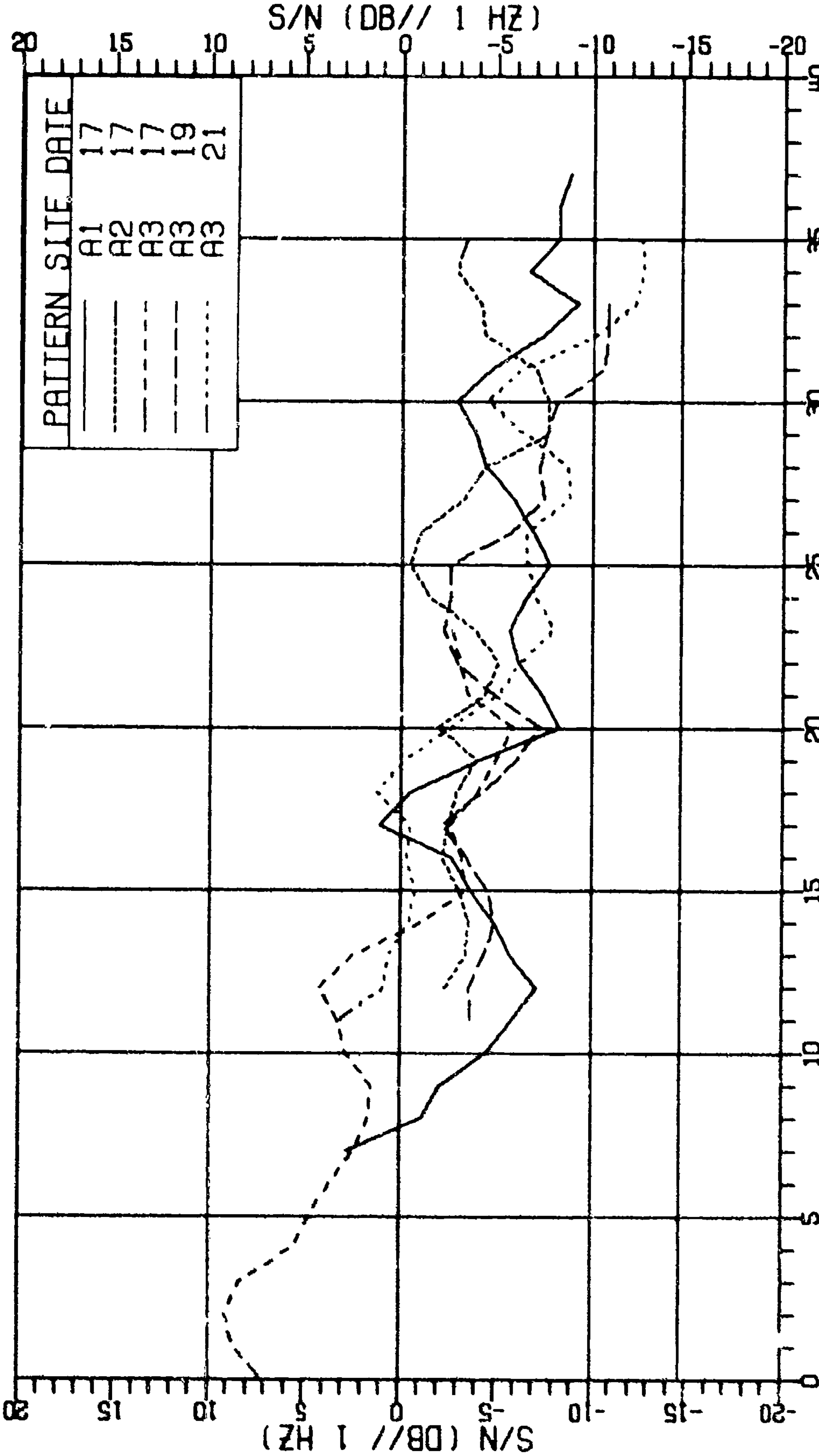

FIGURE III-285
MSS-FVT NEAR BOTTOM DIFFERENCED CARDIOIDS SENSOR
SIGNAL-TO-NOISE RESULTS FOR 70HZ AT 166DB (U)

AS-77-2885

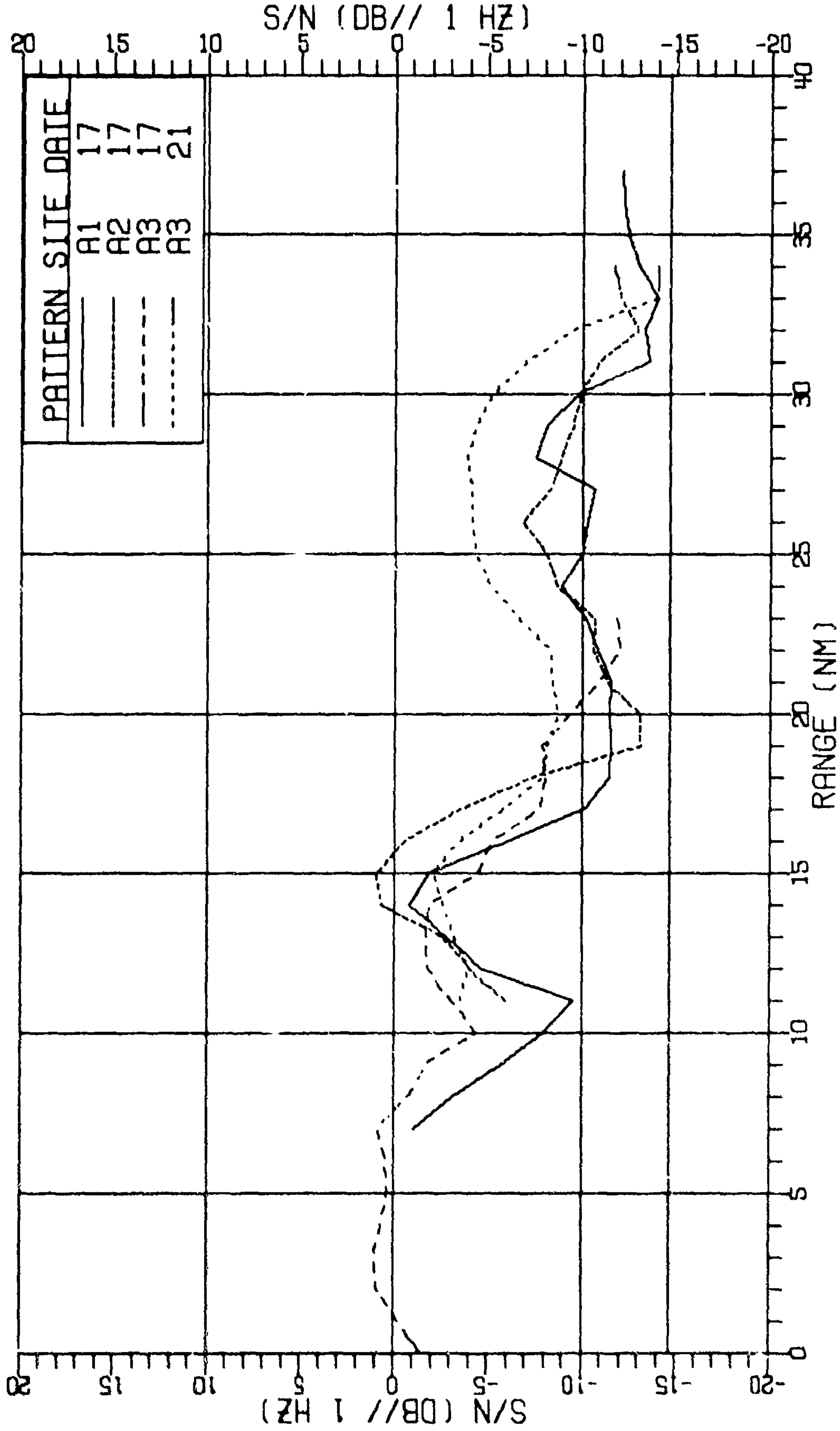

FIGURE III-286
MSS-FVT NEAR BOTTOM OMNIDIRECTIONAL SENSOR
SIGNAL-TO-NOISE RESULTS FOR 170HZ AT 156DB (U)

AS-77-2886

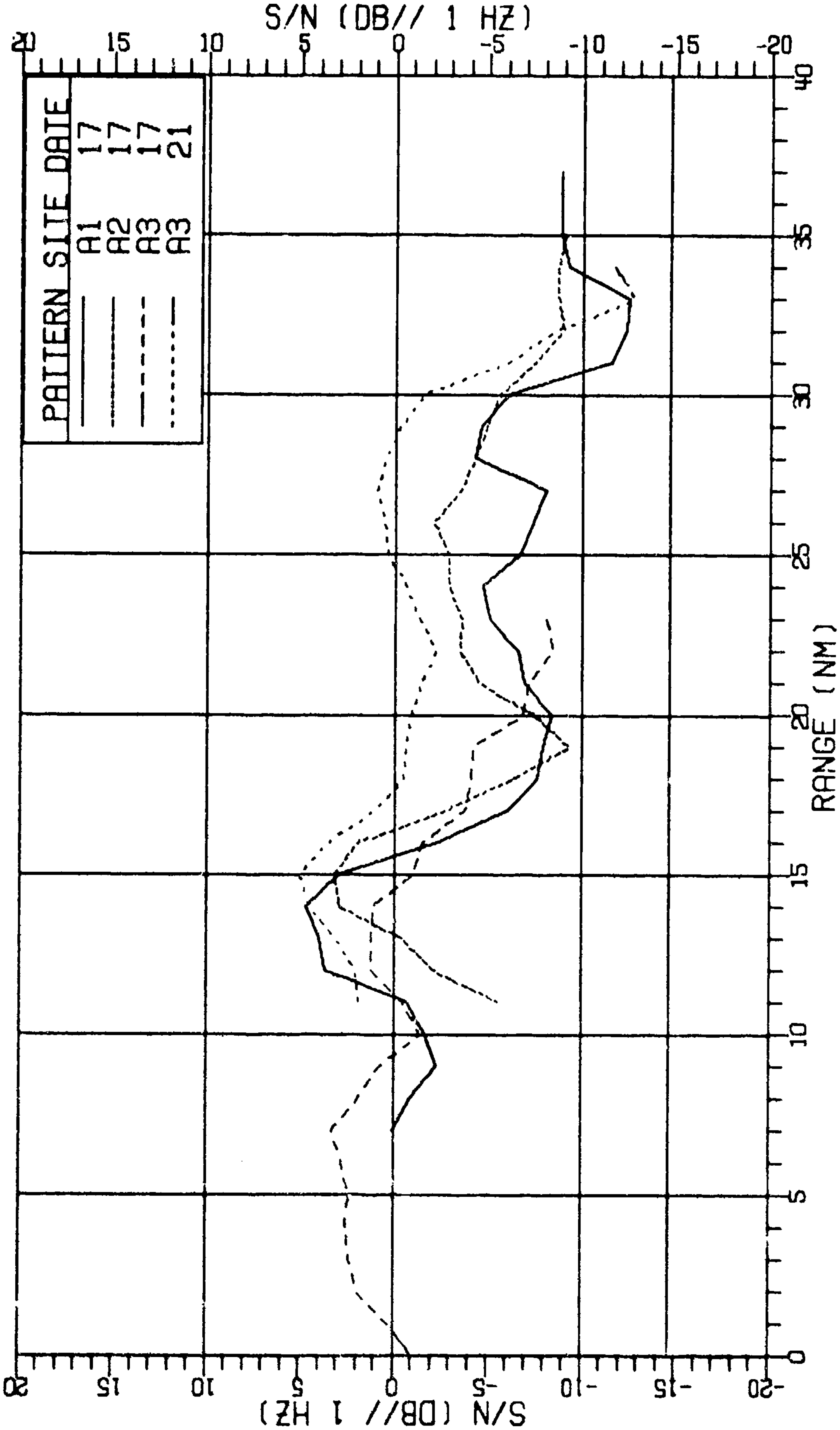

FIGURE III-287
MSS-FVT NEAR BOTTOM SINGLE CARDIOIDS SENSOR
SIGNAL-TO-NOISE RESULTS FOR 170HZ AT 156DB (U)

AS-77-2887

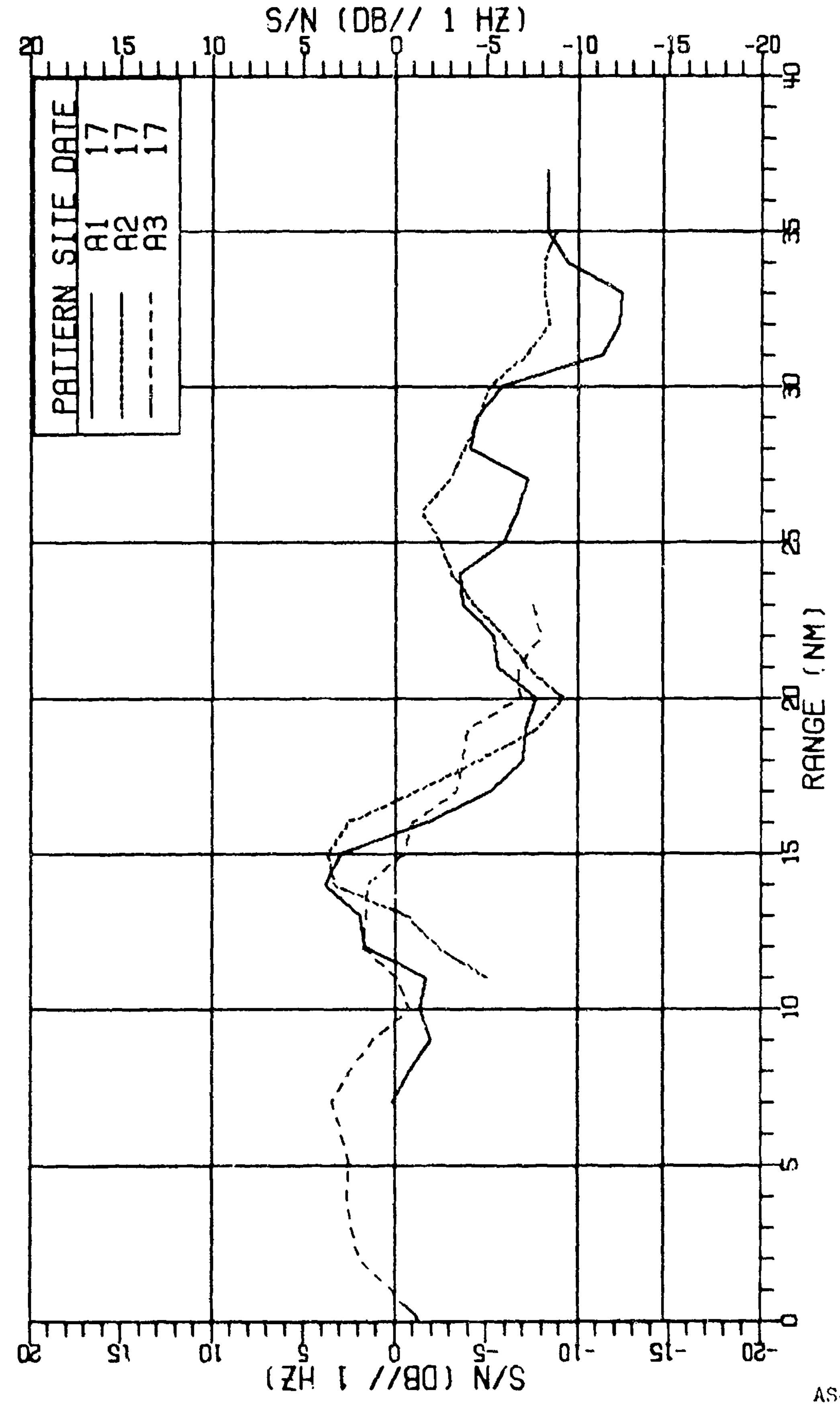

FIGURE III-288
MSS-FVT NEAR BOTTOM MAX GAIN LIMACONS SENSOR
SIGNAL-TO-NOISE RESULTS FOR 170HZ AT 156DB (U)

AS-77-2888

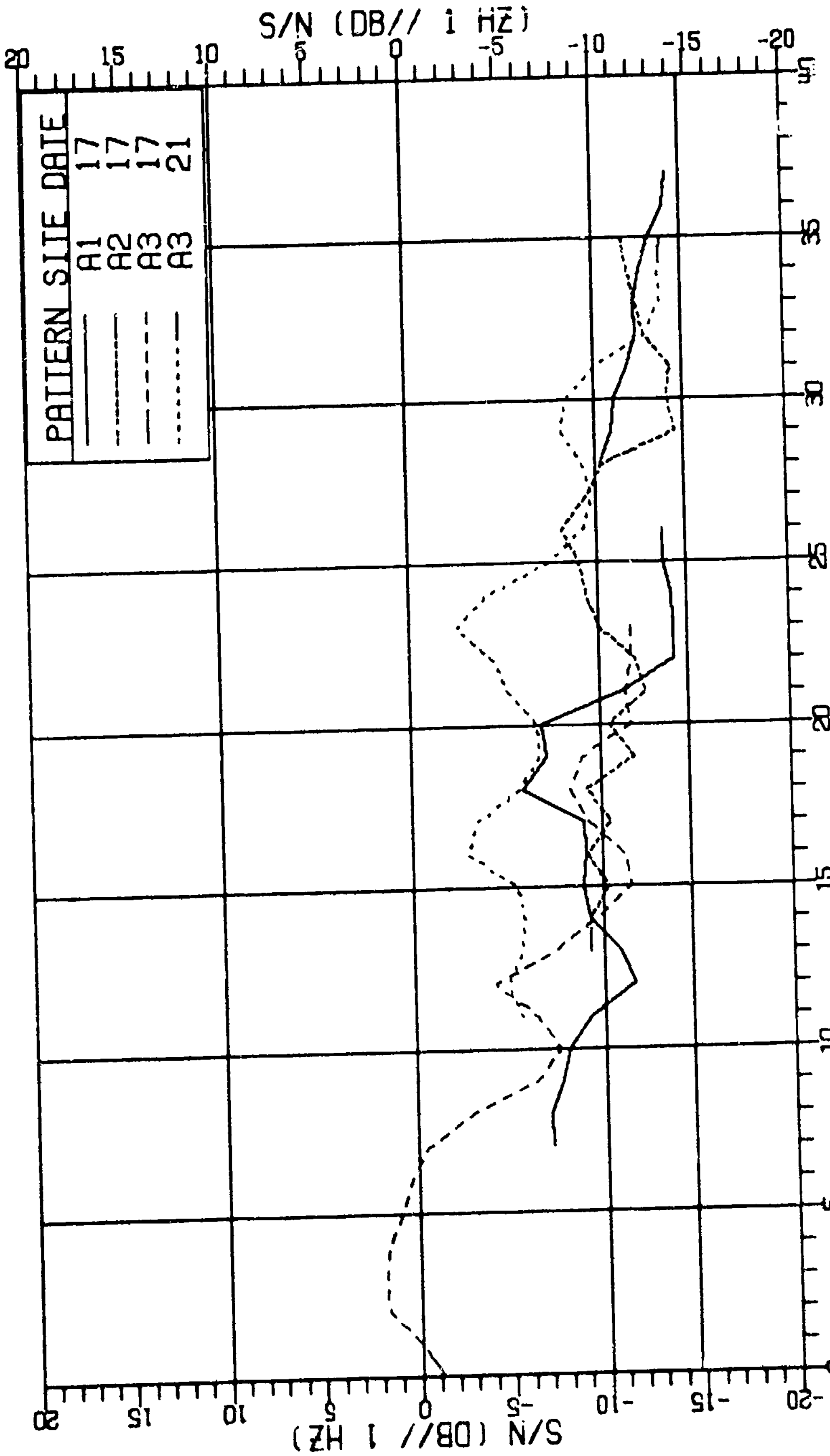

FIGURE III-289
MSS-FVT NEAR BOTTOM VERTICAL DIPOLE SENSOR
SIGNAL-TO-NOISE RESULTS FOR 170HZ AT 156DB (U)

AS-77-2889

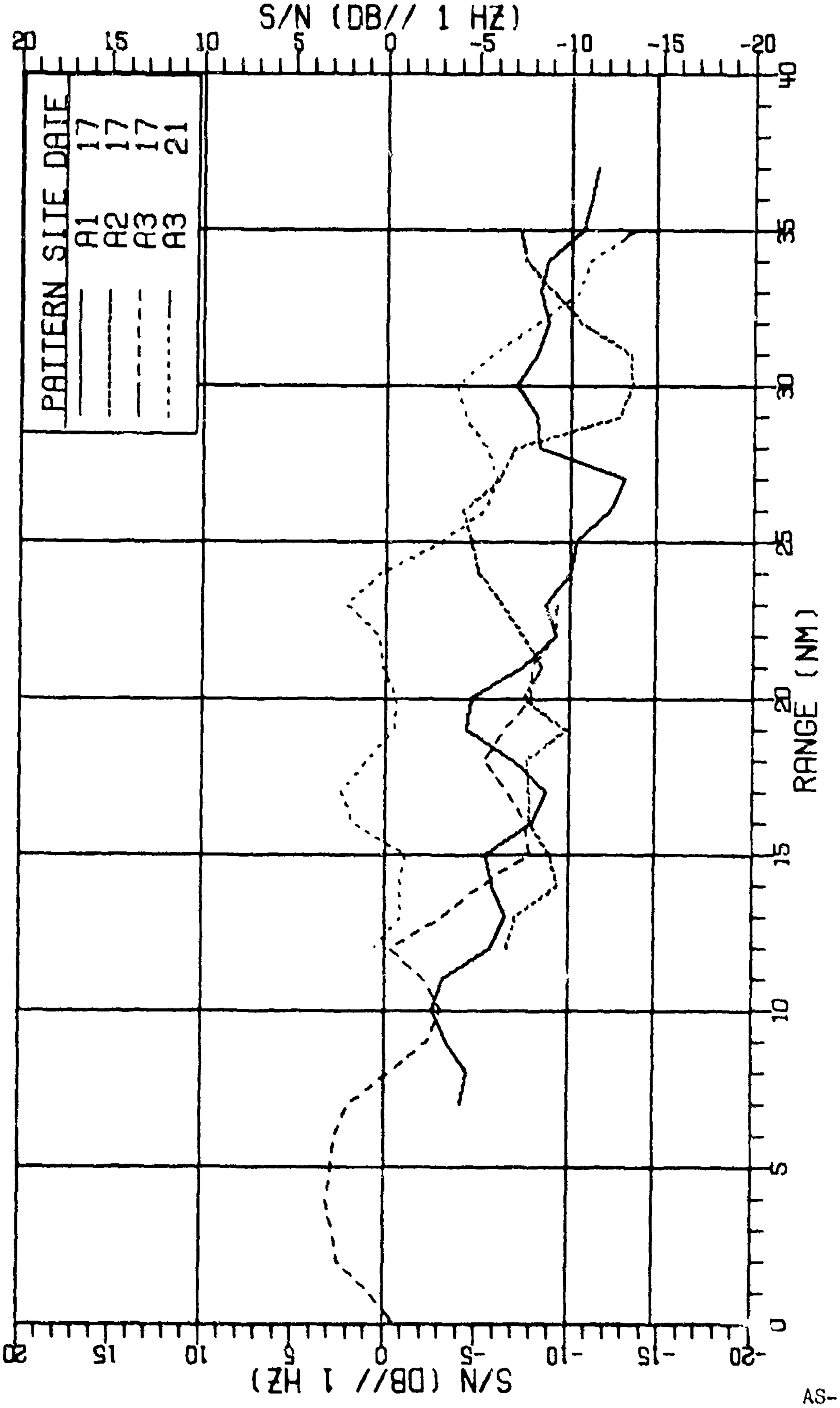

FIGURE III-290
MSS-FVT NEAR BOTTOM DIFFERENCED CARDIOIDS SENSOR
SIGNAL-TO-NOISE RESULTS FOR 170HZ AT 156DB (U)

AS-77-2890

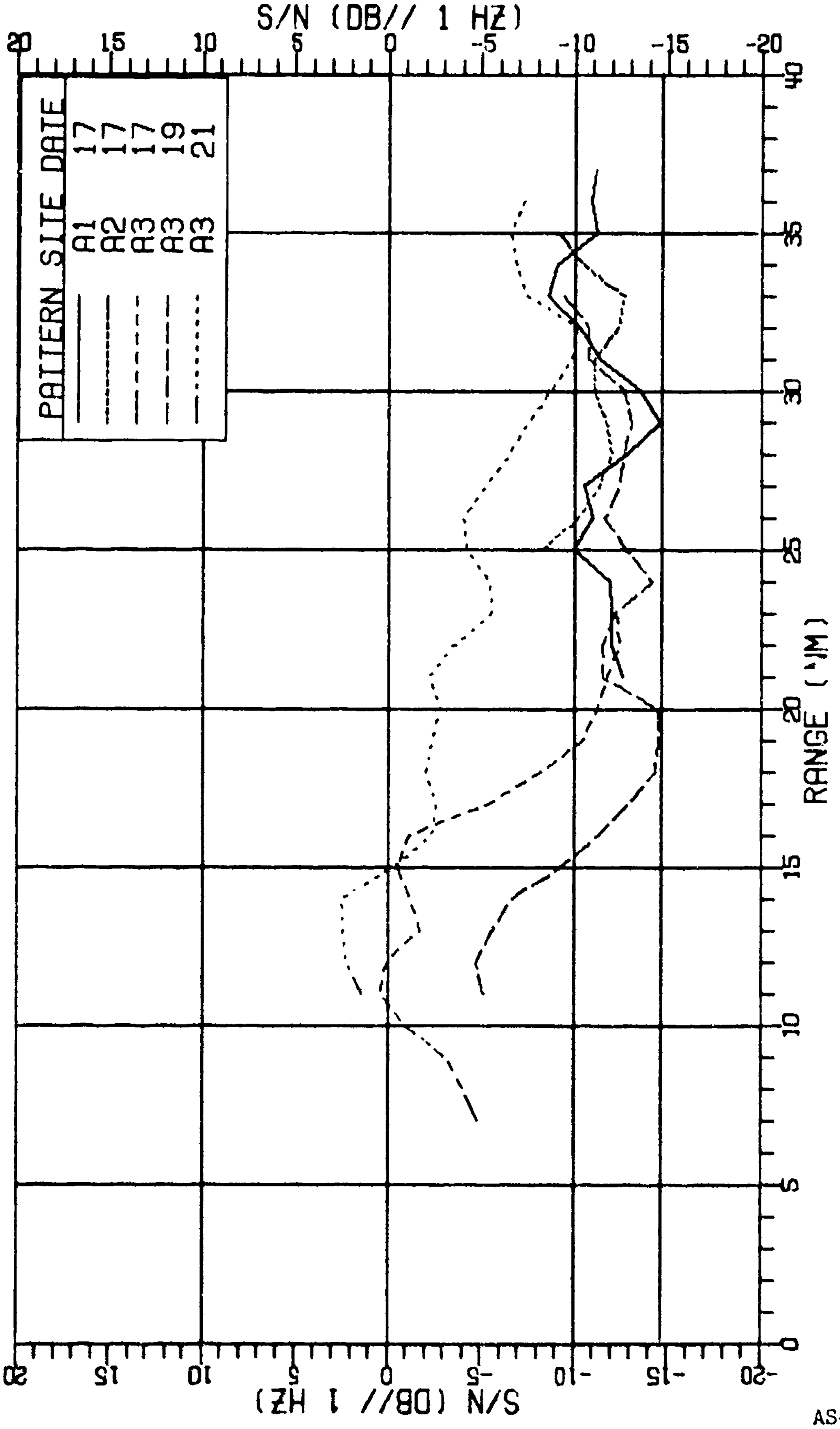

FIGURE III-291
MSS-FVT NEAR BOTTOM OMNIDIRECTIONAL SENSOR
SIGNAL-TO-NOISE RESULTS FOR 335HZ AT 154DB (U)

AS-77-2891

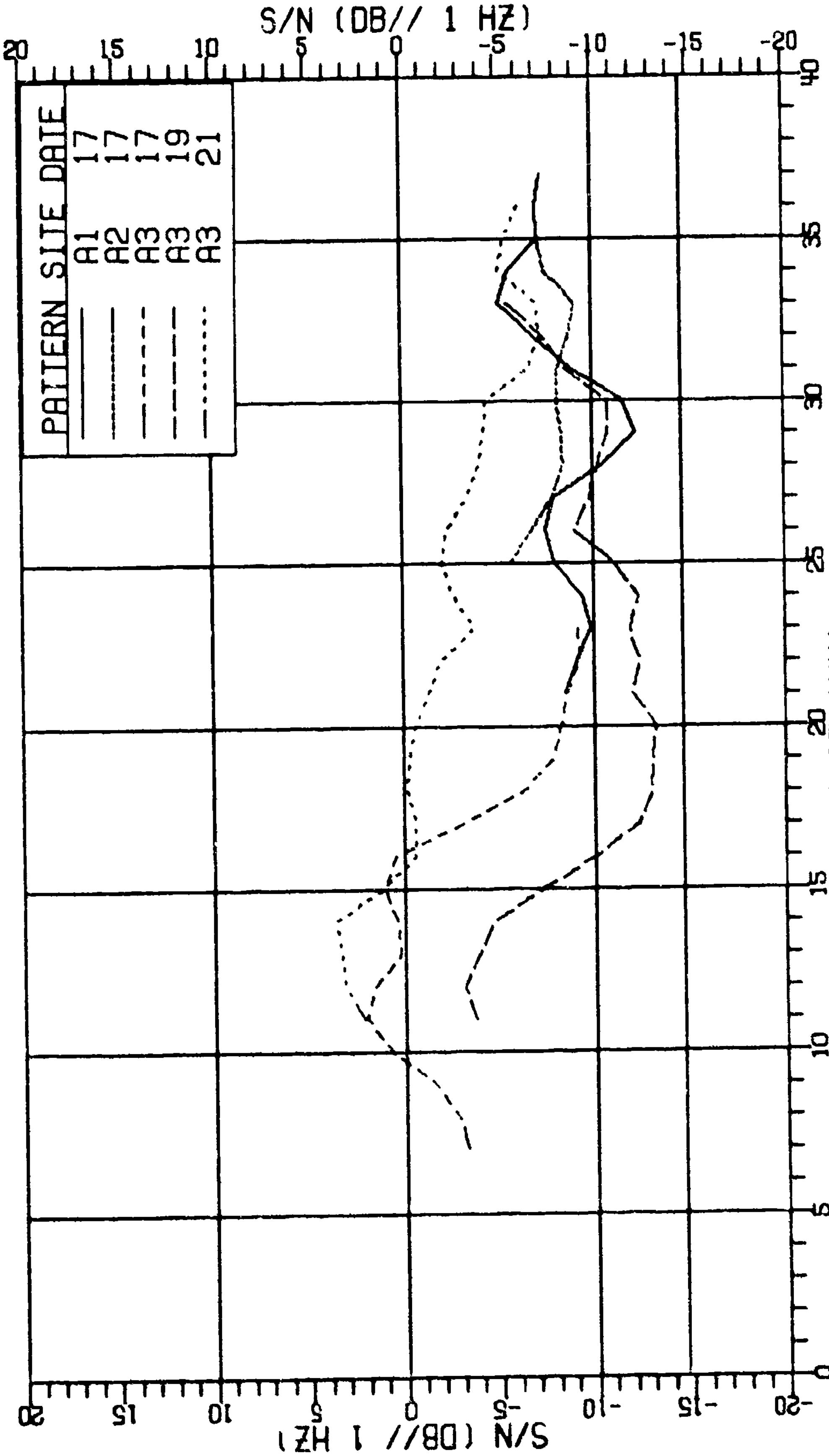

FIGURE III-292
MSS-FVT NEAR BOTTOM SINGLE CARDIOIDS SENSOR
SIGNAL-TO-NOISE RESULTS FOR 335HZ AT 154DB (U)

AS-77-2892

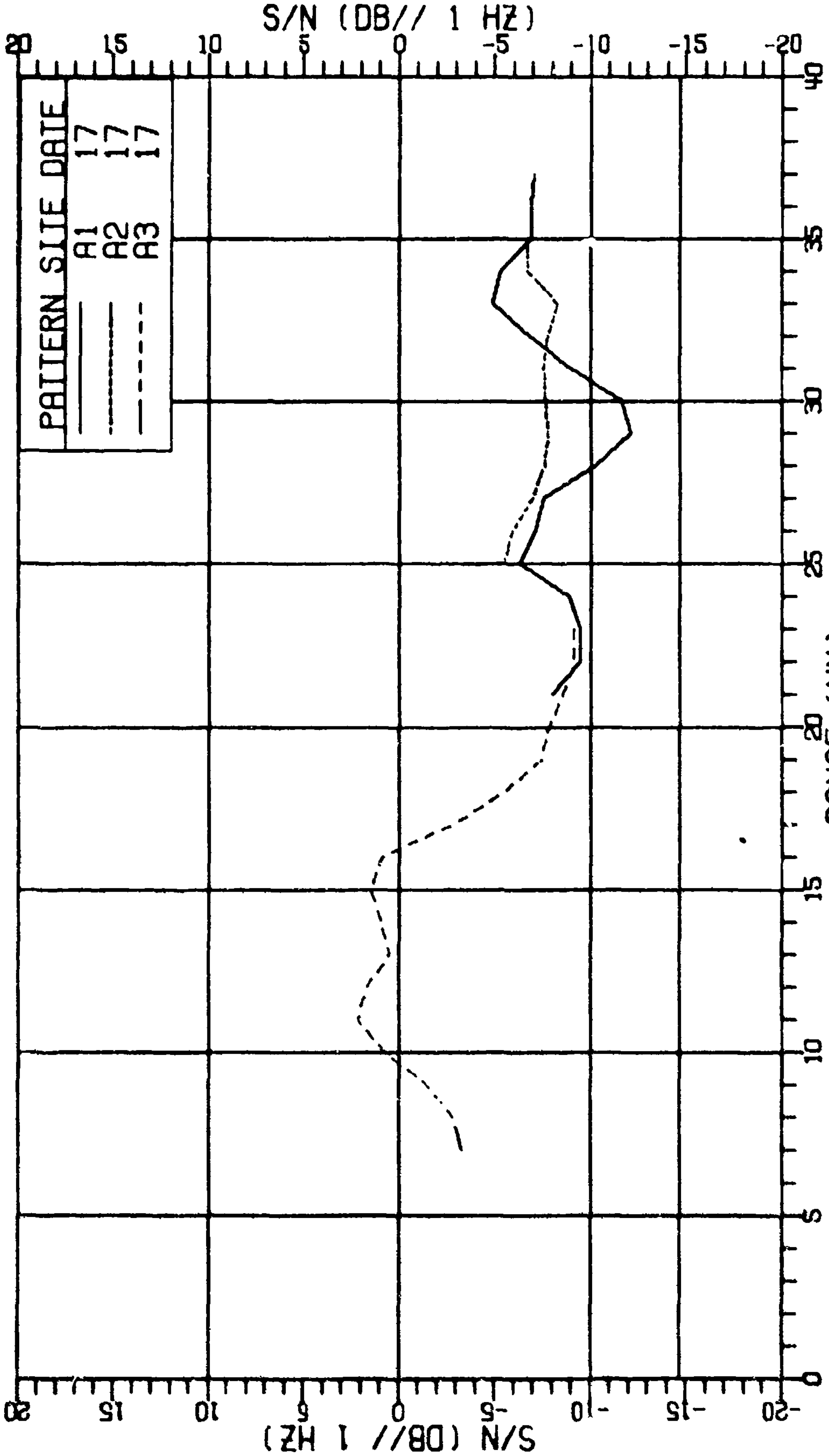

FIGURE III-293
MSS-FVT NEAR BOTTOM MAX GAIN LIMACONS SENSOR
SIGNAL-TO-NOISE RESULTS FOR 335HZ AT 154DB (U)

AS-77-2893

APPENDIX H

NOISE GAIN TIMESERIES CURVES (U)

(FIGURES III-294 - III-301)

(The reverse of this page is blank.)

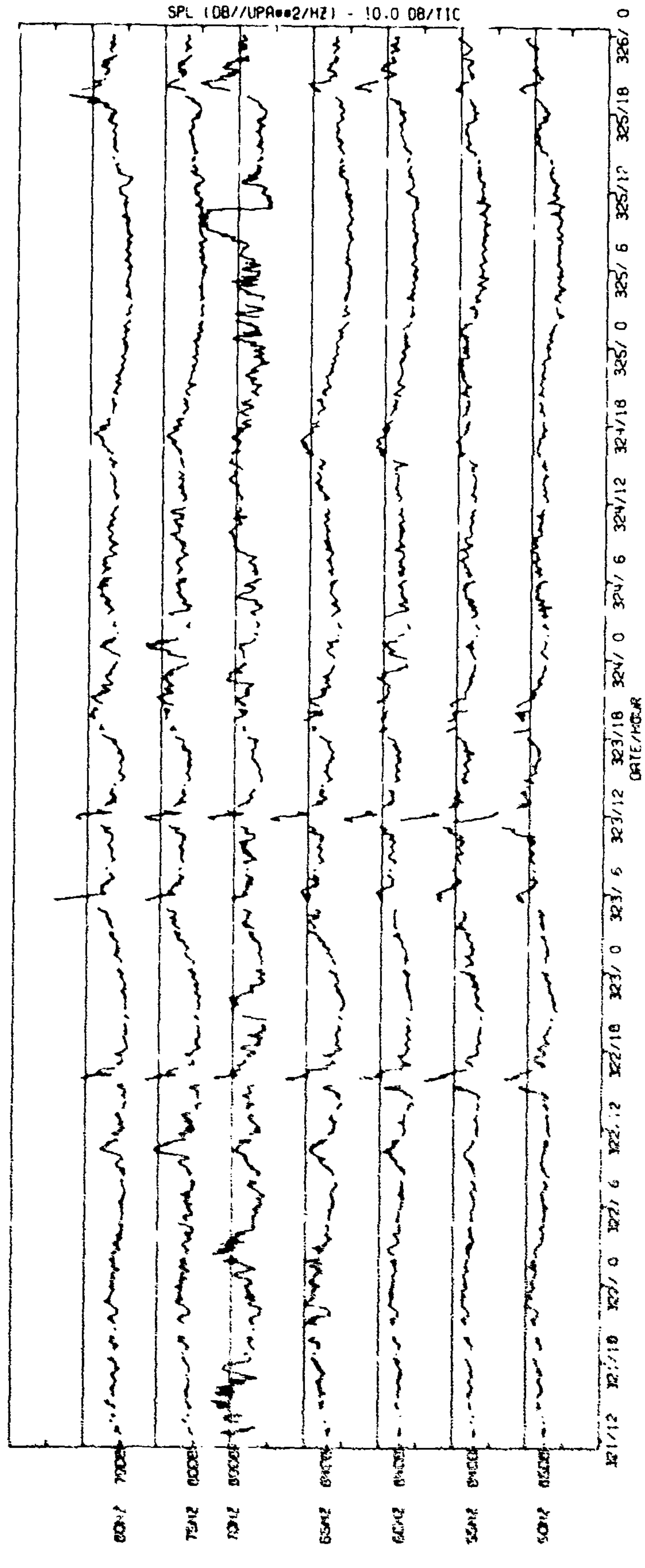

FIGURE II-294
MSS-FVT PHASE II SITE A3 LOW FREQUENCY VERNIER
TIME SERIES OF 5 MIN AVERAGED AMBIENT SOUND FIELD LEVELS
THROUGH 1 HZ BANDS OF THE OMNIDIRECTIONAL SENSOR (U)

AS-77-3387

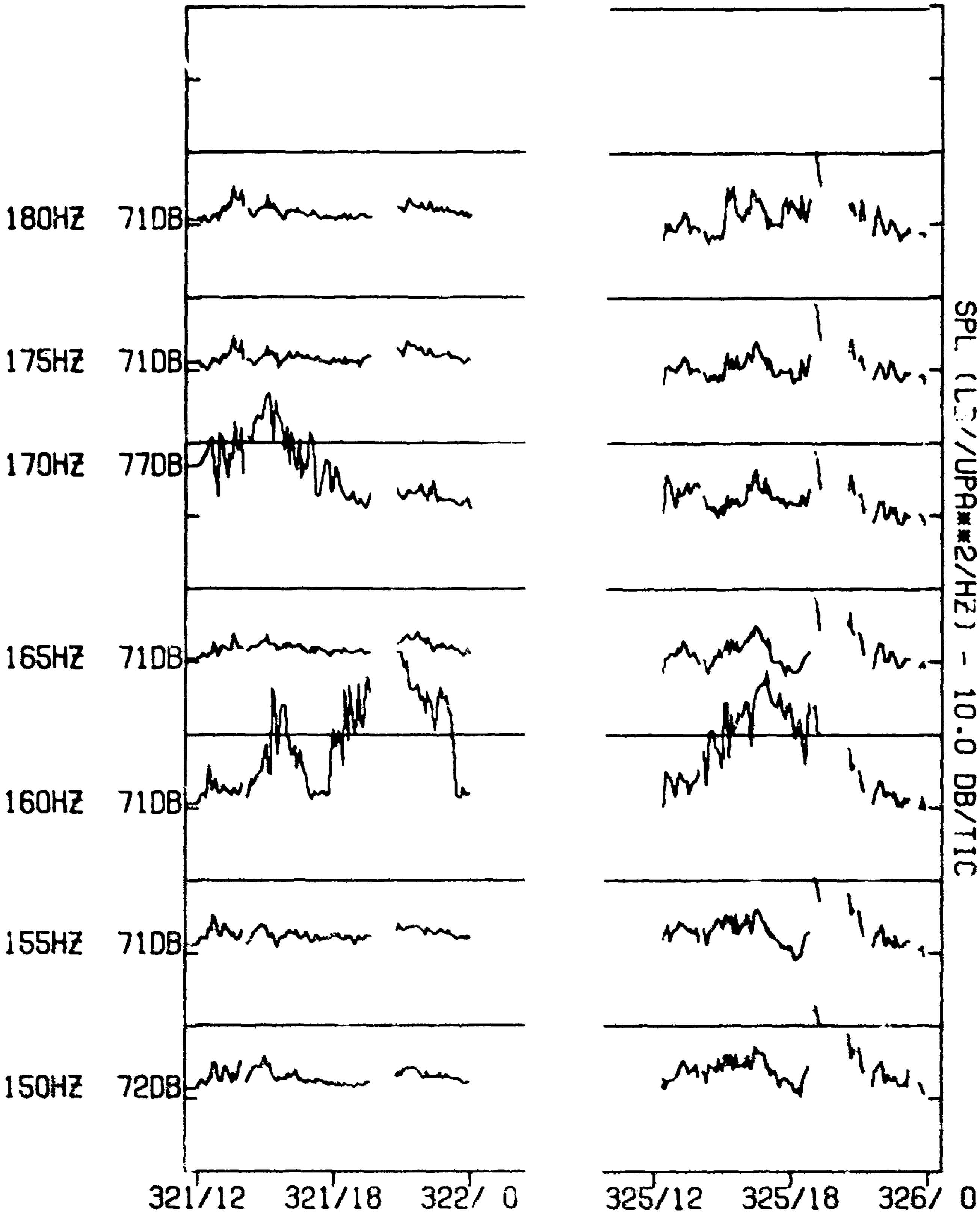

FIGURE III-295
MSS-FVT PHASE II SITE A3 MID FREQUENCY VERNIER
TIME SERIES OF 5 MIN AVERAGED AMBIENT SOUND FIELD LEVELS
THROUGH 1 HZ BANDS OF THE OMNIDIRECTIONAL SENSOR (U)

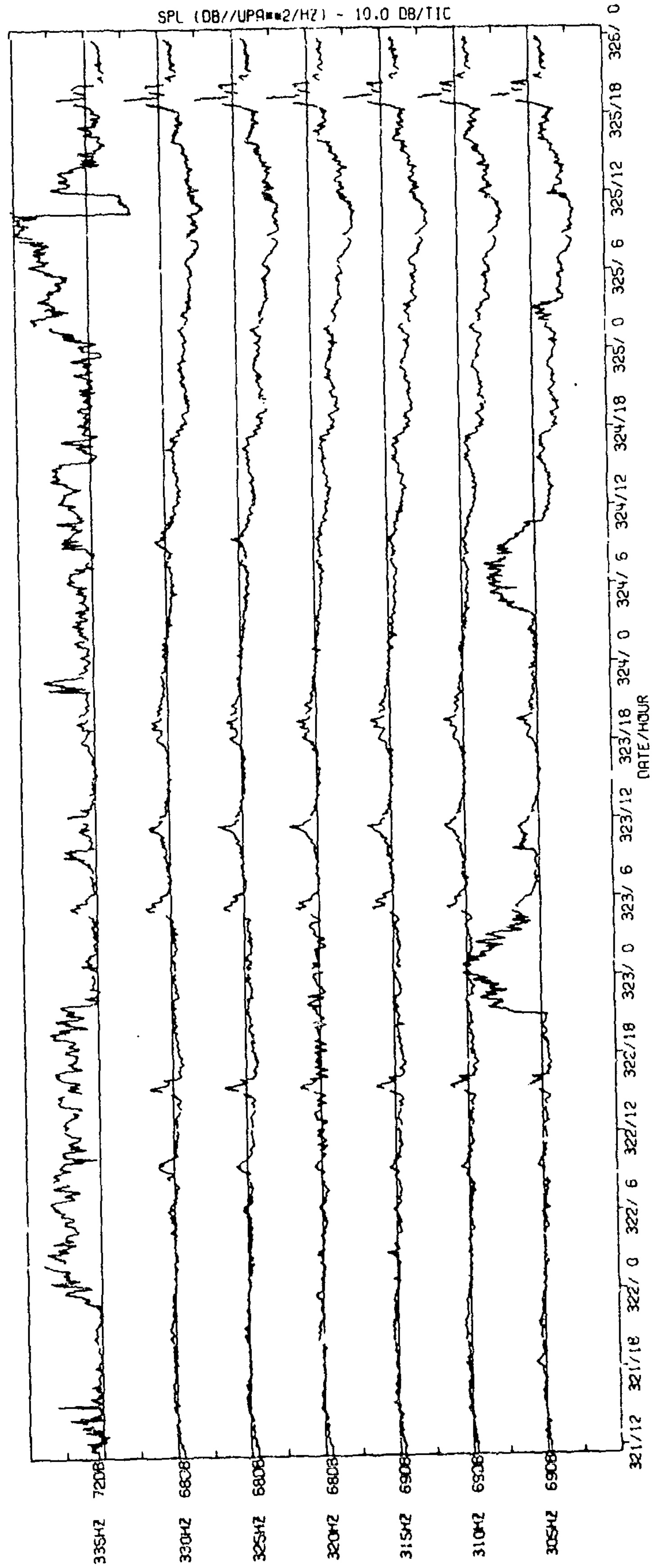

FIGURE III-296
MSS-FVT PHASE II SITE A3 HIGH FREQUENCY VERNIER
TIME SERIES OF 5 MIN AVERAGED AMBIENT SOUND FIELD LEVELS
THROUGH 1 HZ BANDS OF THE OMNIDIRECTIONAL SENSOR (U)

AS-77-3389

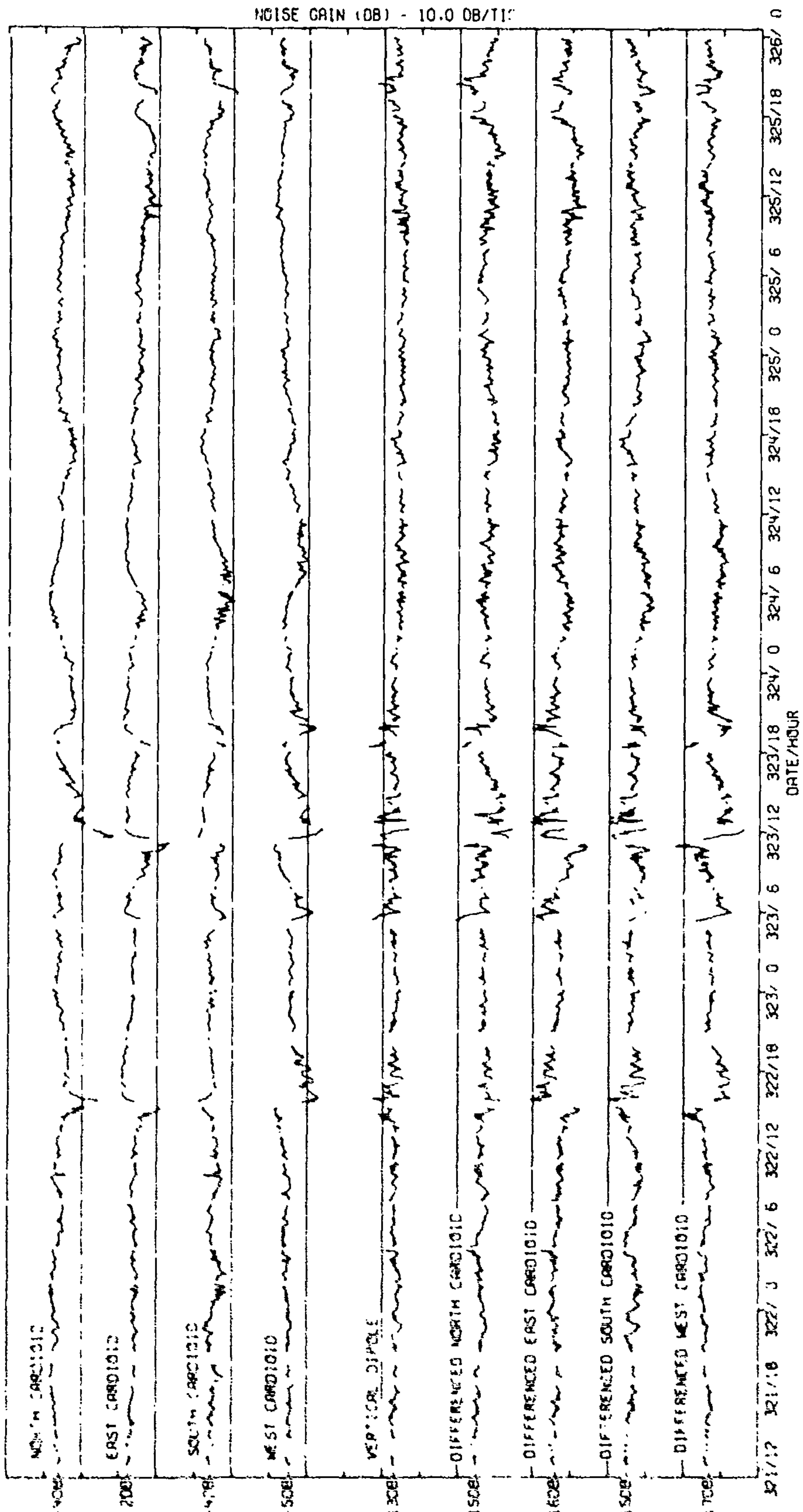

FIGURE III-297
MSS-FVT PHASE II SITE A3 LOW FREQUENCY VERNIER
TIME SERIES OF 5 MIN AVERAGED NOISE GAIN LEVELS
FOR CARDIOID BEAMS AT 50 HZ (U)

AS-77-3390

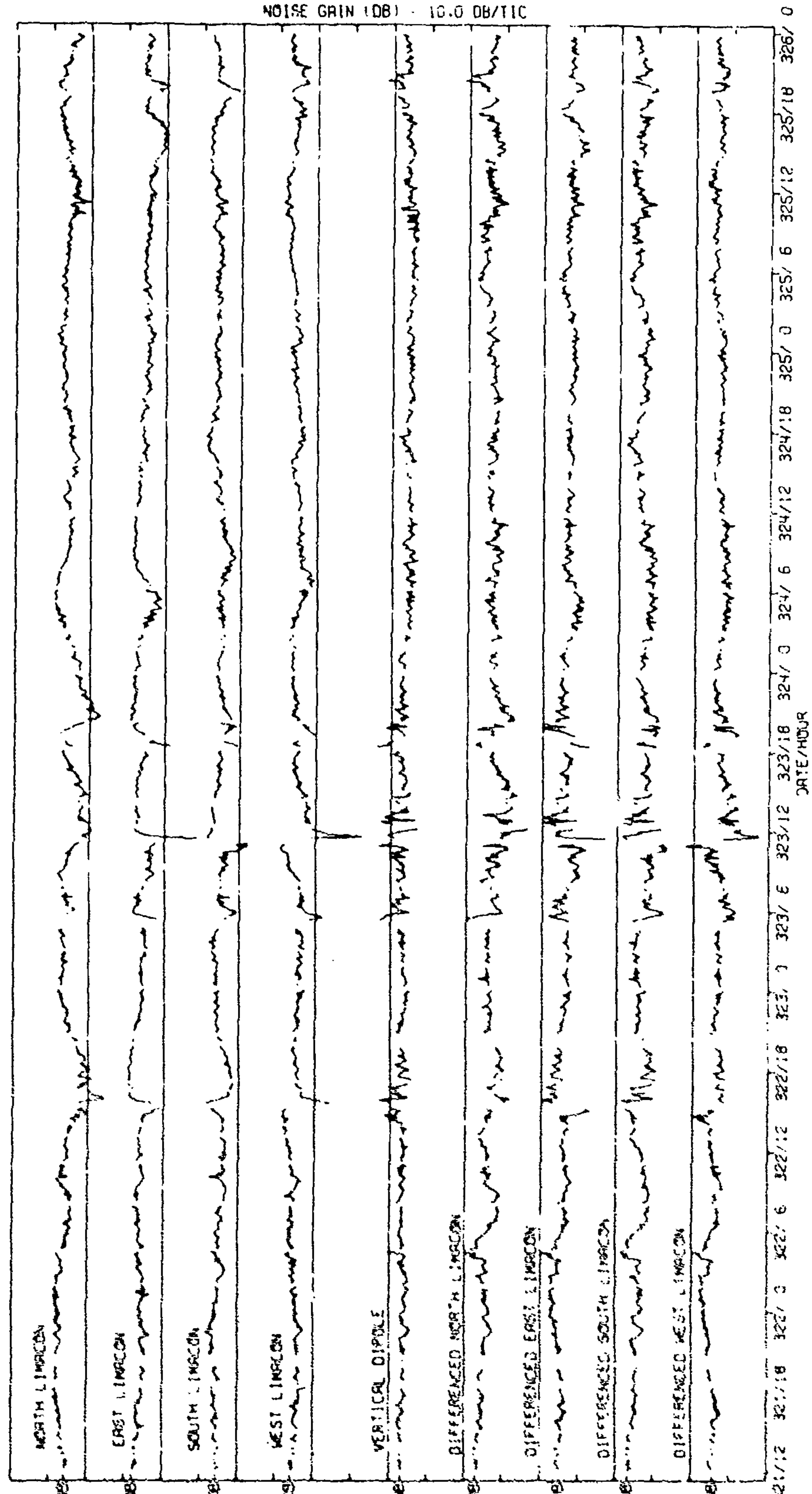

FIGURE III-298
MSS-FVT PHASE II SITE A3 LOW FREQUENCY VERNIER
TIME SERIES OF 5 MIN AVERAGED NOISE GAIN LEVELS
FOR LIMACON (0.33) BEAMS AT 50 HZ (U)

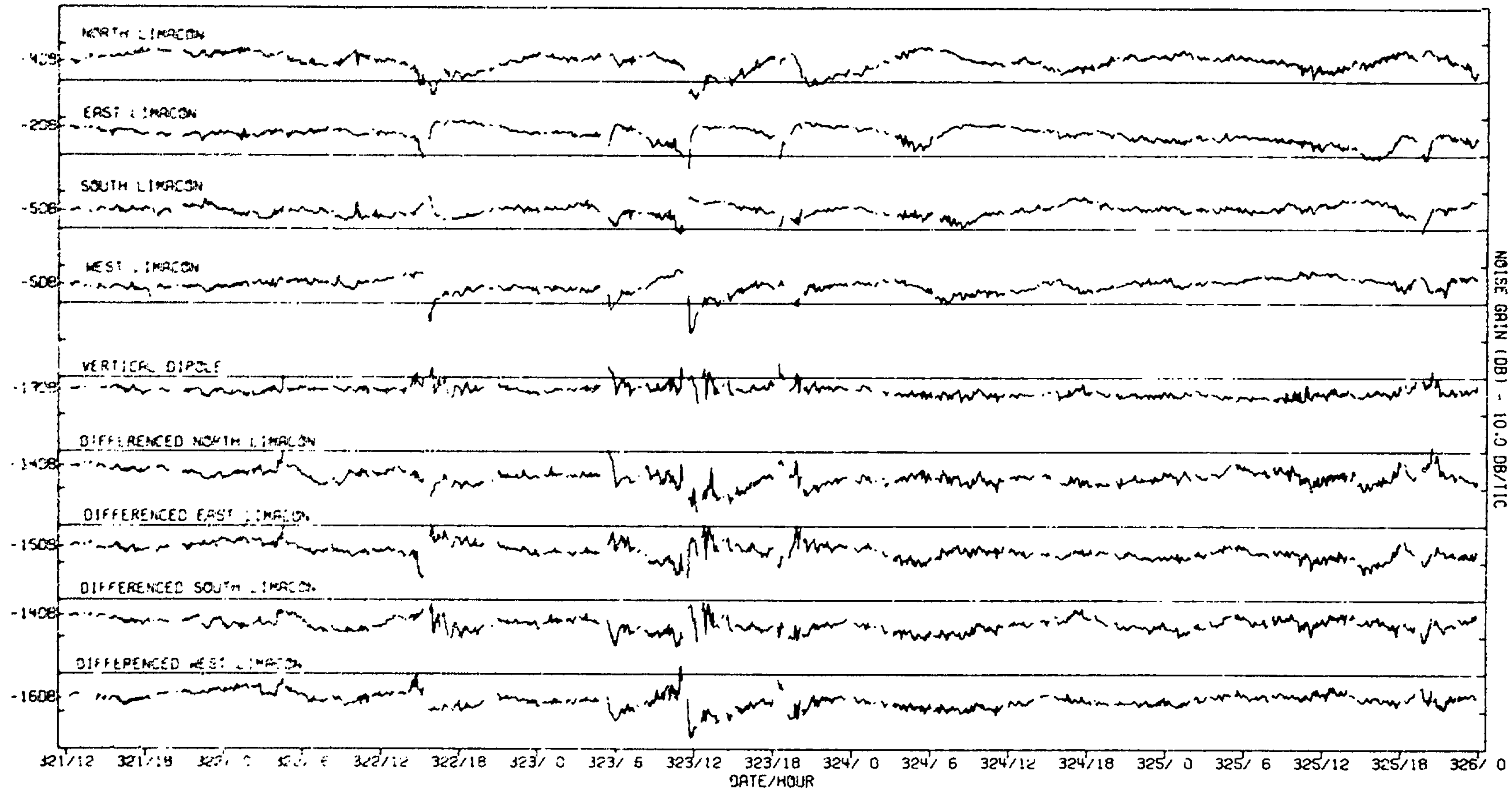

FIGURE III-299
MSS-FVT PHASE II SITE A3 LOW FREQUENCY VERNIER
TIME SERIES OF 5 MIN AVERAGED NOISE GAIN LEVELS
FOR LIMACON (0.50) BEAMS AT 50 HZ (U)

AS-77-3392

CONFIDENTIAL

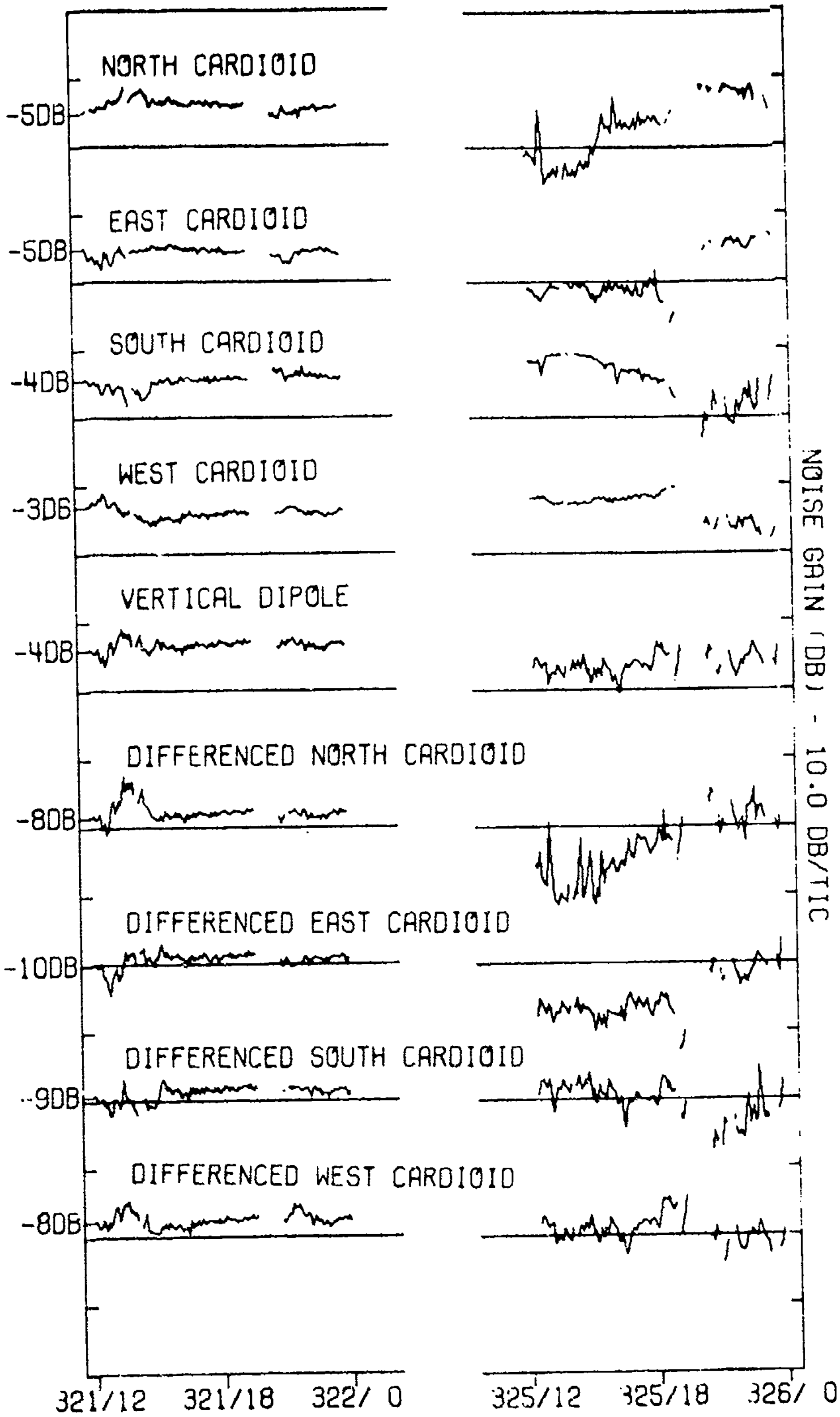

FIGURE III-300
MSS-FVT PHASE II SITE A3 MID FREQUENCY VERNIER
TIME SERIES OF 5 MIN AVERAGED NOISE GAIN LEVELS
FOR CARDIOID BEAMS AT 150 HZ (U)

AS-77-3393

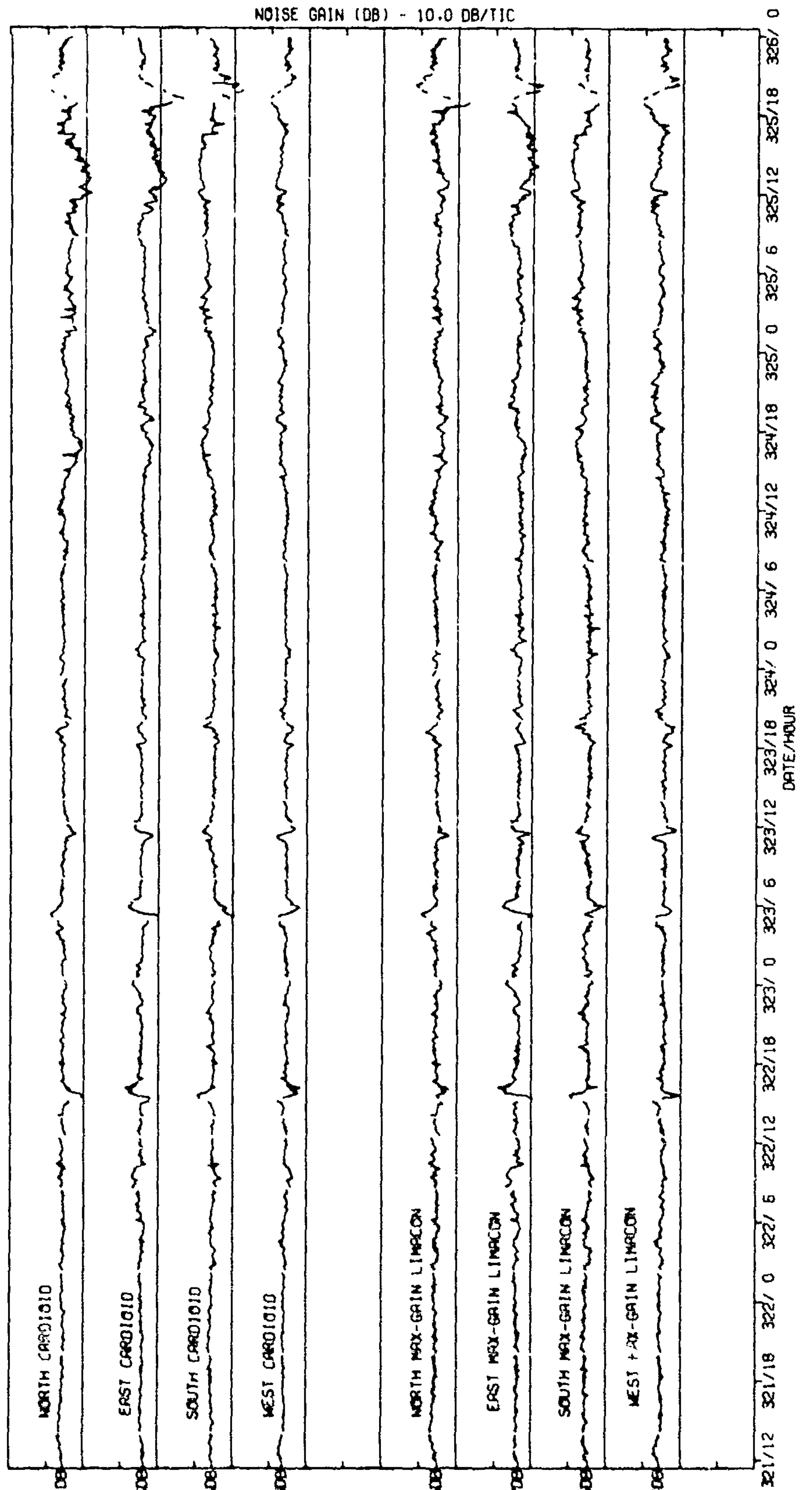

FIGURE III-301
MSS-FVT PHASE II SITE A3 HIGH FREQUENCY VERNIER
TIME SERIES OF 5 MIN AVERAGED NOISE GAIN LEVELS
FOR CARDIOID AND LIMACON (0.33) BEAMS AT 310 HZ (U)

AS-77-3394

APPENDIX I

CLUTTER TIMESERIES CURVES (U)

(FIGURES III-302 - III-312)

(The reverse of this page is blank.)

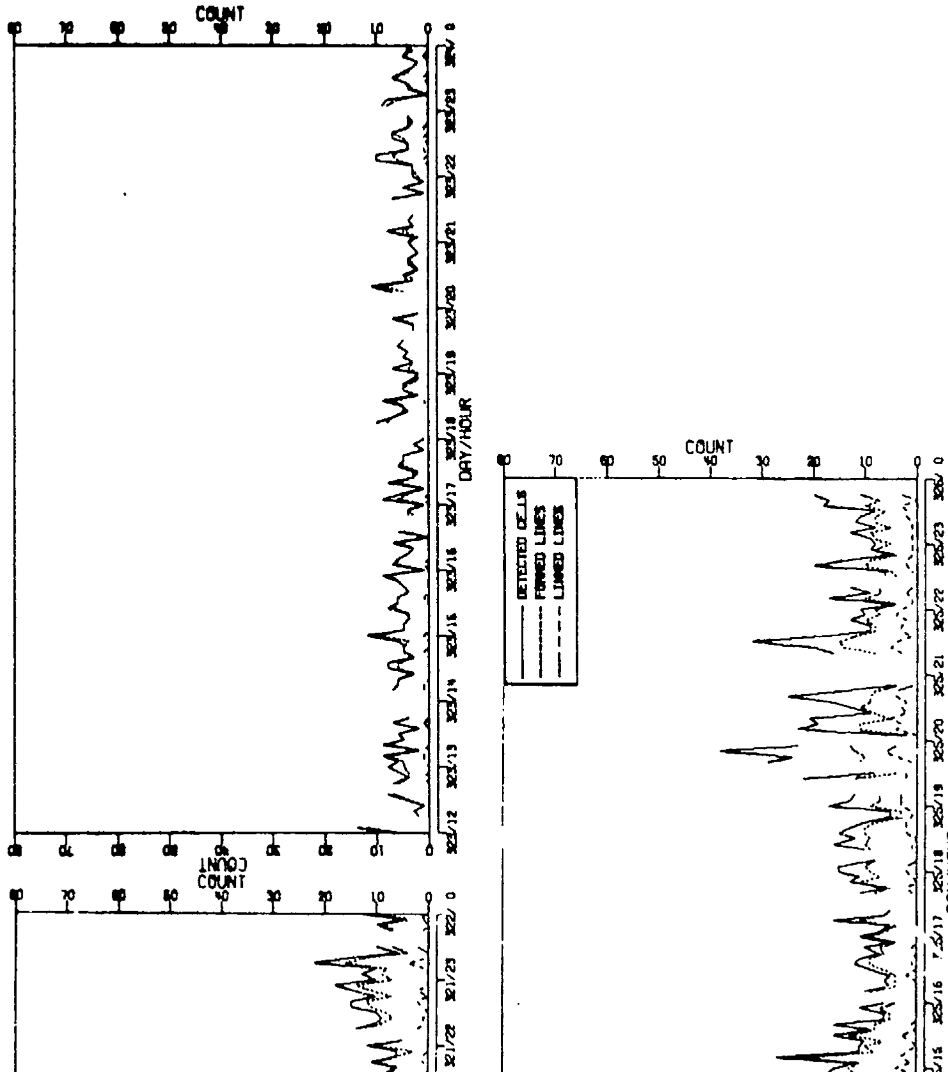

FIGURE III-302
MSS-FVT LOW-FREQUENCY VERNIER CLUTTER RESULTS
FOR THE OMNIDIRECTIONAL SENSOR AT SITE A3
DURING THE PHASE II FIELD EVENTS (U)

AS-77-3395

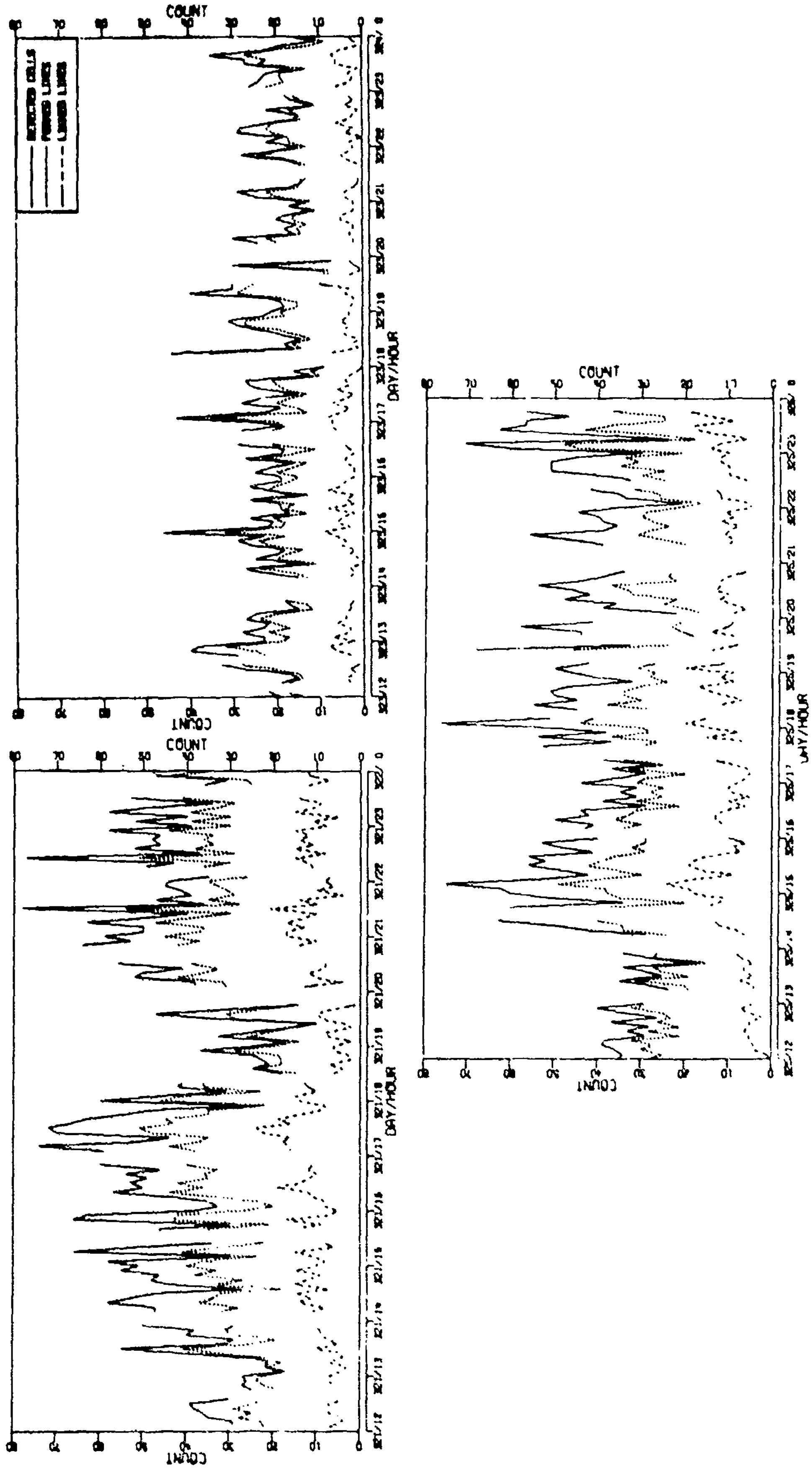

FIGURE III-303
MSS-FVT LOW-FREQUENCY VERNIER CLUTTER RESULTS
FOR THE SINGLE CARDIOIDS SENSOR AT SITE A3
DURING THE PHASE II FIELD EVENTS (U)

AS-77-3396

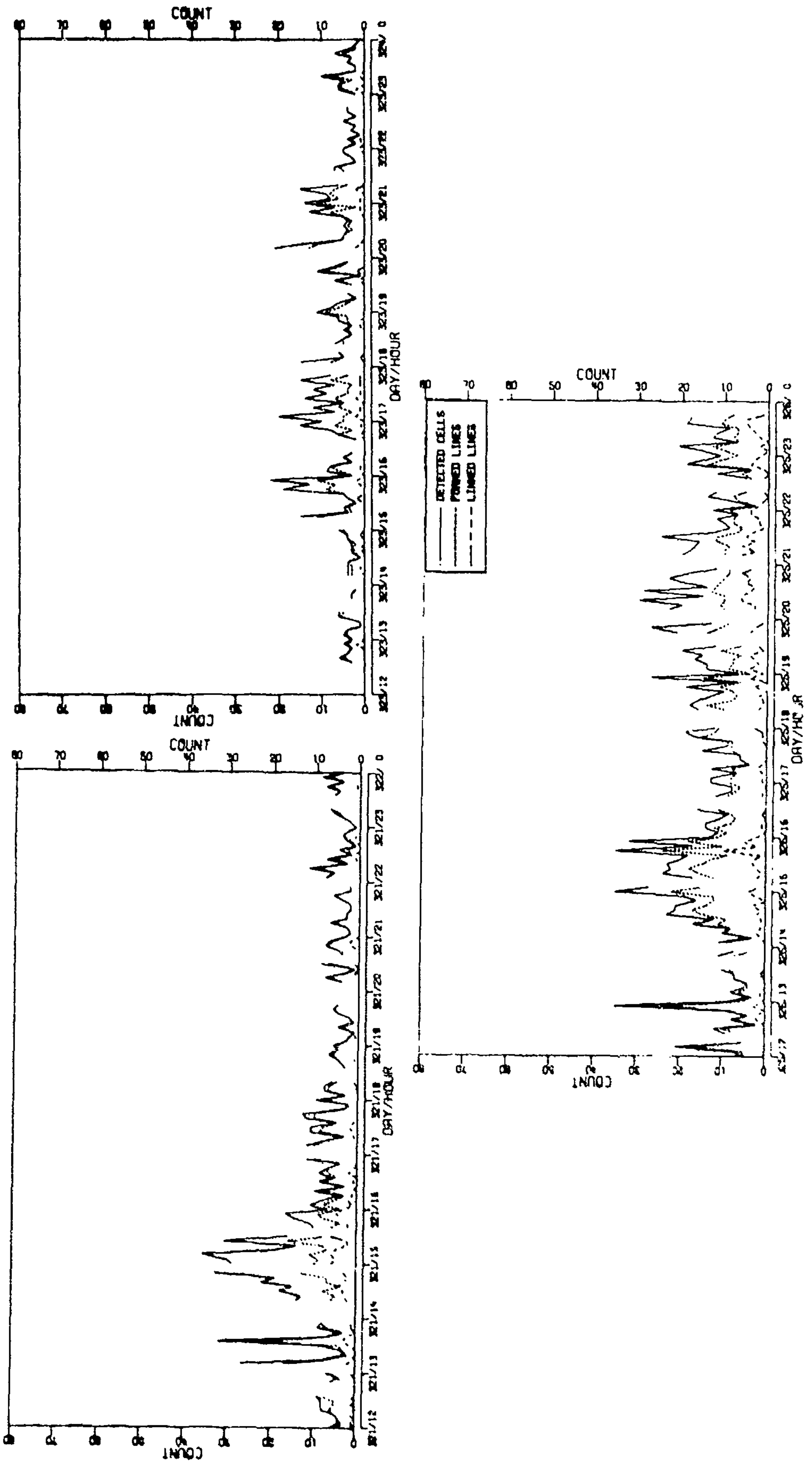

FIGURE III-304
MSS-FVT LOW-FREQUENCY VERNIER CLUTTER RESULTS FOR THE VERTICAL DIPOLE SENSOR AT SITE A3 DURING THE PHASE II FIELD EVENTS (U)

AS-77-3397

CONFIDENTIAL

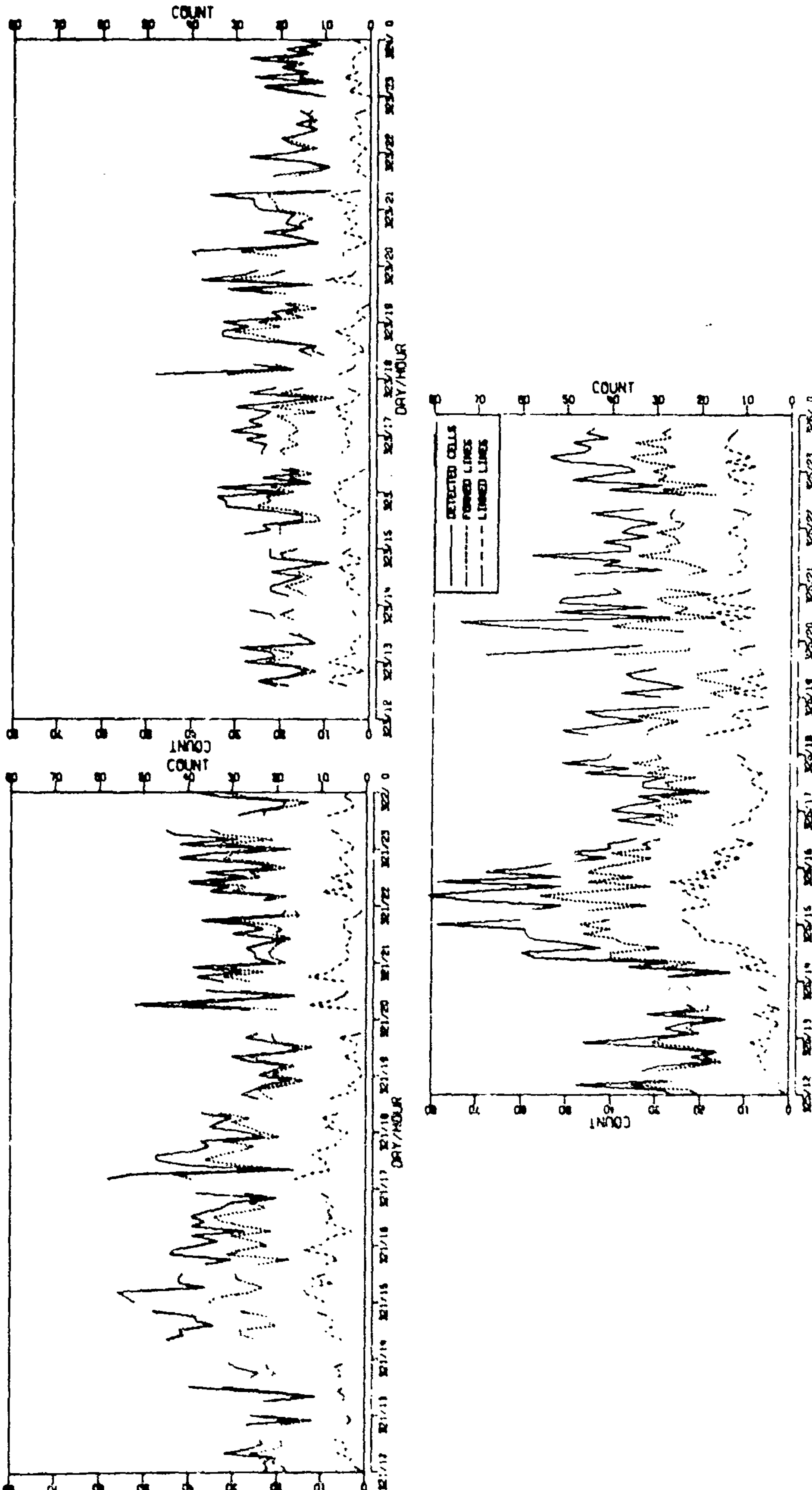

FIGURE III-305
MSS-FVT LOW-FREQUENCY VERNIER CLUTTER RESULTS
FOR THE DIFFERENCED CARDIOIDS SENSOR AT SITE A3
DURING THE PHASE II FIELD EVENTS (U)

AS-77-3398

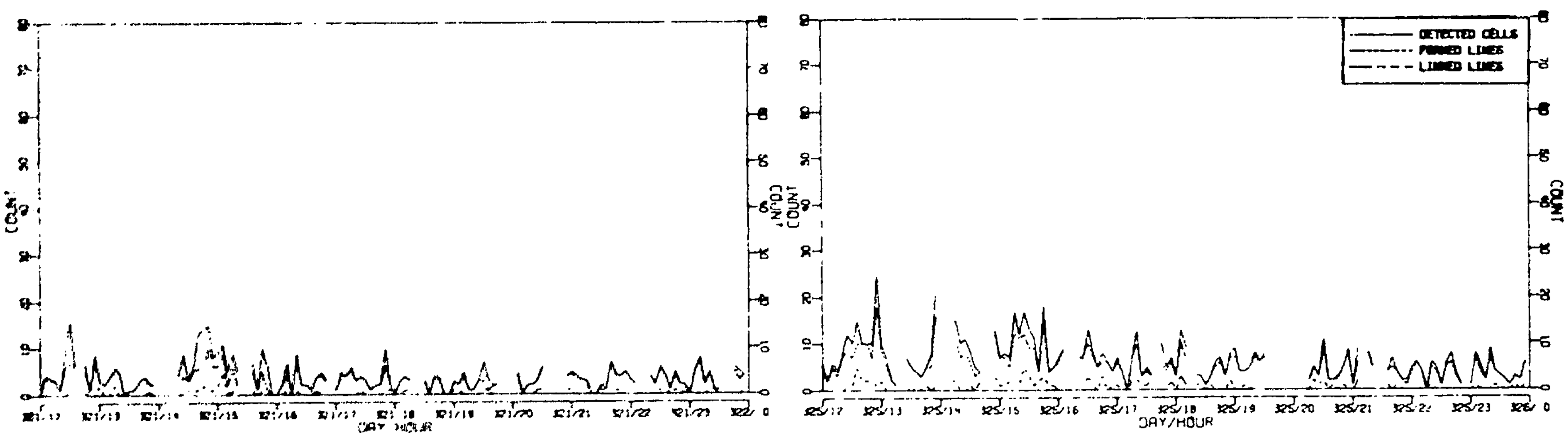

FIGURE III-306
MSS-FVT MID-FREQUENCY VERNIER CLUTTER RESULTS
FOR THE OMNIDIRECTIONAL SENSOR AT SITE A3
DURING THE PHASE II FIELD EVENTS (U)

AS-77-3399

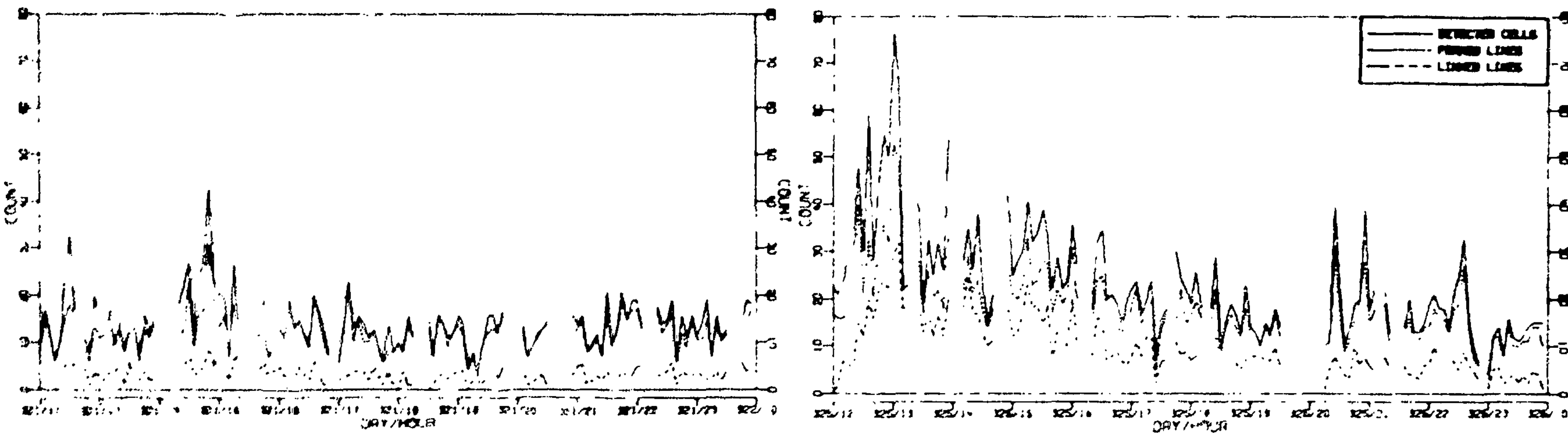

FIGURE III-307
MSS-FVT MID-FREQUENCY VERNIER CLUTTER RESULTS
FOR THE SINGLE CARDIOIDS SENSOR AT SITE A3
DURING THE PHASE II FIELD EVENTS (U)

AS-77-3400

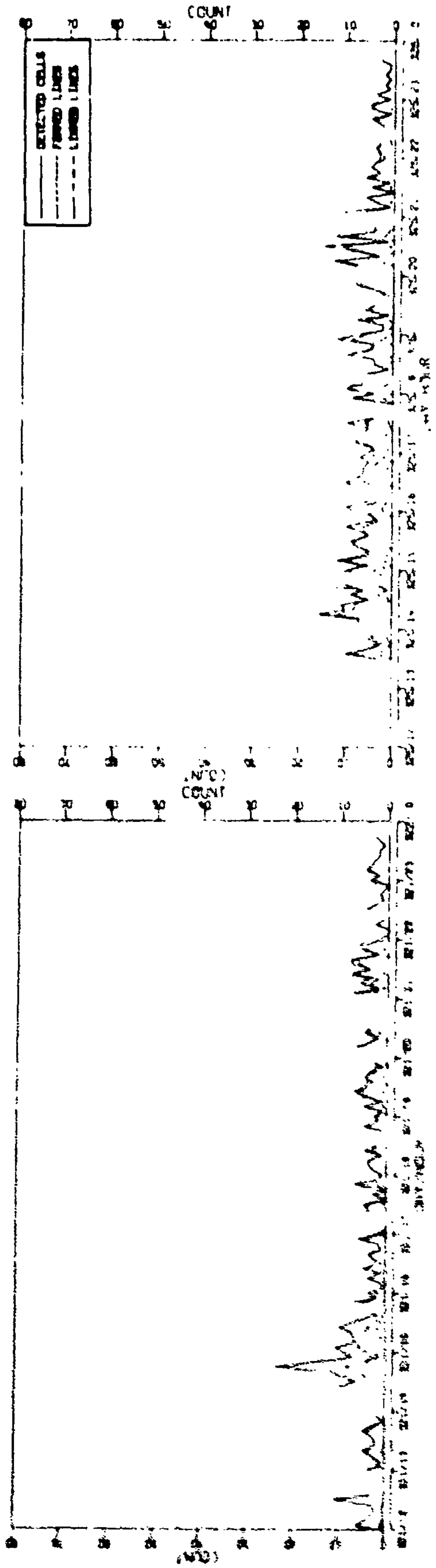

FIGURE III-308
MSS-FVT MID-FREQUENCY VERNIER CLUTTER RESULTS
FOR THE VERTICAL DIPOLE SENSOR AT SITE A3
DURING THE PHASE II FIELD EVENTS (U)

AS-77-3401

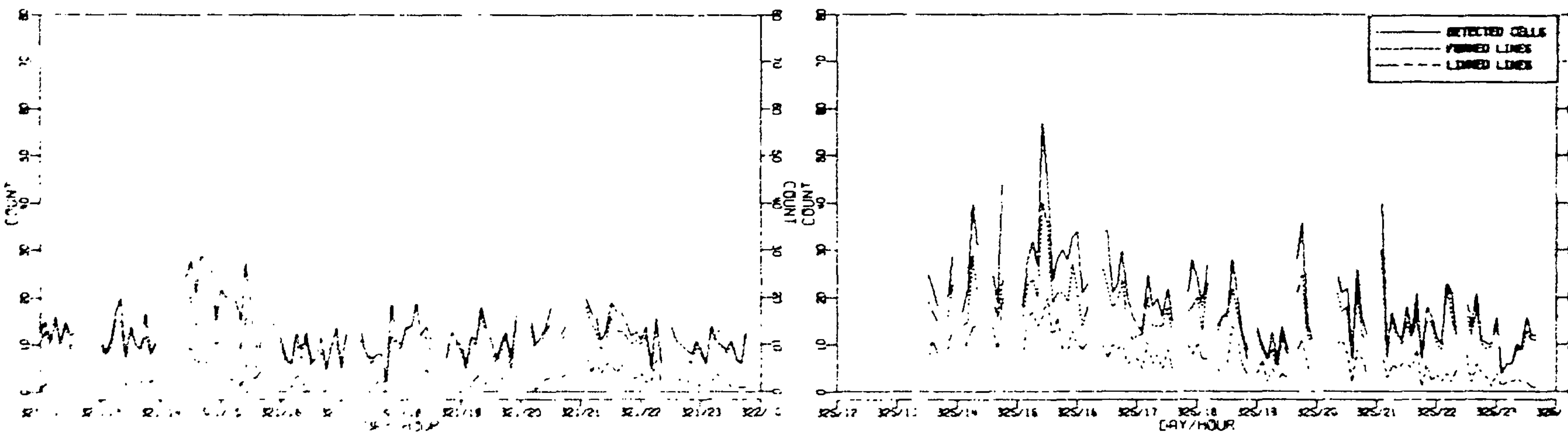

FIGURE III-309
MSS-FVT MID-FREQUENCY VERNIER CLUTTER RESULTS
FOR THE DIFFERENCED CARDIOIDS SENSOR AT SITE A3
DURING THE PHASE II FIELD EVENTS (U)

AS-77-3402

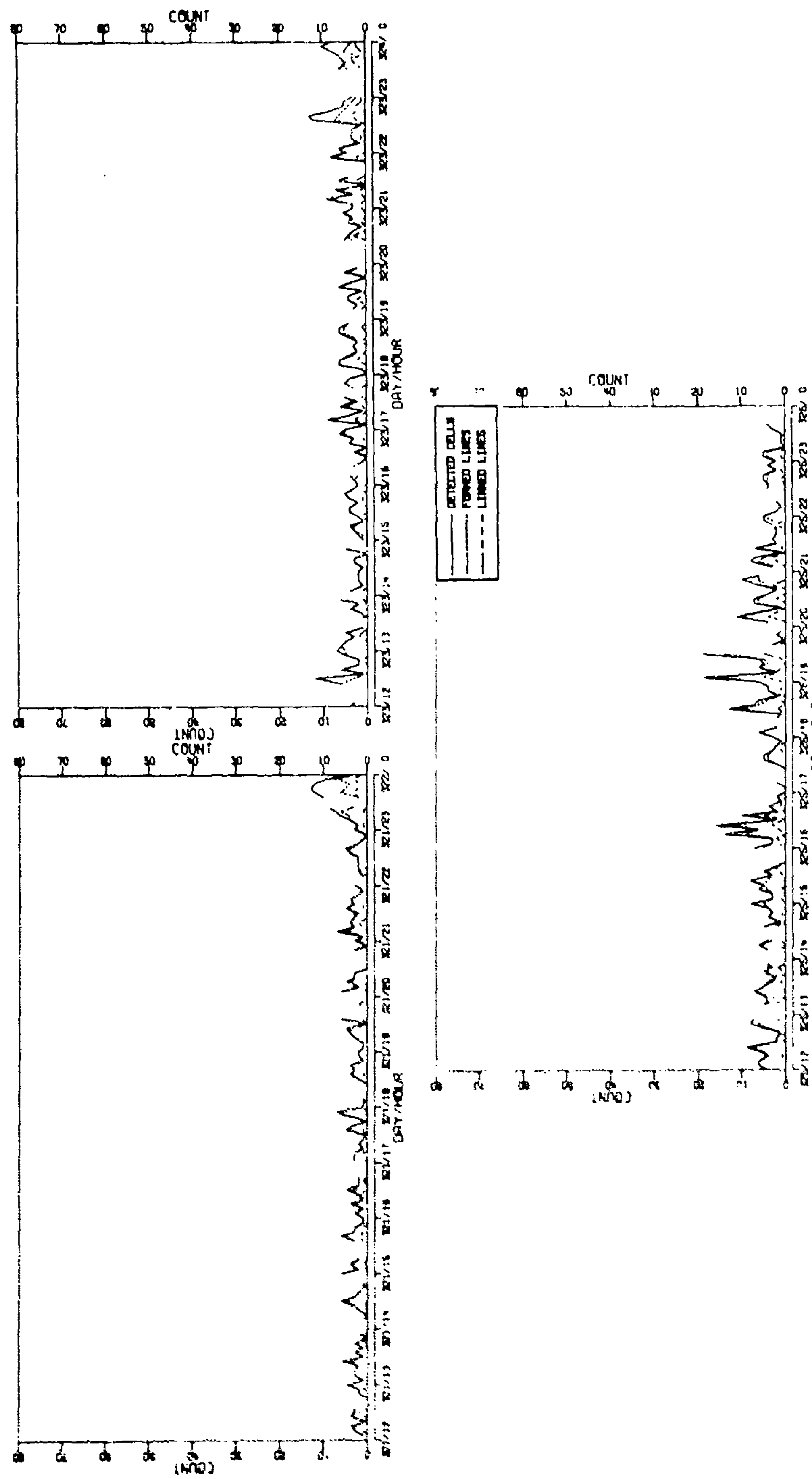

FIGURE III-310
MSS-FVT HIGH-FREQUENCY VERNIER CLUTTER RESULTS
FOR THE OMNIDIRECTIONAL SENSOR AT SITE A3
DURING THE PHASE II FIELD EVENTS (U)

AS-77-3403

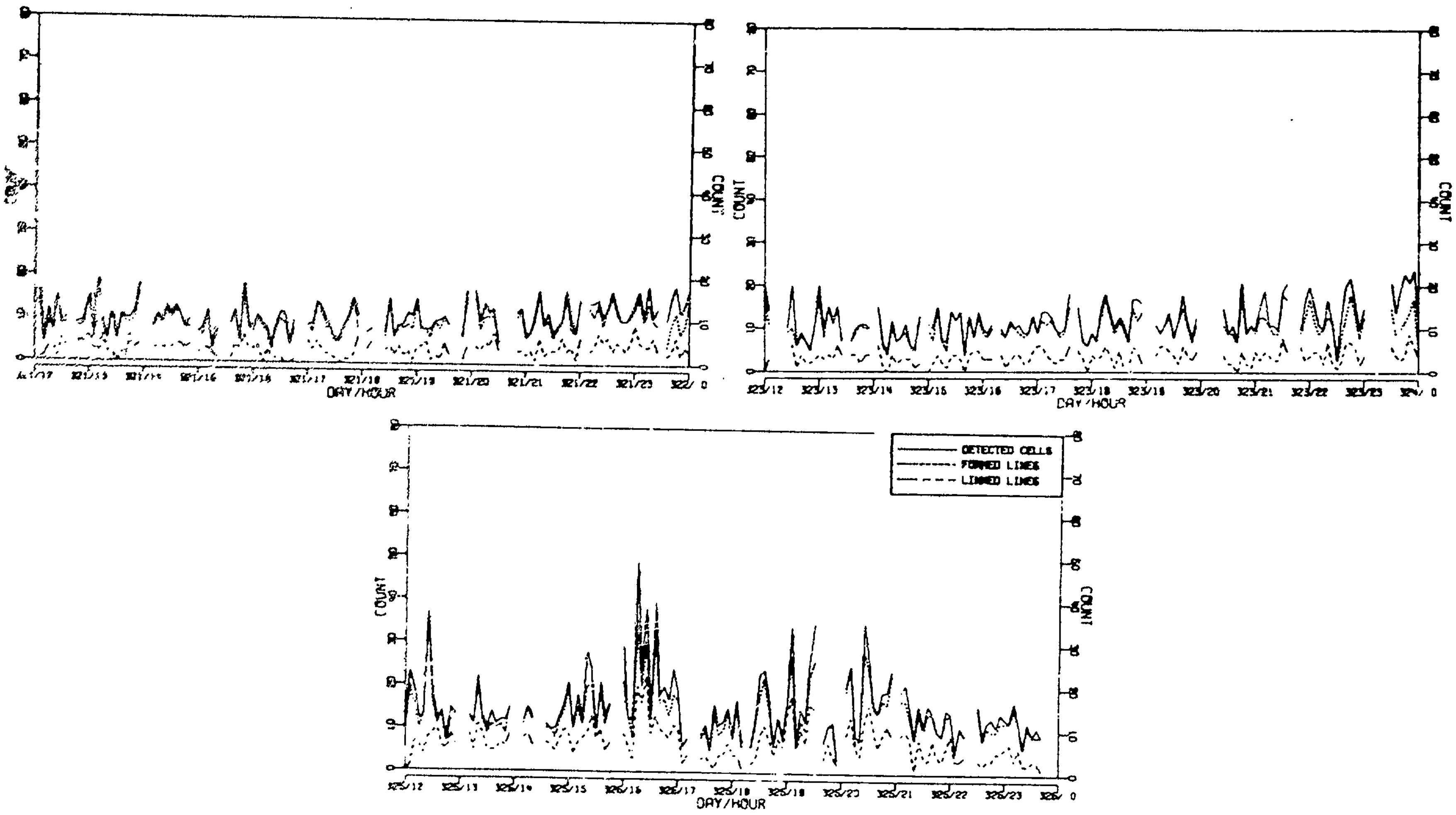

FIGURE III-311
MSS-FVT HIGH-FREQUENCY VERNIER CLUTTER RESULTS
FOR THE SINGLE CARDIOIDS SENSOR AT SITE A3
DURING THE PHASE II FIELD EVENTS (U)

AS-77-3404

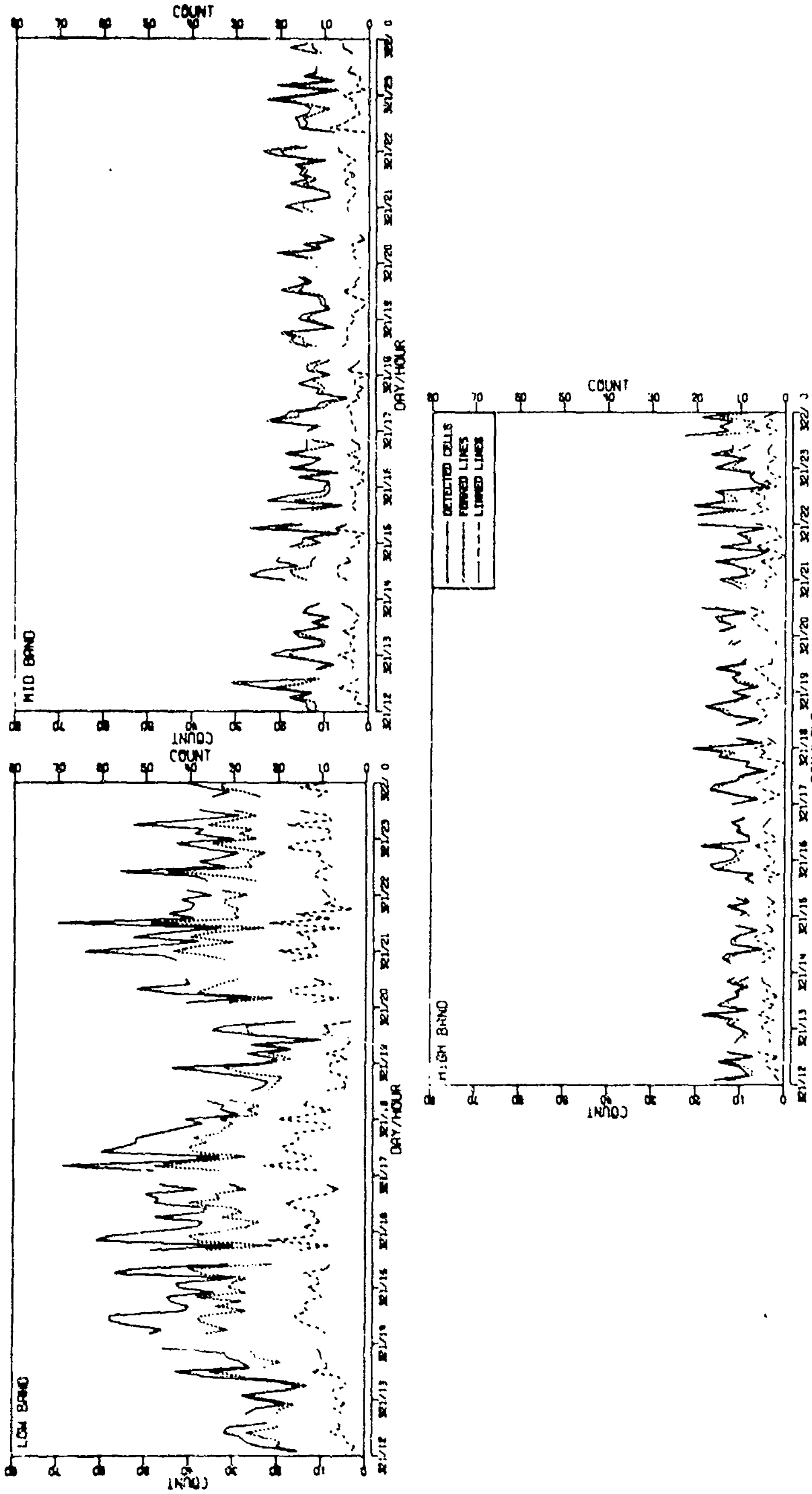

FIGURE III-312
MSS-FVT VERNIER RESOLUTION CLUTTER RESULTS
FOR THE MAX GAIN LIMACONS SENSOR AT SITE A3
DURING THE PHASE II FIELD EVENTS (U)

AS-77-3405

(The reverse of this page is blank.)

APPENDIX J

AMBIENT SOUND FIELD 3D PLOTS

(U) This appendix contains plots of a 3-dimensional representation of the ambient sound field. These plots were generated from vernier resolution calibrated covariance matrices. Only omnidirectional and vertical dipole data were plotted. Such displays are intended to aid the analyst in obtaining an overview of the available data base, in identifying artifacts, and by serving as a guide to later data selection and processing. Each plot covers a 12 h time interval. Each trace represents an intensity average over a 10 min time interval. The data identifier is described below.

II A1 S LBD

- LBD ← Low Band (LBD), Midband (MBD), or High Band (HBD) Data
- S ← Single (S) or Differenced (D) Array
- A1 ← ACODAC Site A1
- II ← Phase II

(The reverse of this page is blank.)

CONFIDENTIAL

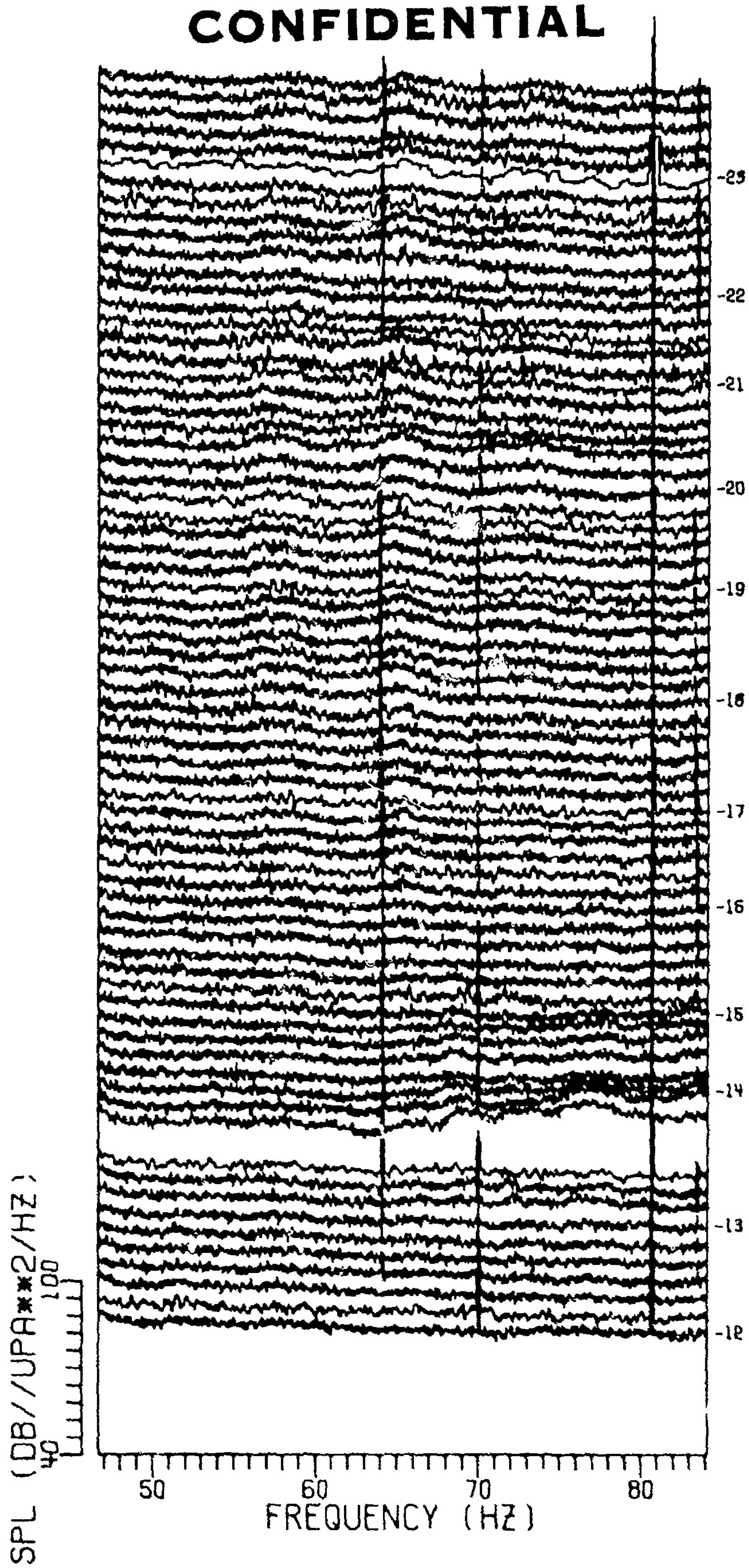

FIGURE III-313

IIA1SLBD 321/12/ 0 - 321/23/55

CONFIDENTIAL

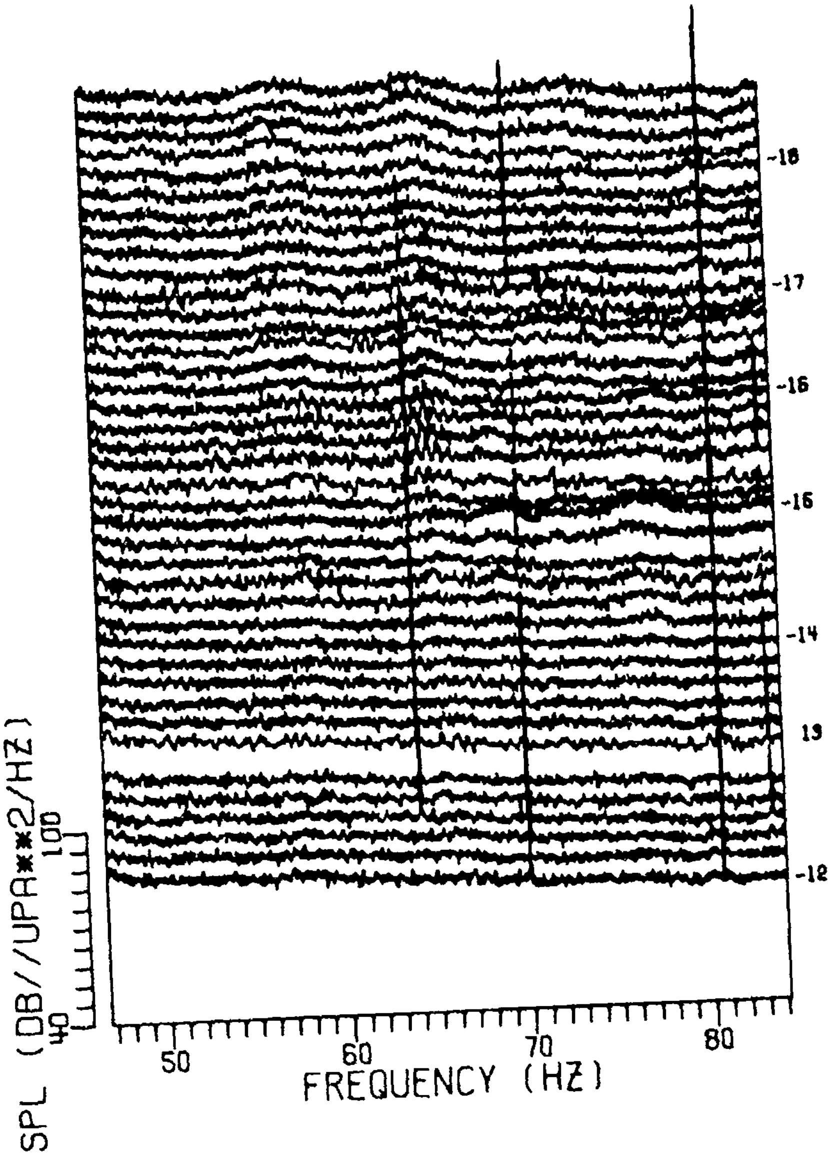

FIGURE III-314

IIA2SLBD 321/12/ 0 - 321/18/55

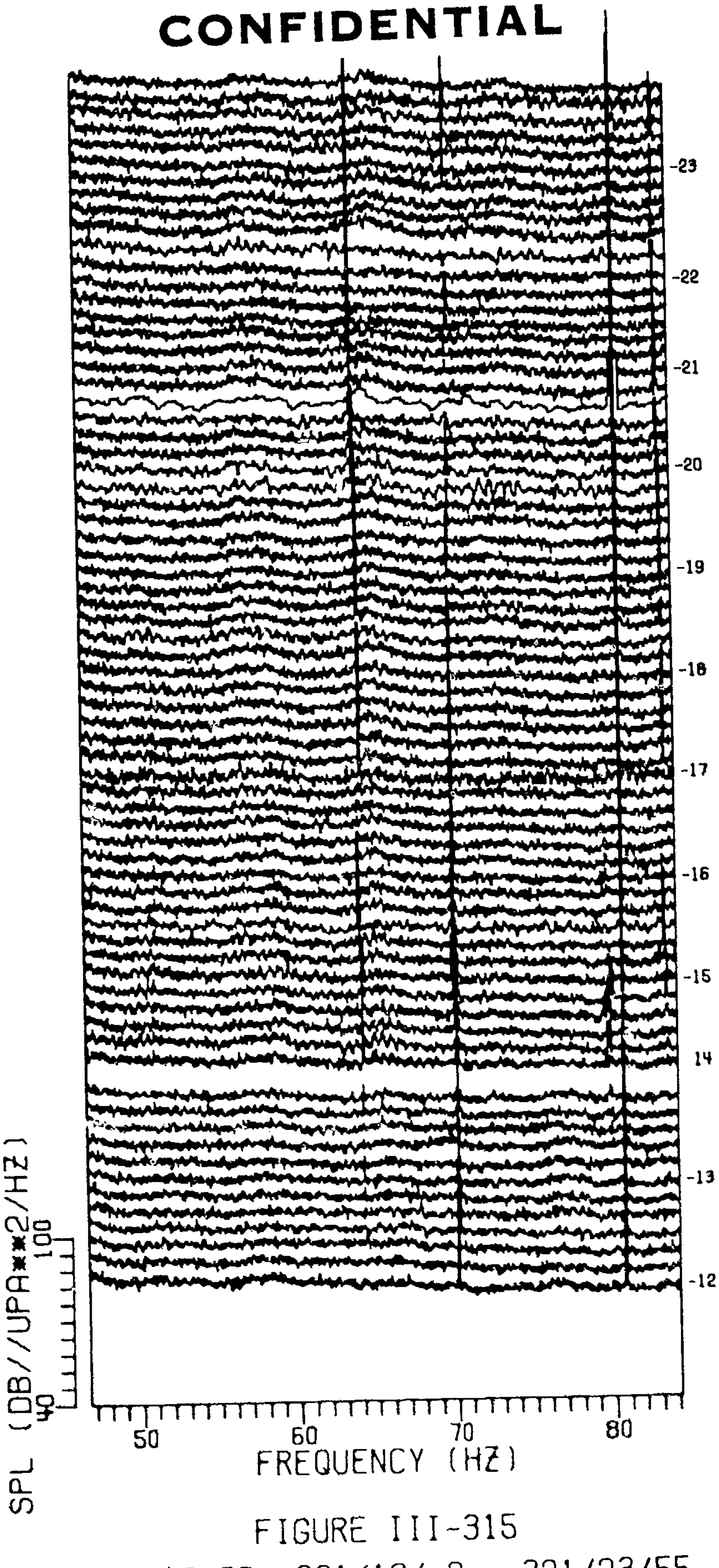

FIGURE III-315

IIA3SLBD 321/12/ 0 - 321/23/55

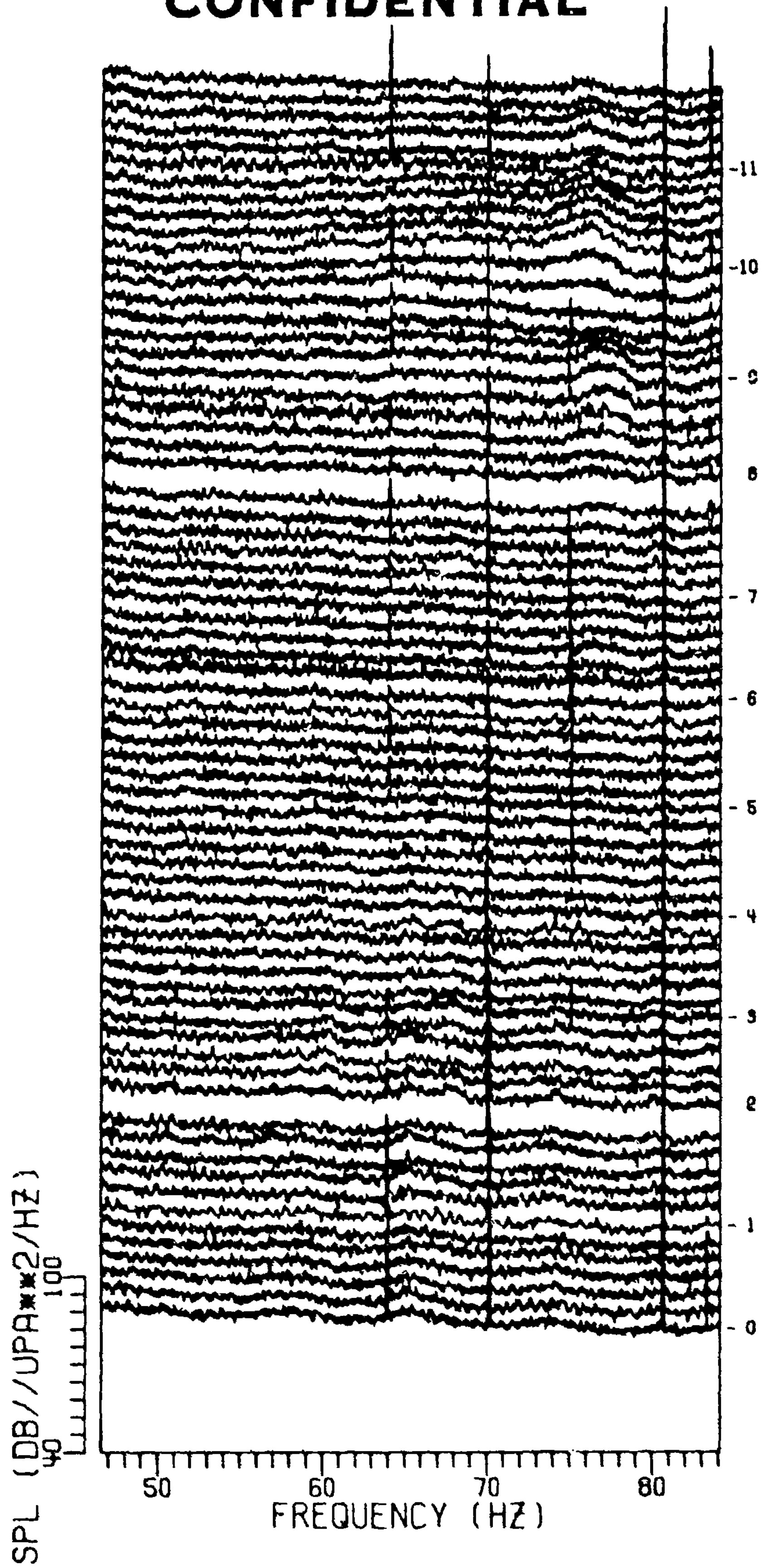

FIGURE III-316

IIA3SLBD 322/ 0/ 0 - 322/11/55

CONFIDENTIAL

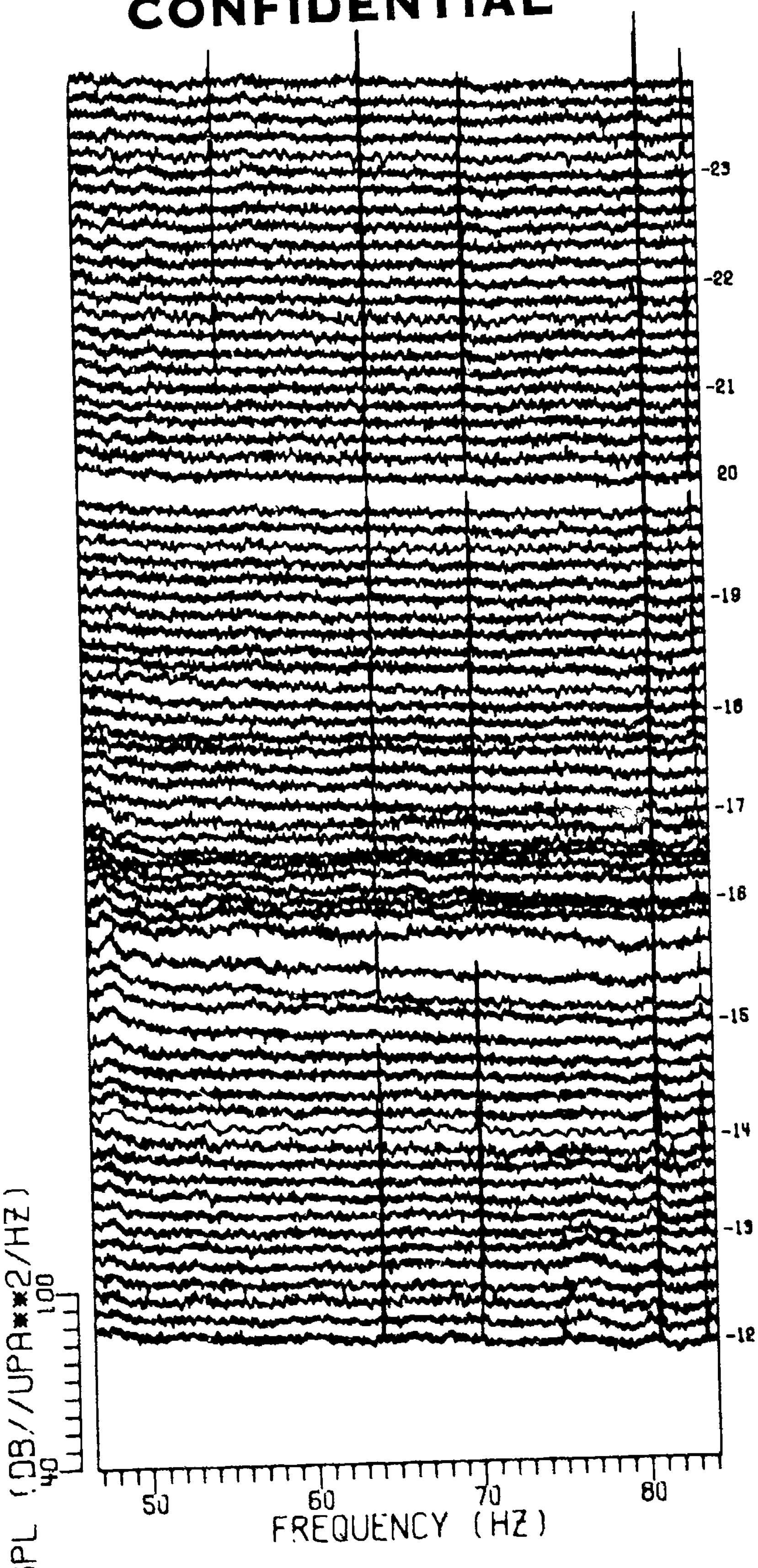

FIGURE III-317

IIA3SLBD 322/12/ 0 - 322/23/55

CONFIDENTIAL

CONFIDENTIAL

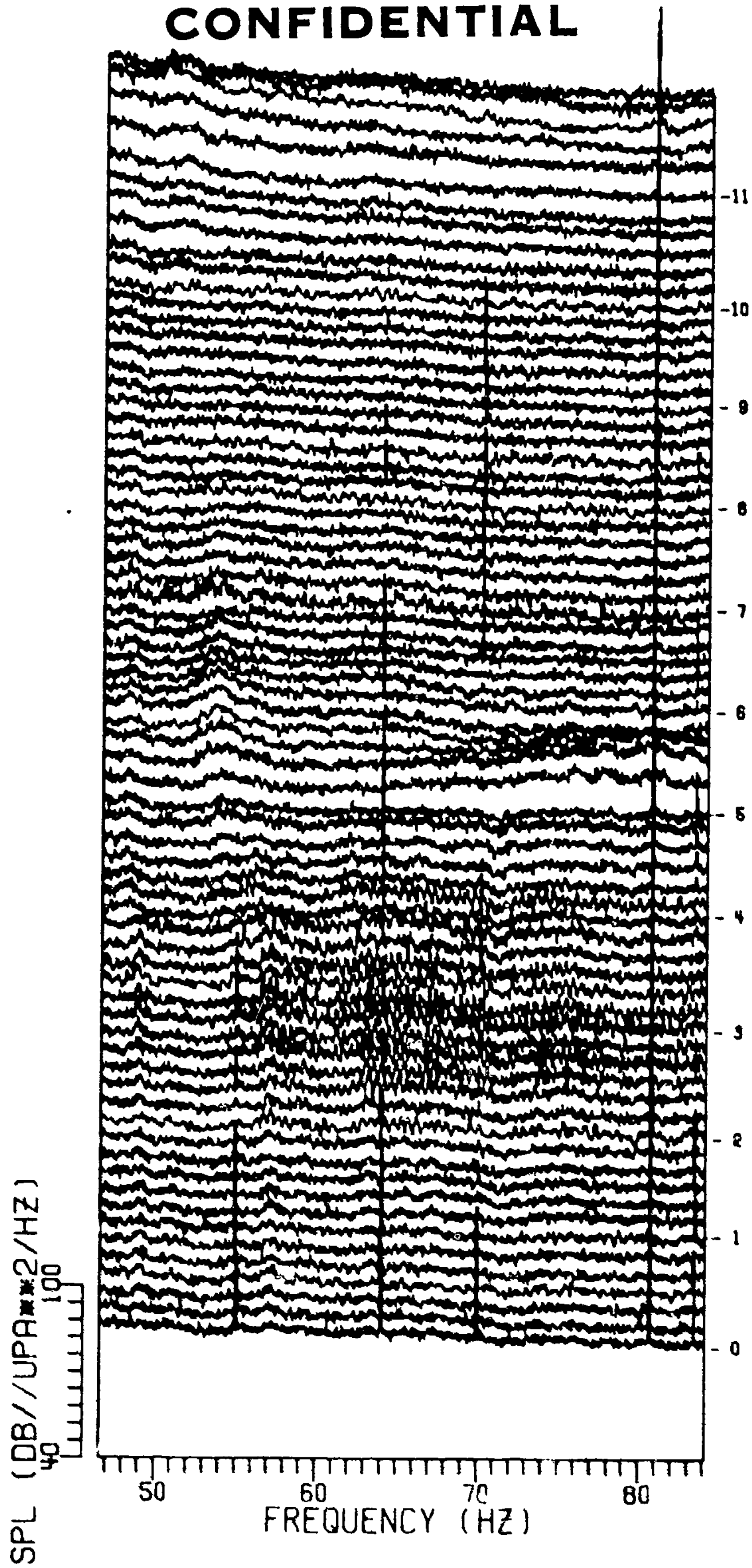

FIGURE III-318

IIA3SLBD 323/ 0/ 0 - 323/11/55

CONFIDENTIAL

CONFIDENTIAL

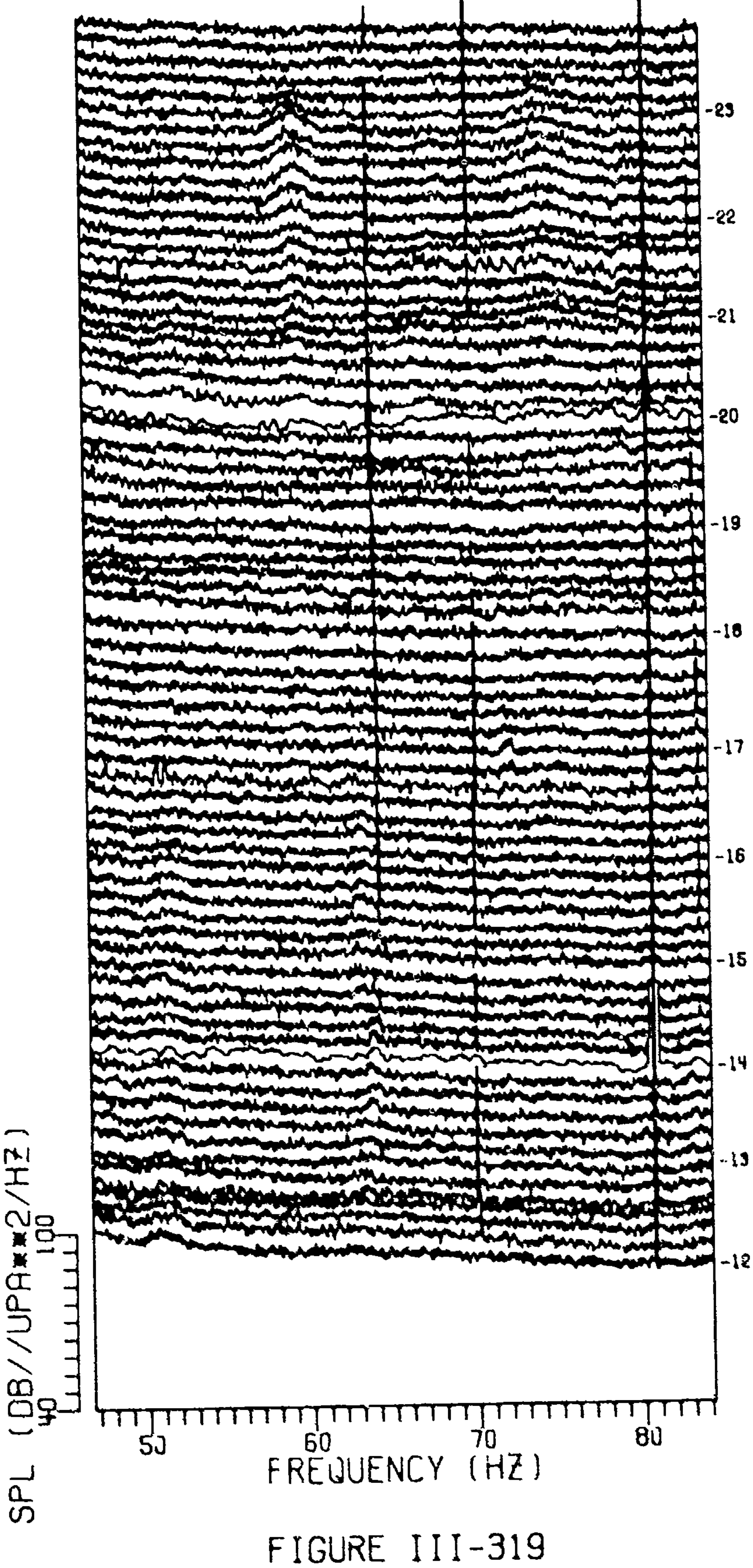

FIGURE III-319

IIA3SLBD 323/12/ 0 - 323/23/55

CONFIDENTIAL

CONFIDENTIAL

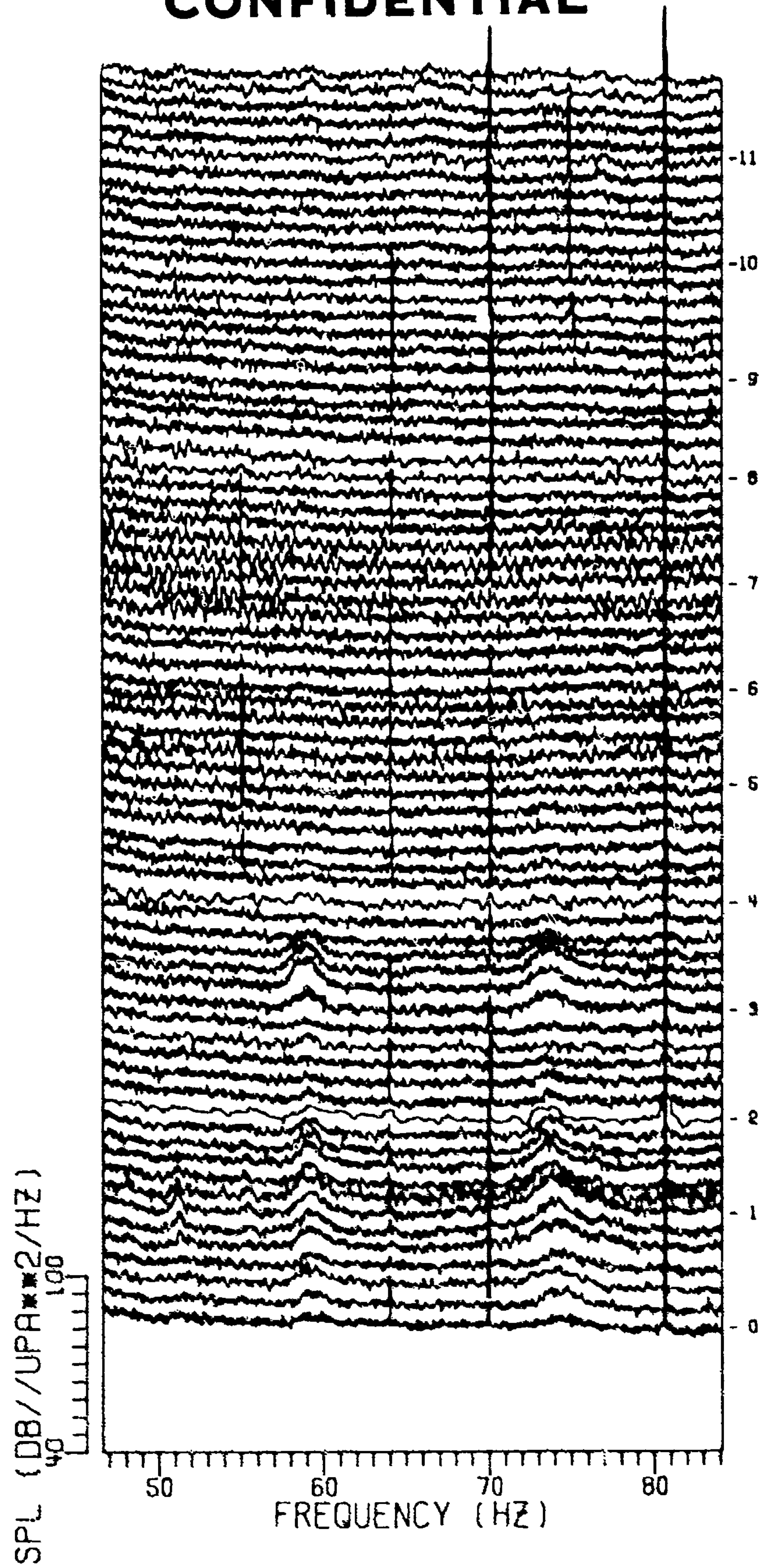

FIGURE III-320

IIA3SLBD 324/ 0/ 0 - 324/11/5(

CONFIDENTIAL

CONFIDENTIAL

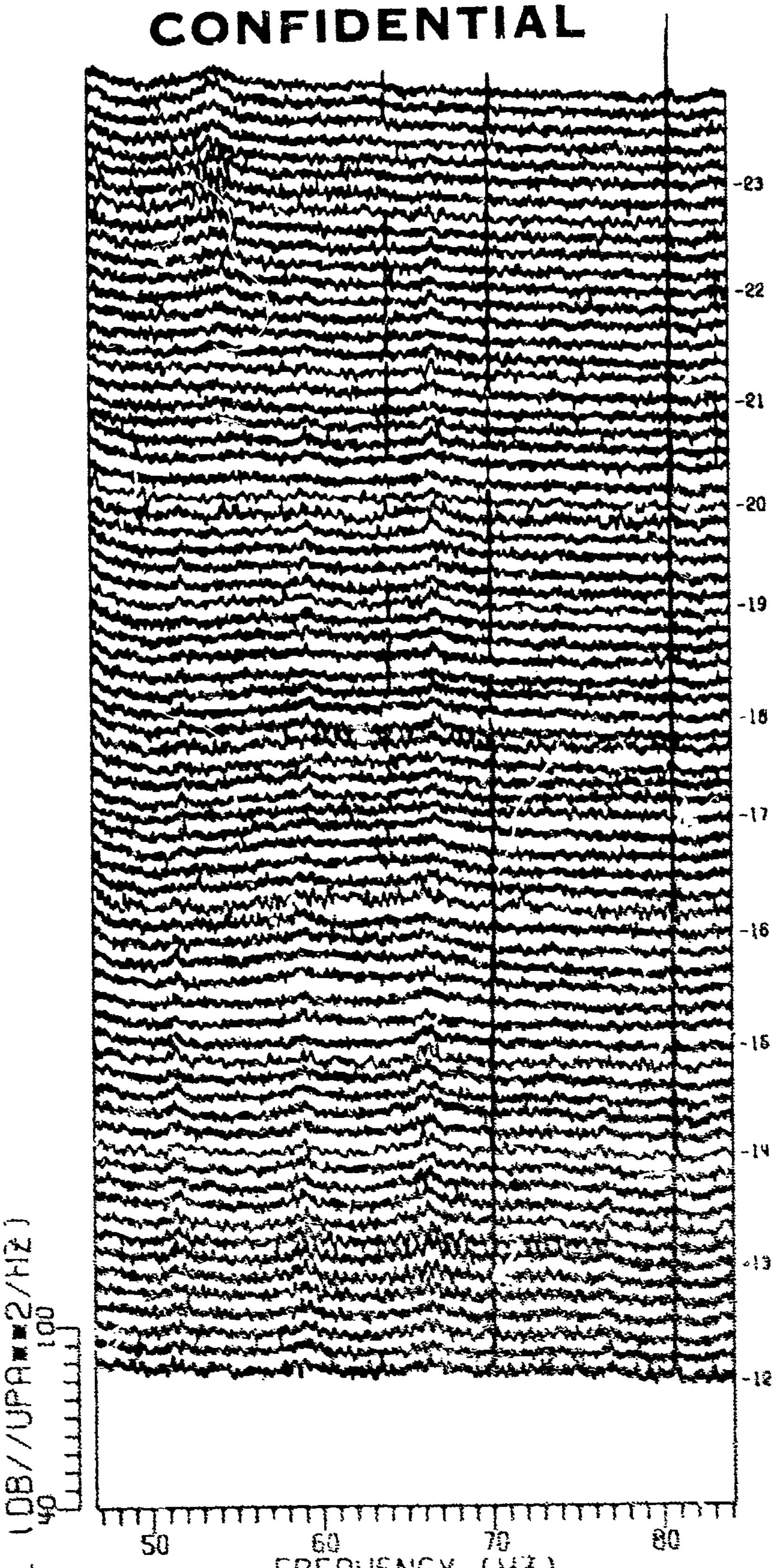

FIGURE III-321

IIA3SLBD 324/12/ 0 - 324/23/55

CONFIDENTIAL

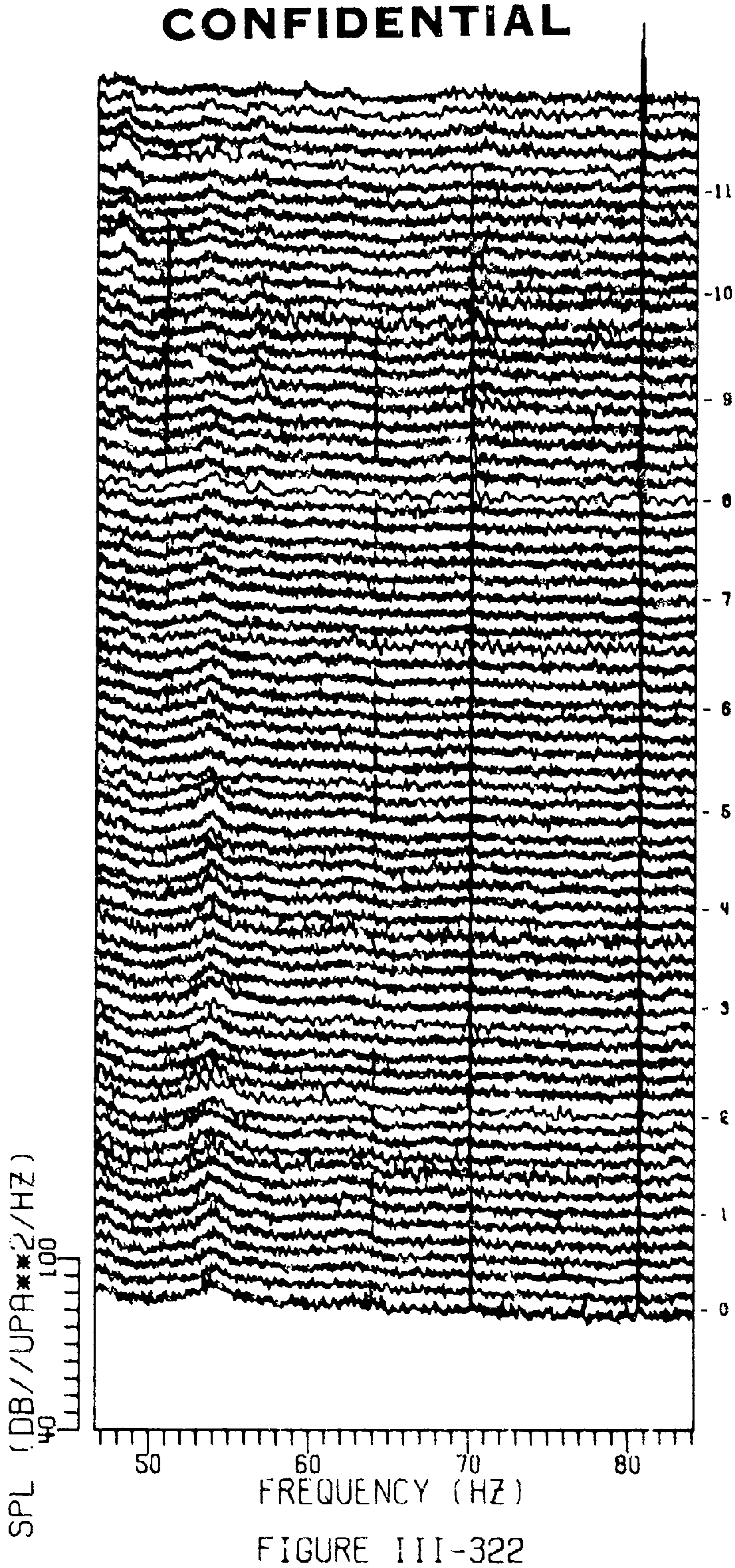

FIGURE III-322

IIA3SLBD 325/ 0/ 0 - 325/11/55

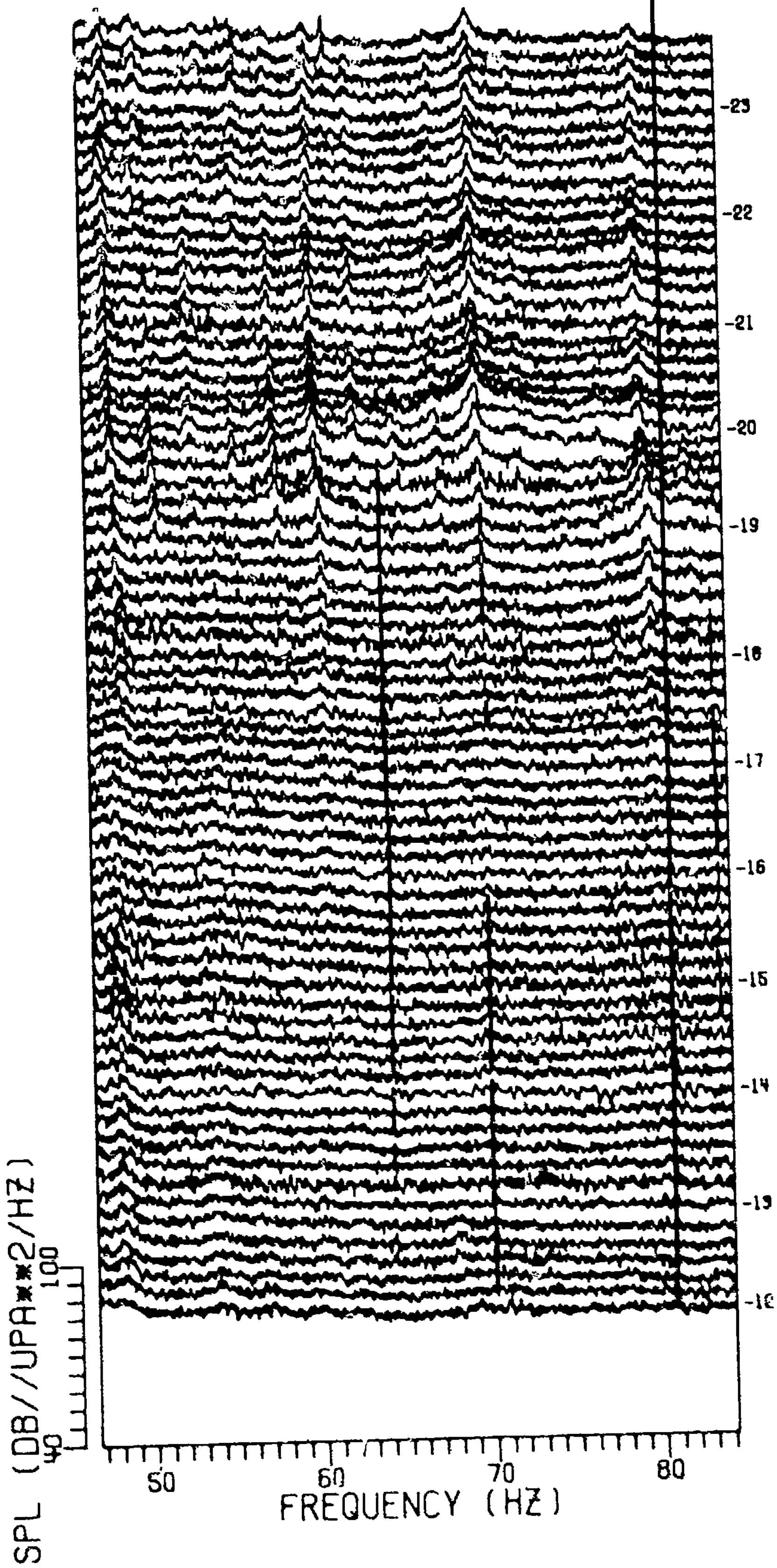

FIGURE III-323

IIA3SLBD 325/12/ 0 - 325/23/55

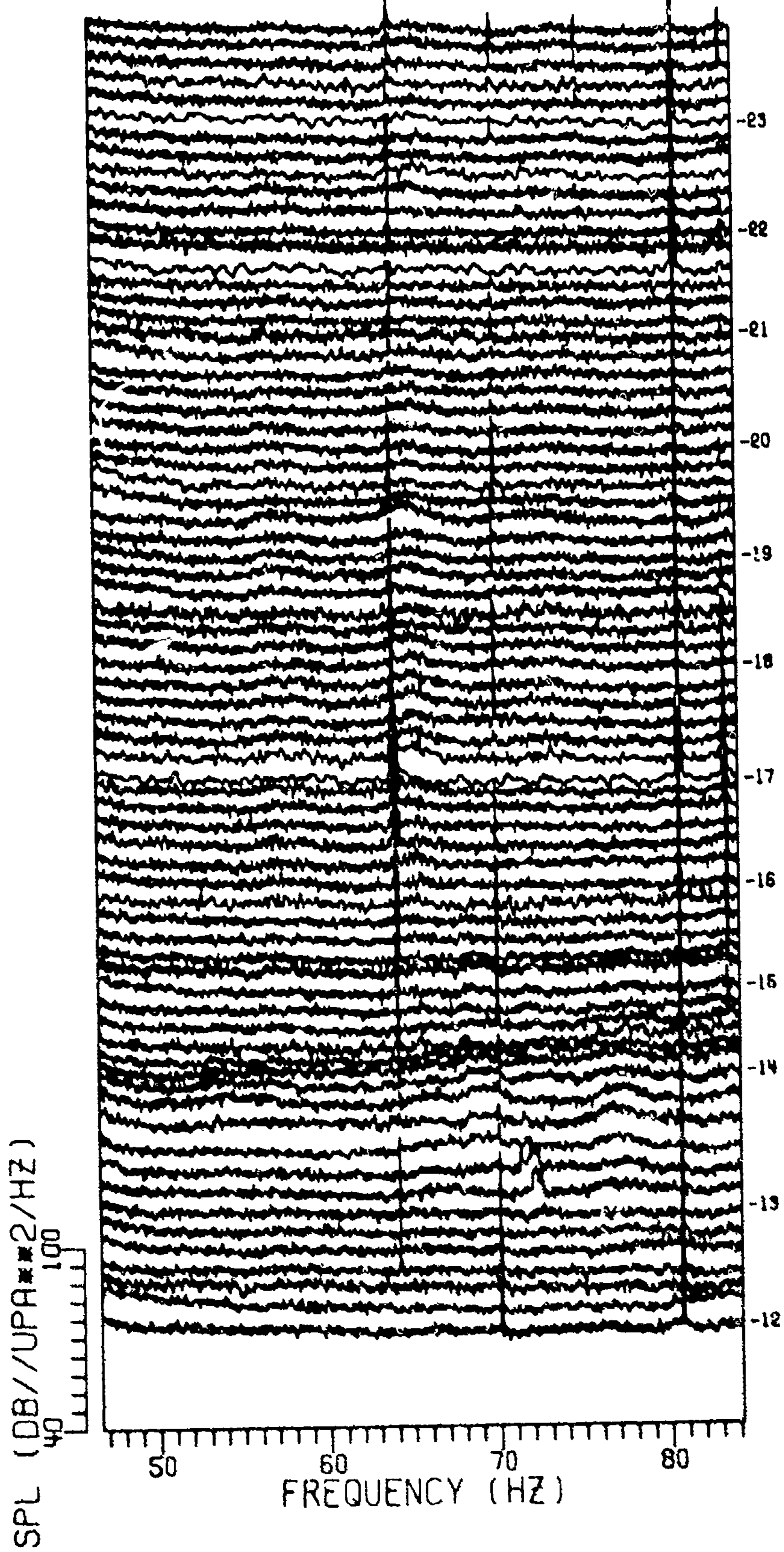

FIGURE III-324
IIA1DLBD 321/12/ 0 - 321/23/55

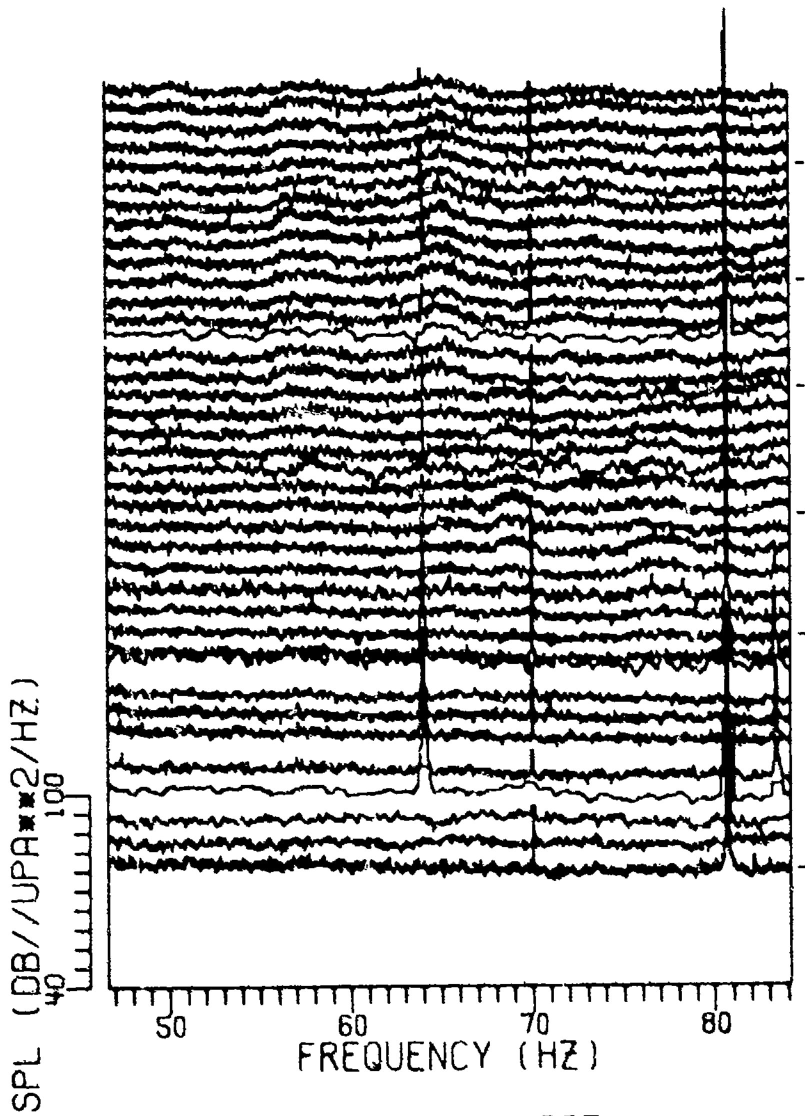

FIGURE III-325
IIA2DLBD 321/12/ 0 - 321/18/55

CONFIDENTIAL

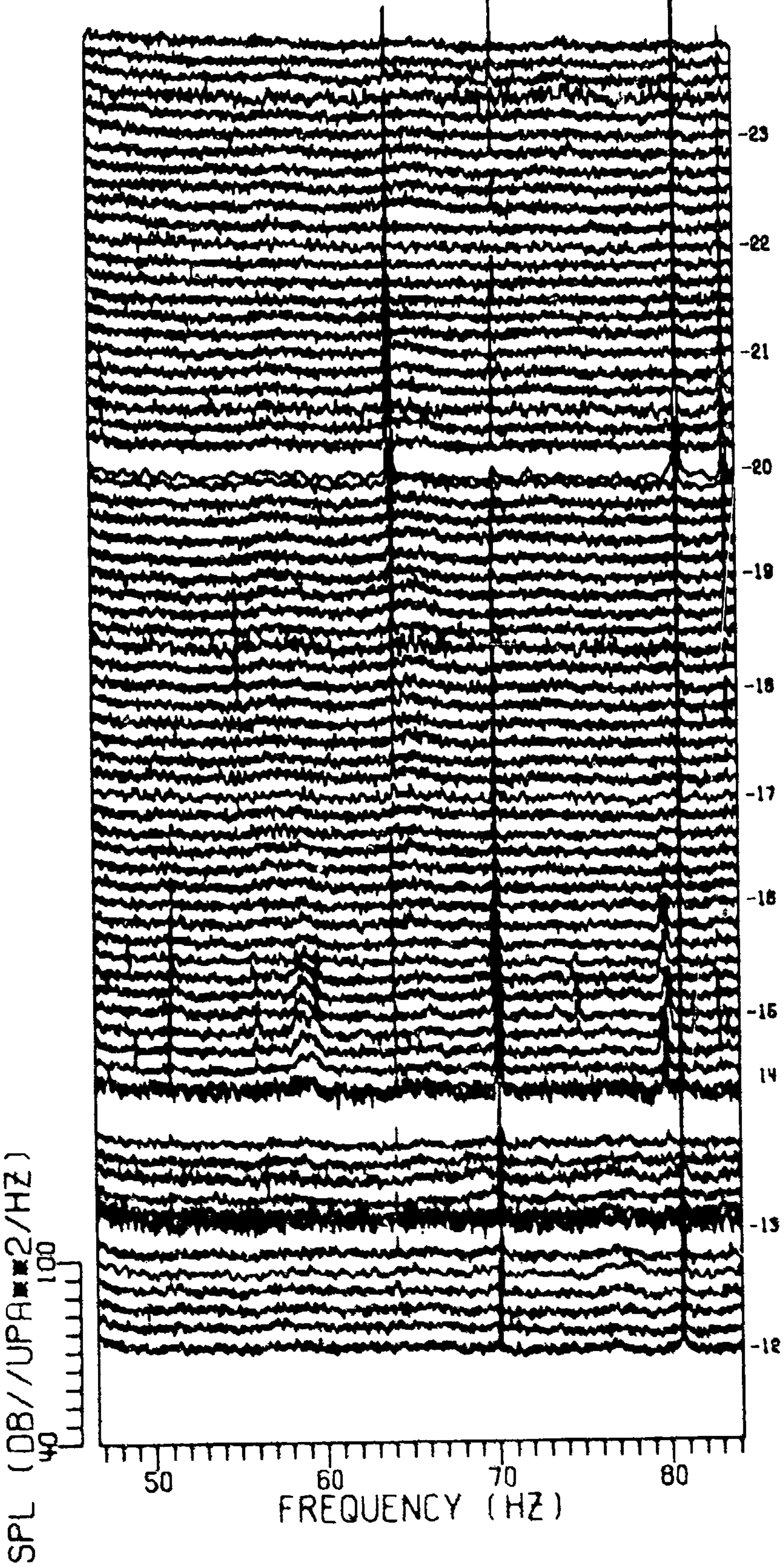

FIGURE III-326

IIA3DLBD 321/12/ 0 - 321/23/55

CONFIDENTIAL

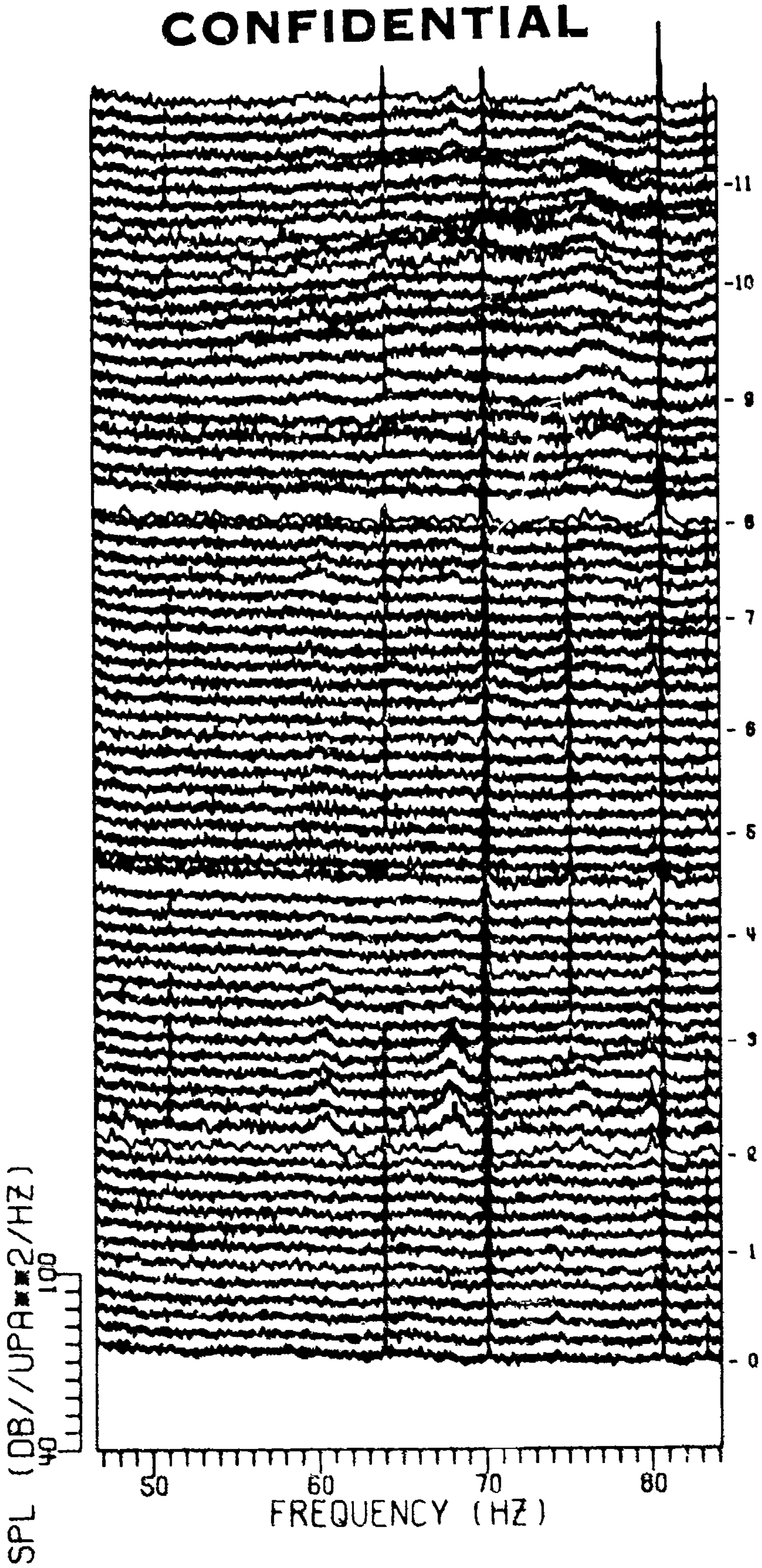

FIGURE III-327

IIA3DLBD 322/ 0/ 0 - 322/11/55

CONFIDENTIAL

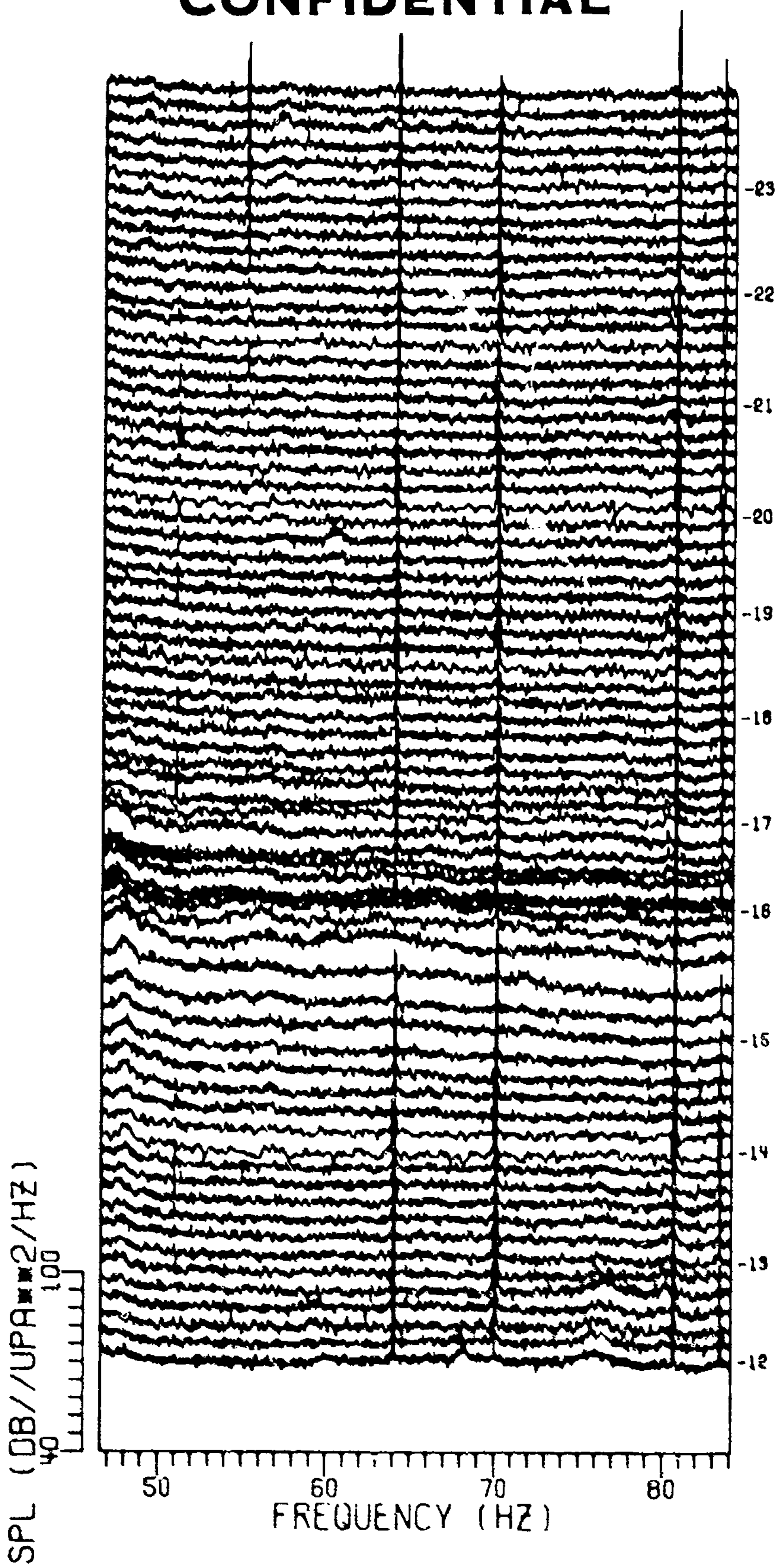

FIGURE III-328

IIA3DLBD 322/12/ 0 - 322/23/55

CONFIDENTIAL

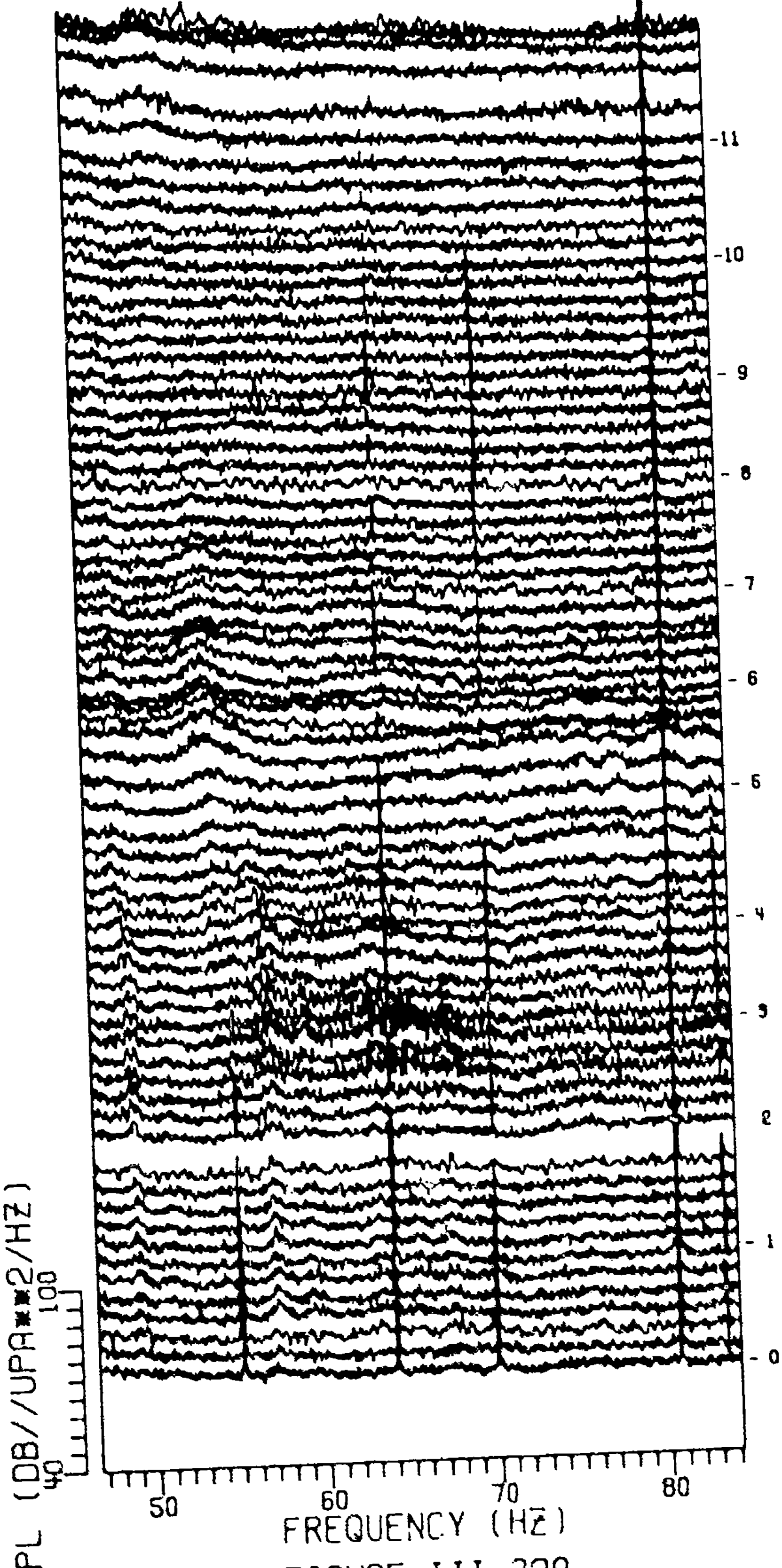

FIGURE III-329

IIA3DLBD 323/ 0/ 0 - 323/11/55

CONFIDENTIAL

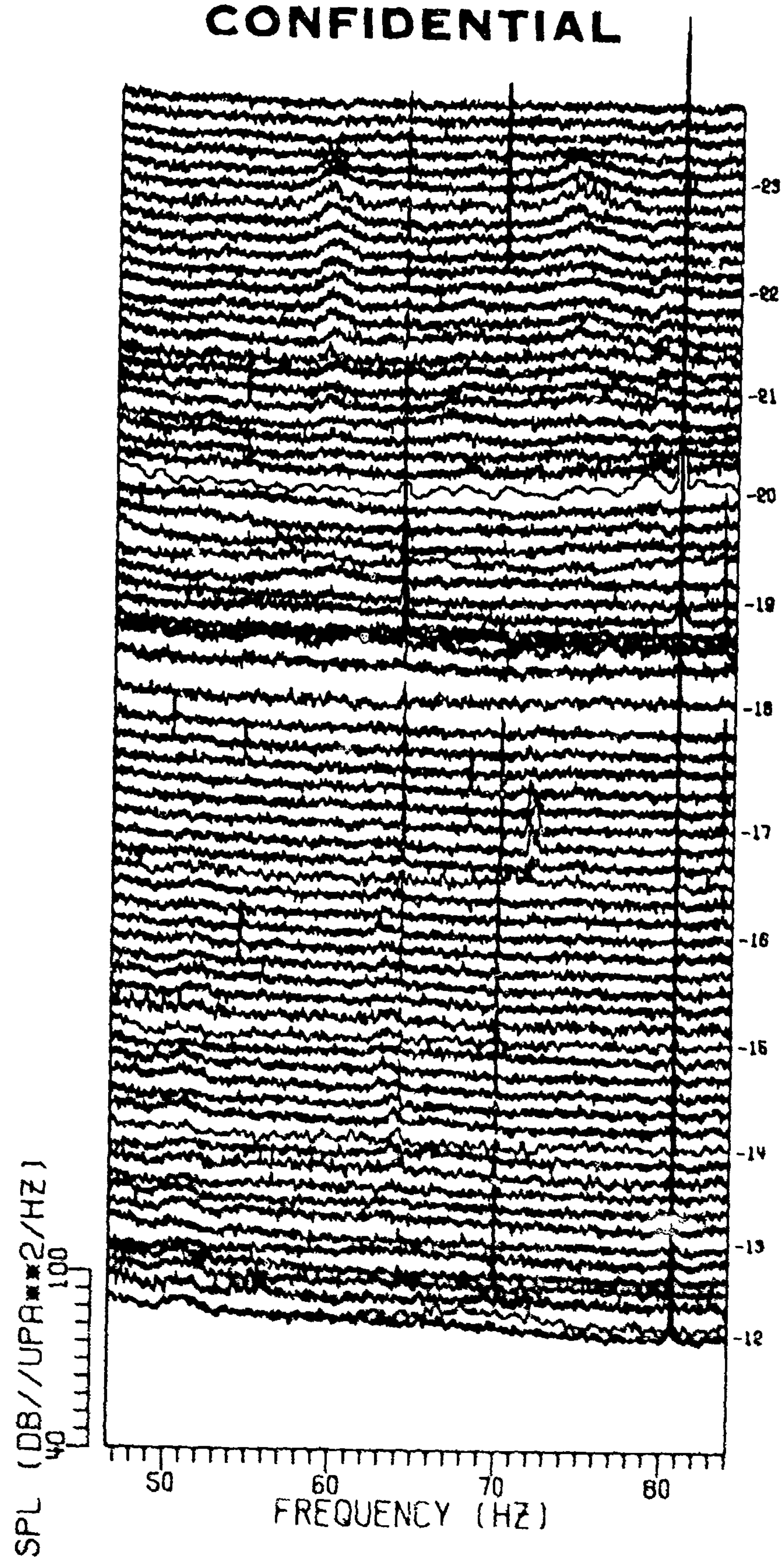

FIGURE III-330
IIA3OLBD 323/12/ 0 - 323/23/55

CONFIDENTIAL

CONFIDENTIAL

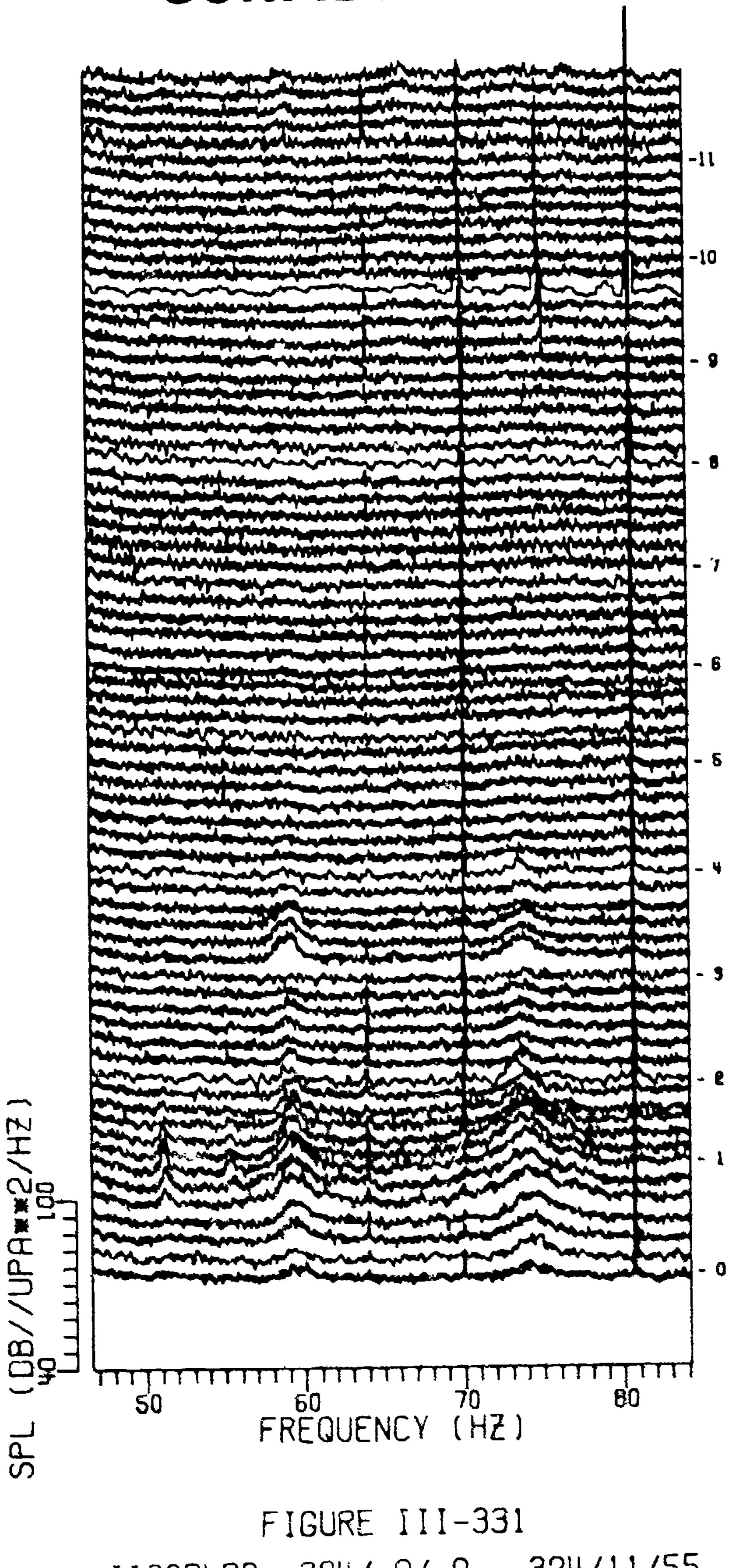

FIGURE III-331

IIA3DLBD 324/ 0/ 0 - 324/11/55

CONFIDENTIAL

CONFIDENTIAL

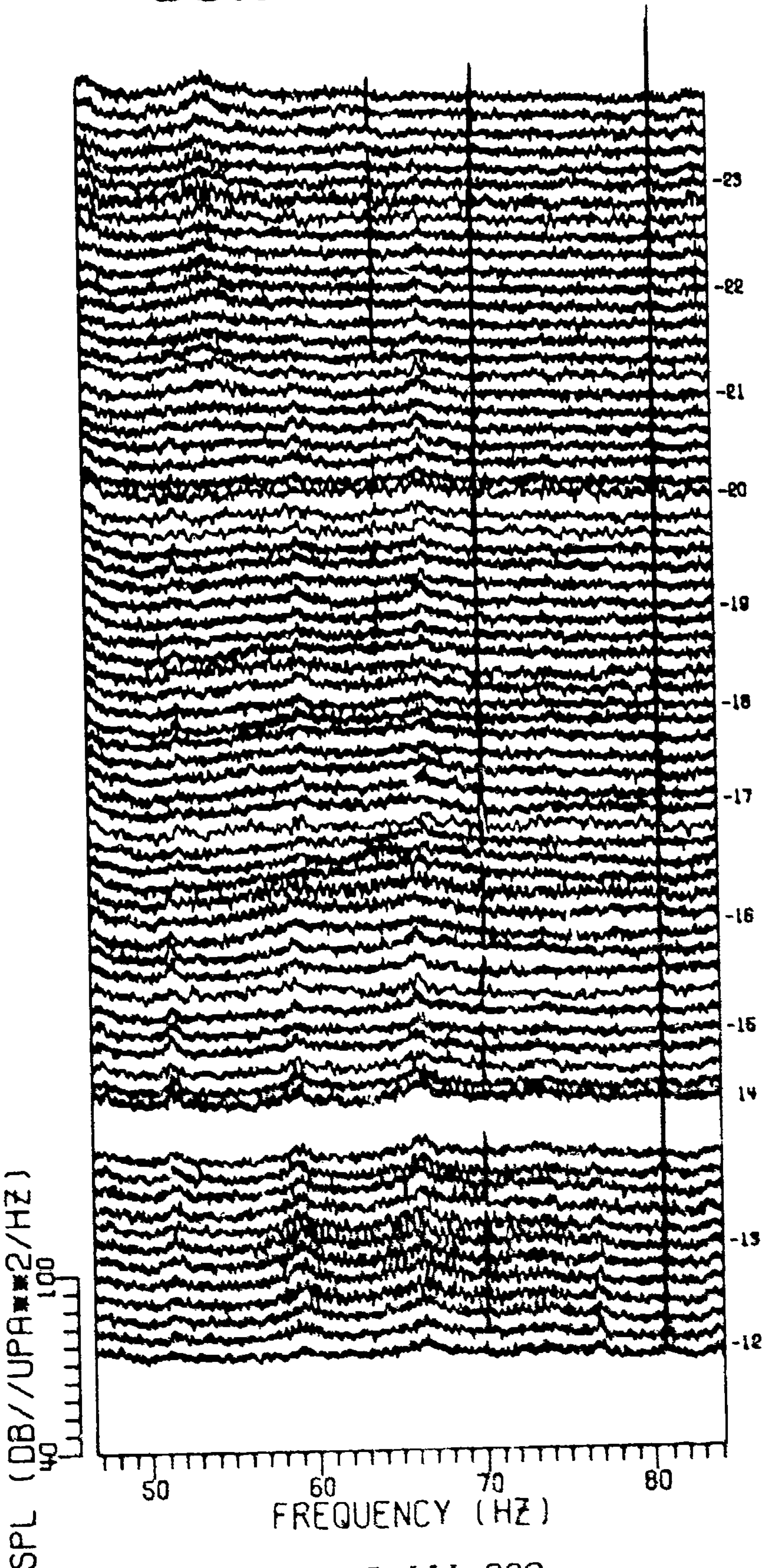

FIGURE III-332

IIA5DLBD 324/12/ 0 - 324/23/55

CONFIDENTIAL

FIGURE III-333
IIA3DLBD 325/ 0/ 0 - 325/11/55

CONFIDENTIAL

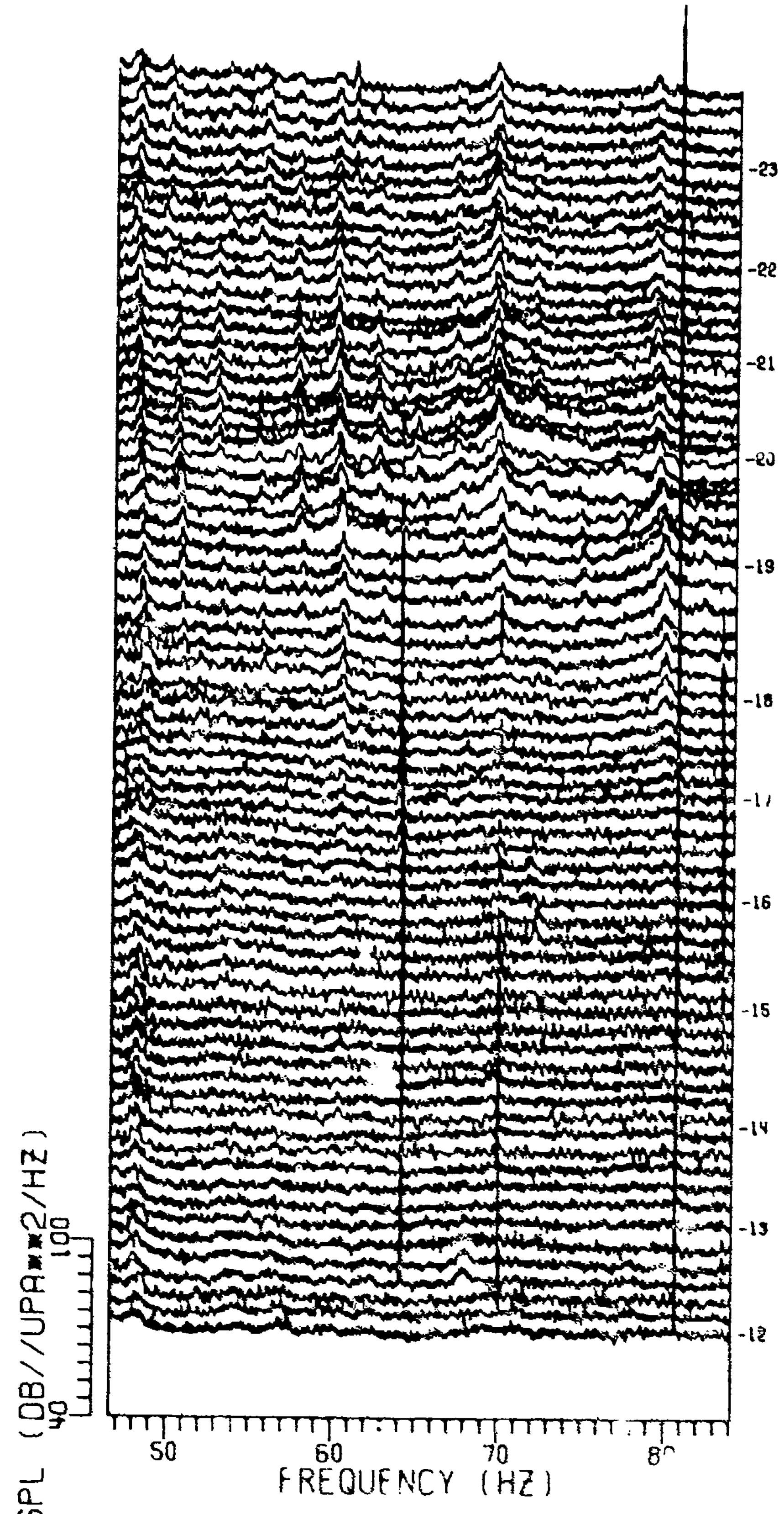

FIGURE III-334

IIA3OLBD 325/12/ 0 - 325/23/55

CONFIDENTIAL

CONFIDENTIAL

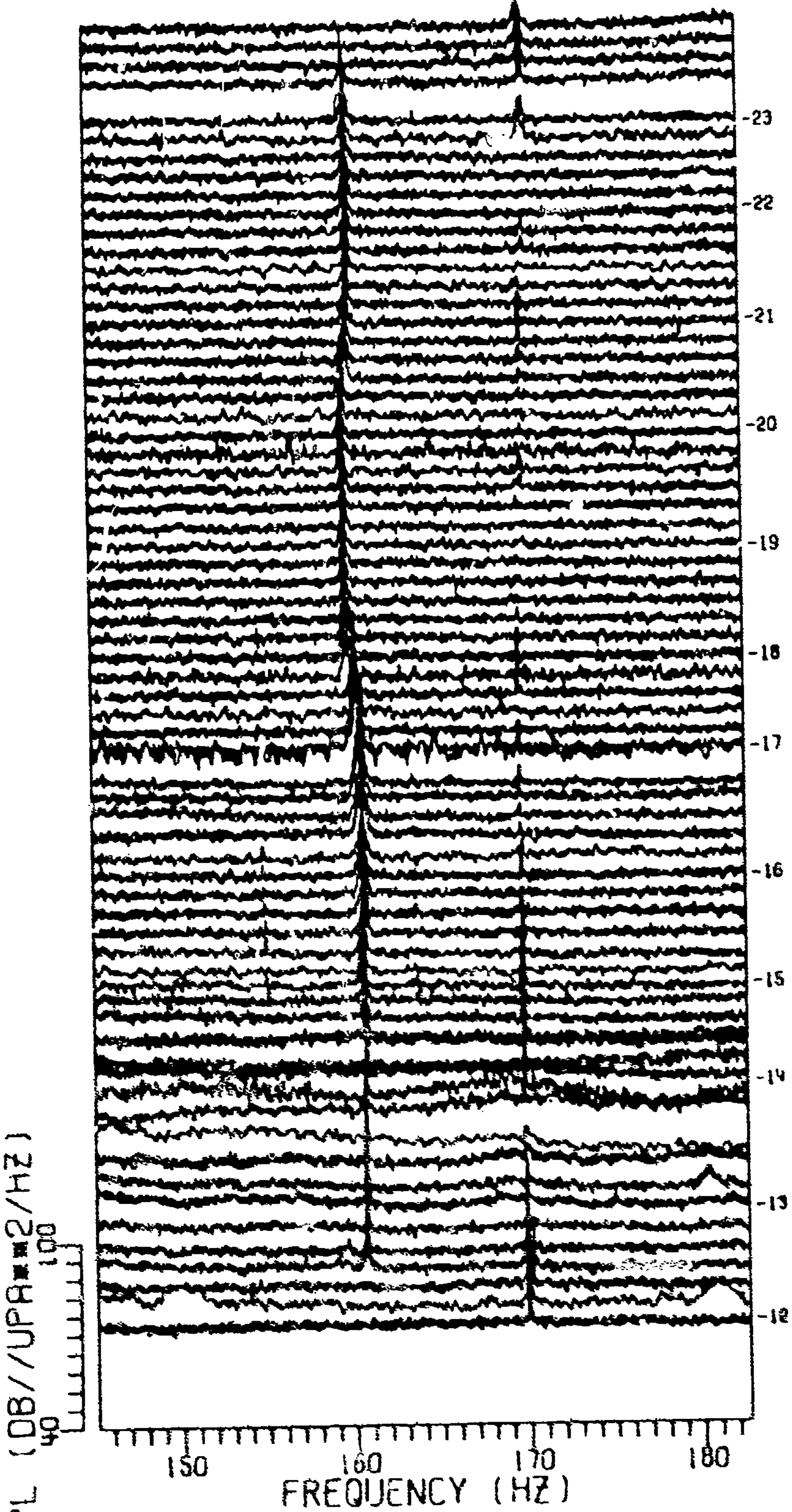

FIGURE III-335

IIA1SMBD 321/12/ 0 - 321/23/55

CONFIDENTIAL

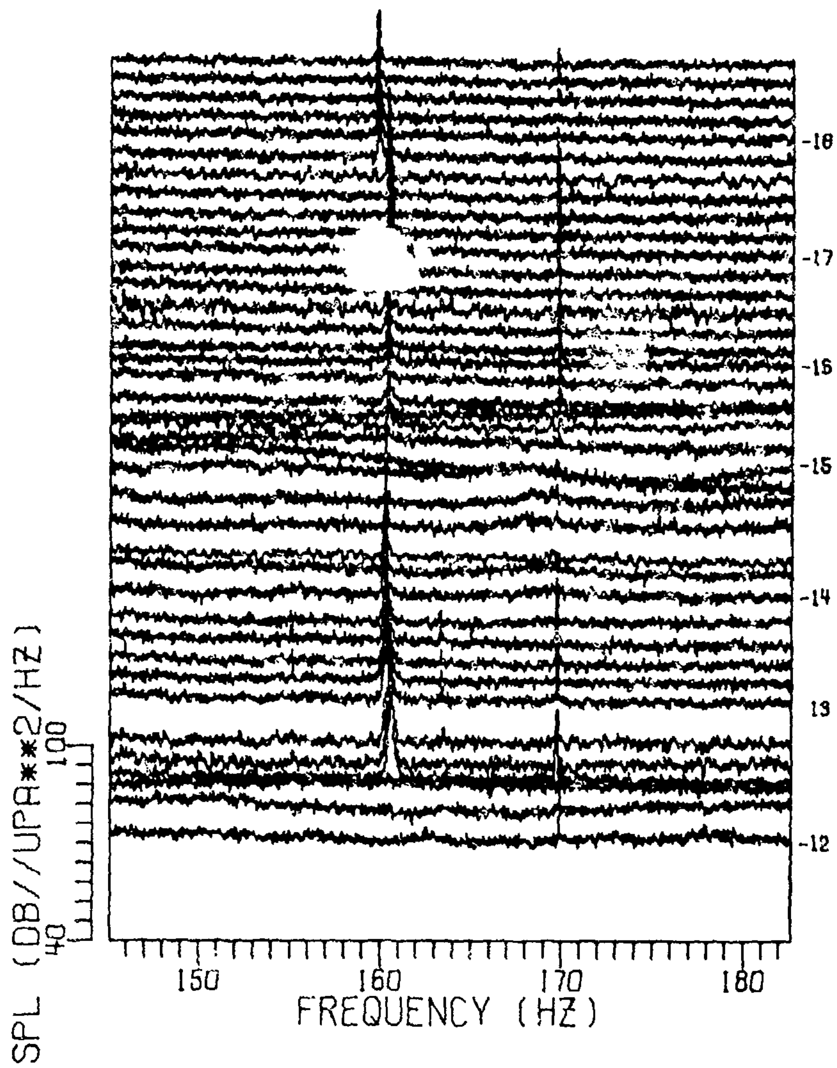

FIGURE III-336
IIA2SMBD 321/12/ 0 - 321/18/55

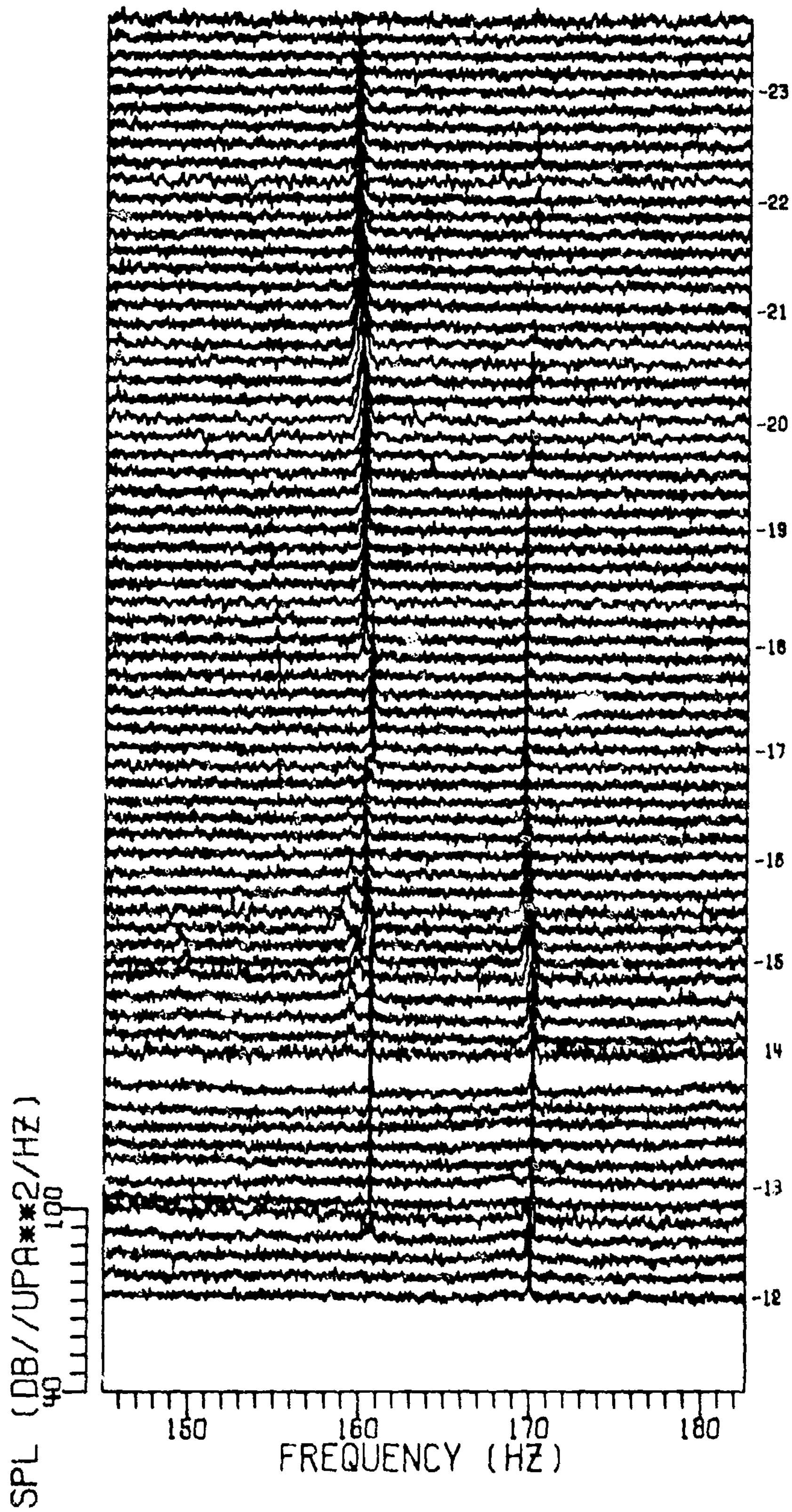

FIGURE III-337

IIA3SMBD 321/12/ 0 - 321/23/55

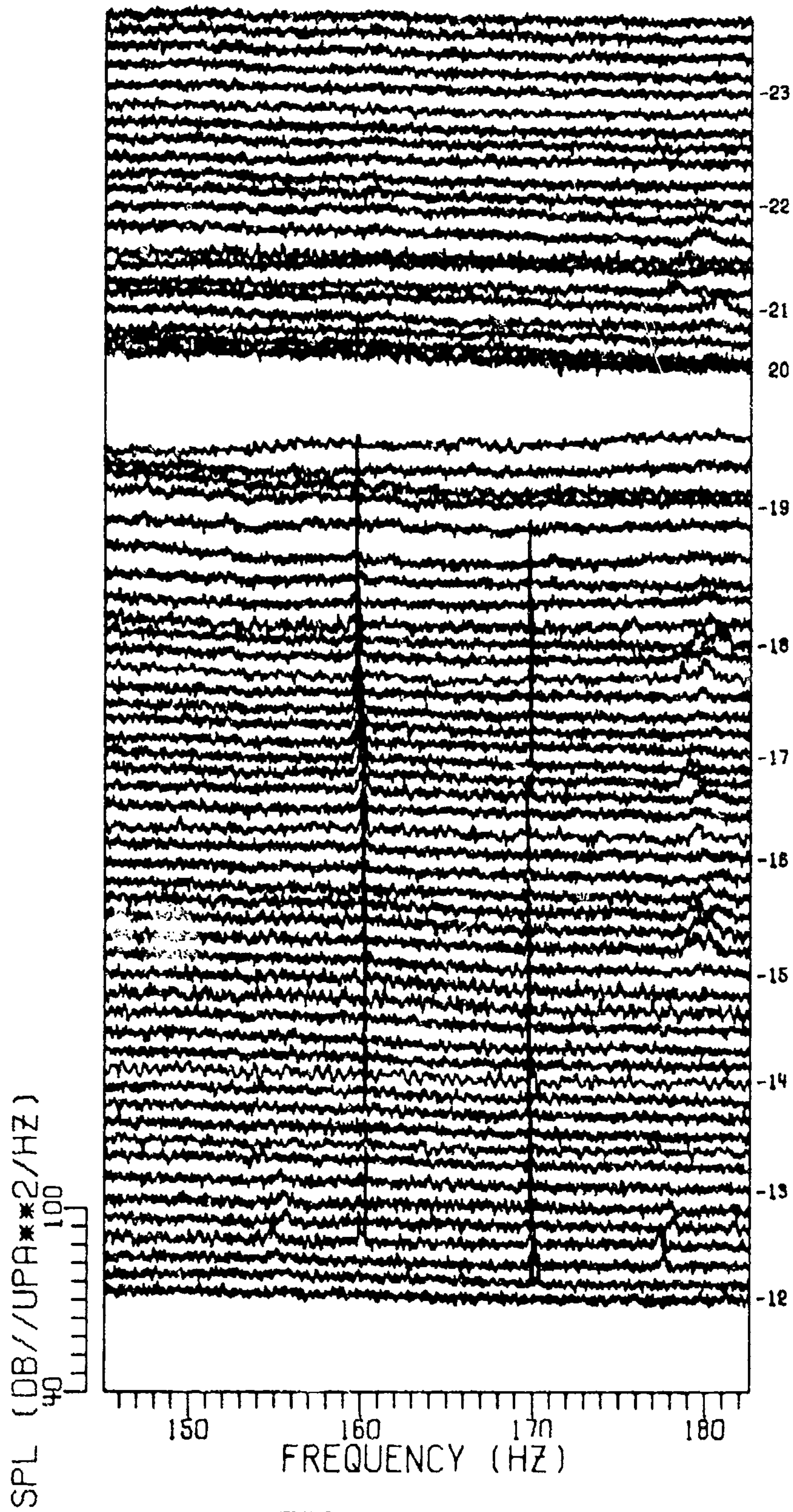

FIGURE III-338

IIA3SMBD 325/12/ 0 - 325/23/55

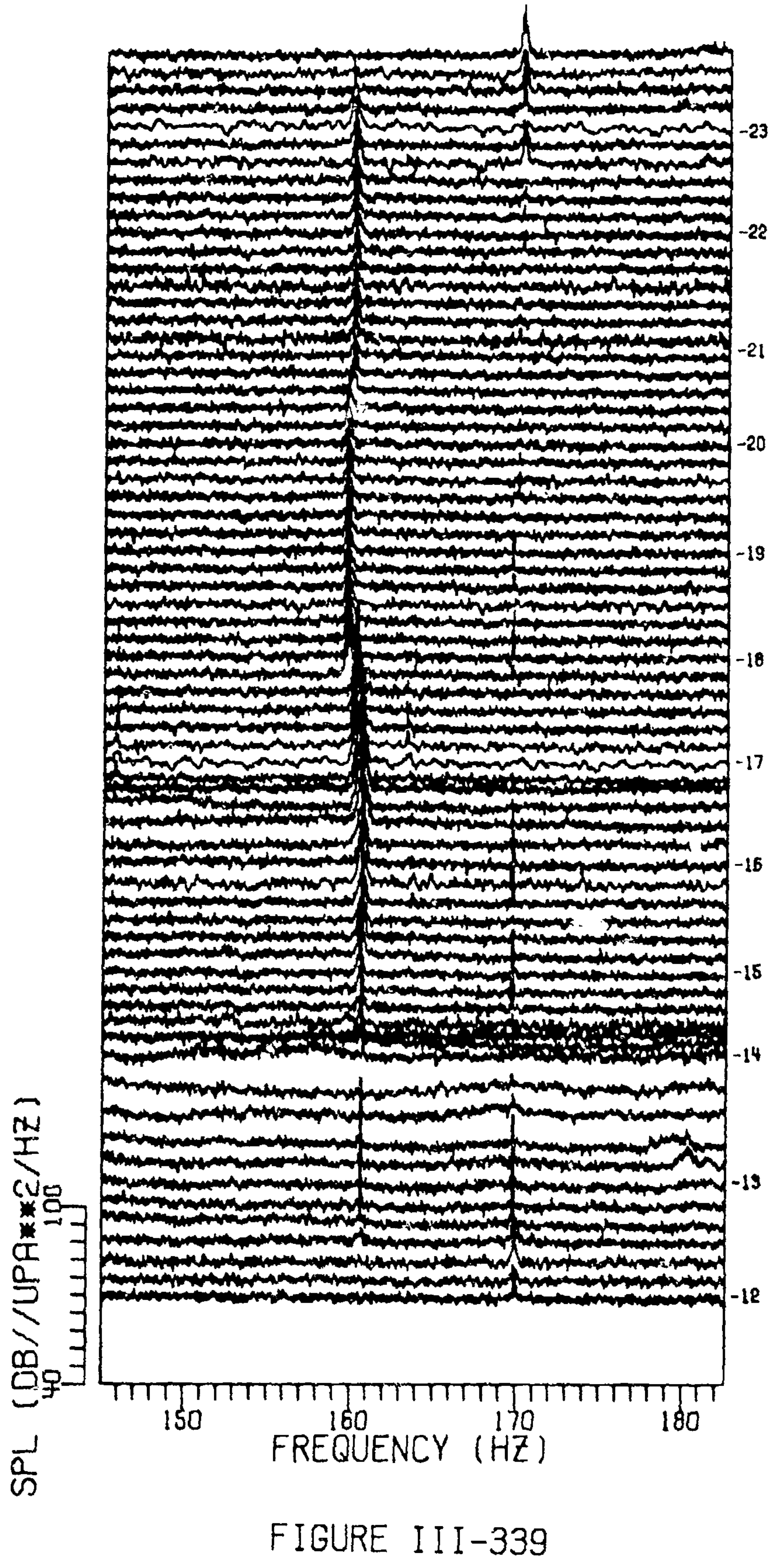

FIGURE III-339

IIA1DMBD 321/12/ 0 - 321/23/55

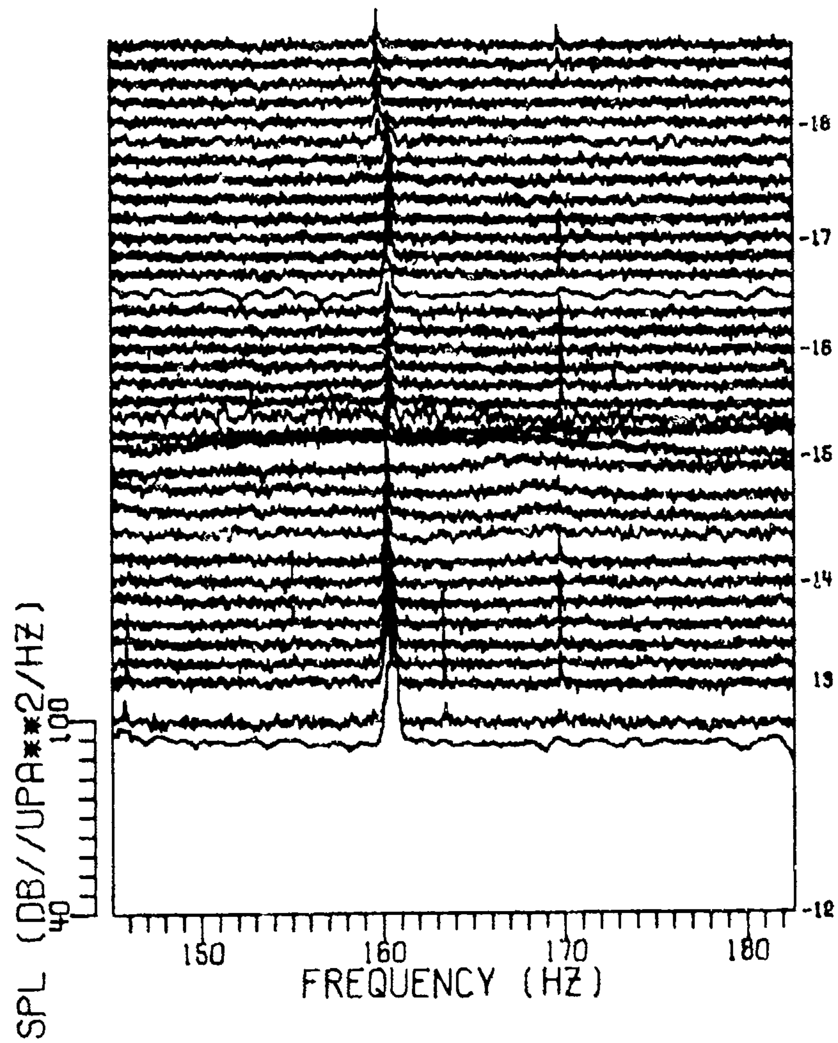

FIGURE III-340
IIA2DMBD 321/12/ 0 - 321/18/55

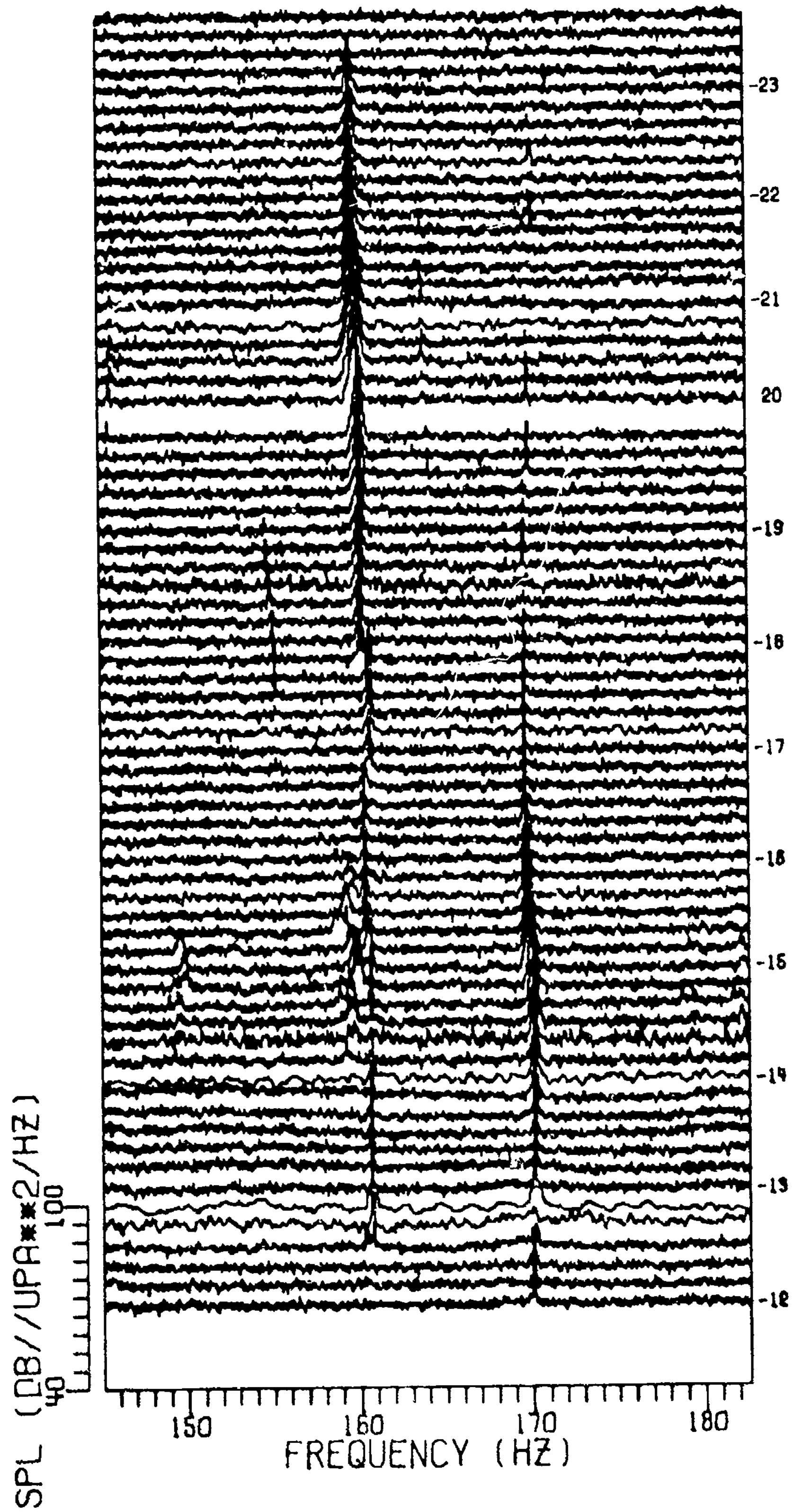

FIGURE III-341

IIA3DMBD 321/12/ 0 - 321/23/55

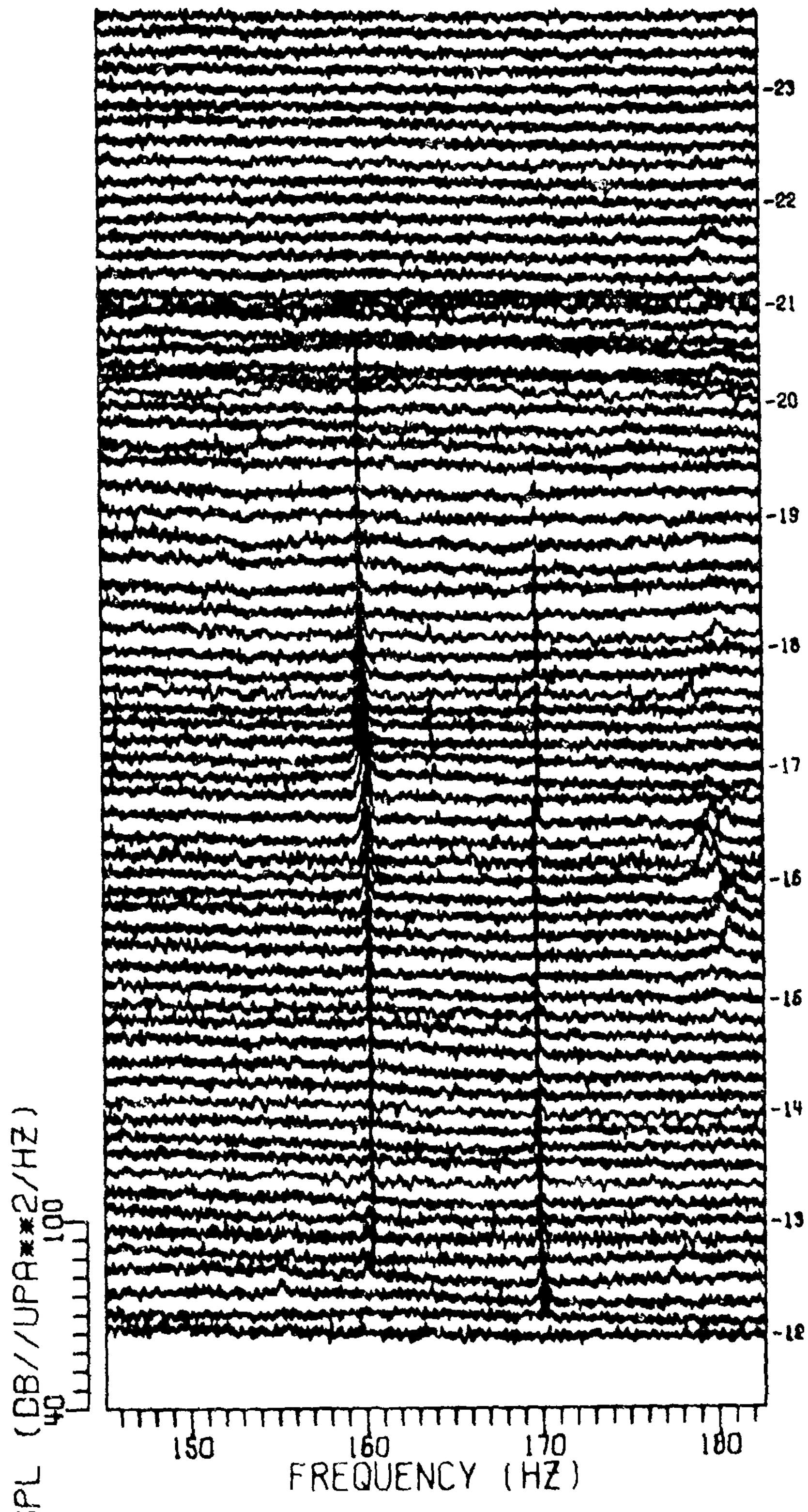

FIGURE III-342

IIA3DMBD 325/12/ 0 - 325/23/55

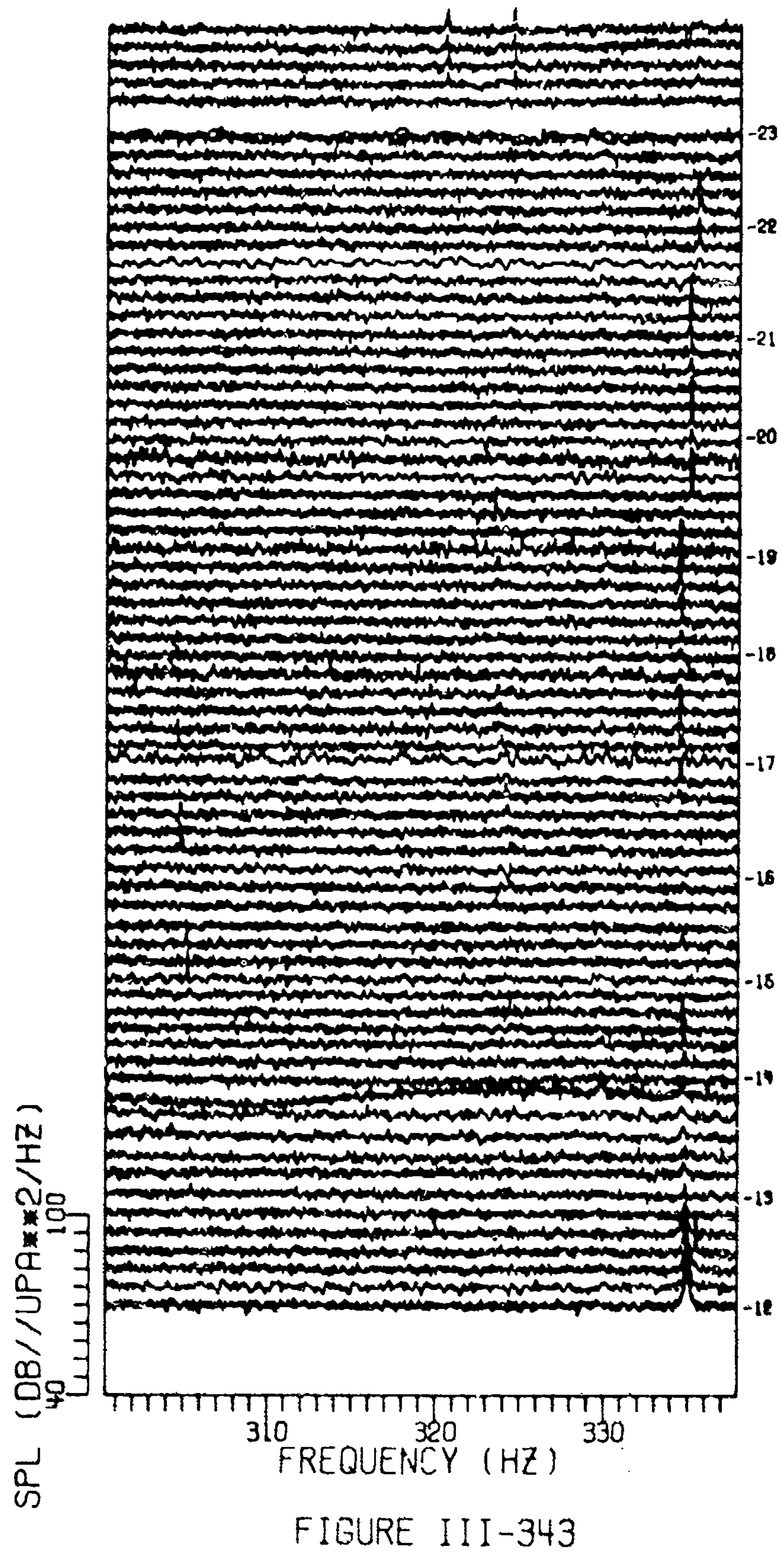

FIGURE III-343

IIA1SHBD 321/12/ 0 - 321/23/55

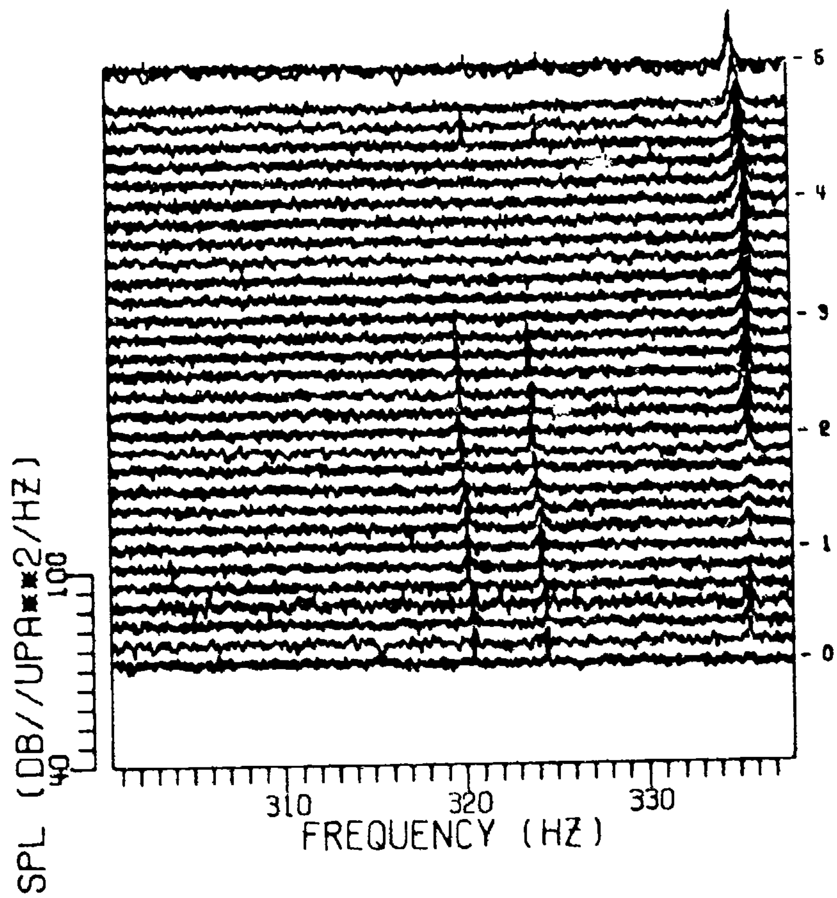

FIGURE III-344

IIA1SHBD 322/ 0/ 0 - 322/ 5/25

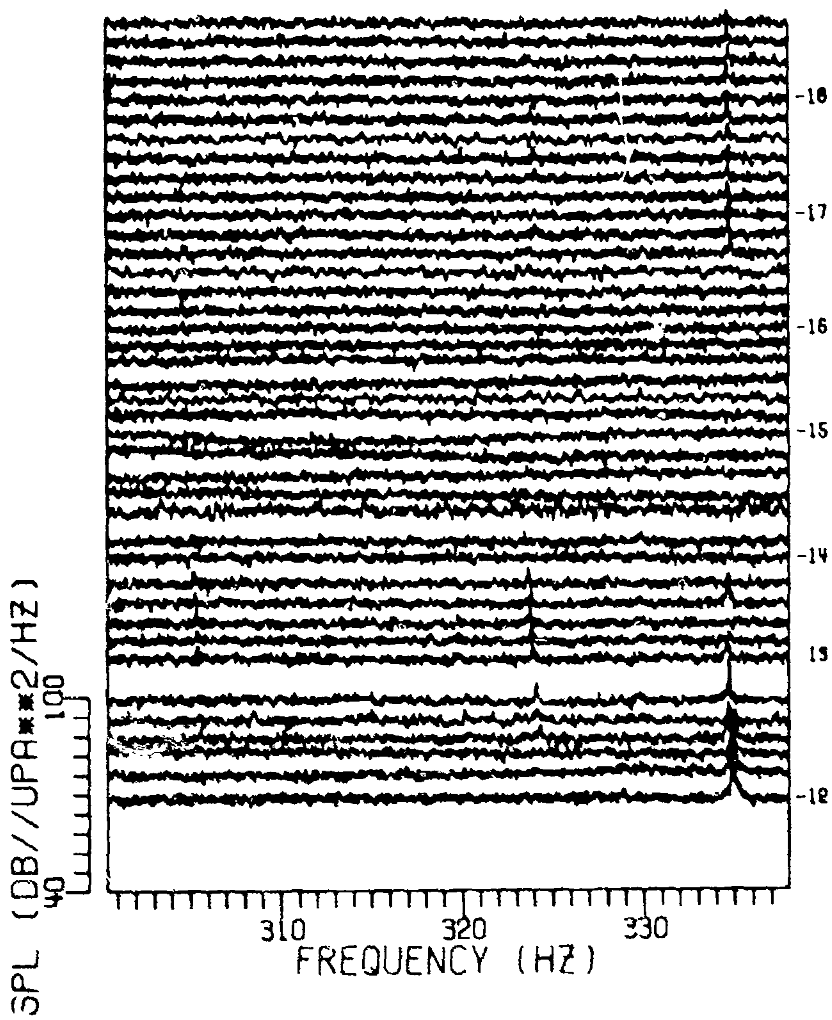

FIGURE III-345

IIA2SHBD 321/12/ 0 - 321/18/55

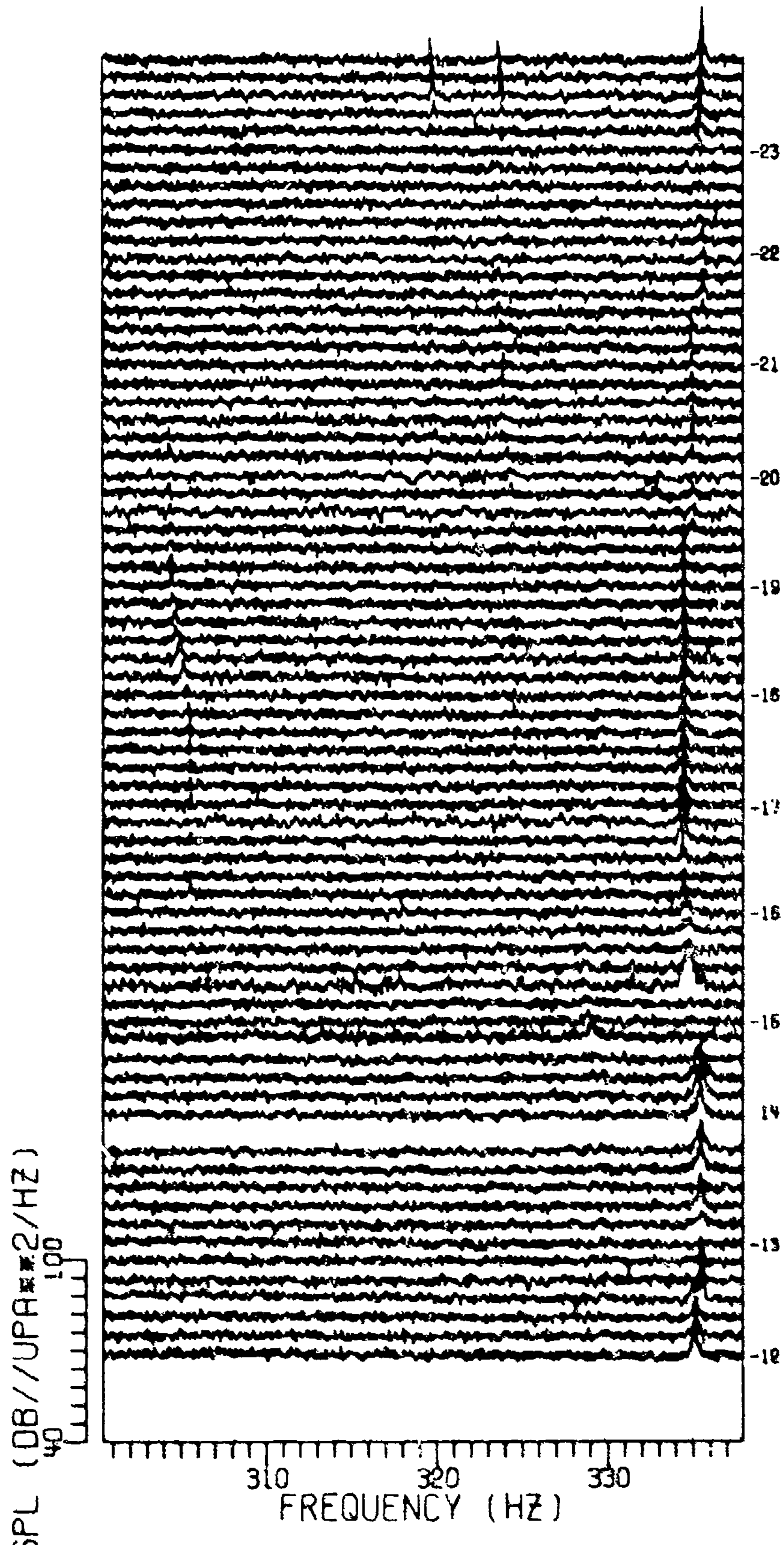

FIGURE III-346

IIA3SHBD 321/12/ 0 - 321/23/55

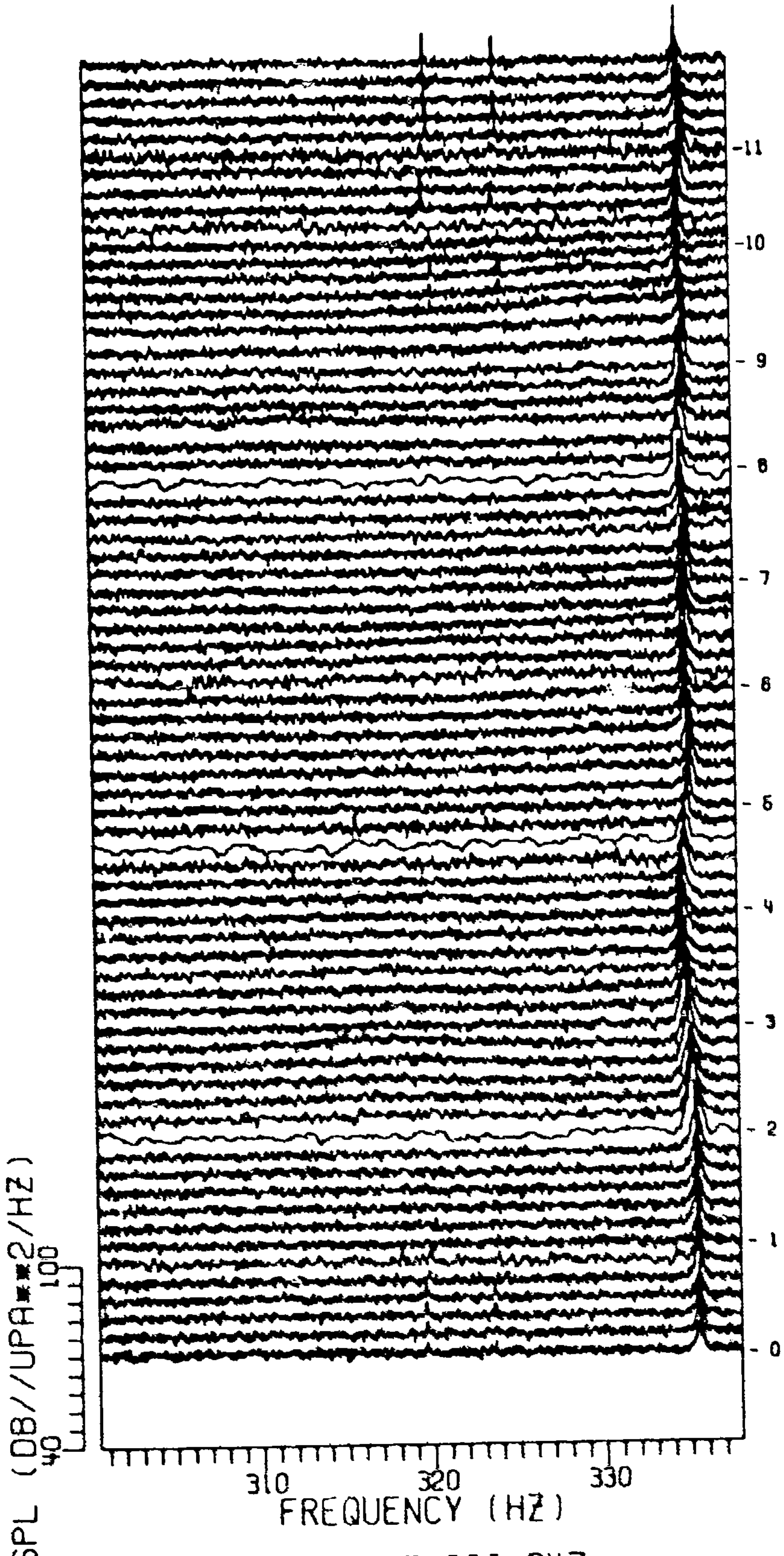

FIGURE III-347

IIA3SHBD 322/ 0/ 0 - 322/11/55

CONFIDENTIAL

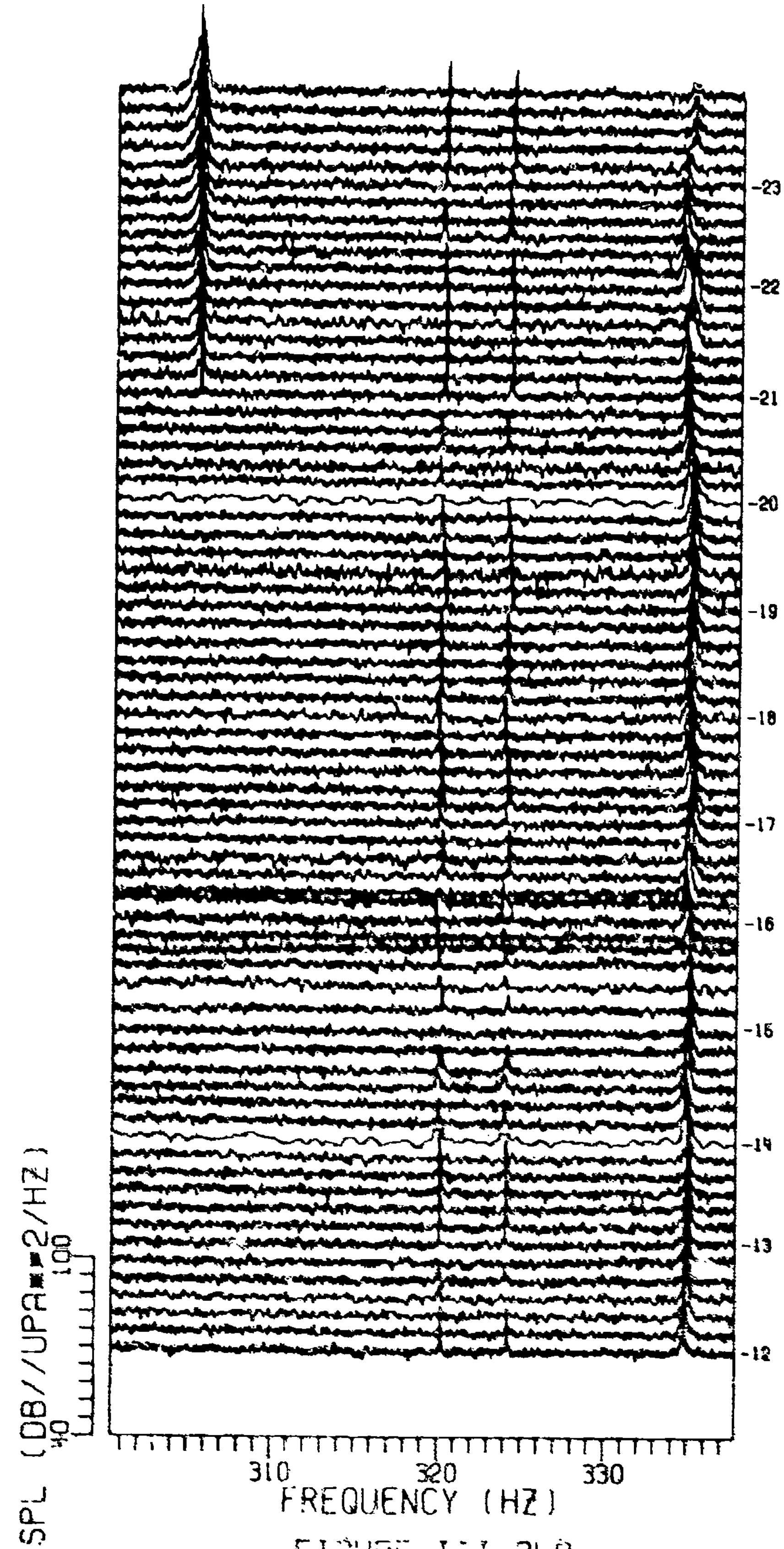

FIGURE III-348

IIA3SHBD 322/12/ 0 - 322/23/55

CONFIDENTIAL

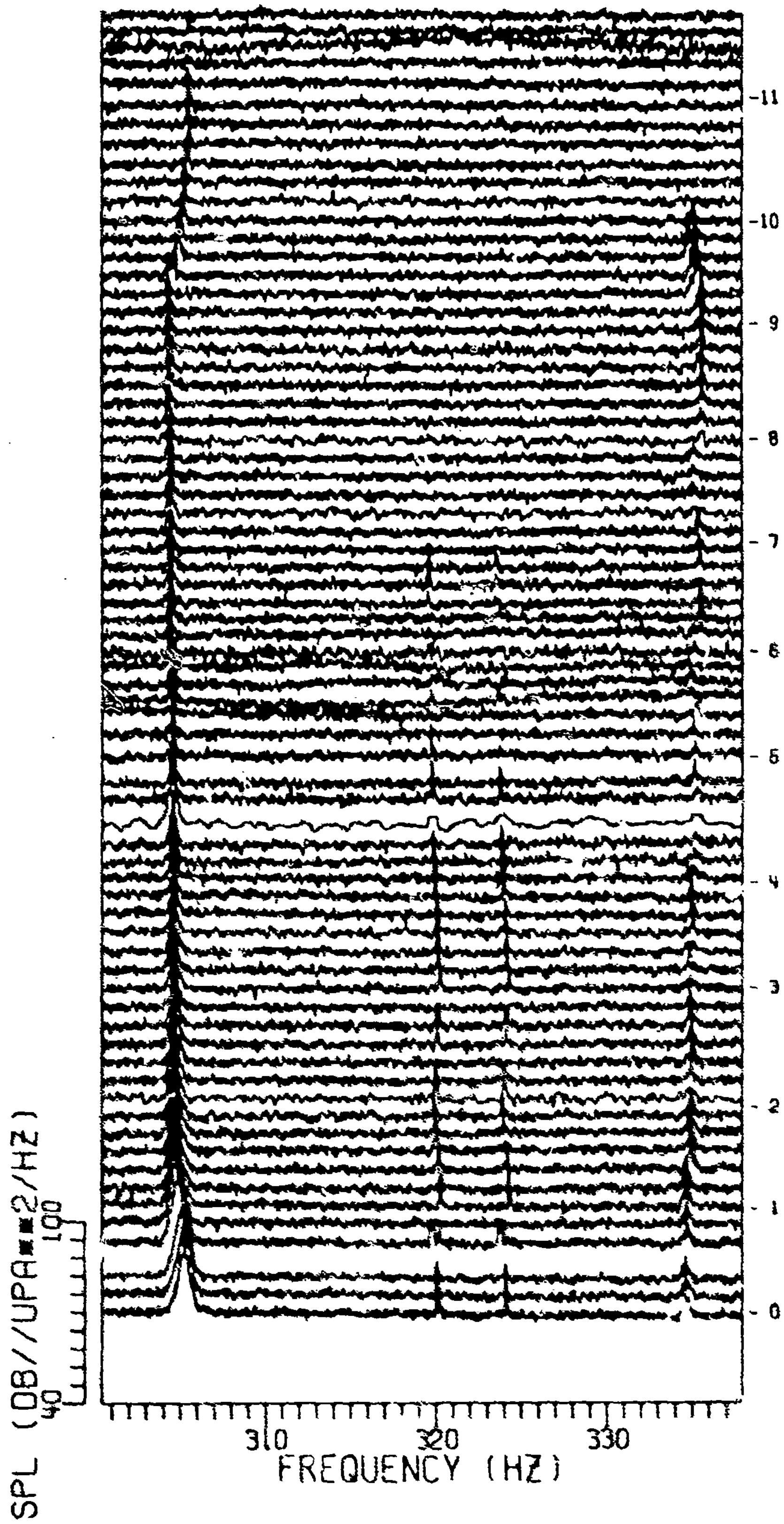

FIGURE III-349

IIA3SHBD 323/ 0/ 0 - 323/11/55

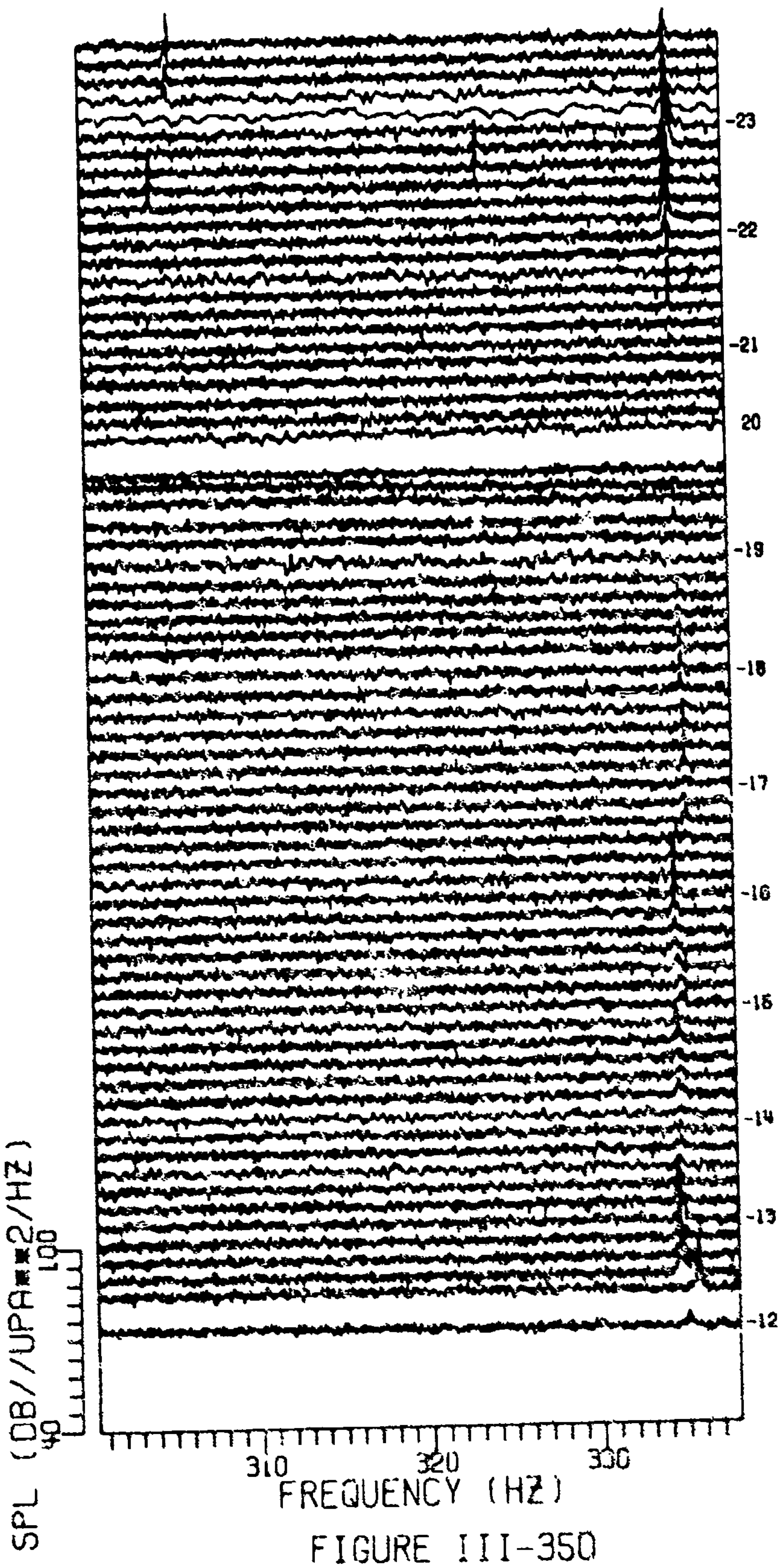

FIGURE III-350

IIA3SHBD 323/12/ 0 - 323/23/55

CONFIDENTIAL

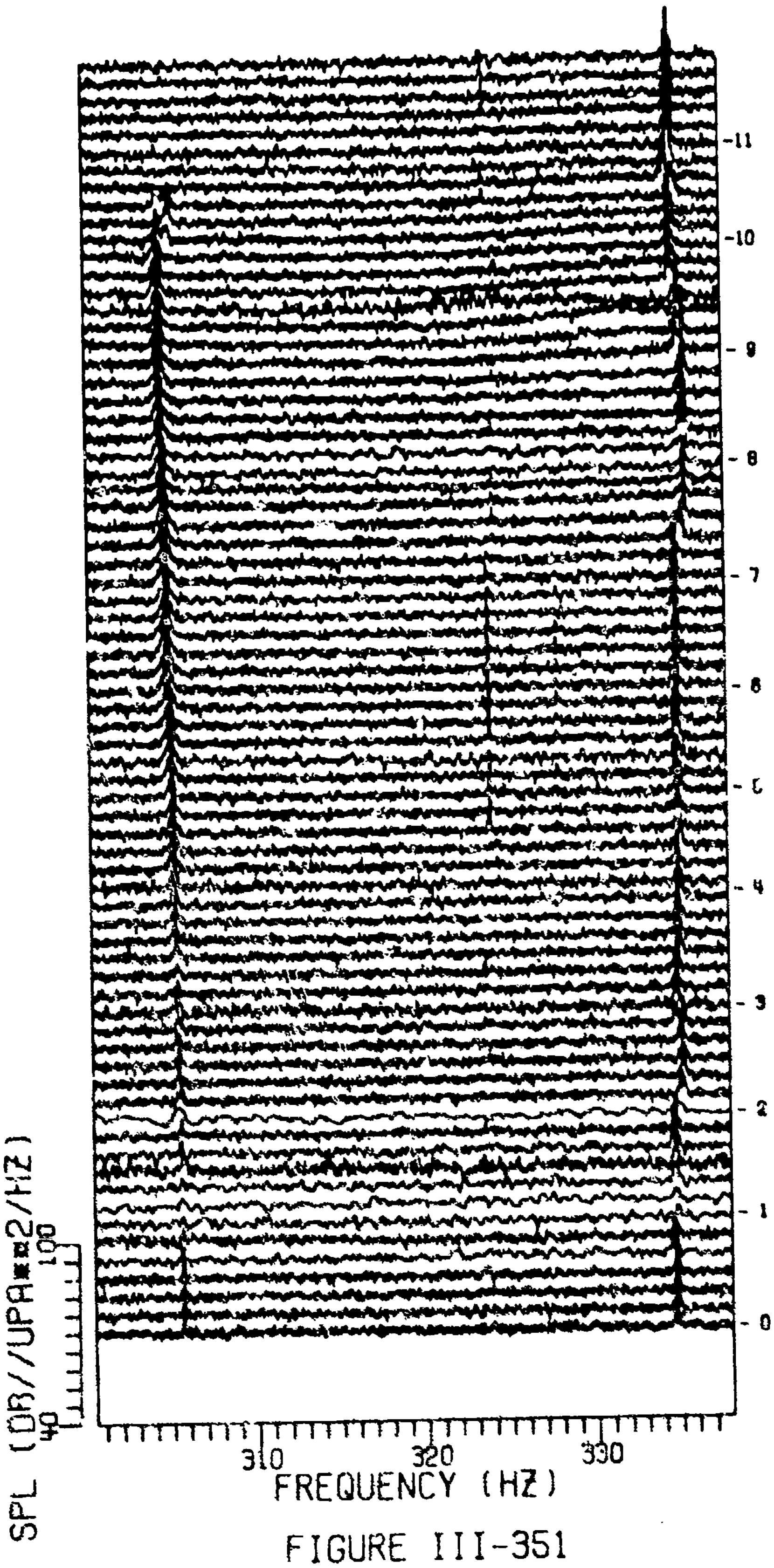

FIGURE III-351

IIA3SHBD 324/ 0/ 0 - 324/11/55

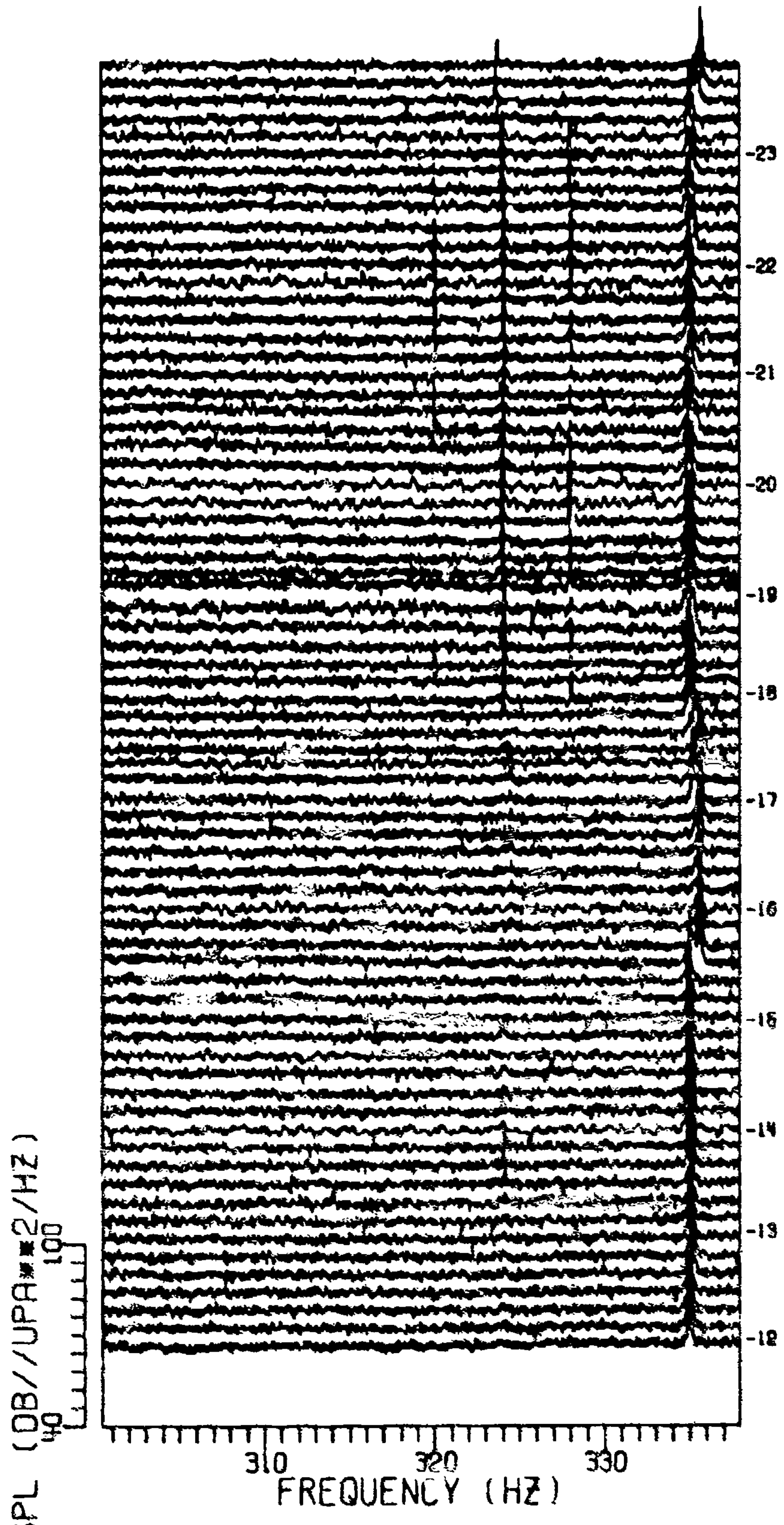

FIGURE III-352

IIA3SHBD 324/12/ 0 - 324/23/55

CONFIDENTIAL

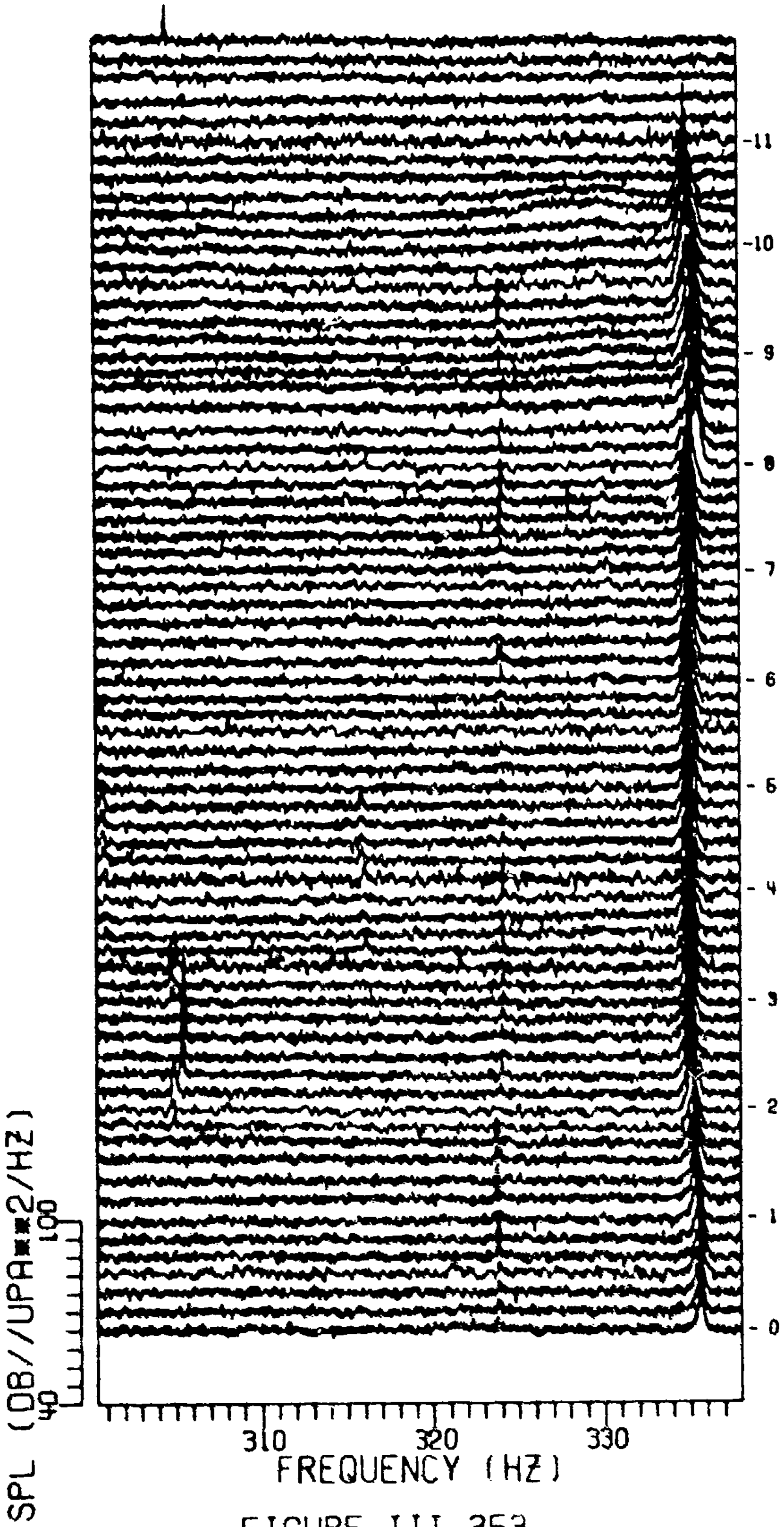

FIGURE III-353

IIA3SHBD 325/ 0/ 0 - 325/11/55

CONFIDENTIAL

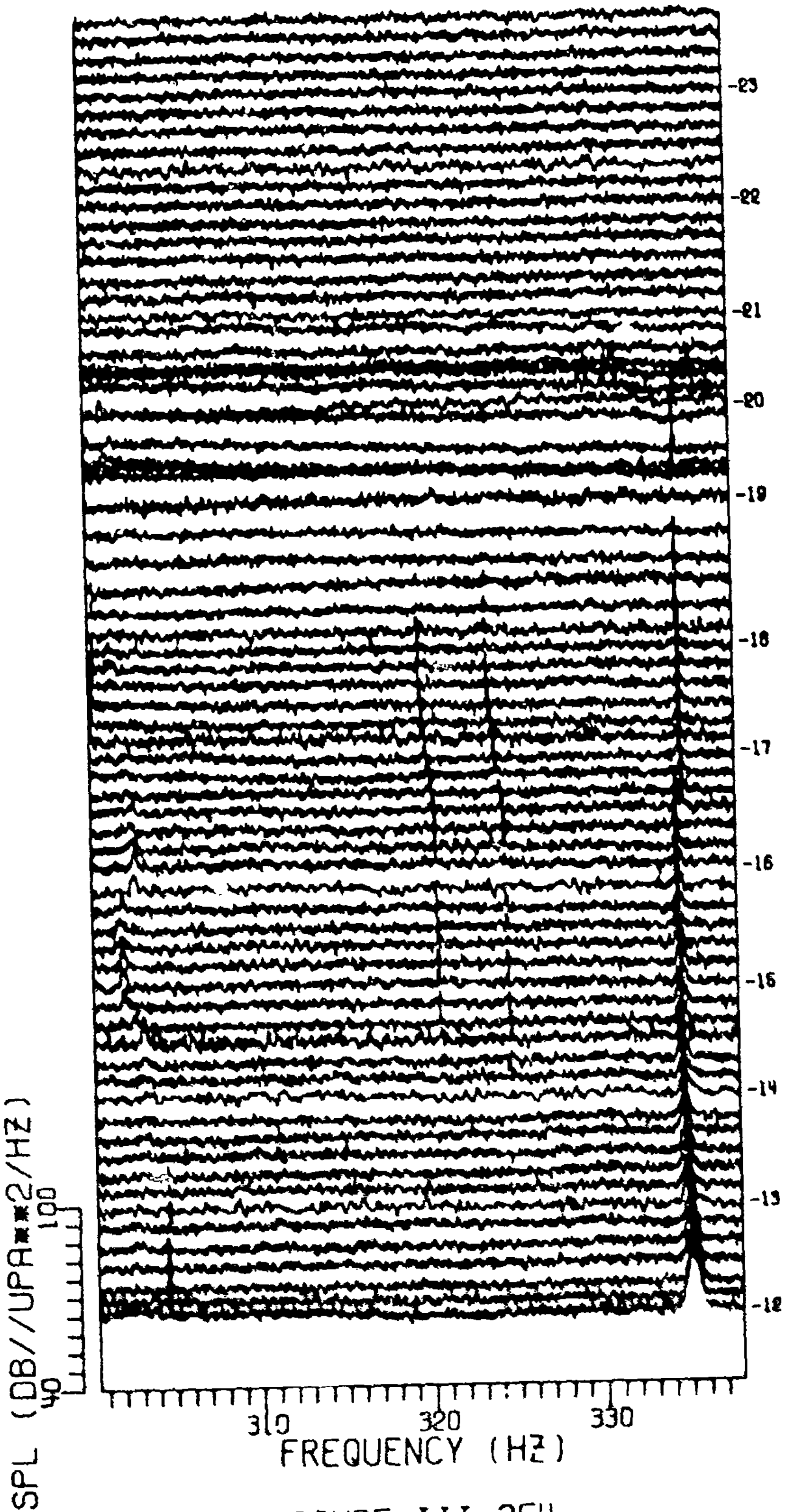

FIGURE III-354
IIA3SHBD 325/12/ 0 - 325/23/55

31 December 1978

DISTRIBUTION LIST FOR
ARL-TR-78-3
FINAL REPORT UNDER CONTRACT N00039-77-C-0003, (ITEMS 0003 AND 0004)
SECRET

Copy No.

	Commander Naval Electronic Systems Command Department of the Navy Washington, DC 20360
1	Attn: PME 124
2	PME 124-30
3	PME 124-40
4	PME 124-60
5	PME 124TA
6	ELEX 320
7	Office of Assistant Secretary of the Navy (RE&S) Room 5E813, Pentagon Washington, DC 20360 Attn: Mr. G. Cann
	Chief of Naval Operations Department of the Navy Washington, DC 20350
8	Attn: OP-095
9	OP-951F
10	OP-951F1
11	OP-981
	Commander Naval Air Development Center Department of the Navy Warminster, PA 18974
12	Attn: Code 3091
13	Code 303
14	Commander Naval Air Systems Command Department of the Navy Washington, DC 20360 Attn: Code PMA-264A

Dist. List for ARL-TR-78-3 under Contract N00039-77-C-0003,
Items 0003 and 0004 (Cont'd)

Copy No.	
15	Commanding Officer Naval Intelligence Support Center 4301 Suitland Road Washington, DC 20390 Attn: Code 222
16	Project Manager Anti-Submarine Warfare Systems Project Office Department of the Navy Washington, DC 20360 Attn: ASW 01T
	Commanding Officer Naval Ocean Research and Development Activity Department of the Navy NSTL Station, MS 39529
17	Attn: S. Marshall, Code 340
18	G. Lewis, Code 500
19 - 20	Commanding Officer and Director Defense Documentation Center Cameron Station, Building 5 5010 Duke Street Alexandria, VA 22314
21	TRW, INC. TRW Defense and Space Systems Group Washington Operation 7600 Colshire Drive McLean, VA 22101 Attn: W. Morley
22	Sanders Associates, Inc. 95 Canal Street Nashua, NH 03606 Attn: L. Gagne
23	Office of Naval Research Resident Representative Room 508, Federal Building Austin, TX 78701
24	Glen E. Ellis, ARL:UT
25	Loyd D. Hampton, ARL:UT

Dist. List for ARL-TR-78-3 under Contract N00039-77-C-0003,
Items 0003 and 0004 (Cont'd)

Copy No.

15	Commanding Officer Naval Intelligence Support Center 4301 Suitland Road Washington, DC 20390 Attn: Code 222
16	Project Manager Anti-Submarine Warfare Systems Project Office Department of the Navy Washington, DC 20360 Attn: ASW 01T
	Commanding Officer Naval Ocean Research and Development Activity Department of the Navy NSTL Station, MS 39529
17	Attn: S. Marshall, Code 340
18	G. Lewis, Code 500
19 - 20	Commanding Officer and Director Defense Documentation Center Cameron Station, Building 5 5010 Duke Street Alexandria, VA 22314
21	TRW, INC. TRW Defense and Space Systems Group Washington Operation 7600 Colshire Drive McLean, VA 22101 Attn: W. Morley
22	Sanders Associates, Inc. 95 Canal Street Nashua, NH 03606 Attn: L. Gagne
23	Office of Naval Research Resident Representative Room 508, Federal Building Austin, TX 78701
24	Glen E. Ellis, ARL:UT
25	Loyd D. Hampton, ARL:UT

Dist. List for ARL-TR-78-3 under Contract N00039-77-C-0003, Items 0003 and 0004 (Cont'd)

Copy No.	
26	Kenneth E. Hawker, ARL:UT
27	Stephen K. Mitchell, ARL:UT
28	Clark S. Penrod, ARL:UT
29	Jack A. Shooter, ARL:UT
30	Library, ARL:UT

DEPARTMENT OF THE NAVY
OFFICE OF NAVAL RESEARCH
875 NORTH RANDOLPH STREET
SUITE 1425
ARLINGTON VA 22203-1995

IN REPLY REFER TO:

5510/1
Ser 321OA/011/06
31 Jan 06

MEMORANDUM FOR DISTRIBUTION LIST

Subj: DECLASSIFICATION OF LONG RANGE ACOUSTIC PROPAGATION PROJECT (LRAPP) DOCUMENTS

Ref: (a) SECNAVINST 5510.36

Encl: (1) List of DECLASSIFIED LRAPP Documents

1. In accordance with reference (a), a declassification review has been conducted on a number of classified LRAPP documents.

2. The LRAPP documents listed in enclosure (1) have been downgraded to UNCLASSIFIED and have been approved for public release. These documents should be remarked as follows:

   Classification changed to UNCLASSIFIED by authority of the Chief of Naval Operations (N772) letter N772A/6U875630, 20 January 2006.

   DISTRIBUTION STATEMENT A: Approved for Public Release; Distribution is unlimited.

3. Questions may be directed to the undersigned on (703) 696-4619, DSN 426-4619.

BRIAN LINK
By direction

Subj: DECLASSIFICATION OF LONG RANGE ACOUSTIC PROPAGATION PROJECT (LRAPP) DOCUMENTS

DISTRIBUTION LIST:

NAVOCEANO (Code N121LC – Jaime Ratliff)
NRL Washington (Code 5596.3 – Mary Templeman)
PEO LMW Det San Diego (PMS 181)
DTIC-OCQ (Larry Downing)
ARL, U of Texas
Blue Sea Corporation (Dr.Roy Gaul)
ONR 32B (CAPT Paul Stewart)
ONR 321OA (Dr. Ellen Livingston)
APL, U of Washington
APL, Johns Hopkins University
ARL, Penn State University
MPL of Scripps Institution of Oceanography
WHOI
NAVSEA
NAVAIR
NUWC
SAIC

Declassified LRAPP Documents

Report Number	Personal Author	Title	Publication Source (Originator)	Pub. Date	Current Availability	Class.
Unavailable	Penrod, C. S., et al.	MOORED SURVEILLANCE SYSTEM FIELD VALIDATION TEST SENSOR PERFORMANCE ANALYSIS. VOLUME I. DATA COLLECTION AND MESUREMENT SYSTEM DESCRIPTION	University of Texas, Applied Research Laboratories	781231	ADC018009	C
Unavailable	Watkins, S. L., et al.	MOORED SURVEILLANCE SYSTEM FIELD VALIDATION TEST SENSOR PERFORMANCE ANALYSIS. VOLUME III. VERNIER RESOLUTION DATA PRODUCTS	University of Texas, Applied Research Laboratories	781231	ADC018373	C
Unavailable	Watkins, S. L., et al.	MOORED SURVEILLANCE SYSTEM FIELD VALIDATION TEST SENSOR PERFORMANCE ANALYSIS. VOLUME II. STANDARD RESOLUTION DATA PRODUCTS	University of Texas, Applied Research Laboratories	781231	ADC018374	C
NORDATN44	Bucca, P. J.	ENVIRONMENTAL VARIABILITY DURING THE CHURCH STROKE II CRUISE FIVE EXERCISE (U)	Naval Ocean R&D Activity	790201	ADC020353; NS; AU; ND	C
NADC7820830	Balonis, R. M.	TEST STEERED VERTICAL LINE ARRAY (TSVLA) MEASUREMENTS FOR BEARING STAKE SURVEYS (U)	Naval Air Systems Command	790301	ADC018003; NS; ND	C
USIControl674779	Williams, W., et al.	REPORT OF THE LRAPP EXERCISE PLANNING WORKSHOP TRACOR INC ROCKVILLE MD 16 - 17 OCTOBER 1978 (U)	Underwater Systems, Inc.	790302	NS; ND	C
NOSCTR357	Hamilton, E. L., et al.	GEOACOUSTIC MODELS OF THE SEAFLOOR: GULF OF OMAN, ARABIAN SEA, AND SOMALI BASIN (U)	Naval Ocean Systems Center	790615	ND	C
Unavailable	Unavailable	RAPIDLY DEPLOYABLE SURVEILLANCE SYST (RDSS) ACOUSTIC VALIDATION TEST (AVT) EXERCISE PLAN (U)	Naval Electronic Systems Command	790625	AU	C
LRAPPRC79027	Brunson, B. A., et al.	GULF OF MEXICO AND CARIBBEAN SEA DATA AND MODEL BASE REPORT (U)	Tracor, Inc.	790701	ADC019153; NS; ND	C
Unavailable	Unavailable	BEARING STAKE BMS DATA QUALITY ASSESSMENT REPORT (U)	University of Texas, Applied Research Laboratories	790705	AU	C
PME12430	Unavailable	RAPIDLY DEPLOYABLE SURVEILLANCE SYSTEM (RDSS) ACOUSTIC VALIDATION TEST (AVT) DATA REDUCTION AND ANALYSIS PLAN (U)	Naval Electronic Systems Command	790815	NS; AU	C
Unavailable	Unavailable	RAPIDLY DEPLOYABLE SURVEILLANCE SYSTEM (RDSS) ACOUSTIC VALIDATION TEST (AVT) EXERCISE PLAN (U)	Naval Electronic Systems Command	790917	AU	C
NOSCTR467	Pedersen, M. A., et al.	PROPAGATION LOSS ASSESSMENT OF THE BEARING STAKE EXERCISE (U)	Naval Ocean Systems Center	790928	ADC020845; NS; AU; ND	C
NOSCTR466	Anderson, A. L., et al.	BEARING STAKE ACOUSTIC ASSESSMENT (U)	Naval Ocean Systems Center	790928	ADC020797; NS; AU; ND	C